Anchorages and Laps in Reinforced Concrete Members under Monotonic Loading

Von der Fakultät für Bauingenieurwesen
der Rheinisch-Westfälischen Technischen Hochschule Aachen
zur Erlangung des akademischen Grades einer Doktorin der Ingenieurwissenschaften
genehmigte Dissertation

vorgelegt von

Janna Caroline Schoening

Berichter: Univ.-Prof. Dr.-Ing. Josef Hegger
Prof. Dr.-Ing. Rolf Eligehausen
Prof. Dr. John Cairns

Tag der mündlichen Prüfung: 21.06.2018

Kurzfassung

Der Verbund zwischen Stahlbetonbewehrung und umgebendem Beton wird durch hohe einzuleitende Zug- oder Druckkräfte stark beansprucht. Bewehrungsstäbe mit großen Stabdurchmessern, die hohe Längskräfte aufnehmen können, aber auch eng angeordnete Bewehrung mit geringer Betondeckung führen zu einer hohen Ausnutzung von Verbundbereichen in Stahlbetonbauteilen. Die Tragfähigkeit der Verbundbereiche wird dabei durch werkstofftechnische, größtenteils aber geometrische Parameter beeinflusst.

Für die zweite Generation des Eurocode 2 wurde eine neue Bemessungsgleichung für die Berechnung erforderlicher Verankerungs- und Übergreifungslängen vorgeschlagen. Dieser Ansatz basiert auf einer Bemessungsgleichung auf Mittelwertniveau, die bei der Erstellung des Model Codes 2010 aus einer umfangreichen Datenbank abgleitet wurde. Eine Überführung des vorgeschlagenen Bemessungsansatzes vom gegebenen Mittelwertniveau auf das Bemessungsniveau, das dem Sicherheitskonzept des Eurocode 0 entspricht, steht bisher noch aus.

Während der aktuelle Eurocode 2 und insbesondere der Nationale Anhang für Deutschland zahlreiche Zusatzregeln zum Einsatz großer Stabdurchmesser > Ø 32 mm enthalten, enthält der Neuvorschlag keine dieser Regeln mehr. Dies wurde zum Anlass genommen, die Notwendigkeit der Zusatzregeln grundlegend zu untersuchen.

Zur Bestimmung des Verbundtragverhaltens von Stahlbetonbauteilen mit großen Stabdurchmessern wurden Beam-End Versuche, Vierpunkt-Biegeversuche mit Übergreifungsstößen und Verankerungsversuche an direkten Auflagern durchgeführt. Dabei stand neben der Untersuchung der Verbundtragfähigkeit insbesondere auch die Rissentwicklung im Fokus. Während Eurocode 2 verschiedene Möglichkeiten zur Rissbreitenreduktion von Querrissen in kontinuierlich bewehrten Stahlbetonbauteilen definiert, sind bisher für Querrissbreiten an Stoßenden und für Längsrisse in Verbundbereichen keine konkreten Angaben enthalten.

Außerdem werden die Parametereinflüsse anhand einer umfassenden Datenbank mit Verankerungs- und Stoßversuchen bestimmt. Diese dient ebenfalls zur Ableitung von Kalibrierwerten für die Bemessungsgleichungen der mittleren Bewehrungsspannung in Verbundbereichen. Bemessungswerte der erforderlichen Verbundlänge werden auf Grundlage einer statistischen Auswertung der Verbunddatenbank und einer anschließenden Anwendung des Verfahrens in Eurocode 0 ermittelt. Neben erforderlichen Kalibrierwerten werden Bewehrungsregeln für hoch ausgenutzte Verankerungen und Übergreifungen vorgeschlagen. Für die Empfehlung praxisgerechter Konstruktionsregeln werden sowohl die Ergebnisse der Tragfähigkeitsuntersuchung als auch der Rissbreitenauswertung herangezogen.

Abstract

In structural concrete members with reinforcing bars subjected to high longitudinal forces, bond zones are highly utilised. The bond strength between reinforcement and surrounding concrete depends on material and geometric parameters. Reinforcement with large-diameter bars bearing high longitudinal forces as well as dense reinforcement positioning further increase the utilisation of bond zones.

For the second generation of Eurocode 2, a new design equation for the calculation of necessary anchorage and lap lengths was proposed. This equation is based on a model for the calculation of mean strength that was derived for Model Code 2010 on the basis of a comprehensive bond database. A transfer of the given design model from mean to design level corresponding with the safety concept of Eurocode 0 is not conducted, yet. While Eurocode 2 and the German National Annex comprise numerous additional rules for the application of large diameter bars Ø > 32 mm, the proposal for the next generation of Eurocode 2 does not include any rules for large diameter bars. For this reason, the necessity of additional rules for large diameter bars is closely investigated in this thesis.

For the determination of the bond behaviour of structural elements with large diameter bars, beam-end tests, four-point bending tests with laps as well as anchorage tests at direct supports were conducted. The fundamental bond behaviour of large-diameter bars was investigated in beam-end tests. Since the additional rules for large-diameter bars are most restrictive for laps, the necessity of these rules were analysed on the basis of four-point bending tests with laps. The actual structural behaviour of end anchorages was tested in anchorages in simply supported beams to account for transverse pressure and densely positioned bars.

While Eurocode 2 defines several possibilities for transverse crack width reduction in continuously reinforced structural elements, specifications for transverse cracks at lap ends and longitudinal cracks are not given. Hence, the key objectives of this thesis are the investigation of developable bar stress in bond zones and the crack development.

Calibration factors for the transfer of mean values to design values are derived from the bond database. Initially, characteristic values of bar stress in bond zones and corresponding model uncertainties are obtained by a statistical evaluation of the test results given in the database. Subsequently, the design value for anchorage and lap lengths is obtained by applying the method according to Eurocode 0. The resulting calibration factor is verified by a level II reliability analysis. Besides the necessary calibration factor, detailing rules for highly utilised anchorages and laps are proposed. The detailing recommendations for practical application are based on the results of experimental load and crack width investigations.

Preface and Acknowledgements

This dissertation was created during my time as research associate at the Institute of Structural Concrete at RWTH Aachen University. It is based on four extensive research projects on bond between reinforcing bars and surrounding concrete. Within these projects, connections of prefabricated members in UHPC (DFG), structural elements with high-strength reinforcement (BBSR) and particularly reinforcement with large diameter bars (AiF) were investigated.

I would like to thank Univ.-Prof. Dr.-Ing. Hegger for the opportunity to work on these projects and for the supervision of this thesis. Despite his many commitments, Professor Hegger has often taken a good deal of time to discuss technical issues together. His advice and his focused way of processing projects has definitely provided support for this work. Prof. Dr. Cairns and Prof. Dr.-Ing. Eligehausen have not only reviewed this thesis, but also conduced toward its success by discussions within the fib task group 2.5 on bond.

During my long time at the institute, I collaborated with many colleagues, whom I would like to thank for the great cooperation. I am very happy that this has resulted in many friendships. My thorough student assistants have contributed to the realisation of the numerous tests. Especially those who have measured and evaluated cracks for hours. For the careful review of this text I would like to thank my colleague Alexander and my brother Timm.

Many thanks are due to my parents, who always stand by my side. The processing of several research projects, the publications, the travels and the finalisation of this dissertation besides the parenting of our children were only possible with the active support of all grandparents, for which I would like to thank them very much.

Most of all, I would like to thank Rahul, who has never questioned the demanding combination of raising children and scientific work, and who is my steady support in all respects.

Aachen, March 2018 Janna Schoening

Notation

Units

Strain: ‰
Force: kN, MN
Stress: MPa
Distance: mm, cm, m

Capital Latin Letters

A_s	cross-sectional area of one bar of the longitudinal reinforcement
$A_{s,calc}$	calculated cross-sectional area of longitudinal reinforcement
$A_{s,prov}$	cross-sectional area of longitudinal reinforcement provided
A_{st}	cross-sectional area of one leg of transverse reinforcement
COV	coefficient of variation
E_c	Young's Modulus of concrete
E_d	design value of action effects
E_k	characteristic value of action effects
E_s	Young's Modulus of reinforcing bar
F	force
F_s	reinforcing bar force
$F_{splitting}$	splitting resistance by concrete cover along the lap length
$F_{stirrup}$	splitting resistance by transverse reinforcement
K	coefficient for efficiency of transverse reinforcement defined in EUROCODE 2
K_{tr}	transverse reinforcement index defined in ACI
M	moment
P_f	failure probability for a certain time period
P_s	reliability of a structure
Q	standard deviation defined in EUROCODE 0
R_d	design value of structural resistance
R_k	characteristic value of structural resistance
R_p	p-quantile of structural resistance
V	shear force
V_δ	coefficient of variation of the errors δ_i defined in EUROCODE 0
V_{fc}	coefficient of variation of concrete strength
V_i	coefficient of variation
V_θ	coefficient of variation of model uncertainty
V_{fc}	coefficient of variation of concrete strength
V_m	coefficient of variation of the design model

$V_{T/P}$ coefficient of variation of the test to prediction ratio

V_{ts} coefficient of variation of uncertainties in the measured loads and differences in the actual material and geometric properties

V_R coefficient of variation for unknown relative rib areas defined by DARWIN

V_R coefficient of variation of resistance

V_x coefficient of variation of a model defined in EUROCODE 0

V_{xi} coefficient of variation of stochastically independent random variables

X_{di} material properties (stochastically independent random variables)

Lowercase Latin Letters

a_{di} design value of a geometrical property

a_{eff} shear span

b width

b slope of the least-squares best fit line

c_b minimum concrete cover as defined in ACI

c_d smallest value of $c_s/2$, c_x and c_y

c_{min} minimum concrete cover

c_{max} maximum concrete cover

c_x side concrete cover

c_y bottom concrete cover

c_s anchored or lapped bar spacing

d effective depth

f_{bm} mean bond strength

f_c concrete compressive strength

f_c' concrete compressive strength as defined in ACI

$f_{c,cube}$ concrete cube strength (200 mm cubes)

f_{ck} characteristic concrete compressive strength

f_{cm} mean concrete compressive strength

f_{ct} tensile strength of concrete

f_{ctd} design tensile strength of concrete

$f_{ctk;0.05}$ characteristic tensile strength of concrete defined as 5%-quantile value

f_{ctm} mean tensile strength of concrete

f_R relative rib area

f_{std} design longitudinal bar stress in bond zones

f_{stm} mean longitudinal bar stress in bond zones

f_y yield strength of reinforcing bars

f_{yk} characteristic yield strength of reinforcing bars

f_{yd} design yield strength of reinforcing bars

g	limit state function
g_{rt}	limit state function
h	height
k_{conf}	effectiveness factor for confinement
k_d	coefficient for efficiency of transverse reinforcement
k_d	coefficient for the effect of bar diameter
$k_{d,n}$	factor for quantile values taking the index of reliability into account
k_m	coefficient for efficiency of transverse reinforcement
k_p	coefficient for reinforcing bar surface
k_q	coefficient for the effect of different steel stress at the lap ends
k_R	coefficient for statistical distribution of resistance
k_v	coefficient for bond conditions
l_0	lap length
l_b	bond or anchorage length
l_t	development length
l_x	distance from centre of support
n_b	number of anchored bars or pairs of lapped bars
n_l	number of legs of confining reinforcement defined in FIB BULLETIN 72
n_{st}	number of items of confining reinforcement within bond length
n_t	number of legs of confining reinforcement
p_{tr}	compression stress perpendicular to the potential splitting plane
r_{ei}	experimental value of a resistance
r_k	characteristic value of resistance defined in EUROCODE 0
r_t	theoretical resistance defined in EUROCODE 0
r_{ti}	theoretical value of a resistance
s_Δ	standard deviation of logarithm of error terms δ_i
s_{st}	longitudinal spacing of confining reinforcement
$s_{r,max}$	maximum possible crack spacing
t_d	coefficient for the effect of bar diameter
t_r	coefficient for the effect of rib geometry
w_k	crack width
w_E	crack width at lap ends
w_{lim}	crack width limit
x	Position in the lap commencing from the lap end
x_{lt}	Position between the cracks commencing from the crack
z	lever arm of internal forces

Greek Letters and Symbols

Ø	bar diameter
$Ø_{eq}$	equivalent bar diameter

α_6	lap factor defined in EUROCODE 2
α_c	confinement contribution provided by concrete cover
α_E	weighting factor for action effects E
$\alpha_{i,EC}$	reduction factors defined in EUROCODE 2
α_Q	coefficient for calibration
α_R	weighting factor for resistance R
α_t	coefficient for the bar diameter
α_{tp}	confinement contribution provided by transverse pressure
α_{tr}	confinement contribution provided by transverse reinforcement
β	index of reliability
β_t	coefficient for strain function
δ_i	error term which defines the model uncertainty defined in EUROCODE 0
Δ_i	logarithm of error terms δ_i
ε_{cm}	mean concrete strain along crack spacing
ε_{sm}	mean steel strain along crack spacing
ε_{sr1}	steel strain between the cracks at crack formation
ε_{sr2}	steel strain in the crack at crack formation
$\varepsilon_{s2,end}$	reinforcement strain at the lap end
ϕ_{ACI}	strength reduction factor defined in ACI CODE 318
ϕ_b	reduction factor for bond
Φ	cumulative distribution function of the standardised normal distribution
γ_c	partial safety factor for concrete
γ_F	safety factor for action effects
γ_{gl}	global safety factor
γ_m	partial safety factor for uncertainties in material properties
γ_M	partial safety factor for uncertainties in material properties and model uncertainties
γ_R	partial safety factor for structural resistance
γ_{Rd}	partial safety factor for model uncertainties in structural resistance
η	conversion factor defined in EUROCODE 0
η_1	coefficient for reinforcement surface
η_2	coefficient for bond conditions
η_3	coefficient for the effect of bar diameter
η_4	coefficient for the characteristic strength of steel reinforcement
η_d	design value of a conversion factor for volume and scale effects
λ	coefficient for light-weight concrete (1.0 for normal concrete)
λ	coefficient for contribution of transverse reinforcement defined in

	EUROCODE 2
μ_E	mean value of action effects
μ_g	mean value
μ_θ	mean value of model uncertainty
μ_R	mean value of resistance
μ_x	mean value of a model defined in EUROCODE 0
θ	inclination of struts
θ	model uncertainty
θ_{di}	model uncertainties within a model with several stochastically independent random variables
ψ_t	coefficient for bond (1.0 for good bond conditions)
ψ_e	coefficient for coated reinforcement
ψ_s	coefficient for bar diameter
ρ_{conf}	ratio of the reinforcement providing confinement
σ_{ctd}	design value of the mean compression stress perpendicular to the potential splitting plane
σ_E	standard deviation of action effects
σ_{fc}	standard deviation of concrete strength
σ_g	standard deviation
σ_R	standard deviation of resistance
σ_s	reinforcing bar stress
$\sigma_{s,max}$	calculated or observed maximum reinforcing bar stress
$\sigma_{s,test}$	reinforcing bar stress obtained in tests
$\sigma_{s,calc}$	reinforcing bar stress calculated according to design models
σ_s^c	concrete contribution
σ_s^{st}	transverse reinforcement contribution

1 Introduction

1.1 Background and Motivation

There is international consensus on many design models for structural concrete elements. However, the harmonisation of code provisions reveals that the structural analysis of some details was conducted very differently in single national codes in the past. The omnipresent anchorage of reinforcing bars is one of the issues still unsolved. At supports of beams and slabs, at curtailed reinforcement and in laps, the question arises, what development length safely anchors the reinforcing bar in the surrounding concrete.

The equations for lap and anchorage length in MODEL CODE 2010 [MC2010] differs from EUROCODE 2 [EC2]. While the equation according to [EC2] is based on MODEL CODE 1990 [MC90], the equation in [MC2010] was derived by a regression analysis described in the Model Code background document on bond [FIB14]. The recently discussed proposal for the next generation of EUROCODE 2 [PT18] contains an equation also based on [FIB14] with a coefficient still under discussion. The resulting lap and anchorage lengths calculated with the equations given in [EC2] and the new proposal [PT18] differ depending on the coefficient used. The design equation for the mean stress in anchorages or laps given in [FIB14] was calibrated with a lap database compiled by the American Concrete Institute and the Institute of Construction Materials at the University of Stuttgart and verified by anchorage tests conducted by AMIN [AMI09]. The influencing parameters for laps and anchorages have been investigated comprehensively in the past, but the design model for lap and anchorage lengths in [MC2010] and the PT1 WORKING DRAFT for the next generation of EUROCODE 2 [PT18] lacks a well-founded derivation of design values. The question arises which coefficient needs to be applied in the equation according to FIB BULLETIN 72 [FIB14] elaborated by fib task group 2.5 for anchorages and laps to safely determine the necessary bond length.

The design model for laps according to the German code for structural concrete published in 1988, DIN 1045 [DEU88] was based on investigations at the Technical University of Munich and at the University of Stuttgart in the 1970s and 1980s. The findings from these investigations were taken into account in the following German codes [DEU08] and [EC2/NA]. The resulting lap lengths were rather long compared to other European codes. The necessity of such lengths was justified by increasing crack widths at lap ends for cyclic loading depending on the lap length. Current investigations by CAIRNS AND ELIGEHAUSEN [CAI14b] showed that the lap design according to EUROCODE 2 [EC2] is partly unsafe. Despite many previous national codes providing shorter lap and anchorage lengths, no major lap or anchorage failure is known.

Bond zones with anchorages and laps are highly utilised, where reinforcing bars are densely positioned and where large diameter bars are used. The necessary bar number in structural members can be reduced by using large diameter bars. The smaller bar or layer number simplifies the placing and compaction of concrete and concurrently enhances the bond quality and durability. During a research project on the investigation of reinforced concrete members with large diameter bars, several issues on laps and anchorages in general arose [HEG15], [HEG18]. The original aim of the conducted research project was the investigation of the numerous additional rules for large diameter bars in EUROCODE 2 [EC2] and its GERMAN NATIONAL ANNEX [EC2/NA]. [EC2] allows for the use of bar diameters up to Ø 40 mm in structural elements without further approval. Depending on the concerned National Annex, bar diameters above a certain limit – the recommended value is Ø 32 mm – underlie additional detailing rules.

Within the research project, the bond behaviour of large diameter bars was investigated by beam-end tests, four-point bending tests with laps and anchorages at direct supports. The replacement of the common pull-out tests by beam-end tests for reinforcement approvals is currently under discussion. Recent investigation showed less scatter in beam-end tests than in pull-out tests [WIL13], but the effort and expenses for beam-end test are higher compared to pull-out test. While the pull-out test is well-suited for the comparison of the bond behaviour of different reinforcement types, it does not reflect real bond zones in structural elements. The question is, whether the beam-end test that rather represents a direct support of a beam, reflects the effects of bond length and confinement in anchorages applied in practice better.

It is known from many lap tests in reinforced concrete members that cracks forming at the lap ends are much wider than cracks in the undisturbed element. [EC2] comprises crack width control for undisturbed structural concrete elements but does not define how to address large crack widths at lap ends. For the bond stress, additional longitudinal cracks can occur in laps and anchorages at high loads and little confinement. [EC2] only states that reinforcing bars shall be anchored so that the bond forces are safely transmitted to the concrete avoiding longitudinal cracking or spalling and that transverse reinforcement shall be provided if necessary. The crack formation both in the transverse and the longitudinal directions does not play a major role for laps with small bar diameters, but for highly utilised cross-sections and large diameter bars, the crack formation becomes increasingly important.

1.2 Aim and Applied Methodology

The aim of this thesis is to investigate the necessity of additional rules for large diameter bars. Furthermore, the thesis aims at the validation of the design model for the bar stress in anchorages and laps according to [FIB14] and the derivation of design values for anchorage and lap lengths.

Chapter 2 presents the basic principles of bond between concrete and ribbed reinforcing bars, as well as the principles of anchorages and lapped splices in reinforced concrete elements. The essential parameters influencing the bond behaviour are described to provide a background for the conducted experimental programme. Since various test specimens for the investigation of bond between concrete and reinforcing bars exist, chapter 2 includes a brief comparison of bond testing methods. Design equations and rules for anchorages and laps including the ultimate and serviceability limit states are given. The current European design code for reinforced concrete structures includes additional rules for large diameter bars described in this chapter. Furthermore, the explanation of the statistical model for the derivation of mean and characteristic crack widths from test specimens is given.

In chapter 3, the beam-end tests, lap and anchorage tests conducted at RWTH Aachen University are documented. The test-specimen design and experimental setup as well as the investigated parameters are described. This chapter presents the applied materials, manufacturing, instrumentation and loading rate of the test specimens. The test results for varying concrete strength, bar diameter, bond length and confinement are given. The test results are compared to the calculated strength and crack widths according to the design models given in Chapter 2. An assessment whether the characteristic crack widths defined in [EC2] covers the large crack widths at the lap ends is given.

Chapter 4 gives a comparison between beam-end tests and beam tests with anchorages and laps. The chapter describes the influences by various parameters observed in the different bond tests. For this purpose, bond strengths obtained in beam-end tests are compared to maximum local bond strengths and bond strengths averaged over the bond length in anchorage and lap tests. The juxtaposition shall clarify whether beam-end tests are suitable for the prediction of bond behaviour in actual structural elements such as in beams with anchorages and laps.

In Chapter 5, a description and analysis of the bond database is shown that provides the basis of the MODEL CODE 2010 [MC2010] formulation for the required anchorage length as described in the fib background document [FIB14]. An adoption of this anchorage design formulation is currently planned for the new EUROCODE 2 generation [PT18]. The database was extended by anchorage tests mostly compiled by AMIN [AMI09] and the own tests described in chapter 3. Since the database evaluation particularly depends on the test results considered, the applied filters and the statistical models are defined. By means of the database, the parameter effects on lap and anchorage strength are analysed. Chapter 5 presents the statistical distribution of the ratio of the test results to the calculated bar stresses according to the design models for anchorages and laps described in chapter 2. Furthermore, a modified design model for mean anchorage and lap strengths is derived.

The database did not include any information on crack width along lapped splices in reinforced concrete elements. Therefore, chapter 6 presents the database extension by information on crack width. The crack width database shows the effects of bond length, bar diameter, reinforcement ratio, confinement and continuous bars on the crack widths at lap ends.

In Chapter 7, the consistent design equation for the mean strength of anchorages and laps for all bar diameters is transferred to design values for anchorage and lap lengths. Previous evaluations of reliability and design values for bond and bar stress in anchorages are presented. Design values for the own model and the model according to [PT18] with own calibration factors derived in chapter 5 are obtained by application of the procedure given in annex D in [EC0]. A level II reliability analysis with COMREL verifies the achievement of the desired index of reliability with the proposed calibration factor.

Chapter 8 illustrates the relation between the design equation and detailing rules for anchorages and laps of straight bars under tension. The detailing includes the percentage of bars anchored or lapped at a section, minimum anchorage lengths, laps of bars with different bar diameters, transverse reinforcement and robustness.

Chapter 9 provides a summary and conclusion of the conducted research on anchorage and lap lengths, a summary on the necessity of additional rules for large diameter bars as well as suggestions for further research.

2 State of the Art on Bond in Concrete

2.1 Bond in Concrete

As a composite material, the structural behaviour of reinforced concrete strongly depends on the bond behaviour between reinforcement and concrete (cf. Figure 2-1, left). In case of deformed reinforcing bars with ribs, the bond is based on contributions by adhesion, shear interlock between the bar deformations (ribs) and the surrounding concrete as well as by friction (cf. Figure 2-1, right). While adhesion contributes to the load transfer at small loads only, the interlock between ribs and concrete lugs becomes activated as soon as a certain slip between reinforcing bar and concrete occurs. The failure of concrete lugs and the following slip increase mobilise friction between reinforcing bar and concrete. Friction does not only result from external transverse pressure acting upon the structural member, but also from concrete shrinkage.

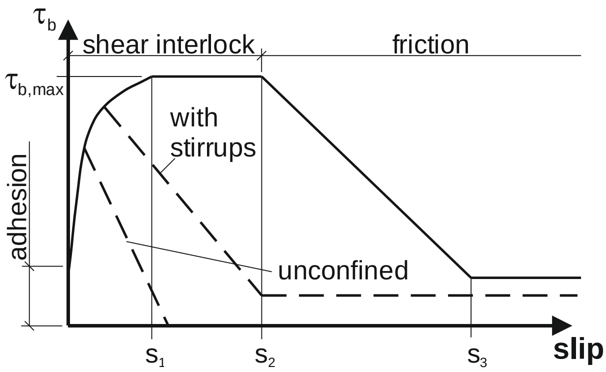

Figure 2-1 Photograph of rib interlock (left) and bond strength τ_b contributions by adhesion, interlock and friction (right)

Tensile forces in reinforcing bars generate local compression cones starting from each rib. For equilibrium, these compression struts lead to tensile cylinder stress (hoop stress) in the surrounding concrete cross-section (cf. Figure 2-2).

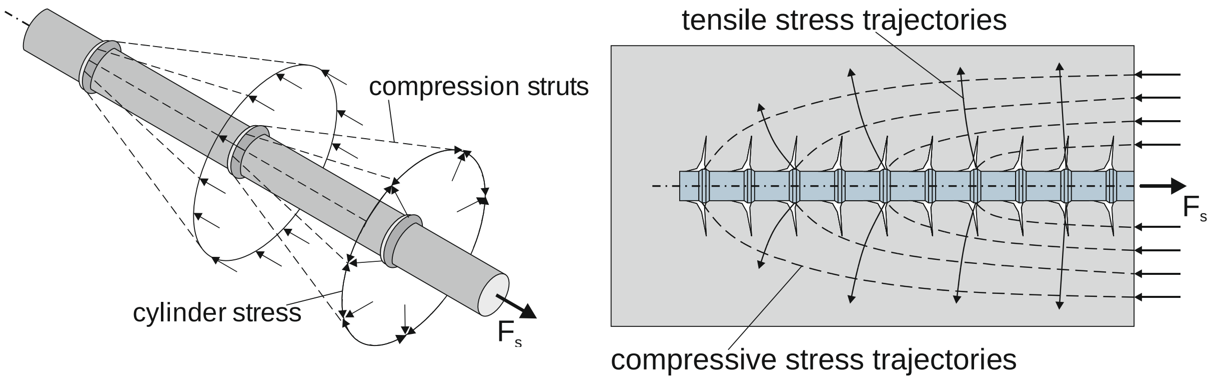

Figure 2-2 Compression struts and cylinder stress (left) and stress trajectories (right) for activated bond between reinforcing bar and surrounding concrete

The bond strength between concrete and reinforcement is usually described by the bond stress τ_b which constitutes an auxiliary unit rather than an actual stress.

$$\tau = \frac{F_s}{U_b \cdot l_b} = \frac{A_s \cdot \sigma_s}{U_b \cdot l_b} = \frac{Ø \cdot \sigma_s}{4 \cdot l_b} \, [\text{MPa}] \tag{2-1}$$

Where

F_s	reinforcing bar force
U_b	bond circumference (= circumference of the reinforcing bar)
l_b	bond length l_b
A_s	cross-sectional area of the reinforcing bar area
σ_s	reinforcing bar stress
Ø	reinforcing bar diameter

Although equation (2-1) suggests that the bond stress τ_b is a force per area, the longitudinal bar force is actually transferred by adhesion, rib interlock as well as friction and does not directly describe force acting upon the area $U_b \cdot l_b$.

High tensile forces in the reinforcing bar lead to either concrete-cone failure or bond failure. Bond failure can be distinguished in pull-out failure and splitting failure. In case the reinforcing bar has sufficient confinement by surrounding concrete, transverse reinforcement or transverse pressure, the concrete lugs between the ribs fail and the reinforcing bar is pulled out of the structural element. If the confinement of the bond zone is not sufficient, the tensile stress of the concrete around the reinforcing bar exceeds the tensile strength of concrete and splitting cracks occur. These cracks lead to a sudden failure where no transverse pressure or reinforcement is present. Transverse reinforcement in the bond zone, e.g. stirrups, does not prevent splitting, but effectively reduces the longitudinal crack widths and can change the failure type from a sudden splitting failure to a pull-out failure at high slip values.

2.2 Slip and Crack Development

The slip between concrete and reinforcing bar s equals the difference between concrete and steel deformation at the same cross-section Δl_s - Δl_c (cf. Figure 2-3).

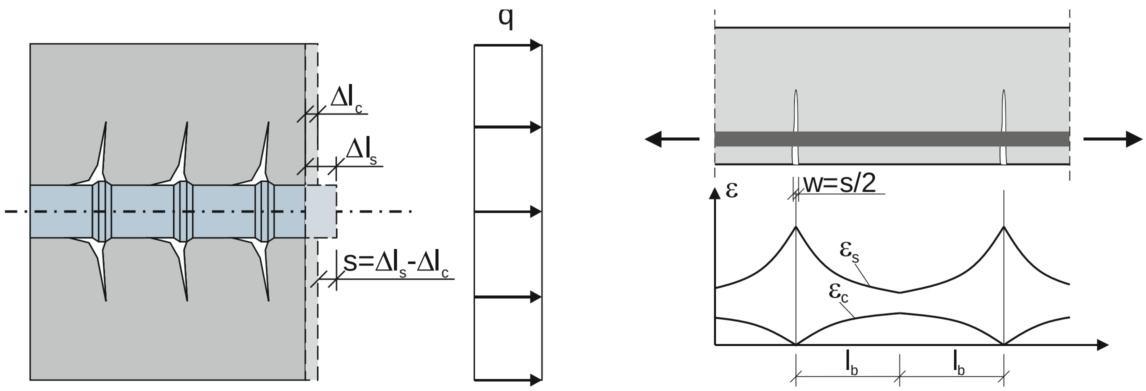

Figure 2-3 Slip s as the difference between steel deformation Δl_s and concrete deformation Δl_c (left) and relation of slip s and crack width w (right)

Besides the bond strength, the reinforcing bar slip at the end of the bond length is another characteristic of the bond behaviour. The bond stiffness is visualised in bond-strength slip curves (cf. Figure 2-1, right). This ratio of bond stress to slip τ_b / s varies for different reinforcement surfaces and concrete types. The reinforcing bar slip also corresponds with half the crack width in structural elements subjected to bending or tensile loads (cf. Figure 2-3, right). Thus, the bond behaviour does not only determine the necessary design of anchorages and laps, but also the crack development of reinforced concrete elements. Both the crack spacing and the crack width depend on bond characteristics.

The maximum bond strength is important for the ultimate limit state design independent from the crack width. For the serviceability limit state, crack control matters and small slip between concrete and reinforcement is necessary. Therefore, different methods for the measurement and evaluation of bond strength can be applied. For crack and deflection control, high bond stiffness at low slip is beneficial. In contrast, the rotation capacity of members under bending increases where bond in the vicinity of flexural cracks disappears after yielding and high steel strain develops [CAI03].

2.3 Differential Equation for Bond

Equation (2-1) is a simplification presuming constant bond stress τ_b along the bond length l_b, while bond strength actually describes the stress differences $\Delta\sigma_s$ and $\Delta\sigma_c$ within an infinitesimal element dx with

$$dx \cdot U_b \cdot \tau_b(x) = \Delta\sigma_s \cdot A_s \Rightarrow \tau_b(x) = \frac{\Delta\sigma_s \cdot A_s}{dx \cdot U_b} \tag{2-2}$$

$$dx \cdot U_b \cdot \tau_b(x) = -\Delta\sigma_c \cdot A_c \Rightarrow \tau_b(x) = -\frac{\Delta\sigma_c \cdot A_c}{dx \cdot U_b} \tag{2-3}$$

The slip at between reinforcing bar and concrete equals

$$s = \Delta l_s - \Delta l_c \tag{2-4}$$

For a linear-elastic material, the differentiations are

$$\frac{ds}{dx} = \frac{\Delta l_s}{dx} - \frac{\Delta l_c}{dx} = \varepsilon_s - \varepsilon_c = \frac{\sigma_s}{E_s} - \frac{\sigma_c}{E_c} \tag{2-5}$$

$$\frac{d^2 s}{d^2 x} = \frac{\Delta\sigma_s}{dx \cdot E_s} - \frac{\Delta\sigma_c}{dx \cdot E_c} \tag{2-6}$$

Introducing equations (2-2) and (2-3) gives

$$\frac{d^2s}{d^2x}=\left(\frac{U_b}{A_s\cdot E_s}-\frac{U_b}{A_c\cdot E_c}\right)\cdot\tau_b\left(x\right)=\frac{4\cdot\tau_b\left(x\right)}{Ø\cdot E_s}\cdot\left(1+\alpha_e\cdot\rho\right) \tag{2-7}$$

With
$\alpha_e = E_s / E_c$
$\rho = A_s / A_c$

The second order differential equation (2-7) can be solved by applying the boundary conditions for reinforcing anchorages or laps. For this purpose, bond strength-slip relations $\tau_b(s)$ must be introduced. Such relations were given in several publications such as [MC2010], [MAR73], [KOE96], [SCH14].

2.4 Influencing Parameters on Bond

2.4.1 Bond Length

The bond stress distribution along reinforcing bars in bond is non-linear. In case the bond length is small, the bond stress decreases rapidly towards the loaded end (cf. Figure 2-4, top left). If the bond length is large, the bond stress drops steadily towards an asymptote (cf. Figure 2-4, bottom left) [WIL13]. The beginning failure of concrete lugs between the ribs towards the loaded end activates lugs at the rear end of the bond length [MAR73].

The non-linear behaviour depends on the softening of the concrete that surrounds the reinforcing bar depending on the crack formation around the tips of the lugs, local crushing of concrete, successive development of radial and longitudinal splitting cracks and formation of cracked shear planes [FIB10].

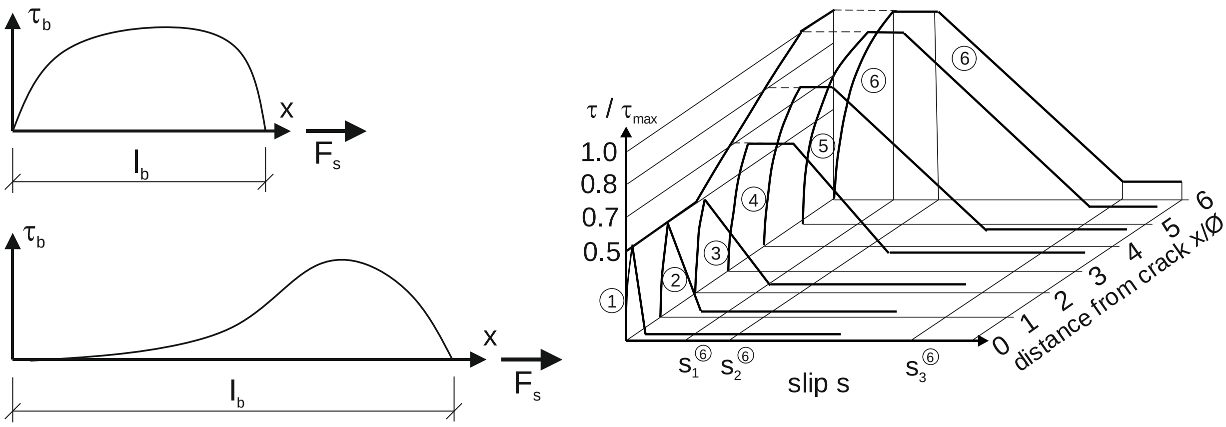

Figure 2-4 Bond stress over bond length for different bond lengths (left) and increasing bond-stress slip curves along the bond length (reproduced from [KRE89]) (right)

Different stress states result at different positions along the bond length (cf. Figure 2-4, left). In the vicinity of cracks, the bond between reinforcement and concrete is deteriorated and the full bond strength is only present at a certain distance of the crack (cf. Figure 2-4, right) [KRE89]. Rear locations along the bond length do not develop the full bond strength where loads are low. As soon as the maximum bond strength is exceeded at the loaded end, the bond between reinforcement and concrete at rear positions of the bond length is activated.

2.4.2 Concrete Strength

Since bond action results from the localised pressure underneath the ribs, it is directly related to the shear component of the interface forces. Additionally, the disseminating compressive struts result in tensile cylinder stress. Bond performance thus depends on both the concrete multi-axial behaviour in compression and on the tensile strength of concrete [FIB10].

For the concrete covers used in practice, bond zones usually fail by splitting and – if confined with transverse reinforcement – by a secondary bar pull-out. Therefore, splitting forces are usually decisive and bond strength is described by the tensile strength of concrete [FIB14].

Both, the bond stiffness $\Delta\tau$ / Δs (cf. Figure 2-1, right) and the bond strength increase by concrete strength are non-linear. Codes usually define bond strength for small slip values to prevent the development of large crack widths. Hence, the bond strength given as the relation of $\tau_b \sim f_c^x$ is usually defined for the initial stiffness with an exponent x between 1/4 and 2/3.

The bond strength of short bond lengths increases with $f_c^{2/3}$, while the increase in bond strength is much smaller for larger bond lengths, since the distribution of the bond strength varies along the bond length. For short bond length and low concrete strength, the bond strength is approximately constant. For high concrete strength and large bond lengths, the bond stress distribution is increasingly non-linear [ELI79].

2.4.3 Bar Diameter

The maximum bar force F_s depends on the cross-sectional area of a reinforcing bar A_s, while the bond strength τ_b is related to the reinforcing-bar circumference U_b. Since the ratio of circumference per cross-sectional area U_b / A_s decreases with increasing bar diameter, large diameter bars presumably offer less bond strength [MAR73]. For a safe transfer of bar force, large diameter bars have higher relative rib areas f_R [DEU09].

For the evaluation of the bar diameter effect, the bond length, the concrete cover and the relative rib area have to be taken into account. The findings in literature on the effect of bar diameter are contradictory. While some authors did not find any effect (e.g. [REH68], [STE07]), others found a slight impairment in bond strength with increasing bar diameter (e.g. [VIW79], [ELI79], [ELI83], [REY82]). Where the cross-sectional dimensions and the bond length are multiples of the bar diameter, the effect of bar diameter is small [ELI83].

TEPFERS [TEP73] conducted a comprehensive test programme on laps and found a decrease in developable bar stress for increasing bar diameters at constant bond length. Considering the ratio of bond length to bar diameter l_0 / Ø in the test results conducted by [TEP73], an effect of bar diameter is not visible.

For increasing bar diameter, the bond stiffness decreases, leading to a softer bond behaviour [VIW79], [UED86], [SCH98b]. This effect results from a smaller available area of concrete lugs for large bar diameters [SCH98b].

2.4.4 Confinement by Concrete Cover

Reinforcing bars with large bar diameters transfer higher loads and lead to increasing tensile stress around the bars. Hence, the concrete cover should increase with increasing bar diameter. The cylinder stress decreases with increasing concrete cover [MAR73]. From a certain multiple of the cover to bar-diameter ratio c / Ø, a concrete cover failure is not decisive, but pull-out failure occurs [MAR73]. The theoretical boundary is the concrete cover that can resist the splitting forces [MAR73]. The transition between splitting and pull-out failure was often found to occur at a concrete cover of 3 · Ø to 5 · Ø [FIB14].

Concrete cover dimensions determine the splitting planes described in [FER69], [FER71], [TEP73], [ORA77], [ELI79]. The failure types describe the potential splitting planes that must be taken into account for evaluation of the effectivity of transverse reinforcement (cf. Figure 2-5).

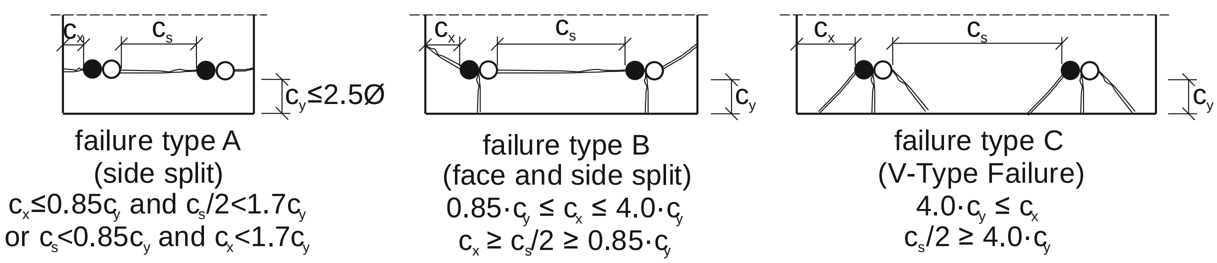

Figure 2-5 Splitting failure modes (reproduced from [ELI79] based on [FER69])

The bar spacing equivalently contributes to the cylinder stress resistance. SCHMIDT-THRÖ [SCH88] conducted pull-out tests with one and two reinforcing bars. The smaller the bar spacing, the larger the irregularities in load application and the larger the difference between the bond behaviour of the two reinforcing bars. The impairment in bond strength increased with smaller bar spacing. Where two bars with wide spacing were tested, the higher bond strength exceeded the bond strength in tests with one bar only. In pull-out tests with two bars and small spacing, the higher bond strength of the two bars equalled the bond strength in one-bar tests [SCH88].

The increase in bond strength by bar spacing has an upper limit [ELI79]. FERGUSON [FER54] found that the bond strength increase of adjacent bars was linear for bar spacing between 1·Ø to 4·Ø. For larger bar spacing, the bond strength increase was less than proportional.

2.4.5 Confinement by Transverse Reinforcement

Transverse reinforcement prevents sudden splitting failure and reduces the splitting crack width considerably. To adequately reduce longitudinal crack widths, transverse bars must have a reasonable spacing. All reinforcing bars only reduce crack widths effectively within their vicinity. Therefore, the transverse bar spacing must not be too wide. On the other hand, the spacing must be wide enough to allow for a good compaction of concrete between the transverse bars. Since the bond stress distribution is non-linear along the bond length, transverse reinforcement is most effective in the highly utilised section of the bond length.

Although transverse reinforcing bars are capable of a longitudinal crack width reduction, they do not yield (e.g. [BUR00], [HEG15]; [ELI79]). Still, some authors found an effect of transverse bar diameter on the obtainable bond strength. In anchorage tests with long bond lengths, the longitudinal crack widths decreased with increasing transverse bar diameter. A linear correlation between transverse bar diameter and bond strength was found [PLI98].

The transverse reinforcement position within the cross-section strongly influences the bond strength increase. While straight bars inside the reinforcing bars do not cross any potential splitting plane, transverse bars positioned within the concrete cover do cross splitting planes and can accordingly contribute to bond strength (cf. Figure 2-5). Since the splitting planes depend on the concrete cover and bar spacing, the effect of transverse reinforcement also depends on the cover dimensions. If the splitting plain is strictly horizontal, only vertical legs lead to a bond strength increase (cf. Figure 2-6). Where splitting cracks develop in the bottom cover, e.g. in slabs with large bar spacing, straight transverse bars are capable of a crack width reduction as well [ORA77]; [CAN05], [ZUO00].

An evaluation of the effectiveness of transverse reinforcement is given in [CAI03] for different positions in the cross-section, different geometric boundary conditions and failure types. Figure 2-6 shows corner and side split failures with effective vertical stirrup legs and face split failure where the horizontal transverse bar crosses the cracks.

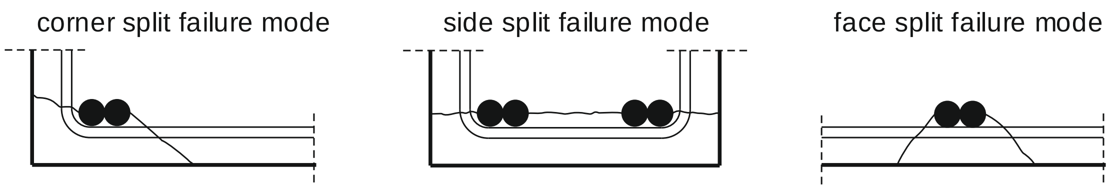

Figure 2-6 Split failure modes (reproduced from [FIB14]) and resisting reinforcement

Besides the crack control, transverse reinforcement also leads to a multi-axial concrete compression at anchored or lapped bars in structural elements under bending. The concrete cover in such elements is subject to additional tensile stress by bursting forces of the longitudinal bars at the lap ends. In this case, transverse reinforcement confines the lap ends and leads to an increase in stress developed by bond. The positive effect of transverse reinforcement equally applies to direct tension members and beams [BUR00].

2.4.6 Confinement by Transverse Pressure

The maximum bond strength is increased by transverse pressure if present. For smooth bars, the bond strength increases linearly with increasing transverse pressure [SCH88], whereas the bond strength increase for deformed bars is non-linear [ROB82], [SCH88], [FIB14]. The effect of transverse pressure increases with increasing slip for deformed bars [UNT65], [SCH88].

SCHMIDT-THRÖ [SCH88] conducted anchorage tests with transverse pressure p varying from p = 0 to p = 20 N/mm². The transverse pressure increased with increasing bar force and was therefore comparable to beam supports. The bond strength increase by transverse pressure was more than 100 % for some test configurations. At high transverse pressure, the longitudinal splitting cracks were controlled by transverse pressure and concrete pry-out was observed. In tests without or small transverse pressure, longitudinal cracks developed above the anchored bars. The transverse pressure perpendicular to the splitting plane reduced the mutual influence of adjacent bars [SCH88].

2.4.7 Further Influencing Parameters

Besides the described bond parameters, several additional parameters influence the bond behaviour. These parameters will be described briefly, but will not be evaluated in detail in this thesis.

For the effect of reinforcing bar position during casting, different bond zones are distinguished [EC2]. The best bond conditions for horizontal bars are close to the bottom of the formwork and for vertical bars when loaded against the casting direction. In both cases the ribs induce compression struts against a less porous mortar [FIB10]. Most codes include a factor for good and poor bond conditions (e.g. [EC2], [MC2010], [ACI14]). If the bond strength is impaired by consolidation of the fluid concrete under the bar, poor bond conditions are presumed [REH61], [MC2010].

In addition to the concrete strength, the aggregate distribution [MAR81], the strength of the aggregate [ZUO00] and the concrete consistency [MAR73] influence the maximum bond strength.

The bond-strength slip relationship is strongly affected by rib geometry that determines the bond stiffness and the splitting tendency. Reinforcing bar ribs are described by the relative rib area f_R. This value is only one reference for the quality of reinforcing bar surfaces, since bond behaviour also depends on the rib angle and the rib filleting. The differences between North American and European rib patterns are not visible in statistical evaluation of bond strength [FIB14].

Reinforced concrete is also influenced by corrosion of the composite materials. Both a deterioration of concrete cover and corrosion of the steel surface influence the bond strength. Corrosion increases the bar diameter and friction, but also leads to the development of longitudinal cracks [FIB10]. A firmly adherent layer of rust before casting is insignificant [MAS90], [FIB10] or even enhances the bond strength at early stages of corrosion [AL-90]. Only at more advanced stages of corrosion, weak material between bar and concrete will reduce the bond strength [CAB94]. Small or delaminated covers increase the tensile cylinder stress and impair the bond strength [COR12], [FIB10].

Furthermore, bond characteristics depend on the loading type. The bearing of the ends of compression bars provides an additional contribution to load transfer [FIB14]. Secondly, the bond stresses in the vicinity of transverse cracks do not occur in compression zones as transverse cracks do not develop. In tension laps, each lapped bar carries half the force of a single bar outside the lap. This is not the case in laps in compression where concrete contributes to the load transfer [FIB14].

Cyclic loads usually do not reduce the developable stress in laps, but increase the slip at the lap ends [REH77]. The slip is significantly influenced by the load history [FIB10]. The deterioration of bond under repeated loading primarily depends on the peak slip [ELI83]. The bond deterioration is not only due to the repeated loading, but also to long term effects [FIB10]. Bond zones under long-term loads corresponding to the serviceability load have the same bond strength as bond zones under a constant load increase until failure [REH77].

2.5 Differences between Anchorages and Laps

Whether design models for necessary bond lengths are equally applicable to both lapped joints and anchorages is an issue that has not been resolved despite many years of effort [FIB14], [REY82]. Compression struts mutually stabilise in the direction of the second bar. Three theories on the inequality of lapped joints and anchorages are distinguished:

- Hydraulic pressure theory by [FER65a] and [TEP73]
- Rib interference by adjacent bars (shielded ribs between the bars)
- Strut-and-tie model with considerable transverse strain at lap ends [BUR00]

The hydraulic pressure theory assumes that the splitting forces generated by a lap are twice those developed in an end anchorage situation and thus lap lengths should be twice the anchorage length [TEP73] (cf. Figure 2-7, left). The slip between the bars is twice the slip between the bars and the concrete, since the bond stress component between the bars is strongly impaired by the slip.

While anchored bars are entirely surrounded by concrete, ribs of lapped bars are impaired, where bars are positioned directly side-by-side. If the ribs towards the second lapped bar do not participate in the load transfer, not the entire circumference contributes to resistance (cf. Figure 2-7, right). In contrast, CAIRNS [CAI96] describes that the distance between lapped bars does not influence the lap strength until the bar strength decreases for spacings between lapped bars of more than 4 · Ø.

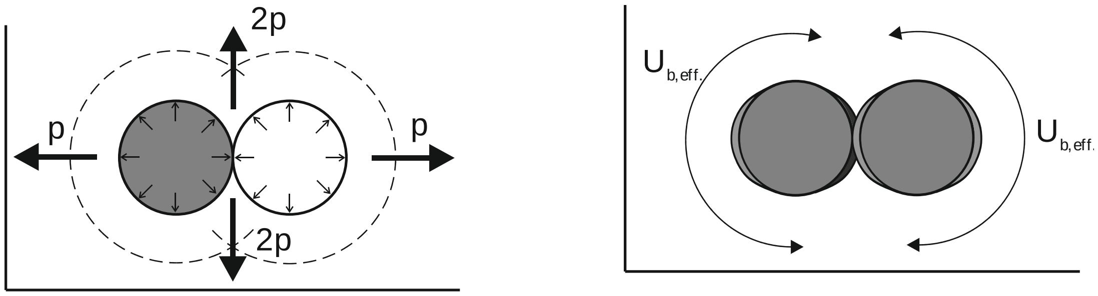

Figure 2-7 Hydraulic pressure theory by [FER65a] and [TEP73] (left) and shielded ribs minimising the bond circumference U_b (right)

BURKHARDT [BUR00] explains the load transfer mechanism with one global and two local strut-and-tie models. All models have ties perpendicular to the lapped bar. Their tensile stresses superimpose and lead to longitudinal cracks (cf. Figure 2-8).

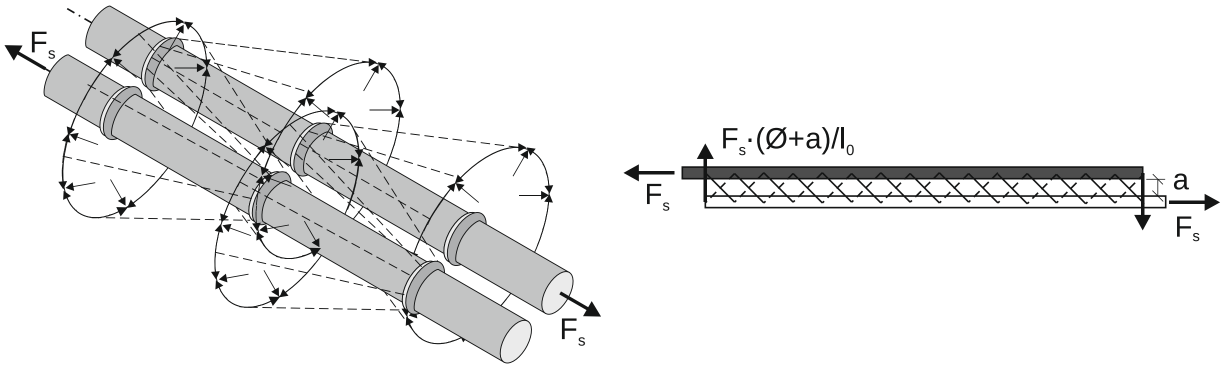

Figure 2-8 Local strut-and-tie-model with cylinder stress (left) and second local strut and tie model with tensile force F_s / (Ø + a) / l_0 between lapped bars (reproduced from [BUR00]) (right)

In contrast, several authors give design equations that are equally applicable to both lapped joints and anchorages [FIB14]. In the test series described in [CAN05]; [ZUO00]; [ORA77] and [REY82], differences between laps and anchorages were not found.

The fact that the current European [EC2] and American [ACI14] codes for structural concrete include a lap factor defining the lap length as a multiple of the anchorage length, while [MC2010] does not include such a factor, demonstrates that this issue was not resolved in the past.

2.6 Test Setups for Bond Investigation

For the investigation of bond in concrete, various test specimens and test-setups exist. RILEM RECOMMENDATION RC5 [RIL82], [RIL83], [AST15] provide standard tests for bond of reinforcing bars in concrete. CAIRNS [CAI02] distinguishes transfer type bond tests and anchorage- or development-type bond tests. The RILEM Pull-Out [RIL83], the RILEM Beam Test [RIL82] and the ASTM Beam-End Test [AST15] are anchorage types (cf. Figure 2-9). Transfer tests with reinforcement stressed in tension at both ends of the bar are used for crack observation mainly [CAI02]. The bond zones in the various test specimens differ by development length and confinement. For the evaluation of bond test results, the afore mentioned influencing parameters must be taken into account.

Most pull-out test specimens have much shorter bond lengths than the required anchorage length for the development of yield strength. Thus, there is usually measurable slip at the unloaded end of the bar and the bond stress is very high.

Besides scientific investigation on bond behaviour, many bond tests are conducted in reinforcing steel industry for technical approvals and regular quality control. For these cases, simple test specimens with little manufacturing complexity and effort are desired.

<u>Pull-Out Test</u>

The most common bond test for reinforced concrete is the pull-out test according to RILEM RECOMMENDATION RC6 [RIL83]. The test specimen is a concrete cube with a height of $10 \cdot Ø$ and a bond length of $5 \cdot Ø$. The bond zone is confined by a cover of $c = 4.5 \cdot Ø$. This test specimen is very simple in fabrication and testing, but it generates unrealistically high bond strengths not comparable to structural elements in practice. The concrete cover is rather large and the planar support generates friction that additionally resists the splitting forces. The test setup according to [RIL83] results in a compression arc (cf. Figure 2-9) that confines the bond zone and leads to increasing bond strength.

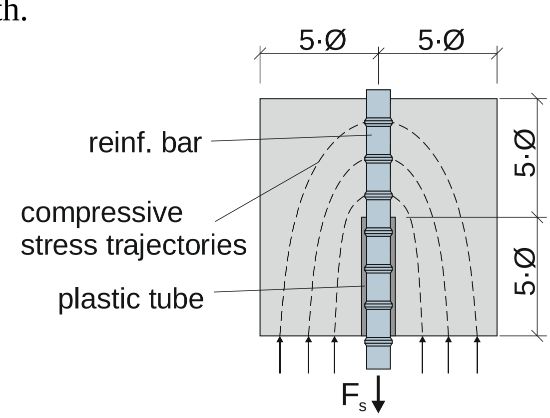

Figure 2-9 Pull-out test according to [RIL83] and resulting compression struts

Beam-End Test

For the investigation of the bond behaviour at the ends of simply supported beams, the beam-end test was developed. This test specimen is standardised in the United States by the American Society for Testing and Materials in ASTM 944-10 [AST15] for the comparison of bond strength of reinforcing bars. This test specimen (cf. Figure 2-10) is also a pull-out test type.

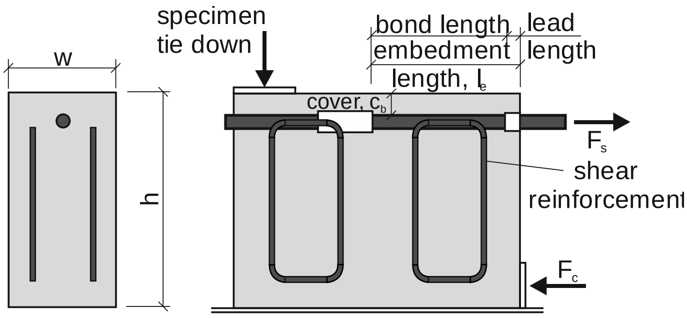

Figure 2-10 Beam-End test with supports (adapted from ASTM 944-10 [AST15])

For the eccentric loading, a bending moment is generated and the test specimen has a compression and tension zone comparable to a simply supported beam (cf. Figure 2-11). In this case, the concrete surrounding the pulled reinforcing bar is also subjected to tension.

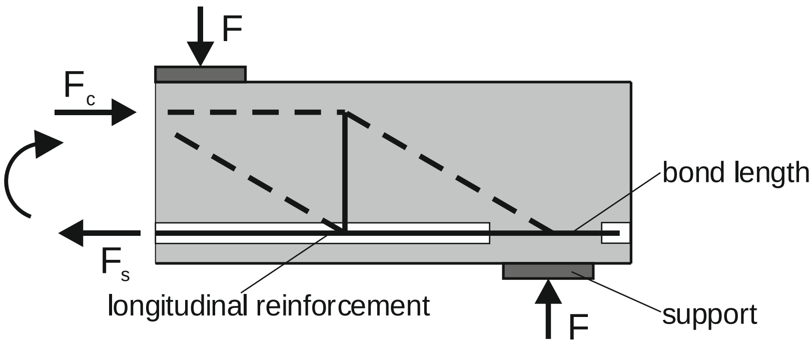

Figure 2-11 Strut-and-tie-model at beam end to visualise the principle of the beam-end test

The length of the standardised test specimen according to [AST15] is 610 mm, while depth and width depend on the bar diameter investigated. The concrete cover and bond length may be varied. The unbonded length at the front of the test specimen is 130 mm to 200 mm. ASTM 944-10 [AST15] defines transverse reinforcement that prevents shear failure, but does not confine the bond zone.

Wildermuth [WIL13] conducted broad investigations on bond test types and concluded that the beam-end test according to [AST15] was more appropriate to test the bond behaviour than the pull-out test according to [RIL83].

In the test setup according to [AST15], the bond zone is not subjected to transverse pressure, while other authors (e.g. [GHA90]) have conducted beam-end tests with transverse pressure as shown in Figure 2-12.

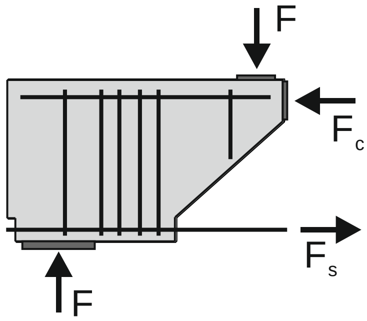

Figure 2-12 Beam-End Test with transverse pressure in the bond zone provided by the support [GHA90], [KEM79], [RAT72]

Beam Test

RILEM RECOMMENDATION RC 5 [RIL82] defines a beam test for the investigation of bond in structural elements under bending. The test specimen consists of two reinforced concrete members linked by a steel hinge. The anchorage length in the tension zone is $l_b = 10 \cdot Ø$. The reinforcing bars are non-bonded at the support; hence, the positive effect of transverse pressure is eliminated. Two test specimen sizes are defined for different reinforcing bar diameters. The concrete cover is 50 mm – Ø / 2 in all tests. Stirrups are positioned for the confinement of the bond zone and for the shear load.

The fabrication and execution of this test specimen is costly and time-consuming. The shear reinforcement ratio is high and a splitting failure of the bond zone is therefore precluded [CAI03]. Additionally, the test type overestimates the bond strength of small diameter bars, since the concrete cover is only partly adjusted for different bar diameters.

Anchorage Tests at Direct Supports

Since bond investigations on the basis of pull-out and beam-end tests are much simpler, entire beam tests with anchorages tested at the support or at curtailed reinforcement were conducted in much smaller numbers. CHAMBERLIN [CHA56] (one bar only), MATHEY [MAT61] (one bar only), RICHTER [RIC84], SCHMIDT-THRÖ [SCH88] and AMIN [AMI09] conducted anchorage tests with simply supported beams. These test specimens include both the positive effect of transverse pressure and – where two or more bars are positioned – the negative effect of densely positioned reinforcement.

Lap Tests in Constant Moment Zone

Besides anchorages at supports and curtailed reinforcement, reinforcing bars are often anchored in laps. The bond behaviour of lapped reinforcing bars is usually tested in four-point bending tests or direct tension members. BETZLE [BET80] described that laps in bending elements are subject to an unfavourable reinforcement bursting (cf. Figure 2-13).

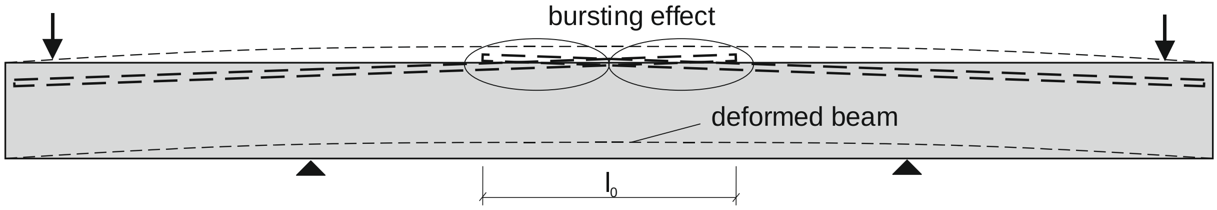

Figure 2-13 Bursting effect in four-point bending test with lapped reinforcement

Figure 2-14 shows the deformation of a four-point bending test with a lap described in chapter 3. The beam end has a deformation of 40 mm at its free end. The deformation at the lap end is 5 mm only. For geometry, the reinforcing bar would have a 55 mm displacement at free deformability of its right-hand side. Thus, the displacement deviation is 50 mm. This deviation equals the impeded deformation of the Ø 40 mm bar. The impeded displacement by 50 mm generates bursting forces within the concrete cover of the beam.

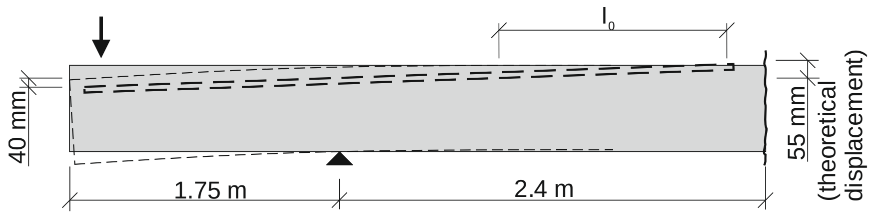

Figure 2-14 Dimensions of bending tests with lapped splices as described in chapter 3

In Figure 2-15, the results of a cantilever with distributed loading and 50 mm displacement is shown.

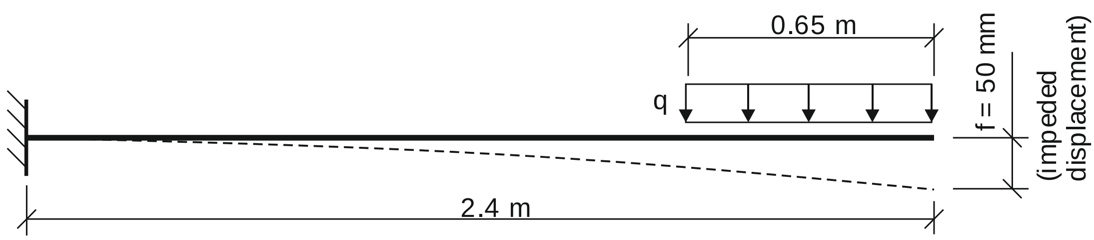

Figure 2-15 Constraint member analogue to reinforcing bar in four-point bending test

The necessary uniformly distributed load to evoke a 50 mm displacement f in a 2.5 m long Ø 40 mm reinforcing bar and a moment of inertia $I_{Ø=40mm} = 125664\ mm^4$, is calculated as follows:

$$f = \frac{1}{E \cdot I} \sum \int M \cdot \overline{M} \rightarrow q = \frac{50mm \cdot 200000N/mm^2 \cdot 125664mm^4}{2.058 \cdot 10^{12} mm^4} = 0.61\,kN/m \qquad (2\text{-}8)$$

The distributed load q acts upon the splitting plane in the concrete cover. Depending on the cover dimensions, different splitting types occur. The left hand side of Figure 2-16 gives the additional load from bursting forces acting upon the surrounding concrete cover for side splitting. Face splitting is shown on the right hand side of Figure 2-16. The figures also give the resulting additional concrete stress $\Delta\sigma_{ct}$. At side splitting, the line load acts upon the horizontal splitting plane. For face splitting, the assumption was made, that the uniformly distributed load acts upon the vertical cracks in the bottom cover only.

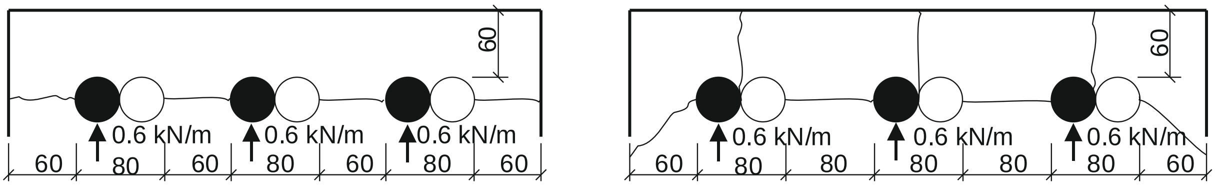

$$\Delta\sigma_{ct} = \frac{3 \cdot 0.6\ \mathrm{N/mm}}{4 \cdot 60\ \mathrm{mm}} = 0.0075\ \mathrm{MPa} \qquad \Delta\sigma_{ct} = \frac{0.6\ \mathrm{N/mm}}{80\ \mathrm{mm}} = 0.0075\ \mathrm{MPa}$$

$$f_{ctm}\left(C30/37\right) = 2.9\ \mathrm{MPa} < 0.0075\ \mathrm{MPa} \qquad v_{Rmi}\left(C30/37\right) = 0.5 \cdot 2.9\ \mathrm{MPa} > 0.01\ \mathrm{MPa}$$

Figure 2-16 Additional tensile stress around lapped reinforcing bars for side splitting (left) and face splitting (right) and resulting additional stress in the concrete cover compared to tensile strength fctm and shear resistance v_{Rmi}

Compared to the mean tensile strength of concrete f_{ctm} of 2.9 MPa and compared to the mean shear resistance at the interface v_{Rmi} of 1.45 MPa for class C30/37 concrete according to [EC2], this additional bursting effect is less than 1 % and therefore negligible.

Lap Tests with Shear

If shear is present within a lap, the moment and consequently the bar stress is not constant along the lap length. Therefore, parts of the lap are less utilised. For the investigation of considerable shear forces within laps, tests with setups other than the four-point bending test were conducted. FERGUSON [FER69]; [FER71] tested specimens conforming to retaining walls with different reinforcement stress at lap ends and introduced a factor increasing the maximum load for laps under non-constant moment that was also applied by [ELI79].

ZEKANY [ZEK81] conducted lap tests with shear and observed little effect of shear on stress developed by bond. Even considerable shear had a small effect on the bond behaviour. In contrast, investigations by REYNOLDS & BEEBY [REY82], LUKOSE ET AL. [LUK82] and ZUO & DARWIN [ZUO98] showed that laps reached higher ultimate loads where shear forces were present.

[FIB14] concludes that the measured differences are too small for consideration in design models. All design models, except [ELI79], neglect the effect of shear.

Further Bond Test Setups

The bond behaviour of reinforcing bars has been investigated for many decades and besides the more common bond tests described before, several further bond test setups such as pull-out tests without transverse pressure [JAN86], anchorage tests in cantilevers [GIL12], column-beam connections [UED86] and at indirect supports [LUN15] have been conducted.

2.7 Large Diameter Bars

2.7.1 Definition of Large Diameter Bars

[EC2] allows for the application of reinforcing bar diameters up to Ø 40 mm and comprises several additional detailing rules for the use of large diameter bars. The definition of the term “large diameter” is a Nationally Determined Parameter (NDP). Large diameters according to [EC2] are greater than the defined value $Ø_{large}$. Table 2-1 exemplarily shows the definition of $Ø_{large}$ for different countries. The additional rules for large diameter bars do not apply in France and in the UK, since [EC2] is valid for bars up to 40 mm only.

Table 2-1 Nationally Determined Parameters [NDP] for large diameter $Ø_{large}$, bar spacing c_s and lap factor α_6 for selected countries

Country	$Ø_{large}$ greater than	k_1 for $c_s = k_1 \cdot Ø$	α_6
Austria	32 mm	1.4	[EC2]
Denmark	32 mm	1.0	[EC2]
France	40 mm	1.0	[EC2]
Germany	32 mm	1.0	Non-contradictory complementary information (NCI)
Netherlands	32 mm	1.0	[EC2]
Spain	32 mm	1.0	[EC2]
United Kingdom	40 mm	1.0	[EC2]

The American Standard [ACI14] allows for the use of bar diameters up to Ø 57 mm without providing additional rules for large diameter bars.

The detailing provisions in [MC2010] apply to reinforcing bar diameters up to Ø 40 mm. Bar diameters above Ø 32 mm shall only be used in exceptional cases and the principles of detailing shall be adapted if necessary [MC2010]. Besides a definition for minimum transverse reinforcement in bond zones, neither the adaptation nor additional rules for large diameter bars are specified. For the increased brittleness of bond behaviour of anchorages and laps with large diameter bars, it is considered prudent to provide double minimum confining reinforcement for bars of size Ø 50 mm [FIB14]. MODEL CODE 2010 [MC2010] thus requires an area of transverse reinforcement equal to that of the total cross sectional area of the bonded bars allowing for a linear increase from size Ø 25 mm to size Ø 50 mm bars.

2.7.2 Origin of Additional Rules for Large Diameter Bars

Structural members reinforced with threaded bars Ø 50 mm, St 420 / 500 were evaluated by REHM [REH75b]. The conducted survey for a specific approval for a power plant in an earthquake zone was based on tests with T-beams with one or two

Ø 50 mm bars conducted at the universities in Munich [REH75a] and Tokyo [KOK72]. From this survey, the additional rules for Ø 50 mm bars were later derived for a general technical approval. The rules were subsequently softened for the approval of Ø 40 mm bars and were also adopted in DIN 1045 [DEU88], EUROCODE 2 [EC2] and its GERMAN NATIONAL ANNEX [EC2/NA].

REHM [REH75b] recommends several rules for the use of Ø 50 mm bars additionally to the code approved at that time. These additional rules included minimum dimensions of the reinforced concrete elements, surface reinforcement for crack width control, reduction of shear capacity, additional reinforcement for compression members and rules for bond zones. The unfavourable slip behaviour of large diameter bars was incorporated by a bond strength reduction factor of 0.8. For anchorages, increased transverse reinforcement was defined to allow for the risk of cover-splitting. Anchorages with straight ends or mechanical devices were only allowed fulfilling increased requirements for the positioning of reinforcement in the longitudinal and transverse directions. The percentage of bars lapped at a section was limited. Since the survey was conducted for an earthquake zone, the fatigue strength of the bars and corresponding fasteners was defined [REH75b].

JUNGWIRTH [JUN77] introduces a model for the design of surface reinforcement. The concrete cover in the tension zone is defined for a direct tension member and the residual member depth for a member under bending.

2.7.3 Additional Rules for Large Diameter Bars

EUROCODE 2 [EC2] defines additional rules for large diameter bars concerning bond strength, crack control, shear, laps and anchorages. Crack control in reinforced concrete members with large diameter bars may be achieved either by using surface reinforcement or by calculation. The area of surface reinforcement $A_{s,surf}$ is defined as a multiple of the area of the tensile concrete external to the links $A_{ct,ext}$ (cf. Figure 2-17).

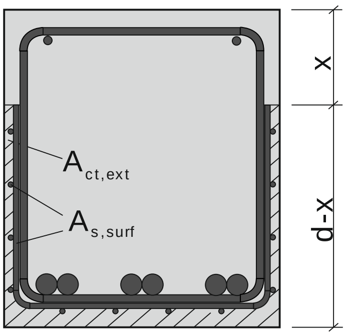

Figure 2-17 Surface reinforcement $A_{s,surf}$ as a multiple of the cross-section under tension external to the links $A_{ct,ext}$ for crack control according to [EC2]

Reinforcing bars should be anchored with mechanical devices or if anchored as straight bars, links should be provided as confining reinforcement. Laps are permissible for limited bar stress and minimum dimensions of the structural element only. Transverse reinforcement additional to that for shear should be provided in the anchorage zones where transverse compression is not present [EC2].

The GERMAN NATIONAL ANNEX [EC2/NA] appends further additional rules for large diameter bars incorporating the findings from the described survey [REH75b]. Minimum dimensions, concrete strength limits, a shear capacity reduction, higher values for the cross-sectional area of surface reinforcement and minimum mandrel diameters. Additionally, further rules for bond zones were defined. Bars may be lapped in members subjected to bending only and the permissible percentage of lapped bars is limited. All members must have direct supports and the longitudinal reinforcement for beams at intermediate supports must be anchored in compression zones. Curtailed bars must exceed the zero-crossing of the envelope of the acting tensile force by the effective depth. Curtailed bars are allowed for members with $h \geq 800$ mm, only [EC2/NA].

Table 2-2 shows an overview of the additional rules defined in [REH75b], [EC2/NA] and [EC2]. The rules given in the column for [EC2] are also valid for the application of [EC2/NA].

Table 2-2 Additional rules for large diameter bars according to [REH75b], [EC2] and [EC2/NA]

	[REH75b]	[EC2/NA]	[EC2]
$Ø_{large}$	50 mm	40 mm	40 mm
Concrete class	-	C20/25 to C80/95	-
Minimum dimensions	-	$15 \cdot Ø$	-
Reduction for shear strength	perm. $\tau_{b,50mm}$ = $0.8 \cdot$ perm. $\tau_{b,DIN\ 1045}$	$0.9 \cdot V_{Rd,c}$	-
Surface reinforcement for crack width control	2 cm²/m	Crack control by surface reinforcement or by calculation $A_{ct,surf} \geq 0.02 \cdot A_{ct,ext}$ (perpendicular to the large diameter bars), $A_{ct,surf} \geq 0.02 \cdot A_{ct,ext}$ (parallel to those bars)	Crack control by surface reinforcement or by calculation $A_{ct,surf} \geq 0.01 \cdot A_{ct,ext}$ (perpendicular to the large diameter bars), $A_{ct,surf} \geq 0.02 \cdot A_{ct,ext}$ (parallel to those bars)
Compression members	Longitudinal bars shall be located in the corner of a stirrup Minimum stirrup diameter: 12 mm Stirrup spacing $s_{st} \leq \{b_{column}/2;\ 350\ mm\}$ Minimum concrete cover $c_{min} = 1 \cdot Ø$	Stirrup spacing $s_{st} \leq \{b_{column}/2;\ 300\ mm\}$ Compression members permissible for dimensions smaller than $15 \cdot Ø$ and concrete classes above C80/95 in case detailed according to [EC2/NA]	-
Minimum mandrel diameter	-	1.0 m	-
Bond strength reduction	perm. $\tau_{b,50mm}$ = $0.8 \cdot \tau_{b,\ DIN\ 1045}$	-	$f_{bd,Ølarge} = (132–Ø)/100$
Laps	Couplers and compression laps are permissible. In deep members, tensile laps with mechanical devices are permissible. Laps staggered where: Longitudinal spacing of lap centres $l_v \geq 1.3 \cdot l_0$	Laps only permissible in members subjected to bending. Maximum percentage of lapped bars: 50 %. Laps staggered where: Longitudinal spacing of lap centres $\geq l_0 \cdot 1.3$	Only in sections with a minimum dimension of 1.0 m or where $\sigma_s \leq 0.8 \cdot f_{yd}$

	[REH75b]	[EC2/NA]	[EC2]
Anchorages	Direct supports are recommended. Curtailed bars shall exceed the zero-crossing of the envelope of the acting tensile force by the effective depth. Curtailed reinforcement and tensile reinforcement for negative moment ends in tension zone shall only be permitted in deep members. 50 % of the bars shall cross the zero-crossing of the moment. Bars with at least $l_v = 1.3 \cdot l_0$ are staggered.	Members must have direct supports. Longitudinal reinforcement for beams at intermediate supports must be anchored in compression zones. Anchorages of straight bars must be designed for the transfer of $\sigma_{sd} = f_{yd}$. Curtailed reinforcement for members with $h \geq 800$ mm, only. Curtailed bars must exceed the zero-crossing of the envelope of tensile force by the effective depth. Bars staggered where: Long. Spacing $\geq l_{b,rqd}$	Anchorages with mechanical devices or straight bars with additional confining reinforcement
Increased transverse reinforcement	Additional transverse reinforcement $A_{tr} \geq 2$ cm²/m (for bond, not only in anchorages), At anchorages: 25 – 30 % of the anchored force, spacing not wider than 200 mm.	Bond securing reinforcement over the entire length, only three bars may be confined by one stirrup. Stirrup cross-section: $A_{Sw} = 0.1 \cdot A_s$ (cm²/m). Spacing: $s \leq 200$ mm. Where shear reinforcement is present and 50 % is provided by stirrups, this additional reinforcement is not necessary. For multi-layer reinforcement, spalling must be secured by edge reinforcement with 0.18 cm²/m	Transverse reinforcement additionally to that for shear provided in the anchorage zones where transverse compression is not present (uniformly distributed in the anchorage zone) Spacing $s_{st} \leq 5 \cdot Ø$ For straight anchorages: Parallel to the tension face: $A_{sh} = 0.25 \cdot A_s \cdot n_1$ Perpendicular to the tension face: $A_{sv} = 0.25 \cdot A_s \cdot n_2$ with A_s = cross sectional area of one anchored bar n_1 = number of layers with bars anchored at the same cross-section in the member n_2 = number of bars anchored in each layer

2.8 State of Standardisation of Bond Zones

Codes for the design of structural members account for the stress developed in bond zones by design models for required anchorage and lap length. The design models have been continuously revised with each new code reissue. [EC2], which is valid since 2004 comprises an anchorage design model previously given in [MC90]. The EC2 Project Team elaborated a new proposal [PT18] for the next generation of [EC2]. Its design model for anchorages and laps was taken from [FIB14], which is the background document on bond for [MC2010]. The Project Team removed the additional provisions regarding large diameter bars according to [EC2] on the basis that size effect is accounted for systematically [PT18]. For laps, [PT18] recommends additional verification of cracking at serviceability limit states in the lap region, particularly for large diameter bars. According to the [PT18] working draft comment, the avoidance of spalling for large diameter bars is a very specific case for structures normally designed according to specific recommendations. For the design model for anchorages and laps, the EC2 Project Team gives provisional calibration factors for the conversion from mean values given in [FIB14] to design values that are still to be validated [PT18].

Code provisions for anchorages and laps can be distinguished between models with bond strength definition and without bond strength. Previous codes gave anchorage and lap lengths depending on a certain bond strength for different concrete classes (cf. [DEU88], [MC90], [EC2]). In contrast, the models according to [ACI14] and [FIB14] were derived from statistical evaluations of test results accounting for the maximum bar strength in anchorages and laps without defining bond strength. For [MC2010], the bond strength was derived from the [FIB14] design model. Bond strength is an auxiliary value that simplifies the design or the comprehension of the design, while it is ultimately not necessary for anchorage and lap design.

As described above, the maximum transferrable bar stress in anchorages and laps depends on many influencing parameters. A preferably simple equation is still desired for structural design. Therefore, the most important influencing parameters must be identified and calibration factors have to be found, which are in agreement with the defined level of safety according to [EC0].

2.9 Design Models for Anchorages and Laps

2.9.1 General

In this section, the design equations for anchorages and laps according to [EC2], [EC2/NA] and [ACI14] are presented. The derivation of the design equations in MODEL CODE 2010 [MC2010] and in the proposal for the next generation of EUROCODE 2 [PT18] from [FIB14] is explained and the design models elaborated by ELIGEHAUSEN [ELI79], BURKHARDT [BUR00], LETTOW [LET06a], ZUO / DARWIN [ZUO00] and CANBAY / FROSCH [CAN06] are shown. For comparability and readability, the symbols of the different models have been changed to the [MC2010] notation, where

l_b	anchorage length
l_0	lap length
f_{cm}	f_{ck} + 8 MPa
c_y	bottom concrete cover
c_x	side concrete cover
c_s	anchored or lapped bar spacing
c_d	$\min\{c_y; c_x; c_s / 2\}$
A_{st}	cross-sectional area of one leg of a confining transverse bar
n_{st}	number of items of confining reinforcement within bond length (e.g. stirrups)
n_l	number of legs of confining reinforcement crossing a potential splitting failure surface at a section
s_{st}	longitudinal spacing of confining reinforcement
n_b	number of anchored bars or pairs of lapped bars in the potential splitting failure surface

The models to determine stresses developable in anchorages or laps are based on experimental and partly on numerical investigations with finite element analysis. The composition of equations, the influencing parameters and the processes for the finding of calibration factors differ. For all models, lap length and concrete strength are the main influencing factors, while their exponents vary among the models. Some models consider the transverse reinforcement contribution by a coefficient; others introduce a summand for transverse reinforcement contribution. All models consider the effect of concrete cover by a cover to bar-diameter ratio. When comparing design models for anchorages and laps, it has to be taken into account that not all influencing parameters are independent of each other.

The models consider the transverse reinforcement contribution quite differently. Some models comprise the number of transverse bars n_{st}, while others comprise the transverse bar spacing s_{st}. The correlation is given by equation (2-9).

$$\Sigma A_{st} = n_{st} \cdot A_{st} = \left(\frac{l_0}{s_{st}} + 1 \right) \cdot A_{st} \approx \frac{l_0 \cdot A_{st}}{s_{st}} \tag{2-9}$$

For side splitting, the horizontal cracking plane is crossed by the number of stirrup legs. Hence, the design models for anchorages include the stirrup leg number n_l if presuming side splitting. In the design models for face splitting, the stirrup cross-section is only considered once as it provides tensile resistance in one face crack only. In this case, the number of stirrup legs is not taken into account (cf. Figure 2-5).

2.9.2 EUROCODE 2

Bond Strength

The design model according to EUROCODE 2 [EC2] for anchorages and laps is based on MODEL CODE 1990 [MC90]. The anchorage length shall be calculated from the bond strength f_{bd} following from

$$f_{bd} = 2.25 \cdot \eta_1 \cdot \eta_2 \cdot f_{ctd} \tag{2-10}$$

The coefficient 2.25 describes the relation of bond strength to the tensile concrete strength. The coefficients η_1 and η_2 take the bond conditions ($\eta_1 = 1.0$ for good bond conditions) and the bar diameter into account with

$$\eta_2 = (132 - Ø) / 100 \tag{2-11}$$

The design concrete strength f_{ctd} is calculated from $f_{ctk;0.05} / \gamma_c$, where $f_{ctk;0,05}$ is limited to the value for C60/75. The design tensile strength of concrete f_{ctd} shall be calculated from the 5%-fractile of the tensile strength of concrete with

$$f_{ctd} = f_{ctk;0,05} / \gamma_c = \alpha_{ct} \cdot 0.7 \cdot 0.3 \cdot f_{ck}^{2/3} / \gamma_c \tag{2-12}$$

The coefficient α_{ct} taking long term and loading effects on the tensile strength into account is a nationally determined parameter (NDP), the recommended value is 1.0. The safety considered in the [EC2] anchorage design model is given in equation (2-12) calculating the bond strength with a 5%-fractile of the tensile strength of concrete divided by the partial safety factor for concrete γ_c being 1.5. The mean bond strength f_{bm} necessary for a comparison of test results is therefore

$$f_{bm} = 2.25 \cdot \eta_1 \cdot \eta_2 \cdot 0.3 \cdot f_{ck}^{2/3} \tag{2-13}$$

Anchorage Length

The value of the basic required anchorage length $l_{b,rqd}$ is

$$l_{b,rqd} = (Ø / 4) \cdot (\sigma_{sd} / f_{bd}) \tag{2-14}$$

The design stress of the bar σ_{sd} is the stress at the cross-section where the anchorage length commences. The design anchorage length l_{bd} is

$$l_{bd} = \alpha_{1,EC} \cdot \alpha_{2,EC} \cdot \alpha_{3,EC} \cdot \alpha_{4,EC} \cdot \alpha_{5,EC} \cdot l_{b,rqd} \geq l_{b,min} \tag{2-15}$$

With

$\alpha_{1,EC}$ coefficient for bar shape ($\alpha_{1,EC} = 1.0$ for straight bars)

$\alpha_{2,EC}$ coefficient for concrete cover with $0.7 \leq \alpha_{2,EC} = 1 - 0.15 \cdot (c_{min} - Ø) / Ø \leq 1.0$ for straight bars with $c_{min} = \{c_s / 2; c_y; c_x\}$

the minimum bar spacing c_s is a NDP that equals $c_s = 1.0 \cdot Ø$ in most European countries, an overview is given in Table 2-1

$\alpha_{3,EC}$ coefficient for transverse reinforcement if present, with

$$0.7 \leq \alpha_{3,EC} = 1 - K \cdot \lambda = 1 - K \cdot (\Sigma A_{st} - \Sigma A_{st,min}) / A_s \leq 1.0 \qquad (2\text{-}16)$$

K takes the efficiency of the transverse reinforcement depending on its location in the section into account (cf. Figure 2-6 and Figure 2-18).
The coefficient λ describes the difference between the cross-sectional area of the transverse reinforcement provided along the anchorage length and the cross-sectional area of the minimum transverse reinforcement $\Sigma A_{st,min}$ with
$\Sigma A_{st,min} = 0.25 \cdot A_s$ (anchorages)
$\Sigma A_{st,min} = 1.0 \cdot A_s \cdot (\sigma_{sd} / f_{yd}) \geq 1.0 \cdot A_s$ (laps)

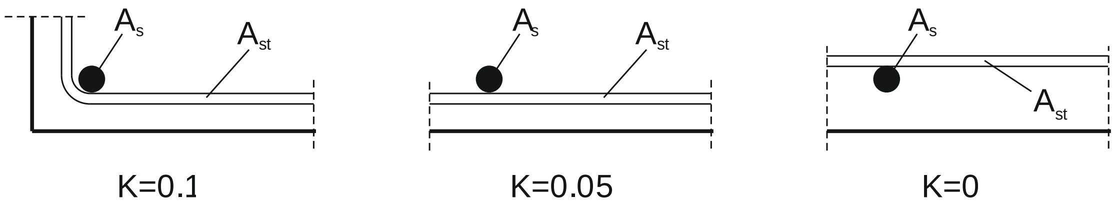

Figure 2-18 Efficiency factor K depending on the positioning of transverse reinforcement (adapted from [EC2])

$\alpha_{4,EC}$ coefficient for welded transverse bars along the anchorage length where present (otherwise $\alpha_{4,EC} = 1.0$)
$\alpha_{5,EC}$ coefficient for transverse pressure p in the plane of splitting. Where present, the anchorage length may be reduced by $0.7 \leq \alpha_{5,EC} = 1 - 0.04 \cdot p \leq 1.0$.

Lap Length

Laps should be staggered and not located in areas of high moments. The clear spacing between lapped bars should not be greater than 4 · Ø or 50 mm. The permissible percentage of lapped bars in tension may be 100 % if all bars are in one layer. For lapped bars in several layers, the percentage should not exceed 50 % [EC2].

The design lap length $l_{b,rqd}$ comprises the basic required anchorage length and coefficients taking the main influencing parameters into account.

$$l_0 = \alpha_{1,EC} \cdot \alpha_{2,EC} \cdot \alpha_{3,EC} \cdot \alpha_{5,EC} \cdot \alpha_{6,EC} \cdot l_{b,rqd} \geq l_{0,min} \qquad (2\text{-}17)$$

The coefficients $\alpha_{1,EC}$ to $\alpha_{5,EC}$ are given above. The coefficient $\alpha_{6,EC}$ for the percentage of bars lapped at a section is determined as follows:

$$1.0 \geq \alpha_{6,EC} = (\rho_l / 25)^{0.5} \leq 1.5 \qquad (2\text{-}18)$$

With
ρ_l percentage of bars lapped at a section

For the concentration of splitting forces at lap ends, [EC2] requires the positioning of transverse reinforcement at the outer sections of the lap length. If the bar diameter of the lapped bars is less than Ø 20 mm or the percentage of lapped bars amounts to less than 25 %, the transverse reinforcement necessary for other reasons may be assumed sufficient. For laps of bars with a diameter greater than or equal to Ø 20 mm, the cross-sectional area of the transverse reinforcement must not be smaller than the cross-sectional area of one lapped bar. For lapped bars with bar diameters larger than Ø 32 mm, the additional rules mentioned in 2.7.1 apply.

Rearrangement for Anchorage and Lap Strength

To calculate the developable steel stress, equation (2-17) must be rearranged. This allows for calculation of test results and comparison of different design models.

$$\sigma_{sd} = \frac{l_0}{Ø} \cdot \frac{4 \cdot f_{bd}}{\alpha_{1,EC} \cdot \alpha_{2,EC} \cdot \alpha_{3,EC} \cdot \alpha_{5,EC} \cdot \alpha_{6,EC}} \qquad (2\text{-}19)$$

For good bond conditions and straight bars without transverse pressure, the mean steel stress can be calculated as follows:

$$\sigma_{sm} = \frac{l_0}{Ø} \cdot \frac{2.7 \cdot f_{ck}^{2/3} \cdot \eta_2}{\alpha_{2,EC} \cdot \left(1 - K \cdot \frac{\Sigma A_{st} - \Sigma A_{st,min}}{A_s}\right) \cdot \alpha_{6,EC}} \qquad (2\text{-}20)$$

2.9.3 German National Annex

The NDPs for anchorage and lap length calculation in Eurocode 2 [EC2] are the coefficient α_{ct} for the tensile strength and the minimum permissible bar spacing c_s (cf. Table 2-1). [EC2/NA] defines $\alpha_{ct} = 1.0$ for bond strength calculation and $c_s = 1.0 \cdot Ø$.

At direct supports, the anchorage length may be calculated with $\alpha_{5,NAD} = 2/3$ taking the transverse pressure into account. [EC2/NA] recommends a simplified cover coefficient $\alpha_{2,NAD} = 1.0$ for anchorages.

For lapped bars with straight ends, the concrete cover orthogonal to the lap plane c_y shall not be taken into account according to [EC2/NA]. The cover used for the calculation of the cover coefficient $\alpha_{2,EC}$ is therefore $c_{min} = \min\{c_s / 2; c_x\}$ for laps. The lap factor $\alpha_{6,NAD}$ depends on the percentage of bars lapped at a section and the bar diameter. Table 2-3 gives the recommended values for $\alpha_{6,NAD}$.

Table 2-3 Coefficient $\alpha_{6,NAD}$ for the percentage of lapped bars under tension according to [EC2/NA]

Bar diameter Ø	Percentage of bars lapped at a section in one layer	
	≤ 33 %	≥ 33 %
< 16 mm	1.2 (1.0)	1.4 (1.0)
≥ 16 mm	1.4 (1.0)	2.0 (1.4)
Values in brackets are valid where $c_s \geq 8 \cdot Ø$ and $c_x \geq 4 \cdot Ø$		

According to [EC2], the transverse reinforcement in laps should be formed by links or U-bars if more than 50 % of the reinforcement is lapped at one section. [EC2/NA] softens this rule defining that transverse reinforcement does not have to consist of links where the distance between adjacent laps c_s is greater than $10 \cdot Ø$ and where the longitudinal spacing of the lap centres of adjacent laps is approximately $0.5 \cdot l_0$.

2.9.4 ACI CODE

The design model given in ACI CODE [ACI14] is based on the design model developed by Orangun et al. [ORA77]. The design anchorage length is

$$l_{bd} = \frac{3}{40} \cdot \frac{f_y}{\lambda \sqrt{f'_c}} \cdot \frac{\psi_t \cdot \psi_e \cdot \psi_s}{\frac{c_b + K_{tr}}{Ø}} \cdot Ø \tag{2-21}$$

With

- λ coefficient for light-weight concrete (1.0 for normal concrete)
- f_c' cylinder concrete strength limited to 69 MPa
- ψ_t coefficient for bond (1.0 for good bond conditions)
- ψ_e coefficient for coated reinforcement (1.0 for uncoated bars)
- ψ_s coefficient for bar diameter (1.0 for bars $\geq$ 22 mm, otherwise 0.8)
- c_b min $\{(c_s + Ø)/2;\ c_y + Ø / 2;\ c_x + Ø / 2\}$, the values $Ø / 2$ have to be added to comply with the chosen notation, since the cover values are related to the bar centres in [ACI14]
- K_{tr} transverse reinforcement index

$$K_{tr} = \frac{40 \cdot A_{st}[\text{in.}^2]}{s[\text{in.}] \cdot n_b} \tag{2-22}$$

$$\frac{c_b + K_{tr}}{Ø} \leq 2.5 \tag{2-23}$$

With

- A_{st} cross-sectional area of all transverse reinforcement within the spacing s_{st} crossing a potential splitting plane [in.²]
- s transverse bar spacing [in.]
- n_b number of anchored or lapped bars

For confinement ratios $(c_b + K_{tr}) / Ø$ above 2.5, pull-out failure becomes more likely and an increase in cover or transverse reinforcement does not lead to increased bond capacity. [DAR95b] found that the bond capacity did not increase for $(c_b + K_{tr}) / Ø > 3.75$, therefore the limit 2.5 gives additional safety [ACI03].

For good bond conditions, uncoated reinforcement and normal-weight concrete, equation (2-21) can be simplified to

$$l_b = \frac{3}{40} \cdot \frac{f_y}{\sqrt{f'_c}} \cdot \frac{\psi_s}{\frac{c_b + K_{tr}}{\text{Ø}}} \cdot \text{Ø}\ [\text{in.}] \tag{2-24}$$

Rearranging for the anchorage strength gives

$$\sigma_s = \frac{40}{3} \cdot \frac{l_b}{\text{Ø}} \cdot \sqrt{f_c'} \cdot \frac{c_b + K_{tr}}{\text{Ø}} \cdot \frac{1}{\psi_s}\ [\text{psi}] \tag{2-25}$$

The development length may be reduced by approximately 30 % if confinement by a compressive reaction is present at simple supports (cf. chapter 9.7.3.8.3 [ACI14])

It must be noted that [ACI14] allows for bar diameters up to 57 mm. The minimum permissible concrete cover is 38 mm in beams and 19 mm in slabs (for Ø 43 mm and Ø 57 mm reinforcing bars: 38 mm). The minimum clear bar spacing is the smaller value of 25 mm or the bar diameter. For large diameter bars, these values are smaller than the [EC2] values that defines minimum bottom and side covers of 1.0 · Ø.

[ACI14] does not permit laps of Ø 43 mm and Ø 57 mm bars for lack of adequate experimental data.

A coefficient for the percentage of bars lapped and the relation between provided and required reinforcement according to [ACI14] is shown in Table 2-4. The coefficient 1.3 is not based on investigations of bond stress, but shall encourage the positioning of laps away from regions of high tensile stress to locations where the cross-sectional area of reinforcement provided is at least twice that required by analysis. Therefore, this coefficient includes a certain safety as well [ACI03].

Table 2-4 Lap length coefficient for the provided reinforcement and the percentage of lapped bars [ACI14]

$A_{s,prov}$ / $A_{s,required}$	Percentage of A_s spliced	Lap length
≥ 2.0	50	max {1.0 · l_b; 305 mm}
	100	max {1.3 · l_b; 305 mm}
< 2.0	All cases	

The design model was validated with tests of small bar diameters with short anchorage and lap lengths, most of which were less than 12 in. (300 mm). Therefore, a factor for bar size γ with γ = 0.8 for Ø 22 mm and smaller bars and 1.0 for larger bar diameters was introduced. ACI COMMITTEE 408 recommends not to use a factor for size effect γ smaller than 1.0 [ACI03].

2.9.5 FIB BULLETIN 72

The background of the bond strength defined in [MC2010] is described in FIB BULLETIN 72 [FIB14]. A semi-empirical design equation for the mean steel stress in lapped bars under tension was derived from 800 tests conducted in Europe, the United States and Asia. The equation for mean anchorage and lap strength representing the validated influencing parameters is given in equation (2-26).

$$f_{stm} = 54 \cdot \left(\frac{f_{cm}}{25}\right)^{0.25} \cdot \left(\frac{25}{Ø}\right)^{0.2} \cdot \left(\frac{l_b}{Ø}\right)^{0.55} \cdot \left[\left(\frac{c_{min}}{Ø}\right)^{0.25} \cdot \left(\frac{c_{max}}{c_{min}}\right)^{0.1} + k_m \cdot K_{tr}\right] \le f_y \quad (2\text{-}26)$$

Where

c_{min} minimum concrete cover: $c_{min} = \min\{c_x; c_y; c_s/2\}$

c_{max} maximum concrete cover: $c_{max} = \max\{c_x; c_s/2\}$

k_m coefficient for efficiency of transverse reinforcement

K_{tr} density of transverse reinforcement

$K_{tr} = n_l \cdot n_{st} \cdot A_{st} / (n_b \cdot Ø \cdot l_b) \le 0.05$

n_l number of legs of a link which crosses the potential splitting failure plane

n_{st} number of transverse links within the lap or anchorage length

n_b number of anchored or lapped bars at the same section

A transverse reinforcement ratio K_{tr} above 0.05 does not increase the bond strength. The factor k_m accounts for the efficiency of transverse reinforcement depending on its position and possible split failure planes according to Figure 2-19. If an anchored bar or lap has a small distance a_l to the next vertical stirrup leg crossing a splitting crack, the transverse reinforcement is most effective. The efficiency decreases by 50 % for horizontal distances a_1 larger than 125 mm or five times the bar diameter. If the transverse reinforcement does not intersect the splitting crack, there is zero effect on bond strength [FIB14].

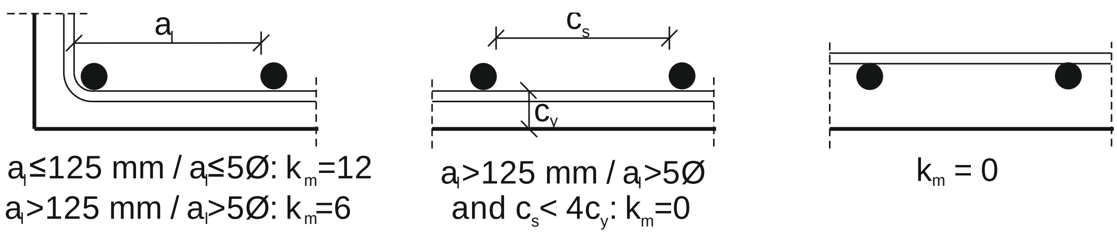

Figure 2-19 Coefficient k_m for efficiency of transverse reinforcement (adapted from [FIB14])

Equation (2-26) is limited to the following boundary conditions, since experimental data outside these boundaries hardly exist.

- $0.5 \le c_{min} / Ø \le 3.5$
- $c_{max} / c_{min} \le 5$
- $25 / Ø \le 2$
- $15\ \text{MPa} \le f_{cm} \le 110\ \text{MPa}$
- $l_0 / Ø \ge 10$
- good bond conditions

Where transverse pressure is present, the stress developed by bond increases to

$$f_{stm,tr} = f_{stm} + 6 \cdot \left(\frac{l_b}{Ø}\right) \cdot p_{tr} < 1.75 \cdot f_{st,0} + 0.8 \cdot \left(\frac{l_b}{Ø}\right) \cdot p_{tr} < 8.0 \cdot \left(\frac{l_b}{Ø}\right) \cdot f_{cm}^{0.5} \qquad (2\text{-}27)$$

Where

p_{tr} mean compression stress perpendicular to the potential splitting failure surface

$f_{st,0}$ mean stress developed by bond for the base conditions of confinement with

$$f_{st,0} = 54 \cdot \left(\frac{f_{cm}}{25}\right)^{0.25} \cdot \left(\frac{l_b}{Ø}\right)^{0.55} \cdot \left(\frac{25}{Ø}\right)^{0.2} \qquad (2\text{-}28)$$

2.9.6 MODEL CODE 2010

Bond Strength for Anchorage and Lap Design

The design bond strength f_{bd} given in MODEL CODE 2010 [MC2010] was derived by rearranging equation (2-26) with a lead coefficient of 41 to allow for the development of the design reinforcement strength f_{yd} = 435 MPa.

To introduce a certain safety margin, two independent models were used to derive design values in [FIB14]. In the first model, the characteristic strength as a 5%-fractile was divided by the partial safety factor for concrete γ_c = 1.5. The characteristic strength was taken as 76 % (54 · 0.76 = 41) of the mean strength. The second model was a statistical analysis with a target probability of failure p_f below 10^{-6} for brittle concrete failure. The statistical model confirmed the simpler model reducing the concrete strength. For the calculation of characteristic bar stress instead of mean stress, the lead coefficient in equation (2-22) was therefore altered from 54 to 41 [FIB14].

The basic bond strength $f_{bk,0}$ in [MC2010] was derived by rearrangement of equation (2-22) with a coefficient of 41. The transverse reinforcement stress f_{stk} was set to 500 / 1.5 = 435 MPa and

$$\frac{l_{b,0}}{Ø} = \left(\frac{f_{yk}}{\gamma_c \cdot 41}\right)^{1.82} \cdot \left(\frac{f_{cm}}{25}\right)^{-0.45} \cdot \left(\frac{25}{Ø}\right)^{-0.36} = 73.5 \cdot \left(\frac{f_{cm}}{25}\right)^{-0.45} \cdot \left(\frac{25}{Ø}\right)^{-0.36} \qquad (2\text{-}29)$$

$$f_{bk,0} = \frac{f_{yd} \cdot Ø}{4 \cdot l_{b,0}} = 1.5 \cdot \left(\frac{f_{cm}}{25}\right)^{0.45} \cdot \left(\frac{25}{Ø}\right)^{0.36} \qquad (2\text{-}30)$$

The values for cover and confining reinforcement corresponding to minimum detailing requirements were introduced and the indices as well as coefficients were rounded to more convenient values. For the calculation of the basic bond strength $f_{bd,0}$ without transverse reinforcement, the coefficient 1.5 was changed to the coefficient η_1 = 1.6. To make allowance for the enhancement in bond strength if minimum confining reinforcement is provided, the value of basic bond strength was increased by 10% and the coefficient η_1 was changed to 1.75 [FIB14]. Equation (2-31) gives the resulting design bond strength f_{bd}.

$$f_{bd} = (\alpha_{2,MC} + \alpha_{3,MC}) \cdot f_{bd,0} - \frac{2 \cdot p_{tr}}{\gamma_{cb}} < 2.0 \cdot f_{bd,0} - \frac{0.4 \cdot p_{tr}}{\gamma_{cb}} < \frac{1.5 \cdot \sqrt{f_{ck}}}{\gamma_{cb}} \tag{2-31}$$

Where

p_{tr} mean compression stress perpendicular to the potential splitting failure surface at ultimate limit state

$$f_{bd,0} = \eta_1 \cdot \eta_2 \cdot \eta_3 \cdot \eta_4 \cdot \left(\frac{f_{ck}}{25}\right)^{0.5} / \gamma_{cb} \tag{2-32}$$

$$\alpha_{2,MC} = \left(\frac{c_{min}}{Ø}\right)^{0.5} \cdot \left(\frac{c_{max}}{2 \cdot c_{min}}\right)^{0.15} \tag{2-33}$$

$$\alpha_{3,MC} = k_d \cdot (K_{tr} - \alpha_t / 50) \tag{2-34}$$

With

γ_{cb} partial safety coefficient for bond $\gamma_{cb} = 1.5$

η_1 coefficient taken as 1.75 for ribbed bars

η_2 coefficient taken as 1.0 for good bond conditions

η_3 coefficient for the effect of bar diameter $\eta_3 = (25 / Ø)^{0.3}$ for $Ø > 25$ mm

η_4 coefficient for the characteristic strength of steel reinforcement being anchored or lapped, taken as 1.0 for $f_{yk} = 500$ MPa

c_{min} minimum concrete cover: $c_{min} = \min\{c_x; c_y; c_s / 2\}$

c_{max} maximum concrete cover: $c_{max} = \max\{c_x; c_s / 2\}$

$0.5 \leq c_{min} / Ø \leq 3.5$

$1.0 \leq c_{max} / c_{min} \leq 5.0$

k_d coefficient for efficiency of transverse reinforcement (cf. Figure 2-20)

K_{tr} $n_l \cdot A_{st} / (n_b \cdot Ø \cdot s_{st})$

n_l number of legs of confining reinforcement crossing a potential splitting failure surface at a section (denominated n_t in [MC2010])

n_b number of anchored bars or pairs of lapped bars in the potential splitting failure surface

α_t coefficient for the bar diameter

$\alpha_t = 0.5$ for $Ø \leq 25$ mm

$\alpha_t = 1.0$ for $Ø = 50$ mm

The factor k_d defined in [MC2010] was derived from k_m in [FIB14] (cf. Figure 2-19) and additionally accounts for the nonlinear relationship between anchorage or lap length and the stress developed in the bar.

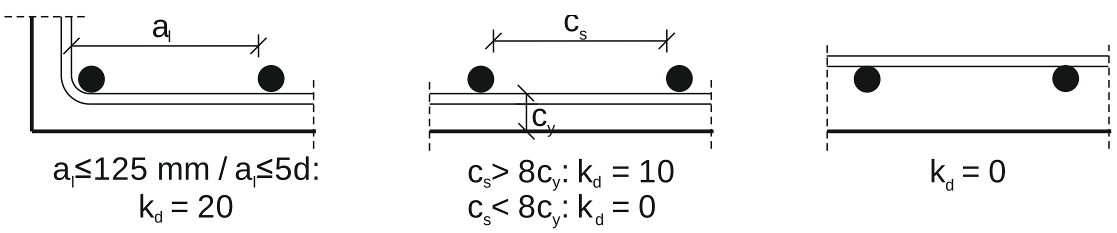

Figure 2-20 Coefficient k_d for efficiency of transverse reinforcement (adapted from [MC2010])

In case the diameter of the anchored bars is smaller than 20 mm and the concrete class is of grade C60 or below, the transverse reinforcement provided for other reasons may be assumed sufficient to satisfy minimum requirements for confining reinforcement without further justification [MC2010]. Otherwise minimum transverse reinforcement has to be positioned with

$$\Sigma A_{st} = n_{st} \cdot n_l \cdot A_{st} \geq \alpha_t \cdot A_{s,cal.} / A_{s,prov} \cdot n_b \cdot A_s \tag{2-35}$$

Where

n_{st} number of items of confining reinforcement within the bond length (denominated n_g in [MC2010])

n_l number of legs of links crossing a potential splitting failure surface at a section (denominated n_t in [MC2010])

α_t coefficient for the bar diameter
$\alpha_t = 0.5$ for $Ø \leq 25$ mm
$\alpha_t = 1.0$ for $Ø = 50$ mm

$A_{s,cal.}$ calculated area of reinforcement required by design

$A_{s,prov.}$ area of reinforcement provided

Anchorage and Lap Length

According to [MC2010], the anchorage length is

$$l_b = \frac{Ø \cdot \sigma_{sd}}{4 \cdot f_{bd}} \tag{2-36}$$

and the lap length is

$$l_0 = \alpha_{4,MC} \cdot \frac{Ø \cdot f_{yd}}{4 \cdot f_{bd}} \tag{2-37}$$

If the calculated reinforcement stress at the ultimate limit state does not exceed 50 % of the characteristic strength of the reinforcement, or no more than 34 % of bars are lapped at the section, the coefficient $\alpha_{4,MC} = 0.7$ may be used; otherwise $\alpha_{4,MC} = 1.0$.

The stress developed in a lap according to [MC2010] may therefore be taken as

$$\sigma_{sd} = \frac{l_0}{Ø} \cdot \frac{4}{\alpha_{4,MC}} \cdot [\left(\alpha_{2,MC} + \alpha_{3,MC}\right) \cdot 1.75 \cdot \left(\frac{25}{Ø}\right)^{0.3} \cdot \left(\frac{f_{ck}}{25}\right)^{0.5} - 2 \cdot p_{tr}] / \gamma_{cb} \tag{2-38}$$

Local Bond-Slip Relationship

Additionally to the design model for anchorage and lap lengths, [MC2010] gives local bond stress-slip relationships. Figure 2-21 gives the values for good bond conditions and bar strain below yield strain.

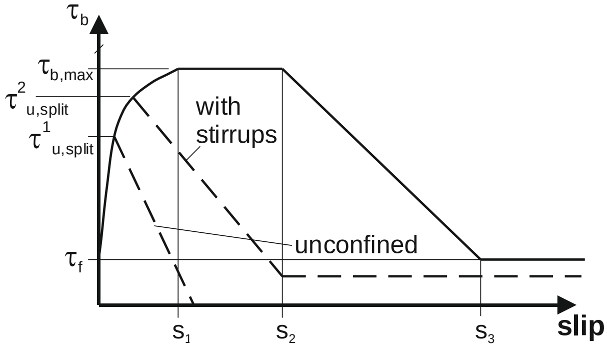

	Pull-Out	Splitting	
		Unconfined	stirrups
τ_{max}	$2.5\sqrt{f_{cm}}$	$7\cdot(f_{cm}/25)^{0.25}$	$8\cdot(f_{cm}/25)^{0.25}$
s_1	1 mm	$s(\tau_{max})$	$s(\tau_{max})$
s_2	2 mm	s_1	s_1
s_3	c_{clear}	$1.2 \cdot s_1$	$0.5 \cdot c_{clear}$
α	0.4	0.4	0.4
τ_f	$0.4\cdot\tau_{max}$	0	$0.4\cdot\tau_{max}$

Figure 2-21 Local bond-slip relationship according to [MC2010]

Where

$\tau_0 = \tau_{max} \cdot (s/s_1)^{\alpha}$ for $0 \le s \le s_1$

$\tau_0 = \tau_{max}$ for $s_1 \le s \le s_2$

$\tau_0 = \tau_{max} - (\tau_{max} - \tau_f) \cdot (s - s_2) / (s_3 - s_2)$ for $s_2 \le s \le s_3$

$\tau_0 = \tau_f$ for $s_3 < s$

c_{clear} clear distance between ribs

Pull-out failure is expected for well confined concrete (concrete cover > 5 · Ø, clear spacing between bars > 10 · Ø) or suitable confining reinforcement. The values for splitting failure are derived from equation (2-26) with l_b / Ø = 5, Ø ≤ 25 mm, c_{max}/c_{min} = 2.0, c_{min} = c_{max} and K_{tr} = 0.02 and

$$\tau_{u,split} = 6.5 \cdot \left(\frac{f_{cm}}{25}\right)^{0.25} \cdot \left(\frac{25}{Ø}\right)^{0.2} \cdot \left[\left(\frac{c_{min}}{Ø}\right)^{0.33} \cdot \left(\frac{c_{max}}{c_{min}}\right)^{0.1} + k_m \cdot K_{tr}\right] \tag{2-39}$$

This splitting bond strength was derived from equation (2-26) with

$$\tau_{u,split} = \frac{Ø}{l_b} \cdot \frac{f_{stm}}{4} = \frac{Ø}{l_b} \cdot \frac{1}{4} \cdot 54 \cdot \left(\frac{f_{cm}}{25}\right)^{0.25} \cdot \left(\frac{25}{Ø}\right)^{0.2} \cdot \left(\frac{l_b}{Ø}\right)^{0.55} \cdot [...] \tag{2-40}$$

$$= \frac{1}{5} \cdot \frac{1}{4} \cdot 54 \cdot \left(\frac{f_{cm}}{25}\right)^{0.25} \cdot \left(\frac{25}{Ø}\right)^{0.2} \cdot (5)^{0.55} \cdot [...] = 6.5 \cdot \left(\frac{f_{cm}}{25}\right)^{0.25} \cdot \left(\frac{25}{Ø}\right)^{0.2} \cdot [...]$$

Furthermore, [MC2010] gives coefficients for the effects of transverse cracking, yielding, transverse stress, longitudinal cracking and cyclic loading.

$$\tau_{b,m} = \tau_0 \cdot \Omega_y \cdot \Omega_{p,tr} \cdot \Omega_{cr} \cdot \Omega_{cyc} \tag{2-41}$$

Where

Ω_y influence of yielding

$\Omega_{p,tr}$ influence of transverse pressure, for compression: $\Omega_{p,tr} = 1 - \tanh(0.2 \cdot p_{tr} / (0.1 \cdot f_{cm}))$

Ω_{cr} influence of longitudinal cracking: $\Omega_{cr} = 1 - 1.2 \cdot w_{cr}$

Ω_{cyc} influence of cyclic loading

For transverse cracking, the bond stress τ is to be reduced by the factor $\lambda = 0.5 \cdot x / Ø \leq 1$ at a distance $x \leq 2 \cdot Ø$ from the crack.

2.9.7 PT1 WORKING DRAFT

For the next generation of EUROCODE 2, the PT1 WORKING DRAFT [PT18] proposes a modified design model on the basis of [FIB14]. The exponents are simplified for ease of use. For good bond conditions, the necessary bond length follows from

$$\frac{l_{bd,req}}{Ø} = 40 \cdot \left(\frac{25\text{ MPa}}{f_{ck}}\right)^{1/2} \cdot \left(\frac{\sigma_{sd}}{435\text{ MPa}} \cdot \frac{\gamma_c}{1.5}\right)^{3/2} \cdot \left(\frac{Ø}{20\text{ mm}}\right)^{1/3} \cdot \left(\frac{1.5 \cdot Ø}{c_{d,conf}}\right)^{1/2} \leq l_{b,min} \quad (2\text{-}42)$$

$$c_{d,conf} = c_d + \left(30 \cdot k_{conf} \cdot \frac{n_l \cdot A_{st}}{n_b \cdot Ø \cdot s_{st}} + 8 \cdot \sigma_{ctd} / \sqrt{f_{ck}}\right) \cdot Ø \leq 3.75 \cdot Ø \quad (2\text{-}43)$$

With

k_{conf} effectiveness factor

- $k_{conf} = 1.0$ for confinement reinforcement crossing the potential splitting plane (maximum distance from leg to anchored bar $\leq 5 \cdot Ø$)
- $k_{conf} = 0.25$ for transverse reinforcement within the cover cy with ($c_s \geq 8 \cdot Ø$)
- $k_{conf} = 0$ in other circumstances

σ_{ctd} design value of the mean compression stress perpendicular to the potential splitting plane

$l_{b,min}$ $15 \cdot Ø$ for anchorages and $20 \cdot Ø$ for laps

If tension laps are positioned in zones where the yield strength shall be exceeded, the laps are to be designed for $1.2 \cdot \sigma_{sd}$. Alternatively, confining reinforcement or a reduction of lapped bars to a percentage of 50 % or smaller is required.

The coefficients 40, 30 and 8 in equations (2-42) and (2-43) are still to be validated with a reliability analysis [PT18]. Rearranging for the developable stress in anchorages gives

$$f_{std,PT} = 435 \cdot \frac{1.5}{\gamma_c} \cdot \left(\frac{f_{ck}}{25\text{ MPa}}\right)^{\frac{1}{3}} \cdot \left(\frac{20}{Ø}\right)^{\frac{2}{9}} \cdot \left(\frac{l_b}{40 \cdot Ø}\right)^{\frac{2}{3}} \cdot \left(\frac{c_{d,conf}}{1.5 \cdot Ø}\right)^{\frac{1}{3}} \quad (2\text{-}44)$$

2.9.8 ELIGEHAUSEN

ELIGEHAUSEN [ELI79] developed a design model for stress developed in laps based on 550 tests from several publications, including 325 tests with ineffective or no inner transverse reinforcement. The design model distinguishes between beam type members (split failure type A and B) and slab type members (split failure type C). For split failure modes, [ELI79] provides an model adding the concrete and transverse reinforcement contributions. The bar stress developed σ_s is defined as

$$\sigma_s = \sigma_s^c + \sigma_s^{st} \quad (2\text{-}45)$$

With
σ_s^c concrete contribution
σ_s^{st} transverse reinforcement contribution

If the relation of horizontal concrete cover to vertical concrete cover is small ($c_x \leq 0.85 \cdot c_y$), failure type A (cf. Figure 2-5) occurs. Cracks parallel to the longitudinal reinforcement originate in the horizontal lap plane. The concrete contribution may be taken as

$$\sigma_s^c = 5.3 \cdot \left(\frac{0.5 \cdot c_s + c_x}{\text{Ø}} \right)^{0.5} \cdot f_{c,cube}^{0.5} \cdot \left(\frac{l_0}{\text{Ø}} \right)^{2/3} \cdot k \tag{2-46}$$

With
$k = k_d \cdot k_q \cdot k_v \cdot k_p$
k_d coefficient for the effect of bar diameter: $0.75 \leq k_d = \sqrt{10/\text{Ø}} \leq 1.2$
k_q coefficient for the effect of different steel stress at the lap ends: $k_d = 2 / (1+k_1)$ and $k_1 = \frac{\min \sigma_e}{\max \sigma_e} \geq 0.6$
k_v coefficient taken as 1.0 for good and 0.8 for poor bond conditions
k_p coefficient taken as 1.0 for conventionally ribbed bars
$f_{c,cube}$ concrete compressive strength obtained from 200 mm cubes

Failure type B (face-and-side split, cf. Figure 2-5) occurs in laps with large horizontal concrete cover ($0.85 \cdot c_y < c_x \leq 4.0 \cdot c_y$) and small clear spacing between laps ($1.7 \cdot c_y \leq c_s \leq 2.0 \cdot c_x$). In this case, the concrete contribution σ_s^c to the steel stress is

$$\sigma_s^c = 5.8 \cdot \left(\frac{2 \cdot c_x}{c_y} \right)^{1/4} \cdot \left(\frac{c_y}{\text{Ø}} \right)^{1/2} \cdot f_{c,cube}^{1/2} \cdot \left(\frac{l_0}{\text{Ø}} \right)^{2/3} \cdot k \tag{2-47}$$

Failure type C (V-type failure) is expected in laps in slab type elements with small side effect ($c_x \geq 4.0 \cdot c_y$) and clear bar spacing $c_s > 8.0 \cdot c_y$. The concrete contribution to the developable reinforcing bar stress σ_s^c is given as:

$$\sigma_s^c = \alpha_c \cdot \left(\frac{c_y}{\text{Ø}} \right)^{1/2} \cdot f_{c,cube}^{1/2} \cdot \left(\frac{l_0}{\text{Ø}} \right)^{2/3} \cdot k \tag{2-48}$$

Where
α_c coefficient for calibration:
$\alpha_c = 9.75$ for $c_y \leq 2.5 \cdot \text{Ø}$
$\alpha_c = 12.27$ for $c_y > 2.5 \cdot \text{Ø}$

The increase in bar stress in laps by transverse reinforcement is taken into account independent from the failure type. The calibration coefficient α_Q in equation (2-49) was obtained by finite element analysis.

$$\sigma_s^{st} = \alpha_Q \cdot \sqrt{\Sigma A_{st} / A_s \cdot f_{yt}} \cdot k_q \qquad (2\text{-}49)$$

With

α_Q coefficient for calibration:

- $\alpha_Q = 6.0 \cdot \sqrt{2}$ for stirrups around one bar
- $\alpha_Q = 6.0$ for stirrups around two bars
- $\alpha_Q = 1.8$ for straight transverse reinforcement outside the lap
- $\alpha_Q = 0$ for transverse reinforcement inside the lap

f_{yt} transverse-reinforcement stress limited to 300 MPa

k_q see above

The design model according to [ELI79] includes a safety factor $\nu = 2.1$, since lap failure is usually brittle. This factor is included in the calibration factors given in equations (2-46) to (2-48). The value 2.1 was defined in [DEU88] and corresponds to an averaged load safety factor of approximately $(\gamma_g + \gamma_q) / 2 = (1.35 + 1.5) / 2 = 1.4$ and a partial safety factor for concrete of 1.5 according to the [EC2] safety concept $(1.4 \cdot 1.5 \approx 2.1)$.

2.9.9 BURKHARDT

BURKHARDT [BUR00] extended the [ELI79] design model for high strength concrete. 538 tests were analysed including 191 tests with concrete cube strength above 50 MPa and the reinforcing bar stresses in laps limited to 1.2 times the yield strength.

$$\sigma_s = \sigma_s^c + \sigma_s^{st} \leq 1.2 \cdot f_y \qquad (2\text{-}50)$$

For the 5%-fractile of the concrete contribution σ_s^c, BURKHARDT [BUR00] obtained a calibration factor $\alpha = 28.5$ by a regression analysis of 233 beam tests (59 with high strength concrete). This design model is limited to laps with good bond conditions. For the calculation of the mean reinforcing stress, the coefficient $\alpha_6 = 28.5$ is replaced by 38.

$$\sigma_{s;0,05}^c = 28.5 \cdot f_c^{1/4} \cdot \left(\frac{l_0}{Ø}\right)^{1/2} \cdot \left(\frac{c_d}{Ø}\right)^{1/5} \cdot k \qquad (2\text{-}51)$$

Where

c_d minimum concrete cover: $c_d = \min\{c_x; c_y; c_s / 2\}$

$k = k_d \cdot k_p$ (see ELIGEHAUSEN [ELI79]), with $0.75 \leq k_d = \sqrt{10/Ø} \leq 1.0$

The positive effect of confinement by transverse reinforcement increases for higher concrete strength [BUR00]. Accordingly, the transverse reinforcement contribution includes the concrete strength. The calibration factor $\alpha = 3.2$ for the 5%-fractile given in equation (2-52) was obtained by a regression analysis of 224 tests (124 with high strength concrete). The mean transverse reinforcement contribution to the reinforcing bar stress, can be obtained by replacing the coefficient 3.2 by 4.2.

$$\sigma_{s;0,05}^{st} = 3.2 \cdot f_c^{1/4} \cdot \sqrt{\frac{n_t}{n_b} \cdot \frac{\Sigma A_{st}}{A_s} \cdot f_{yt}} \cong 3.2 \cdot f_c^{1/4} \cdot \sqrt{\frac{l_0 \cdot n_l \cdot A_{st} \cdot f_{yt}}{s_{st} \cdot n_b \cdot A_s}} \tag{2-52}$$

The design reinforcing bar stress given in equation (2-53) was obtained by considering the safety factors for concrete $\gamma_c = 1.5$, high strength concrete $\gamma_c' = 1 / (1.1 - f_{ck} / 500)$ and steel $\gamma_s = 1.15$.

$$\sigma_{sd} = 28.5 \cdot f_c^{1/4} \cdot \left(\frac{\gamma_s \cdot l_0}{\gamma_c \cdot \gamma_c' \cdot Ø} \right)^{1/2} \cdot \left(\frac{c_d}{Ø} \right)^{1/5} \cdot k + 3.2 \cdot f_c^{1/4} \cdot \sqrt{\frac{l_0 \cdot n_l \cdot A_{st} \cdot f_{yt}}{s_{st} \cdot n_b \cdot A_s}} \tag{2-53}$$

2.9.10 LETTOW

LETTOW [LET06a] analysed laps with finite element models and compared the results to test results from literature and existing design models. He derived a new design model for the mean steel stress in laps, whereas the same failure types as ELIGEHAUSEN [ELI79] were distinguished. The calibration factor $\alpha_{A/B} = 11.1$ was found from a regression analysis of 67 beam tests. The model presumes a simplified relation between clear lap spacing and horizontal concrete cover $c_s / c_x = 2.0$. Equation (2-54) gives the mean reinforcement stress in beam-type members with side effect ($c_x / c_y \leq 4$).

$$\sigma_{sm} = 11.1 \cdot f_{cm}^{2/5} \cdot \left(\frac{l_0}{Ø} \right)^{3/5} \cdot \left[\left(\frac{c_x}{c_y} \right)^{1/4} \cdot \left(\frac{c_y}{Ø} \right)^{1/2} \right] \cdot k_u \cdot k_v \tag{2-54}$$

The mean reinforcement stress in slab-type members without side effect ($c_x / c_y > 4$) is given by equation (2-55).

$$\sigma_{sm} = 13.9 \cdot f_{cm}^{2/5} \cdot \left(\frac{l_0}{Ø} \right)^{3/5} \cdot \left[\left(\frac{c_y}{Ø} \right)^{1/2} \right] \cdot k_u \cdot k_v \tag{2-55}$$

Where

k_u coefficient for confinement
 $1.1 \cdot (l_0 / s_{st})^{1/10}$
 1.0 where stirrups are not present

k_v coefficient for bond
 0.95 for bond with increased splitting tendency (high ribs, large f_R values)
 1.0 for all other cases and for a concrete cover $c_y < 1.2 \cdot c_x$

In contrast to ELIGEHAUSEN [ELI79] and BURKHARDT [BUR00], LETTOW [LET06a] chose a coefficient k_u to consider the effect of transverse reinforcement. Conforming with BURKHARDT [BUR00], [LET06a] considered tests with stirrups only. The design model established in [LET06a] does not include any safety factors, since it was derived to recalculate test results and finite element results on mean level.

2.9.11 Zuo and Darwin

The design model by Zuo and Darwin [ZUO00] is based on experimental investigations including 64 lap tests with different concrete strengths and relative rib areas. In addition to the experiments, a regression analysis was conducted for 367 tests with and without transverse reinforcement. Conforming with [ELI79], the lap strength consists of a concrete and a transverse reinforcement contribution with

$$\sigma_s = \sigma_s^c + \sigma_s^{st} \tag{2-56}$$

The concrete contribution σ_s^c is given by

$$\sigma_{sm}^c = \left[59.8 \cdot l_0 \cdot \frac{(c_{min} + 0.5 \cdot Ø)}{A_s} + 2350\right] \cdot \left(0.1 \cdot \frac{c_{max}}{c_{min}} + 0.9\right) \cdot f_c^{1/4}\,[\text{psi}] \tag{2-57}$$

With

$c_{max} = \max\{c_{min,ZD}; c_y\}$

$c_{min} = \min\{c_{Z/D}; c_y\}$

$c_{min,ZD} = \min\{c_s/2;\ 6.4\text{ mm};\ c_x\}$

$c_{max} / c_{min} \leq 3.5$

Zuo and Darwin [ZUO00] found that the concrete strength has a different effect on the transverse reinforcement contribution than on the concrete contribution. The transverse reinforcement contribution σ_s^{st} may be calculated as follows

$$\sigma_{sm}^{st} = \left(31.14 \cdot t \cdot \frac{n_{st} \cdot A_{st}}{n_b \cdot A_s} + \frac{3.99}{A_s}\right) \cdot f_c^{3/4}\,[\text{psi}] \tag{2-58}$$

Where

$t = t_d \cdot t_r$

t_d coefficient for the effect of bar diameter: $t_d = 0.78 \cdot Ø + 0.22$ [in.]

t_r coefficient for the effect of rib geometry: $t_r = 9.6 \cdot f_R + 0.28$

The relative rib area f_R ranges from 0.056 to 0.086, leading to values for t_r between 0.82 to 1.11 with an average value of 0.98 [DAR95b]. For simplicity, the coefficient t_r is taken as 1.0 in the comparison of design models in chapter 5.

Equations (2-57) and (2-58) were derived from test results and thus give mean values. The equations for design values given in [ZUO00] include calibration factors with a strength reduction factor $\phi_{Z/D}$ of 0.9.

2.9.12 Canbay and Frosch

Canbay and Frosch [CAN05] verified their model for the ultimate lap load by 480 lap tests with and without transverse reinforcement. The maximum lap strength at splitting failure including the contribution by transverse reinforcement is defined as

$$\sigma_s = \frac{F_{split} + F_{st}}{n_b \cdot A_s \cdot \tan\beta} = \frac{2.75}{n_b \cdot A_s} \cdot \left(F_{split} + F_{st}\right)\left[ksi\right] \qquad (2\text{-}59)$$

Where

F_{split} splitting resistance by concrete cover along the lap length [kip]

F_{st} splitting resistance by transverse reinforcement [kip]

θ inclination of struts initiating at the rib flanks (20 ° provided optimal results)

Canbay and Frosch [CAN06] distinguish side (cf. Figure 2-22, left) and face splitting types (cf. Figure 2-22, left).

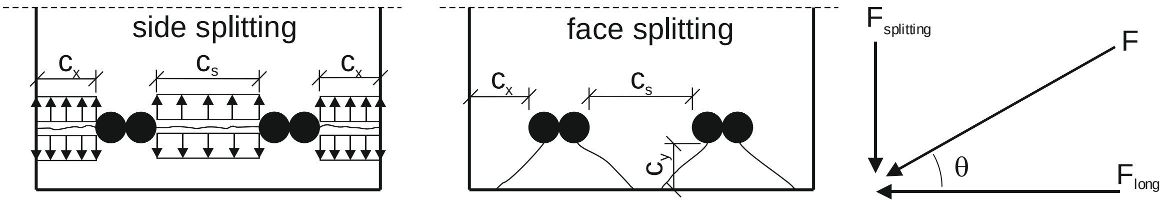

Figure 2-22 Side splitting (left), face splitting (centre) and force distribution at bond forces (right) (adapted from [CAN06])

The tensile concrete stress around the bars is presumed to be linear along the lap length. The non-linearity of the bond strength along the lap length is considered by introducing an efficient lap length l_0*. The side-splitting force $F_{split,\,side}$ is

$$F_{split,\,side} = l_0^* \cdot \left[2 \cdot c_x{}^* + 2 \cdot c_s{}^* \left(n_b - 1\right)\right] \cdot 6 \cdot f_c^{1/2}\ \left[kip\right] \qquad (2\text{-}60)$$

For face-splitting, the splitting force $F_{split,\,face}$ is

$$F_{split,\,face} = l_0^* \cdot \left[2 \cdot c_y{}^* \cdot \left(0.1 \cdot \frac{c_x}{c_y} + 0.9\right) + 2 \cdot c_y{}^* \left(n_b - 1\right) \cdot \left(0.1 \cdot \frac{c_s}{2} \cdot \frac{1}{c_y} + 0.9\right)\right] \cdot 6 \cdot f_c^{1/2} \qquad (2\text{-}61)$$

With

c_y*, c_x*, $(c_s / 2)$* coefficients for the efficiency of concrete cover at linear stress distribution

$$c_i{}^* = c_i \cdot . \frac{0.77}{\sqrt{c_i / Ø}} \leq c_i$$

l_0* coefficient for the efficiency of lap length at linear stress distribution

$$l_0{}^* = l_0 \cdot \frac{9.51}{\sqrt{l_0 / Ø \cdot f_c^{1/4}}} \leq l_0$$

Transverse reinforcement generates additional resistance in the failure plane of splitting. Equation (2-62) gives the splitting force $F_{st,\,side}$ provided by transverse reinforcement. This equation includes the leg number n_l crossing the splitting plane for side splitting (cf. Figure 2-22).

$$F_{st,\,side} = n_{st} \cdot n_l \cdot A_{st} \cdot f_{yt} \cdot \left[\frac{n_b \cdot f_c^{1/2}}{170} \right] \; [\text{kip}] \tag{2-62}$$

For face split failures, the transverse reinforcement crosses the splitting plane at each bar, therefore equation (2-63) defining the splitting force $F_{st,\,face}$ includes the bar number n_b instead of the leg number n_l.

$$F_{st,\,face} = n_{st} \cdot n_b \cdot A_{st} \cdot f_{yt} \cdot \left[\frac{n_b \cdot f_c^{1/2}}{170} \right] [\text{kip}] \tag{2-63}$$

The recommended transverse bar yield strength f_{yt} is 62 MPa.

In the development of the design equation (2-59), a safety factor of 1.2 was used. Without the safety factor, 50 % of the calculated strengths were unsafe. By using the factor 1.2, only 10 % of the unconfined and 16 % of the confined tests did not reach their yield strength. This accounts for a nominal yield strength equal to 414 MPa and lap lengths designed according to the proposed model [CAN05].

2.9.13 Summary

Table 2-5 compares the considered effects of concrete strength, bar diameter and bond length for anchorages and laps in good bond conditions of uncoated reinforcement. A more detailed table on the considered design models is given in appendix A. The design equations for the necessary anchorage and lap length in [EC2] and [MC2010] include the characteristic concrete cylinder strength. The design models given in [ACI14], [FIB14], [BUR00], [LET06a], [ZUO00] and [CAN06] comprise a mean concrete cylinder strength. Only the design model established by ELIGEHAUSEN [ELI79] is based on the mean concrete cube strength.

Table 2-5 Comparison of consideration of parameters in design models for anchorages and laps

Design Model	Bond length	Concrete strength	Bar diameter	Lap factor
[EC2]	$l_b^{1.0}$	$f_{ck}^{2/3}$	(132 - Ø) / 100	1.0 – 1.5
[EC2/NA]	$l_b^{1.0}$	$f_{ck}^{2/3}$	(132 - Ø) / 100	1.5 – 2.0
[ACI14]	$l_b^{1.0}$	$f_{cm}^{1/2}$	0.8 or 1 (Ø ≥ 22 mm)	1.0 – 1.3
[FIB14]	$l_b^{0.55}$	$f_{cm}^{1/4}$	$(25 / Ø)^{0.2}$	1.0
[MC2010]	$l_b^{0.55}$	$f_{ck}^{1/2}$	$(25 / Ø)^{0.3}$	0.7 – 1.0
[PT18]	$l_b^{0.67}$	$f_{ck}^{1/3}$	$(20 / Ø)^{2/9}$	1.0
[ELI79]	$l_b^{0.67}$	$f_{cm,cube}^{1/2}$	$(10 / Ø)^{0.5}$	1.0
[BUR00]	$l_b^{0.50}$	$f_{cm}^{1/4}$	$(10 / Ø)^{0.5}$	1.0
[LET06a]	$l_b^{0.60}$	$f_{cm}^{2/5}$	-	1.0
[ZUO00]	$l_b^{1.0}$	$f_{cm}^{1/4}$	0.78 · Ø + 0.22 [in.]	1.0
[CAN06]	$l_b^{0.50}$	$f_{cm}^{1/2}$	-	1.0

2.10 Limit State of Cracking

2.10.1 Definition of Crack Width

The bearing behaviour of structural concrete elements under bending and tension is characterised by the development of cracks. Cracks impair the structural elements' aesthetics, but contribute to the utilisation of the material properties of concrete and reinforcing steel. Only in case the crack widths exceed certain limiting values, the cracks impair the durability and bond strength of structural concrete elements. [EC2] provides values for the calculated crack widths w_k that depend on exposure classes. The limiting value should be established accounting for the proposed application and type of the structure as well as for the costs of crack limitation [EC2].

Even satisfying the detailing rules according to [EC2] cannot prevent single cracks that exceed the calculated crack width. The rules for crack control shall not guarantee the explicit compliance of a defined crack width, but avoid the occurrence of single large cracks [EC2]. The exact crack width can hardly be calculated, since the existing crack models include simplifications, loads as well as materials are not perfectly distributed and the execution quality is not constant [DEU12].

For the evaluation of crack widths, the distribution of crack widths along the crack length as well as along the structural element length has to be considered. While the reinforcement reduces the crack width in its vicinity, the crack width increases at increasing distance from the reinforcement. According to the GUIDE TO GOOD PRACTICE FOR CRACK MEASUREMENTS published by the German Society for Concrete and Construction Technology [DEU06], the value w_k calculated according to [EC2] equations does not correspond to the crack width at the concrete surface, but conforms with a mean crack width over the effective depth of the reinforcement. Therefore, the crack control procedure can only control the crack width in the vicinity of the reinforcement in bond [EC2] (cf. Figure 2-23, left).

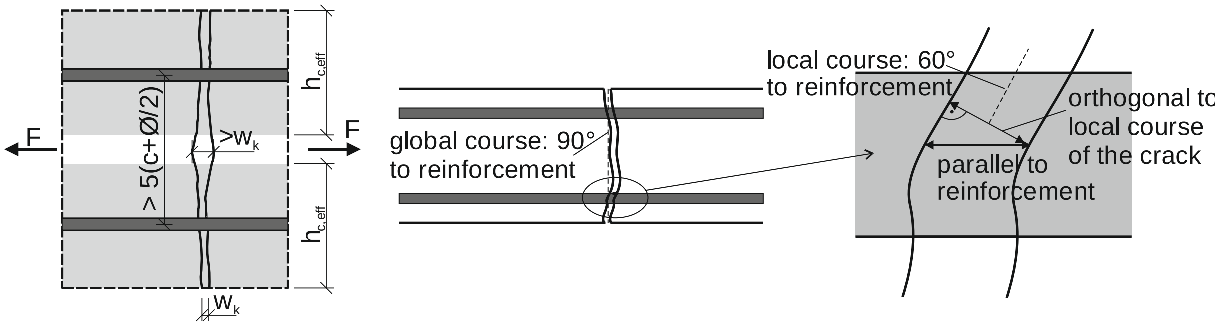

Figure 2-23 Calculated crack width w_k (left) and crack measurement parallel to reinforcement versus orthogonal to crack course (right)

The GUIDE TO GOOD PRACTICE [DEU06] defines the crack width w_{test} as the distance between the two edges of the crack measured orthogonally to the course of the crack at the concrete surface. It is not clear whether the local or the global course of the crack is meant (cf. Figure 2-23, right). The direction of the measurement however influences the resulting value of the crack width. Measuring cracks orthogonally to the locally inclined crack gives a smaller crack width than measuring parallel to the tensile reinforcement (cf. Figure 2-23, right).

Since the crack width is not constant over the crack length, the crack width shall be measured at several locations. According to [DEU06], the recommended spacing for the measurement should not exceed the mean stirrup spacing in the structural element and all visible cracks exceeding 0.05 mm shall be measured.

Bending crack widths are not constant over the crack depth but decrease in the direction of the compression zone (cf. Figure 2-24). In structural elements under bending, the crack width should therefore be measured at several locations along the perimeter of the effective area of the reinforcement. When calculating characteristic values from the crack measurements, the number of measurements affects the results. The smaller the number of measurements, the larger the characteristic crack width. MARTIN ET AL. [MAR80] found that the statistical distribution of bending cracks is wider than the distribution of direct cracks.

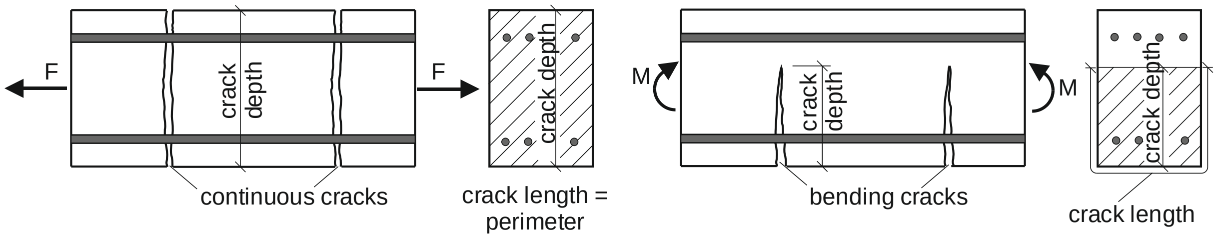

Figure 2-24 Front view and cross-section with crack formation in structural members subjected to direct tension (left) and bending (right)

[MC2010] defines the calculated crack width w_d as the crack width at the height of the reinforcement. The crack width in the extreme fibre $w_{d,ex}$ may be calculated from:

$$w_{d,ex} = w_d \cdot \frac{h - x}{d - x} \tag{2-64}$$

With
x height of the compression zone

Because [EC2] considers the crack width w_k as a mean value over the effective depth, crack width measurements at the extreme fibre, at the height of the reinforcement and at the effective height $h_{c,eff}$ are reasonable. The location of the crack measurement has to be considered in the crack width evaluation (cf. Figure 2-25, right). Measuring crack widths at a distance corresponding to the stirrup spacing (in accordance with [DEU06]) in wide elements under bending, results in large crack widths, since several cracks are measured in the extreme fibre of the cross section (cf. Figure 2-25, left).

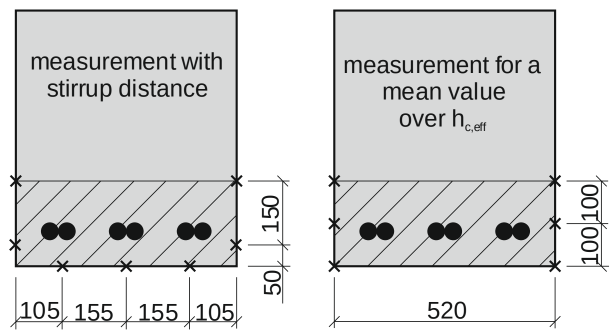

Figure 2-25 Crack measurement locations according to [DEU06] (left)) and [DEU12] (right)

2.10.2 Crack Phases in Structural Concrete

Cracking of structural concrete elements can be distinguished in two phases: the crack formation phase and the stabilised cracking phase. Crack formation starts as soon as the tensile strength of the concrete is reached. With increasing load, the stiffness of the structural element decreases and the number of cracks stabilises. Figure 2-26 shows the strain state in both phases of reinforcement and surrounding concrete.

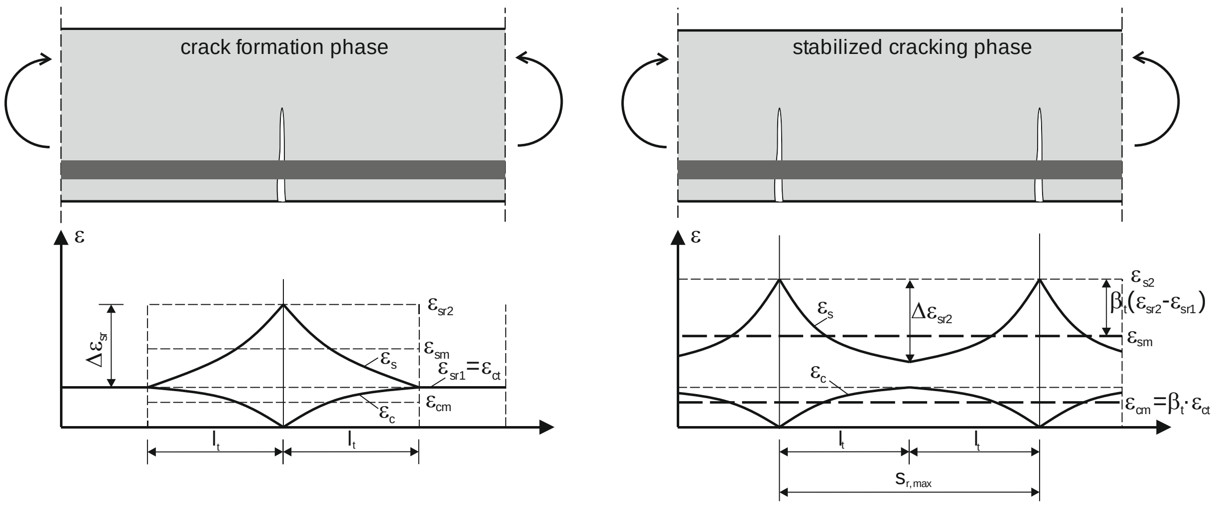

Figure 2-26 Crack formation phase (left) and stabilised cracking phase (right) (reproduced from [ZIL10])

Where

l_t	development length
$s_{r,max}$	maximum possible crack spacing
ε_{cm}	mean concrete strain along crack spacing
ε_{sm}	mean steel strain along crack spacing
ε_{ct}	concrete strain
ε_{sr1}	steel strain halfway between the cracks in the crack formation phase
ε_{sr2}	steel strain at the location of the crack in the crack formation phase
$\Delta\varepsilon_{sr}$	difference between steel strain at the crack and halfway between the cracks in the crack formation phase ($\Delta\varepsilon_{sr} = \varepsilon_{sr2} - \varepsilon_{sr1}$)
ε_{s2}	steel strain at the location of the crack in the stabilised cracking phase
β_t	coefficient for strain function

The crack width can be calculated from the crack spacing and the difference in steel and concrete strain. At the crack formation phase, the concrete and steel strain between the cracks have the same value. The crack spacing is greater than twice the development length l_t.

$$a \geq 2 \cdot l_t \approx \frac{\sigma_{s2} \cdot \varnothing}{2 \cdot \tau_{sm}} \tag{2-65}$$

Where σ_{s2} is the steel stress after cracking. The steel stress σ_{s2} cannot exceed $f_{ct} \cdot E_s / E_c$.

The difference in steel and concrete strains during the crack formation phase is:

$$\varepsilon_{sm} - \varepsilon_{cm} = (1 - \beta_t) \cdot \frac{\sigma_{s2}}{E_s} \tag{2-66}$$

Where β_t is 0.6 for short-term loading and 0.4 for long-term loading.

At the stabilised cracking phase, the concrete stress σ_c between the cracks remains below the tensile strength of concrete f_{ct}. The crack spacing varies between l_t and $2 \cdot l_t$. A new crack occurs, when the cracking force F_{cr} is transferred over l_t.

$$s_{r,max} = 2 \cdot l_t = 2 \cdot \frac{F_{cr}}{\tau_{sm} \cdot U_s} \approx \frac{f_{ct} \cdot \varnothing}{2 \cdot \tau_{sm} \cdot \rho_{s,eff}} \tag{2-67}$$

The difference in steel and concrete strain at the stabilised cracking phase is:

$$\varepsilon_{sm} - \varepsilon_{cm} = \frac{\sigma_{s2}}{E_s} - \beta_t \cdot \frac{f_{ct}}{\rho_{s,eff} \cdot E_s} \cdot (1 + \alpha \cdot \rho_{s,eff}) \tag{2-68}$$

2.10.3 Models for the Calculation of Characteristic Crack Spacing

Models for the calculation of crack width can be distinguished in classical and continuous models. While classical crack models consider the stabilised cracking phase only, continuous crack models consider both the crack formation and the stabilised cracking phases. The crack theory given in DIN 1045-1 [DEU08], [EUR91] and [EC2] belongs to the classical crack theory that has been described by REHM AND MARTIN [REH68], SCHIEßL [SCH98a] and MARTIN ET AL. [MAR80] in German literature. The continuous crack theory given in DIN 1045 [DEU88], [MC90] and [EC2/NA] was also described by KÖNIG AND TUE [KOE96].

The tensile stresses have to be transferred from the reinforcing bar into the concrete. Close to the crack location, the bond between reinforcement and concrete is disrupted over a length depending on the concrete cover. The crack spacing depends on the length of the disrupted bond commencing from the crack and accordingly on the concrete cover (cf. Figure 2-27).

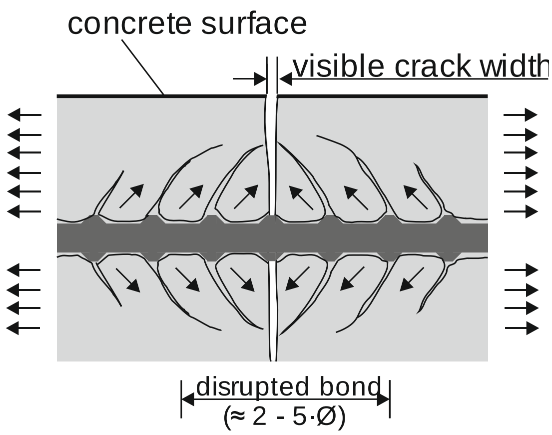

Figure 2-27 Disrupted bond length at cracks in elements under tension or bending (adapted from [ZIL10])

Several authors (e.g. [REH68], [MAR80]) and [EC2] consider the concrete cover by an addend to equation (2-67):

$$s_{r,max} = k_1 \cdot c + k_2 \cdot k_3 \cdot \frac{Ø}{\rho_{s,eff}} \tag{2-69}$$

Where k_1 is a factor for the disrupted length, k_2 is a factor for the bond strength and k_3 a factor for the strain distribution.

2.10.4 Characteristic Values of Crack Spacing and Crack Width

For the largest possible crack spacing in the stabilised cracking phase, denoted $s_{r,max}$, mean and characteristic values have to be distinguished. The characteristic crack spacing can be calculated by multiplying the mean crack spacing with a certain conversion factor or by introducing mean and characteristic values for bond strength. The crack spacing equations in [EUR91], [EC2] and [MC2010] are based on [REH68] with

$$s_{rk} = k_4 \cdot s_{rm} = k_4 \cdot \left(50 + 0.25 \cdot k_1 \cdot k_2 \cdot \frac{Ø}{\rho_{eff}} \right) \tag{2-70}$$

Where the factor k_1 is 0.8 for ribbed bars and k_2 is 0.5 for bending. The conversion factor k_4 is 1.7, which corresponds with a coefficient of variation (COV) V_x of 40 % with

$$s_{rk} = s_{95\,\%} = s_{rm} \cdot \left(1 + k_{95\,\%} \cdot V_x\right) = s_{rm} \cdot \left(1 + 1.645 \cdot 0.4\right) = s_{rm} \cdot 1.7 \tag{2-71}$$

The original EUROCODE 2 published in 1991 [EUR91] comprises the same conversion factor designated β. For load induced cracking, β equals 1.7. The characteristic crack spacing is given by

$$s_{rk,ENV} = \beta \cdot s_{rm} = \beta \cdot \left(50 + 0.25 \cdot k_1 \cdot k_2 \cdot \frac{Ø}{\rho_{eff}} \right) \tag{2-72}$$

The crack spacing according to [EC2] follows from

$$s_{rk,EC2} = 3.4 \cdot c + k_1 \cdot k_2 \cdot 0.425 \cdot \frac{Ø}{\rho_{eff}} \tag{2-73}$$

This equation also corresponds with the formulation according to [REH68] with a conversion factor of 1.7 for the transformation from mean to characteristic crack spacing when a concrete cover c = 25 mm is assumed (3.4 · c = 85 mm = 1.7 · 50):

$$s_{rk,EC2} = 1.7 \cdot \left(50 + 0.25 \cdot k_1 \cdot k_2 \cdot \frac{Ø}{\rho_{eff}} \right) \tag{2-74}$$

The [EC2] crack spacing is thus a characteristic crack spacing derived from the mean crack spacing and the conversion factor 1.7. According to equation (2-71), this factor corresponds with a 95% quantile and a COV of 40%.

A conversion factor for the calculation of characteristic values can also be found in [MC90] and [EC2/NA]. The following crack spacing equation for stabilised cracking is given in [MC90] and [EC2/NA].

$$s_{rk,MC90} = s_{rk,NAD} = 2 \cdot l_t = \frac{f_{ct} \cdot Ø}{2 \cdot \tau_{sm} \cdot \rho_{s,eff}} \tag{2-75}$$

Applying the bond strength $\tau_{sm} = 2.25 \cdot f_{ct}$ results in the mean crack width, while a bond strength $\tau_{sm} = 1.8 \cdot f_{ct}$ represents the characteristic value of the crack width as 75% quantile [MC90]. Thus, the relation between mean and characteristic value is 2.25 / 1.8 = 1.25. Accordingly, the crack spacing defined in [EC2/NA] and [MC90] is a characteristic value calculated from the mean value multiplied with a conversion factor of 1.25 instead of 1.7. The factor 1.25 approximately corresponds with a COV V_x of 40 % with

$$s_{rk} = s_{75\%} = s_{rm} \cdot \left(1 + k_{75\%} \cdot V_x\right) = s_{rm} \cdot \left(1 + 0.675 \cdot 0.4\right) = s_{rm} \cdot 1.27 \tag{2-76}$$

The procedure for statistical analysis of crack width measurements is not clearly defined in codes or guidelines. From the literature review, the following coherence was identified:

- The crack spacing s_{rk} according to [EC2] is a characteristic crack spacing equal to $1.7 \cdot s_{rm}$. The factor 1.7 corresponds with a 95%-fractile value and a COV of 40%.
- The crack spacing s_{rk} according to [EC2/NA] and [MC90] is a characteristic crack spacing derived from $1.25 \cdot s_{rm}$. The value 1.25 corresponds with a 75%-fractile value and a COV of 40 %.

2.10.5 Statistical Distribution of Crack Widths

For a statistic evaluation, the probability distribution of the sample and the desired confidence level have to be defined. The quantiles can be obtained with equation (2-77) for a normal distribution or with equation (2-78) for a log-normal distribution.

$$X_k = m_x \cdot (1 + k_n \cdot V_x) \tag{2-77}$$

$$X_k = m_x \cdot \exp(\mu + k_n \cdot \sigma) \tag{2-78}$$

The symbols are given below. The k_n-factors depend on the required quantile, the number of measurements, the probability distribution of the population and the desired confidence level.

Quantile values of crack measurements can be calculated from those tabulated k_n-factors given in DIN ISO 16269 [DEU14]. These tables are valid for the normal and log-normal distributions. BERGMEISTER [BER99] found in a χ^2-test that the crack spacing has a log-normal distribution, while the crack width has a gamma distribution. The tables given in [EC0] for the calculation of characteristic values were derived from Bayesian procedures with vague prior distributions [EC0] and can therefore not be compared exactly to the classic statistical analysis. For simplification, the evaluation of crack measurements in chapter 3 was accomplished with log-normal distributions for crack spacing and crack width. When presuming a log-normal distribution, the logarithmised crack widths have a normal distribution. The mean value m_x, the standard deviation s_x, the COV V_x and the quantile values X_k of the crack width can be calculated with equations (2-78) to (2-81).

$$m_x = \exp\left(\mu + \frac{\sigma^2}{2}\right) \tag{2-79}$$

$$s_x = \exp\left(\mu + \frac{\sigma^2}{2}\right) \cdot \sqrt{\exp\left(\sigma^2\right) - 1} \tag{2-80}$$

$$V_x(x) = \frac{m_x}{s_x} = \sqrt{\exp\left(\sigma^2\right) - 1} \tag{2-81}$$

Where μ and σ are the mean value and the standard deviation of the logarithmised measured crack widths $\ln(w_{test})$.

2.10.6 Evaluation of Crack Width Measurements in Literature

In the numerous published crack investigations, the crack width has certainly been measured in different locations (extreme fibre or at the height of the reinforcement) and in different directions (orthogonally to the local course of the crack or parallel to the reinforcement under tension). Besides different methods for practical crack measurements, two different definitions of 95% quantile values have been found in literature.

Some authors define the 95%-quantile of a measurement as the crack width that only 5% of the measurements exceed [DEU06], [EMP16]. This definition disrespects the number of measurements, the statistical distribution of the sample and the COV. Other authors use a statistical analysis as described above to calculate the 95%-quantile from the crack width sample. [MAR80], [REH68], [EC2], [MC2010] and their preceding documents are based on such statistical analyses. The two definitions of quantile values may lead to the same results depending on the number of measurements, the statistical distribution and the COV V_x.

KÖNIG AND TUE [KOE96] directly compare mean crack widths instead of 95%-quantiles. Since many test reports give mean values only, they determine the mean calculated crack width of their crack model from the maximum crack width. The conversion is done based on the mechanical crack model rather than on a statistical analysis.

Since the crack width w_k according to [EC2] is calculated from a 95% quantile for crack spacing, the crack width is larger than the crack width w_k according to [EC2/NA], which is calculated from a 75% quantile for the maximum crack spacing.

2.10.7 Acceptance Criteria for Measured Crack Widths

For the evaluation of mean and quantile values from crack width samples, acceptance criteria have to be applied. The GUIDE TO GOOD PRACTICE [DEU06] defines permissible percentages of exceedance of the allowable crack width. The evaluation of maximum exceedances of single measurements should be done with engineering expertise. For the durability of the structure, single crack widths shall not exceed 0.4 mm to 0.5 mm [DEU12]. Based on the capability of the crack width equation [DEU06] gives the following permissible percentages of exceedance:

- w_k = 0.4 mm (maximum 5 % exceedance)
- w_k = 0.3 mm (maximum 10 % exceedance)
- w_k = 0.2 mm (maximum 20 % exceedance)

In this case, the 95%-quantile of the crack width sample is defined as the crack width that only 5% of the measurements exceed disrespecting the number of measurements, the statistical distribution and the COV.

SCHIEẞL [SCH98a] recommends that mean values of the data set of crack measurements must fall below the defined limiting value w_{max} and that the largest crack width, defined as the 95%-quantile of the sample may not exceed the limiting value by more than 30 % ($w_{test,95\%} \leq 1.3 \cdot w_{max}$). The 95% quantiles are determined by a classic statistical analysis.

2.10.8 Crack width for Different Bar Diameters

Where a combination of bar diameters is used in a section, the different bond behaviour of the bar diameters must be taken into account. According to [EC2], an equivalent bar diameter $Ø_{eq}$ should be used in this case. For a section with n_1 bars of diameter $Ø_1$ and n_2 bars of diameter $Ø_2$, the following expression shall be used in equation (2-69)

$$Ø_{eq} = \frac{n_1 \cdot Ø_1^2 + n_2 \cdot Ø_2^2}{n_1 \cdot Ø_1 + n_2 \cdot Ø_2} \tag{2-82}$$

The same equivalent bar diameter $Ø_{eq}$ shall be used according to [MC2010].

2.10.9 Crack Width in Reinforcement Laps

Besides considering the maximum reinforcing bar stress, laps should be evaluated concerning the crack formation. Transverse cracks develop due to tensile loads and longitudinal cracks develop due to bond forces in the lap zone. Transverse crack widths at lap ends are always larger than in the undisturbed zone. The crack widths in the lap are smaller than the crack widths in the undisturbed member, since the reinforcement ratio is higher in laps. While the crack control for structural concrete elements is regulated in [EC2], detailed information on the permissible crack width at lap ends is not given. The cracks at lap ends develop due to the stiffness change and the slip of the tensile reinforcement in the lap. At high forces and small concrete cover, longitudinal cracks occur, which commence from the highly utilised lap ends. The longitudinal crack width can be controlled effectively by transverse reinforcement, but not prevented.

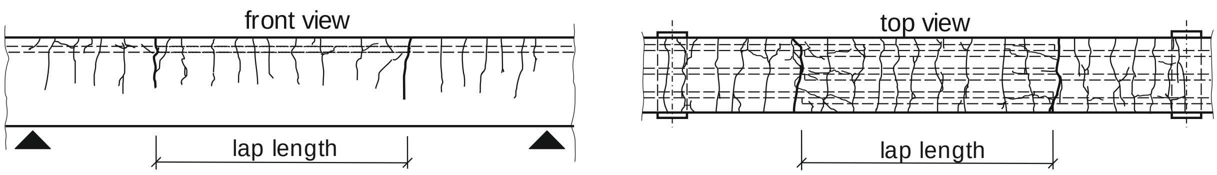

Figure 2-28 Typical crack formation between the supports in four-point bending tests with laps at steel stress between service loads and ultimate loads

Many reports on laps in reinforced concrete elements have been published, but little test numbers with measured or documented crack widths at lap ends are known.

BETZLE [BET81] conducted four-point bending tests with laps and documented the crack width at the lap ends. Up to the allowable bending moment $M_{all.}$, BETZLE observed bending cracks only. Longitudinal cracks developed at loads above $M_{all.}$. The crack width at the lap ends was 30 % to 50 % above the undisturbed bending zone for 16 mm and 28 mm bars. For large bar spacing and small bar diameters, the crack width at the lap end corresponded with the crack width in the undisturbed bending zone. Test specimens with increased lap length had larger crack widths at the lap ends than shorter laps [BET81].

ELIGEHAUSEN [ELI79] gives a model for the calculation of crack width at lap ends based on the crack width in the undisturbed element and the reinforcement slip in the lap.

The crack width w_E at the lap end is the sum of the slip of the reinforcement in the lap and the steel deformation outside the lap [ELI79]. The slip at the lap end can be calculated from the slip at the lap centre plus the slip of the bar and the surrounding concrete. At the lap end, the slip of the bar s_{le} and the surrounding concrete equals half the mean crack width w_m in the undisturbed element. The crack width at the lap end is

$$W_{le} = s_{1e} + 0.5 \cdot w_m \tag{2-83}$$

The slip is the difference between steel and concrete deformation and can be calculated from

$$s(x) = s_0 + \int_0^x \varepsilon_s \cdot dx - \int_0^x \varepsilon_c \cdot dx \tag{2-84}$$

ELIGEHAUSEN [ELI79] solved the differential equation numerically with a linear multistep method. The step length was $\Delta x \leq 0.1 \cdot Ø$. The unknown boundary conditions (steel stress, deformations and crack width if cracks are located in the lap) and the crack width w were varied until the difference of the steel stresses fell below a defined limit. In long laps and for small steel strain, only the outer parts of the lap length contribute to the load transfer, while the lap centre acts like a beam with doubled reinforcement ratio.

ELIGEHAUSEN [ELI79] recommends accepting crack widths at lap ends that are 25% larger than the crack width limits w_{lim} for the 95%-quantiles. The derived acceptable crack widths at lap ends are

- $w_E \leq 0.25$ mm for $w_{lim} = 0.2$ mm
- $w_E \leq 0.38$ mm for $w_{lim} = 0.3$ mm
- $w_E \leq 0.50$ mm for $w_{lim} = 0.4$ mm

The crack widths in structural concrete members with laps can therefore be evaluated by the general crack width acceptance criteria defined in codes (e.g. [EC2], [EC2/NA], [MC2010]) by the criteria defined in the guide to good practice [DEU06] and in [SCH98a] and by the explicit crack width acceptance criteria for laps defined by [ELI79].

Strain in Reinforcement Laps

The reinforcement strain in laps comprises both the strain decrease by the load transfer from one bar to the other and the strain development between transverse cracks. The strain at a crack ε_{crack} within the lap is

$$\varepsilon_{crack} = \varepsilon_{s2,end} - \frac{x}{l_0} \cdot \varepsilon_{s2,end} \tag{2-85}$$

With

$\varepsilon_{s2,end}$ Reinforcement strain at the lap end

x Position in the lap starting from the lap end

Test results have shown that the reinforcement strain is rather constant in the inner third of the lap length. The load transfer takes place at the lap ends while the inner length does not contribute to the load transfer. This changes as soon as the lap length is very short or in case the bond has been deteriorated at the lap length and the inner part of the lap is activated. While the real strain distribution in the lap is non-linear [BUR00], the function can be approximated with a linear decrease having a plateau at the lap centre, with tri-linear or non-linear functions.

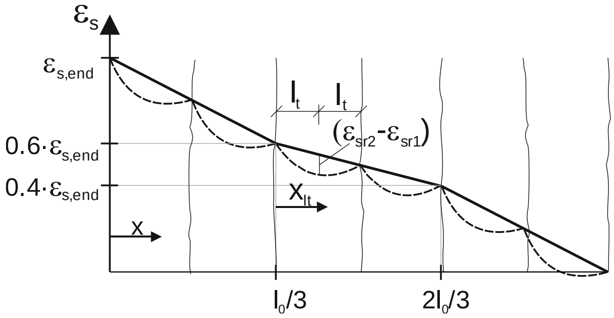

Figure 2-29 Tri-linear strain function in a lap considering cracks

In the stabilised crack phase, the structural concrete member remains uncracked between the cracks. The strain between the cracks reaches the values of the cracked state in the cracks only (cf. Figure 2-29, right). The strain in the lap between the cracks can be calculated with equation (2-86).

$$\varepsilon_{si} = \varepsilon_{s2,end} - \frac{x}{l_0} \cdot \varepsilon_{s2,end} - 0.6 \cdot \left(\varepsilon_{sr2} - \varepsilon_{sr1}\right) \cdot \frac{x_{lt}}{l_t} \qquad (2\text{-}86)$$

With

ε_{sr1} steel strain between the cracks at crack formation

$$\varepsilon_{sr1} = \varepsilon_{ct} \qquad (2\text{-}87)$$

ε_{sr2} steel strain in the crack at crack formation

$$\varepsilon_{sr2} = \frac{A_{c,eff} \cdot f_{ct}}{A_s \cdot E_s} \qquad (2\text{-}88)$$

x_{lt} position between the cracks commencing from the crack

l_t transfer length or half the crack spacing

The bond strength in the lap can be derived from the strain difference as follows

$$\tau_i = \frac{Ø \cdot E_s \cdot \left(\varepsilon_{s,i} - \varepsilon_{s,i-1}\right)}{4 \cdot l_i} \qquad (2\text{-}89)$$

3 Bond tests

3.1 General

The bond behaviour of reinforcing bars with large diameters was investigated by means of 44 beam-end tests, twelve anchorage tests at simply supported beams and 17 four-point bending tests with lapped bars. The bond stress-slip relationships of the reinforcing bars and the crack formation in the bond zone were determined in beam-end tests. Six test specimens were cast to test the anchorage at each side resulting in twelve anchorage tests. Lapped splices were investigated by three reinforcing bars lapped in the constant bending moment zone of four-point flexural tests. Besides the determination of the bond stress, crack widths and deformations were measured. The test programmes conducted during the AiF projects 16992 N and 18821 N funded by the German Federation of Industrial Research Associations are described in more detail in [HEG15] and [HEG18]. Drawings of all test specimens are provided in the annex A.2.

3.2 Materials

For the specimens of tests under bending and most beam-end tests, ready-mixed concrete was used. For some beam-end tests, the concrete was mixed in the laboratory, while the same concrete mixture was used in both cases (Table 3-1). The mean concrete properties are given in the appendix.

Table 3-1 Concrete Mixture

Cement [kg/m³]	Water [kg/m³]	Super-plasticiser [kg/m³]	Aggregate (sum) [kg/m³]	Aggregate 0 – 2 [kg/m³]	Aggregate 2 – 8 [kg/m³]	Aggregate 8 – 16 [kg/m³]
285	180	1.0	1869	748	467	654

In the beam-end and lap test specimens, the lapped longitudinal reinforcement was located at the bottom of the formwork to generate good bond properties. During testing, all test specimens were placed upside-down for a simpler crack observation.

All reinforcing bars were customary reinforcement of class B500B. In [DEU09], the relative rib area f_R is defined as 0.052 for Ø 10 mm reinforcing bars and as 0.056 for reinforcing bars of Ø 20 mm and larger. These values are usually exceeded due to the manufacturing process. The relative rib areas of the large diameter bars was between 0.06 and 0.08. The appendix gives an overview of the measured relative rib areas and mean steel properties.

3.3 Beam-End Tests

3.3.1 Test-Specimen Dimensioning and Test-Setup

The bond strength of large diameter bars was investigated by 22 beam-end test series with two tests each. The effects of bar diameter, concrete strength, bond length and confinement were tested.

The specimens were tested according to [AST15], but modified by choosing all dimensions depending on the investigated reinforcing bar diameter. For comparability, the angle of the strut in the test specimen was kept constant for all bar diameters. The test specimen height was h = 14 · Ø, the length l = 20 · Ø and the width b = 8 · Ø (cf. Figure 3-1).

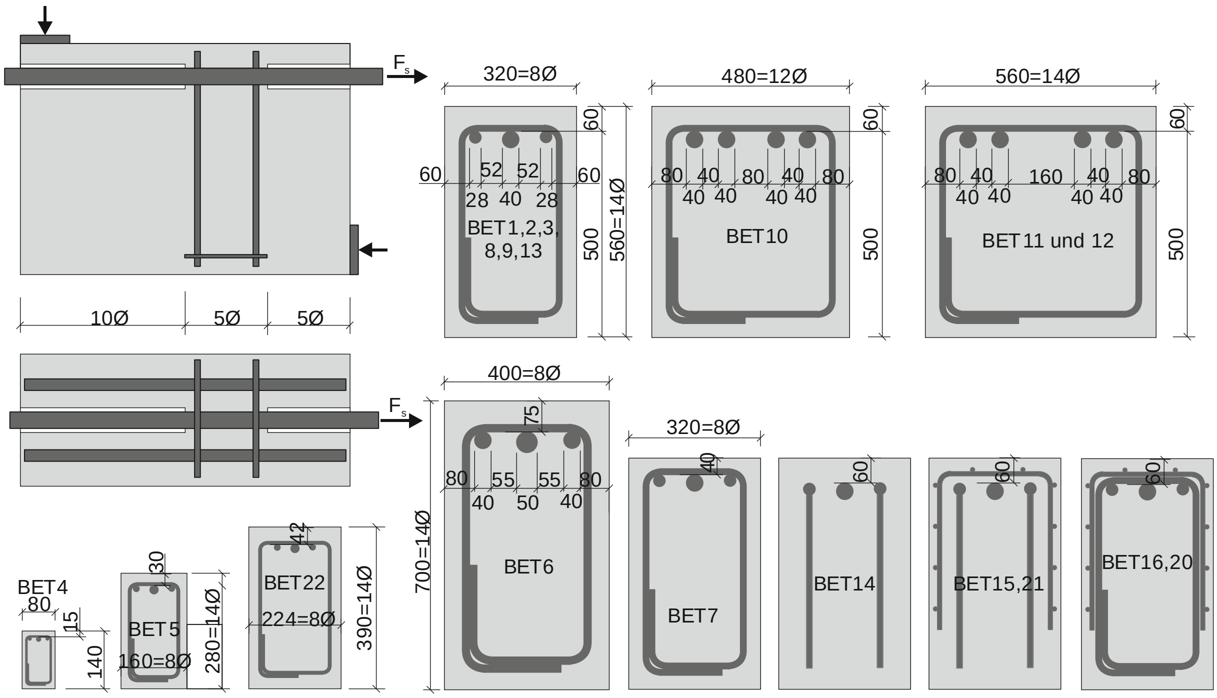

Figure 3-1 Beam-end test specimen dimensions, typical front and top view (left) and cross-sections for BET-1 to BET-22 (right)

For comparability with pull-out specimens from literature, the bond length was $l_b = 5 \cdot Ø$. The chosen bond length is sufficiently short to presume a constant bond strength over the bond length and sufficiently long to avoid large scatter in test results. To preclude cone type concrete failure at the load application, the unbonded length $l_{ub} = 5 \cdot Ø$ was chosen in accordance with [WIL13].

The test specimens contained additional reinforcement for the load transfer from the bond zone to the support at the rear part of the test specimen. This reinforcement was adopted from [AST15]. Most beam-end test specimens contained stirrups in the bond zone also used as shear reinforcement. To provide shear reinforcement in the test specimens without transverse reinforcement in the bond zone according to [AST15], the stirrups were turned by 90°. The stirrup spacing in the bond zone conformed with the stirrup spacing in the lapped splices in the four-point bending tests.

For the eccentric loading of the beam-end test specimen in this test setup, a vertical support is necessary to carry arising forces from the generated bending moment. The test specimen has a planar support on the lab floor and a reaction plate on the rear top (cf. Figure 3-2). This reaction plate was supported by a cross-beam anchored with threaded bars in the floor. A compression reaction plate was positioned at the bottom of the test-specimen front. The dimensions of the front and top reaction plates were determined in dependence on the investigated bar diameter.

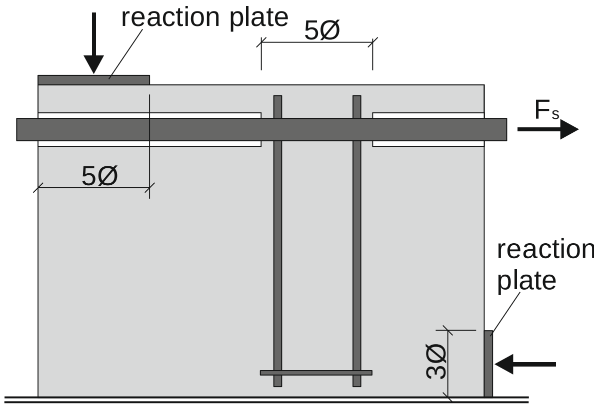

Figure 3-2 Photograph of beam-end test setup (left) and test specimen drawing with reaction plate dimensions (right)

3.3.2 Test Parameter

Table 3-2 gives an overview of the conducted test-series with two tests per series. BET-1 was the reference test specimen with 30 MPa concrete strength, bar diameter 40 mm, 60 mm concrete cover (1.5 · Ø) and a bond length of 5 · Ø. The test series BET-2 and BET-3 were conducted with increased concrete strength. Different bar diameters were tested in the test series BET-4 (10 mm) to BET-6 (50 mm) and BET-22 (28 mm). For test BET-7, the concrete cover was decreased from 1.5 · Ø to 1.0 · Ø. Test series BET-9, BET-20 and BET-21 were conducted to investigate the effect of transverse pressure on the bond behaviour. The effect of bar spacing was tested in BET-10 and BET-11 with two reinforcing bars tested in one test specimen with a bar spacing of 2 · Ø and 4 · Ø, respectively. The width of the test specimens was 12 · Ø and 14 · Ø, respectively. Test series BET-12 was conducted with bent reinforcing bars. The bar distance was 4 · Ø and thus corresponds with BET-11. To investigate the effect of different bond lengths in BET-17, the bond length was increased from 200 mm (5 · Ø) to 400 mm (10 · Ø).

For the large number of transverse reinforcement rules in [EC2], the effect of transverse reinforcement was investigated by several beam-end tests. The reference test specimens BET-1 and BET-13 had two 14 mm stirrups with a 140 mm spacing in the bond zone. During the conducted beam-end tests, the effects of stirrup diameter

(BET-8, BET-16 and BET-18), stirrup spacing (BET-14 and BET-19) and surface reinforcement (BET-15) were investigated.

Beam-end tests BET-1 to BET-12 were conducted with reinforcing bars from the rolling mill Annahütte while tests BET-13 to BET-22 were conducted with reinforcing bars from the rolling mill Badische Stahlwerke. For a comparison, BET-13 was tested with the same parameters as BET-1.

Table 3-2 Test parameter of the beam-end tests

Test	Ø	f_{cm}	A_{st}	A_{st}/A_s	c	Bar number
	[mm]	[MPa]	[mm]	[-]	[-]	[-]
BET-1	40 mm	36.5/29.3	Ø 14 / 140	1.0	1.5· Ø	1
BET-2	40 mm	55.4	Ø 16 / 150	1.0	1.5· Ø	1
BET-3	40 mm	104.0	Ø 16 / 120	1.0	1.5· Ø	1
BET-4	10 mm	34.0/39.6	Ø 6 / 40	1.0	1.5· Ø	1
BET-5	20 mm	35.7/36.5	Ø 8 / 90	1.0	1.5· Ø	1
BET-6	50 mm	29.9	Ø 16 / 130	1.0	1.5· Ø	1
BET-7	40 mm	32.0	Ø 14 / 140	1.0	1.0· Ø	1
BET-8	40 mm	34.3	Ø 10 / 140	0.5	1.5· Ø	1
BET-9[1)]	40 mm	38.2	Ø 14 / 140	1.0	1.5· Ø	1
BET-10	40 mm	36.4/41.8	Ø 14 / 140	1.0	1.5· Ø	2
BET-11	40 mm	37.3	Ø 14 / 140	1.0	1.5· Ø	2
BET-12	40 mm	29.5	Ø 14 / 140	1.0	1.5· Ø	2 (bend)
BET-13	40 mm	30.5	Ø 14 / 140	1.0	1.5· Ø	1
BET-14	40 mm	50.5	0	0	1.5· Ø	1
BET-15	40 mm	50.4	surf	0	1.5· Ø	1
BET-16	40 mm	31.1	Ø 16 / 140 surf	1.0	1.5· Ø	1
BET-17[2)]	40 mm	31.1	Ø 14 / 140	1.0	1.0· Ø	1
BET-18	40 mm	50.5	Ø 10 / 140 surf	0.5	1.5· Ø	1
BET-19	40 mm	50.5	Ø 8 / 80	0.5	1.5· Ø	1
BET-20[1)]	40 mm	37.7	Ø 14 / 140 surf	1.0	1.5· Ø	1
BET-21[1)]	40 mm	37.7	surf	0	1.5· Ø	1
BET-22	28 mm	51.0	Ø 8 / 80	1.0	1.5· Ø	1

[1)] transverse pressure
[2)] bond length $l_b = 10 \cdot Ø$

3.3.3 Measurements and Test Procedure

The pull-out force generated by the hydraulic cylinder, the slip between the concrete and the reinforcing bar at the loaded and unloaded sides as well as the crack formation in the transverse and longitudinal directions on the test-specimen top were continuously recorded with displacement transducers (cf. Figure 3-3). During the tests with two reinforcing bars (BET-10 to BET-12), the steel strain of both bars was measured with additional displacement transducers. In tests BET-8 to BET-12, the stirrup strain was measured with strain gauges.

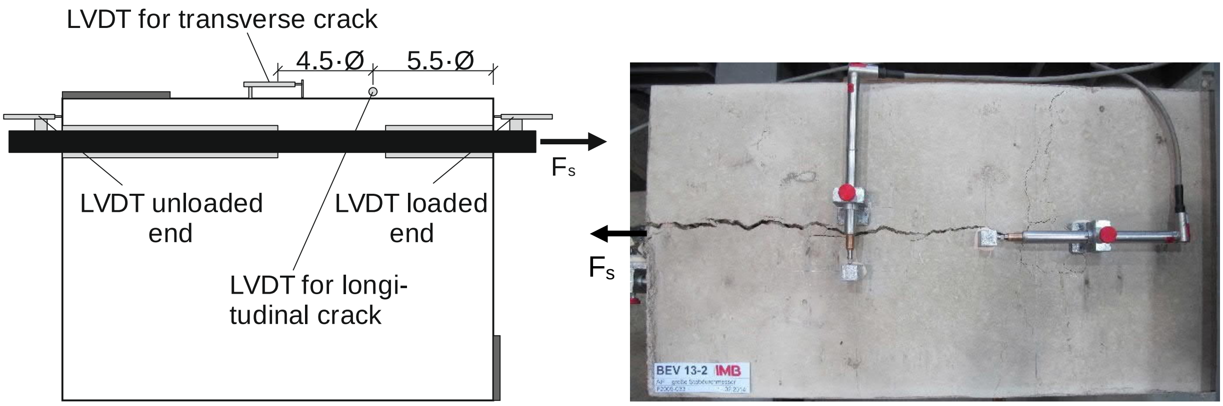

Figure 3-3 Drawing of displacement-transducer (DT) position (left) and photograph of DTs in test BET-13-2 (right)

The reinforcing bars were pulled load-controlled with hydraulic cylinders until the slip at the unloaded side of the bond zone reached 5 mm. The loading rate of the beam-end tests was $\Delta\sigma$ = 40 MPa/min. This rate correlates with [RIL83] and [AST15] as described in [HEG15].

3.3.4 Test Results

The bond strength was proportional to $f_{ck}^{2/3}$ (cf. Figure 3-5). Since the concrete strength attains values between 26.4 MPa and 38.2 MPa, the bond strength values are given normalised with the factor $(38 / f_{cm})^{2/3}$. The bond strength $\tau_{0.1}$ is the bond stress measured at 0.1 mm slip and τ_{max} is the maximum bond strength with the corresponding slip s_{max}. All slip values discussed in this chapter are slip values at the free end of the bar. Table 3-3 gives the mean bond strength of the beam-end test series. The following diagrams show comparisons with codes, where the calibration factors for bar diameter were set to 1.0. All bond strength slip relationships are documented in [HEG15] and [HEG18].

Table 3-3 Bond strength at 0.1 mm slip, maximum bond strength, slip values at maximum bond strength (at free end of reinforcing bar) and corresponding coefficients of variation V_i obtained in two beam-end tests each

Test	Parameter[1)]	$\tau_{0.1} \cdot \left(\frac{38}{f_{cm}}\right)^{2/3}$	$V_{\tau 0.1}$	$\tau_{max} \cdot \left(\frac{38}{f_{cm}}\right)^{2/3}$	$V_{\tau max}$	s_{max}	ν_{smax}
		[MPa]	[%]	[MPa]	[%]	[mm]	[%]
BET-1 (reference)	Ø=40 mm, C30, c=1.5· Ø	9.3	9.3	11.8	10.2	0.61	26.7
BET-2	f_{cm}=55 MPa	8.0	1.6	11.1	5.6	0.63	4.5
BET-3	f_{cm}=104 MPa	8.7	2.7	9.4	11.1	0.75	7.5
BET-4	Ø =10 mm	8.7	26.8	14.4	17.0	0.66	42.4
BET-5	Ø =20 mm	10.8	23.8	14.6	13.9	2.20	80.9
BET-6	Ø =50 mm	9.5	0.1	11.8	1.4	0.56	10.1
BET-7	c=1.0· Ø	8.4	-	9.7	0.0	0.54	-
BET-8	$\Sigma A_{st}/A_s$=0.5	8.8	-	10.3	0.0	0.49	-
BET-9	p_{max}=6 MPa	11.0	1.2	16.2	2.8	1.92	86.0
BET-10	n=2, a=2· Ø	5.1	22.4	6.9	15.0	0.53	72.8
BET-11	n=2, a=4· Ø	7.0	4.1	9.2	1.7	0.65	19.0
BET-12	bend, a=4· Ø	-	-	8.1	7.4	0.54	2.1
BET-13	reference	9.3	6.7	11.5	0.7	0.54	22.5
BET-14	$\Sigma A_{st}/A_s$=0	8.1	0.4	10.2	8.7	0.51	13.9
BET-15[2)]	$\Sigma A_{st}/A_s$=0	8.3	7.5	10.6	0.4	0.40	10.6
BET-16[2)]	$\Sigma A_{st}/A_s$=1.3	11.2	4.8	13.8	0.7	0.73	17.4
BET-17	l_b=10·Ø	7.8	9.7	10.8	1.6	0.73	1.9
BET-18[2)]	$\Sigma A_{st}/A_s$=0.5	8.6	5.4	11.0	9.8	0.49	7.3
BET-19	$\Sigma A_{st}/A_s$=0.5	8.2	5.5	11.7	14.9	0.69	21.7
BET-20[2)]	p_{max}=10 MPa	17.2	11.9	26.7	0.9	2.60	48.4
BET-21[2)]	p_{max}=12 MPa	15.6	-	30.7	-	1.54	-
BET-22	Ø =28 mm	8.5	6.0	12.2	15.8	0.51	26.6

[1)] Unless otherwise stated: Ø = 40 mm, c = 1.5 · Ø, $\Sigma A_{st} / A_s$ = 1.0 if positioned likewise along a lap according to chapter 3.4 (α_6 = 1.5: l_0 = 1310 mm with 8 stirrups Ø 14 mm positioned at the outer thirds of the lap with a spacing of 140 mm, 8 · 1.54 cm² / 12.56 cm² = 1.0)

[2)] With surface reinforcement

The maximum bond strength was reached in BET-3-1 with τ_{max} = 22.1 MPa at a cylinder compressive strength of 104 MPa. The corresponding rebar stress was 440 MPa. Hence, the reinforcing bars in the beam-end tests were loaded well below their yield strength.

Crack Formation

Firstly, a crack at the unloaded end of the bond length l_b developed perpendicular to the reinforcing bar during the beam-end test (cf. Figure 3-4, crack 1). Secondly, a crack parallel to the reinforcing bar developed from the loaded side of the bar to the unloaded side (cf. Figure 3-4, crack 2).The transverse crack proceeded on the side of the test specimen diagonally to the bottom front side of the test specimen (cf. Figure 3-4, crack 3). Moreover, diagonal cracks in the direction of the rear support appeared on the top side (cf. Figure 3-4, crack 4). Only just before bond failure, radial cracks were observed at the front side of some test specimens.

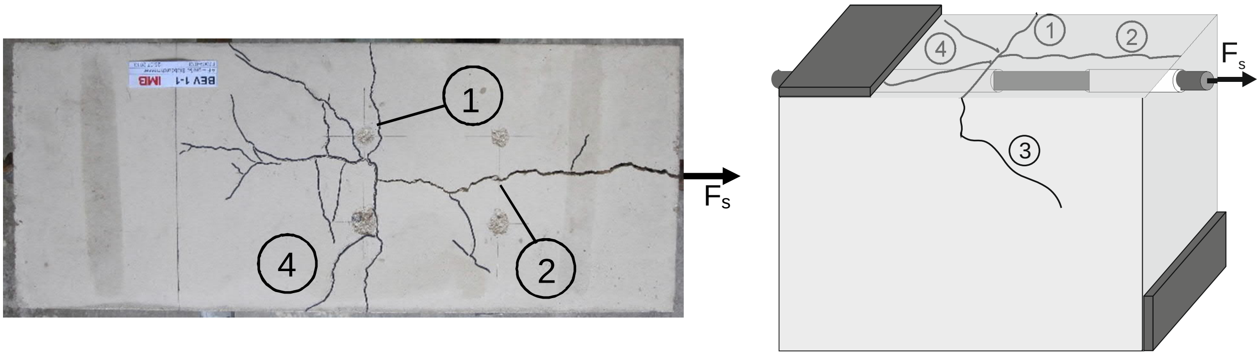

Figure 3-4 Top-view of BET-1-1 with scheme of crack formation (left) and 3-D crack scheme (right)

The longitudinal and transverse cracks were smaller than 0.1 mm for a reinforcing bar stress of 160 MPa. When the maximum reinforcing bar stress (about 200 MPa) was reached, the longitudinal cracks were 0.2 mm and the transverse cracks about 0.4 mm wide. The service stress at about 320 MPa, where the crack width was measured during the four-point bending tests, was only reached in beam-end tests with high strength concrete (BET-2 and BET-3).

Effect of Compressive Strength

The maximum bond strength was rather proportional to $f_{ck}^{2/3}$ as proposed in [EC2] than to $f_{cm}^{0.25}$ as proposed in [MC2010]. In contrast, the bond strength at 0.1 mm slip corresponds with a lower exponent. Figure 3-5 gives a comparison of tests results with the bond strength according to equation (2-10) [EC2] and equation (2-39) [MC2010]. The bond strength f_{bd} in the model according to [EC2] was calculated for a mean tensile concrete strength f_{ctm}. The coefficients for bar diameter, cover and transverse reinforcement according to [EC2] and [MC2010] were taken into account in the equations. The cover $c_y = 1.5 \cdot Ø$ increases the calculated bond strength in comparison to the minimum concrete cover $c_y = 1.0 \cdot Ø$. To enable the comparison of results for the evaluation of other influencing parameters, the bond strength was normalised with

$\tau_{i,norm.} = \tau_{i,test} \cdot (38 / f_{cm})^{2/3}$ corresponding with [EC2]. A bond strength plateau observed in tests with high strength concrete was described in [HEG15].

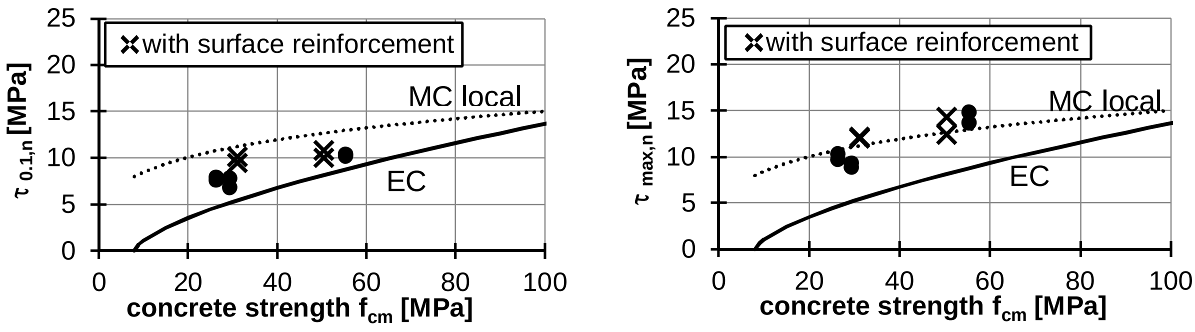

Figure 3-5 Effect of concrete compressive strength on bond strength at s = 0.1 mm (left) and at τ_{max} (right) in comparison with design bond strengths according to [EC2] and [MC2010]

Effect of Bond Length

The bond strength averaged over the bond length decreased with increasing bond length. The decrease was 16 % for the bond strength at 0.1 mm slip for a bond length of $10 \cdot Ø$ (BET-17) compared to $5 \cdot Ø$ (BET-1). The maximum bond strength decreased by 9 %.

Effect of Bar Diameter

To investigate the effect of bar diameter, beam-end tests with reinforcing bar diameters of Ø 10 mm, Ø 20 mm, Ø 28 mm, Ø 40 mm and Ø 50 mm were conducted with a concrete cover $c_y = c_x = 1.5 \cdot Ø$. Beam-end test BET4-1 with a 10 mm reinforcing bar had a pull-out failure with an intact concrete cover. Beam-end test BET4-2, also reinforced with one 10 mm bar, had a splitting failure with the described crack formation, but the crack width was much smaller than for bars with larger diameters.

The bond strength slightly decreased with increasing bar diameter (cf. Figure 3-6). The low bond strength of the 10 mm test specimen at 0.1 mm slip was unexpected, Figure 3-6 thus includes the values obtained in [WIL13] as well. The variation of test results decreased for larger bar diameters.

The relative rib area did not increase with increasing bar diameter. In contrast to previous findings [REH61], [MAR73], [STE07], a bar diameter effect was visible. The slip at maximum bond strength did not increase for large diameter bars.

A comparison of the bond strength reduction by bar diameter obtained from the beam-end tests shows that the bond stress at 0.1 mm slip is captured well by the [EC2] equation for decreasing bond strength $\eta_2 = (132 - Ø) / 100$. The maximum bond strength of the 10 mm bars conforms with [WIL13], while the bond stress at 0.1 mm slip is unexpectedly low. Figure 3-6 gives the test results in relation to the mean values of the 20 mm bar ($\eta_2(20\text{ mm}) = 1.0$). For the bond strength obtained in tests conducted by WILDERMUTH [WIL13] τ_w, the effects of concrete strength, concrete cover c_w and bond length were described with

$$\tau = \tau_W \cdot \left(\frac{38}{f_{cm}}\right)^{2/3} \cdot \left(\frac{c_{own} \cdot Ø}{c_w \cdot Ø}\right)^{1/4} \cdot c(l_b) = \tau_W \cdot \left(\frac{38}{f_{cm}}\right)^{2/3} \cdot \left(\frac{1.5 \cdot Ø}{2.0 \cdot Ø}\right)^{1/4} \cdot c(l_b) \qquad (3\text{-}1)$$

Where the coefficient $c(l_b)$ takes the bond length into account. The bond length in the tests described in [WIL13] was 10 · Ø. The own tests showed a decrease in bond strength for increasing bond length from 5 · Ø to 10 · Ø. The coefficient for the consideration of bond length $c(l_b)$ was 1.19 for the bond strength at 0.1 mm slip and 1.09 for the maximum bond strength (cf. “Effect of Bond Length”).

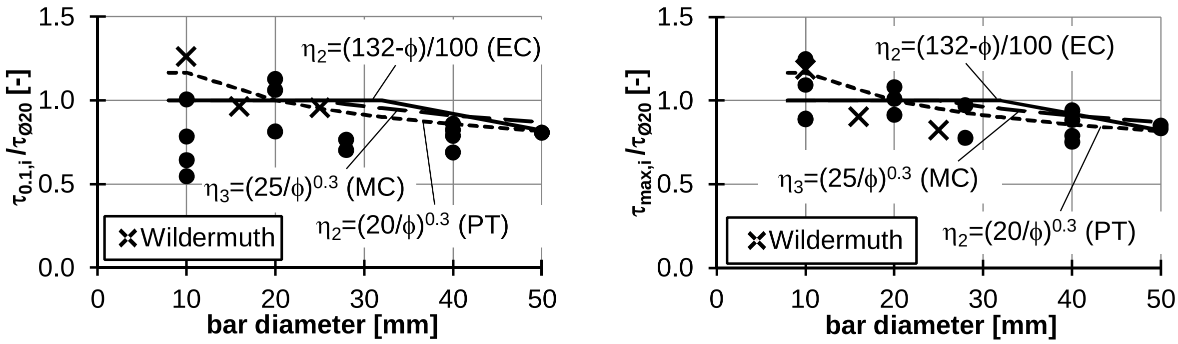

Figure 3-6 Effect of bar diameter on bond strength at 0.1 mm slip (left) and on maximum bond strength (right) (values given in relation to the values for the 20 mm bar) and consideration of bar diameter in [EC2], [MC2010], [PT18]

Effect of Rib Geometry

The bond strength of the 40 mm reinforcing bars from two different rolling mills with relative rib areas $f_{R,1}$ = 0.064 and $f_{R,2}$ = 0.079 was comparable [HEG15]. The scatter within the bond strength of one rolling mill (3 %) was about the same as the scatter between different rolling mills. Hence, the test results are independent from the manufacturer of the investigated reinforcing bars.

Effect of Concrete Cover and Bar Spacing

The standard concrete cover c = 1.5 · Ø = 60 mm was reduced to c = 1.0· Ø = 40 mm in test series BET-7. For both covers, a splitting failure was observed. The reduction in bond strength with smaller concrete cover was 10 % at 0.1 mm slip and 18 % for the maximum bond strength. The crack formation was comparable for both covers. The concrete cover c_d defined in codes is the smaller value of bottom and side concrete cover and half the bar spacing. Figure 3-7 illustrates a comparison between tests BET-1 and BET-2 with different bottom covers as well as tests BET-10 and BET-11 with different bar spacing in comparison to the reduction factors given in [EC2] and [MC2010].

In case larger concrete covers are chosen, the required bond length $l_{b,req}$ may be reduced by the coefficient $\alpha_2 = 1 - 0.15 \cdot (c_d - Ø) / Ø$. The smallest allowable concrete cover according to [EC2] is the bar diameter. Figure 3-7 shows that the equation according to [EC2] is a good approximation to account for the improvement in bond strength by concrete cover.

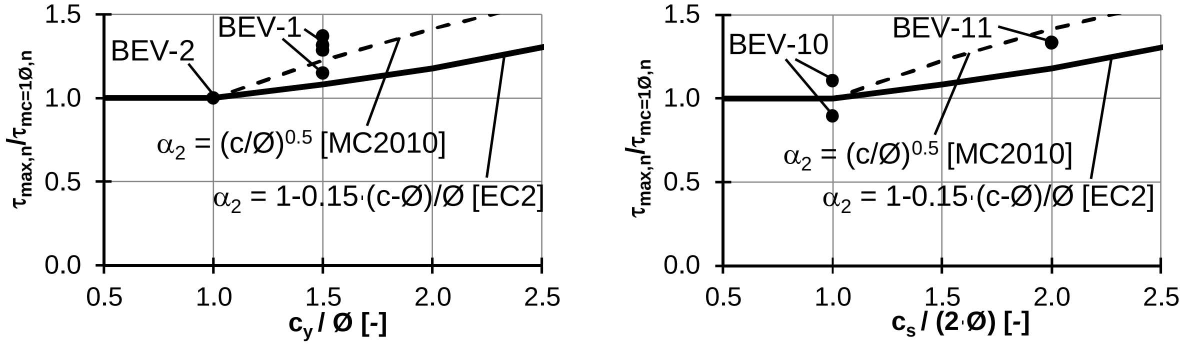

Figure 3-7 Effect of the concrete-cover to bar-diameter ratio on maximum bond strength (left) and effect of the bar-spacing to bar-diameter ratio on maximum bond strength (right), values given in relation to the values for c_i / Ø = 1.0

When two bars were positioned next to each other, one bond zone failed first, while the second reinforcing bar still transferred load (BET-10 and BET-11). For the evaluation of bond strength, the smaller bond strength of the bar failing first is documented here.

The bond strength at 0.1 mm slip was reduced for two bars with a 2 · Ø spacing from 9.3 MPa to 5.1 MPa (45 % decrease) and with a 4 · Ø spacing to 7.0 MPa (25 % decrease) (cf. Figure 3-8). The maximum bond strength τ_{max} was reduced for the allocation of two bars with a 2 · Ø spacing from 11.8 MPa to 6.9 MPa (41 % decrease) and with a 4 · Ø spacing to 9.2 MPa (22 % decrease).

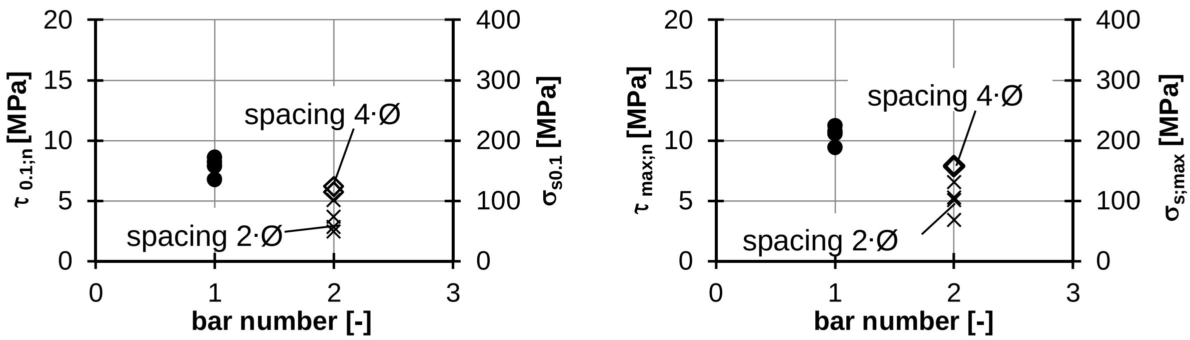

Figure 3-8 Effect of the bar number on bond strength at 0.1 mm slip (left) and on maximum bond strength (right)

The bond strength of a single bar obtained in beam-end tests is up to 30 % higher than the mean bond strength calculated from [EC2]. However, the measured bond strength of two adjacent bars with the smallest allowable spacing ($c_s = 2 \cdot Ø$) is comparable to the values calculated according to [EC2].

$$\tau = 2.25 \cdot 0.3 \cdot \left(f_{cm}\right)^{2/3} \cdot \frac{132\text{ mm} - 40\text{ mm}}{100\text{ mm}} = 6.5\text{ N / mm}^2 \tag{3-2}$$

Own investigations and test results described in literature show that the bond strengths obtained in pull-out tests are well above the bond strengths defined in [EC2]. This finding also applies to the comparison of calculated mean values that were derived from the calculated design values in [EC2]. The common clustering of several adjacent bars positioned at small bar spacing justifies the small bond strengths defined in [EC2]. The beam-end test results show a strong decrease in developable stress of reinforcing bars if more than one bar is anchored.

The crack formation for beam-end tests with two adjacent bars corresponds to the crack formation of the beam-end tests with one bar, but with one longitudinal crack above each loaded bar. The crack width above the reinforcing bar that failed first was visibly greater.

<u>Effect of Transverse Reinforcement</u>

The positioning of transverse reinforcement did not increase the maximum bond strength significantly, but the load did not drop as suddenly as for splitting failure where stirrups are not present. When the concrete tensile strength is reached within the cover, the stirrups are activated and enable a bar pull-out.

The increase in maximum bond strength by positioning stirrups was 15 % in case 3 Ø 8 mm bars were placed in the bond zone with a 80 mm spacing (BET-1, BET-13 and BET-19 with stirrups, BET-14 without). Unexpectedly, test series BET-8 did not show any increase in bond strength, although two 10 mm bars with a 140 mm spacing were positioned in the bond zone (cf. Figure 3-9). [EC2] considers the transverse reinforcement cross-section, only, even though it is known from previous bond tests that the stirrup spacing has a significant influence.

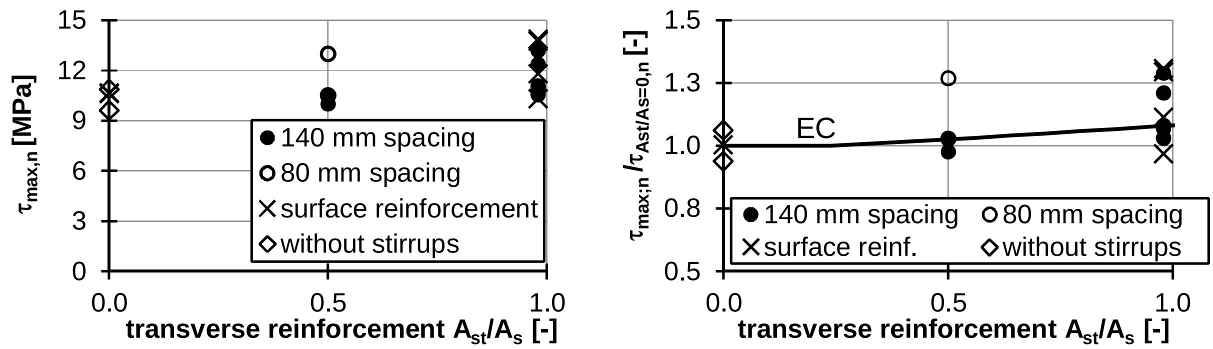

Figure 3-9 Effect of transverse reinforcement on maximum bond strength (left) and maximum bond strength in relation to the unconfined test specimen in comparison with [EC2] without taking $\Sigma A_{st,min}$ into account (right)

The required bond length according to [EC2] can be reduced where transverse reinforcement is positioned. A comparison between measured and calculated bond strength according to [EC2] is given in Figure 3-9 (right). The test results are given related to the mean value $\tau_{m,Ast/As=0}$ of the test series where $\Sigma A_{st}/A_s = 0$ (BET-14).

Effect of Surface Reinforcement

Although providing additional transverse reinforcement in the bond zone, the surface reinforcement did not lead to increasing bond strength in test specimens BET-15 without stirrups (cf. Figure 3-10, left). The test results of BET-16 and BET-18 with stirrups and surface reinforcement were contradictory. While the transverse reinforcement of the surface reinforcement was positioned directly at the stirrups in BET-16, the transverse legs were positioned between the stirrups in BET-18 (cf. Figure 3-10, right). Accordingly, an improved bond behaviour was expected for BET-18. But when normalising the test results, BET-18 only reached 11.0 MPa maximum bond strength, while BET-16 had a bond strength of 13.8 MPa.

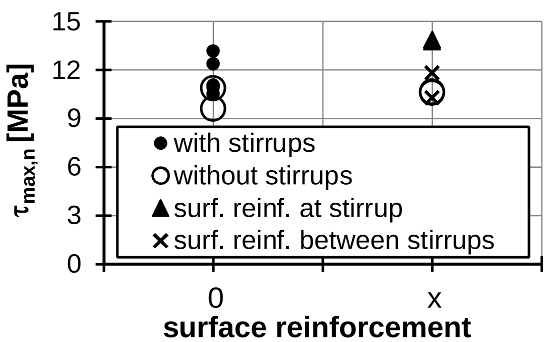

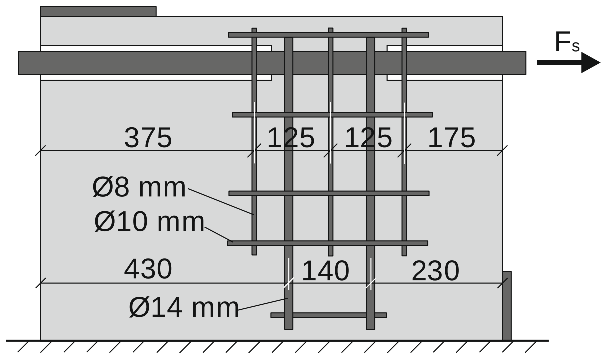

Figure 3-10 Effect of surface reinforcement on maximum bond strength (left) and positioned surface reinforcement in BET-18 (right)

Effect of transverse pressure

For beam-end tests BET-9, BET-20 and BET-21, transverse pressure was generated in the bond zone by locating the vertical support directly over the bond zone (cf. Figure 3-11). The steel sheet for the test specimen tie-down that indirectly provided the transverse load had dimensions that correspond with the bond length and the width of the test specimen (320 mm x 200 mm). The transverse pressure was increased continuously with the reinforcing bar load and therefore corresponds with the stress state of anchorages of longitudinal reinforcement at beam ends. The loading of the cross-beam at the vertical support was measured continuously with one load cell each at the two threaded bars visible in Figure 3-2. The transverse pressure calculated from the load cells was:

$$p = (F_1 + F_2) / (b \cdot l_b) \tag{3-3}$$

For the geometry of the beam-end test that is given in Figure 3-11 (left), the sum of the forces measured by the load cells was expected to be about

$$F_1 + F_2 = F_s \cdot \frac{(360+60)\,\text{mm}}{240\,\text{mm}} = F_s \cdot 1.75 \tag{3-4}$$

In contrast, the test results showed that the sum of the forces measured by the load cells was rather equal to $1.05 \cdot F_s$ and conformed with a stress distribution shown in Figure 3-11 (right)

$$F_1 + F_2 \approx F_s \cdot 1.05 \approx F_s \cdot \frac{(360+20)\text{mm}}{347\text{mm}} \tag{3-5}$$

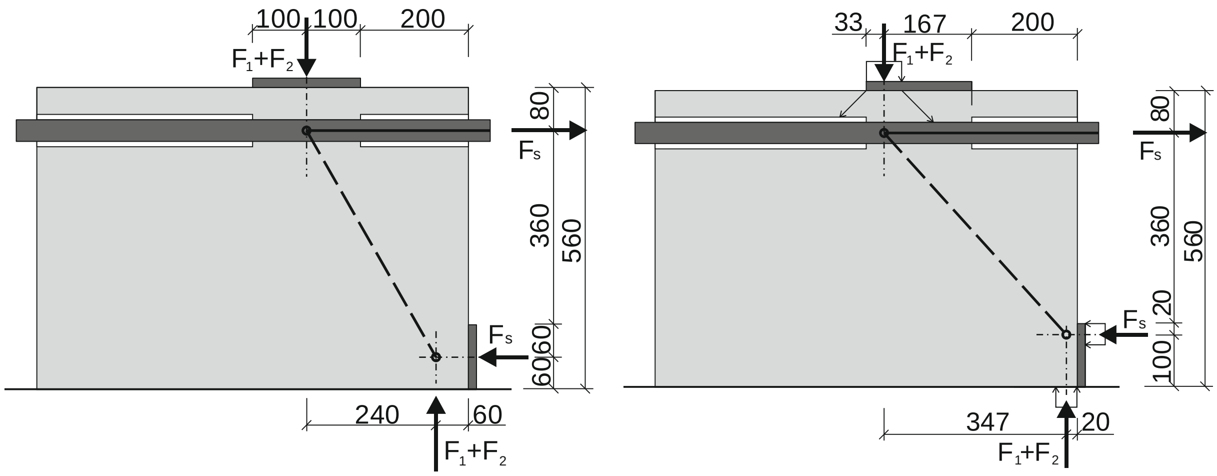

Figure 3-11 Test-setup (left) of beam-end test BET-9 with transverse pressure and expected ratio of bar force F_s to sum of load cell forces F_1+F_2 (left) as well as observed ratio of bar force Fs to sum of load cell forces F_1+F_2 (right)

For the eccentric loading of the test specimen, the reaction-plate loading was not uniform but eccentric as visible in Figure 3-11. Therefore, not the entire reaction plate length l_b was activated to transfer the transverse pressure, instead the geometry of the test specimen resulted in transverse pressure given by

$$p = (F_1 + F_2) / \left(b \cdot \frac{2 \cdot l_b}{3} \right) = 1.05 \cdot F_s / \left(b \cdot \frac{2 \cdot l_b}{3} \right) = 1.05 \cdot \sigma_s \cdot A_s / \left(b \cdot \frac{2 \cdot l_b}{3} \right) \tag{3-6}$$

All beam-end tests with transverse pressure were tested with a Ø 40 mm bar, where p resulted in $0.06 \cdot \sigma_s$.

For this modified test setup, no transverse crack appeared at the end of the bond length. The longitudinal crack parallel to the loaded reinforcing bar was more ramified than in the tests without transverse pressure. At the front side of the test specimens, two diagonal cracks proceeded from the reinforcing bar to the top side of the test specimen and one vertical crack in the direction of the compression plate at the test specimen bottom (cf. Figure 3-12).

Figure 3-12 Crack formation at top (left) and front side (right) in beam-end test BET-9-1 with transverse pressure

Figure 3-13 (left) gives the maximum bond strength in beam-end tests with and without transverse pressure. The transverse pressure p = 6.3 MPa in BET-9 lead to a 37 % increase in maximum bond strength. Figure 3-13 gives the ratio of maximum bond strength of tests with transverse pressure to maximum bond strength without transverse pressure and the consideration in [EC2].

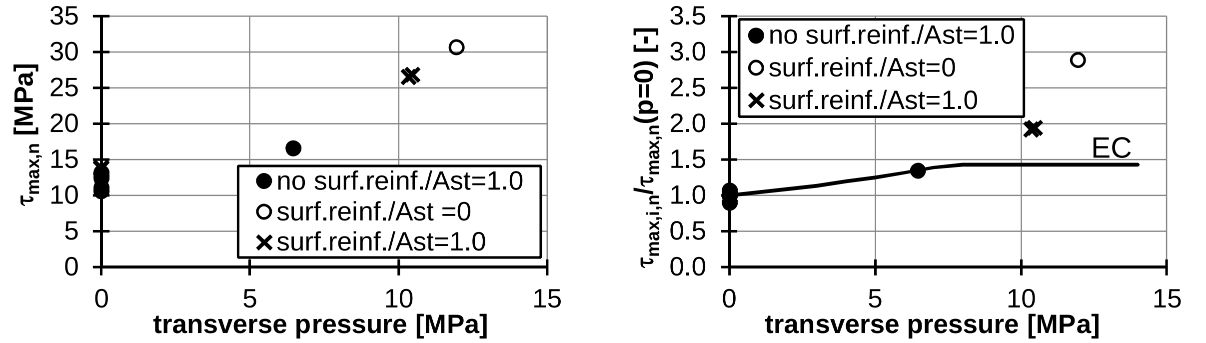

Figure 3-13 Effect of transverse pressure on maximum bond strength (left) and maximum bond strength in relation to the test specimen without transverse pressure (right)

The bond strength reduction for transverse pressure in the bond zone by the coefficient $\alpha_5 = 1 - 0.04 \cdot p$ according to [EC2] conforms with the test results without surface reinforcement. According to [EC2], the compression stress in reinforced concrete members shall not exceed 60 % of the concrete strength (18 MPa for f_{cm} = 30 MPa).

<u>Beam-end Tests with Bends</u>

Test series BET-12 with a 40 mm reinforcement-bar bend was described in [HEG15].

3.4 Lap Tests

3.4.1 Test Setup and Dimensioning

The performance of reinforcement laps in highly utilised sections was analysed by 17 four-point bending tests. The test specimen dimensions were chosen for three Ø 40 mm reinforcing bars lapped at the same section. The beam was supported symmetrically by two supports 3.5 m apart. The length of the beam was necessary to load the three reinforcing bars in the constant moment zone until their yield strength was reached. The distance between the lap ends and the support was at least twice the effective depth in all tests (cf. Figure 3-14).

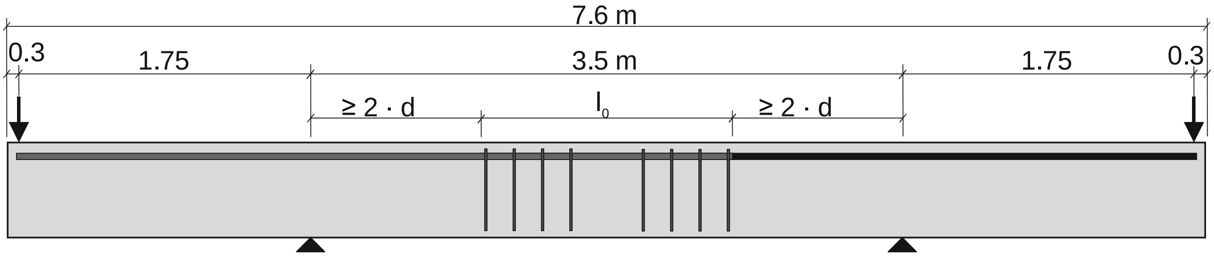

Figure 3-14 Test setup of four-point bending tests with 40 mm reinforcing bars

Figure 3-15 shows the cross-sections of beam T3 with 1.5 · Ø concrete cover and a bar distance of c_s = 2.0 · Ø, T5 with c = 1.0 · Ø and c_s = 4.0 · Ø, and T7 with surface reinforcement. The test specimen width is the sum of three lapped splices with Ø 40 mm reinforcing bars, the concrete cover and the bar distance. The beam depth was designed for yielding of the reinforcing before failure of the compression zone.

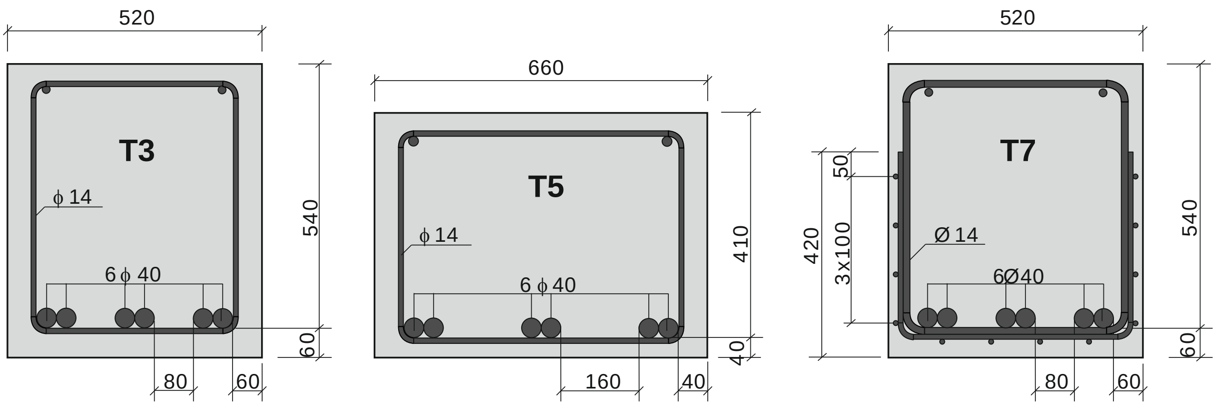

Figure 3-15 Cross-sections of beam tests T3 (left), T5 (centre) and T7 (right)

The bond length was calculated for a mean bond strength according to [EC2].

$$l_0 = \alpha_1 \cdot \alpha_2 \cdot \alpha_3 \cdot \alpha_5 \cdot \alpha_6 \cdot \frac{Ø \cdot f_{ym}}{4 \cdot f_{bm}} = \alpha_6 \cdot \frac{Ø \cdot f_{ym}}{4 \cdot f_{bm}} \tag{3-7}$$

With

$f_{bm} = 2.25 \cdot \eta_1 \cdot \eta_2 \cdot f_{ctm} = 2.25 \cdot f_{ctm}$

$\alpha_1 = \alpha_2 = \alpha_3 = \alpha_5 = \eta_1 = \eta_2 = 1.0$

The mean concrete strength f_{ctm} and the experimentally determined yield strength f_{ym} was used for the calculation.

3.4.2 Test Parameter for the Lap Tests

Table 3-4 contains an overview of the dimensions of beam test specimens. The lap lengths were dimensioned without consideration of bar diameter (η_2 = 1.0). The lap factors α_6 were chosen according to [EC2] (α_6 = 1.5) and [EC2/NA] respectively (α_6 = 2.0).

Table 3-4 Concrete strength f_{cm}, dimensions (b/h), confinement and lap length of the beam tests with laps

Test	f_{cm}	Cross-section (b/h)	Bar-Ø	Bars lapped	Transverse reinforce-ment	Stirrup spacing s_{st}	Concrete cover c	Lap factor α_6	Lap length l_0	
[-]	[-]	[mm]	[mm]	[%]	[-]	[mm]	[-]	[-]	[-]	[m]
T 1	40.2	520/600	40	100	8 Ø 14	130	1.5· Ø	1.5	33· Ø	1.31
T 2	32.5	500/600	40	100	8 Ø 14	130	1.0· Ø	1.5	33· Ø	1.31
T 3	33.0	520/600	40	100	8 Ø 14	180	1.5· Ø	2.0	44· Ø	1.75
T 4	59.9	500/350	40	100	8 Ø 14	130	1.0· Ø	1.5	23· Ø	0.93
T 5	34.6	660/450	40	100	8 Ø 14	180	1.0· Ø	1.5	33· Ø	1.31
T 6	39.2	520/600	40	100	14 Ø 14	90	1.5· Ø	2.0	44· Ø	1.75
T 7	34.5	540/600	40	100	8 Ø 14[1]	180	1.5· Ø	2.0	44· Ø	1.75
T 8	36.8	650/600	50	100	10 Ø 16	160	1.5· Ø	2.0	42· Ø	2.07
T 9	40.0	540/600	40	100	8 Ø 14[1]	130	1.5· Ø	1.5	33· Ø	1.31
T 10	40.5	540/600	40	100	8 Ø 14[2]	130	1.5· Ø	1.5	33· Ø	1.31
T 11	37.3	540/600	40	100	-[1]	-	1.5· Ø	1.5	33· Ø	1.31
T 12	33.6	540/600	40	33	8 Ø 14	100	1.5· Ø	1.15	25· Ø	1.00
T 13	32.5	540/600	40	66	8 Ø 14	130	1.5· Ø	1.5	33· Ø	1.31
T 15	38.4	540/600	28/40	100	6 Ø 12[1]	130	1.5· Ø	1.0/1.5	22·Ø	0.90
T 16	34.4	540/600	28/40	100	8 Ø 14	130	1.5· Ø	1.5/2.1	33· Ø	1.31
T 17	38.3	380/400	28	100	6 Ø 12	140	1.5· Ø	1.5	33· Ø	0.90
T 18	39.6	380/400	28	100	6 Ø 12[1]	140	1.5· Ø	1.5	33· Ø	0.90

[1] surface reinforcement

[2] additional reinforcement at lap end

Test T1 was conducted with 1.5 · Ø = 60 mm concrete cover and a lap factor α_6 = 1.5. The lap length resulted in 1310 mm or 33 · Ø. In test T2, the concrete cover was reduced to 1.0 · Ø = 40 mm. The effect of lap length was investigated by test T3. The lap length for T3 was calculated with the lap factor $\alpha_6 = 2.0$ according to [EC2/NA] and resulted in 1750 mm or $l_0 = 43 \cdot Ø$. Since the yield strength was reached with $l_0 = 43 \cdot Ø$, this length was chosen in tests T6 to T8, too. To investigate the necessary lap detailing for shorter laps, tests T9 to T18 were tested with $l_0 = 33 \cdot Ø$.

In all tests, a cylinder compressive strength of 30 MPa was aimed for. Only for test T4, a cylinder compressive strength of 60 MPa was planned. The remaining parameters for T4 were equal to test T2 ($c = 1.0 \cdot Ø = 40$ mm and $\alpha_6 = 1.5$). Test T5 was conducted with increased longitudinal bar spacing.

Stirrups were positioned at the outer thirds of the lap length in all tests. The effect of smaller stirrup spacing was investigated by test T6. Tests T7, T9 and T11 were conducted with surface reinforcement as shown in Figure 3-16. In test T11, surface reinforcement according to [EC2] was positioned, but the test specimen did not contain stirrups along the lap length.

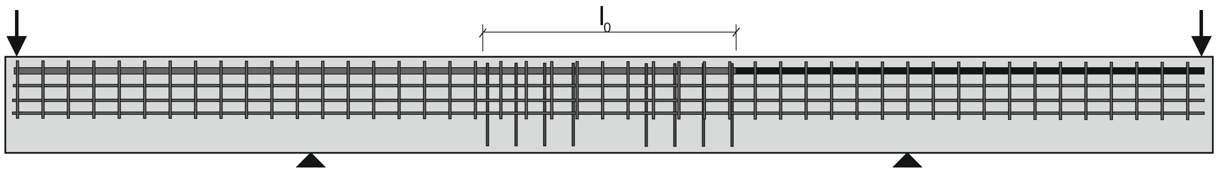

Figure 3-16 Four-point bending test T7 with surface reinforcement

While in most tests 100 % of the bars were lapped, test T12 was a 33 % lap and T13 a 66 % lap both with three bars in total. Tests T15 and T16 were combined laps with 40 mm and 28 mm bars. The effect of bar diameter was investigated in tests T8, T17 and T18. Test T8 was conducted with three Ø 50 mm reinforcing bar diameters and tests T17 and T18 with three Ø 28 mm bars. For these tests, the beam dimensions were adjusted (cf. Figure 3-17).

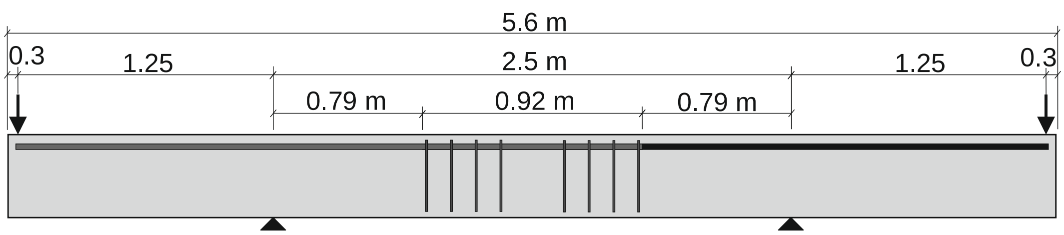

Figure 3-17 Test setup of four-point bending tests with Ø 28 mm reinforcing bars

3.4.3 Measurements and Test Procedure

For the evaluation of stress developed by bond and of crack formation in the lap zone during the loading, the following values were measured:

- Hydraulic cylinder load
- Beam deflection by displacement transducers (WA) WA D1 to WA D3 underneath the hydraulic cylinders and at the beam centre (u [mm])

– Reinforcing bar strain by strain gauges (SG) at the longitudinal reinforcement along the lap length (ε_s [‰])
– Transverse reinforcing bar strain by strain gauges (SG) at the stirrups (ε_{st} [‰])
– Concrete strain with strain gauges Be1 to Be4 and displacement transducers B1 and B2 at the concrete surface at the lapped splice, at the supports or between lap and support (ε_c [‰])
– Transverse concrete strain with an extensometer with a 100 mm base at the extreme fibre and at the test specimen side at the height of the longitudinal reinforcement (ε_c [‰])
– Slip measurement at the end of the lapped splice with steel rods WA S1 and WA S2 in tests T1 to T8 (cf. [HEG15])
– Beam rotation with displacement transducers at the beam faces WA V1 and WA V2
– Crack width with a digital crack magnifier at 160 MPa, 320 MPa and 400 MPa steel stress (w [mm])
– Crack spacing (s [mm])

Figure 3-18 illustrates the measurements for beam T1.

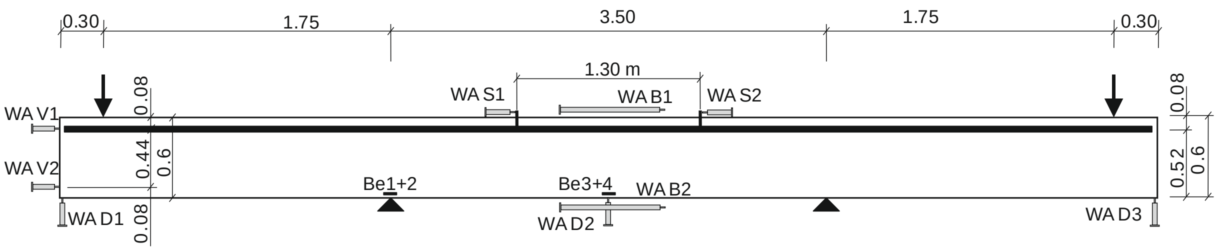

Figure 3-18 Measurement instrumentation for lap test specimen T1

The increase in crack width was measured with a PEAK digital crack magnifier WIDE STAND MICRO (cf. Figure 3-19, (a)). The possible accuracy of the crack width measurement with the digital crack magnifier was 0.001 mm. This precision not necessary in structural concrete elements. While crack widths were measured from 0.01 mm, the following statistical evaluation includes crack widths wider than 0.05 mm only. This bottom limit was defined, since the coefficient of variation (COV) of the measurement was otherwise well above the standard deviation known from published crack measurements. This conforms with [DEU06] requiring a measuring precision of 0.05 to 0.1 mm for crack width meters and 0.05 mm for crack magnifiers.

The crack widths were measured at sharp crack edges at the concrete surface parallel to the direction of the tensile reinforcement independently from the local crack course. However, this agreement influences the measured crack widths.

To evaluate the crack width correctly, the crack width measurement had to be conducted at exactly the same location, since the crack width is not constant over the crack length (cf. Figure 3-19, (b)). Therefore, five axes (a-e) were marked with a cutter line before testing (cf. Figure 3-19, (c)). Three axes (c-e) were on the top side of the test specimen above the lapped reinforcement to compare the crack width above laps positioned in the beam corner and cross-sectional beam centre (cf. Figure 3-19, (d)). Two axes were located at the test specimen's side, one at the height of the longitudinal reinforcement and one at the effective height of the longitudinal reinforcement $h_{c,eff} = 2.5 \cdot (h - d)$. A digital photograph of the crack was taken at the intersection of a crack with the axes at each load level. The crack width was determined using the software METRIC for the evaluation of the photographs.

Compared to measurements with a crack width meter, this procedure offers the possibility to review the development of the crack width. All flexural cracks between the supports of the beam were measured.

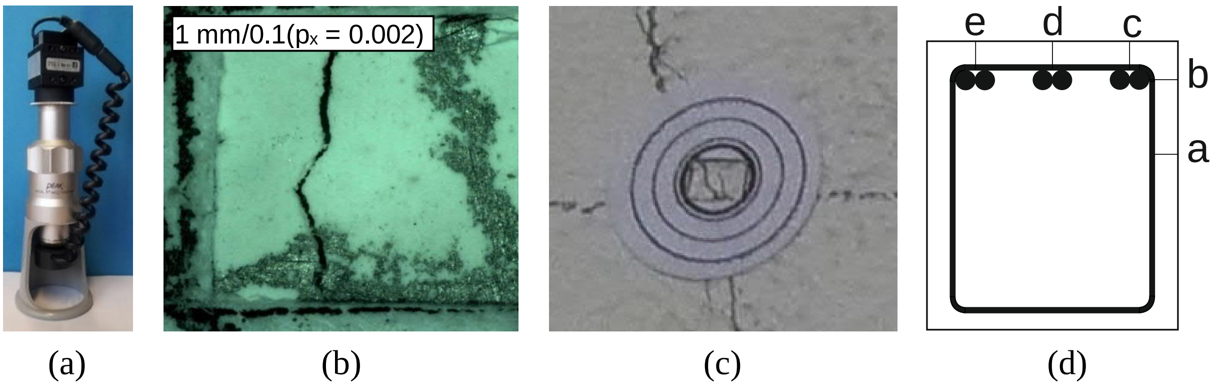

Figure 3-19 Labelled intersection of crack and measuring axis (a); crack magnifier (b); digital photograph of a crack (c); axis for measurement (d)

The crack measurement at the height of the reinforcement (80 mm) was close to the centre of the effective depth (100 mm). To compare mean values over $h_{c,eff}$, the measurements in axes c to e were averaged. The three crack measurements (axis a, axis b and mean value of axes c to e) were used for a statistical evaluation in tests T1 to T8 (cf. Figure 2-25, c)). The locations for crack measurements were reduced to axes b, c and d in tests T9 to T18. The statistical evaluation was therefore done with the averaged crack width in axis c and d multiplied with the factor 0.69. This factor was derived from a mean crack depth h_{cr} = 320 mm as shown in Figure 3-20.

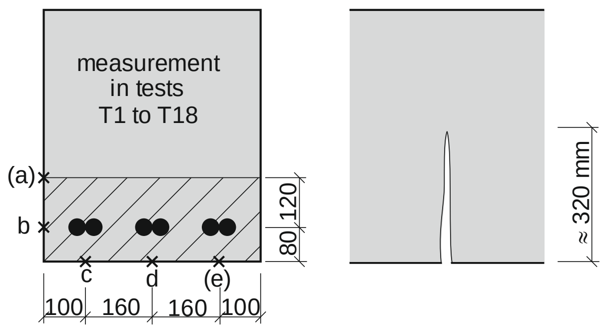

$$\frac{h_{cr} - h_{c,eff}/2}{h_{cr}} = \frac{320 - 100}{320} = 0.69$$

Figure 3-20 Crack measurement locations in the conducted tests and crack width over mean crack depth

The loading was increased by 80 MPa steps for the longitudinal reinforcement. The testing speed was 20 MPa / min. To determine the reinforcement stress, the strain distribution was calculated with a parabola-rectangle diagram for concrete under compression according to [EC2]. At first, the specimens were loaded force-controlled and displacement-controlled after reaching the service load.

3.4.4 General Test Results

In most tests without surface reinforcement lap failure was observed, only tests T6 to T8 failed in bending. The test specimens with surface reinforcement failed in the compression zone or were unloaded. Test T11 was an exception, since the lap failed for the lack of stirrups, although surface reinforcement was present. The failure type was defined by crack formation during the test and by a comparison of ratios M_{test} / M_u (Table 3-5). M_u is the moment for which the experimentally determined yield strength of the longitudinal reinforcement is reached. The tests exceeding the calculated stress developed by bond (taking mean material properties into account) had a compression zone failure or were unloaded. In case the lap failed before reaching yield strength, considerable hoop stress and longitudinal cracks formed in the lap zone and the concrete cover spalled off (cf. Figure 3-21, left).

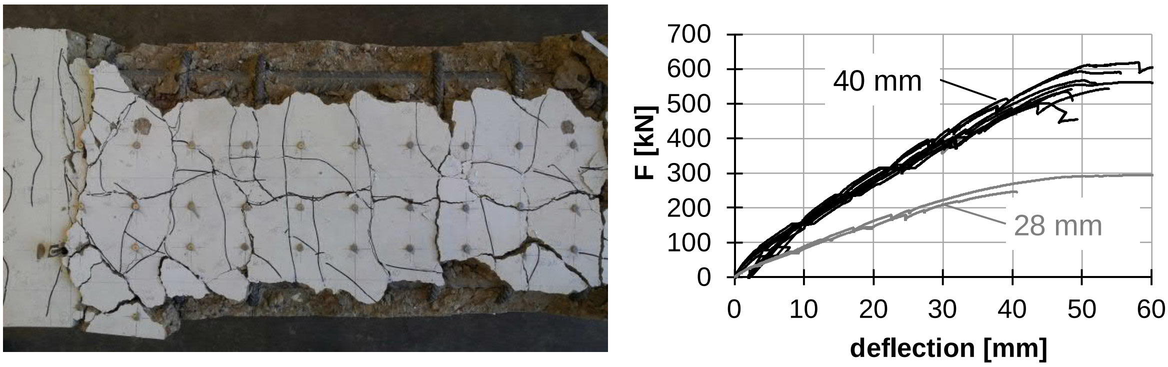

Figure 3-21 Crack formation an spalling in T4 (left) and deflection of flexural tests under the load application (right)

The failure did not occur at three reinforcing bars at a time, but started at one lapped rebar. The lap initiating the failure was the intermediate lap in some tests and a side lap in other tests. The yield strength was developed in the lapped splices with a lap factor α_6 = 2.0.

The beam deflection was largely independent of the test parameters (cf. Figure 3-21, right). For T4, T5 and T8 the deflections slightly differed from the remaining tests for changed cross-section dimensions. In tests T1 and T2 with short lap lengths, the deflections at the load application were smaller than in the tests with large bond length.

Table 3-5 Comparison of calculated bending moment M_u with maximum bending moment obtained in tests M_{test}

Test	Bar-Ø	Concrete cover c	Lap factor α_6	Transverse reinf. ratio A_{st}/A_s	Concrete strength f_{cm}	Max. bar stress σ_s	M_{test}	M_u	M_{test}/M_u
	[mm]				[MPa]	[MPa]	[kNm]	[kNm]	[%]
T1	40	1.5·Ø	1.5	1.0	40.2	495	872	980	89
T2	40	1.0· Ø	1.5	1.0	32.5	473	834	1000	83
T3	40	1.5· Ø	2.0	1.0	33.0	555	965	964	100
T4	40	1.0· Ø	1.5	1.0	59.9	532	505	537	94
T5[3]	40	1.0· Ø	1.5	1.0	34.6	552	706	735	96
T6	40	1.5· Ø	2.0	1.7	39.2	> 580	1022	998	102
T7	40	1.5· Ø	2.0	1.0[1]	34.5	> 580	1119	990	113
T 8	50	1.5· Ø	2.0	1.0	36.8	556	1397	1343	104
T 9	40	1.5· Ø	1.5	1.0[1]	40.0	> 580	1078	990	109
T 10	40	1.5· Ø	1.5	1.0[2]	40.5	> 580	1000	996	100
T 11	40	1.5· Ø	1.5	0.0[1]	37.3	520	903	988	91
T 12	40	1.5· Ø	1.15	1.0[4]	33.6	510	884	979	90
T 13	40	1.5· Ø	1.5	1.0[5]	32.5	545	942	974	97
T 15	28/40	1.5· Ø	1.0/1.5	1.0[1]	38.4	582	993	991	100
T 16	28/40	1.5· Ø	1.5/2.1	1.0	34.4	562	968	980	99
T 17	28	1.5· Ø	1.5	1.0	38.3	565	313	315	99
T 18	28	1.5· Ø	1.5	1.0[1]	39.6	> 583	374	315	119

[1] surface reinforcement
[2] additional reinforcement at lap end
[3] longitudinal bar spacing a = 4 · Ø
[4] 33 % bars lapped
[5] 66 % bars lapped

The longitudinal reinforcement strain was recorded with strain gauges. The largest strain increase was observed in the first third of the lap from the bar end, while a strain plateau was located in the central part of the lap (representative illustration for test T3 given in Figure 3-22). In the rear third of the lap length, the steel strain increased again. The plateau in the centre was more distinct for smaller loads. For higher lap loads, the central part of the lap contributed more to the load transfer. Meeting the expectations, half the reinforcing bar load was transferred at the centre of the lap. The tested variation in lap length and confinement did not result in clear differences in the reinforcing-bar strain distribution over the lap length.

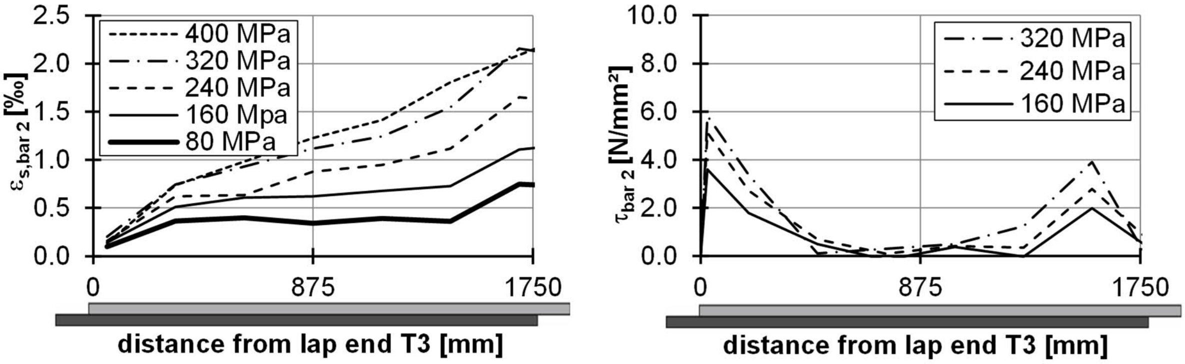

Figure 3-22 Reinforcing bar strain (left) and bond strength (right) in test T3 along the lap length l_0 = 1750 mm

The bond strength calculated from the measured reinforcement strain is given in Figure 3-22. For a longitudinal stress of 320 MPa, the bond stress was up to 6 MPa at the end of the lap length conforming to the steel strain distribution along the lap length. All test specimens had significant transverse concrete strain in the first and last third of the lap length. The intermediate third in the middle of the lap length remained nearly unstrained.

The stirrup with a 40 mm distance from the lap end had the highest strain in all test specimens (cf. Figure 3-23). The stirrup strain remained below 1 ‰ in all tests, therefore the transverse reinforcement did not yield. In test T3, the stirrups were located at 4 cm, 22 cm, 40 cm and 58 cm from the lap end.

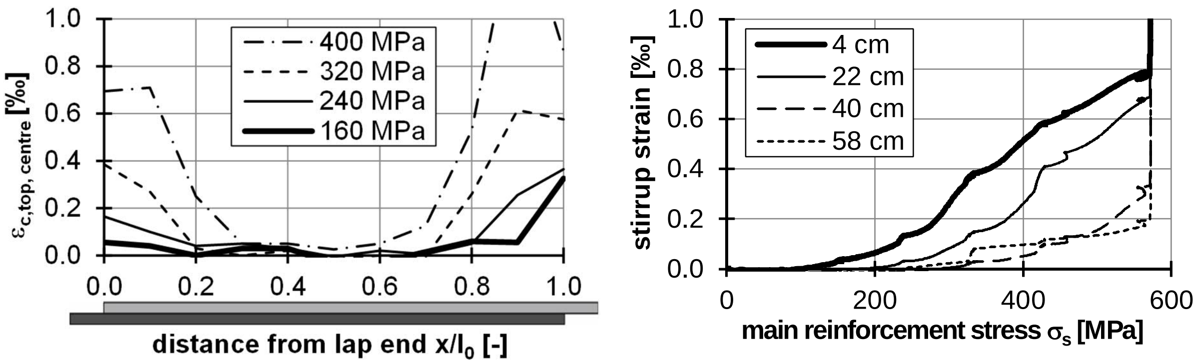

Figure 3-23 Transverse concrete strain over relative lap length (left); stirrup strain over longitudinal reinforcement stress at different positions from the lap end (right) in test T3

3.4.5 Maximum Bar Strength in Lap

<u>Influence of Lap Length and Effect of Percentage of Bars Lapped at a Section</u>

The influence of lap length was investigated in tests T1 and T3 with three Ø 40 mm reinforcing bars lapped at the same section and a concrete strength of 30 MPa. The concrete covers c_y and c_x were 1.5 · Ø (60 mm) and the bar spacing c_s was 2.0 · Ø. The transverse reinforcement was positioned according to [EC2] with $\Sigma A_{st} = 1.0 \cdot A_s$. The increase in lap factor from $\alpha_6 = 1.5$ for test T1 ([EC2]) with l_0 = 33 · Ø to $\alpha_6 = 2.0$ for test T3 ([ELI79]; [EC2/NA]) with l_0 = 44 · Ø led to an increase in maximum bar stress

σ_s. A positive effect of lap length was not observed in tests T7 and T9 where surface reinforcement was positioned. Test specimens T7 and T9 were unloaded when the yield strength of the bars was reached (cf. Figure 3-24).

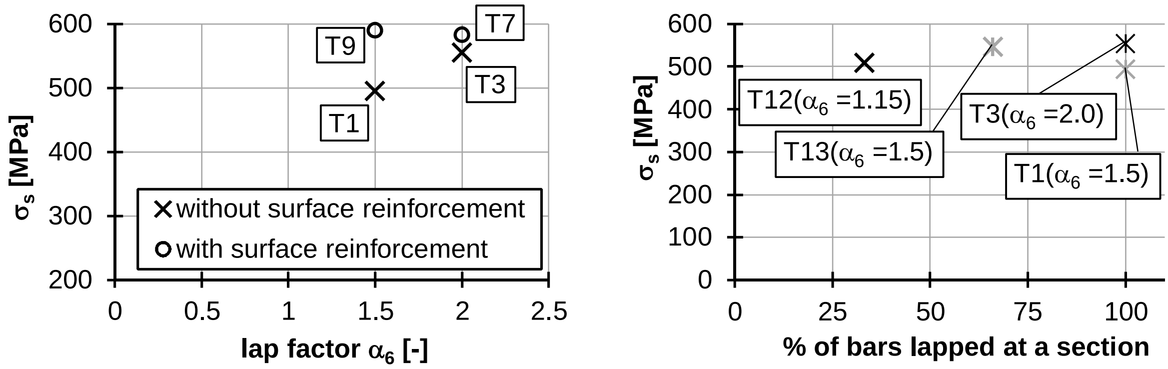

Figure 3-24 Influence of lap factor (left) and influence of percentage of bars lapped at a section (right) on the maximum steel stress for Ø 40 mm, $f_{cm} \approx 30$ MPa, $c_y = c_x = 1.5 \cdot Ø$, $c_s = 2.0 \cdot Ø$, $\Sigma A_{st} = 1.0 \cdot A_s$

The percentage of bars lapped at a section ρ_l was reduced in tests T12 and T13 to 33 % and 66 %, respectively. The lap factors α_6 according to [EC2] were applied. For the continuous bars, the failure in tests T12 and T13 was less brittle than in tests T1 and T3 with 100%-laps.

For the 33%-lap (T12), the lap length l_0 was calculated with $\alpha_6 = 1.15$ resulting in $l_0 = 1000$ mm. This lap reached the same ultimate steel stress as test T1 with three bars lapped at a section and a lap factor $\alpha_6 = 1.5$. The lap length of the 66%-lap (T13) was calculated with $\alpha_6 = 1.5$ resulting in $l_0 = 1310$ mm. The reinforcing bar stress in test T13 with $\alpha_6 = 1.5$ and $\rho_l = 66\%$ reached the same value as test T3 with $\alpha_6 = 2.0$ and $\rho_l = 100\%$ (cf. Figure 3-24).

Influence of Concrete Strength

The influence of concrete strength was investigated by tests T2 and T4 with a bar diameter of Ø 40 mm and a lap factor $\alpha_6 = 1.5$. The lap length was 1310 mm ($l_0 = 33 \cdot Ø$) in test T2 and 920 mm in test T4 ($l_0 = 23 \cdot Ø$). The concrete cover values c_y and c_x were $1.0 \cdot Ø$ (40 mm), the bar spacing c_s was $2.0 \cdot Ø$ and the sum of the transverse reinforcement ΣA_{st} equalled $1.0 \cdot A_s$. The increase in concrete cylinder strength from 33 MPa (T2) to 60 MPa (T4) led to an increase in bar stress developed by 14 % ($\sigma_{s,T4}$ / $\sigma_{s,T2}$ = 532 MPa / 473 MPa) at a concrete cover of $1.0 \cdot Ø$ and a transverse reinforcement ratio $\Sigma A_{st}/ A_s = 1.0$.

Figure 3-25 shows the transverse concrete strain $\varepsilon_{c,top,centre}$ in the extreme fibre above the lap in the centre along its lap length. The strain is small in the lap centre and increases strongly towards both lap ends in test T2. In contrast to test T2 with normal strength concrete, very small transverse concrete strain at the lap end was observed in test T4 with high strength concrete.

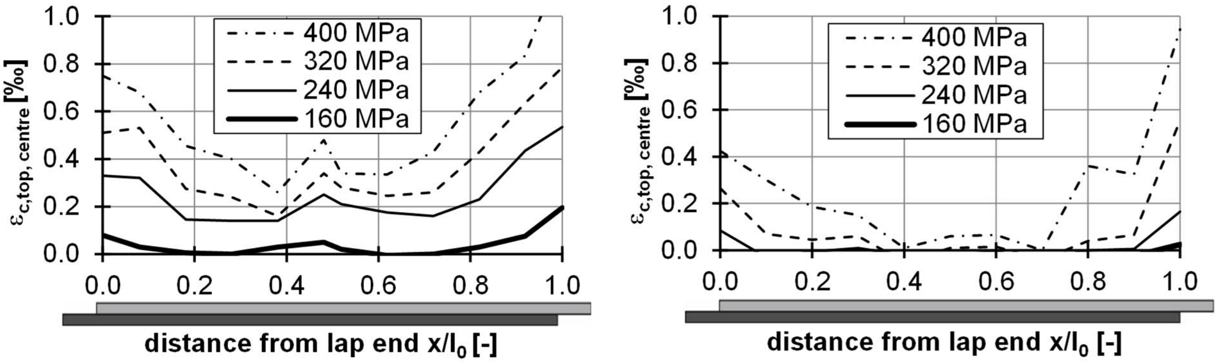

Figure 3-25 Transverse concrete strain in the lap zone with normal (left, T2) and high strength concrete (right, T4)

Influence of Bar Diameter

The influence of bar diameter was evaluated by tests T3 and T8 with a lap factor $\alpha_6 = 2.0$ and by tests T1 and T17 with a lap factor $\alpha_6 = 1.5$. Both tests were conducted with concrete covers $c_y = c_x = 1.5 \cdot Ø$, $c_s = 2.0 \cdot Ø$ and $f_{cm} \approx 30$ MPa. The transverse reinforcement ($\Sigma A_{st} = 1.0 \cdot A_s$) corresponded with [EC2]. The maximum steel stress in the lap tests with Ø 40 mm (T3) and Ø 50 mm (T8) bars was very similar (cf. Figure 3-26). The different yield strengths of the reinforcement bars with Ø 40 mm and Ø 50 mm must be taken into account. The Ø 50 mm reinforcement bars had a 540 MPa yield strength and a ratio M_{test} / M_u of 1.13 with $\sigma_{s,test} > 540$ MPa. The yield strength of the Ø 40 mm bar equalled 570 MPa, but the ratio M_{test} / M_u was only 1.0, although the maximum bars stress obtained in the test $\sigma_{s,test}$ was 568 MPa.

For the decreased lap length, the maximum stress obtained in test T1 was smaller than in T3. Unlike the similar behaviour observed in tests T3 (Ø 40 mm) and T8 (Ø 50 mm), the steel stress in test T17 with Ø 28 mm bars was 14 % ≙ 70 MPa higher than in the comparable test with Ø 40 mm bars (test T1) (cf. Figure 3-26).

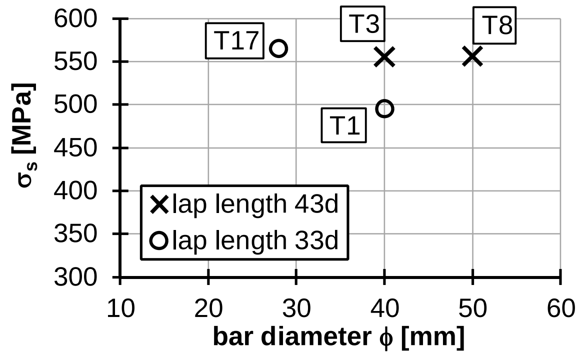

Figure 3-26 Effect of bar diameter on maximum bar stress for $\alpha_6 = 2.0$, $f_{cm} \approx 30$ MPa, $c_y = c_x = 1.0$, $c_s = 2.0$, $\Sigma A_{st} = 1.0 \cdot A_s$

Calculating the averaged bond strength τ_a over the lap length, a bond strength decrease with increasing bar diameter becomes visible (cf. Figure 3-27, left). This effect is reduced if the non-linear ratio of lap length to bar stress $\sigma_s \sim l_0^{0.55}$ according to [FIB14] is taken into account (cf. Figure 3-27, right).

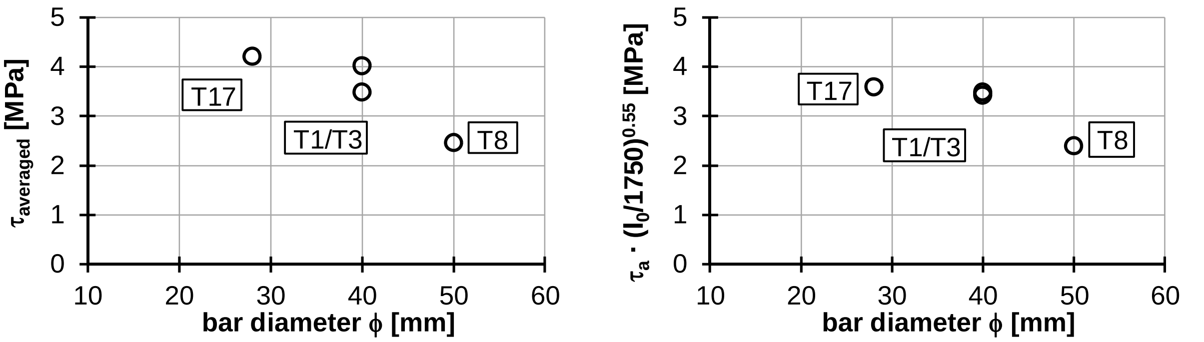

Figure 3-27 Effect of bar diameter on averaged bond strength τ_a for $\alpha_6 = 2.0$, $f_{cm} \approx 30$ MPa, $c_y = c_x = 1.0$, $c_s = 2.0$, $\Sigma A_{st} = 1.0 \cdot A_s$

Influence of Concrete Cover

The influence of concrete cover was investigated by tests T1 and T2 with a concrete strength of about 30 MPa (Ø = 40 mm, $\alpha_6 = 1.5$, $c_s = 2.0 \cdot Ø$, $\Sigma A_{st} = 1.0 \cdot A_s$). The increase in concrete cover from 1.0 · Ø = 40 mm in test T2 to 1.0 · Ø = 60 mm in test T1 lead to an increase in maximum bar stress developed by bond by 7 %.

For concrete covers exceeding 1.0 · Ø bar diameter, the lap length may be reduced by the factor $\alpha_2 = 1 - 0.15 \cdot (c_d - Ø) / Ø$ according to [EC2]. The effect of concrete cover on the ultimate bar stress developed in the Ø 40 mm laps corresponds with the formulation for α_2 (cf. Figure 3-28). For the increased concrete cover from 40 mm to 60 mm, the lap length may be reduced by the factor $\alpha_2 = 1 - 0.15$ (60 mm – 40 mm) = 0.93. This value approximately conforms with the decrease in ultimate bar stress of test T2 in comparison with test T1 by the factor 83 / 87 = 0.96.

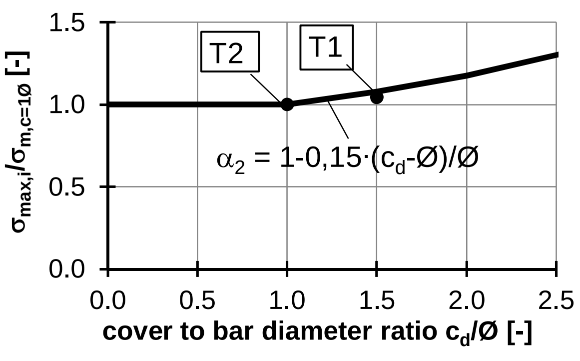

Figure 3-28 Influence of concrete cover on maximum bar stress for Ø 40 mm, $\alpha_6 = 1.5$, $f_{cm} = 30$ MPa, $c_s = 2.0$, $\Sigma A_{st} = 1.0 \cdot A_s$ compared to the reduction factor α_2 according to [EC2]

Test T2 with a concrete cover of 1.0 · Ø had higher transverse concrete strain in the lap centre than test T3 with a concrete cover of 1.5 · Ø. The transverse strain in test T3 with 1.5 · Ø = 60 mm was very small in the central part (cf.Figure 3-29).

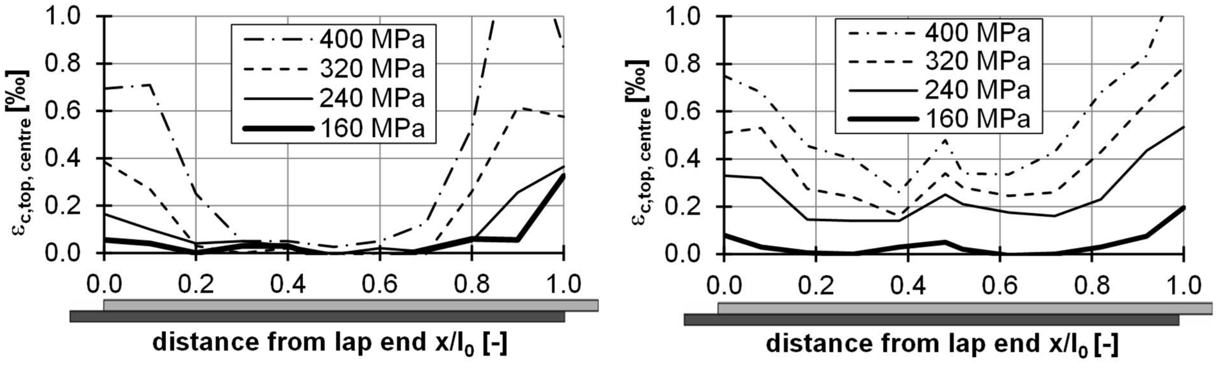

Figure 3-29 Transverse concrete strain for 1.5 · Ø (left, T3) and 1.0 · Ø (right, T2) concrete cover in the extreme fibre

Influence of Longitudinal Bar Spacing

By means of tests T2 and T5, the effect of bar spacing was tested with three Ø 40 mm bars lapped at the same section (α_6 = 1.5) and a concrete strength of about 30 MPa. The bottom and side covers were 1.5 · Ø (60 mm) and the transverse reinforcement ΣA_{st} was 1.0 · A_s. The increase in bar spacing from 2.0 · Ø = 80 mm in test T2 to 4.0 · Ø = 160 mm in test T5 lead to an increase in maximum bar strength by 20 %.

The clear spacing between laps shall be at least 2.0 · Ø according to [EC2]. By an increase of the clear spacing, the required lap length may be multiplied with a reduction factor $\alpha_2 = 1 - 0.15 \cdot (c_d - Ø) / Ø$ (cf. Figure 3-30). The increase in bar spacing at constant horizontal and vertical concrete cover is not captured by [EC2], since the smaller value of half the bar spacing and the concrete cover $c_d = \min \{c_x, c_y, c_s / 2\}$ is used for the calculation of α_2. Figure 3-30 shows a comparison of the test results with $c_d = c_s / 2$.

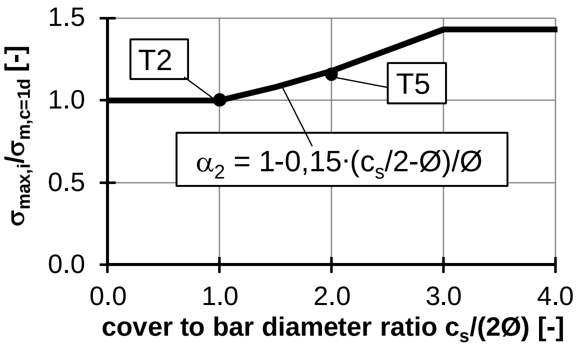

Figure 3-30 Effect of bar spacing on maximum bar stress for Ø 40 mm, α_6 = 1.5, f_{cm} = 30 MPa, $c_y = c_x$ = 1.0, ΣA_{st} = 1.0 · A_s

For the increased bar spacing from 40 mm to 80 mm, the lap length may be reduced by α_2 = 1 – 0.15 · (80 mm – 40 mm) / 40 mm = 0.85 according to [EC2]. This value conforms to the decrease in maximum bar stress with the ratio $\sigma_{max, T5} / \sigma_{max, T2}$ = 555 MPa / 473 MPa = 0.85 (cf.Figure 3-30).

Greater bar spacing led to a decrease in stirrup strain (cf. Figure 3-31). Strain gauges were located at the horizontal stirrup legs between two lapped splices. By the increased concrete area between the laps in test T5, the stirrup contribution was smaller than in test T2.

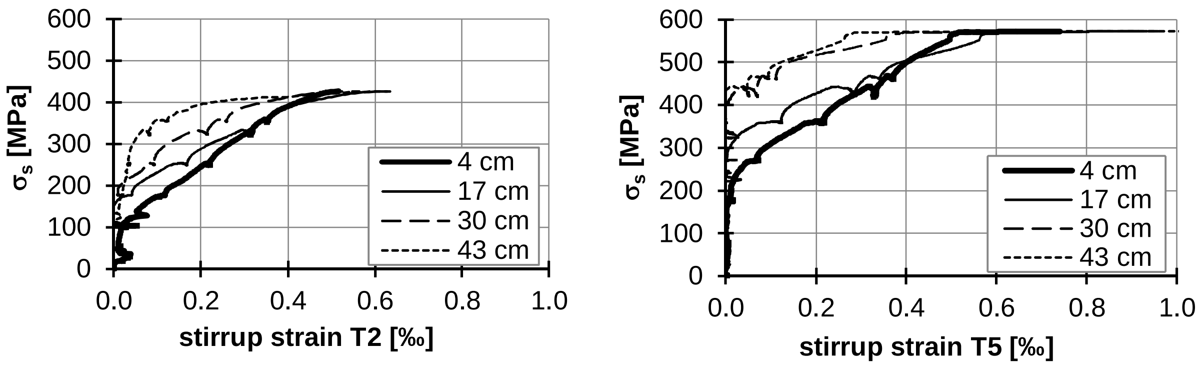

Figure 3-31 Steel stress in the longitudinal reinforcement vs. stirrup strain for lap spacing $c_s = 2 \cdot Ø$ (T2, left) and lap spacing $c_s = 4 \cdot Ø$ (T5, right) for stirrups located at 4 cm, 17 cm, 30 cm and 43 cm distance from the lap end

Influence of Transverse Reinforcement and Surface Reinforcement

The influence of transverse reinforcement was investigated by tests T3 and T6. Both tests were conducted with three Ø 40 mm bars with a lap factor $\alpha_6 = 2.0$ and a concrete strength of about 30 MPa. The bar spacing c_s was $2.0 \cdot Ø$ and the cover c_y was $1.5 \cdot Ø$. The increase in bar stress developed by bond due to increased transverse reinforcement from $\Sigma A_{st} / A_s = 1.0$ (T3) to $\Sigma A_{st} / A_s = 1.7$ (T6) was 5 % (cf. Figure 3-32).

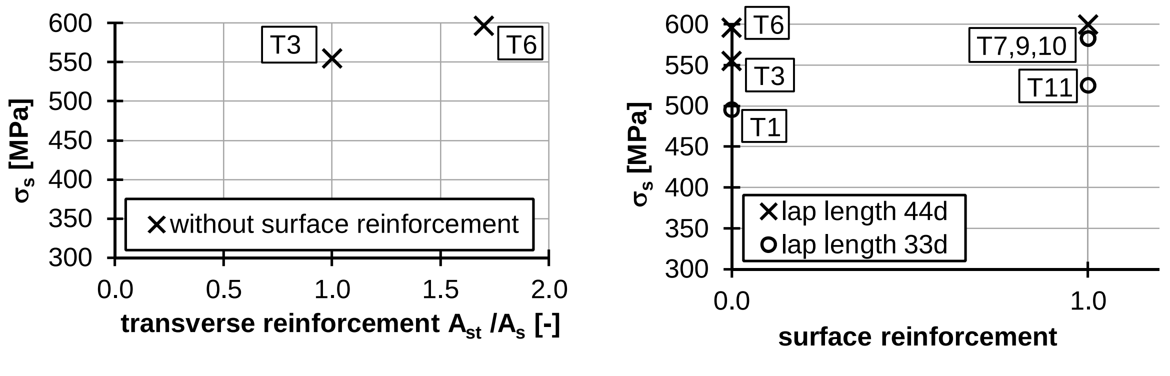

Figure 3-32 Effect of transverse reinforcement ratio A_{st}/A_s (left) and of surface reinforcement (right) on maximum bar stress for Ø = 40 mm, f_{cm} = 30 MPa, $c_y = c_x = 1.5$, $c_s = 2.0$

In tests T7, T9, T11 and T18, the effect of surface reinforcement was investigated. The cross-sectional area of the surface reinforcement was calculated according to [EC2] and [EC2/NA], respectively. In test T7, both the longitudinal and the transverse surface reinforcement was Ø 10 mm with a 100 mm spacing. These values conform to 2 % of the cross-sectional beam area under tension outside the stirrups according to [EC2/NA].

The cross-sectional area of the surface reinforcement in tests T9, T11 and T18 conforms to [EC2]. In this case, the longitudinal surface reinforcement equals 2 % of the cross-sectional beam area under tension outside the stirrups, while the transverse surface reinforcement equals 1 % of this area. These percentages gave Ø 10 mm bars with a 100 mm spacing in the longitudinal direction and Ø 8 mm bars with a 125 mm spacing in the transverse direction for tests T9 and T11. In test T18, the percentages resulted in Ø 8 mm bars with a 90 mm spacing for the longitudinal surface reinforcement and in Ø 8 mm bars with a 200 mm spacing for the transverse surface reinforcement. All test specimens with surface reinforcement were unloaded once the yield strength was reached.

In test T11, surface reinforcement was positioned, but no stirrups along the lap length. The maximum bar stress was slightly higher than in beam T1 with stirrups but without surface reinforcement (cf. Figure 3-32, right). In contrast to stirrups, the surface reinforcement in the direction orthogonal to the lapped reinforcement did not confine the bond zone sufficiently. This behaviour can be explained by insufficient anchorage of the U-bars of the surface reinforcement in comparison to closed stirrups (cf. Figure 3-15, right).

In test T10, stirrups required according to [EC2] and additional longitudinal reinforcement of 12 Ø 10 mm bars with a length of 60 cm at the lap ends for crack control were positioned. The cracks were reduced effectively at the lap ends, but wide cracks occurred at the ends of the additional reinforcement. As a result of this measure, the ultimate bar force increased by 17 % in comparison to test T1 ($\sigma_{s,T10}$ / $\sigma_{s,T1}$ = 580 MPa / 495 MPa) and the yield strength of the lapped bars was reached (cf. Figure 3-32).

According to [EC2], the sum of the transverse reinforcement area ΣA_{st} shall be larger than the area of one lapped bar A_s. The provided transverse reinforcement shall be positioned at the outer thirds of the lap (cf. Figure 3-33, left). In case more than the required minimum transverse reinforcement is provided, the required lap length can be reduced by the factor $\alpha_3 = 1 - k \cdot (\Sigma A_{sl} - \Sigma A_{st,min}) / A_s$. The minimum transverse reinforcement $A_{st,min}$ according to [EC2] is $1.0 \cdot A_s$ for lapped bars. The increase in maximum bar stress in tests T6 and T7 with increased transverse reinforcement conforms with the formulation according to [EC2] (cf. Figure 3-33, right).

The transverse reinforcement ratio A_{st} / A_s in Figure 3-33 (right) was calculated including the cross-sectional area of the transverse surface reinforcement. According to [EC2/NA], surface reinforcement may be taken into account for the required transverse reinforcement large diameter bars.

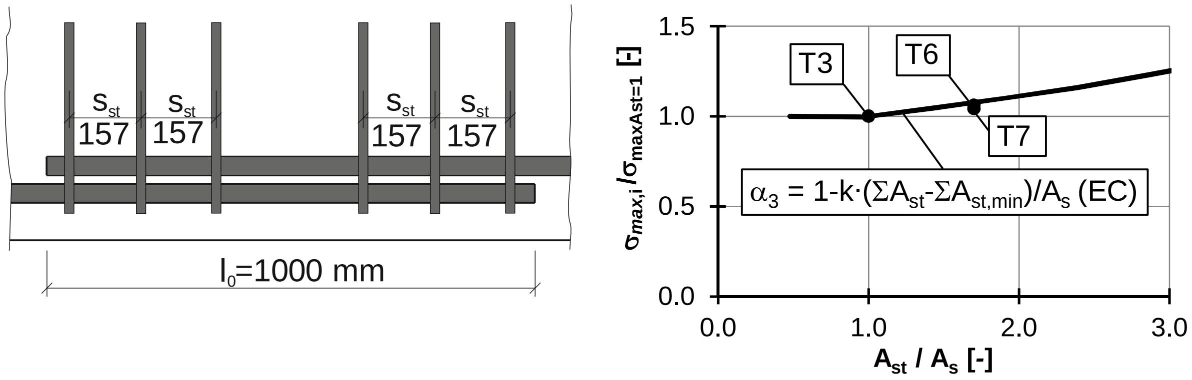

Figure 3-33 Typical transverse reinforcement positioning along the lap length according to [EC2] (left) and effect of transverse reinforcement on maximum bar stress for Ø 40 mm, α_6 = 2.0, c_y = c_x = 1.0, c_s = 2.0, f_{cm} =30 MPa, $Ø_{st}$ = 14 mm (right)

The redistribution of bond stress over the lap length depends on the concrete strength, the reinforcing bar surface and the transverse reinforcement. In tests T6 and T7 with increased transverse reinforcement, only the outer sections of the lap contributed to the load transfer. With increased loading, the lap centre increasingly contributes to the load transfer. This behaviour conforms with the observations in test T3 with transverse reinforcement according to [EC2]. The transverse concrete strain at the lap end was smaller in test T7 with surface reinforcement than in test T3 (cf. Figure 3-34).

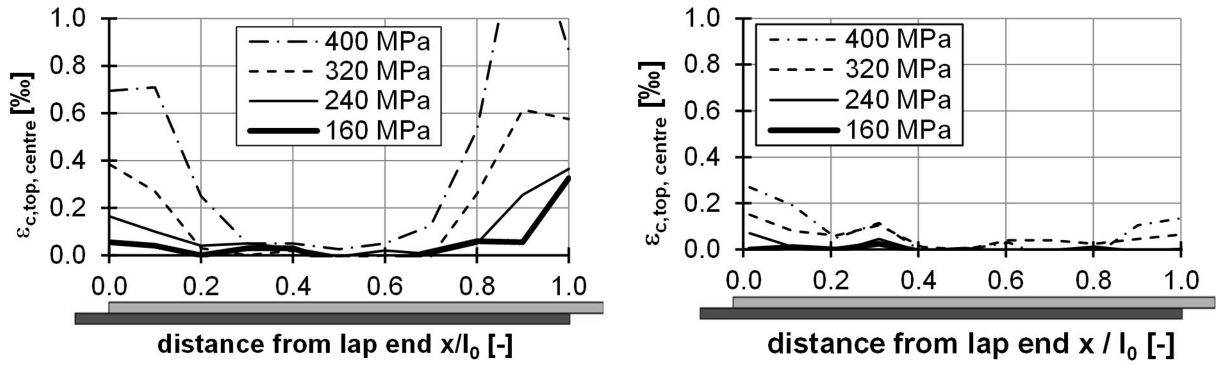

Figure 3-34 Transverse concrete strain without (left, T3) and with surface reinforcement (right, T7) vs. relative distance from lap length x / l_0

The surface reinforcement orthogonal to the longitudinal reinforcement contributed to the transverse load resistance in the lap zone. This lead to a transverse-strain reduction of the stirrups in test T7 (cf. Figure 3-35).

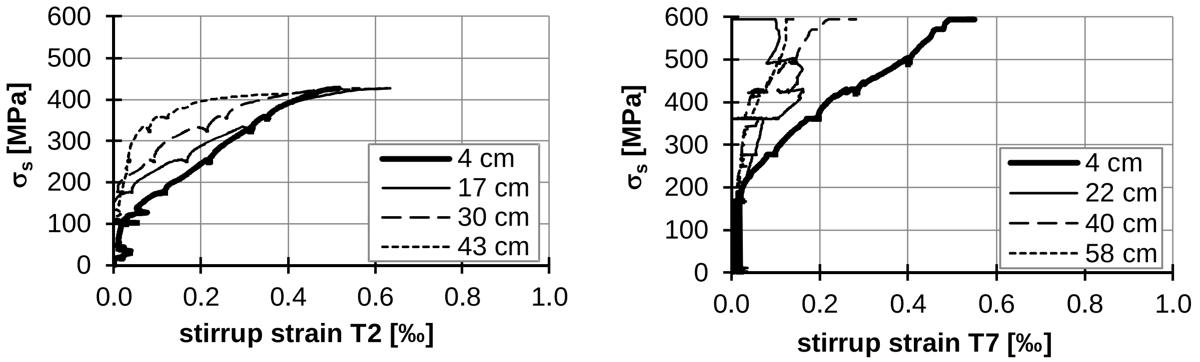

Figure 3-35 Steel stress in the longitudinal reinforcement vs. stirrup strain with transverse reinforcement only (T2, left) and with transverse as well as surface reinforcement (right, T7) for stirrups located at 4 cm, 17 cm, 30 cm and 43 cm distance from the lap end

Effect of Bar Diameter Combination

The influence of laps with different bar diameters was tested with a combination of three Ø 40 mm bars lapped with six Ø 28 mm bars in tests T15 and T16. The total cross-sectional area of the reinforcement was 37.7 cm² (Ø 40 mm bars) and 36.9 cm² (Ø 28 mm bars), respectively. In test T16, the lap length was calculated with a lap factor $\alpha_6 = 1.5$ for the Ø 40 mm bar, resulting in a lap length of 1310 mm (l_0 / Ø = 33). The bar diameter combination led to an increase by 14 % in maximum bar stress in comparison with a lap with Ø 40 mm bars only. In test T15, the possibility of a lap length reduction by positioning of surface reinforcement was tested. In this case, the lap length was calculated with a lap factor $\alpha_6 = 1.0$ for the Ø 40 mm bar, resulting in a lap length of 900 mm (l_0 / Ø = 23). The chosen lap length of 900 mm is very close to the lap length calculated with the lap factor $\alpha_6 = 1.5$ for the Ø 28 mm bar (l_0 = 920 mm and l_0 / Ø = 33). This lap detailing enabled a beam loading up to the yield strength of the Ø 40 mm reinforcing bars (cf. Figure 3-36).

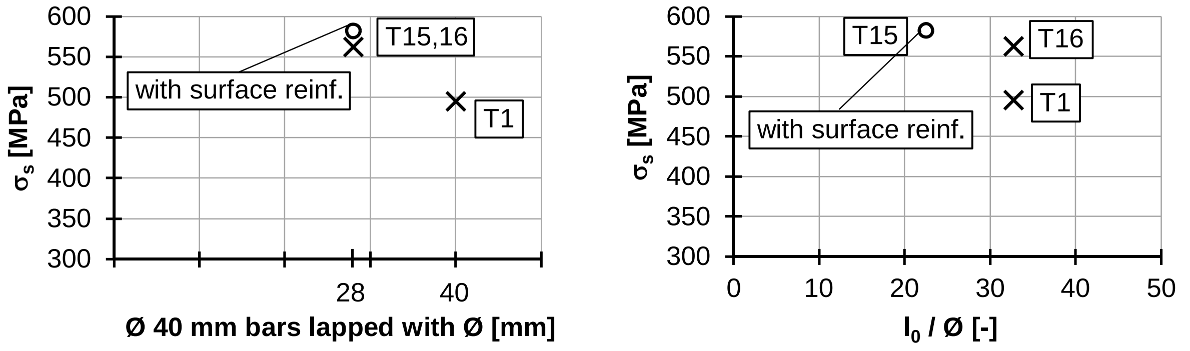

Figure 3-36 Maximum bar stress vs. bar diameter (left) and lap length l_0 / Ø (right) for $Ø_1$ = 40 mm and $Ø_2$ = 28 mm, $f_{cm} \approx 30$ MPa, $c_y = c_x = 1.5$, $c_s = 2.0$, $\Sigma A_{st} = 1.0 \cdot A_s$

3.4.6 Crack Formation in Four-Point Bending Tests

Initially, the dead weight of the test specimens and the applied load led to bending cracks above the supports. During further loading, bending cracks formed in the entire zone of constant bending moment between the supports (cf. Figure 3-37, 1). The crack spacing and the crack widths were visibly smaller in the lap zone than outside (cf. Figure 3-37, 2). The largest crack width was observed at the ends of the lap (cf. Figure 3-37, 3). Once the service loads were exceeded, longitudinal cracks developed parallel to the longitudinal reinforcement in the lap region starting from the lap ends (cf. Figure 3-37, 4). These longitudinal cracks were both visible in the extreme fibre of the beam and at the beam's side at the height of the longitudinal reinforcement.

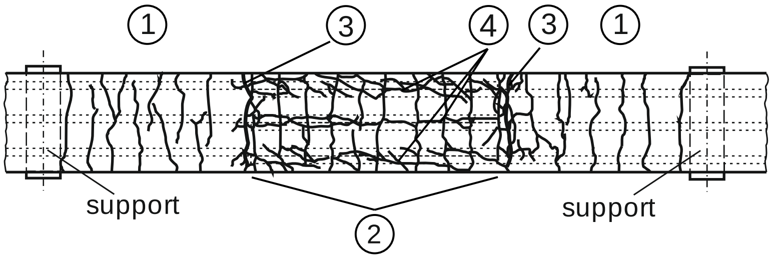

Figure 3-37 Crack formation of test T2 at the top side of the test specimen

Figure 3-38 shows the crack formation in test T3 with Ø 40 mm reinforcement, a lap factor α_6 = 2.0, concrete cover c = 1.5 · Ø and transverse reinforcement according to [EC2]. Since longitudinal cracks developed in the bottom cover as well as in the side cover, the splitting type was face-and-side splitting.

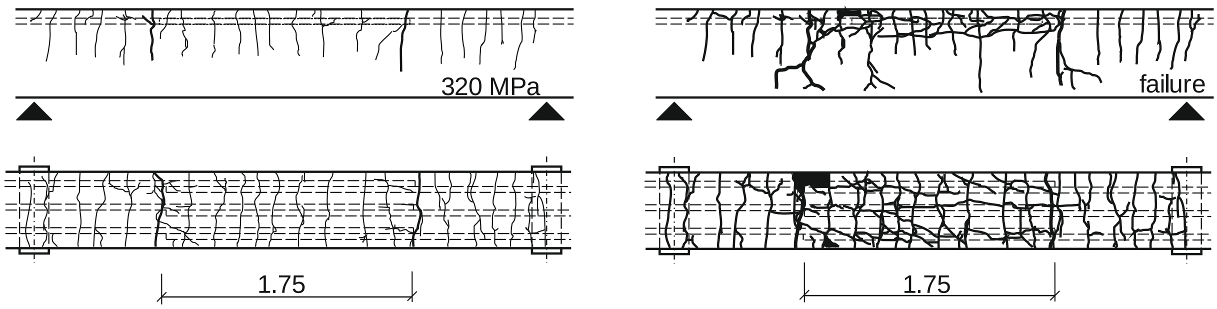

Figure 3-38 Crack development of test T3 (α_6 = 2.0, l_0 = 1.75 m) without surface reinforcement at σ_s = 320 MPa (left) and at failure (σ_s = 550 MPa) (right)

By the positioning of surface reinforcement according to the additional rules for large diameter bars in [EC2] (cf. Figure 2-17), the crack widths were reduced effectively. Figure 3-39 shows the crack formation in test T7 with surface reinforcement. The lap factor, concrete cover and transverse reinforcement conforms with test T3 in Figure 3-38. The use of surface reinforcement with bars parallel to the longitudinal reinforcement lead to significant decrease in lap-end crack widths at service stress.

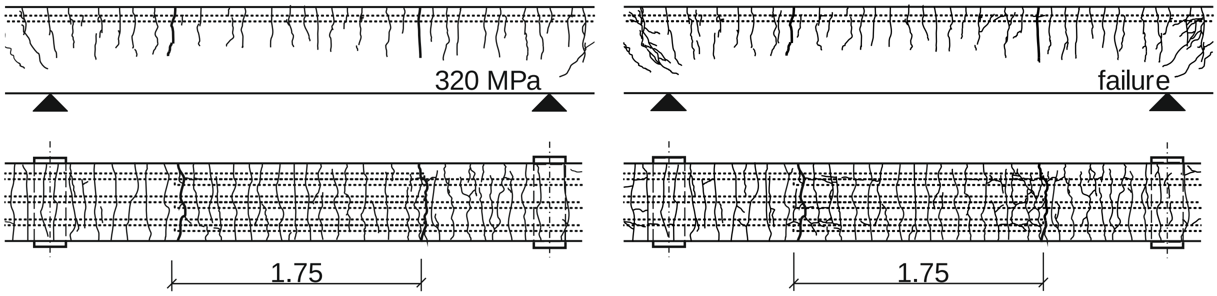

Figure 3-39 Crack development of test T7 (α_6 = 2.0, l_0 = 1.75 m) with 2 % surface reinforcement at σ_s = 320 MPa (left) and before unloading (σ_s > 570 MPa) (right)

An overview of the measured crack widths and crack spacing is given in Table 3-6.

Table 3-6 Mean and characteristic crack widths w for the four-point bending tests at 320 MPa steel stress with w_{beam} = crack width along the entire beam length, w_{ud} = crack width along the undisturbed length and w_{end} = crack width at lap end ($w_{95\%} = w_m \cdot (1 - 1.645 \cdot V_w)$)

Test	Test parameter	$w_{m,beam}$	$w_{95\%,beam}$	$w_{m,ud}$	$w_{95\%,ud}$	$w_{m,end}$	$w_{max,end}$
		[mm]	[mm]	[mm]	[mm]	[mm]	[mm]
T1	c=1.5·Ø, α_6 = 1.5	0.21	0.59	0.23	0.50	0.36	0.59
T2	c=1.0· Ø, α_6 = 1.5	0.19	0.45	0.19	0.37	0.44	0.68
T3	c=1.5· Ø, α_6 = 2.0	0.18	0.39	0.21	0.46	0.28	0.40
T4	as T2 with 60 MPa	0.16	0.36	0.17	0.37	0.24	0.40
T5	asT2 with a = 4 · Ø	0.23	0.58	0.26	0.60	0.47	0.90
T6	as T3 with more stirrups	0.20	0.46	0.21	0.43	0.43	0.75
T7	as T3 with surf. reinfor.	0.10	0.17	0.11	0.18	0.18	0.23
T8	as T3 with Ø 50 mm	0.16	0.49	0.24	0.55	0.61	0.70
T9	as T1 with surf. reinf.	0.11	0.19	0.12	0.21	0.12	0.29
T10	as T1 with add. reinf.	0.14	0.33	0.18	0.38	0.20	0.24
T11	As T9 without stirrups	0.09	0.17	0.10	0.18	0.12	0.20
T12	as T3 with 33 % lap	0.19	0.45	0.18	0.40	0.32	0.48
T13	as T3 with 66 % lap	0.16	0.37	0.18	0.40	0.24	0.35
T15	28/40 mm, surf.reinf.	0.08	0.15	0.09	0.15	0.10	0.16
T16	28/40 mm	0.16	0.37	0.21	0.50	0.24	0.38
T17	as T3 with 28 mm	0.16	0.38	0.17	0.40	0.32	0.49
T18	as T17 with surf. reinf.	0.08	0.17	0.09	0.18	0.16	0.27

The crack width in the extreme fibre $w_{m,cde}$ is considered with an averaged value of the crack width measurements in axes c, d and e (cf. Figure 3-40, left), since the crack widths at the intermediate lap (measuring axis d), and at the lap in the corner of the beam did not differ significantly (measuring axis c and e).

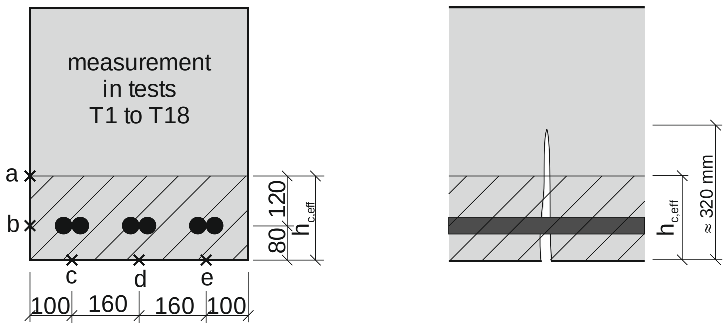

Figure 3-40 Crack measurement locations in the conducted lap tests (left) and crack depth (right) at $\sigma_s = 320$ MPa

The vertical position of the reinforcement (axis b) approximately equals half the effective height $h_{c,eff}/\,2$ of the reinforcement according to [EC2]. For a presumed linear crack width opening, the averaged crack width over the effective height equals the crack width at the height of the reinforcement. Therefore, the measured crack width w is given as an averaged crack width over the effective height $h_{c,eff}$ by

$$w_{T1-T8} = w\left(\frac{h_{c,eff}}{2}\right) = \frac{w_a + w_b + w_{m,cde}}{3} \tag{3-8}$$

The crack widths in tests T9 to T18 were measured in axes c and d in the extreme fibre and in axis b at the height of the reinforcement only. To calculate the averaged crack widths over the height of $h_{c,eff}$, the crack widths in the extreme fibre were multiplied with the factor 0.69 (cf. Figure 3-20).

$$w_{T9-T18} = w\left(\frac{h_{c,eff}}{2}\right) = \frac{w_{m,cd} \cdot 0.69 + w_b}{2} \tag{3-9}$$

The crack widths in tests with surface reinforcement were measured at the same load levels as in the tests without surface reinforcement. By the allocation of surface reinforcement, the reinforcement ratio of the test specimens was increased and the reinforcement stress was actually decreased by 20 % for the same load levels. Hence, the crack widths of the test specimens without surface reinforcement were measured at 160 MPa, 320 MPa and 400 MPa, while the crack widths of the test specimens with surface reinforcement were measured at 130 MPa, 260 MPa and 330 MPa.

Table 3-6 gives an overview of the mean and characteristic crack widths. The crack width w_{beam} accounts for the entire beam including the lap and the lap ends. The crack width w_{ud} is the crack width in the undisturbed length of the beam between the lap and the supports. These crack widths conform to a reinforced concrete element without laps and are therefore directly comparable to the crack widths calculated by codes. The crack width w_{end} is the crack width at the ends of the lap.

Comparison of Measured Crack Widths in the Undisturbed Beam with Codes

Table 3-7 gives mean and fractile values of the crack widths calculated with the equations given in [EC2], [EC2/NA] and [MC2010] as well as the test results in the undisturbed zone of the test specimen. For evaluation, the measured crack widths are given as 75%-fractiles and 95%-fractiles calculated with a log-normal distribution for crack width. The 95%-fractiles have to be compared to the [EC2] values and the 75%-fractiles have to be compared to the [EC2/NA] and [MC2010] values (cf. chapter 2.10).

Table 3-7 Crack widths in the beam tests at 320 MPa rebar stress in the undisturbed length of the beam and calculated values according to [EC2], [EC2/NA] and [MC2010] under consideration of surface reinforcement

	Test results			EC (95%) and EC2/NAD (75%)			MC(75%)
	$w_{m,ud}$	$w_{75\%,ud}$	$w_{95\%,ud}$	$w_{m,EC}=w_{m,EC/NAD}$	$w_{k,EC}$	$w_{k,EC2/NAD}$	$w_{k,MC}$
	[mm]	[mm]	[mm]	[mm]	[mm]	[mm]	[mm]
T1	0.23	0.28	0.50	0.31	0.52	0.41	0.57
T2	0.19	0.23	0.37	0.22	0.37	0.30	0.41
T3	0.21	0.26	0.46	0.30	0.52	0.41	0.56
T4	0.17	0.21	0.37	0.21	0.36	0.29	0.40
T5	0.26	0.33	0.60	0.25	0.42	0.39	0.50
T6	0.21	0.26	0.43	0.29	0.50	0.39	0.54
T7	0.11	0.13	0.18	0.18	0.30	0.16	0.28
T8	0.24	0.31	0.55	0.37	0.63	0.49	0.69
T9	0.12	0.15	0.21	0.17	0.30	0.16	0.27
T10	0.18	0.22	0.38	0.30	0.50	0.40	0.55
T11	0.10	0.12	0.18	0.18	0.31	0.16	0.29
T12	0.18	0.23	0.40	0.31	0.52	0.42	0.58
T13	0.18	0.22	0.40	0.31	0.53	0.42	0.58
T15	0.09	0.10	0.15	0.18	0.31	0.16	0.29
T16	0.21	0.26	0.50	0.31	0.52	0.42	0.58
T17	0.17	0.22	0.40	0.21	0.36	0.29	0.39
T18	0.09	0.11	0.18	0.13	0.22	0.12	0.21

The effect of additional surface reinforcement is taken into account by an equivalent bar diameter $Ø_{eq} = \Sigma n_i^2 \cdot Ø_i^2 / (\Sigma n_i \cdot Ø_i)$ for the effect of bar diameter combination in [EC2], [EC2/NA] and [MC2010]. The surface reinforcement influences the equivalent bar diameter $Ø_{eq}$, the reinforcement ratio $\rho_{s,eff}$ and the reinforcing bar stress σ_s. In the test specimens with surface reinforcement, the concrete cover of the Ø 40 mm bar was taken into account.

The comparison of the characteristic crack widths calculated according to [EC2], [EC2/NA] and [MC2010] with the 95%- fractile values of the measured crack widths in the undisturbed beam length is given in Figure 3-41. In this figure, the surface reinforcement in tests T7, T9, T11, T15 and T18 is not taken into account for a first comparison.

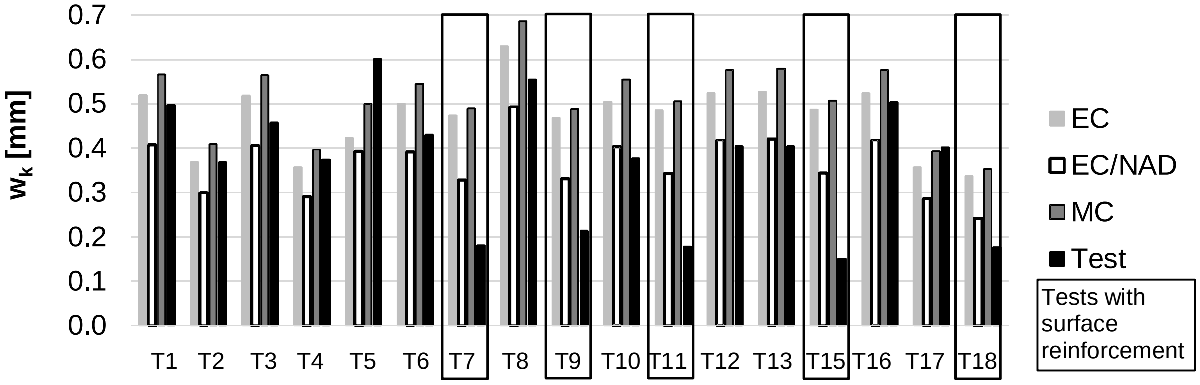

Figure 3-41 Characteristic crack widths (95%-fractile values) obtained in the undisturbed length of tests T1 to T18 and characteristic calculated crack width according to [EC2], [EC2/NA] and [MC2010] for σ_s = 320 MPa without consideration of surface reinforcement

Considering the effects of surface reinforcement for tests T7, T9, T11, T15 and T18 gives the characteristic crack widths according to [EC2], [EC2/NA] and [MC2010] that are shown in Figure 3-42.

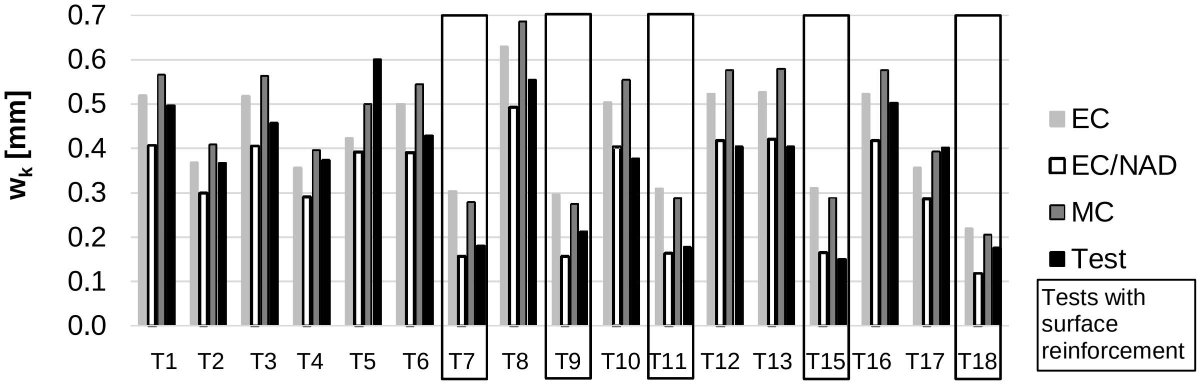

Figure 3-42 Characteristic crack widths (95%-fractile values) obtained in the undisturbed length of tests T1 to T18 and characteristic calculated crack width according to [EC2], [EC2/NA] and [MC2010] under consideration of surface reinforcement (within σ_s, $\rho_{s,eff}$ and $Ø_{eq}$)

Figure 3-43 shows the mean calculated crack widths obtained in the undisturbed length $w_{95\%,ud}$ in tests and according to [EC2], [EC2/NA], [MC2010] under consideration of the surface reinforcement. The mean values $w_{m,EC}$ were obtained by dividing the values w_k calculated from [EC2] by 1.7. The crack widths calculated from [EC2/NA] and [MC2010] were divided by 1.25 to obtain the mean values $w_{m,EC2/NAD}$ and $w_{m,MC}$. These factors are derived in chapter 2.10. Considering the conversion factors, the crack widths according to [EC2] and [EC2/NA] are very similar. The mean crack width according to [MC2010] is larger than the other values, since [MC2010] uses a conversion factor of 1.25 only and includes an addend for the deteriorated bond zone close to the cracks. This addend leads to larger calculated crack widths. The [EC2] values are closer to the measured values for lower concrete cover (T2, T4 and T5).

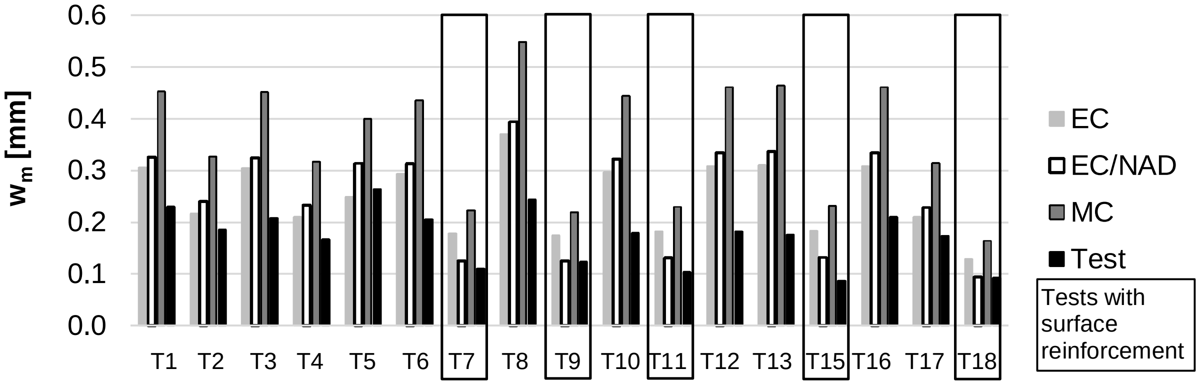

Figure 3-43 Mean crack widths obtained in the undisturbed length in tests T1 to T18 and mean calculated crack width according to [EC2], [EC2/NA] and [MC2010] under consideration of surface reinforcement

Figure 3-44 shows the ratio of the mean measured crack widths $w_{m,ud}$ in the undisturbed length at the load that conforms to σ_s = 320 MPa (with surface reinforcement: σ_s = 260 MPa) to the calculated crack widths $w_{m,EC}$ applying a conversion factor of 1.7. [EC2] presumes a maximum crack spacing equal to twice the development length of the reinforcement (cf. Figure 2-26). The real crack spacing in the stabilised cracking phase in structural elements is a value between one and two times the development length. Since the crack width is proportional to the crack spacing, the test results $w_{m,ud}$ should be in the range of the calculated value $w_{m,EC}$ and 50 % of this value. Figure 3-44 shows that this requirement is met for all tests except T5.

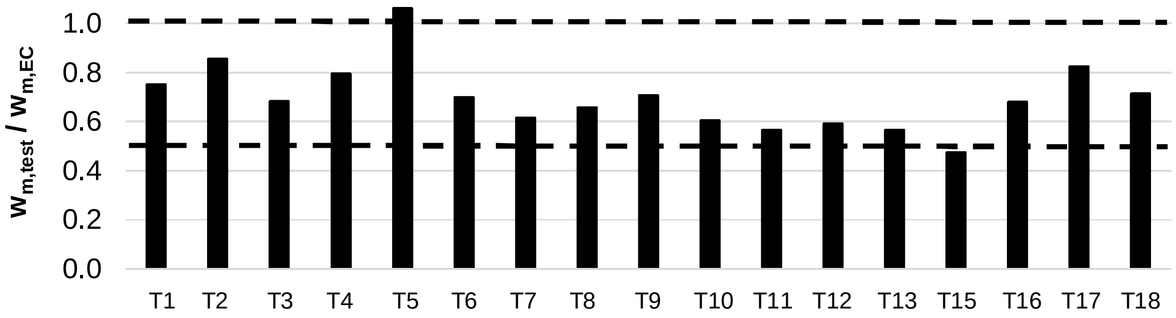

Figure 3-44 Relation of mean crack widths measured in the undisturbed length in tests to mean crack widths calculated from [EC2] with $w_{m,EC} = w_{k,EC} / 1.7$ at $\sigma_s = 320$ MPa (tests with surface reinforcement $\sigma_s = 260$ MPa) under consideration of surface reinforcement

The strain difference $\varepsilon_{sm} - \varepsilon_{cm}$ for the calculation of crack widths according to [EC2] equals the strain difference according to [EC2/NA]. The ratios of the mean crack widths measured in the beam tests $w_{m,test}$ to the calculated crack widths according to [EC2/NA] $w_{m,NAD}$ at $\sigma_s = 320$ MPa (with surface reinforcement: $\sigma_s = 260$ MPa) are given in Figure 3-45. A conversion factor 1.25 was applied for $w_{m,NAD} = w_{k,NAD} / 1.25$. In this case, the ratio $w_{m,test} / w_{m,NAD}$ falls below 1.0 in test T5, since the concrete cover is not taken into account in the crack spacing equation in [EC2/NA] ($s_{r,max} = Ø_{eq} / (3.6 \cdot \rho_{s,eff})$). Contrary to the crack spacing equation according to [EC2] ($s_{r,max} = k_3 \cdot c + k_1 \cdot k_2 \cdot k_4 \cdot Ø_{eq} / \rho_{s,eff}$), the crack spacing according to [EC2/NA] does not consider the smaller concrete cover in test T5 and the ratio $w_{m,test}/w_{m,NAD}$ is smaller than $w_{m,test}/w_{m,EC2}$.

In contrast, the ratios $w_{m,test} / w_{m,calc}$ for tests T7, T9, T11, T15 and T18 are higher when calculated according to [EC2/NA] than according to [EC2]. This effect is also due to the consideration of concrete cover in the crack spacing equation in [EC2]. When taking the equivalent bar diameter $Ø_{eq}$ into account, the crack spacing according to [EC2/NA] decreases stronger than the [EC2] crack spacing. Therefore, the crack width according to [EC2/NA] also decreases strongly, and the ratio $w_{m,test} / w_{m,NAD}$ increases.

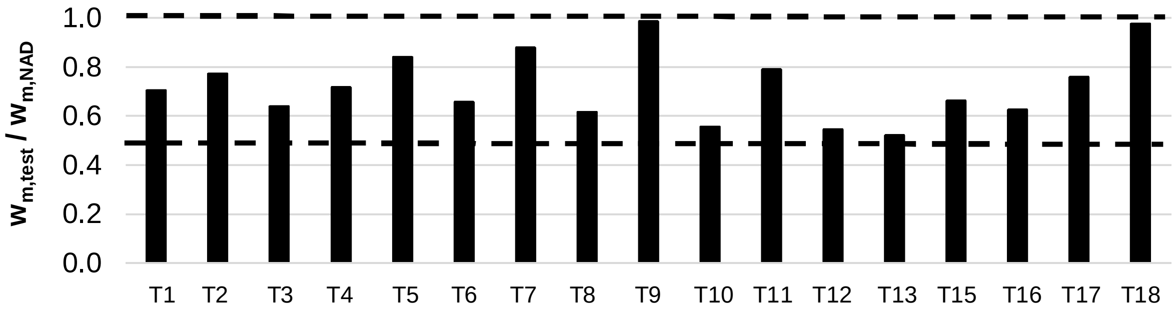

Figure 3-45 Relation of mean crack widths measured in the undisturbed length in tests $w_{m,test}$ to mean crack widths in the undisturbed length $w_{m,NAD}$ calculated from [EC2/NA] with $w_{m,NAD} = w_{k,NAD} / 1.25$ at $\sigma_s = 320$ MPa (tests with surface reinforcement $\sigma_s = 260$ MPa) under consideration of surface reinforcement

Figure 3-46 shows the ratio $w_{m,test}$ / $w_{m,MC}$ of the mean measured crack widths at the load that conforms to σ_s = 320 MPa (with surface reinforcement: σ_s = 260 MPa) to the calculated crack widths according to [MC2010] applying a conversion factor of 1.25. The test values are approximately half the calculated values instead of expected values between 0.5 and 1.0.

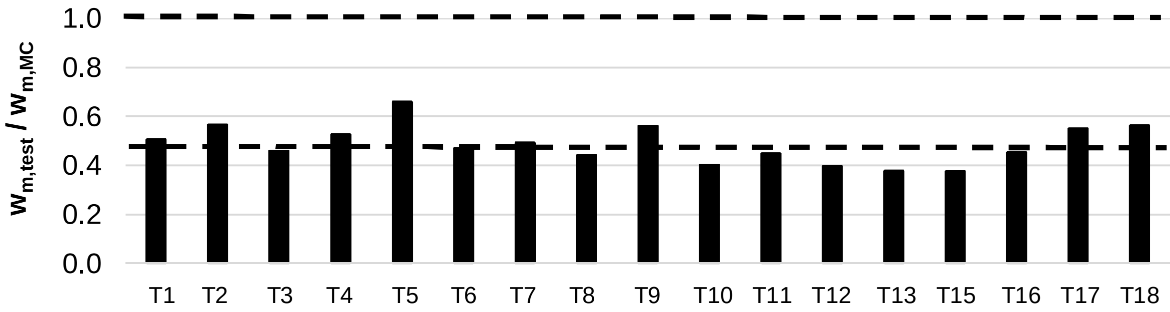

Figure 3-46 Relation of mean crack widths $w_{m,test}$ measured in the undisturbed length in tests to mean crack widths calculated from [MC2010] with $w_{m,MC} = w_{k,MC}$ / 1.25 at σ_s = 320 MPa (tests with surface reinforcement σ_s = 260 MPa) under consideration of surface reinforcement

Influence of Concrete Strength

The increase in concrete strength in test T4 (58 MPa instead of 38 MPa) lead to reduced crack widths in the undisturbed beam length, in the lap and at the ends of the lap (cf. Figure 3-47, left). The mean crack widths at the lap ends at 320 MPa were 0.66 mm for 38 MPa and 0.48 mm for 58 MPa. The decrease in crack width for higher concrete strength can be explained by the increasing bond strength and concrete contribution in tension between cracks for higher concrete strength. Figure 3-47 shows the crack widths in the lap (“lap”) at the lap ends (“end”) and in the undisturbed beam (“ud”).

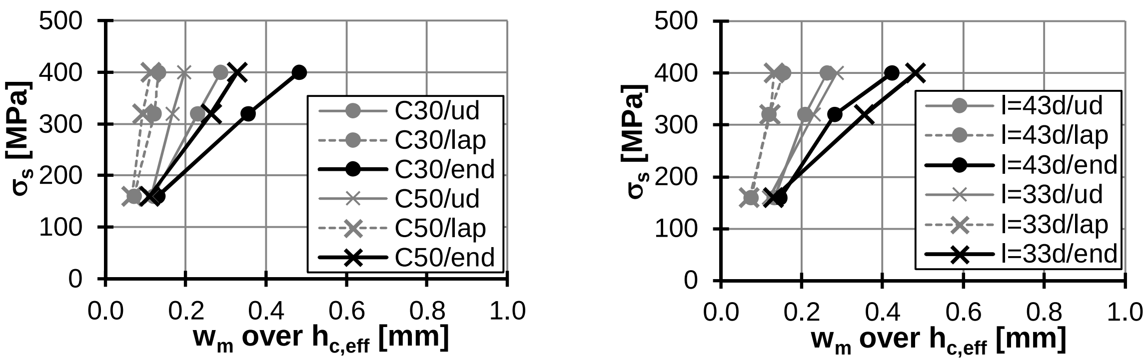

Figure 3-47 Effect of concrete strength (left) and lap length (right) on mean crack widths w_m in the lap (lap), at the lap ends (end) and in the undisturbed beam (ud)

Influence of lap length

The mean crack widths of tests T1 with a lap length l_0 = 33 · Ø and T3 with a lap length l_0 = 43 · Ø are given in Figure 3-47 (right). The lap length in the tested range under static loading has no effect on the crack width at the lap ends. The mean crack width at 320 MPa at the lap ends was 0.66 mm for l_0 = 33 · Ø and 0.61 mm for l_0 = 43 · Ø. The mean crack width averaged over the beam length is smaller in the beam with the longer lap, since a longer part of the beam has the doubled reinforcement ratio. The mean crack width along the entire beam is 0.21 mm for the beam with the lap length of 1310 mm (lap proportion 1310 mm / 3500 mm = 37 %). The mean crack width along the beam with the 1750 mm lap is 0.18 mm (lap proportion 1750 / 3500 = 50 %).

Influence of Bar Diameter

The bar diameter mainly influences the crack width at the lap ends. In lap tests T1 (Ø 40 mm), T3 (Ø 40 mm), T8 (Ø 50 mm) and T17 (Ø 28 mm), the concrete cover was a multiple of the bar diameter (c = 1.5 · Ø). For the increasing concrete cover with increasing bar diameter, the influence of the bar diameter in the tests conducted is related to the influence of the concrete cover. While the effect of bar diameter is small when comparing the mean crack width in the undisturbed beam, the mean crack width at the lap end is significantly higher for the 50 mm reinforcing bar (cf. Figure 3-48, left). The maximum crack widths at the lap ends show the same effect.

Influence of Surface Reinforcement

Surface reinforcement effectively reduced the crack widths in the undisturbed beam, within the lap and at the lap ends as shown in Figure 3-48 (right). This effect is even more pronounced for the fractile values of the crack width and for the maximum values. The maximum crack widths at the lap ends at 320 MPa are 0.61 mm without (T3) and 0.26 mm with surface reinforcement (T7).

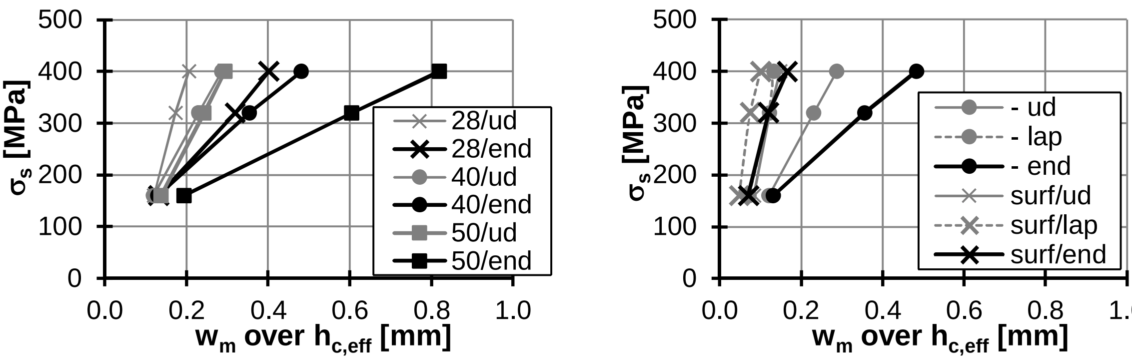

Figure 3-48 Effect of bar diameter (left) and surface reinforcement (right) on mean crack widths w_m in the lap (lap), at the lap ends (end) and in the undisturbed beam (ud)

Test specimen T10 contained additional reinforcement at the lap ends to reduce the crack width at the lap ends. This additional reinforcement conformed with the longitudinal surface reinforcement but only had a length of 60 cm. This reinforcement effectively reduced the crack width at the lap ends, but lead to large crack widths at the ends of the additional reinforcement. Hence, this additional reinforcement only transfers the large crack width from the lap end towards the undisturbed beam and the lap and is therefore not recommended.

Influence of Cover and Lap Spacing

A reduced concrete cover of 1.0 · Ø (T2) instead of 1.5 · Ø (T1) led to a slight decrease in mean crack width in the undisturbed beam and in the lap. This corresponds with the additional term in crack-spacing equations for bond deterioration determined by the size of the concrete cover described in chapter 2.10. In contrast, the mean crack width at the lap ends was higher for the smaller concrete cover (cf. Figure 3-49, left). The maximum crack widths at the lap ends at 320 MPa were comparable for both covers (0.68 mm for c = 1.0 · Ø and 0.66 mm for c = 1.5 · Ø).

In tests T1 and T5, the lap distance was increased from c_s = 2 · Ø to c_s = 4 · Ø. This lead to a decrease in reinforcement ratio (ρ = 3.6 % for c_s = 2 · Ø and ρ = 2.8 % for c_s = 4 · Ø). The mean crack widths at 320 MPa in the undisturbed beam increased with decreasing reinforcement ratio (cf. Figure 3-49, right). This observation conforms with the crack width theory, expecting smaller crack width for increasing reinforcement ratio. The mean crack width at the lap end was about the same size for both reinforcement ratios, or lap distances respectively. In contrast, the maximum crack width at 320 MPa was significantly higher for the smaller reinforcement ratio at the lap ends (T2 (c_s = 2 · Ø, ρ = 3.6%): w_{max} = 0.68 mm, T5 (c_s = 4 · Ø, ρ = 2.8%): w_{max} = 0.9 mm).

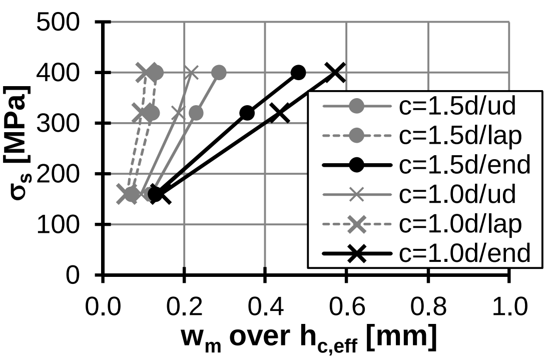

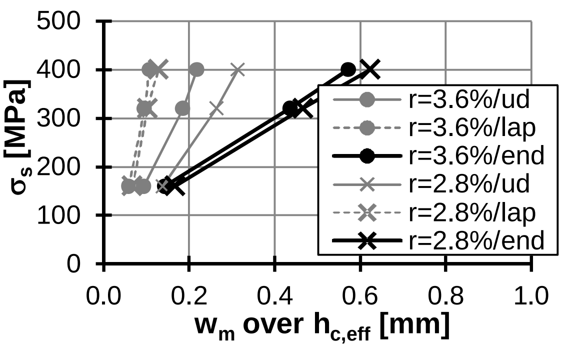

Figure 3-49 Effect of concrete cover c (left) and reinforcement ratio ρ (right) on mean crack widths w_m in the lap (lap), at the lap ends (end) and in the undisturbed beam (ud)

Effect of Transverse Reinforcement

Tests T3 and T6 were conducted with different stirrup numbers in the laps. The stirrups were concentrated at the lap ends in all tests. Test T3 had eight stirrups in the lap, four were positioned at each lap end. Test T6 had seven stirrups at each lap end. The effect of stirrup number is shown in Figure 3-50 (left). The mean and maximum crack widths at 320 MPa at the lap ends were higher for more stirrups per lap end. The crack widths in the undisturbed beam and in the lap were the same in both tests. Transverse reinforcement is therefore not capable of a crack width reduction at lap ends.

Effect of Percentage of Bars Lapped at a Section

Test T12 had one lapped reinforcing bar and a lapped bar proportion of 33 %, only. Test T13 had a lapped-bar percentage of 66% with two lapped bars. For the smaller reinforcement ratio within the lap, the 33 % and 66 % laps had larger crack widths within the lap. When less than 100 % of bars were lapped at a section, the mean crack width at the lap ends decreased (cf. Figure 3-50, right). The mean crack widths at 320 MPa in the undisturbed beam was the same for the tests with 33 % , 66 % and 100 %.

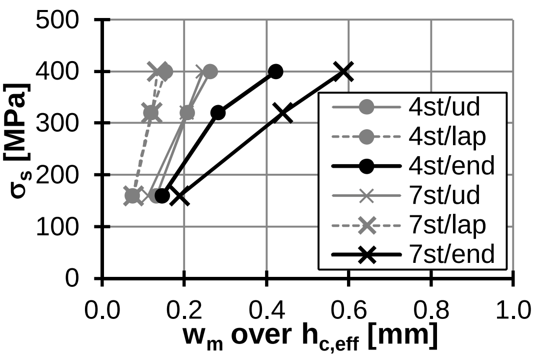

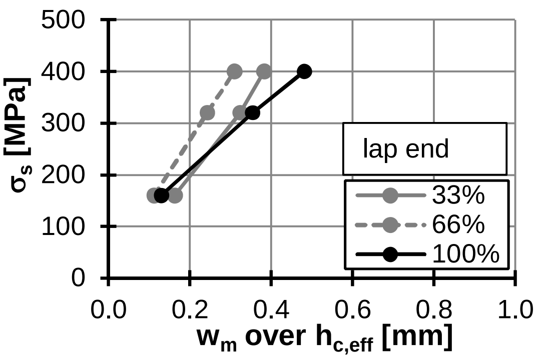

Figure 3-50 Effect of stirrup number (left) and percentage of bars lapped at a section at lap ends (right) on mean crack widths w_m in the lap (lap), at the lap ends (end) and in the undisturbed beam (ud)

Effect of Bar Diameter Combination

In test T15 and T16, three 40 mm bars were lapped with six 28 mm bars. Test T16 without surface reinforcement is compared to test T3 with Ø 40 mm bars and to test T17 with Ø 28 mm bars. The crack widths in the undisturbed beam were smallest for the 28 mm bars, both in test T17 and in test T16 at the beam side with the 28 mm bars. Figure 3-51 (left) gives the crack width for the combined beam at the 40 mm bar side (40 / (28) mm in Figure 3-51, left) and at the 28 mm bar side ((40) / 28 mm in Figure 3-51, left). The mean crack width at the lap ends of the combined lap was even smaller than at the lap ends of the 28 mm bar (Figure 3-51, right).

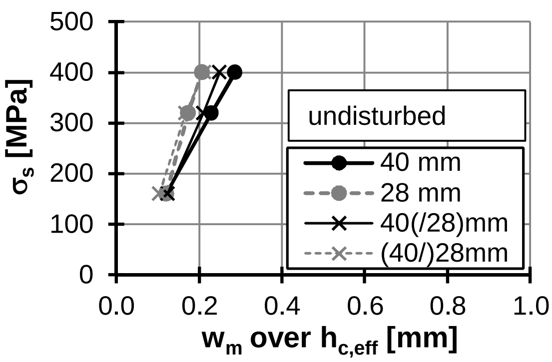

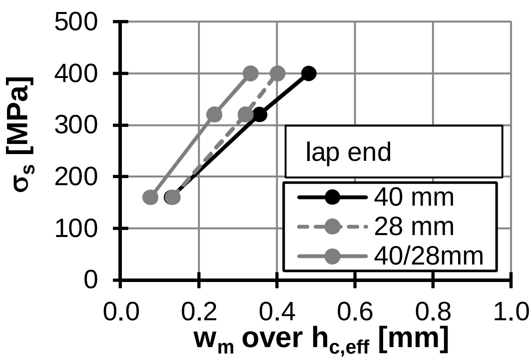

Figure 3-51 Effect of bar diameter combination on mean crack widths in the undisturbed beam (left) and at the lap ends (right)

Effect of Loading Type

The effects of long-term and cyclic loads were not investigated within the test programme described. Cyclic loads and long-term effects deteriorate the bond between concrete and reinforcing steel and increase the slip at the lap ends [REH77], [FIB10]. While crack widths were independent from the lap length in the described lap tests under monotonic loading, crack widths at lap ends subjected to cyclic loads do depend on the lap length [ELI79].

3.4.7 Conclusion on Crack Width in Laps

The crack width evaluation for monotonic loading showed that the crack widths at lap ends may be reduced by increasing concrete strength, bar diameter reduction and continuous reinforcing bars. The lap length and the positioning of transverse reinforcement did not influence the crack widths at lap ends in the conducted lap tests under monotonic loading. In contrast, the lap length does influence the crack width at lap ends under sustained or cyclic loading [ELI79].

The experimentally determined crack widths are compared to the acceptance criteria according to EUROCODE 2 [EC2], the GUIDE TO GOOD PRACTICE [DEU06], SCHIEßL [SCH98a] and ELIGEHAUSEN [ELI79] that were described in chapter 2.10.

Table 3-8 gives a comparison of the characteristic crack widths obtained in tests T1 to T18 and the maximum crack widths at the lap ends with the characteristic crack widths according to [EC2].

Table 3-8 Characteristic crack widths measured in the lap tests at σ_s = 320 MPa (w_{beam} = crack width along the entire beam length, w_{ud} = crack width along the undisturbed length), maximum crack width at lap end $w_{max,end}$ and according to [EC2] under consideration of surface reinforcement

Test	Test parameter	$w_{95\%,beam}$	$w_{95\%,ud}$	$1.25 \cdot w_{95\%,ud}$	$w_{max,end}$	$w_{k,EC}$
		[mm]	[mm]	[mm]	[mm]	[mm]
T1	c=1.5·Ø, α_6 = 1.5	0.59	0.50	0.63	0.59	0.52
T2	c=1.0· Ø, α_6 = 1.5	0.45	0.37	0.46	0.68[1]	0.37
T3	c=1.5· Ø, α_6 = 2.0	0.39	0.46	0.58	0.40	0.52
T4	as T2 with 60 MPa	0.36	0.37	0.46	0.40	0.36
T5	as T2 with c_s = 4 · Ø	0.58	0.60	0.75	0.90[1]	0.42
T6	as T3 with more stirrups	0.46	0.43	0.54	0.75[1]	0.50
T7	as T3 with surf. reinfor.	0.17	0.18	0.22	0.23[1]	0.30
T8	as T3 with Ø 50 mm	0.49	0.55	0.69	0.70[1]	0.63
T9	as T1 with surf. reinf.	0.19	0.21	0.26	0.29[1]	0.30
T10	as T1 with add. reinf.	0.33	0.38	0.47	0.24	0.50
T11	as T9 without stirrups	0.17	0.18	0.23	0.20	0.31
T12	as T3 with 33 % lap	0.45	0.40	0.50	0.48	0.52
T13	as T3 with 66 % lap	0.37	0.40	0.50	0.35	0.53
T15	28/40 mm, surf.reinf.	0.15	0.15	0.19	0.16	0.31
T16	as 28/40 mm	0.37	0.50	0.63	0.38	0.52
T17	as T3 with 28 mm	0.38	0.40	0.50	0.49	0.36
T18	as T17 with surf. reinf.	0.17	0.18	0.23	0.27[1]	0.22

[1] value exceeds $1.25 \cdot w_{95\%,ud}$

Comparison with Acceptance Criteria According to EUROCODE 2 [EC2]

[EC2] does not define maximum crack widths, but gives a design method to calculate the necessary reinforcement for different acceptable crack widths. The comparison of the crack widths measured in the tests with the characteristic crack widths according to [EC2] in Table 3-8 shows that the characteristic crack widths in the tests were smaller than the calculated crack width in the undisturbed length of the beam, but also along the entire beam length. The maximum crack widths at the lap ends exceed the calculated crack widths according to [EC2]. The maximum crack widths at the lap ends represent single values, while the characteristic values according to [EC2] represent 95%-fractile values that allow for small crack numbers exceeding this value.

The crack widths in tests T2 and T5 with a concrete cover of 40 mm (1 · Ø) exceeded the characteristic values according to [EC2] when considering the entire beam length. In both tests, the 95% quantiles $w_{k95\%,test}$ were above the calculated crack widths $w_{k,EC}$ in all parts of the beam.

In the tests with surface reinforcement (T7, T9, T11, T15, T18), the characteristic crack widths were smaller than 0.2 mm when considering the entire beam length (Table 3-6). The measured crack widths were also smaller than the characteristic values according to [EC2] taking the equivalent bar diameter, the smaller bar stress and the increased reinforcement ratio into account.

Comparison with Acceptance Criteria According to SCHIEßL [SCH98a]

SCHIEßL [SCH98a] recommends that the mean value of the data set of crack measurements shall be smaller than the defined limiting value w_{lim} and that the largest crack width - defined as the 95%-fractile of the sample - may not exceed the limiting value by more than 30 % ($w_{test,95\%} \leq 1.3 \cdot w_{lim}$). In contrast, the 95%-fractiles are determined by a classical statistical analysis with $w_{k,95\%} = w_m \cdot (1+1.645 \cdot V_x)$.

In the tests without surface reinforcement, the largest 95%-fractile value of the crack width including the lap end was 0.59 mm in test T1 (cf. Table 3-8). The requirement $w_{test,95\%} \leq 1.3 \cdot w_{lim}$ according to SCHIEßL [SCH98a] would therefore be met when defining w_{lim} = 0.45 mm. In the tests with surface reinforcement, the requirement that the largest crack width falls below 1.3-times the limiting value would be met for w_{lim} = 0.15 mm.

Comparison with Acceptance Criteria According to ELIGEHAUSEN [ELI79]

ELIGEHAUSEN [ELI79] recommends accepting crack widths at lap ends that are 25% larger than the crack width limits w_{lim} for the 95%-quantiles. The maximum crack widths at the lap ends exceeding 25 % of the 95%-fractile values along the entire beam length are indicated in Table 3-8. The maximum crack width at the lap ends in the test specimens with surface reinforcement T7, T9 and T18 exceed 1.25-times the 95%-fractile values, but the absolute values are small. For the test specimens without surface reinforcement, the acceptance criteria is not met in tests with small concrete cover T2 and T5, but neither in test T6 with increased transverse reinforcement.

Comparison with Acceptance Criteria According to GUIDE TO GOOD PRACTICE [DEU06]

Single crack widths shall not exceed 0.4 mm to 0.5 mm [DEU12] and the percentages of exceedance shall not be larger than the following values [DEU08], [DEU06]:

- $w_{k,lim.}$ = 0.4 mm (maximum 5 % exceedance)
- $w_{k,lim.}$ = 0.3 mm (maximum 10 % exceedance)
- $w_{k,lim.}$ = 0.2 mm (maximum 20 % exceedance)

In this case, the number of crack widths above the given limits is counted disrespecting the statistical distribution and the COV of the crack width measurement.

Table 3-9 gives a comparison of the percentages of crack widths measured in the tests below the limits $w_{k,lim.}$ with the defined crack width limits according to [DEU06]. The acceptance criteria are described in chapter 2.10.7. For example, where a crack width limit of 0.3 mm is defined, 90 % of the measured crack widths shall fall below this value [DEU06]. In all test specimens with surface reinforcement, the acceptance criteria were met. For test specimens without surface reinforcement, the criteria were not met in many cases.

Table 3-9 Comparison of the percentages of characteristic crack widths below $w_{k,lim}$ to the limits according to [DEU06] (bold values do not comply with the acceptance criteria)

	Percentages of crack widths below $w_{k,lim.}$					
	entire beam length			undisturbed length of beam		
	$w_{k,lim.} \leq$ 0.4 mm	$w_{k,lim.} \leq$ 0.3 mm	$w_{k,lim.} \leq$ 0.2 mm	$w_{k,lim.} \leq$ 0.4 mm	$w_{k,lim.} \leq$ 0.3 mm	$w_{k,lim.} \leq$ 0.2 mm
[DEU06] limits	*0.95*	*0.9*	*0.8*	*0.95*	*0.9*	*0.8*
T1	**0.91**	**0.83**	**0.55**	**0.90**	**0.77**	**0.45**
T2	**0.94**	0.94	**0.58**	1.00	1.00	**0.50**
T3	0.97	**0.87**	**0.68**	0.97	**0.84**	**0.52**
T4	**0.71**	**0.67**	**0.40**	0.98	0.92	**0.55**
T5	**0.89**	**0.68**	**0.53**	**0.89**	**0.61**	**0.39**
T6	**0.92**	**0.86**	**0.63**	0.97	**0.88**	**0.50**
T7[1]	1.00	1.00	0.99	1.00	1.00	1.00
T8	**0.89**	**0.83**	**0.67**	**0.88**	**0.75**	**0.42**
T9[1]	1.00	1.00	0.97	1.00	1.00	0.95
T10	1.00	0.92	**0.77**	1.00	0.94	**0.65**
T11[1]	1.00	1.00	0.98	1.00	1.00	0.98
T12	0.95	**0.85**	**0.68**	0.95	**0.87**	**0.68**
T13	0.98	0.91	**0.72**	0.97	**0.88**	**0.64**
T15[1]	1.00	1.00	0.98	1.00	1.00	0.96
T16	0.98	0.94	**0.67**	1.00	1.00	**0.59**
T17	0.97	**0.86**	**0.77**	1.00	**0.86**	1.00
T18[1]	1.00	1.00	0.96	1.00	1.00	0.97

[1] with surface reinforcement

Conclusion on Crack Widths in Lap Tests with Ø 40 mm Bars

- The mean measured crack widths are smaller than the mean calculated values according to [EC2], [EC2/NA] and [MC2010].
- The characteristic measured crack widths are not always smaller than the characteristic values calculated according to [EC2], [EC2/NA] and [MC2010], since the COV of the crack measurement along the entire beam including the lap was higher than 0.4.
- The calculated crack widths according to [EC2] and [EC2/NA] meet the test results better than [MC2010] that gives values well above the measured crack widths.
- The crack widths for a concrete cover $1.5 \cdot Ø = 60$ mm obtained in tests were similar to the calculated values, while the crack widths for a concrete cover $1.0 \cdot Ø = 40$ mm were larger than the calculated values. The effect of cover seems therefore overestimated in [EC2].
- For tests with surface reinforcement, the crack widths can be obtained from the design equations in [EC2] and [EC2/NA] with the equivalent bar diameter $Ø_{eq}$, the increased reinforcement ratio and the decreased bar stress.
- Surface reinforcement reduces the characteristic crack width (95%-fractile values) along the beam length to values below 0.2 mm.
- The maximum crack widths at lap ends exceed 1.25-times the 95%-fractile values of the crack widths along the entire beam length in some tests with and without surface reinforcement.
- The defined maximum percentages of crack widths exceeding the limits according to [DEU06] are met in the tests with surface reinforcement, but not in the test specimens without surface reinforcement.
- The maximum crack widths at the lap ends exceed the calculated values according to [EC2] and [EC2/NA], but are still acceptable, since the calculated values represent 95%-fractile values instead of maximum permissible values.

3.5 Anchorage Tests

3.5.1 Test-Specimen Dimensioning and Test-Setup

In [EC2], different required bond lengths and detailing rules are applied for anchorages and laps. The additional rules for large diameter bars in [EC2] are more restrictive for laps, but some additional rules apply to anchorages as well. To investigate the necessity of these rules and to clarify the differences between anchorages and laps, twelve anchorage tests were conducted. In structural elements, reinforcing bars are anchored at curtailed reinforcement and at the ends of beams and slabs. While anchorages at beam or slab supports benefit from transverse pressure, curtailed reinforcement lacks additional confinement by transverse pressure. The conducted beam-end tests also correspond to simply supported beam ends. To account for their frequent occurrence and for a direct comparison with the beam-end test results, anchorages were tested under transverse pressure in simply supported beams.

For the investigation of highly utilised anchorages, small concrete covers and bar spacings were chosen resulting in quite narrow test specimen. The specimen depth and reinforcement were designed to preclude bending and shear failure. The shear span does not influence the force to be anchored at the support. Where loads are close to the support, a certain percentage of the shear load is transferred directly into the support, but the full longitudinal reinforcing bar force has to be anchored at the support. The load was positioned close to the support with a shear span M / (V · d) = V · 1.0 / (V · 0.62) = 1.6. Six beams were cast and tested at each side. The tested setup had a cantilever to prevent an anchorage failure at the non-tested side of the specimen.

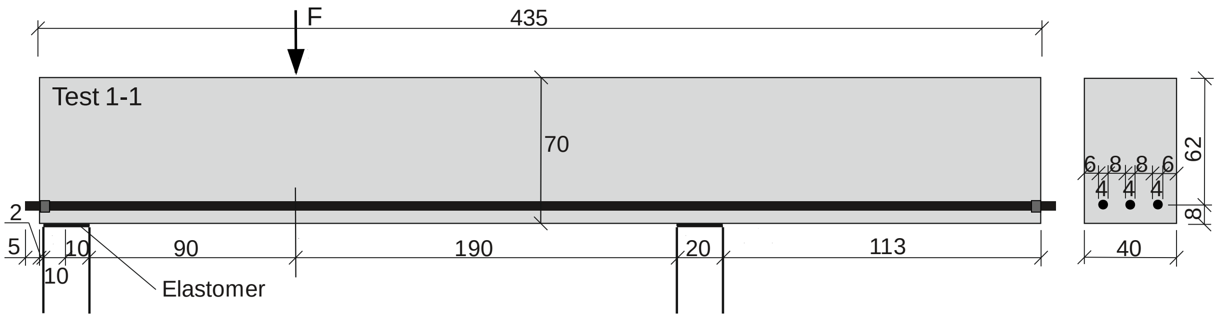

Figure 3-52 Test-setup of anchorage test V-1-1

The anchorage length $l_b = 5 \cdot Ø = 200$ mm was chosen in accordance with the beam-end tests. The mean bond strength according to [EC2] was calculated from

$$f_{bm} = 2.25 \cdot f_{ctm} = 2.25 \cdot 0.3 \cdot (30\ \text{MPa})^{2/3} = 6.5\ \text{MPa} \tag{3-10}$$

Taking the effect of transverse pressure with an increase in bond strength by 3/2 into account gives the maximum bar stress

$$\sigma_s = \frac{l_b \cdot 4 \cdot f_{bm}}{Ø} = \frac{200\ \text{mm} \cdot 4 \cdot 3/2 \cdot 6.5\ \text{Mpa}}{40\ \text{mm}} = 195\ \text{MPa} \tag{3-11}$$

The bar stress at the front edge of the support is

$$\sigma_s = \frac{\Delta F_{Ed} + F_s(M)}{A_s} = \frac{V_{max} \cdot \left(\frac{\cot\theta}{2} + \frac{l_x}{z}\right)}{A_s} \tag{3-12}$$

With

V_{max} maximum shear force at the support

θ inclination of struts

l_x distance from the centre of the support

z lever arm of internal forces

[EC2] defines the anchorages length commencing from the front edge of the support (cf. Figure 3-53, left). Corresponding to the crack theory for reinforced concrete members, each crack spacing in bending represents a value between one and two times the development length of the reinforcing bars. The anchorage length would therefore commence from the last bending crack from the support (cf. Figure 3-53, right). To investigate anchorages with and without defined lengths, some tests had cracks induced by a steel sheet at the front edge of the support.

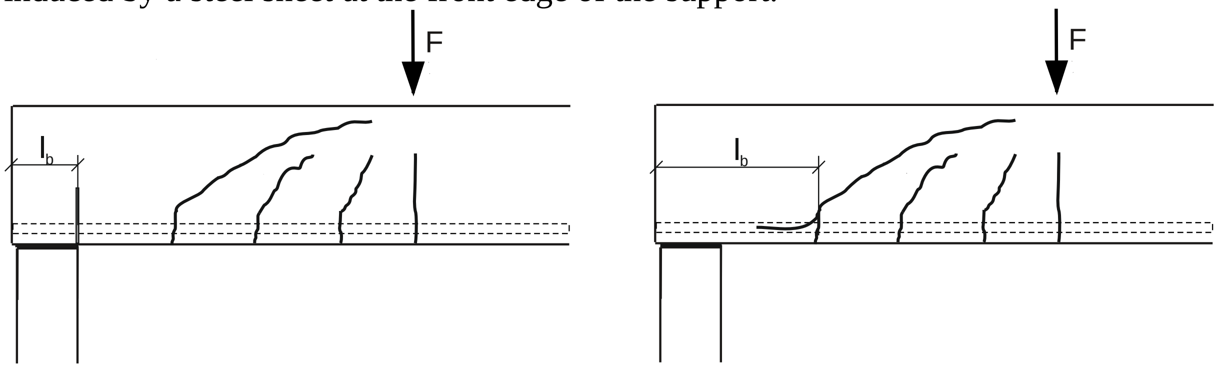

Figure 3-53 Bond length with (left) and without induced crack (right)

3.5.2 Test Parameter

In all anchorages, the longitudinal reinforcement anchored above the support consisted of three B500 reinforcing bars with Ø 40 mm. The concrete cover was consistently chosen to 1.5 · Ø corresponding with the beam-end and lap tests. The bar spacing was tested with 1 · Ø (V2 and V3), which corresponds with the minimum bar spacing according to most codes, and with an increased spacing of 2 · Ø. The mean concrete compression strength aimed for was 38 MPa. For a comparison, a mean strength of 60 MPa was tested in test V2.

In tests V1-2, V2-1, V2-2, V3-1 and V3-2, cracks were induced at the front edge of the support (cf. Figure 3-53, left).

In practice, anchorage lengths are longer than 5 · Ø, since the design bond strength f_{bd} is taken into account during design. The effect of anchorage length was tested by means of test specimen V-4 with a 440 mm bond length corresponding to the design bond strength f_{bd} for C30/37 according to [EC2]. The bond strength reduction for bar diameter in equation (2-10) was not taken into account ($\eta_2 = 1.0$).

$$l_b = \frac{Ø \cdot \sigma_{sd}}{4 \cdot f_{bd}} = \frac{40 \text{ mm} \cdot 195 \text{ MPa}}{4 \cdot 3/2 \cdot 3.04 \text{ MPa}} \approx 440 \text{ mm} \tag{3-13}$$

Where

$$f_{bd} = 3 / 2 \cdot 2.25 \cdot 0.3 \cdot 0.7 \cdot (30 \text{ MPa})^{2/3} / 1.5 = 3 / 2 \cdot 3.04 \text{ MPa} \tag{3-14}$$

In test specimen V5, the 40 mm bars were supplemented by two 28 mm bars. While in test V5-1 two straight 28 mm bars were positioned, a 28 mm bar-diameter bend was positioned in test V5-2. Table 3-10 summarises the test parameter of the conducted anchorage tests.

Test V6 was conducted to investigate the effect of transverse reinforcement within the anchorage length. While surface reinforcement according to [EC2] and stirrups were positioned in V6-1, test V6-2 was tested with two stirrups only.

Table 3-10 Overview of the conducted anchorage tests: anchored bars, concrete cover c_x and c_y, concrete strength f_{cm}, anchorage length l_b, bar spacing c_s and further parameters

Test	Anchored bars	c_x / Ø = c_y /Ø	f_{cm}	l_b / Ø	c_s / Ø	Stirrups	Induced crack	Additional reinforcement
	[mm]	[-]	[MPa]	[-]	[-]	[mm]		[mm]
V1-1	3 Ø 40	1.5	39.1	5.0	2.0	-	-	-
V1-2	3 Ø 40	1.5	39.1	5.0	2.0	-	x	-
V2-1	3 Ø 40	1.5	60.4	3.6	1.0	-	x	-
V2-2	3 Ø 40	1.5	60.4	3.6	1.0	2 Ø 14	x	-
V3-1	3 Ø 40	1.5	35.2	5.0	1.0	-	x	-
V3-2	3 Ø 40	1.5	35.2	5.0	1.0	2 Ø 8	x	-
V4-1	3 Ø 40	1.5	32.9	11.0	2.0	3 Ø 12	-	-
V4-2	3 Ø 40	1.5	32.9	11.0	2.0	-	-	-
V5-1	3 Ø 40	1.5	37.0	5.0	2.0	2 Ø 14	-	2 Ø 28 (straight)
V5-2	3 Ø 40	1.5	37.0	5.0	2.0	2 Ø 14	-	1 Ø 28 (bend)
V6-1	3 Ø 40	1.5	36.5	5.0	2.0	2 Ø 14[1]	-	-
V6-2	3 Ø 40	1.5	36.5	5.0	2.0	2 Ø 14	-	-

[1] plus surface reinforcement

3.5.3 Measurements and Test Procedure

The anchorage tests were loaded force-controlled up to 700 kN and displacement-controlled at higher loads. The deflection (DT1), the crack opening (DTCr) at the induced cracks and the slip (DTS) at the reinforcing bars were measured with displacement transducers. Strain gauges were applied to the reinforcing bars to record the strain along the anchorage length and the stirrup strain if positioned. The transverse concrete strain was measured with strain gauges and extensometers with a base distance of 100 mm (cf. Figure 3-54).

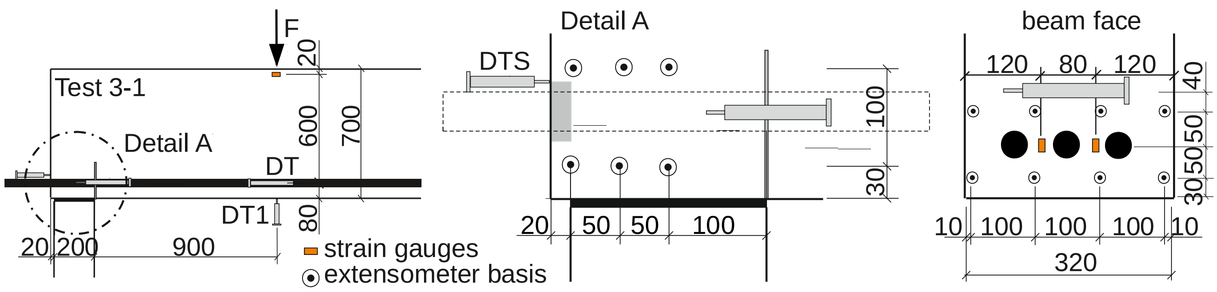

Figure 3-54 Instrumentation of anchorage test T3-1: side view (left), detail A (centre) and front view (right)

The increase in crack width was measured with a PEAK digital crack magnifier WIDE STAND MICRO (cf. Figure 3-19, (a)). The crack widths were measured at the height of the longitudinal reinforcement parallel to its direction. A digital photograph of the crack was taken at the intersection of a crack with the axis at each load level. Subsequently, the crack widths were determined using the software METRIC for the evaluation of the photographs. The bar stress σ_s calculated with equation (3-12) for each load level is given in Table 3-11.

Table 3-11 Load levels for crack measurements and corresponding bar stress σ_s and bond stress τ_b

Load Level	f_{cm}	l_b	V	$\cot\theta$	l_x	z	F_s	σ_s	τ_b
	[MPa]	[mm]	[kN]	[-]	[m]	[m]	[kN]	[MPa]	[MPa]
1	38	200	117	3.00	0.10	0.59	196	52	2.6
2	38	200	320	2.93	0.10	0.59	523	139	6.9
3	38	200	467	2.01	0.10	0.59	550	146	7.3
4	38	200	613	1.73	0.10	0.59	636	169	8.4

3.5.4 Test Results

Most test specimens failed by splitting within the anchorage length at the beam ends. The splitting was visible at the beam faces and at the bottom of the beam end above the support. Three tests (V2-1, V2-2 and V4-1) had substantial anchorage capacities and failed in the compression zone. The values of the averaged bond strength over the bond length l_b obtained in the test τ_{max} and the normalised, averaged bond strength $\tau_{max,n} = \tau_{max} \cdot (38 / f_{cm})^{2/3}$ are given in Table 3-2.

The bar stress F_s was calculated from

$$F_s = \Delta F_{Ed} + F_s(M) = V_{max} \cdot \left(\frac{\cot\theta}{2} + \frac{l_x}{z} \right) \qquad (3\text{-}15)$$

Table 3-12 Test results (maximum shear load V_{max}, inclination of compression strut θ, distance from the centre of the support l_x, lever arm of internal forces z, bar force F_s, maximum bar stress σ_{max} at the front edge of the support, and averaged bond strengths τ_{max} and $\tau_{max,n}$)

Test	f_{cm}	V_{max}	$\cot\theta$	$l_x = l_b/2$	z	F_s	σ_{max}	τ_{max}	$\tau_{max,n}$
	[MPa]	[kN]	[-]	[m]	[m]	[kN]	[MPa]	[MPa]	[MPa]
V1-1	39.1	1063	1.45	0.10	0.56	960	255	12.7	12.5
V1-2	39.1	1042	1.45	0.10	0.56	944	250	12.5	12.3
V2-1	60.4	>1106	1.37	0.07	0.45	933	> 248	> 17.2	>12.6
V2-2	60.4	>1103	1.37	0.07	0.45	931	> 247	> 17.2	>12.6
V3-1	35.2	679	1.51	0.10	0.56	635	169	8.4	8.9
V3-2	35.2	987	1.40	0.10	0.56	867	230	11.5	12.1
V4-1	32.9	>1299	1.39	0.22	0.59	1393	> 370	> 8.4	> 9.2
V4-2	32.9	1166	1.42	0.22	0.59	1266	336	7.6	8.4
V5-1	37.0	1373	1.39	0.10	0.585	1189	238	11.9	12.1
V5-2	37.0	1301	1.40	0.10	0.59	1134	227	11.3	11.5
V6-1	36.5	1230	1.41	0.10	0.59	1080	286	14.3	14.7
V6-2	36.5	1125	1.44	0.10	0.59	1001	266	13.3	13.6

Crack Development

While considerable shear cracks developed in the shear span, a shear failure was prevented by heavy transverse reinforcement. At high loads, the shear cracks proceeded into the anchorage towards the support. The distance between the front edge of the support and the first bending crack presumably also contributes to the anchorage length. The distance of the first bending crack to the front edge of the support was between 50 mm in tests V5-1 and V5-2 up to 250 mm in test V6-1. At failure, a large crack width was observed at a crack leading to the front edge of the support in all tests (cf. Figure 3-55).

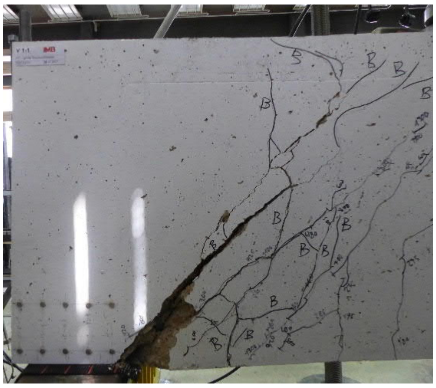

Figure 3-55 Crack pattern in test V1-1 without induced crack (left) and test V1-2 with induced crack (right) after failure

For this reason, the evaluation of test results is conducted with an anchorage length equal to the length of the support only. The distance from the front edge of the support to the first bending crack was not considered in the evaluation.

Splitting cracks occurred at the face and bottom side of the test specimen. Most anchorages remained uncracked in the test specimen sides. Longitudinal cracks parallel to the longitudinal reinforcement at the test specimen sides were only observed in tests V1-2, V4-2, V5-2 and V6-2. The anchorages in tests V2-1, V2-2 and V4-1 remained uncracked.

Figure 3-56 shows examples of crack patterns at the bottom side of the test specimens. In tests V3-1 and V3-2 with small bar spacing ($c_s = 1.0 \cdot Ø$) three longitudinal cracks developed in the bottom cover c_y (cf. Figure 3-56, left). In test V3-2, the longitudinal crack widths were reduced by the positioned transverse reinforcement. The crack development in V1-1 and V1-2 was independent from the positioned steel sheet. Both tests V1 had a bar spacing $c_s = 2.0 \cdot Ø$ and did not include transverse reinforcement. In contrast to test V3, the splitting failure changed into a combined concrete cone pry-out and splitting failure in V1 (cf. Figure 3-56, left centre) . The splitting cracks outside the support were still visible. In tests V6-2 with stirrups and V6-1 with stirrups and additional surface reinforcement, no cracks developed below the intermediate bar. While V6-2 still had a combined concrete cone pry-out and splitting failure (cf. Figure 3-56, right centre), the positioned surface reinforcement lead to a mere concrete cone pry-out (cf. Figure 3-56, right).

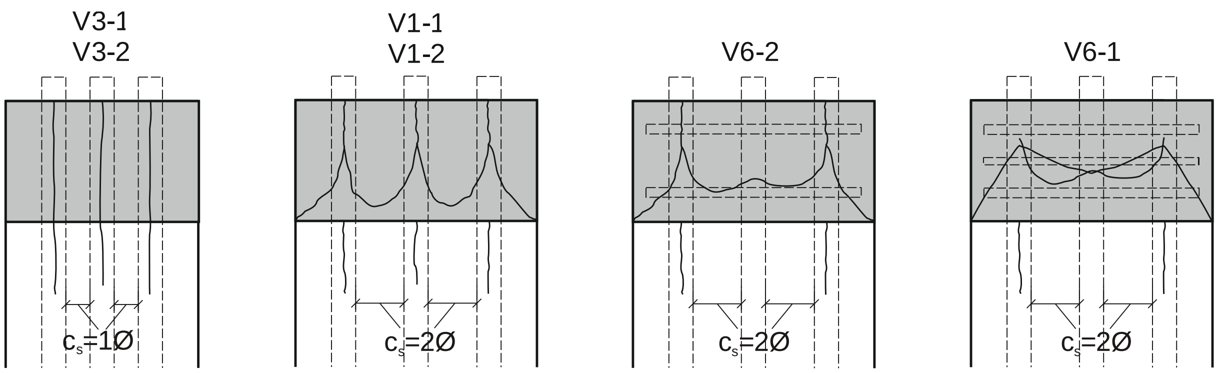

Figure 3-56 Crack patterns at the bottom side of test V3-1/V3-2 with small bar spacing ($c_s = 1 \cdot Ø$), test V1-1/V1-2 ($c_s = 2 \cdot Ø$) without stirrups, test V6-2 with $c_s = 2 \cdot Ø$ and stirrups and test V6-1 with $c_s = 2 \cdot Ø$, stirrups and surface reinforcement

Tests V3-1 and V3-2 both had an unfavourable steel sheet geometry for the induced crack and unfavourably bundled cables for the instrumentation. Therefore, a T-shaped crack pattern occurred at the test specimen face above the anchored bars. Around the bars, a face-split failure was observed, while a side split failure was expected [HEG18].

Reinforcing Bar Strain within the Anchorage Length

The distribution of steel strain ε_s along laps observed in the four-point bending tests (cf. Figure 3-22) conformed to previous findings. For anchorages in simply supported beams, detailed investigations of the strain distribution have not been conducted, yet. Thus, several strain gauges were applied to the anchored bars in the conducted tests to generate information on the strain decrease at end anchorages.

Figure 3-57 gives the theoretical bar force F_s according to equation (3-15) at the support as the sum of the bar force resulting from the bending moment $F_s(M)$ and the additional force ΔF_s resulting from shear. The stress values were calculated with a cross-sectional area of the reinforcing bars of $A_s = 3771$ mm². Figure 3-57 also gives the theoretical reinforcing bar stress $\sigma_s = F_s / A_s$ and corresponding bar strain ε_s at different positions. For cotθ = 1.45, V = 1600 kN · 2/3 and z = 0.56 m.

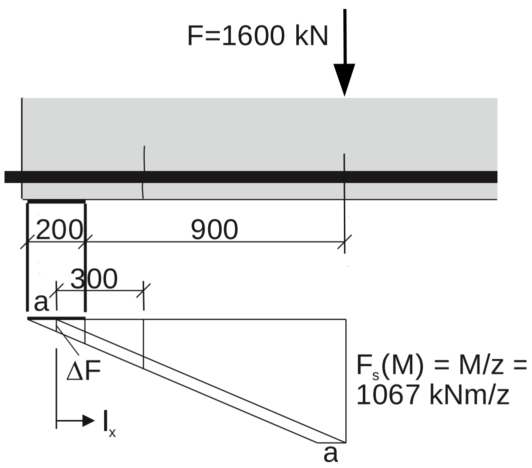

		end	centre	front	crack
position l_x	[mm]	-100	0	100	300
M	[kNm]	0	0	107	320
$F_s(M)$	[kN]	0	0	249	744
ΔF_s	[kN]	0	754	754	754
F_s	[kN]	0	754	1003	1498
σ_s	[MPa]	0	200	266	397
ε_s	[‰]	0	1.0	1.33	1.99

Figure 3-57 Bending moment M, bar force F_s, bar stress σ_s and bar strain ε_s at the support

Figure 3-58 shows the measured steel strain in tests V1-1 without and V1-2 with an induced crack at the front edge of the support. For the short anchorages tested, a linear strain increase was presumed for the anchored bars. The strain measurements in the anchorage tests without induced crack (cf. Figure 3-58 to Figure 3-61) indicate that the bar force is not anchored linearly at the support, but greater parts are transferred towards the end of the anchorage length and between the front edge of the support and the first bending crack.

Figure 3-58 (right) shows that the strain distribution is slightly different in tests with steel sheets inducing a crack at the front edge of the support. In this case, the measured steel strain ε_s at the front edge of the support equals the theoretical value (1.3 ‰ for V = 1560 kN, cf. Figure 3-57). While the surrounding concrete contributed to the longitudinal load transfer in test V1-1 without steel sheet, the cross-section at the front edge of the support in test V1-2 coincided with a crack without concrete contribution to load transfer. Therefore, the measured steel strain in test V1-1 is higher than in test V1-2 (cf. Figure 3-58).

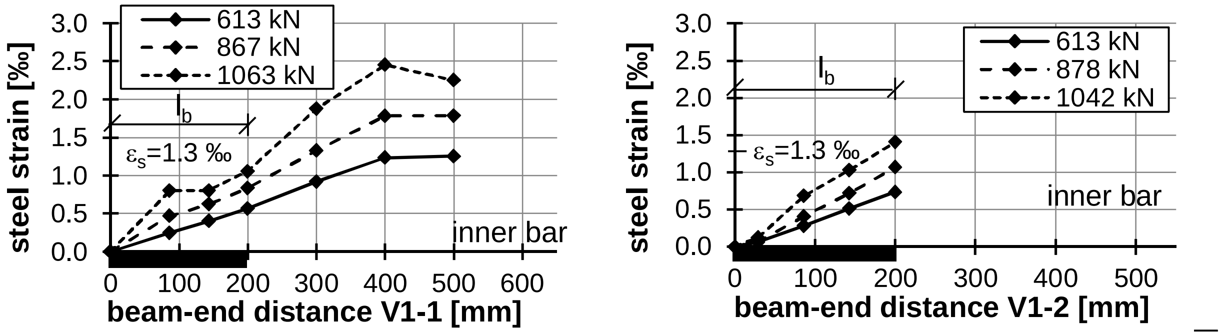

Figure 3-58 Steel strain in test V1-1 without steel sheet for induced crack (left) and steel strain in test V1-2 with induced crack (right)

When positioning stirrups along the anchorage length (tests V6-1 and V6-2), the longitudinal reinforcing bar strain at the front edge of the support decreases (cf. Figure 3-58, left and Figure 3-59). Since the steel strain is smaller within the support in tests V6-1 and V6-2 with stirrups, the reinforcing bar stress increases stronger before the support. Thus, the anchorage length in the test specimens without induced crack begins at the first bending crack before the support.

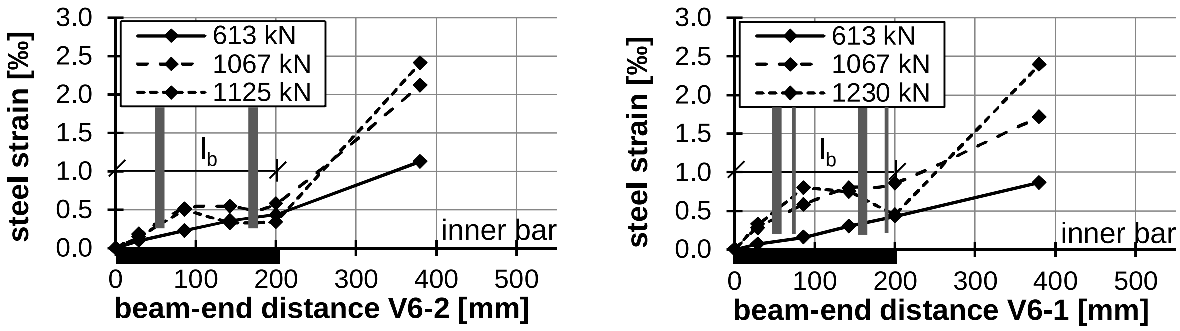

Figure 3-59 Steel strain in test V6-2 with stirrups (left) and in test V6-1 with stirrups and additional surface reinforcement (right)

The stronger steel strain increase towards the end of the beam (and the anchorage) was observed both in tests with anchorage lengths of 5.0 · Ø (V1 and V6) and 11.0 · Ø (V4) (cf. Figure 3-60).

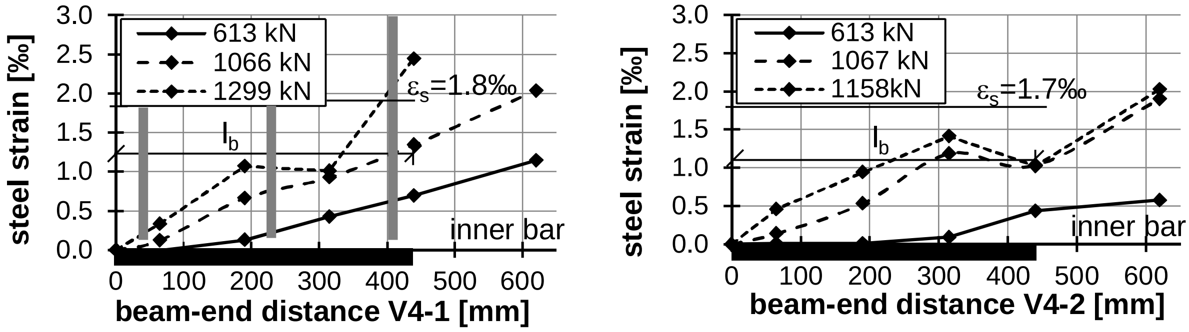

Figure 3-60 Tests V4-1 with increased anchorage length (l_b = 440 mm, first bending crack about 30 mm from support) with stirrups (left) and V4-2 with increased anchorage length (l_b = 440 mm, first bending crack within anchorage length) without stirrups (right)

In test V4-1with stirrups, the first bending crack appeared at a distance of approximately 30 mm from the front edge of the support. Test V4-2 without stirrups had a bending crack even commencing into the anchorage length.

The calculated reinforcing bar strain at maximum shear load ε_s = 1.8 ‰ (V4-1, V_{max} = 1299 kN) and ε_s = 1.7 ‰ (V4-2, V_{max} = 1158 kN) is given in Figure 3-60. Test V4-1 with stirrups reaches this reinforcing bar strain at maximum load, while the strain in test V4-2 without stirrups remains well below the calculated value.

Effect of Bond Length

For comparison, the anchorage length is defined as the length of the support in the tests with and without induced crack. The length of the support of the Ø 40 mm bars was 200 mm (l_b / Ø = 5.0) in tests V1-1, V1-2, V6-1 and V6-2, but 440 mm (l_b / Ø = 11.0) in tests V4-1 and V4-2. The transferrable bar stress increased with increasing bond length. In the test specimens without transverse reinforcement (V1-1 and V4-2), the maximum shear force increased by 10 %. In the test specimens with transverse reinforcement (V6-2 and V4-1), the maximum shear force increased by more than 15 %. Test specimen V4-1 reached the capacity of the hydraulic cylinder (2 MN) and could not be loaded further. The normalised, averaged bond stress over the bond length was smaller in long anchorages ($\tau_{max,n,11\cdot Ø}$ ≈ 8.4 MPa and $\tau_{max,n,5\cdot Ø}$ ≈ 12.5 MPa).

Figure 3-61 shows the bond stress distribution over both anchorage lengths calculated from the steel strain measurements with discrete strain gauges. The maximum local bond strength calculated from the strain measurements was about 18 MPa in both cases. The 440 mm anchorage had a longer intermediate section with constant bar stress not contributing to the load transfer (cf. Figure 3-61, right).

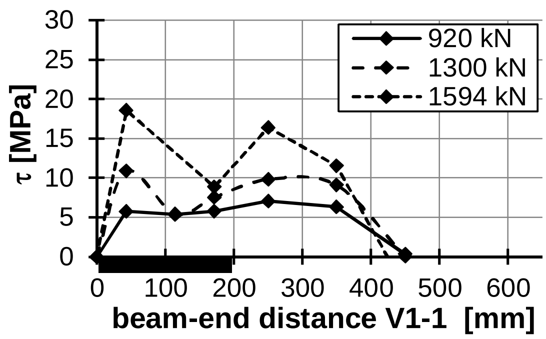

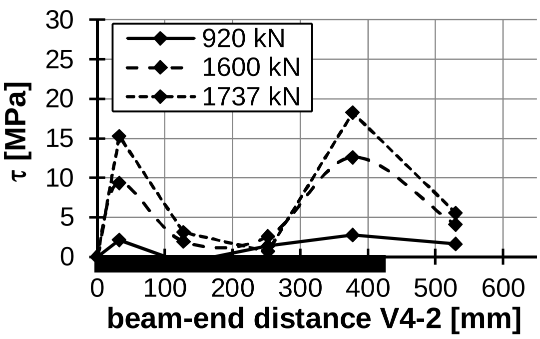

Figure 3-61 Local bond stress τ vs. the distance from the beam-end in test V1-1 with 200 mm anchorage length (left) and in test V4-2 with 440 mm anchorage length (right) calculated from strain measurements

Effect of Induced Crack

When inducing a bending crack at the front edge of the support, the maximum shear force did not change. Test specimen V1-1 reached a shear force equal to 1063 kN and V1-2 a shear force equal to 1042 kN. Despite the longer anchorage length consisting of the length of the elastomer plus the distance to the first bending crack in test V1-1, the maximum load was not higher than in test V1-2, where the anchorage length was defined by the steel sheet. The steel strain at the induced crack was slightly increased compared to the undisturbed anchorage, since the surrounding concrete contributed to the load transfer at the front edge of the support (cf. Figure 3-58).

Effect of Concrete Strength

The test specimens V2 and V3 were tested with different concrete strength and adapted anchorage length. The concrete strength of V2 was 60.4 MPa and the anchorage length 144 mm. In test V3, the anchorage length was 200 mm at a concrete strength of 35.2 MPa. The concrete cover and bar spacing were the same in both tests. The concrete under the load application failed in both tests V2. The maximum transferrable shear force in tests V2-1 and V2-2 ($f_{cm} = 60.4$ MPa) was more than 1100 kN ($\tau_b > 17$ MPa, $\sigma_s > 248$ MPa). The maximum strength was not reached, since the test specimen failed in compression at the load application.

Tests V3-1 and V3-2 reached a shear force of 679 kN (without stirrups) and 987 kN (2 Ø 8 mm stirrups) respectively. Presuming a failure of test V2-1 close to 1100 kN, the observed bond strength increase corresponds to the model according to [FIB14]. The comparison on the basis of the design model according to [FIB14] allows for the consideration of the different anchorage lengths. The bar stress obtained in test V3-1 (169 MPa) corresponds with a theoretical bar stress of 230 MPa for test V2 with

$$\sigma_{V2} = \sigma_{V3-1} \cdot \left(\frac{f_{cm,V2}}{f_{cm,V3}}\right)^{0.25} \cdot \left(\frac{l_{b,V3}}{l_{b,V2}}\right)^{0.55} = 169 \cdot \left(\frac{60.4}{35.2}\right)^{0.25} \cdot \left(\frac{200}{145}\right)^{0.55} = 231\,\text{MPa} \qquad (3\text{-}16)$$

Effect of Bar Spacing

The bar spacing was varied in tests V1 ($c_s = 2.0 \cdot Ø$) and V3 ($c_s = 1.0 \cdot Ø$). For the unfavourable steel sheet geometry in test V3, the test results are not directly comparable. The ratio of the maximum shear load in tests V3-1 and V1-2 is 679 kN to 1042 kN (cf. Table 3-12) which represents a decrease by 35 % for smaller bar spacing.

Effect of Transverse Reinforcement

Tests V1-1 and V6-2 had the same bar spacing c_s, similar concrete strength f_{cm} and same anchorage length l_b, but different confinement by transverse reinforcement. Test V1-1 did not contain any stirrups and test V6-2 had two 14 mm bars along the 200 mm anchorage length. The normalised maximum bond strength $\tau_{b,n} = \tau_{max} \cdot (38 / f_{cm})^{2/3}$ in the test specimen with stirrups reached 13.6 MPa and the test specimen without stirrups reached 12.7 MPa. The concrete strength was very similar in both tests. The strength increase was only 7 %, but the stirrups prevented splitting below the intermediate bar in test V6-2.

Effect of Surface Reinforcement

The positioning of surface reinforcement led to a 8 % increase in bond strength. Test V6-2 reached a shear load of 1125 kN and a maximum bond strength τ_{max} of 13.3 MPa, while test V6-1 with surface reinforcement reached 1230 kN and 14.3 MPa, respectively. The bond failure type changed from a splitting failure to a concrete cone pry-out as visible in Figure 3-62.

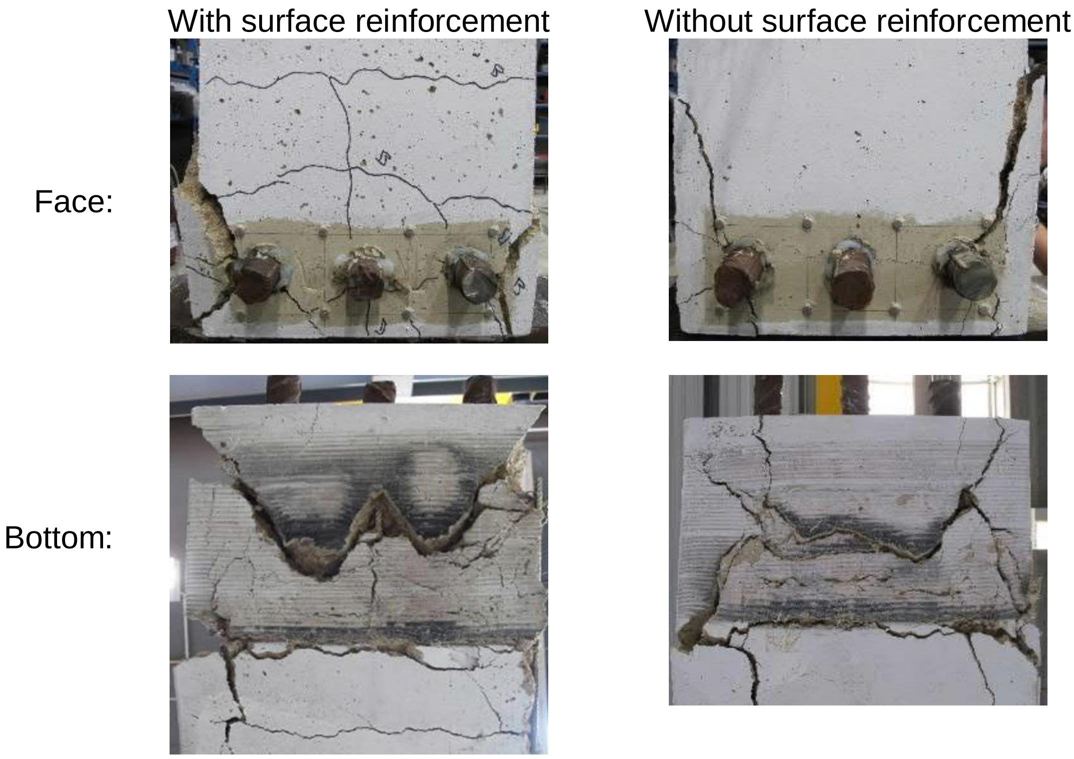

Figure 3-62 Crack patterns in test V6-2 at the front and bottom sides with surface reinforcement (left) and test V6-1 without surface reinforcement (right)

Effect of Additional Reinforcement (Ø 28 mm bars)

In test V5, two additional Ø 28 mm bars were positioned to increase the anchorage capacity. In test V5-1, two straight Ø 28 mm bars and in test V5-2 one Ø 28 mm bend were provided (cf. annex A.2.4.5). The shear capacity increased from 1125 kN in test V6-2 with the same anchorage length, concrete strength and stirrup number to 1373 kN (straight) and 1300 kN (bent), respectively. The maximum averaged bond stress did not increase, since the additional loads were transferred by the Ø 28 mm bars. The forces ΔF_{Ed} were distributed to five reinforcing bars. Thus, the strain in the surrounding concrete was reduced and higher ultimate loads were reached. Although the shear capacity increased, the maximum local bond stress in test V5-1 was 15 MPa and therefore smaller than the local bond stress in test V6 with 18 MPa. Figure 3-63 shows the steel strain (left) in the Ø 40 mm (top) and Ø 28 mm bars (bottom) and the bond strength calculated from the strain measurements (right). The measured values in the Ø 40 mm and Ø 28 mm bars approximately equal the calculated strain value $\varepsilon_s = 1.2$ % at $V_{max} = 1373$ kN.

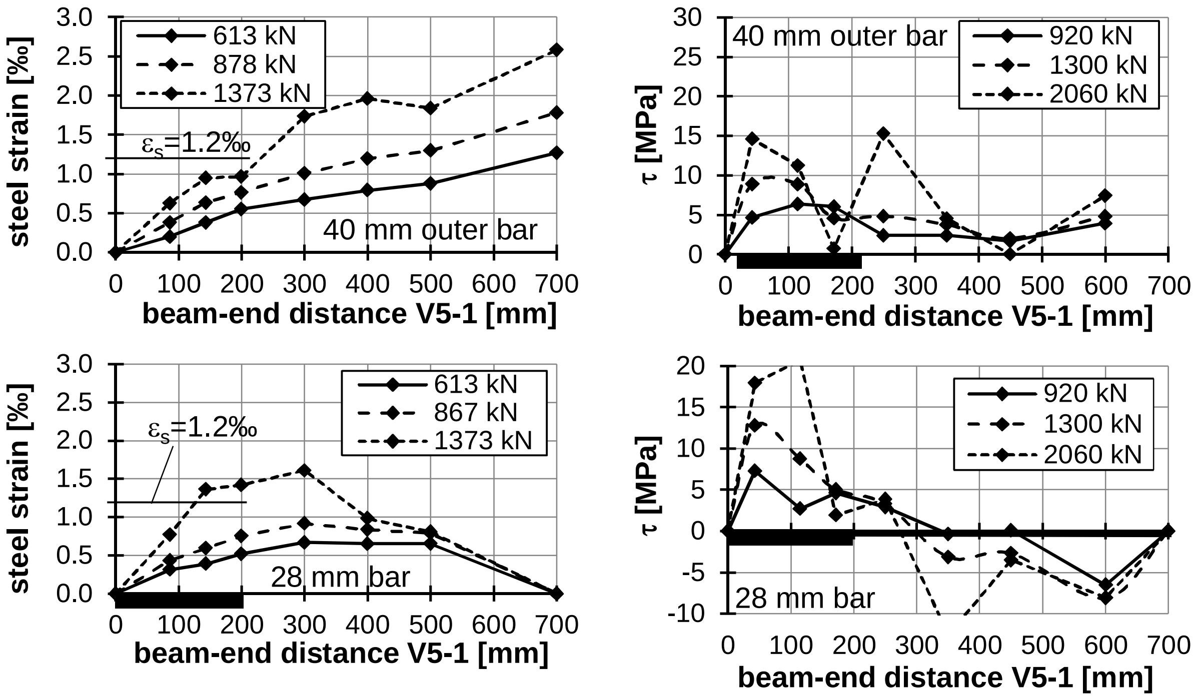

Figure 3-63 Steel strain (left) and bond strength (right) calculated from the steel strain in test V5-1 for the 40 mm bar (top) and the 28 mm bar (bottom)

3.6 Necessity of Additional Rules for Large Diameter Bars

The following experimental results were obtained concerning the necessity of additional rules for large diameter bars:

- A bond strength reduction with increasing bar diameter is reasonable
- Minimum dimensions for large diameter bars (15 · Ø according to [EC2/NA] and 1 m for laps according to or [EC2]) are not required
- The definition of bar stress in laps with large diameter bars $\sigma_s \leq 0.8 \cdot f_{yd}$ [EC2] is reasonable, where surface reinforcement is not provided
- The longitudinal surface reinforcement 2 % · $A_{ct,ext}$ [EC2/NA] resulted in slightly smaller crack widths than with 1 % · $A_{ct,ext}$ [EC2], but for both values, the mean yield strength of the bars was attained in lap tests and the 95%-fractile value of the crack widths was smaller than 0.2 mm (transverse surface reinforcement: 2 % · $A_{ct,ext}$ according to [EC2] and [EC2/NA])
- Transverse reinforcement is strongly recommended in anchorages and laps, while the attained bar stress was only increased by 5 % to 7 %, the bond behaviour was more robust as concrete splitting was mitigated
- It is not required to design anchorages for $\sigma_{sd} = f_{yd}$ in any case [EC2/NA], since the anchorage test designed with σ_{sd} = 195 MPa, transverse reinforcement and transverse pressure did not fail
- Contrary to the definition in [EC2/NA], the percentage of lapped bars may exceed 50 %. Continuous bars do contribute to robustness, but robustness can also be attained by transverse reinforcement, surface reinforcement and long bond lengths

4 Bond Strengths Obtained in Different Test Specimens

4.1 General

The comparison of test results obtained by the different test setups outlines the transferability from small-scale tests to actual structural elements. The following analysis of test results accounts for the different influencing parameters.

Increasing bond lengths result in reduced averaged bond stress τ_a over the bond length. Hence, pull-out and beam-end tests with a bond length of e.g. $5 \cdot Ø$ usually give greater averaged bond strength than structural members with lap lengths of about $40 \cdot Ø$. Test setups with transverse pressure in the bond zone – such as anchorages in simply supported beams – obtain higher bond strengths than bond tests without the positive effect of transverse pressure. According to [EC2/NA], transverse pressure at beam ends leads to a bond strength increase up to 50 %. Additionally, the realisable bar spacing c_s influences the test results. Adjacent reinforcing bars obtain less bond strength than widely spaced bars or single bar tests, such as pull-out or beam-end tests.

From the strain measurements during lap and anchorage tests, local bond strengths were calculated. The maximum values of the local bond strength values $\tau_{l,n}$ in the lap tests are comparable to the averaged values in beam-end tests. Hence, averaged normalised bond strengths $\tau_{a,n}$ and normalised local bond strengths, which were obtained by strain measurements at discrete positions in the lap and anchorage tests, are compared. For a comparison of test results, the individual concrete strength of the test specimens must be taken into account. Although certain concrete strength values are aimed for in practice, it is not possible to meet the exact strength requirements at the day of testing. Therefore, test results τ_b are normalised with a reference concrete strength $f_{cm,ref}$ and an exponent x that appropriately describes the ratio of bond strength to concrete compression strength as described in chapter 4.3.

4.2 Effect of Bond Length

EUROCODE 2 [EC2] presumes a constant bond strength for different bond lengths, while [FIB14] and [PT18] include a reduction factor for bond strength with increasing bond length. The proposed relationship in [FIB14] does not capture the small bond strength decrease in the beam-end tests (in tests with $5 \cdot Ø$ and $10 \cdot Ø$ respectively), but a comparison with the lap tests in Figure 4-1 shows that the relationship is reasonable for longer bond lengths. The maximum bond strengths obtained in beam-end tests and lap tests were normalised with $(38 / f_{cm})^{2/3}$ and $(38 / f_{cm})^{0.25}$, respectively. The graph representing the qualitative relationship between bond length and bond strength according to [EC2] is the mean bond strength obtained in the beam-end tests with $l_b = 5 \cdot Ø$. The qualitative graph for [FIB14] equals $\tau_{max} = \tau_{max,5Ø} (1/l_b) \cdot 0.55$. The anchorage test results are not shown here, since the bond zones were subjected to transverse pressure.

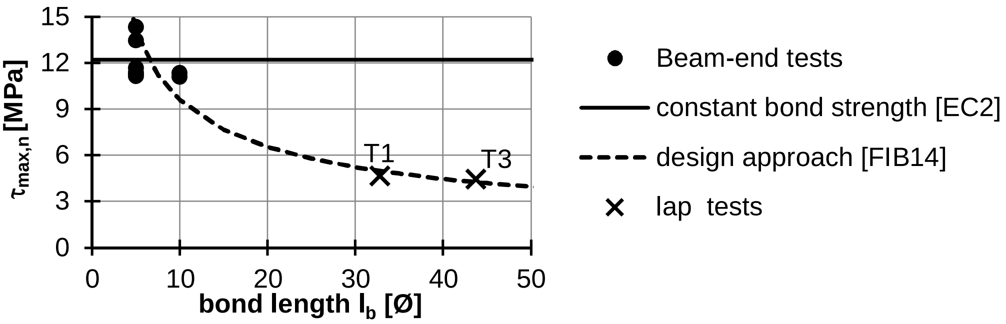

Figure 4-1 Comparison between maximum bond strength obtained in beam-end and lap tests with qualitative bond strengths according to [EC2] and [FIB14]

4.3 Effect of Bar Diameter

A decrease in bond strength with increasing bar diameter was observed both in beam-end tests and in lap tests (cf. Figure 4-2).

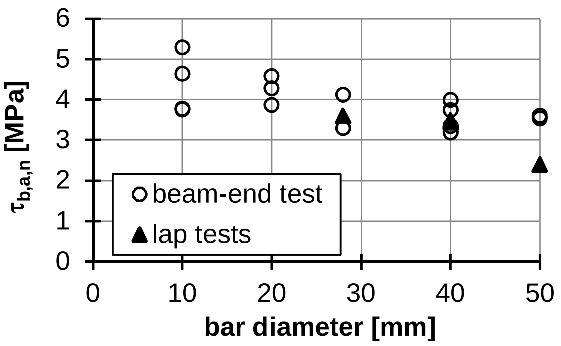

Figure 4-2 Averaged and normalised bond strength vs. bar diameter in beam end-tests and lap tests

For a comparison, the bond strength is normalised with a mean concrete strength f_{cm} of 38 MPa and a bond length of 44 · Ø.

$$\tau_{b,a,n} = \frac{\sigma_s \cdot Ø}{4 \cdot l_b} \cdot \left(\frac{l_b}{44}\right)^{0.55} \cdot \left(\frac{38\ \mathrm{MPa}}{f_{cm}}\right)^{0.67} \tag{4-1}$$

In the lap tests, increasing crack widths at the lap ends were measured for increasing bar diameters. Since the ratio of the concrete cover to the bar diameter c / Ø was constant, the measured crack widths also depend on the concrete cover. The crack width increase at the lap ends is presumably due to the increasing cover rather than to the increasing bar diameter.

Since all anchorage tests were conducted with 40 mm bars, an effect of bar diameter was not investigated in the anchorage tests.

4.4 Effect of Concrete Strength

The test results $\tau_{b,t}$ are normalised with a reference concrete strength $f_{cm,ref}$ and an exponent x that appropriately describes the ratio of bond strength to concrete compression strength.

$$\tau_{b,n} = \tau_{b,t} \cdot \left(\frac{f_{cm,ref}}{f_{cm,t}} \right)^{x} \tag{4-2}$$

The beam-end tests conducted showed a good correlation between concrete strength and bond strength for an exponent x = 2/3, conforming with [EC2]. Thus, for the following comparison of test results, the results from beam-end tests (BET) $\tau_{b,n,BET}$ and anchorage tests $\tau_{b,n,ancho}$ are normalised with equation (4-3). The reference concrete strength $f_{cm,ref}$ was set to 38 MPa representing the concrete class aimed for (C30/37).

$$\tau_{b,n,BET} = \tau_{b,n,ancho} = \tau_{b,t} \cdot \left(\frac{38\ \text{MPa}}{f_{cm,t}} \right)^{0.67} \tag{4-3}$$

In contrast, the model for the calculation of lap strength proposed in [FIB14], gives an exponent of x = 0.25 for the effect of concrete strength. This relation was also found in lap tests described in chapter 3.4. The difference can be explained by the varying bond lengths. While most beam-end and anchorage tests had bond lengths of 5 · Ø, the laps were tested with 33 · Ø to 43 · Ø.

This observation conforms with the findings by ELIGEHAUSEN in [ELI79]. The bond strength of short bond lengths increases with $f_c^{2/3}$, while the increase in bond strength is much smaller for larger bond lengths, since the distribution of bond stress is increasingly non-linear with increasing bond lengths.

In the following comparison, the bond strengths obtained in lap tests $\tau_{b,lap}$ are normalised with equation (4-4).

$$\tau_{b,n,lap} = \tau_{b,lap} \cdot \left(\frac{38\ \text{MPa}}{f_{cm,t}} \right)^{0.25} \tag{4-4}$$

4.5 Effect of Transverse Pressure

The anchorages tested in simply supported beams were always subjected to transverse pressure, while the lap tests were not subjected to transverse pressure. Therefore, the effect of transverse pressure was investigated in the beam-end tests by a modification of test setup (cf. chapter 3.3.1).

Table 4-1 gives the averaged normalised bond strength $\tau_{b,a,n}$ taking the concrete strength according to equations (4-3) and (4-4) into account. Additionally, the normalised local bond stress is given that was obtained by strain measurements at discrete positions in the lap and anchorage tests. Since crack widths correspond to twice the slip of reinforcing bars at the crack location, the slip at the maximum load $s(\tau_{max})$ measured in beam-end tests is compared to the crack width in the lap and anchorage tests in Table 4-1.

Table 4-1 Normalised and averaged bond strength $\tau_{b,a,n}$, normalised local bond stress $\tau_{b,l,n}$ and corresponding slip s or crack width w for beam-end tests and lap tests (width of transverse crack at the end of the bond length) with varying transverse pressure p

		Transverse pressure p	f_{cm}	$\tau_{b,a,n}$	$\tau_{b,l,n}$	$s(\tau_{max})$	$w(\tau_{max})$
		[MPa]	[MPa]	[MPa]	[MPa]	[mm]	[mm]
Beam-end tests	BET-1	0	38.2	11.8	-	0.68	0.38
	BET-9	6.0 MPa	27.9	16.2	-	-	-
Lap tests	T1	0	40.2	3.7	10.9	-	0.76
	T3	0	33.0	3.3	13.3	-	0.66
Anchorage tests	V3-1	15.4 MPa	35.2	12.1	27.1	-	0.22
	V6-2	14.1 MPa	36.5	13.7	24.3	-	-

The observed bond strength increase for transverse pressure was 40 % in the beam-end tests. Beam-end tests without transverse pressure and laps can be used for a comparison of small-scale and real-scale test setups without transverse pressure. For the non-linear effect of bond length, the direct comparison of averaged bond strengths along the bond length is not recommended. Instead, the averaged bond strength $\tau_{b,a,n}$ in beam-end test BET-1 (11.8 MPa) without transverse pressure is compared to the maximum local bond stress $\tau_{b,l,n}$. These values are in the same range as the maximum local bond strength $\tau_{b,l,n}$ measured in the lap tests without transverse pressure (10.9 MPa and 13.3 MPa respectively). In both test setups, the vertical concrete cover was $1.5 \cdot Ø$ and Ø 14 mm stirrups were positioned with a 130 mm spacing.

The averaged bond strength $\tau_{b,a,n}$was not higher in the anchorage tests, although substantial transverse pressure was present. This effect is partly based on the strain distribution within the anchorage of the simply supported beam (cf. chapter 3.5.4). The maximum local bond strength measured in the anchorage tests was 50 % higher than the average bond strength $\tau_{b,a,n}$ measured in beam-end test BET-9 with transverse pressure (cf. Table 4-1). Another reason for the non-conformity of averaged values $\tau_{a,n}$ of anchorages and beam-ends with transverse pressure is the fact that three densely spaced adjacent bars were tested at the anchorage. Figure 4-3 shows the ratio of bond strengths in tests without transverse pressure to tests with transverse pressure and the consideration of its effect according to [EC2] and [EC2/NA]. The beam-end and anchorage test results in Figure 4-3 are normalised with $(f_{cm} / 38)^{2/3}$. The increase in bond strength for transverse pressure according to [EC2/NA] is 1.5-times the bond strength without transverse pressure and the increase according to [EC2] is the smaller value of $1 / 0.7$ and $1 / (1 - 0.04 \cdot p)$.

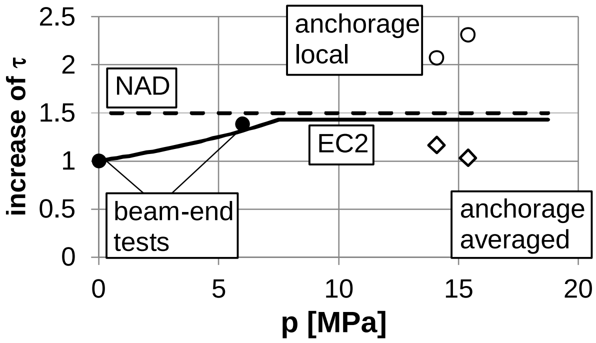

Figure 4-3 Bond strength increase for transverse pressure in beam-end tests and anchorage tests and bond strength increase for transverse pressure according to [EC2] and [EC2/NA]

4.6 Effect of Concrete Cover

Table 4-2 gives a comparison of bond strengths normalised with equations (4-3) and (4-4) averaged over the respective bond lengths. The averaged bond strength $\tau_{b,a,n}$ obtained in lap tests is considerably smaller than the one obtained in beam-end tests. The local bond stress measured in the lap tests were in the same range as the averaged bond strength in beam-end tests.

The maximum bond strength of the beam-end test $\tau_{b,a,n}$ with a bottom cover c_y of $1.0 \cdot Ø$ (BET-7, τ_b = 9.7) was 18 % smaller than with a bottom cover of $1.5 \cdot Ø$ (BET-1, τ_b = 11.8 MPa). In lap tests, the increase in bond strength averaged over the bond length $\tau_{b,a,n}$ and the local increase in bond strength $\tau_{b,l,n}$ due to concrete cover was within the test specimens' scatter (3 %). It should be noted that the local bond strength $\tau_{b,l,n}$ calculated on the basis of measurements with strain gauges during lap tests does not give the precise bond stress along the lap length.

Table 4-2 Normalised averaged bond strength $\tau_{b,a,n}$ vs. bond length, normalised local bond stress calculated from steel strain $\tau_{b,l,n}$ and corresponding slip s or crack width w for beam-end tests and lap tests (width of transverse crack at the end of the bond length) with varying concrete cover c_y

		Bottom cover c_y	f_{cm}	$\tau_{b,a,n}$	$\tau_{b,l,n}$	$s(\tau_{max})$	$w(\tau_{max})$
		[-]	[MPa]	[MPa]	[MPa]	[mm]	[mm]
Beam-end tests	BET-1	$1.5 \cdot Ø$	27.9	11.8	-	0.68	0.38
	BET-7	$1.0 \cdot Ø$	32.0	9.7	-	0.54	1.26
Lap tests	T1	$1.5 \cdot Ø$	40.2	3.7	10.9	-	0.76
	T2	$1.0 \cdot Ø$	32.5	3.8	10.7	-	0.76

Figure 4-4 (left) shows the ratios of the bond strength to the reference bond strength obtained in tests with the minimum bottom cover $c_y = 1.0 \cdot Ø$. The figure also illustrates the consideration of bottom cover in [EC2], [EC2/NA] and [FIB14]. For a profound comparison of design models with the experimental influence of the bottom cover c_y, a broader variation of c_y would be necessary. The effect of concrete cover is given as the ratio of maximum bond stress to the bond stress of the test with c_y / Ø = 1.0 and c_s / Ø = 2.0, respectively. The positive effect of concrete cover on bond strength is neglected in [EC2/NA] and is therefore represented by the value 1.0 in Figure 4-4. The bond strength increase for increasing concrete cover according to [EC2] is the smaller value of 1 / 0.7 and / /(1 - 0.15 · (c_i - 1)). The increase in bond strength defined in [FIB14] is represented by the factor $(c_i / Ø)^{0.25}$ in Figure 4-4.

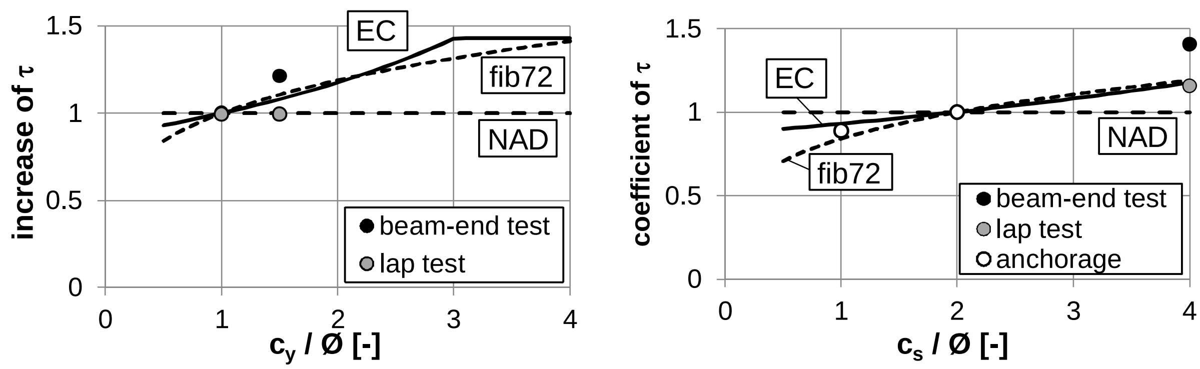

Figure 4-4 Bond strength increase vs. bottom cover c_y (left) and bar spacing c_s (right) in beam-end tests, lap tests and anchorage tests

Table 4-3 compares of bond strengths normalised with equation (4-3) and averaged over the respective bond length for different bar spacing. Beam-end test BET-10 with a bar spacing $c_s = 2 \cdot Ø$ showed quite a small bond strength $\tau_{b,a,n}$ which was presumably caused by load-application issues. In the lap and anchorage tests, the test specimens with greater bar spacing obtained higher averaged bond strengths $\tau_{b,a,n}$, but the local bond stress $\tau_{b,l,n}$ was not higher.

Table 4-3 Normalised averaged bond strength $\tau_{b,a,n}$ vs. bond length, normalised local bond stress calculated from steel strain $\tau_{b,l,n}$ and corresponding slip s or crack width w for beam-end tests and lap tests (width of transverse crack at the end of the bond length) with varying bar spacing c_s

		Bar spacing c_s	f_{cm}	$\tau_{b,a,n}$	$\tau_{b,l,n}$	$s(\tau_{max})$	$w(\tau_{max})$
		[-]	[MPa]	[MPa]	[MPa]	[mm]	[mm]
Beam-end tests	BET-10	2.0 · Ø	36.4	6.9	-	0.87	1.50
	BET-11	4.0 · Ø	37.3	9.2	-	0.65	0.96
Lap tests	T2	2.0 · Ø	32.5	3.8	10.7	-	0.76
	T5	4.0 · Ø	34.6	4.3	9.8	-	0.59
Anchorage tests	V3-2	1.0 · Ø	35.2	12.1	27.2	-	0.21
	V6-2	2.0 · Ø	36.5	13.7	24.2	-	-

In contrast to beam-end specimens without transverse pressure, anchorages in simply supported beams are positively influenced by transverse pressure, while the narrow bar spacing has a negative effect on the bond strength. Figure 4-4 (right) shows the ratios of bond strength to reference bond strength obtained in tests with the minimum bar spacing $c_s = 2.0 \cdot Ø$ and the consideration of bar spacing according to [EC2], [EC2/NA] and [FIB14]. The reference values were 6.9 MPa (for the beam-end tests), 3.8 MPa (for the lap tests) and 13.7 MPa for the anchorage tests. The positive effect of bar spacing on bond strength was confirmed by the test results.

For the different test-setup, the effect of bar spacing on bond strength in beam-end tests and anchorage tests is not directly comparable. The maximum bond strength of the single bars without transverse pressure was 11.8 MPa in the beam-end tests (BET). The bond strength of two adjacent bars without transverse pressure with $4.0 \cdot Ø$ spacing reached 9.2 MPa and with $2.0 \cdot Ø$ spacing 6.9 MPa. From these results, the bond strength can be extrapolated for $1.0 \cdot Ø$ spacing with the effect of transverse pressure according to [EC2].

$$\tau_{max,BET,c_s=1.0\cdot Ø} = \frac{6.9-(9.2-6.9)/(4-2)\cdot 1}{\min\{0.7;(1-0.04\cdot 15\,\text{Mpa})\}} = 8.2 \text{ MPa} \tag{4-5}$$

This value is only 8 % smaller than the obtained bond strength of 8.9 MPa in test V3-1 with a bar spacing $c_s = 1 \cdot Ø$.

The beam-end and anchorage tests with a bar spacing of $c_s = 2 \cdot Ø$ can be compared directly. When taking the transverse pressure according to [EC2] into account, the maximum bond strength in BET-10 can be obtained from test V1-2 with

$$\tau_{max,V1-2,c_s=2\cdot Ø} = \frac{12.3\,\text{MPa}}{\min\{1/0.7;1/(1-0.04\cdot 15\,\text{Mpa})\}} = 8.6 \text{ MPa} \tag{4-6}$$

This value is 25 % higher than the maximum bond strength τ_{max} = 6.9 MPa observed in beam-end test BET-10 with the same spacing ($c_s = 2.0 \cdot Ø$). It must be noted that the anchored bars act as a group in the anchorage tests, while Table 3-3 for the beam-end test specimen with two adjacent bars only gives the maximum bond strength of the bar that failed first. The bond strength in the second bar and therefore also the bond strength of the entire anchored bar group was actually higher.

4.7 Effect of Transverse Reinforcement

The transverse reinforcement was varied in the three test types to investigate the effect on bond strength within the test series, but also to investigate the comparability of the transverse reinforcement effect in different test specimens. Table 4-4 summarises the effect of transverse reinforcement observed in the three test types. Unexpectedly, the beam-end tests without transverse reinforcement and with 2 Ø 10 mm stirrups (BET-8) had the same averaged bond strength (10.3 MPa). In the beam-end tests with 2 Ø 14 mm stirrups (BET-1) and 3 Ø 8 mm stirrups (BET-19), the bond strength increased by about 15 % (11.7 MPa) in both cases.

Table 4-4 Normalised bond strengths $\tau_{b,a,n}$ and $\tau_{b,l,n}$ and corresponding slip s or crack width w for beam-end tests and lap tests (width of transverse crack at the end of the bond length) with varying transverse reinforcement A_{st}

		Transverse reinforcement	f_{cm}	$\tau_{b,a,n}$	$\tau_{b,l,n}$	$s(\tau_{max})$	$w(\tau_{max})$
			[MPa]	[MPa]	[MPa]	[mm]	[mm]
Beam-end tests	BET-1	2 Ø 14	27.9	11.8	-	0.68	0.38
	BET-8	2 Ø 10	34.3	10.3	-	0.49	0.50
	BET-14	0	50.5	10.2	-	0.51	0.66
	BET-19	3 Ø 8	50.5	11.7	-	0.79	0.74
Lap tests	T3	Ø 14 /180	33.0	3.3	13.3	-	0.66
	T6	Ø 14 /90	39.2	3.4	4.7	-	0.66
Anchorage tests	V3-1	0	35.2	8.9	27.7	-	-
	V3-2	2 Ø 8	35.2	12.1	27.7	-	0.21
	V1-1	0	39.1	13.6	24.3	-	-
	V6-2	2 Ø 14	36.5	12.5	21.2	-	-
	V4-1	3 Ø 12	32.9	9.3	18.5	-	-
	V4-2	0	32.9	8.4	20.0	-	-

The normalised averaged bond strengths $\tau_{b,a,n}$ obtained in lap test T3 with minimum transverse lap reinforcement according to [EC2] had the same value as in test T6 with reduced stirrup spacing (90 mm instead of 180 mm). The negligible effect of transverse bar spacing in the lap tests was not expected and might be due to the high level of transverse reinforcement in both test specimens.

In the anchorage tests, the test specimens V3-2 with and V3-1 without transverse reinforcement both reached the same maximum local bond strength $\tau_{b,l,n}$ (27.5 MPa). The bond strength averaged over the bond length $\tau_{b,a,n}$ was smaller in anchorages without transverse reinforcement. For a spacing of 2 · Ø and anchorage lengths of 200 mm (V1-1 and V6-2), the bond strength increase for the positioning of transverse reinforcement was 9 %. For anchorages with a 1 · Ø spacing and an anchorage length of 200 mm, the bond strength increase for transverse pressure was 36 % (V3-2 and V3-1). The considerable bond strength increase by transverse reinforcement in test V3-2 might be caused by the unfavourable geometry of the crack-inducing steel sheet. In the anchorage test with a spacing of 2 · Ø and an anchorage length of 440 mm, the compression zone under the load application failed before the anchorage and the effect of transverse reinforcement within the anchorage length could not be evaluated.

Figure 4-5 gives a comparison of bond strength over transverse reinforcement ratio obtained in beam-end tests, lap tests and anchorage tests. For the beam-end tests and anchorage tests, the bond strength is divided by the bond strength for

$\Sigma A_{st,min} / A_s = 0.25$. For lap tests, the bond strength is divided by the bond strength for the ratio $\Sigma A_{st,min} / [A_s \cdot (\sigma_{sd} / f_{yd})] = 1.0$. Both minimum transverse reinforcement values conform with [EC2].

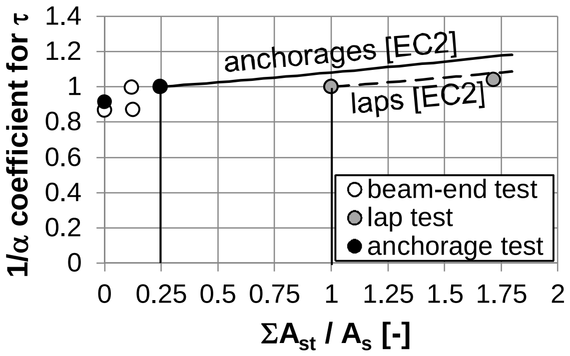

Design anchorage and lap lengths according to [EC2] may be reduced by $\alpha_{3,EC}$:

$$0.7 \leq 1 - K \cdot \frac{\sum A_{st} - \sum A_{st,min}}{A_s} \leq 1.0$$

The coefficient for τ equals $1/\alpha_{3,EC}$ with K (cf. Figure 2-6 and Figure 2-18)

Figure 4-5 Bond strength increase vs. ratio of transverse reinforcement cross-section to the cross-sectional area of one lapped or anchored bar $\Sigma A_{st} / A_s$

4.8 Predictability of Bond Behaviour by Beam-End Tests

The conducted tests should clarify whether beam-end tests are suitable for the prediction of bond behaviour of structural concrete members such as beams. The failure modes in beam-end, anchorage and lap tests were comparable. Beam-end tests show a single longitudinal crack in the bottom cover of the loaded bar (face split failure). The anchorages also developed a face split failure (three cracks in the bottom cover above three anchored bars) for small confinement by transverse reinforcement. In case transverse reinforcement or even surface reinforcement was positioned in the anchorages, the failure type changed from splitting to a pry-out of the reinforcing bars. The lap test failure was a face-and-side split failure type.

Since the non-linear distribution of bond strength along the lap length leads to considerable differences between laps and anchorages, parameter effects are not straight comparable. While the exponent 2/3 for the concrete strength captures the bond strength in beam-end tests correctly, lap tests revealed that the exponent 1/4 for concrete strength captures the bond strength better for long bond lengths.

Since a uniform load application to more than one bar is difficult to realise in beam-end tests, the testing of groups of reinforcing bars in one or more layers is easier at end anchorages of simply supported beams or in laps. The observed bond strength decrease for decreased bar spacing was about 15 % in anchorages and laps, while the decrease was up to 40 % for the weaker of the two reinforcing bar in beam-end tests. This seems to be caused by the load application and should be noted for further analysis.

Transverse pressure led to an increase in bond strength by 40 % in the beam-end tests conducted. The averaged bond strength along the anchorage length $\tau_{b,a,n} \approx 13$ MPa was not much higher than the bond strength in beam-end tests without transverse pressure (about 12 MPa). The negative effect of grouped reinforcing bars with little spacing superimposed the positive effect of transverse pressure. The local bond strength $\tau_{b,l,n}$

calculated from strain measurements in anchorage tests was more than twice as much as the bond strength without transverse pressure. Such high values were only observed locally and cannot be reached along the entire anchorage length.

The slight increase in averaged bond strength $\tau_{b,a,n}$ observed in beam-end tests for the positioned transverse reinforcement conforms with the increase investigated in anchorages, while it seems to be more beneficial in laps without transverse pressure.

The beam end-test is therefore capable to predict different parameter effects on bond capacity in bond zones. For a correct capture of the effect of adjacent bars with small spacing, a uniform load application must be planned thoroughly.

In beam-end tests, the transverse crack at the end of the bond length is reduced by the continuous reinforcement shown in Figure 3-1. Still, the widths of the transverse crack at the end of the bond length (denominated crack 1 in Figure 3-4) measured in beam-end tests resemble the crack width dimensions obtained at lap ends. Since a wide range of transverse crack widths was observed at the end of the bond length in beam-end tests for equal parameters, parameter effects are not clearly visible. In contrast, parameter effects on crack width are clearly visible within the lap length and in the undisturbed length of lap tests. While the concrete strength, the presence of continuous bars and the bar diameter influence the crack widths at the lap ends, the change in stiffness prevails.

5 Database for the Ultimate Limit State

5.1 Database Filter

In this chapter, a comparison of the described test results and design models with a lap and anchorage database is presented. The database was originally compiled by ACI COMMITTEE 408 [ACI01] and FIB TASK GROUP 2.5 [FIB05] and comprises more than 800 tests with anchorages and laps. Annex A.3 provides drawings and tables of the anchorage and lap tests included in the database.

The database comprises several lap investigations. The first major lap investigations were conducted by FERGUSON ET AL. in the 1950s and 1960s at the University of Texas at Austin [FER65a], [FER65c], [FER69]; [FER62]; [FER65b]. The European investigations were performed in the 1970s by TEPFERS [TEP73] as well as REHM AND ELIGEHAUSEN [REH77] in Gothenburg and Stuttgart, respectively. For new materials such as high-strength reinforcement, high-strength concrete and epoxy-coated reinforcing bars, new test programmes were conducted during the 1990s (e.g. [DAR95a], [ZUO00], [DAR95b], [AZI99], [AZI93], [DEV91], [CHO91], [KAD94], [BUR00]). All of these investigations comprise more than 20 lap tests each, but the test programme described in [TEP73] was the largest investigation performed including 173 tests.

The tests in the original database include different concrete strength, bar diameter, yield strength, rib area, lap length and confinement as well as bottom, top and side bars. Most tests are four-point bending tests with laps in the constant moment zone, but different test-setups are covered as well. The database does not comprise tests with:

- Anchorages with bends and hooks
- Coated bars
- Lapped bars with different bar diameters
- Pull-out tests
- Anchorages under compression

The original database comprises anchorages and laps in poor bond conditions and laps where less than 100 % of the bars are lapped. In the course of this evaluation, these cases were excluded from the database and described briefly in chapter 8.1.

[FIB14] defines a database filter, which was mostly applied for the following evaluation as well. The own filtered database comprises only test specimen where:

- 20 MPa < f_{cm} < 110 MPa (the lower limit is representative of practice and the upper limit represents a limit of experimental data)
- l_0 / Ø ≥ 15 for laps (representative of practice)
- 0.95 ≤ c_{min} / Ø < 3.5 (the lower limit is representative of practice and the upper limit represents a limit of experimental data)

- c_{max} / $c_{min} \leq 5$ (limit of experimental data)
- $K_{tr} \leq 0.05$ (little increase in bond strength above this value)
- $\sigma_{s,test}$ / $f_{ym} > 1.2$ (otherwise failure probably not attributable to bond)
- $n_b > 1$ (otherwise no mutual influence of adjacent bars)

The database was extended by the anchorage test data compiled by AMIN [AMI09]. Since the stress to be developed in anchorages is usually much lower than the yield strength, shorter anchorages were allowed in the own database.

The cover values correspond with the minimum cover and bar spacing c_{min} according to [EC2] and [MC2010] (1.0 · Ø). Without consideration of durability requirements, the minimum cover defined in [ACI14] is 38 mm for Ø 43 mm (0.88 · Ø) bars. In slabs, the minimum cover is 19 mm for bar diameters up to Ø 36 mm (0.53 · Ø) according to [ACI14]. Cover dimensions in existing structures often do not fulfil current cover requirements. The performance of anchorages and laps with smaller covers was described by SCHENKEL [SCH98b] (with cover ratios c_y / Ø from 0 to 1.9).

The maximum bar stress $\sigma_{s,test}$ was extracted from the individual publications by Fib task group 2.5. The reinforcing bar stresses of the tests conducted at IMB were calculated with a parabola-rectangle diagram for concrete stress. The aim of lap tests is usually to reach the mean yield strength f_{ym} without prior failure and certain ability for load increase above the yield strength to obtain ductile behaviour. Test specimens included in the database with lapped-bar stress well above the yield strength probably failed in shear or bending rather than in bond. Therefore, test results with bar stresses above $1.2 \cdot f_{ym}$ were excluded from the database.

The database also comprised anchorage and lap tests with one bar only. The bond strength of single bars is higher than for several lapped or anchored bars, since cover and bar spacing influence the bond strength (cf. chapters 3.3.4, 3.4.4, 3.5.4 and 5.3.4). Therefore, tests with one bar only were excluded in the following evaluation. Additionally, structural elements with one bar only do not represent structural elements in practice. The database was described and evaluated in several publications [BUR00], [ACI01]; [ACI03], [LET06b],[BUR00]; [CAI14b]; [FIB14]; [LET06a]; [LET06b]. Table 5-1 gives an overview of the database test numbers used for these publications. The publications including statistical analyses of the database were used to check the results of the database evaluation in this thesis. The appendix of this thesis contains tables and drawings of the single test programmes included in the database.

Table 5-1 Test numbers in original and filtered database (transverse reinforcement = links)

	[ACI01]	[FIB05]	[FIB05] filtered	[LET06b]	[FIB14]	[CAI14b]	Own data-base	Own data-base filtered
Overall test number	478	807	561	793	582		1230	669
Tests with links	286	392	299	391	306		396	239
Tests without links	192	415	262	402	276		839	430
Lap tests	453	782	546		543	445	781	457
Lap tests with links	272	378	290		288	221	388	231
Lap tests without links	181	404	256		255	224	393	226
Anchorage tests	25[1]	25[1]	15[1]		39		449[2]	212[2]
Anchorage tests with links	14	14	9		18		74	8
Anchorage tests without links	11	11	6		21		449	204

[1] the original database contained anchorages described in [CHA56] and [MAT61]

[2] including [CHA56], [MAT61], the tests described in chapter 3.5 and [AMI09]

When comparing the test results in the database with the calculated values of the described design models, it appears that the database includes a number of outliers. Particularly the following tests results deviated from the majority of tests:

- Test results of laps in a cantilever with very large concrete cover were not comparable to four-point bending tests (conducted by FERGUSON [FER65b]).
- Tests conducted by TEPFERS [TEP73] with f_R = 0.12 partly give very high maximum bar stresses.
- Tests conducted by HAMAD AND MANSOUR [HAM96] where the lapped bars were not directly adjacent do not conform with the calculated strength. If the lap spacing increases, the spacing between the lapped bars decreases in their test setup. The splitting plane remains the same in both cases. The high bar stresses obtained in tests were unexpected, since the spacing was wide but the concrete covers c_x and c_y were very small.
- Outliers also result from an early termination of the test specimen loading. Some tests have probably been stopped as soon as the yield strength was reached. Excluding tests in case the strengths obtained in tests $\sigma_{s,test}$ is greater than the yield strength f_{ym} and the calculated value $\sigma_{calc,EC2}$ is greater than 1.2

$\sigma_{s,test}$, leads to exclusion of 10 test specimens from the database (tests described in [AZI99] and [TEP73]).

5.2 Statistical Database Evaluation for Different Design Models

The following tables give comparisons of the maximum bar stresses found in tests $\sigma_{s,test}$ with the calculated mean reinforcing bar stresses according to the described design models for laps and anchorages $\sigma_{s,i}$. The mean value of the model uncertainty of the design models is denominated θ and the coefficient of variation (COV) of the model uncertainty is denominated V_θ.

The [FIB14] design model correlates very well with the test results. Due to a slightly different database used here, the standard deviation is even smaller than in [FIB14] (Table 5-2).

Table 5-2 Statistical data for [FIB14] equation (2-26) presuming a log-normal distribution

$\sigma_{s,test}$ / $\sigma_{sm,fib14}$	All laps	Laps without links	Laps with links	Anchorages at indirect supports	Anchorages at direct supports	All results
mean value θ	0.99	0.99	1.00	1.02	0.99	1.00
standard deviation	0.131	0.135	0.128	0.168	0.184	0.135
COV V_θ	0.132	0.136	0.128	0.165	0.186	0.136
minimum	0.65	0.65	0.65	0.63	0.44	0.63
5% characteristic ratio	0.79	0.78	0.80	0.77	0.72	0.79
number of results	457	226	231	47	165	669

For the evaluation of the design model according to [EC2], the test results were compared to the mean lap strength derived in equation (2-20) that was calculated with a mean bond strength f_{bm} according to [EC2] in equation (2-13). The analysis indicates that laps without links often do not reach the calculated lap strength (cf. Table 5-3). The design model according to [EC2] requires minimum reinforcement in laps so that laps without links do not conform with the requirements.

The [EC2] design model for laps was calibrated with bar stress values close to the yield strength, therefore different filters for the yield strength were applied in the database analysis. Where the filter was $\sigma_s < 1.2 \cdot f_{ym}$, the COV was 0.305 for 457 laps (cf. Table 5-3). Applying a filter $0.8 \cdot f_{ym} < \sigma_s < 1.2 \cdot f_{ym}$ left 291 lap test results and gave a COV of 0.312. The COV was reduced to 0.272 when applying a bar-stress filter of $0.82 \cdot f_{ym} < \sigma_s < 0.92 \cdot f_{ym}$ (92 lap tests). Since the first change did not result in a significant decrease of the COV and the second change left a much smaller test number, the original filter $\sigma_s < 1.2 \cdot f_{ym}$ was kept throughout the analysis.

Table 5-3 Statistical data for equation (2-20) with mean bond strength according to (2-13) [EC2] (presuming a log-normal distribution)

$\sigma_{s,test}$ / $\sigma_{s,EC2}$	All laps	Laps without links	Laps with links	Anchorages at indirect supports	Anchorages at direct supports	All results
mean	0.95	0.91	1.00	0.99	1.23	1.02
standard deviation	0.290	0.300	0.263	0.283	0.315	0.324
COV	0.305	0.332	0.265	0.286	0.256	0.316
minimum	0.33	0.33	0.39	0.44	0.44	0.33
5% characteristic ratio	0.56	0.51	0.63	0.60	0.79	0.59
number of results	457	226	231	47	165	669

Cairns and Eligehausen [CAI14b] try to overcome the deficiency of EUROCODE 2 [EC2] by means of a lap-factor modification and by an additional factor taking the yield strength into account. This leads to a shift of the data points into the safety zone. When only the increased lap factor $\alpha_6 = 2.5$ for a percentage of lapped bars larger than 50 % instead of $\alpha_6 = 1.5$ according to EUROCODE 2 [EC2] is taken into account, the mean value, the standard deviation, the minimum value and the 5% characteristic ratio equal the values in Table 5-3 multiplied by the factor 2.5/1.5. The values of the COV do not change.

When both the increased lap factor $\alpha_6 = 2.5$ for a percentage of lapped bars larger than 50 % ($\alpha_6 = 2.3$ for the 50 % and 66 % laps in the database) and the proposed factor for the effect of stress to be developed are considered, the statistical data given in Table 5-5 results. The coefficients of variation increase in comparison to the original EUROCODE 2 [EC2] design model.

Table 5-4 Statistical data for equation (2-20) according [EC2] (presuming a log-normal distribution) with $\alpha_6 = 2.5$ and factors for different yield stress of bars according to [CAI14b]

$\sigma_{s,test}$ / $\sigma_{sm,EC2,[CAI4b]}$	All laps	Laps without links	Laps with links
mean value θ	1.55	1.46	1.63
standard deviation	0.557	0.548	0.542
COV V_θ	0.360	0.375	0.333
minimum	0.54	0.55	0.54
5% characteristic ratio	0.82	0.75	0.91
number of results	457	226	231

The design model according to [EC2/NA] differs from the design model according to [EC2], since the concrete cover is not taken into account and lap factors are higher (cf. chapter 2.9.3). Hence, laps designed according to [EC2/NA] reach a higher safety level. The [EC2/NA] and [EC2] design models have much higher coefficients of variation than the design model according to [FIB14] (cf. Table 5-5).

Table 5-5 Statistical data for equation (2-20) with mean bond strength according to (2-13) [EC2/NA], where α_2 and α_6 deviate from [EC2] (presuming a log-normal distribution)

$\sigma_{s,test}$ / $\sigma_{sm,NAD}$	All laps	Laps without links	Laps with links	Anchorages at indirect supports	Anchorages at direct supports	All results
mean value θ	1.30	1.21	1.39	1.15	1.18	1.26
standard deviation	0.414	0.376	0.430	0.356	0.280	0.381
COV V_θ	0.318	0.311	0.310	0.309	0.238	0.303
minimum	0.44	0.44	0.52	0.47	0.44	0.44
5% characteristic ratio	0.74	0.70	0.81	0.67	0.78	0.74
number of results	457	226	231	47	165	669

Besides the design models yet evaluated in this chapter, the design model proposed in [PT18] that was derived from [FIB14] (cf. 2.9.7) was analysed as well. Since [PT18] gives a design lap and anchorage length only, the design equation was rearranged for the design lap and anchorage strength $f_{std,PT18}$ in equation (2-44). To find calibration factors for the mean lap and anchorage strength $f_{stm,PT18}$, the own database was used. The calibration factor 40 in the design equation (2-44) was changed to 31 to obtain mean strength values. This calibration factor gave the best correlation with test results. The statistical evaluation of the design model according to [PT18] with the own derived calibration factors is described in more detail in 5.6.3.

Furthermore, the coefficient for the transverse reinforcement ratio in design equation (2-44) was modified. While [PT18] gives a coefficient of 31, the own evaluation gave much better correlation when the coefficient was changed to 60.

$$f_{stm,PT17} = 435\ \text{MPa} \cdot \left(\frac{f_{cm}}{25\ \text{MPa}}\right)^{\frac{1}{3}} \cdot \left(\frac{20}{Ø}\right)^{\frac{2}{9}} \cdot \left(\frac{l_b}{31 \cdot Ø}\right)^{\frac{2}{3}} \cdot \left(\frac{c_{d,conf}}{1.5 \cdot Ø}\right)^{\frac{1}{3}} \qquad (5\text{-}1)$$

With

$$c_{d,conf} = c_d + Ø \cdot \left(60 \cdot k_{conf} \cdot \rho_{conf} + 8 \cdot \sigma_{ctd} / \sqrt{f_{ck}}\right) \leq 3.75 \cdot Ø \qquad (5\text{-}2)$$

With this modification, the ratio $\sigma_{s,test}$ / $\sigma_{sm,PT}$ given in Table 5-7 resulted.

Table 5-6 Statistical data for equation (5-4) according to [PT18] with own calibration factors (presuming a log-normal distribution)

$\sigma_{s,test}$ / $\sigma_{sm,PT}$	All laps	Laps without links	Laps with links	Anchorages at indirect supports	Anchorages at direct supports	All results
mean value θ	0.99	0.99	0.99	1.09	0.98	0.994
standard deviation	0.156	0.171	0.138	0.229	0.191	0.172
COV V_θ	0.157	0.173	0.139	0.209	0.195	0.173
minimum	0.56	0.60	0.56	0.60	0.53	0.53
5% characteristic ratio	0.76	0.73	0.78	0.76	0.70	0.74
number of results	457	226	231	47	165	669

The mean anchorage and lap strength according to [ACI14] was calculated by dividing the design values with the safety factor 0.9 (cf. chapter 7.3). Since the lap factor 1.3 is also described as a safety factor in [ACI03], this value is not taken into account in the calculation of the mean bar stress in laps. For anchorages at direct supports, the stress value was multiplied with 1.3, since the confinement by a compression reaction may be taken into account according to [ACI14]. The reinforcing bar stress obtained in most tests was higher than the calculated values according to the [ACI14] design model. The model especially underestimates the developable bar stress in anchorages (Table 5-7). Since the obtained mean value θ is well above 1.0, the design values for anchorages according to [ACI14] divided by 0.9 do not represent the mean values obtained in the database.

Table 5-7 Statistical data for equation (2-25) according to [ACI14] approximating a mean level by division with the safety factor 0.9 and disrespecting the lap factor 1.3 (presuming a log-normal distribution)

$\sigma_{s,test}$ / $\sigma_{sm,ACI}$	All laps	Laps without links	Laps with links	Anchorages at indirect supports	Anchorages at direct supports	All results
mean value θ	1.07	1.04	1.11	1.42	1.90	1.30
standard deviation	0.262	0.265	0.250	0.406	0.450	0.462
COV V_θ	0.244	0.256	0.225	0.285	0.237	0.355
minimum	0.70	0.70	0.73	0.65	0.99	0.65
5% characteristic ratio	0.70	0.66	0.75	0.87	1.26	0.69
number of results	457	226	231	47	165	669

The statistical data for the ratio of bar stress in lap tests to calculated bar stress according to the design models given in [ELI79], [BUR00], [LET06a], [ZUO00] and

[CAN05] is summarised in Table 5-8. MARX [MAR15] conducted a comparison of the design models described.

Table 5-8 Statistical data for mean reinforcing bar stress in laps given in [ELI79], [BUR00], [LET06a], [ZUO00], [CAN05] (presuming a log-normal distribution)

$\sigma_{s,test}$ / $\sigma_{sm,calc}$	[ELI79]		[BUR00]		[LET06a]		[ZUO00]		[CAN05]	
	without links	with links	without links	with links	without links	with links	without links	with links	without links	with links
mean value θ	0.98	1.00	1.04	0.94	0.98	0.92	0.97	1.08	1.03	1.08
standard deviation	0.22	0.20	0.17	0.14	0.22	0.20	0.15	0.30	0.18	0.29
COV V_θ	0.23	0.20	0.17	0.15	0.23	0.22	0.16	0.28	0.17	0.27
minimum	0.56	0.58	0.67	0.52	0.48	0.47	0.54	0.44	0.67	0.54
5% characteristic ratio	0.66	0.71	0.78	0.74	0.66	0.63	0.74	0.66	0.77	0.68
number of results	226	231	226	231	226	231	226	231	226	231

The coefficients of variation of the model uncertainty θ of the model elaborated in [ELI79] are much higher (V_θ = 0.23 and 0.20) than in the original evaluation (V_θ = 0.13). BURKHARDT [BUR00] refined the model according to [ELI79], which was originally limited to a concrete strength of 65 MPa, for high-strength concrete and therefore captures the effect of increasing concrete strength more precisely [MAR15].

The design model defined in [LET06a] is the least complex equation, but the test results were slightly overestimated in this evaluation and the coefficients of variation are higher compared to the [FIB14] equation. [ZUO00] and [CAN05] also validated their models with the database of the ACI Committee 408 [ACI01].

The approximate conformity of the described design models shows that different theoretical models for the load transfer are capable of describing the bearing behaviour of anchorages and laps.

All models given in Table 5-5 have smaller coefficients of variation than [EC2], [EC2/NA] and [ACI14], but the coefficients of variation of the models according to [FIB14] and [PT18] with own calibration factors are still smaller.

5.3 Database Evaluation of Parameter Effects in Lap Tests

For a more detailed evaluation of the design models, the effects of the single influencing parameters must be taken into account. Table 2-5 gives an overview of the effects of bond length l_b, concrete strength f_{cm} and bar diameter Ø according to different design models described.

All design models were derived from experimental or numerical investigations. Below, the parameter effects given in the filtered database and in selected publications of large comprehensive test series are presented. For a comparison of the test results, different parameters are summarised to certain value ranges (Table 5-9).

Table 5-9 Value ranges for transverse reinforcement, concrete strength f_{cm}, lap length l_0, concrete cover c_y and c_x and bar spacing c_s

	Transverse reinforcement	f_{cm}	l_0 / Ø	c_y / Ø and c_x / Ø	c_s / Ø
	[-]	[MPa]	[-]	[-]	[-]
Range of values	with without	20 - 30 30 - 45 45 - 65 65 - 100	15 - 22 22 - 30 30 - 40 > 40	0.95 - 1.4 1.5 - 2.4 2.5 - 3.4 > 3.5	1.95 - 2.4 2.5 - 3.4 > 3.5

5.3.1 Lap Length

The design models in [EC2], [EC2/NA], [ACI14] and [ZUO00] presume a linear relationship of lap length and lap strength, whereas the design models in [FIB14], [ELI79], [LET06a], [BUR00] and [CAN05] consider a nonlinear correlation.

For the evaluation of the tests without transverse reinforcement included in the database, the exponent of the lap-length to bar-diameter ratio is 0.37 (cf. Figure 5-1, left). These tests include laps in beams with concrete strength between 20 MPa and 120 MPa (cf. Figure 5-1, right).

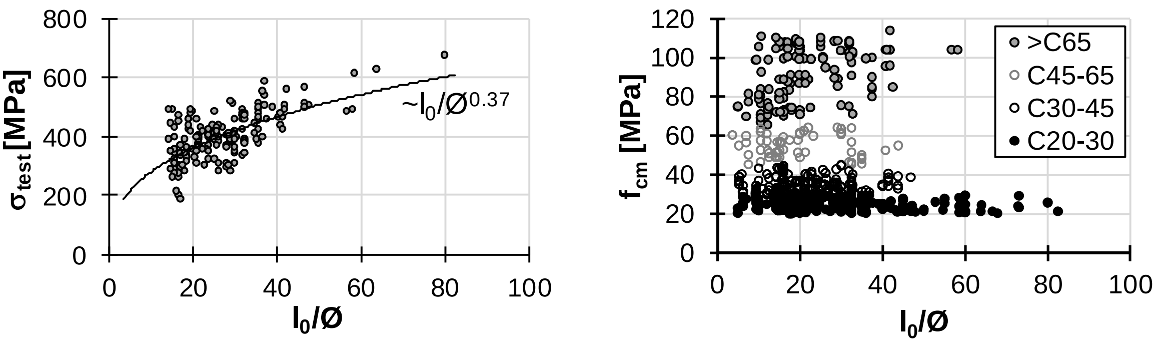

Figure 5-1 Effect of lap-length to bar-diameter ratio on bar stress for laps σ_{test} without transverse reinforcement (left) and concrete strength distribution in the database (right)

For laps with 20 MPa – 30 MPa concrete strength and bar spacing $c_s \geq 4 \cdot Ø$, an exponent of 0.40 reflects the test results best (cf. Figure 5-2, left). The bar stress in laps with 30 - 45 MPa concrete strength and $c_s \geq 4 \cdot Ø$ is best described by $(l_0 / Ø)^{0.33}$ (cf. Figure 5-2, right).

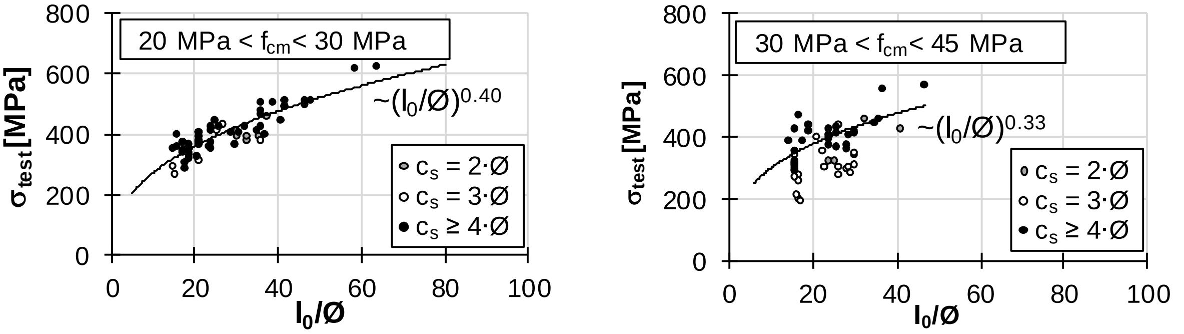

Figure 5-2 Effect of lap-length to bar-diameter ratio on maximum bar stress σ_{test} for 20 MPa < f_{cm} < 30 MPa (left) and 30 MPa < f_{cm} < 45 MPa (right)

Evaluating individual publications of comprehensive test programmes gives exponents for the lap-length to bar-diameter ratio of about 0.55 for [FER65c], [AZI93] and [TEP73] (cf. Figure 5-3), while the test results in [REH77] are rather captured with the exponent 0.26 (cf. Figure 5-4, right).

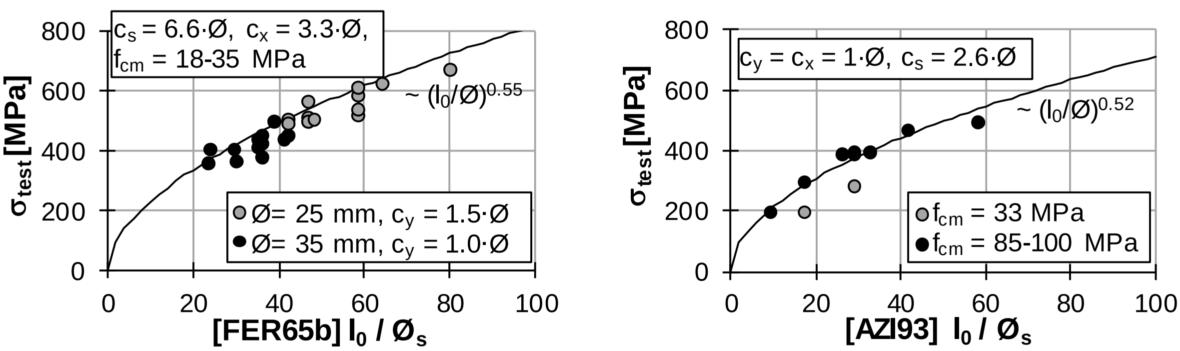

Figure 5-3 Effect of lap-length to bar-diameter ratio on maximum bar stress σ_{test} obtained in test programmes conducted by FERGUSON [FER65c] (left) and AZIZINAMINI [AZI93] (right)

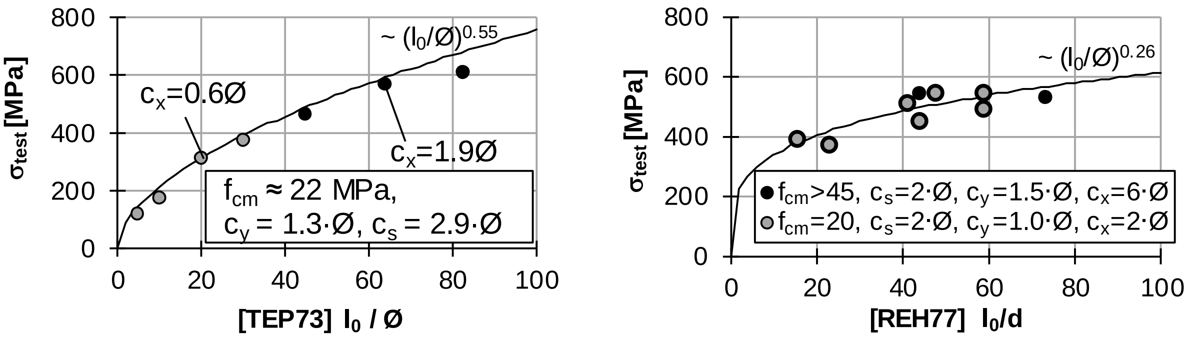

Figure 5-4 Effect of lap-length to bar-diameter ratio on maximum bar stress σ_{test} obtained in test programmes conducted by TEPFERS [TEP73] (left) and REHM [REH77] (right)

This comparison indicates, that the linear design models in [EC2], [EC2/NA], [ACI14] and [ZUO00] overestimate the effect of lap length on obtainable lap strength. The comparison of the ratios of experimental to theoretical values over l_0 / Ø validates this finding (cf. Figure 5-5).

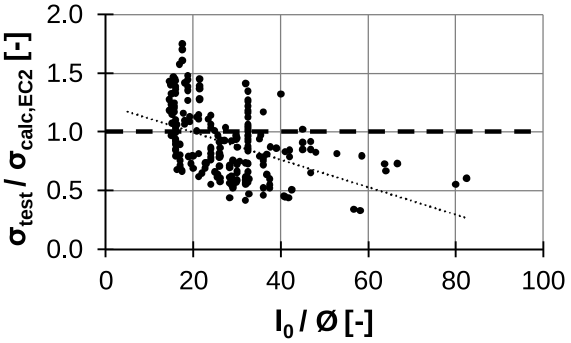

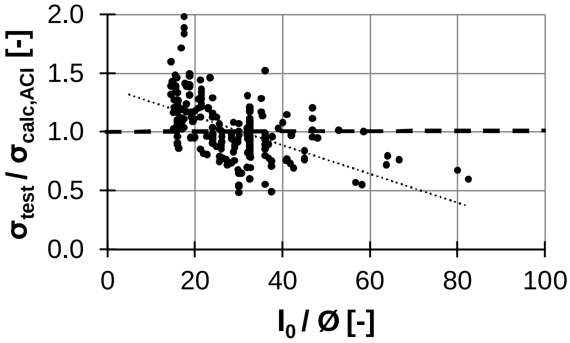

Figure 5-5 Comparison of maximum bar stress in tests to the calculated bar stress according to [EC2] (left) and[ACI03]; [ACI14] (right)

Other design models consider the effect of lap-length to bar-diameter ratio with an exponent smaller than 1.0 [ELI79] [BUR00], [LET06a], [CAN05] and [FIB14] (cf. Figure 5-6, left) and capture the effect of lap length better (cf. Figure 5-6 , right).

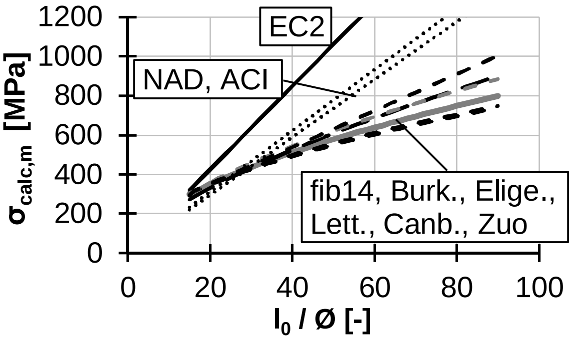

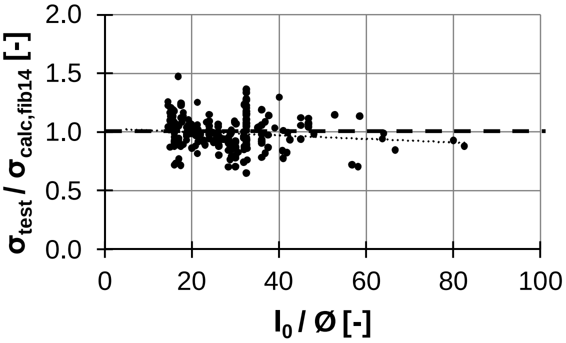

Figure 5-6 Calculated bar stress obtainable in laps according to the considered design models for Ø = 25 mm; $c_x = c_y = 1.5 \cdot Ø$; $c_s = 3 \cdot Ø$ (left) and comparison of maximum bar stress in tests to the calculated bar stress according to [FIB14] (right)

5.3.2 Concrete Strength

Design models for lap or anchorage length either directly comprise the concrete strength or consider the bond strength as a multiple of the tensile strength of concrete. The design model according to [EC2] considers the concrete strength with an exponent of 2/3 for normal strength concrete, while other design models consider a smaller effect of concrete strength on bond and lap strength by applying exponents between 0.25 and 0.5 for the concrete strength. Table 2-5 gives an overview of exponents applied in the described design models.

When evaluating the effect of concrete strength on the lap strength, the ratio of lap length to bar diameter as well as the concrete cover have to be considered. Figure 5-7 shows the lap strength over the concrete strength for certain covers and lap lengths within the filtered database. The individual test results were obtained in different publications. In both cases, the relationship of concrete cover to lap strength is captured well by the exponent 0.28.

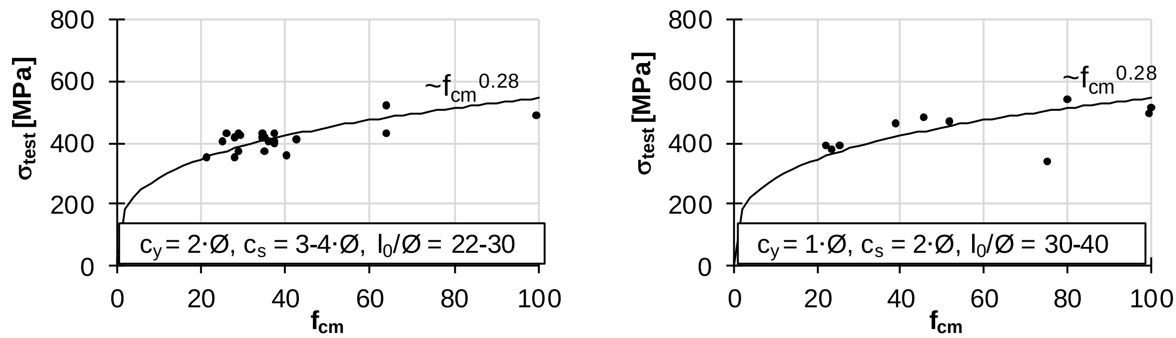

Figure 5-7 Effect of concrete strength on maximum bar stress σ_{test} at medium bottom cover and bar spacing (left) and at small bottom cover and bar spacing (right) without transverse reinforcement

Similar exponents for the effect of concrete strength f_{cm} are obtained by separately evaluating the test series described in [FER65c], [TEP73], [AZI93] and [AZI99]. Exponents between 0.18 [AZI99] and 0.34 [AZI93] were found.

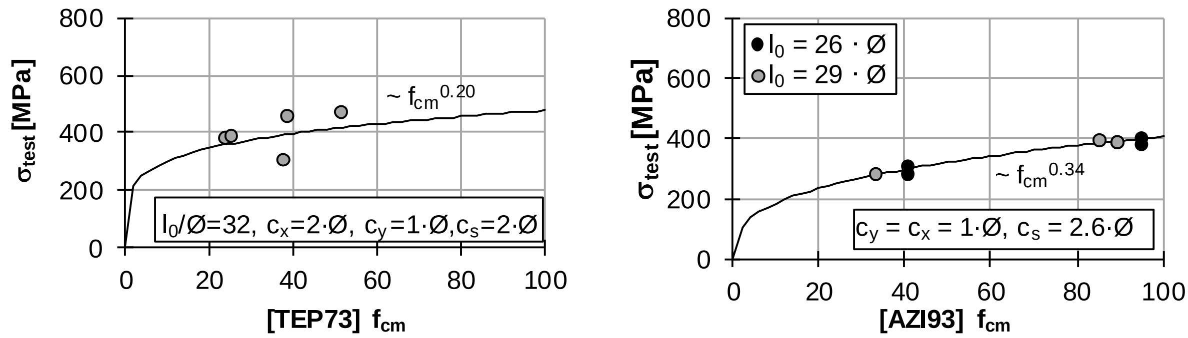

Figure 5-8 Effect of concrete strength on maximum bar stress σ_{test} obtained in test programmes conducted by [TEP73] (left) and [AZI93] (right)

EUROCODE 2 [EC2] accounts for concrete strength with an exponent 2/3 up to a limit concrete strength f_{cm} = 68 MPa. (cf. Figure 5-9, left). The course of the bar stress according to EUROCODE 2 [EC2] reflects the definition of the tensile concrete strength f_{ctm} that changes for concrete classes above C50/60.

The calculated bar stress in the bond zone with increasing concrete strength is much higher than the values calculated according to other design models. The necessary lap length depending on the concrete strength is thus smaller (cf. Figure 5-9, right). The maximum bar stress according to [EC2] is higher than the bar stress according to [EC2/NA] in Figure 5-9 (left), since the lap factor α_6 for the 25 mm bar equals 1.5 in [EC2/NA] instead of α_6 = 2.0 [EC2].

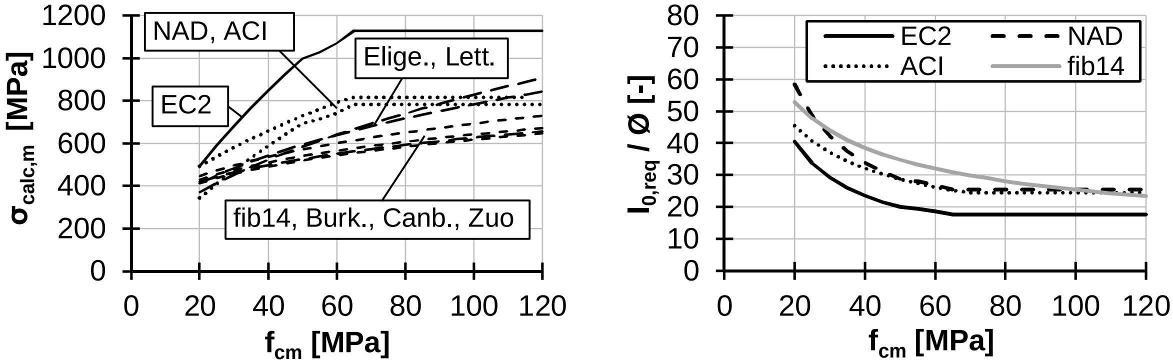

Figure 5-9 Theoretical maximum bar stress vs. concrete strength according to the considered design models for $l_0 = 40 \cdot Ø$ (left) and required mean lap length for $\sigma_s = 500$ MPa (right) according to [EC2], [EC2/NA], [ACI14] and [FIB14] with Ø = 25 mm, $c_y=c_x=c_s/2=1.5 \cdot Ø$

The [FIB14] design model with the exponent 0.25 conforms with the test results much better than [EC2] with the exponent 2/3 (cf. Figure 5-10). Hence, [EC2] substantially overestimates the lap strength at high concrete strength.

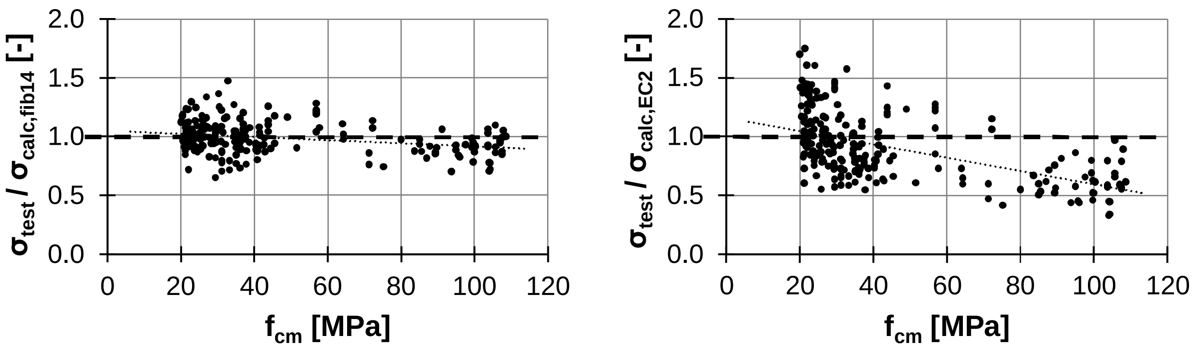

Figure 5-10 Comparison of maximum bar stress in tests to calculated bar stress according to [FIB14] (left) and [EC2] (right)

In this work, design models are evaluated with equal consideration of concrete strength for laps with and without transverse reinforcement. However, some authors found that the effect of concrete strength increases if transverse reinforcement is present (e.g. [CAN05], [ZUO00]).

5.3.3 Bar Diameter

For the evaluation of bar diameter effect, the lap length and the concrete strength as well as the concrete-cover to bar-diameter ratio must be taken into account. Tests with constant covers at changing bar diameters are suitable to investigate the effect of bar diameter. Where the concrete cover is a multiple of the bar diameter, the concrete cover strongly correlates with the lap strength. The concrete cover effect is greater than the bar diameter effect. CHINN [CHI55], FERGUSON [FER65a] and TEPFERS [TEP73] conducted tests with constant cover values at changing bar diameters.

Figure 5-11 (left) compares the ratio of the maximum bond strength as average over the bond length obtained in tests ([CHI55], [FER65a] and [TEP73]) to the maximum bond strength of the 25 mm bar with the calculated averaged bond strength according to [FIB14] and [EC2]. The lap lengths and concrete strengths were taken into account with

$$\tau_{b,a,n} = \frac{Ø \cdot \sigma_s}{4 \cdot l_b} \cdot \left(\frac{28}{l_b}\right)^{0.55} \cdot \left(\frac{25}{f_{cm}}\right)^{0.25} \tag{5-3}$$

The slight decrease in bond strength with increasing bar diameter is captured well by [FIB14]. Both, [FIB14] and [EC2] neglect the positive effect for small bar diameters. Figure 5-11 (right) illustrates a decrease in lap strength with increasing bar diameter.

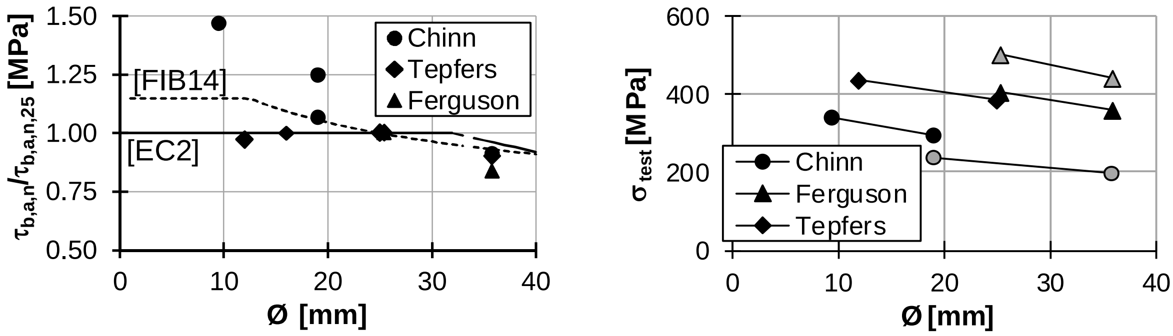

Figure 5-11 Effect of bar diameter on ratio of normalised averaged bond strength $\tau_{b,a,n}$ to normalised averaged bond strength of the 25 mm bar $\tau_{b,a,n,25}$ and on maximum bar stress in tests σ_{test} for the parameters given in Table 5-10

Table 5-10 Parameters in investigations shown in Figure 5-11

	n_b	l_0	f_{cm}	c_y	c_x	c_s
[CHI55]	1	15 · Ø	30 MPa	38 mm (grey)	1.5 · Ø	
[CHI55]	1	15 · Ø	30 MPa	15 mm (black)	c_x = 4 · Ø	
[FER65a]	2	24 · Ø (black)	30 MPa	c_y = 42 mm	1.7 · Ø	3.3 · Ø
[FER65a]	2	40 · Ø (grey)	30 MPa	c_y = 38 mm	4 · Ø	
[TEP73]	2	35 · Ø	22 MPa	2 – 3 · Ø	2 – 3 · Ø	4 - 6 · Ø

The effect of bar diameter is taken into account in [EC2] for bar diameters greater than 32 mm. The design model given in [FIB14] considers the bar diameter starting from 12.5 mm. The design models according to the NATIONAL ANNEX OF EUROCODE 2 (NAD) [EC2/NA] and [ACI14] comprise two different factors that depend on the bar diameter. For this reason, steps appear for [EC2/NA] and [ACI14] in Figure 5-12 (left and right).

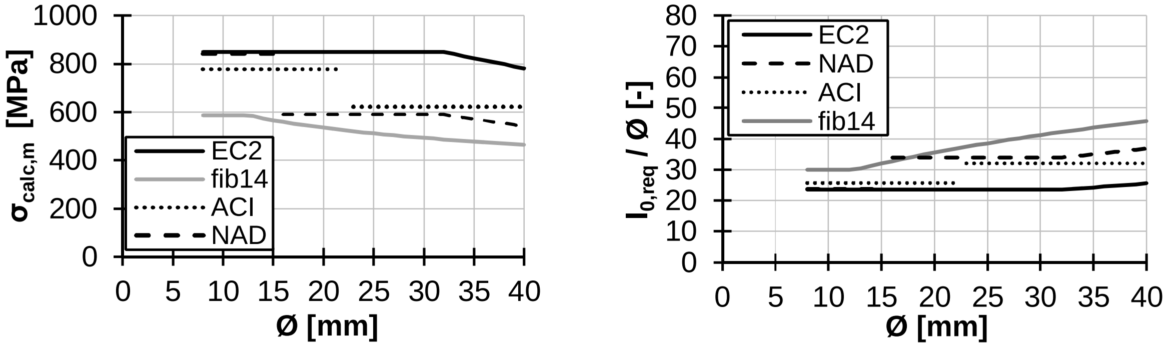

Figure 5-12 Calculated maximum lap strength vs. bar diameter for $l_0 = 40 \cdot Ø$ (left) and required mean lap length depending on bar diameter for $\sigma_s = 500$ MPa (right) according to [EC2], [EC2/NA], [ACI14] and [FIB14] with $f_{cm} = 40$ MPa; $c_y = c_x = 1.5 \cdot Ø$; $c_s = 3 \cdot Ø$

The lap strength is overestimated by [FIB14] and [EC2] for reinforcing bars with diameters above 20 mm (cf. Figure 5-13). The model according to [EC2] overestimates the overall lap strength and does not take the positive effect of small bar diameters into account. The model is uneconomic for small diameter bars and increasingly unsafe for larger diameters. The effect of the bar diameter is superimposed by the consideration of lap length. Tests with large diameters often have longer lap lengths and chapter 5.3.1 shows that the bar-stress increase with increasing lap length is overestimated by [EC2].

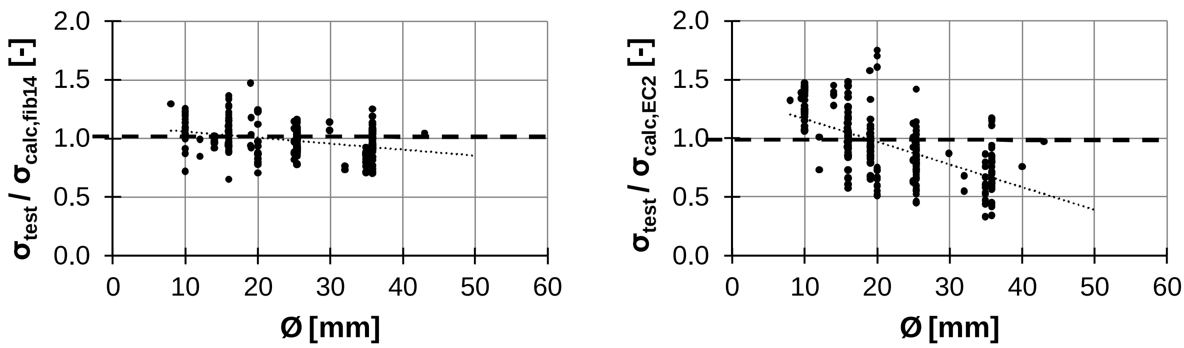

Figure 5-13 Relation of maximum bar stress in tests to calculated bar stress according to [FIB14] (left) and [EC2] (right)

5.3.4 Concrete Cover

The cover dimensions determine the splitting modes described in chapter 2.4.4. While small bottom covers c_y cause face splitting, small bar spacing c_s and small side cover c_x evoke side splitting. Since the bar or lap spacing c_s contributes to the load transfer of two bars or laps, the spacing is accounted for by c_s / 2. Thus, many design models only consider a minimum cover value $c_{min} = \min \{c_y; c_x; c_s/2\}$. To analyse the effect of concrete cover, the lap-length to bar-diameter ratio and the concrete strength are classified according to Table 5-9. Figure 5-14 shows the effect of bar spacing c_s on lap strength for different lap lengths at f_{cm} = 20 MPa to 30 MPa (left) and the effect of bottom cover c_y at f_{cm} = 30 MPa to 45 MPa (right) for the filtered database. The exponents of 0.12 and 0.47 given in the diagrams capture the test results best. For spacings of lapped bars above 10 · Ø, the lap strength does not increase any further.

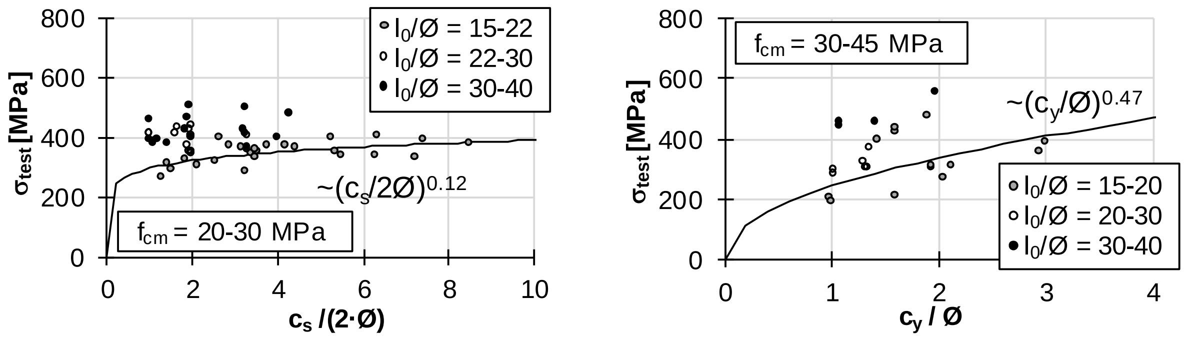

Figure 5-14 Effect of bar spacing c_s (left) and bottom cover c_y (right) on maximum bar stress σ_{test}

The effect of cover was investigated by several authors. Figure 5-15 gives the maximum bar stress over the bar spacing c_s measured in test programmes described in [REH77] and [AZI99]. While the test results by REHM [REH77] are captured with an exponent of 0.39 for c_s / 2 · Ø, the exponent must be higher for the tests conducted with high strength concrete by AZIZINAMINI [AZI99]. Figure 5-15 indicates that the positive effect of bar spacing c_s increases with increasing concrete strength.

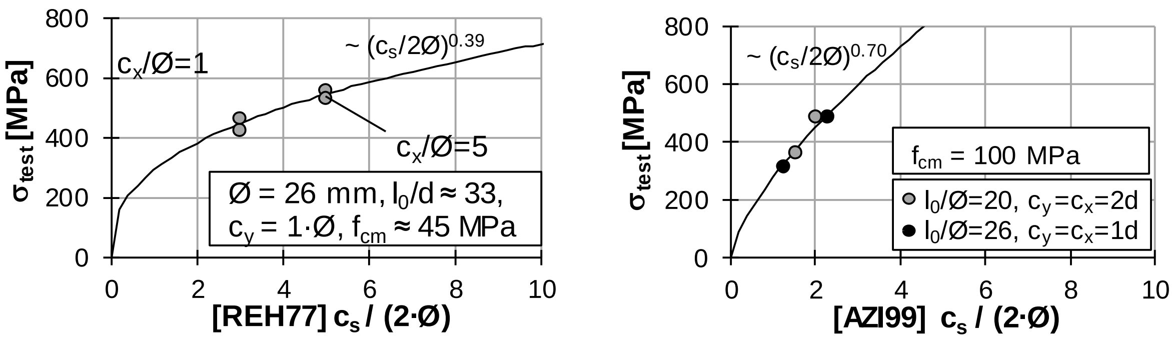

Figure 5-15 Effect of cover on maximum bar stress σ_{test} obtained in test programmes conducted by REHM [REH77] and AZIZINAMINI [AZI99]

The design model described in [ACI14] comprises a linear relationship of concrete cover and lap strength. The design model for laps in [FIB14] uses a smaller exponent with 0.25. In [EC2/NA], the effect of concrete cover and bar spacing is also covered by the lap factor α_6. This factor may be reduced for cover to bar-diameter ratios c_{min} / Ø ≥ 4 (cf. Figure 5-16).

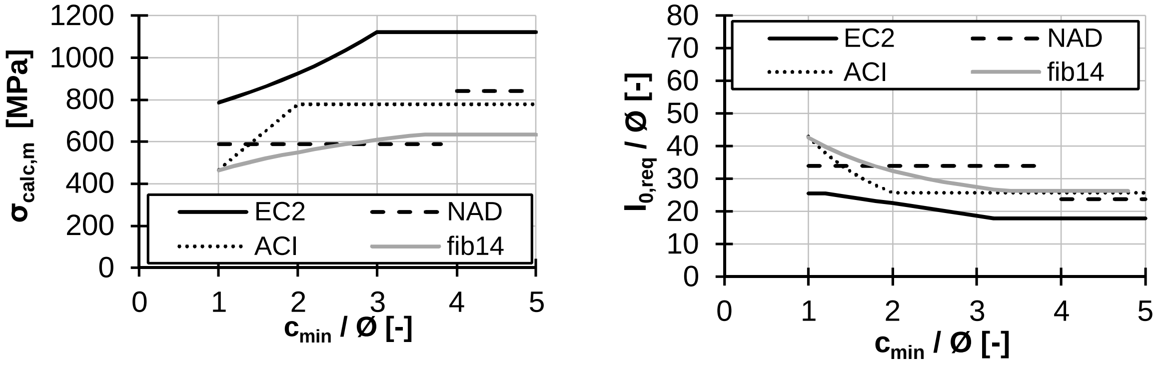

Figure 5-16 Calculated, maximum lap strength over minimum concrete cover for $l_0 = 40 \cdot Ø$ (left) and required lap length for $\sigma_s = 500$ MPa (right) depending on minimum cover with $Ø = 25$ mm and $f_{cm} = 40$ MPa

Both design models given in [EC2] and [FIB14] slightly underestimate the lap strength for small cover to bar diameter ratios (cf. Figure 5-17). Table 5-3 indicates that the design model for laps according to [EC2] overestimates the lap strength. Figure 5-17 (left) shows that the model is particularly unsafe for small cover to bar diameter ratios. The ratio of σ_{test} / $\sigma_{calc,\ fib14}$ over c_{min} / Ø with an exponent of 0.25 in [FIB14] is shown in Figure 5-17 (right).

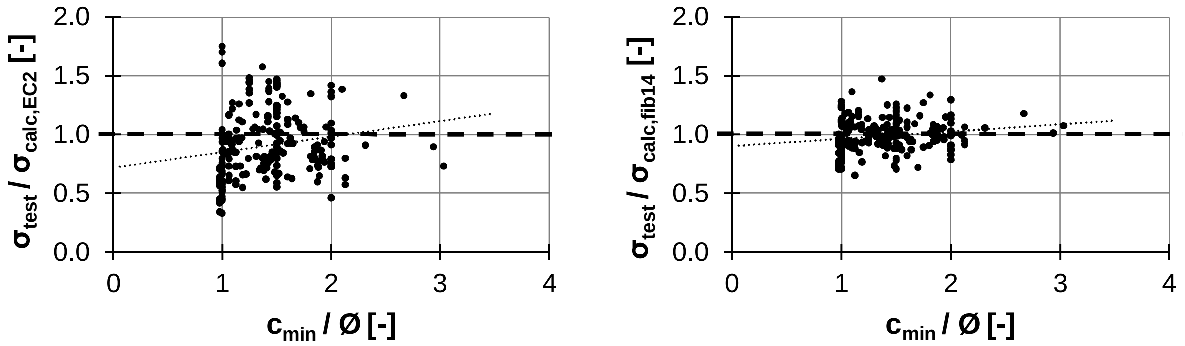

Figure 5-17 Relation of maximum bar stress in tests to calculated bar stress according to [EC2] (left) and [FIB14] (right) for different cover to bar-diameter ratios $c_{min} = \min\{c_y; c_x; c_s/2\}$

The design model according to [FIB14] (cf. equation (2-26)) considers the ratio of maximum cover to minimum cover c_{max} / c_{min}, while the other design models described in chapter 2.9 neglect the effect of this ratio. Figure 5-18 illustrates the ratio of estimated to calculated strength over the ratio c_{max} / c_{min} for [FIB14]. When neglecting the ratio (cf. Figure 5-18, left), the lap strength is underestimated for ratios c_{max} / c_{min} above 1.5. Including $(c_{max} / c_{min})^{0.1}$ results in good conformity with test results (cf. Figure 5-18, right).

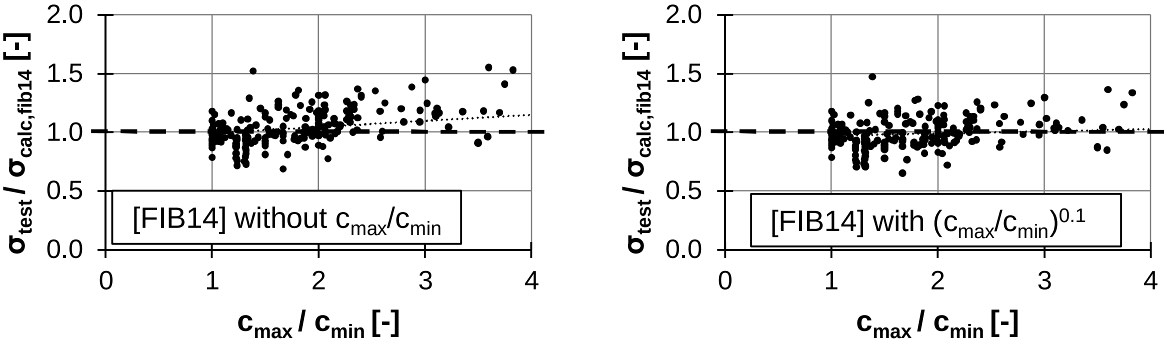

Figure 5-18 Ratio of σ_{test} / $\sigma_{calc,fib14}$ without consideration of c_{max} / c_{min} according to [FIB14] (left) and with consideration of c_{max} / c_{min} (right)

Where the ratio c_{max} / c_{min} is not taken into account for the sake of simplicity of the design model, the COV and the mean value increase (cf. Table 5-11).

Table 5-11 Statistical data for [FIB14] equation (2-26) with and without consideration of c_{max} / c_{min} presuming a log-normal distribution

$\sigma_{s,test}$ / $\sigma_{s,fib14}$	Laps with consideration of $(c_{max}/c_{min})^{0.1}$ according to [FIB14]	Laps without consideration of c_{max}/c_{min}
mean value θ	0.99	1.04
standard deviation	0.131	0.148
COV V_θ	0.132	0.142
minimum	0.65	0.65
5% characteristic ratio	0.79	0.82
number of results	457	457

5.3.5 Transverse Reinforcement

Test Series with Transverse Reinforcement in the Database

The effect of transverse reinforcement can be described either by the transverse bar spacing s_{st} or by the total cross-sectional area of the transverse reinforcement ΣA_{st} within the bond length. Figure 5-19 shows the effect of transverse bar spacing on maximum bar stress for the filtered database tests with transverse reinforcement. The bar stress decreases with increasing bar spacing, but the scatter is quite high.

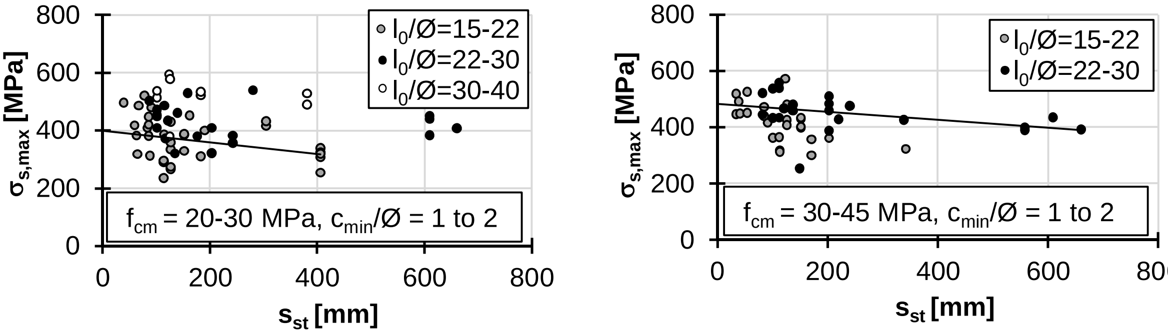

Figure 5-19 Effect of transverse bar spacing s_{st} on maximum bar stress σ_{test} at f_{cm} = 20-30 MPa (left) and at f_{cm} = 30 – 45 MPa (right)

The transverse bar spacing was varied in [AZI99], [REZ92], [REH77] and [ZUO98]. All publications show a slight decrease in ultimate bar stress for decreasing transverse bar spacing s_{st} (cf. Figure 5-20).

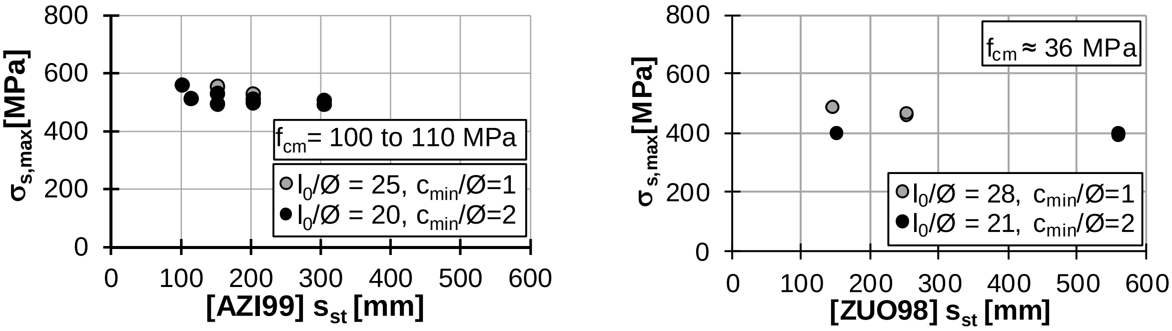

Figure 5-20 Effect of transverse bar spacing on maximum bar stress σ_{test} obtained for different transverse bar spacing in test programmes by [AZI99] and [ZUO98]

[EC2] accounts for the effect of transverse reinforcement by the ratio $\Sigma A_{st} / A_s$. This model accounts for both the total cross-sectional area of the transverse reinforcement A_{st} as well as for the transverse bar spacing within $n_{st} \approx (l_0/s_{st} + 1)$. Figure 5-21 illustrates that the maximum bar stresses in the lap database increase with an increasing ratio $\Sigma A_{st} / A_s$ as well as the strong correlation of maximum lap strength with the cross-sectional area of the transverse reinforcement.

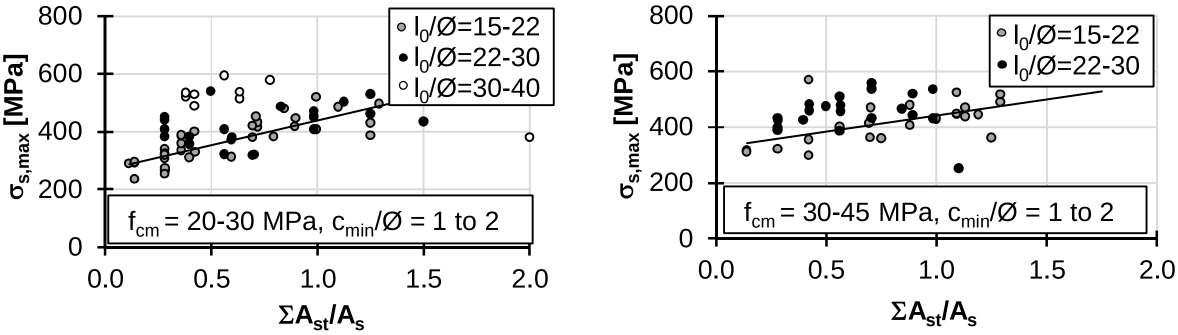

Figure 5-21 Effect of transverse-reinforcement to longitudinal-reinforcement ratio on maximum bar stress σ_{test} at f_{cm} = 20 - 30 MPa (left) and at f_{cm} = 30 - 45 MPa (right)

Design Models for the Consideration of Transverse Reinforcement

Transverse reinforcement increases the ultimate bond strength and reduces the brittleness of bond failure by adding resistance after concrete cover splitting. Resistance at splitting failure is only provided where transverse reinforcement crosses the splitting plane. It is therefore essential to estimate the splitting failure types according to chapter 2.2 (cf. Figure 5-22) before choosing the position of transverse reinforcement. While transverse reinforcement within the bottom cover adds resistance for face split failures, only vertical legs provide resistance for side split failures. According to [FIB14], face splitting changes to a side splitting type where the anchored bars or laps are positioned with a spacing smaller than 8 · Ø.

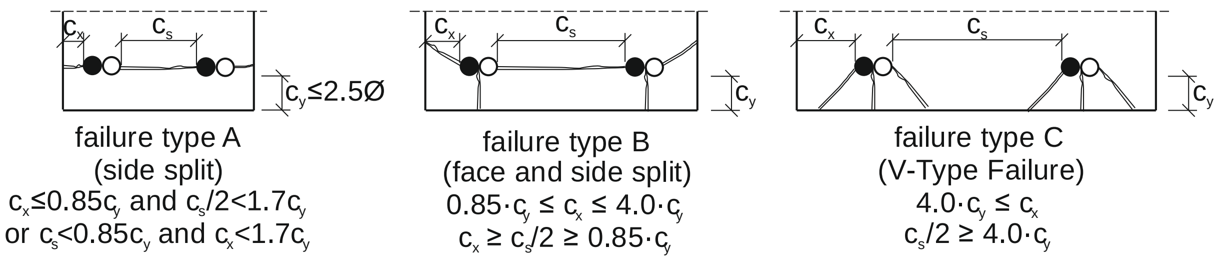

Figure 5-22 Splitting failure modes (reproduced from [ELI79] based on [FER69])

The codes described in chapter 2.9 account for the transverse reinforcement in different manners. Table 5-12 gives an overview of the design equations for the transverse reinforcement contribution. The equations are described in more detail in chapter 2.9. The effect of confining reinforcement is either taken into account by reducing the necessary lap or anchorage length l_b, by an increase in bond strength τ_b or by an increase in lap and anchorage strength f_{stm}.

Table 5-12 Contribution of transverse reinforcement to bar stress in anchorages and laps applied in selected codes

Code	Transverse reinforcement contribution	Note
[EC2] $l_{bd} = l_b \cdot \alpha_3$	$\alpha_{3,EC} = 1 - K \cdot \lambda = 1 - K \cdot \left(\frac{\sum A_{st} - \sum A_{st,min}}{A_s} \right)$ $\sum A_{st} = n_{st} \cdot A_{st}$ n_{st} = number of transverse bars	K defined in Figure 2-18 $\Sigma A_{st,min} = 0.25 \cdot A_s$ (anchorages) $\Sigma A_{st,min} = A_s \cdot (\sigma_{sd} / f_{yd}) \geq 1.0 \cdot A_s$ (laps)
[FIB14] $f_{stm} =$ $f_{stm,0} \cdot [A_{c+Ktr}]$	$\left[\left(\frac{c_{min}}{Ø} \right)^{0.25} \cdot \left(\frac{c_{max}}{c_{min}} \right)^{0.1} + k_m \cdot K_{tr} \right]^{1.82}$	k_m defined in Figure 2-19 n_t = number of transverse bars n_l = number of legs of transverse reinforcement n_b = number of bars anchored or lapped
[MC2010] $f_{bd} =$ $(\alpha_3+\alpha_2) \cdot f_{bd,0}$	$\alpha_{3,MC} = k_d \cdot (K_{tr} - \alpha_t / 50)$ $K_{tr} = \frac{n_t \cdot A_{st}}{n_b \cdot Ø \cdot s_t}$ Minimum transverse reinforcement: $\Sigma A_{st} = n_{st} \cdot n_t \cdot A_{st} \geq \alpha_t \cdot A_{s,cal.} / A_{s,prov} \cdot n_b \cdot A_s$ For $Ø \leq 20$ mm and concrete class $\leq$ C60: Transverse reinforcement provided for other reasons sufficient to satisfy minimum requirements for confining reinforcement without further justification	k_d defined in Figure 2-20 (additionally accounts for the non-linear relationship between anchorage and lap length and the stress developed in the bar) $\alpha_t = 0.5$ for $Ø \leq 25$ mm $\alpha_t = 1.0$ for $Ø = 50$ mm $A_{s,cal.}$ = required reinforcement cross-section $A_{s,prov.}$ = provided reinforcement cross-section
[PT18] $f_{stm} =$ $f_{stm,0} \cdot (c_{d,conf})^{1/3}$	$\left(\frac{c_d}{1.5 \cdot Ø} + \frac{1}{1.5} \cdot \left(30 \cdot k_{conf} \cdot \rho_{conf} + 8 \cdot \frac{\sigma_{ctd}}{\sqrt{f_{ck}}} \right) \right)^{1/3}$ $\rho_{conf} = \frac{\sum A_{s,conf}}{n_b \cdot Ø \cdot l_b} = \frac{n_t \cdot \pi \cdot Ø_t^2}{4 \cdot n_b \cdot s \cdot Ø}$	σ_{ctd} is the design value of transverse pressure k_{conf} defined in chapter 2.9.7
[ACI14] $l_{bd} =$ $l_b \cdot Ø/(c_b+K_{tr})$	$\frac{Ø}{c_b + K_{tr}} \geq \frac{1}{2.5}$ $K_{tr} = \frac{40 \cdot A_{st}[in.^2]}{s[in.] \cdot n_b}$	A_{st}: cross-sectional area of all transverse reinforcement within the spacing s crossing a potential splitting plane

The sum of the cross-sectional area ΣA_{st} depends on the transverse bar number considered. Equations (5-4) and (5-5) give the bar number for transverse bars located in the outer sections of the lap (cf. Figure 5-23, left and equation (5-4)) and distributed over the entire lap length (cf. Figure 5-23, right and equation (5-5)).

$$\text{Lap ends: } \Sigma A_{st} = n_{st} \cdot A_{st} = 2 \cdot \left(\frac{l_b}{3 \cdot s_{st}} + 1 \right) \cdot A_{st} \neq \frac{l_b}{s_{st}} \cdot A_{st} \tag{5-4}$$

$$\text{Distributed: } \Sigma A_{st} = n_{st} \cdot A_{st} = \left(\frac{l_b}{s_{st}} + 1 \right) \cdot A_{st} \neq \frac{l_b}{s_{st}} \cdot A_{st} \tag{5-5}$$

The difference between the calculated and actual transverse bar spacing increases with decreasing transverse bar number. Since laps and anchorages shall be short and the transverse bar number shall be small, there is a considerable difference between the bar spacing s_{st} and the bar spacing obtained from l_b / n_{st} (cf. Figure 5-23), where $n_{st} = 2 \cdot (l_b / (3 \cdot s_{st}) + 1)$ or $n_{st} = (l_b / s_{st} + 1)$.

This difference results in different coefficients of variation at the evaluation of design models. The evaluation of the model according to [FIB14] given in Figure 5-27 shows that the design model was presumably calibrated with the ratio l_b / n_{st}, since inserting the transverse bar spacing s_{st} gave an increased spread of the ratio between test results to calculated values.

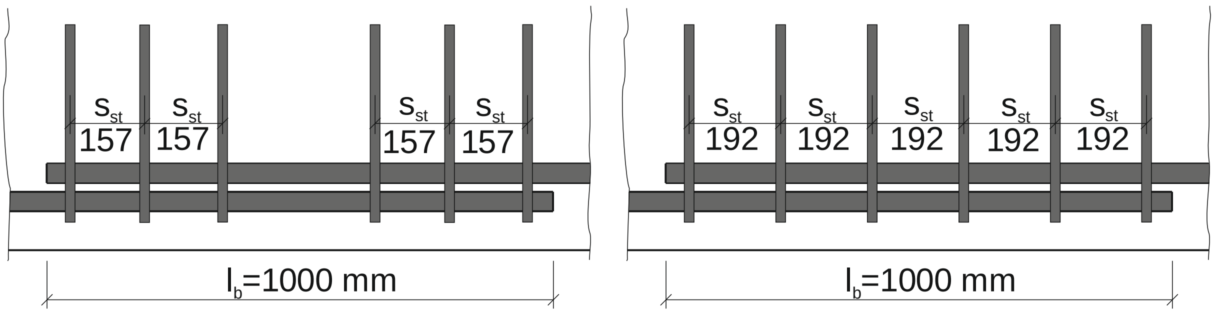

Figure 5-23 Visualisation of the difference between the calculated transverse bar spacing $s_{st,calc} = l_b / n_{st} = l_b / 6 = 167$ mm and the actual values $s_{st.lb/3} = 157$ mm (left) and $s_{st.lb} = 192$ mm (right) respectively

To evaluate the different models for the consideration of transverse reinforcement, the calculated lap strengths are compared to the lap test results documented in the database. The filtered database only comprises eight anchorage tests with transverse reinforcement. For this small number, anchorages with transverse reinforcement are not analysed here. The design model according to [EC2] correlates well with the results, but increasingly overestimates the strength for higher stress levels (cf. Figure 5-24). This is not caused by transverse reinforcement, but by the neglection of the non-linear strength increase with rising lap length in the design model according to [EC2].

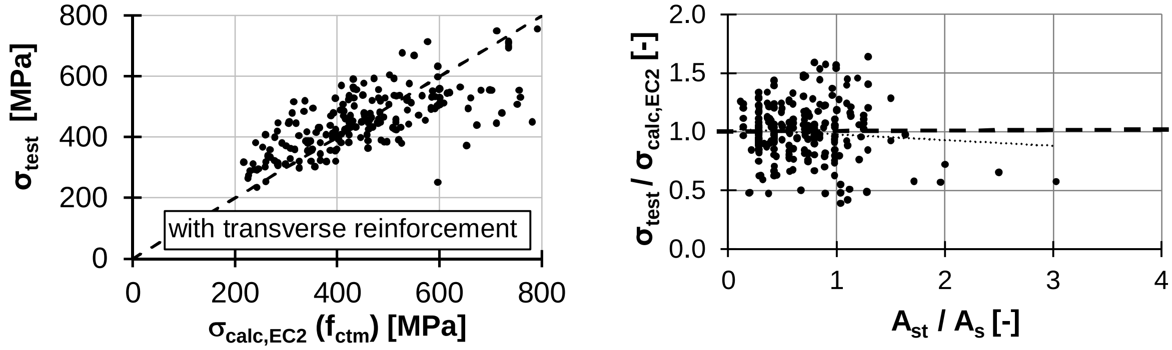

Figure 5-24 Comparison of measured lap strength $\sigma_{s,test}$ to calculated lap strength σ_{calc} according to [EC2] for laps with transverse reinforcement (left) and ratio $\sigma_{s,test}$ / σ_{calc} according to [EC2] vs. ratio of transverse reinforcement area to longitudinal reinforcement A_{st}/A_s (right)

As shown in Figure 5-25, the design model according to [ACI14] underestimates the lap strength of laps with transverse reinforcement. The overestimation is visible for all transverse reinforcement ratios A_{st} / A_s. For values A_{st} / A_s below 1.2, the influence of transverse reinforcement is generally well captured, while the scatter is relatively high.

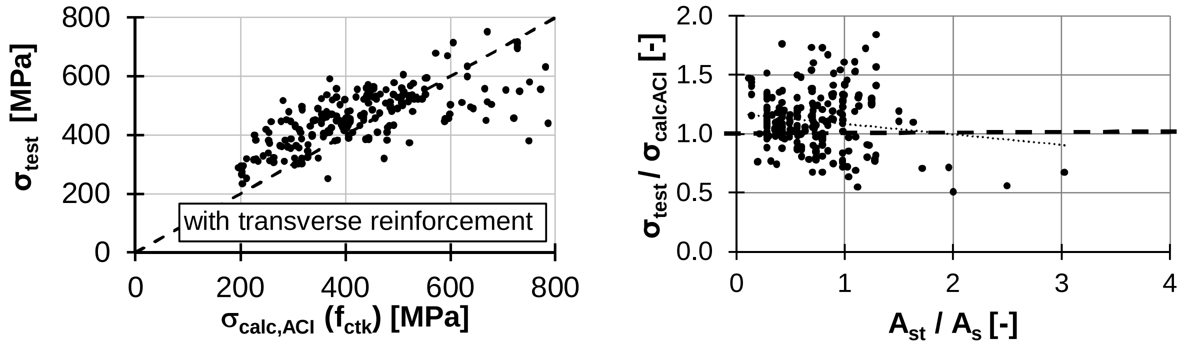

Figure 5-25 Comparison of measured lap strength σ_{test} to calculated lap strength σ_{calc} according to [ACI14] for laps with transverse reinforcement (left) and ratio σ_{test} / σ_{calc} according to [ACI14] vs. ratio A_{st} / A_s (right)

The design model according to [MC2010] was evaluated taking the characteristic value of the tensile strength of concrete $f_{ctk,0.05}$ into account The lap strength was multiplied by 1.7 to estimate mean values. The scatter is rather high when comparing the measured strength to the calculated strength according to [MC2010] (cf. Figure 5-26).

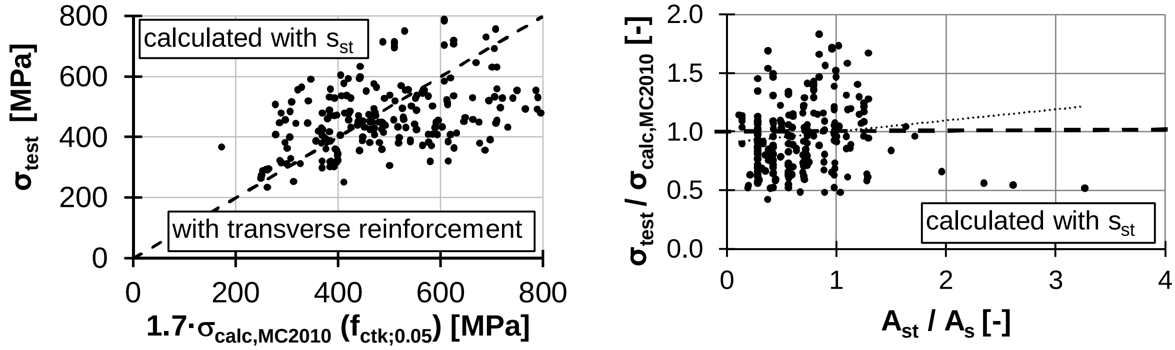

Figure 5-26 Comparison of measured lap strength $\sigma_{s,test}$ to calculated lap strength $\sigma_{calc,EC}$ according to [MC2010] for laps with transverse reinforcement (left) and ratio $\sigma_{s,test}$ / σ_{calc} according to [MC2010] vs. ratio A_{st} / A_s (right)

The design model defined in [MC2010] is based on the design model for mean strengths according to [FIB14]. While [FIB14] defines the effect of transverse reinforcement using the ratio of bond length to transverse bar number l_b / n_{st}, a footnote also allows for the use of the transverse bar spacing s_{st} instead. A comparison of test results with the calculated values according to [FIB14] is given in Figure 5-27. The evaluation of the ratio σ_{test} / $\sigma_{calc,fib14}$ shows a strong dependence on the value s_{st} and l_b / n_{st} respectively. In case the lap strength is calculated with the actual transverse bar spacing s_{st}, the scatter is much higher than applying the ratio l_b / n_{st} instead of s_{st}. Especially for small transverse bar numbers, these values are not equal (cf. Figure 5-23).

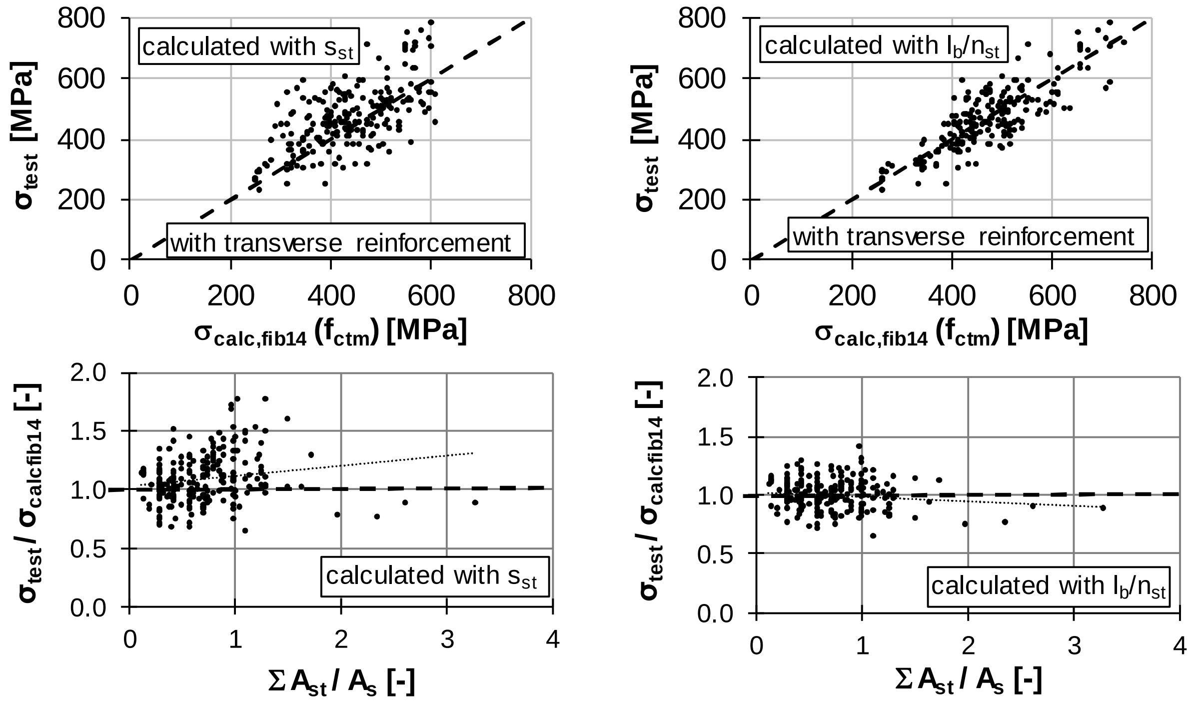

Figure 5-27 Comparison of measured lap strength σ_{test} to calculated lap strength σ_{calc} according to [FIB14] (top) and ratio σ_{test} / σ_{calc} according to [FIB14] vs. ratio of transverse reinforcement area to longitudinal reinforcement area ΣA_{st} / A_s (bottom), the values were calculated with s_{st} (left) and l_b / n_{st} (right), respectively

The COV of the model uncertainty V_θ of the design model according to [FIB14], where the contribution of transverse reinforcement is calculated from l_b / n_{st}, is smaller than the model uncertainty of the [EC2] and [ACI14] design equations.

Besides the design models yet evaluated in this chapter, the design model proposed in [PT18] that was derived from [FIB14] (cf. 2.9.7) was analysed as well. Since [PT18] gives a design lap and anchorage length only, the design equation was rearranged for the design lap and anchorage strength $f_{std,PT18}$ in equation (2-44). To find calibration factors for the mean lap and anchorage strength $f_{stm,PT18}$, the own database was used. In chapter 5.2, the calibration factor 40 in the design equation (2-44) was changed to 31 in equation (5-1) to obtain mean strength values. Furthermore, the coefficient for the transverse reinforcement ratio in design equation (2-44) was modified in equation (5-2). While [PT18] gives a coefficient of 30, the own evaluation gave much better correlation when the coefficient was changed to 60.

With this modification, the ratio $\sigma_{s,test}$ / $\sigma_{calc,PT}$ shown in Figure 5-28 resulted. The influence of transverse reinforcement is captured well with the modification described. The scatter of laps with links is even smaller than for laps without links and the influence of applying s_{st} or l_b / n_{st} is much smaller than for the equation according to [FIB14].

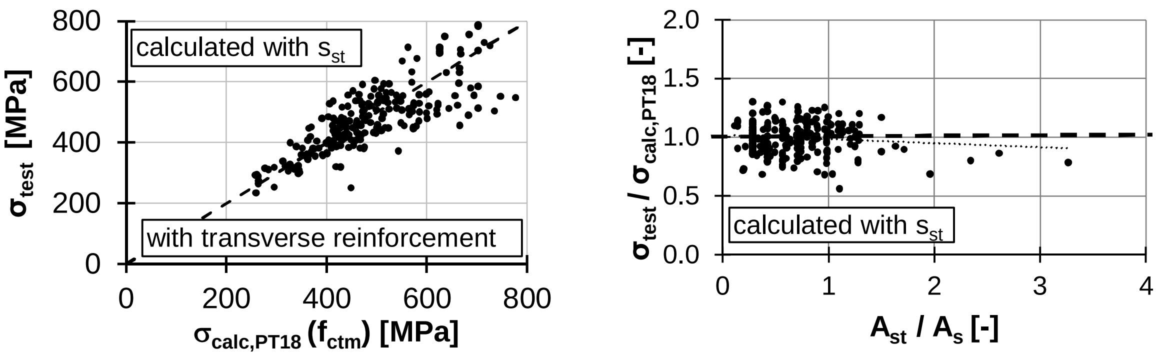

Figure 5-28 Comparison of measured lap strength σ_{test} to calculated lap strength σ_{calc} according to [PT18] with own calibration factors (left) and ratio σ_{test} / $\sigma_{calc,PT18}$ vs. ratio of transverse reinforcement area to longitudinal reinforcement area A_{st} / A_s (right)

The statistical data of the ratio of the maximum bar stress in lap tests with transverse reinforcement to the calculated bar stress is given in chapter 5.2. With $V_\theta = 0.128$, the model uncertainty θ of the design model according to [FIB14] has the smallest COV and represents the lap test results with transverse reinforcement best. The design model according to [PT18] including the own modified calibration factor has a slightly higher COV of model uncertainty θ ($V_\theta = 0.144$). Both models capture the test results in the database better than the design model according to [EC2] that has a COV of the model uncertainty $V_\theta = 0.265$.

Figure 5-29 shows the required lap length over the cross-sectional area of the transverse reinforcement A_{st} and the transverse bar spacing s_{st} (with $s_{st} = n_{st}$ / l_0). The design models for the effect of transverse reinforcement according to [FIB14] and [EC2/NA] give similar results, while the required lap length according to [EC2] is much shorter. The different required lengths according to [EC2] and [EC2/NA], result from the different lap factors α_6.

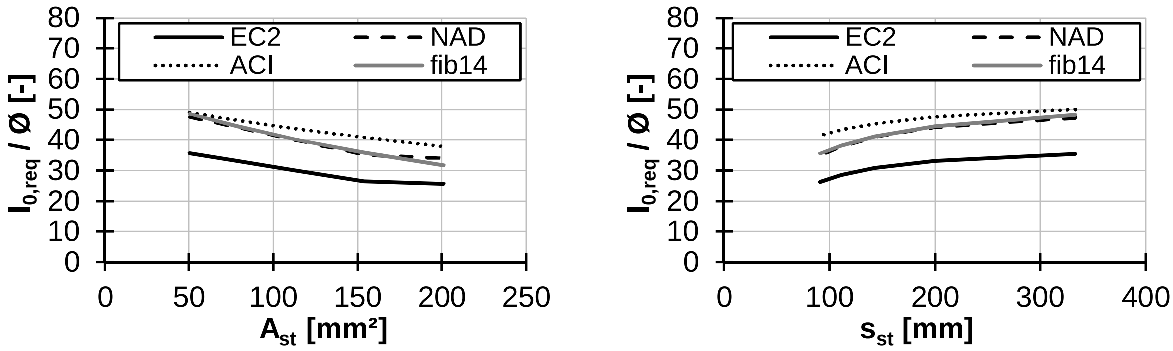

Figure 5-29 Required lap length depending on the cross-section of the transverse reinforcement (left) and depending on the spacing of the transverse reinforcement (right) for Ø = 25 mm; f_{cm} = 40 MPa; $c_y = c_x = 1.5 \cdot Ø$; $c_s = 3 \cdot Ø$; σ_s = 500 MPa

5.3.6 Yield Strength

Reinforcing bars with high yield strength require longer lap and anchorage lengths to develop the full bar force. Thus, the effect of yield strength correlates with the effect of lap length. Often, high-yield strength bars also feature high relative rib areas. FERGUSON AND BREEN [FER65a] tested bars with different yield strengths without documenting the relative rib area. A correlation of yield strength in tests described in [FER65a] to maximum bar stress is not visible in Figure 5-30 (left). The bond stress as average over the bond length slightly decreases for increasing yield strength. The bond strength for f_y = 680 MPa decreases with increasing bond length (cf. Figure 5-30, right).

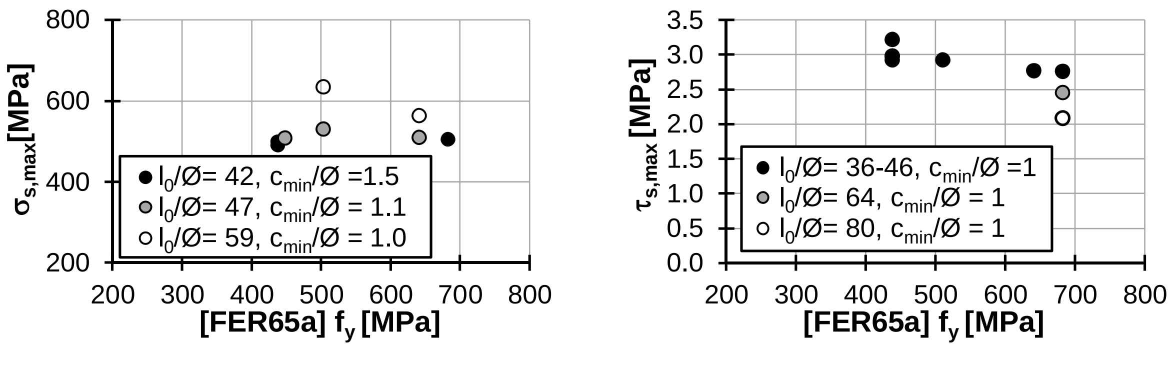

Figure 5-30 Maximum bar stress vs. yield strength for different lap-length to bar-diameter ratios (left) and averaged maximum bond strength vs. yield strength (right) in [FER65a]

The design model according to [FIB14] slightly underestimates the lap strength for yield strengths above 600 MPa (cf. Figure 5-31, left). This effect does not correlate with the effect of lap length, since it was visible for all ratios l_0 / Ø from 5.0 to 82.5 that the high-strength reinforcing bars (f_y > 600 MPa) were tested with. The design model according to [EC2] overestimates the lap strength independently from the yield strength (Figure 5-31, right).

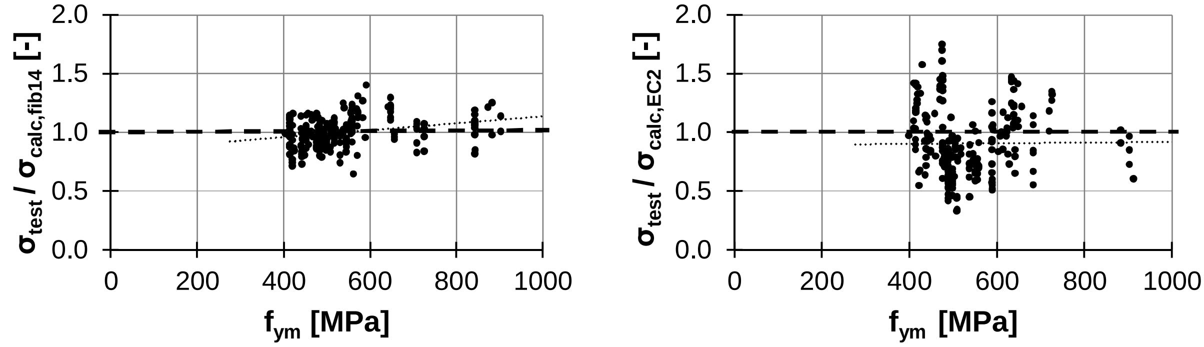

Figure 5-31 Comparison of the maximum bar stress in tests to the calculated bar stress according to [FIB14] (left) and [EC2] (right) for different yield strengths

Since the described design models do not consider the yield strength, the calculated lap strength and the necessary lap lengths are constant for all yield strengths.

5.3.7 Summary of Parameter Effects

A comparison of the database and selected publications gave the exponents for parameter effects given in Table 5-13.

Table 5-13 Exponents of influencing parameters found in the database and in selected publications

	l_0	f_{cm}	c_{min}	c_y	c_s	c_x	s_{st}	A_{st}
without links	$l_0^{\,0.45}$	$f_{cm}^{\,0.25}$	$c_{min}^{\,0.4\text{ to }0.45}$	$c_y^{\,0.4}$	$c_s^{\,0.2}$			
with links	$l_0^{\,0.4\text{ to }0.9}$	$f_{cm}^{\,0.30}$	$c_{min}^{\,0.5}$	$c_y^{\,0.5}$	$c_s^{\,0.2}$		$s_{st}^{\,-0.15}$	$A_{st}^{\,0.2\text{ to }0.6}$
[AZI95]	$l_0^{\,0.4}$						$s_{st}^{\,-0.1}$	
[AZI99]	$l_0^{\,0.5}$						$s_{st}^{\,-0.1\text{ to }0.15}$	
[AZI93]	$l_0^{\,0.5}$	$f_{cm}^{\,0.3}$						
[CHI55]	$l_0^{\,0.6}$					$c_x^{\,0.1\text{ to }0.3}$		
[FER65a]	$l_0^{\,0.55}$							
[KAD94]	$l_0^{\,0.6\text{ to }0.7}$	$f_{cm}^{\,0.2}$		$c_y^{\,0.4}$				
[OLS90]	$l_0^{\,0.6\text{ to }0.7}$	$f_{cm}^{\,0.1\text{ to }0.4}$						
[REH77]	$l_0^{\,0.4}$				$c_s^{\,0.4}$		$s_{st}^{\,-0.25}$	
[TEP73]	$l_0^{\,0.4\text{ to }0.6}$	$f_{cm}^{\,0.3}$					$s_{st}^{\,-0.1}$	
[TRE89]			$c_{min}^{\,0.3}$				$s_{st}^{\,-0.1}$	
[ZUO98]							$s_{st}^{\,-0.1}$	
[FIB14]	$l_0^{\,0.55}$	$f_{cm}^{\,0.25}$	$c_{min}^{\,0.25}$					

Since the different authors used quite different lap test parameters, the observed effects of single parameters differ strongly. This explains the different exponents for the parameter effects in different design codes. The database evaluation for laps showed good conformity of the parameter effects in tests with the design model according to [FIB14].

5.4 Database Evaluation of Parameter Effects in Anchorages

The database described above mainly includes lap tests. The design model according to [FIB14] was calibrated with the lap database and validated with anchorage test results compiled by AMIN [AMI09]. According to [FIB14], the design model is equally applicable to both laps and one-bar anchorages. For an evaluation of the design models for anchorages, a database including the test results compiled by AMIN [AMI09], additional test results obtained by RICHTER [RIC84] and the own anchorage tests described in chapter 3.5 was created. The database includes 449 anchorage test specimen, 316 of which are tests with more than one anchored bar. For the application in practice, only test results with at least two bars are included in the statistical evaluation. 253 of these tests were subjected to transverse pressure and 63 tests were conducted without transverse pressure. Applying the filter defined in chapter 5.1 leaves 165 tests with transverse pressure and 47 tests without transverse pressure in the anchorage test database.

5.4.1 Reinforcing Bar Stress Calculation

The anchorage tests with transverse pressure correspond to end anchorages of simply supported beams. Some tests in the database have a load application at the end of the anchorage length, while other tests have a longer shear span (cf. Figure 5-32). Besides beams, rectangular and diagonal beam-end tests (cf. Figure 2-12) are included in the database.

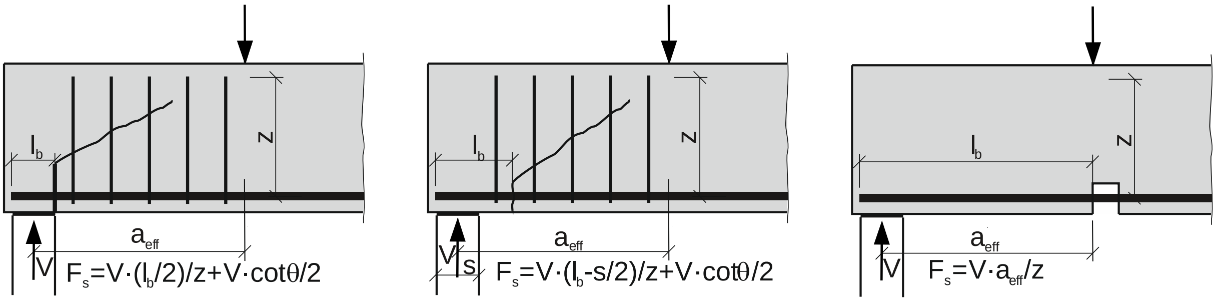

Figure 5-32 Anchorage test with induced crack at the front edge of the support (left), with bending crack with a certain distance to the front edge of the support (centre) and with bond breaker below the load application (right)

In the tests with a bond breaker (cf. Figure 5-32, right), the steel strain can be measured directly. In the tests without bond breaker – corresponding with actual structural elements – the strain measurement at the beginning of the anchorage length l_b is not always possible. The theoretical bond length starts at the front edge of the support, while the bond zone actually starts at the crack in the vicinity of the support. Since the exact position of the last bending crack is random, it is difficult to measure the steel strain in this crack with discrete strain gauges.

Alternatively, the steel strain can be determined by calculation. If the anchorage length is equal to the distance between the support and the position of the load application a_{eff} (cf. Figure 5-32, right), the theoretical steel strain is

$$\sigma_s = \frac{F_s}{\sum A_s} = \frac{V \cdot a_{eff}}{z \cdot \sum A_s} \tag{5-6}$$

In the test specimen, where the anchorage length does not stretch up to the position of the load application (cf. Figure 5-32, left and centre), the reinforcing bar stress to be developed is calculated from the bending moment at the crack in the vicinity of the support (or at the induced crack) and from the additional force from shear theory.

$$\sigma_s = \frac{F_s}{\sum A_s} = \frac{1}{\sum A_s}\left(\frac{M}{z} + \frac{V \cdot \cot\theta}{2}\right) \tag{5-7}$$

With

$$\cot\theta = \frac{1.2}{1 - \frac{V_{Ed}}{V_{Rd,cc}}} \tag{5-8}$$

θ inclination of the strut according to [EC2]
$V_{Rd,cc}$ concrete contribution according to [EC2]

5.4.2 Transverse Pressure

Design Models for the Consideration of Transverse Pressure

The anchorage test data has to be distinguished between tests with transverse pressure and tests without transverse pressure. End anchorages in simply supported beams are subjected to transverse pressure, while curtailed reinforcement is usually not.

The effect of transverse pressure is taken into account by the coefficient $1 / \alpha_5 = 1 - 0.04 \cdot p_{tr}$ in [EC2], while the design model according to [EC2/NA] accounts for transverse pressure by the constant factor 3/2.

[FIB14] gives a different model for the consideration of transverse pressure. While the design model accounts for the non-linear effect of anchorage length for the contributions of transverse reinforcement and cover, it linearly accounts for the anchorage length within the calculation of the transverse pressure contribution with

$$f_{stm,tr} = f_{stm} + 6 \cdot \frac{l_b}{Ø} \cdot p_{tr} < 1.75 \cdot f_{stm} + 0.8 \cdot \frac{l_b}{Ø} \cdot p_{tr} < 8 \cdot \frac{l_b}{Ø} \cdot \sqrt{f_c} \tag{5-9}$$

Where

$$f_{stm,tr} = f_{stm} + \Delta f_{stm} = f_{stm} + \Delta f_b \cdot 4 \cdot l_b / Ø \tag{5-10}$$

The anchorage strength increase is based on the assumption that the bond strength increases by $\Delta f_b = 1.5 \cdot p_{tr}$ for small transverse pressure approximately equal to the tensile strength of the concrete applied. The increase reduces to $\Delta f_b = 0.2 \cdot p$ for higher transverse pressure. Figure 5-33 shows the increase in anchorage strength by transverse pressure defined in [FIB14].

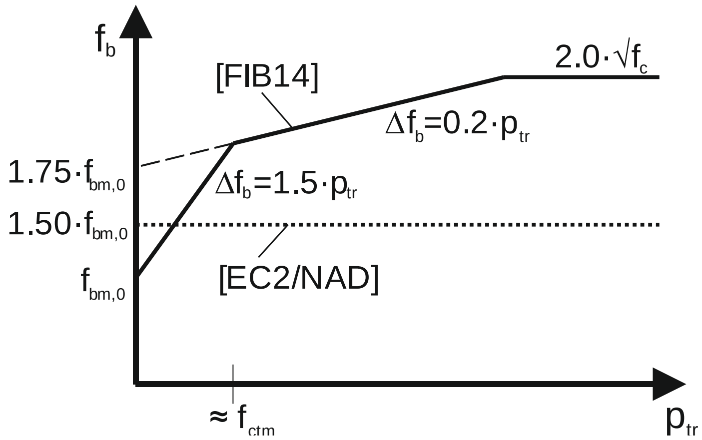

Figure 5-33 Increase of mean bond strength by transverse pressure p_{tr} according to [FIB14]

The design model for the consideration of transverse pressure in [FIB14] is applied in a slightly modified manner in [MC2010] (cf. equation (2-31)).

The Project Team [PT18] defined a design model accounting for transverse pressure in the proposal for the next generation of EUROCODE 2 based on [FIB14] that is given in equations (2-42) to (2-44) .

While [PT18] considers the non-linearity of bond-strength along the lap length, [FIB14] and [MC2010] – although based on the non-linear model – define the bar stress by the linear equation $f_{st} = 4 \cdot f_{bd} \cdot l_b / Ø$. This model requires a constant influence of transverse pressure along the anchorage length l_b.

Tests Series with Transverse Pressure in the Database

The anchorage tests with transverse pressure in the database comprise the data compiled by [AMI09] and were complemented by the tests conducted by RICHTER [RIC84] as well as with the tests in chapter 3.5. For the different test setup, the test results obtained in [CAI96] are not included in the database (cf. Figure 5-39). Figure 5-34 shows a comparison of anchorage test results with transverse pressure in comparison to the design model according to [FIB14].

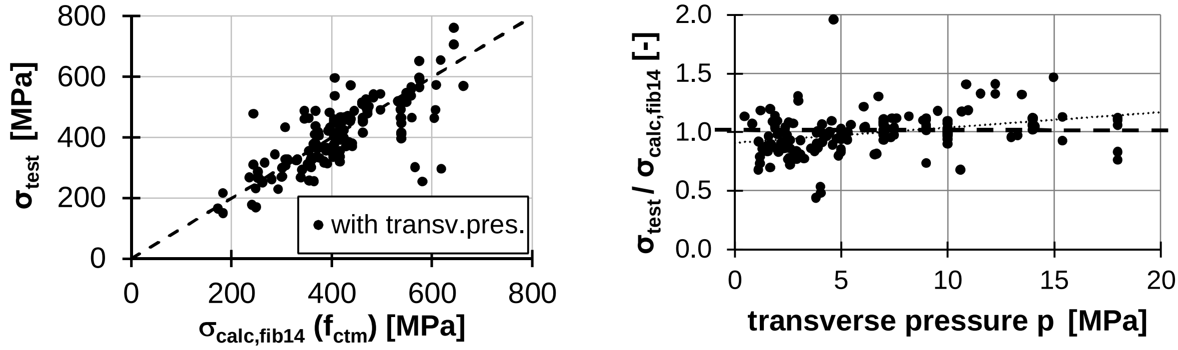

Figure 5-34 Maximum bar stress obtained in tests with transverse pressure σ_{test} in comparison with the calculated stress according to [FIB14] (left) and relationship between σ_{test} / $\sigma_{calc,fib14}$ and transverse pressure (right)

The upper limit of bond strength increase by transverse pressure in equation (5-9) is defined by the square root of the concrete strength. For a detailed analysis of the impact of transverse pressure, the limits defined in equation (5-9) were evaluated. The limit $f_{stm} > 8 \cdot l_b / Ø \cdot f_{ck}^{0.5}$ is decisive if the transverse pressure is higher than 2.6 MPa.

Figure 5-35 (left) shows that the tests described in chapter 3.5 with short anchorage lengths $l_b / Ø = 5$ conform with [FIB14], while the results of the anchorages with $l_b / Ø = 11$ to 12 are not met by the design model. In the test series conducted by RICHTER [RIC84] and the tests described in chapter 3.5, transverse pressure was always present, therefore, a comparison of ultimate anchorage strength without transverse pressure is not possible.

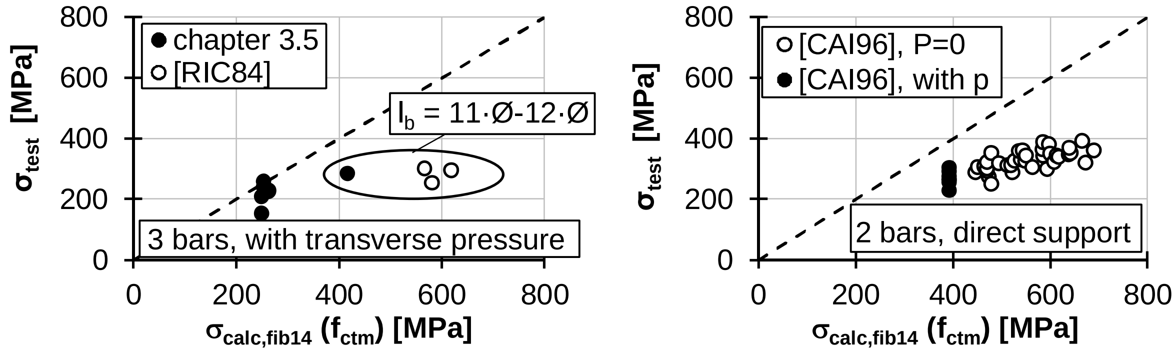

Figure 5-35 Maximum bar stress obtained in tests with transverse pressure vs. calculated stress according to [FIB14] for tests described in [RIC84] and chapter 3.5 (left) and for tests described in [CAI96] (right)

CAIRNS AND JONES [CAI96] conducted tests with and without transverse pressure. The results of both test types do not conform to the design model according to [FIB14] design model (cf. Figure 5-35, right).

The PROJECT TEAM proposal [PT18] summarises the confining effects of concrete cover, transverse reinforcement and transverse pressure within the factor $c_{d,conf}$ in equation (2-42). The value c_d for minimum concrete cover in equation (2-42) is replaced by the sum of the three confining effects. This model takes the non-linear effect of anchorage length for all contributions by confinement into account. Equation (5-31) gives the sum of the confinement contributions with a modified coefficient for the contribution of transverse reinforcement.

Figure 5-36 shows a comparison of anchorage test results with transverse pressure in comparison to the design model according to [PT18]. For the evaluation, the own calibration factors for the model according to [PT18] described in chapter 5.6.4 were applied. This measure does not change the influence of transverse pressure. This design model considers the transverse pressure with an exponent of 1/3. The effect of transverse pressure is underestimated for transverse pressures above 5 MPa.

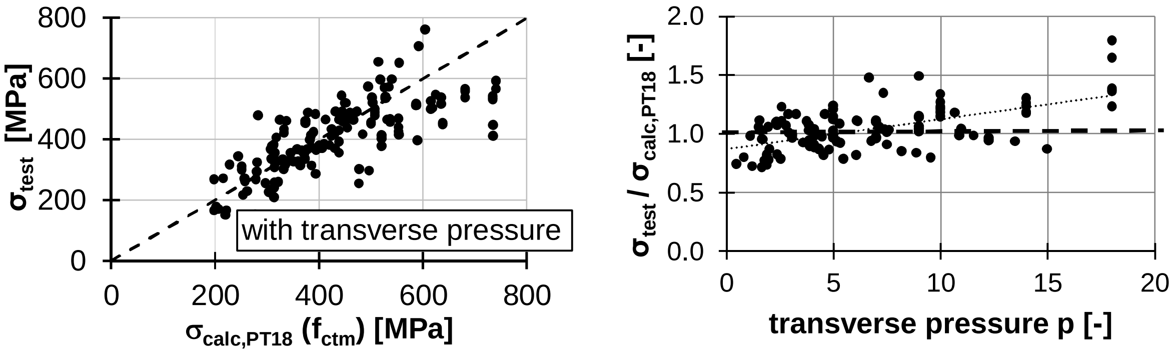

Figure 5-36 Maximum bar stress in tests with transverse pressure σ_{test} in comparison with the calculated stress according to [PT18] $\sigma_{calc,PT18}$ (left) and ratio σ_{test} / $\sigma_{calc,PT18}$ (right)

Anchorage tests conducted by BATAYNEH [BAT93], CAIRNS AND JONES [CAI96], JENSEN [JEN82] and RICHTER [RIC84] as well as the tests described in chapter 3.5 had transverse pressure confining the bond zone and at least two adjacent bars tested. The ratio of anchorage strength obtained in tests to the calculated strength without transverse pressure according to [FIB14] $\sigma_{s,test}$ / $\sigma_{fib,\ p=0}$ is given in Figure 5-37. The stress developed in the bond zone increases non-linearly with increasing transverse pressure. Since the scatter of the ratio $\sigma_{s,test}$ / $\sigma_{fib,\ p=0}$ is large, the investigations by different authors are evaluated individually.

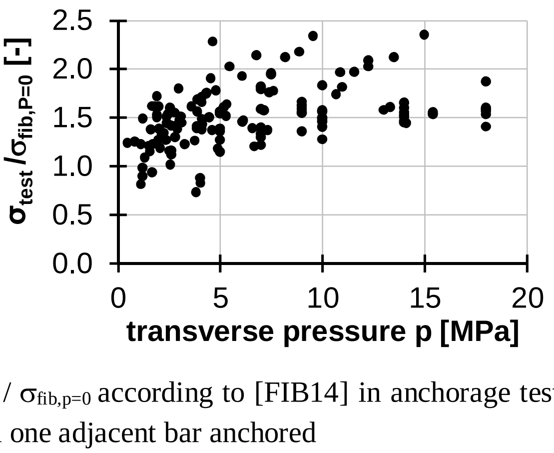

Figure 5-37 Ratio of $\sigma_{s,test}$ / $\sigma_{fib,p=0}$ according to [FIB14] in anchorage tests with transverse pressure p and more than one adjacent bar anchored

While the tests described in [RIC84] and in chapter 3.5 do not have a broad variation of transverse pressure, [BAT93] and [JEN82] comprise several tests with different transverse pressure values. The ratios of measured strength to estimated strength according to [FIB14] $\sigma_{s,test}$ / $\sigma_{fib,p=0}$ are given in Figure 5-38.

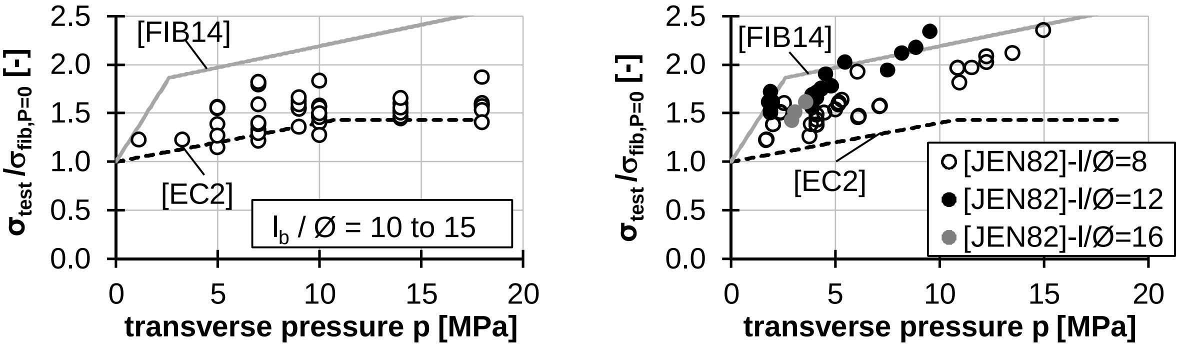

Figure 5-38 Ratio of $\sigma_{s,test}$ / $\sigma_{fib,p=0}$ in tests conducted by BATAYNEH [BAT93] (left) and JENSEN [JEN82] (right)

The reports on the tests conducted by BATAYNEH [BAT93] and JENSEN [JEN82] are not available to the author, but the test setups are described in [AMI09]. While JENSEN [JEN82] used beam-end test specimens, the tests conducted by BATAYNEH [BAT93], were direct tension members with transverse pressure (cf. Figure 5-39) .

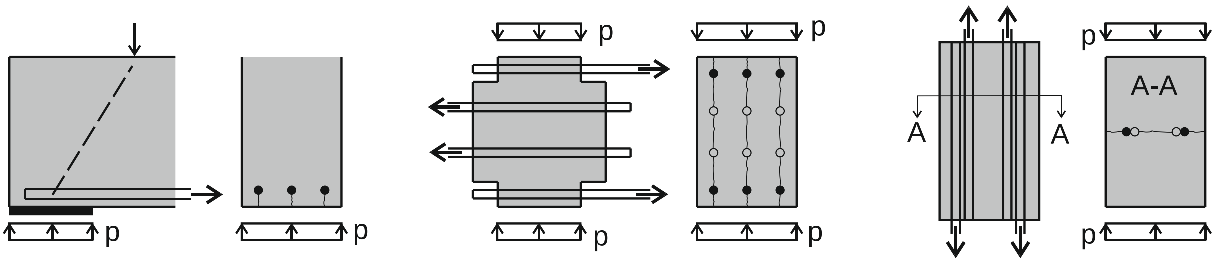

Figure 5-39 Test specimens with transverse pressure: beam-end type specimen (left), test conducted by BATAYNEH [BAT93] (centre) and tests conducted by CAIRNS AND JONES [CAI96] (right)

In contrast, CAIRNS AND JONES [CAI96] varied the transverse pressure at low values between 0.5 MPa and 2.5 MPa (cf. Figure 5-40).

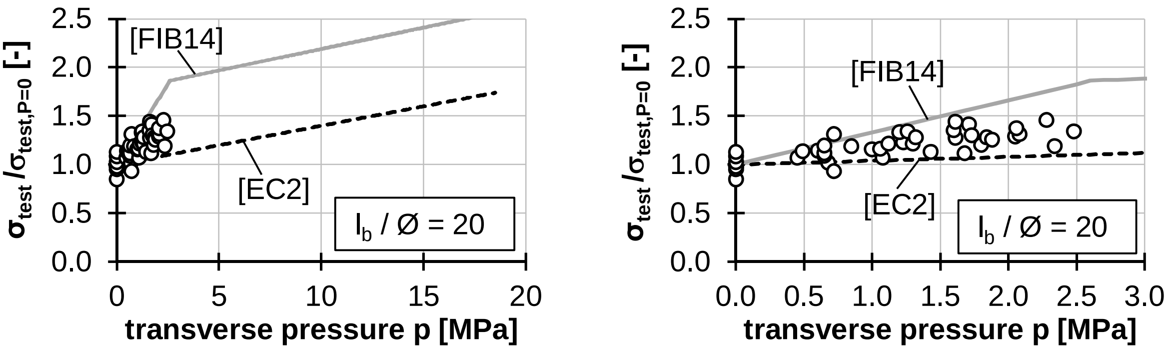

Figure 5-40 Ratio of $\sigma_{s,test}$ / $\sigma_{fib,p=0}$ in tests conducted by CAIRNS AND JONES [CAI96] with different scaling of the x-axis

CAIRNS AND JONES [CAI96] tested laps in direct tension members with very large bottom cover. The concrete strength only varied slightly in the test programmes. The lap length was 10 · Ø to 15 · Ø in [BAT93], 8 · Ø to 16 · Ø in [JEN82] and 20 · Ø in [CAI96]. The cover values were different, but these basic parameters (c_x, c_y, c_s, l_b, f_{cm}) are considered within the calculated values $\sigma_{fib,p=0}$ according to [FIB14].

For both the beam-end tests and the direct tension members, the results of long anchorages are only captured well with a non-linear model for lap length. In some test setups, the transverse pressure acts in the direction of the splitting cracks, while it acts orthogonally to the direction of the splitting cracks in other test setups (cf. Figure 5-39). The own anchorage tests developed vertical cracks in the bottom cover (cf. Figure 3-56, and Figure 5-39, left). This crack formation is even facilitated by the acting transverse pressure. Likewise, the face splitting cracks in the test specimens conducted by BATAYNEH [BAT93] are facilitated by the acting transverse pressure (cf. Figure 5-39, centre). In contrast, the transverse pressure acts orthogonal to the side splitting cracks that develop in the test specimens used by CAIRNS AND JONES [CAI96]. For the large bottom cover, face splits in the same direction as the transverse pressure are unlikely (cf. Figure 5-39, right). This fact might explain the higher increase in ultimate strength by transverse pressure observed in [CAI96] than for other test specimens. The specimens tested by [CAI96] without transverse pressure reached much lower stresses than calculated by [FIB14].

5.4.3 Parameter Effects for Anchorages

Most authors varied the transverse pressure and the concrete cover values in anchorage tests, while the concrete strength and the anchorage length were kept constant. Hence, only little data is available for an evaluation of the influence of anchorage length on developable bond stress.

Anchorage Length

Figure 5-41 (left) shows the effect of anchorage length on maximum bar stress in tests conducted by AMIN [AMI09] and in the tests described in chapter 3.5. The anchorage length effect can be described with the exponents 0.20 and 0.30, respectively.

Bar Diameter

BATAYNEH [BAT93] investigated the effect of bar diameter on the maximum bar stress. Figure 5-41 (right) compares the ratio of the maximum bond strength as average over the bond length obtained in tests [BAT93] $\tau_{b,a,n}$ to the maximum bond strength of 25 mm bars $\tau_{b,a,n,25}$ with the calculated averaged bond strength according to [FIB14] and [EC2]. The lap lengths and concrete strengths were taken into account with

$$\tau_{b,a,n} = \frac{Ø \cdot \sigma_s}{4 \cdot l_b} \cdot \left(\frac{10}{l_b}\right)^{0.55} \cdot \left(\frac{31}{f_{cm}}\right)^{0.25} \tag{5-11}$$

BATAYNEH [BAT93] conducted tests with bar diameters 8 mm, 12 mm and 16 mm. Since the values in [FIB14] refer to 25 mm bars, the value for the 25 mm bar was extrapolated.

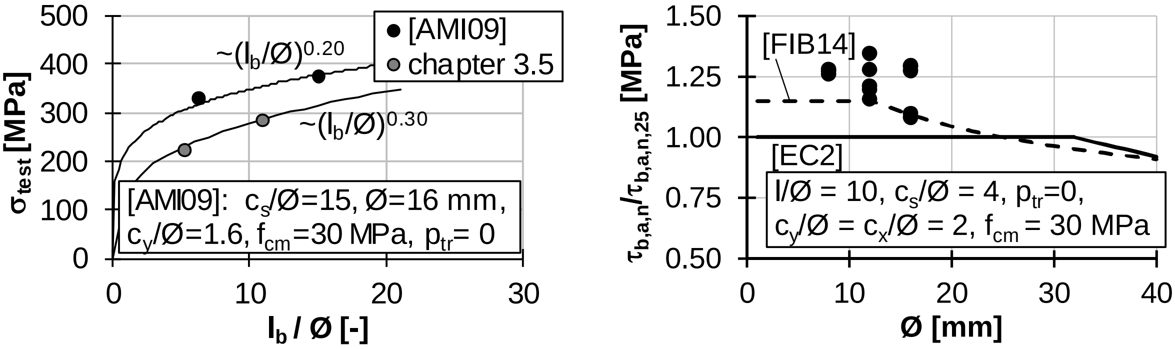

Figure 5-41 Effect of anchorage length on maximum bar stress in [AMI09] (left) and effect of bar diameter on normalised averaged bond strength $\tau_{b,a,n}$ to normalised averaged bond strength of the 25 mm bar $\tau_{b,a,n,25}$ in [BAT93] (right)

Concrete Cover

KEMP AND WILHELM [KEM79] investigated the effect of concrete cover on the maximum bar stress. They conducted tests with varying bottom cover c_y only (cf. Figure 5-42, left) and tests, where all cover values (c_y, c_x and c_s) were varied. For the latter, the parameter $c_{min} = \min \{c_s, c_x, c_y\}$ is used to describe the test results in Figure 5-42 (right). In both cases, the test results are captured with an exponent of 0.4 for the effect of cover.

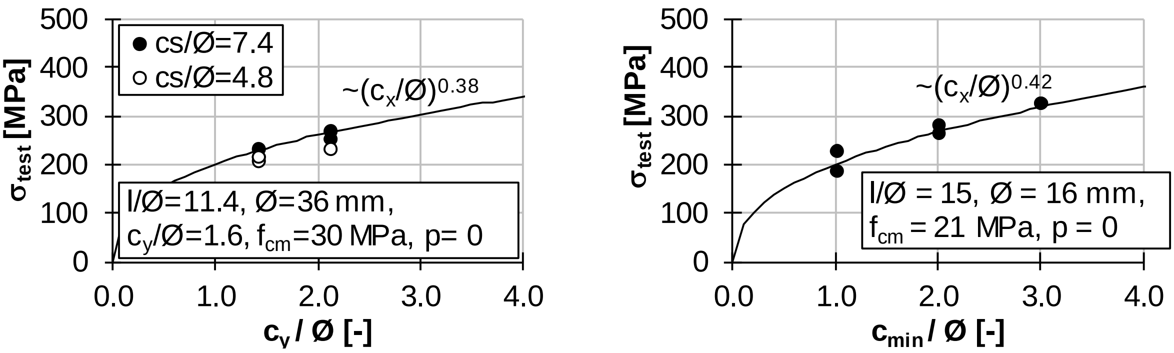

Figure 5-42 Effect of bottom cover (left) and minimum cover $c_{min} = \min \{c_s, c_x, c_y\}$ (right) on maximum bar stress in tests conducted by KEMP AND WILHELM [KEM79]

AMIN [AMI09] performed anchorage tests with varying side cover c_x. For transverse bar pressure above 2.7 MPa, the effect of concrete cover conforms to the findings in [KEM79] so that an exponent of about 0.4 describes the influence of cover correctly. In contrast, the influence of concrete cover at transverse pressure below 2.7 MPa was much smaller in the tests conducted by AMIN [AMI09] (cf. Figure 5-43).

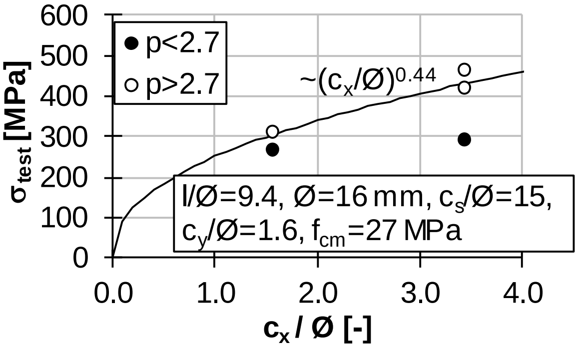

Figure 5-43 Effect of side cover on maximum bar stress obtained in anchorage tests conducted by AMIN [AMI09]

Transverse Pressure

The bond strength increase for transverse pressure is shown in Figure 5-44. BATAYNEH [BAT93] found an increase in bond strength of $0.25 \cdot p_{tr}$ for transverse pressure between 5 MPa and 18 MPa (cf. Figure 5-44, left). In contrast, RATHKJEN [RAT72] found an increase in bond strength by $1.0 \cdot p_{tr}$ for smaller transverse pressure between 1.6 MPa and 6.8 MPa. REGAN [REG97] observed an increase by transverse pressure of $2 \cdot p_{tr}$ for transverse pressure up to 1.7 MPa (cf. Figure 5-44, right). These values are comparable to the values given in [FIB14], where the increase in bond strength due to transverse pressure equals $1.5 \cdot p_{tr}$ for small transverse pressure values and $0.2 \cdot p_{tr}$ for higher transverse pressure [fib14].

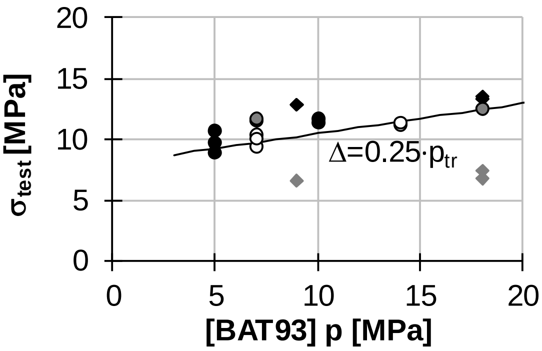

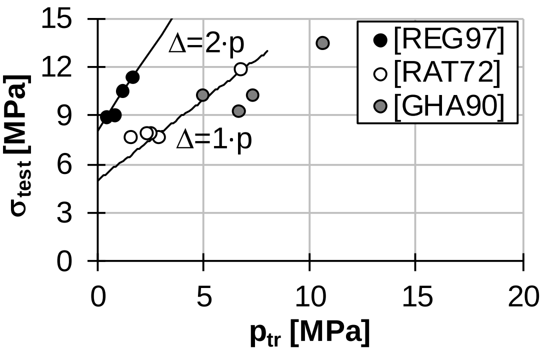

Figure 5-44 Effect of transverse pressure on bond strength for different test parameter according to [BAT93] (left) and [REG97], [RAT72], [GHA90] (right)

Summary of Parameter Effects

Table 5-14 summarises the parameter effects for anchorages found by selected authors. The exponents describing the effect of concrete cover in anchorages conform to the values obtained for laps (cf. Table 5-13). The effect of bar diameter also complies with the findings for laps. While the exponent describing the effect of lap length is about 0.5 for laps, a smaller exponent was found for anchorage lengths. It must be noted that only little anchorage test numbers with varying anchorage length at constant parameters were documented in literature.

Table 5-14 Exponents of influencing parameters for maximum bar stress found in anchorage tests in selected publications and own findings

	l_b / Ø	Ø	c_y	c_x	c_{min}
[AMI09]	$(l_b / Ø)^{0.20}$			$c_x^{\ 0.44}$	
Chapter 3.5	$(l_b / Ø)^{0.30}$				
[BAT93]		$Ø^{-0.27}$			
[KEM79]			$c_y^{\ 0.38}$		$c_{min}^{\ 0.42}$

5.4.4 Statistical Evaluation of Design Models for Anchorages

Table 5-15 summarises the data obtained in the statistical evaluation of the design models according to [FIB14], [EC2] and [EC2/NA] for anchorages with and without transverse pressure in the database described in chapter 5.1.

Table 5-15 Statistical data for anchorages without (indirect support) and with (direct support) transverse pressure presuming a log-normal distribution

	[FIB14]		[EC2]		[EC2/NA]	
σ_{test} / $\sigma_{s,calc}$	Anchorages at indirect supports	Anchorages at direct supports	Anchorages at indirect supports	Anchorages at direct supports	Anchorages at indirect supports	Anchorages at direct supports
mean value θ	1.02	0.99	0.99	1.23	1.15	1.18
standard deviation	0.168	0.184	0.283	0.315	0.356	0.280
COV V_θ	0.165	0.186	0.286	0.256	0.309	0.238
minimum	0.63	0.44	0.44	0.44	0.47	0.44
5% characteristic ratio	0.77	0.72	0.60	0.79	0.67	0.78
number of results	47	165	47	165	47	165

The statistical evaluation of the design model according to [FIB14] is in good agreement with the anchorage test results, but shows an increased COV (0.165 without transverse pressure and 0.186 with transverse pressure) in comparison to the lap test results (Table 5-2). The test results obtained by RICHTER [RIC84] and some anchorage tests described in chapter 3.5 are not well captured by the design model (cf. Figure 5-45, left). These tests have comparatively long anchorage lengths (11 · Ø and 12.4 · Ø) and no induced crack at the end of the anchorage length. Therefore, the distance between the front edge of the support and the first bending crack also contributes to the available length for the development of the bar force. When removing the four tests from the database, the mean value of the ratio σ_{test} / $\sigma_{calc,fib}$ for anchorages with transverse pressure is 1.0 and the COV is reduced from 0.186 in Table 5-15 to 0.165. This measure however contradicts the applicability of the design model according to [FIB14] for anchorages, since the removed tests represent most common anchorages in simply supported beams.

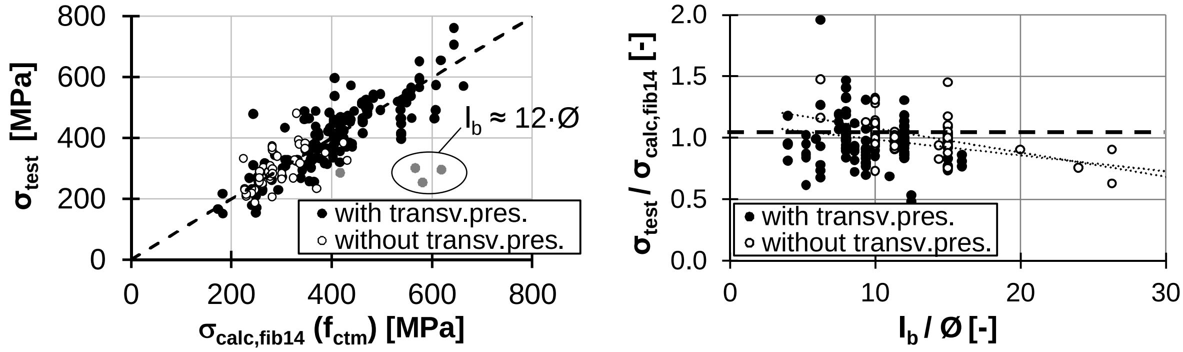

Figure 5-45 Reinforcing bar stress obtained in anchorage tests vs. calculated bar stress according to [FIB14] (left) and ratio of bar stress in tests to calculated bar stress according to [FIB14] for different anchorage lengths (right)

Although [FIB14] accounts for the non-linear effect of anchorage length on reinforcing bar stress, the model overestimates the bar stress in anchorages with long anchorage lengths (cf. Figure 5-45, right). The effects of concrete strength f_{cm}, bar diameter Ø, concrete cover c_{min} and transverse pressure p_{tr} are captured correctly by the design model according to [FIB14] (cf. Figure 5-46).

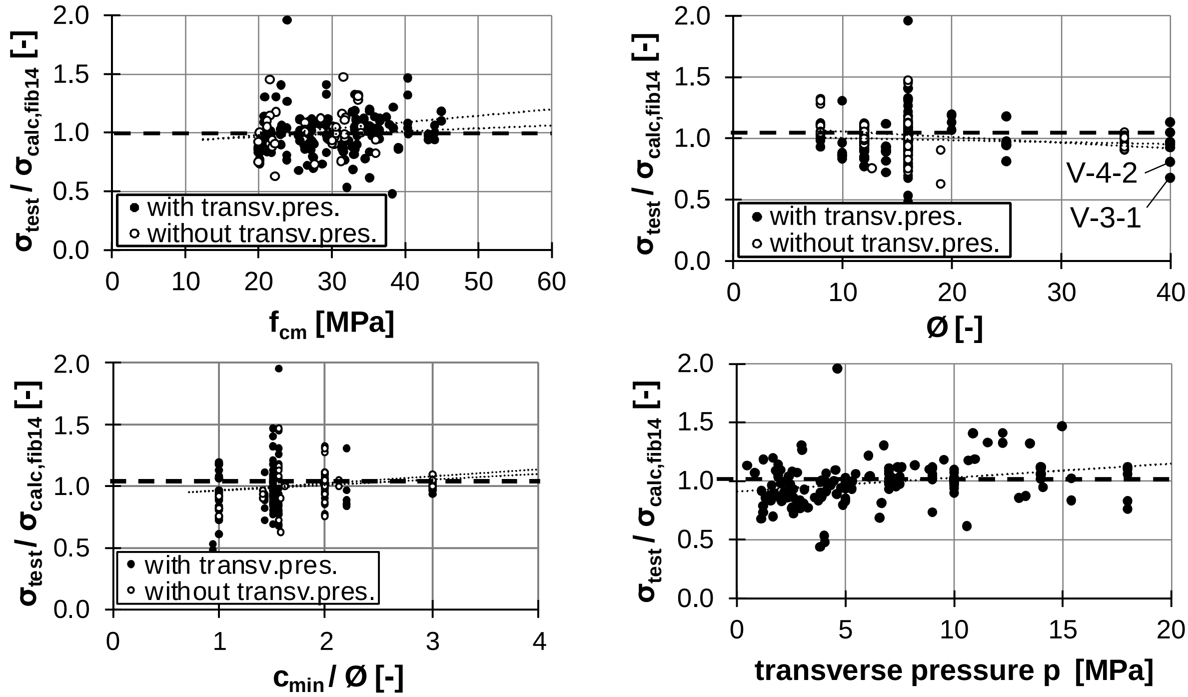

Figure 5-46 Ratio of maximum bar stress in tests to calculated bar stress according to [FIB14] for different concrete strengths f_{cm} (top, left), bar diameters Ø (top, right), concrete covers c_{min} (bottom, left) and transverse pressure p_{tr} (bottom, right)

The design models according to [EC2] and [EC2/NA] underestimate the maximum bar stress of anchorages at direct supports (Table 5-15). For anchorages with and without transverse pressure, the standard deviation is about the same as the standard deviation for laps. These design models overestimate the obtainable bar stress for tests with comparably long anchorage lengths of 25 · Ø and 26 · Ø (cf. Figure 5-47). The comparison of test results and values calculated according to [EC2] and [EC2/NA] is given in Figure 5-47 and Table 5-5. The ratios $\sigma_{s,test}$ / $\sigma_{calc,EC2}$ and $\sigma_{s,test}$ / $\sigma_{calc,NAD}$ also differ for test specimen without transverse pressure, since the concrete cover is taken into account differently (cf. chapter 2.9.3).

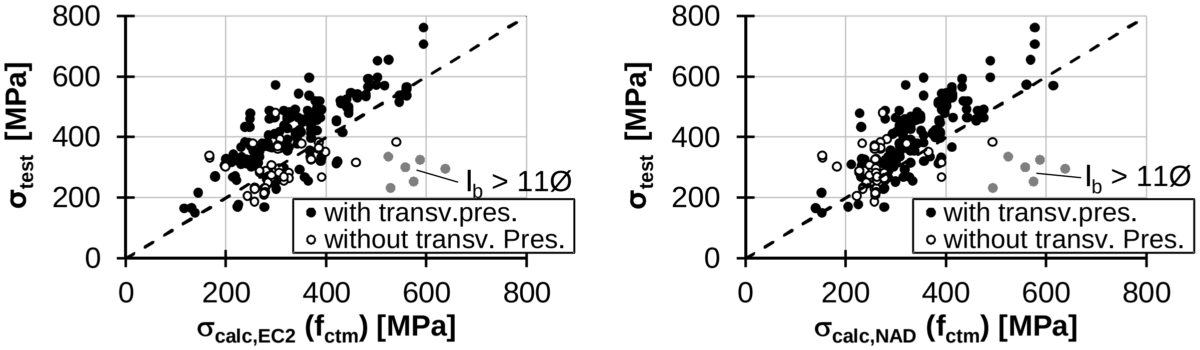

Figure 5-47 Maximum bar stress obtained in anchorage tests with and without transverse pressure vs. calculated bar stress according to [EC2] (left) and according to [EC2/NA] (right)

The design model for mean anchorage strengths according to ACI [ACI14] (dividing the equation given in the code by the factor 0.9, cf. chapter 5.2) underestimates the maximum bar stress in anchorages (cf. Figure 5-48). In contrast, the maximum bar stress was overestimated for two tests with long anchorage lengths. The mean value θ_{ACI} of the ratio $\sigma_{s,test}$ / $\sigma_{calc,ACI}$ is much higher for anchorages (V_θ = 1.42 and 1.90, respectively) than for laps (V_θ = 1.07). Table 5-7 gives an overview of the statistical data for the design model according to [ACI14].

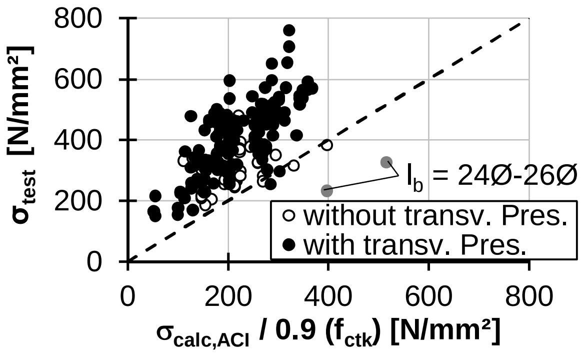

Figure 5-48 Reinforcing bar stress obtained in anchorage tests vs. calculated bar stress [ACI14]

5.5 Comparison of own Tests with Database

Besides the validation of existing design models, the database compiled here enables a validation of the own test results described in chapters 3.4 and 3.5. Figure 5-49 compares the anchorage test results (left) and the lap test results (right) with the database.

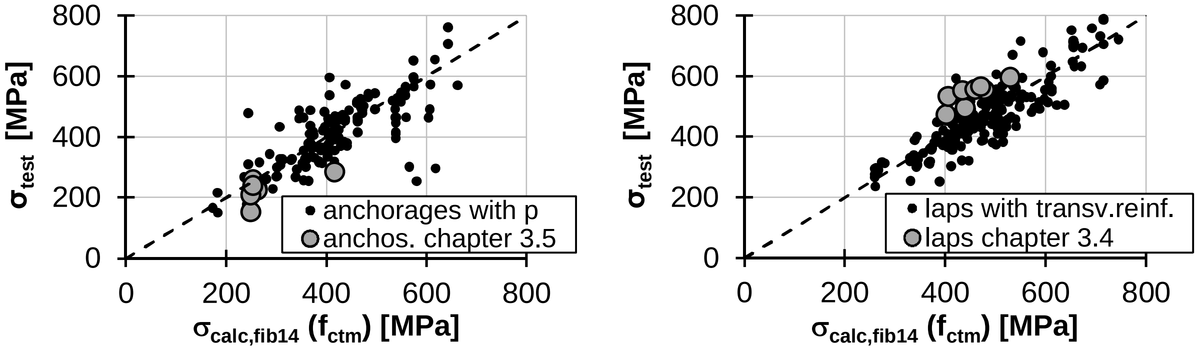

Figure 5-49 Maximum bar stress obtained in anchorage tests described in chapter 3.5 and in the anchorages with transverse pressure in the database (left) and maximum bar stress obtained in lap tests described in chapter 3.4 with the laps with transverse reinforcement in the database (right)

A total of 12 anchorage tests was conducted, but only seven tests are considered in the database. Two tests included additional reinforcement (V5-1 and V5-2) and three anchorages did not fail and were therefore excluded from the database (V2-1, V2-2 and V4-1). The anchorage tests without transverse reinforcement both with $l_b = 5 \cdot Ø$ (V3-1) and $l_b = 11 \cdot Ø$ (V4-2) reached considerably smaller maximum bar stress than calculated with the design model according to [FIB14]. For the test with the short bond length (V3-1), this was presumably caused by the unfavourable steel sheet geometry that was used to induce a crack at the front edge of the support. The test specimen with the increased bond length (V4-2) had the longest anchorage length tested and did not include a crack induction. The database evaluation showed that all tests in the database with long anchorage lengths and transverse pressure are overestimated by the design model according to [FIB14] that takes the positive effect of transverse pressure over a linearly considered anchorage length into account.

From the 17 lap tests conducted in total, only eight tests are considered in the database. Conforming with the filter described in chapter 5.1, the test specimens with surface reinforcement (T7, T9, T10, T11 and T18), a percentage of lapped bars smaller than 100 % (T12 and T13) and with a bar diameter combination (T15 and T16) were excluded from the database. The parameter effects on maximum bar stress obtained in the tests conform well with the design model according to [FIB14]. All lap tests showed slightly higher maximum lap strength than the average lap strength in the database (cf. Figure 5-49, right).

5.6 Own Design Model for Anchorages and Laps

Although the design model according to [FIB14] captures both laps and anchorages quite well, slightly different factors for the contributions of transverse reinforcement and transverse pressure are proposed. Besides the own model based on [FIB14], own calibration factors for the design model according to [PT18] were derived. These two design models for the mean bar stress in anchorages and laps best fit the test results. Therefore, these models for mean bar-stress values provide the basis for the derivation of design values in chapter 7.4.

5.6.1 Consideration of Transverse Reinforcement

<u>Positioning of Transverse Reinforcement in Anchorages and Laps</u>

For the non-linear strain distribution in laps, it is recommended to position the transverse reinforcement not along the entire lap length, but at the outer thirds of the lap (cf. Figure 5-50, left). In case the transverse reinforcement is distributed along the lap length, the bars in the centre of the lap length are not activated.

A distribution along the outer thirds of anchorages is not reasonable, where anchorage lengths are small. Therefore, for anchorages a uniform reinforcement positioning distributed along the entire anchorage length is recommended (cf. Figure 5-50, right).

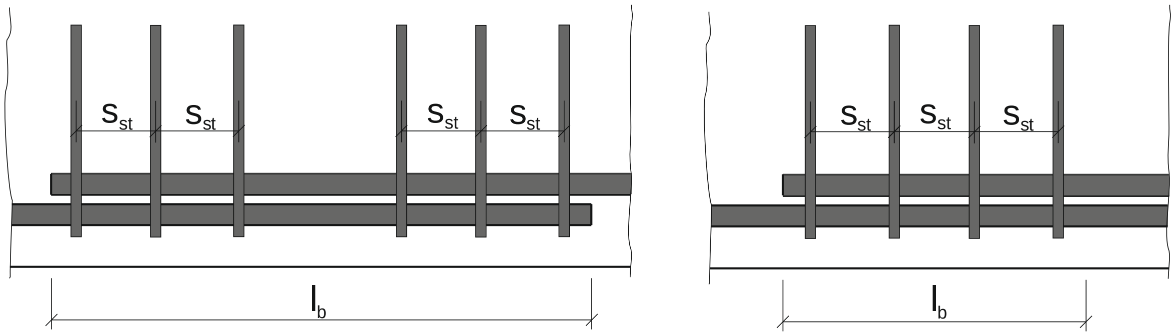

Figure 5-50 Recommended transverse reinforcement distribution for long anchorage lengths, e.g. in laps (left) and for short anchorage lengths (right)

The effect of transverse reinforcement can be described by the transverse bar spacing s_{st} or the number of bars n_{st}. Anchorage lengths and thirds of lap lengths are usually small (cf. Figure 5-50) and the ratio of the bond length to the stirrup number l_b / n_{st} does not equal the transverse bar spacing s_{st}. For this reason, the consideration of transverse reinforcement by transverse bar number or transverse bar spacing does lead to different results as described in chapter 5.2.5.

Since the bar spacing s_{st} does not equal l_b / n_{st} and the transverse reinforcement distribution shall be non-uniform in laps, a calculation of required lap length with s_{st} is recommended. It is also more comprehensible not to calculate the design bond length l_{bd} with a transverse reinforcement contribution defined by the bond length itself. Equation (5-12) gives the proposed factor α_{tr} for the contribution of transverse reinforcement in the design equation for anchorage and lap strength.

$$\alpha_{tr} = k_m \cdot \rho_{conf} = k_m \cdot \frac{A_{st}}{\text{Ø} \cdot s_{st}} \tag{5-12}$$

With k_m according to [FIB14] (cf. Figure 5-53)

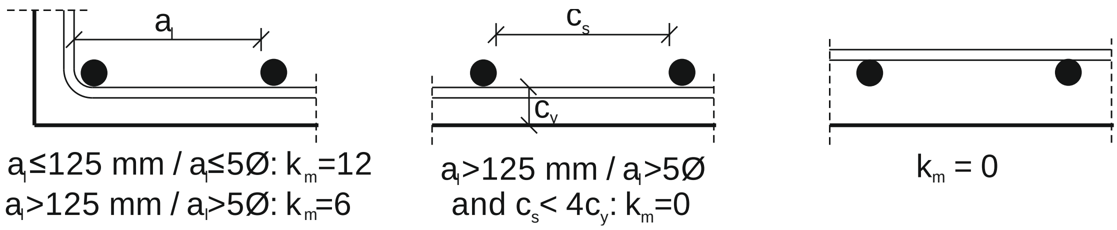

Figure 5-51 Coefficient k_m for efficiency of transverse reinforcement (adapted from [FIB14])

Equation (5-12) neglects the leg number of the transverse reinforcement n_l and the anchored or lapped bar number n_b that are both included in the [FIB14] design equation. Although stirrups cross the potential splitting plane in side-split-failures twice, their horizontal leg only contributes to face-split-failures once (cf. Figure 2-5 and Figure 2-6). It is therefore necessary to consider the transverse reinforcement only once. Still, the positioning of stirrups is necessary, since side-split-failures are not prevented by transverse bars within the vertical cover. The removal of the leg number crossing the potential splitting plane n_l is also recommended, since the exact splitting plane may not be known during design.

The consideration of the number of the anchored or lapped bar n_b would only be necessary in case one transverse bar would only contribute to one longitudinal crack. Instead, the transverse reinforcement does not yield (cf. chapter 3 and [FIB14]), but only contributes to the confinement of the bond zone. Therefore one transverse bar contributes not only to the crack width reduction of several longitudinal cracks, but also to the confinement of several adjacent lapped or anchored bars.

Minimum Transverse Reinforcement

For the control of longitudinal splitting cracks and for an increase in ultimate bond strength, a certain minimum transverse reinforcement is recommended. Confining reinforcement introduces a modest amount of ductility into the failure mechanism. Although splitting failure is only prevented by continuous longitudinal bars, transverse reinforcement reduces longitudinal crack widths and reduces the scatter of the ultimate lap or anchorage strength. Transverse reinforcement positioned for other reasons (such as shear, confinement in columns, transverse longitudinal reinforcement in slabs) may also contribute to bond strength. Transverse reinforcement is only redundant where the cover to bar-diameter ratio is high or in case transverse pressure significantly contributes to confinement of the bond zone [FIB14]. For the specification of minimum confining reinforcement, the bursting forces caused by bond are considered.

CANBAY AND FROSCH [CAN05] give a definition of bursting forces F_{split} depending on the bar force F_s and the angle of the compression struts θ commencing from the ribs given in equation (5-13). For the analysis conducted, they recommend an angle θ = 20°.

$$F_{split} = F_s \cdot \tan\theta = 0.36 \cdot F_s \qquad (5\text{-}13)$$

This value approximately agrees with the perception that the vertical component of the bond strength τ_b is distributed over the area enclosed by bar diameter and bond length $Ø \cdot l_b$ (cf. Figure 5-52 and equation (5-14)).

$$F_{split} = \tau_b \cdot Ø \cdot l_b = \frac{F_s}{U_b \cdot l_b} \cdot Ø \cdot l_b = \frac{F_s}{\pi \cdot Ø \cdot l_b} \cdot Ø \cdot l_b = 0.32 \cdot F_s \qquad (5\text{-}14)$$

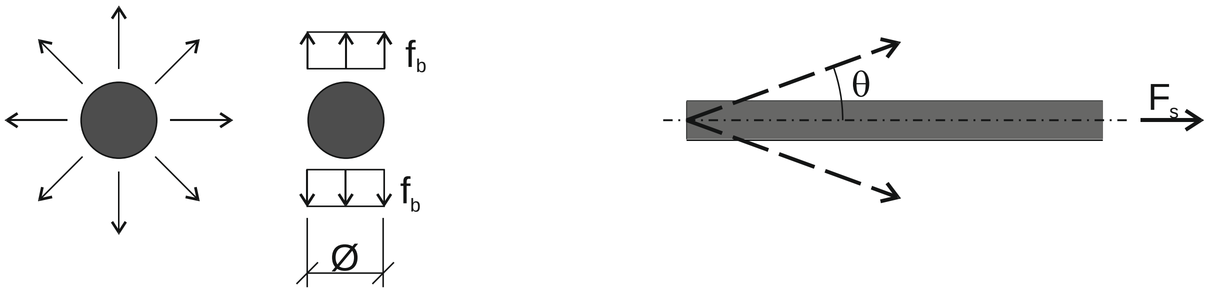

Figure 5-52 Approximation of confinement force F_{split} orthogonal to the anchored bar according to [FIB14] (left) and according to [CAN05] (right)

Since the bond stress is neither uniformly distributed around the bar circumference nor along the lap length, it is recommended in [FIB14] that confining reinforcement should resist at least half the total force transferred by bond instead of 36 % or 32 %. If the full yield strength of a bar is to be anchored and links are of the same grade, then a total area of transverse reinforcement of at least half the total cross-sectional area of the bonded bars should be supplied within the lap or anchorage length. The minimum total area is

$$\sum A_{st,min} = 0.5 \cdot A_s \qquad (5\text{-}15)$$

Taking the small transverse bar stress obtained in several tests into account increases the required cross-sectional area of the transverse reinforcement to

$$\sum A_{st,min} = n_{st} \cdot A_{st} = 0.5 \cdot A_s \cdot \frac{435}{250} \approx 1.0 \cdot A_s \qquad (5\text{-}16)$$

Where the transverse reinforcement is positioned in the outer thirds of the lap length (cf. Figure 5-50, left), the transverse bar spacing is defined by

$$s_{st} = \frac{l_b}{1.5 \cdot n_{st} - 3} \qquad (5\text{-}17)$$

The distance between the lap or anchorage end and the position of the first transverse reinforcing bar shall equal the longitudinal bar diameter. This distance is neglected during design. Since the transverse bar spacing should be wide enough to allow for good concrete compaction, the positioning of transverse bars within the outer thirds should neither imply too little transverse bar spacing. For compaction it is advisable to provide a transverse bar spacing s_{st} of 80 mm or more. Therefore, a regular distribution of transverse reinforcement makes more sense if the design anchorage or lap length is small (cf. Figure 5-50, right). In bond zones with a design length below 250 mm, the positioning of uniformly distributed transverse reinforcement is recommended with

$$s_{st} = \frac{l_b}{n_{st} - 1} \tag{5-18}$$

<u>Maximum Transverse Reinforcement</u>

The contribution of transverse reinforcement to the maximum bar stress in bond zones is limited. The upper limits defined in codes were derived from the original formulation by ORANGUN [ORA77], where

$$\frac{1}{500} \cdot \frac{A_{st} \cdot f_{ytr}}{s_{st} \cdot Ø} \leq 3.0 \rightarrow \text{with } f_{ytr} = 20.000 \text{ ksi} \rightarrow \frac{A_{st} \cdot 40}{s_{st} \cdot Ø} \leq 3.0 \tag{5-19}$$

ACI CODE 318 [ACI14] defines a combined upper limit for the contributions of concrete cover and transverse reinforcement given in equation (5-20). Applying the minimum permissible concrete cover c_b / Ø = 0.5, the upper limit for confinement is 2.0.

$$\frac{c_b + K_{tr}}{Ø} = \frac{c_b}{Ø} + \frac{40 \cdot A_{st}\left[\text{in.}^2\right]}{Ø \cdot s_{st}\left[\text{in.}^2\right] \cdot n_b} \leq 2.5 \tag{5-20}$$

Expanding the maximum contribution by transverse reinforcement in equation (5-21) defined in [FIB14] by the factor 40, shows the approximate conformity with the limits defined in [ACI14] and [ORA77].

$$\frac{A_{st}}{s_{st} \cdot Ø} \leq 0.05 \rightarrow \frac{40 \cdot A_{st}}{s_{st} \cdot Ø} \leq 2.0 \tag{5-21}$$

5.6.2 Consideration of Transverse Pressure

<u>New Proposal for the Consideration of Transverse Pressure</u>

The resulting conformity of test results with the design model according to [FIB14] is very good, but the calculated additional strength by transverse pressure only depends on the actual transverse pressure for transverse pressure up to 2.6 MPa. For this reason, the design model was modified towards a model, where the actual transverse pressure defines the contribution of transverse pressure.

Since the test results indicate a stronger increase in bond strength for low transverse pressure, a non-linear model for the consideration of the transverse pressure effect is recommended within the factor α_{tp} where

$$\alpha_{tp} = 0.32 \cdot p_{tr}^{0.4} \tag{5-22}$$

Inserting α_{tr} and α_{tp} to the design equation gives

$$f_{stm,mod} = 54 \cdot \left(\frac{f_{cm}}{25}\right)^{0.25} \cdot \left(\frac{l_b}{Ø}\right)^{0.55} \cdot \left(\frac{25}{Ø}\right)^{0.2} \cdot \left[\alpha_c + \alpha_{tr} + \alpha_{tp}\right] \tag{5-23}$$

In the own model in equation (5-23), the transverse pressure contribution is

$$f_{stm,p,mod} = 54 \cdot \left(\frac{f_{cm}}{25}\right)^{0.25} \cdot \left(\frac{l_b}{Ø}\right)^{0.55} \cdot \left(\frac{25}{Ø}\right)^{0.2} \cdot 0.32 \cdot p_{tr}^{0.4} \tag{5-24}$$

In contrast, [FIB14] gives a linear transverse pressure contribution multiplied with the linear value l_b / Ø.

$$f_{stm,p} = 6 \cdot \frac{l_b}{Ø} \cdot p_{tr} \tag{5-25}$$

A comparison of anchorage test results with transverse pressure in comparison to the own model given in equation (5-23) is shown in Figure 5-53.

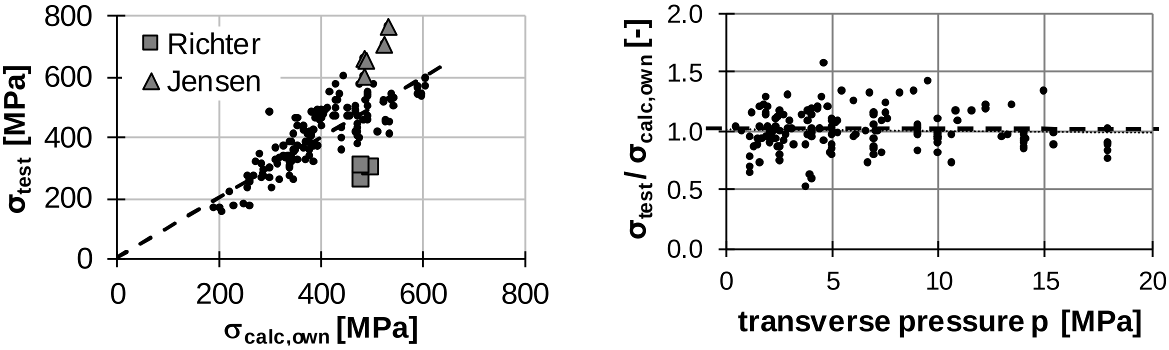

Figure 5-53 Maximum bar stress obtained in tests with transverse pressure $\sigma_{s,test}$ in comparison with the calculated stress according to the own modified model $\sigma_{calc,own}$ (left) and relationship between $\sigma_{s,test}$ / $\sigma_{calc,own}$ and transverse pressure (right)

Figure 5-53 (left) illustrates the good conformity with test results if the non-linear influence of anchorage length on the transverse pressure contribution is taken into account. Only tests conducted by JENSEN [JEN82] and RICHTER [RIC84] are not sufficiently covered by the design model. The consideration of transverse pressure with the proposed exponent of 0.4 conforms to the test results as shown in Figure 5-53 (right).

The design model according to [FIB14] overestimates the ultimate anchorage strength with transverse pressure for long anchorages (cf. Figure 5-34). This effect is not visible in the design model according to the own modified model.

5.6.3 Own Model for Mean Bar Stress in Anchorages and Laps

The own model based on [FIB14] given in equation (5-26) sums up the contribution by concrete cover (equation (5-27)) and the own proposal for the contributions of transverse reinforcement (equation (5-28)) and transverse pressure (equation (5-29)).

$$f_{stm,mod} = 54 \cdot \left(\frac{f_{cm}}{25}\right)^{0.25} \cdot \left(\frac{l_b}{Ø}\right)^{0.55} \cdot \left(\frac{25}{Ø}\right)^{0.2} \cdot \left[\alpha_c + \alpha_{tr} + \alpha_{tp}\right] \tag{5-26}$$

$$\alpha_c = \left(\frac{c_{min}}{Ø}\right)^{0.25} \cdot \left(\frac{c_{max}}{c_{min}}\right)^{0.1} \tag{5-27}$$

$$\alpha_{tr} = k_m \cdot \rho_{conf} = k_m \cdot \frac{A_{st}}{Ø \cdot s_{st}} \tag{5-28}$$

$$\alpha_{tp} = 0.32 \cdot p_{tr}^{0.4} \tag{5-29}$$

Where $f_{ck} = f_{cm} - 8$ MPa, $A_{st} \cdot n_{st} \geq A_s$ and $k_m = 7$ or 4 according to Figure 5-54.

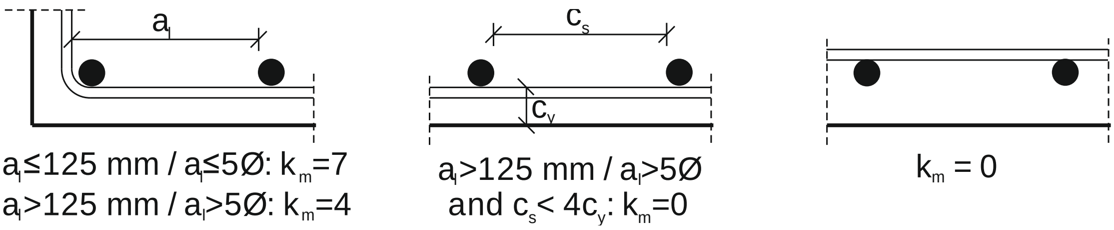

Figure 5-54 Coefficient k_m for efficiency of transverse reinforcement (reproduced from [FIB14])

5.6.4 Design Model According to [PT18] with own Calibration Factors

The model given in [PT18] is rearranged for the calculation of bar stress developed by bond and the own calibration factors 31 for the ratio l_b / Ø and 60 for k_{conf} are derived from the database. The mean stress follows from equation (5-30).

$$f_{stm,PT} = 435 \cdot \left(\frac{f_{cm}}{25\ \text{MPa}}\right)^{\frac{1}{3}} \cdot \left(\frac{20}{Ø}\right)^{\frac{2}{9}} \cdot \left(\frac{l_b}{31 \cdot Ø}\right)^{\frac{2}{3}} \cdot \left(\frac{c_{d,conf}}{1.5 \cdot Ø}\right)^{\frac{1}{3}} \tag{5-30}$$

With

$$c_{d,conf} = c_d + \left(60 \cdot k_{conf} \cdot \frac{n_l \cdot A_{st}}{n_b \cdot Ø \cdot s_{st}} + 8 \cdot \sigma_{ctd} / \sqrt{f_{ck}}\right) \cdot Ø \leq 3.75 \cdot Ø \tag{5-31}$$

k_{conf} see 2.9.7

The coefficients 31 and 60 are determined in this thesis on the basis of the database with $f_{ck} = f_{cm} - 8$ MPa. Since [PT18] defines the required design bond length, the original equation (2-42) includes a coefficient of 40 instead of 31 for mean values. The coefficient of 29 is derived from tests confined by concrete cover only. For the contribution of transverse reinforcement, [PT18] gives a coefficient of 31 instead of 60 in equation (2-43). The own coefficient of 60 is chosen in this thesis on the basis of tests with transverse reinforcement. The coefficient of 8 for the transverse pressure contribution, which is given in equation (2-43) [PT18] as well, was confirmed by the tests in the database with transverse pressure. Applying the coefficients of 31, 60 and 8 gives the statistical values shown in Table 5-16.

5.6.5 Statistical Evaluation of Models for Mean Bar Stress in Bond Zones

Table 5-16 gives the statistical data of the own model based on [FIB14] and the modified model according to [PT18] with own calibration factors. The data is required for the evaluation of the applicability of the design models and for the derivation of design values.

Table 5-16 Statistical data (presuming a log-normal distribution) for models for mean anchorage strength calculated with equations (5-26) and (5-30) (tr.r. = transverse reinforcement and tr.p. = transverse pressure)

$\sigma_{test}/\sigma_{sm,calc}$	Own model based on [FIB14]					Model according to [PT18] with own calibration factors				
	Laps with tr. r.	Laps without tr. r.	Anchor. without tr. p.	Anchor. With tr. p.	All tests	Laps with tr. r.	Laps without tr. r.	Anchor. without tr. p.	Anchor. With tr. p.	All tests
Mean θ	1.01	0.99	1.03	1.00	1.00	0.99	0.99	1.09	0.98	0.99
Standard deviation	0.130	0.135	0.172	0.166	0.145	0.138	0.171	0.229	0.191	0.172
COV V_θ	0.129	0.136	0.168	0.165	0.144	0.139	0.173	0.209	0.195	0.173
Minimum	0.60	0.65	0.63	0.53	0.53	0.56	0.60	0.60	0.53	0.53
5% ratio	0.81	0.78	0.77	0.76	0.78	0.78	0.73	0.76	0.70	0.74
Number of results	231	226	47	165	669	231	226	47	165	669

The following diagrams show comparisons of the consideration of parameter effects in the design models according to [EC2], [EC2/NA], [ACI14], [FIB14], [PT18] with own calibration factors and the own model based on [FIB14].

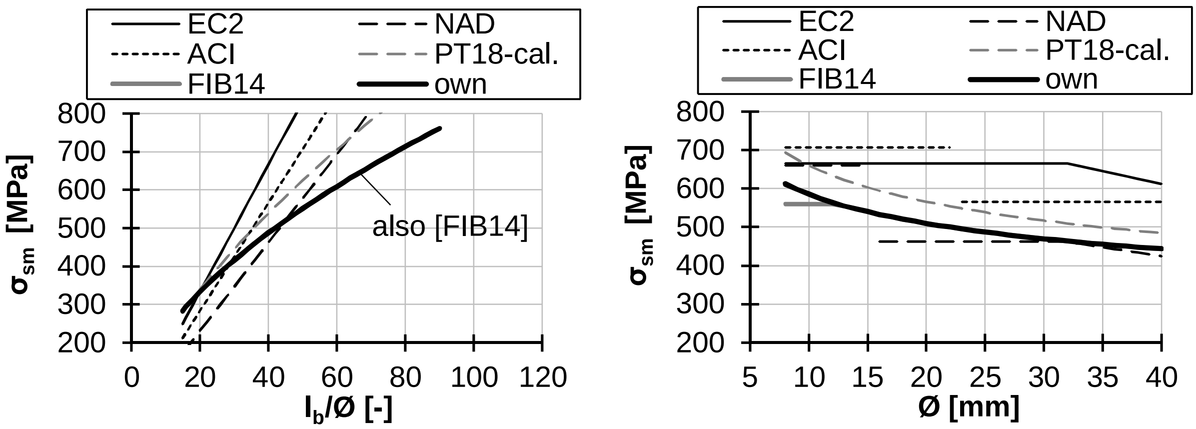

Figure 5-55 Mean bar stress in bond zones calculated according to [EC2], [EC2/NA], [ACI14], [FIB14], [PT18] with own calibration factors according to equation (5-30) and own model according to equation (5-26), all equations with f_{cm} = 33 MPa and $c_{min} = 1.5 \cdot Ø$, Ø = 25 mm (left) and $l_b = 40 \cdot Ø$ (right)

The effects of concrete strength and minimum cover (c_{min} = min {c_y, c_x, c_s / 2}) are shown in Figure 5-56. The influence of concrete strength has an upper limit in the models according to [EC2], [EC2/NA] and [ACI14]. The strength increases most in the model according to [EC2] and [EC2/NA], since the concrete strength is taken into account with the exponent 2/3, while the model according to [FIB14] only takes the concrete strength with an exponent of 0.25 into account (cf. Figure 5-56 and Table 2-5).

The concrete cover is also considered differently within the design equations. [EC2/NA] has a simplified, but conservative model that neglects the positive effect of concrete cover (cf. Figure 5-56, right).

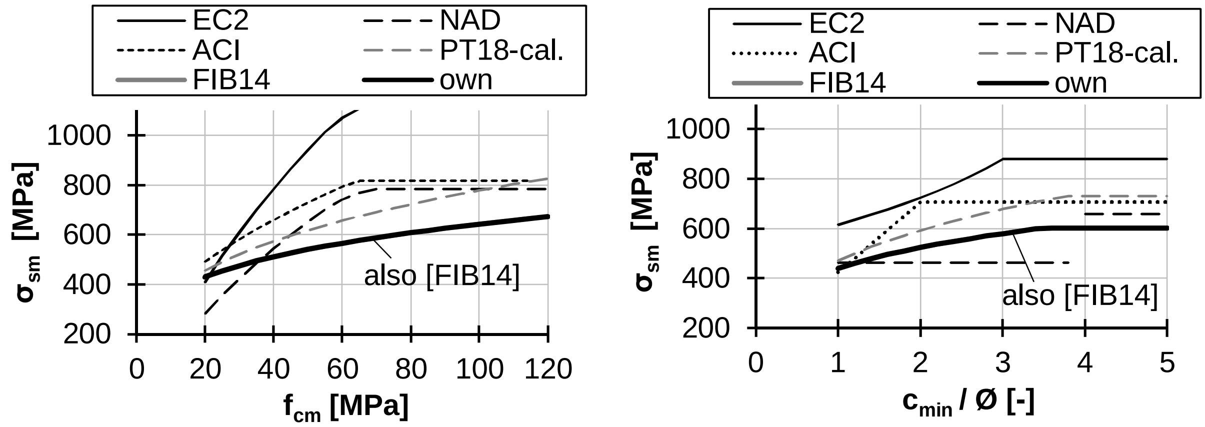

Figure 5-56 Mean bar stress in bond zones calculated according to [EC2], [EC2/NA], [ACI14], [FIB14], [PT18] with own calibration factors according to equation (5-30) and own model according to equation (5-26), all equations with Ø = 25 mm and l_b = 40 · Ø, c_{min} = 1.5 · Ø (left) and f_{cm} = 33 MPa (right)

Figure 5-57 shows the influences of transverse reinforcement (left) and transverse pressure (right).

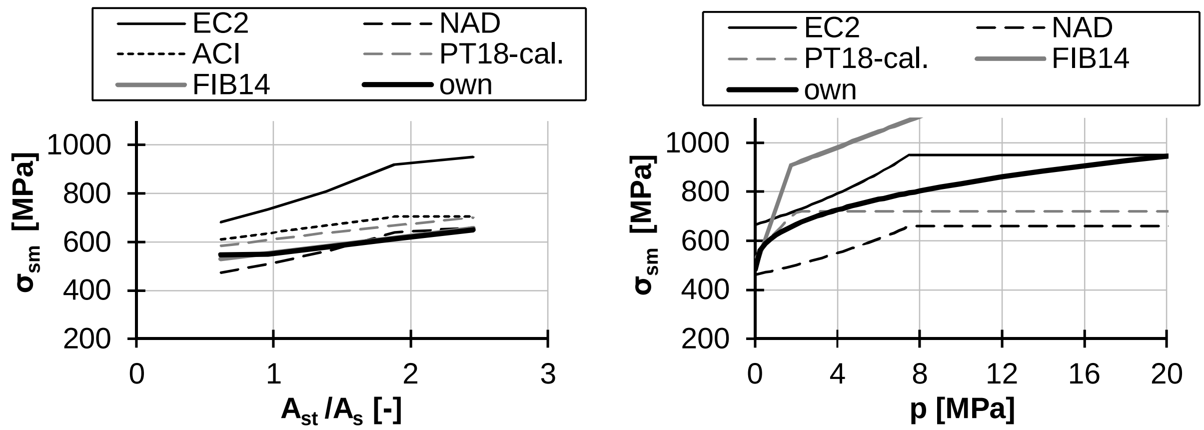

Figure 5-57 Mean bar stress in bond zones calculated according to [EC2], [EC2/NA], [FIB14], [PT18] with own calibration factors according to equation (5-30) and own model according to equation (5-26), all equations with Ø = 25 mm, l_b = 40 · Ø, c_{min} = 1.5 · Ø and f_{cm} = 33 MPa, left: n_{st} = 6, s_{st} = 167 mm and increasing transverse bar diameter

The increase in stress developed by bond for increasing transverse reinforcement is very similar in this comparison. The design equation according to [FIB14] overestimates the anchorage strength increase caused by transverse pressure. The model has an upper limit defined by concrete strength that is not reached for the evaluated parameters (cf. Figure 5-57, right).

<u>Comparison of Modified Design Models for Transverse Pressure</u>

Figure 5-58 shows the effect of non-linearity for two calculations of ultimate stress developed in lapped or anchored bars. The example is calculated for an anchorage of Ø 25 mm bars with $l_b = 40 \cdot Ø$ (Figure 5-58, left) and $l_b = 10 \cdot Ø$ (Figure 5-58, right). Both examples are calculated without transverse pressure, a concrete strength $f_{cm} = 33$ MPa and a minimum concrete cover of $1.5 \cdot Ø$. The own derived calibration factor for the mean value in the design model according to [PT18] in equation (5-30) is 31 for both anchorage lengths.

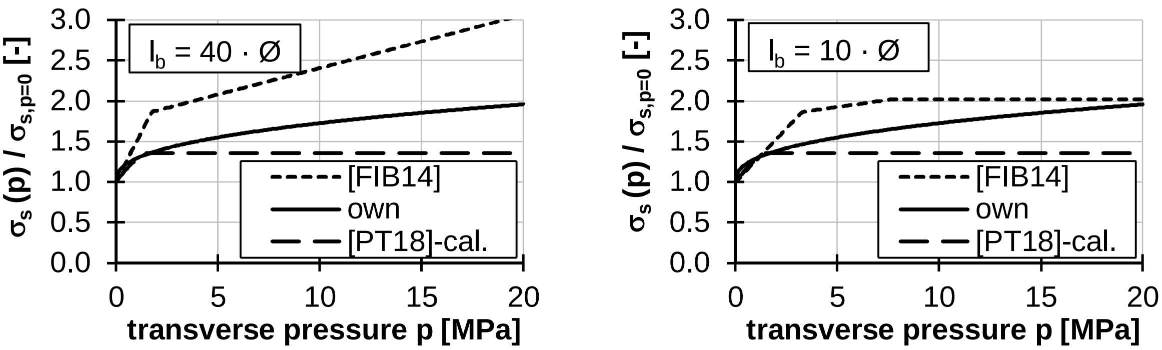

Figure 5-58 Ratio of ultimate bar stress in anchorages with transverse pressure to ultimate bar stress in anchorages without transverse pressure $\sigma_s(p) / \sigma_{s,p=0}$ vs. transverse pressure p for $l_b = 40 \cdot Ø$ (left) and $l_b = 10 \cdot Ø$ (right); $f_{cm} = 33$ MPa; $c_{min} = 1.5 \cdot Ø$; Ø = 25 mm

The mean values and coefficients of variation for the model according to [FIB14], for the own model based on [FIB14] and for the model according to [PT18] with the own derived calibration factors in comparison with the test results with transverse pressure are given in Table 5-17.

Table 5-17 Statistical data (presuming a log-normal distribution) for anchorage tests with transverse pressure calculated with equations (5-9), (5-23) and (5-30)

$\sigma_{test} / \sigma_{sm,calc}$	[FIB14]	Own based on [FIB14]	[PT18] calibrated
Mean value θ	0.99	1.00	0.98
Standard deviation	0.184	0.166	0.191
COV V_θ	0.186	0.165	0.195

6 Lap Database for the Limit State of Cracking

6.1 General

The large crack widths observed at the lap ends in chapter 3.4 comply with observations by several authors. Although laps were investigated by many authors in the past, only some documented the crack widths in the test specimens. For a parameter study on crack widths at lap ends, a database for crack width measurements was compiled. The database includes 93 lap tests conducted by BETZLE [BET81], BURKHARDT [BUR00], CYLLOK [CYL06], FERGUSON [FER65a] , REHM [REH77] and THOMPSON [THO75] as well as the own tests described in chapter 3.4.

Since each test specimen has two lap ends only, there is a limited number of crack measurements available for statistical evaluation. Accordingly, it is reasonable to compare maximum or mean crack widths at the lap ends instead of fractile values. For the different strength and robustness of the laps, the crack widths were measured at different reinforcing bar stresses. THOMPSON [THO75] measured the crack width at about 250 MPa and the own tests described in chapter 3.4 were measured at 320 MPa bar stress. The other authors used bars stress levels between these boundaries. For a comparison, the crack widths were extrapolated with the reinforcing bar stress ratio 320 MPa / $\sigma_{s,test,i}$.

The crack widths were measured at different locations along the cross-sectional perimeter. While some authors also measured the crack width at the sides of the test specimens at the height of the reinforcement, all authors measured the crack width in the extreme fibre of the particular concrete cross-section. Therefore, the following evaluation compares the parameter effects for the crack widths in the extreme fibre.

The larger the bar diameter, the greater the change in stiffness at a lap end. According to REHM [REH77] crack widths at lap ends are not wider than in the undisturbed parts of the beam for reinforcing bars with Ø ≤ 14 mm and $l_0 \geq 1.6 \cdot l_{b,req}$ for static and cyclic loading.

6.2 Parameter Effects

6.2.1 Lap Length

Conforming with the test results in chapter 3.4, neither BURKHARDT [BUR00], nor REHM AND ELIGEHAUSEN [REH77] found an effect of lap length on the crack widths at lap ends in laps subjected to static loading (cf. Figure 6-1). The tests conducted by FERGUSON [FER65a] and THOMPSON [THO75] neither show a clear effect of lap length on crack width at the lap ends. BETZLE [BET81] described that the lap length has no effect, while his test results give different crack widths at the lap ends. Figure 6-1 shows no correlation of lap length and crack width at the lap ends at 320 MPa when evaluating single test series with equal test parameters.

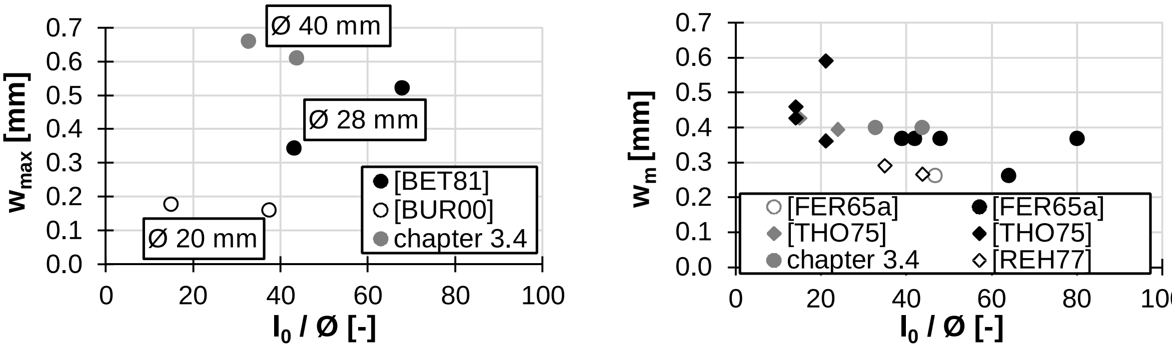

Figure 6-1 Influence of lap-length to bar-diameter ratio l_0 / Ø on maximum crack width at the lap end (left) and on mean crack width at the lap end (right) at 320 MPa

In contrast, REHM AND ELIGEHAUSEN [REH77] found that crack widths at lap ends are influenced by the lap length if subjected to cyclic or long-term loads.

6.2.2 Concrete Cover

The bottom concrete cover c_y influences the effective height of the reinforcement $h_{c,eff}$. Accordingly, the effect of bottom cover strongly correlates with the effect of reinforcement ratio within the effective height of the reinforcement. Figure 6-2 shows an increase in crack width at the lap ends at 320 MPa with increasing bottom cover in tests conducted by [FER65a] and [THO75]. In the own tests described in chapter 3.4 this effect was not visible. The effect conforms with the effect of cover in reinforced concrete members with continuous reinforcement, where increasing bottom cover leads to an increase in crack widths.

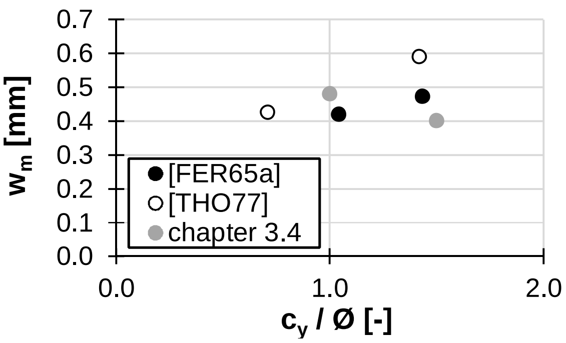

Figure 6-2 Influence of concrete-cover to bar-diameter ratio c_y / Ø on mean crack width at the lap end at 320 MPa

6.2.3 Reinforcement Ratio

The tests conducted by BETZLE [BET81], CYLLOK [CYL06], FERGUSON [FER65a] and THOMPSON [THO75] show an increase in crack width at the lap ends for smaller bar spacing and thus increasing reinforcement ratio in the effective height. The maximum crack widths at the lap ends in the own tests did not meet this expectation, but were 0.68 mm in the lap with a reinforcement ratio of 3.6 % and 0.90 mm in the test with a reinforcement ratio of 2.8 % (cf. chapter 3.4.6). However, the effect was negligible for the mean crack widths at the laps ends with 0.44 mm for ρ_{eff} = 3.6 % and 0.47 mm for ρ_{eff} = 2.8 %. Figure 6-3 shows the crack widths at the lap ends at 320 MPa for different reinforcement ratios. The crack widths at the lap ends increase with increasing reinforcement ratios. This contradicts the behaviour of undisturbed structural concrete members that develop smaller crack widths at higher reinforcement ratios. The change in stiffness at the lap ends is more pronounced for higher reinforcement ratios and thus generates larger crack widths.

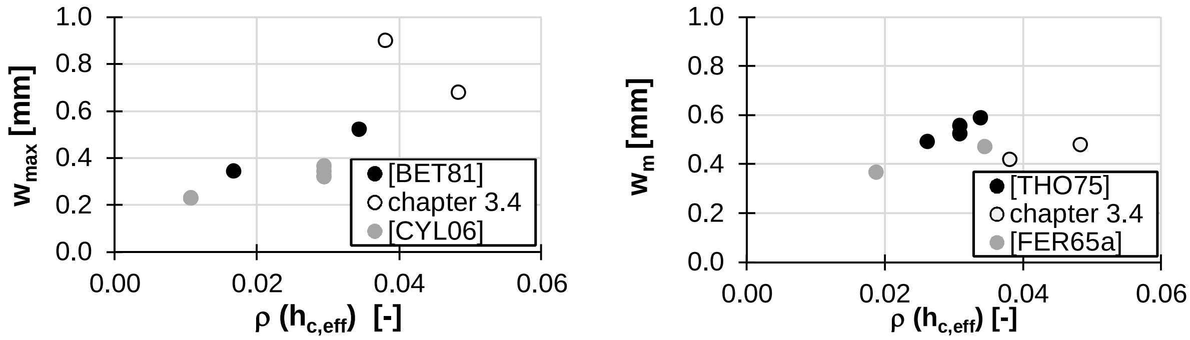

Figure 6-3 Influence of reinforcement ratio depending on the effective height of the reinforcement $h_{c,eff}$ on the maximum crack width (left) and on the mean crack width (right) at 320 MPa

6.2.4 Bar Diameter

Figure 6-4 (left) illustrates the influence of bar diameter on the maximum crack width at the lap end at 320 MPa at a constant ratio of c_y / Ø. The test results described in chapter 3.4 and in [BUR00] indicate an increase in crack widths at the lap ends for increasing bar diameter for constant values of c_y / Ø. Taking the effect of cover into account, the effect of bar diameter is slightly smaller. In contrast, Figure 6-4 (right) shows the influence of bar diameter on crack width at the lap end at 320 MPa at constant bottom cover c_y. BETZLE [BET81] and FERGUSON [FER65a] found increasing crack widths at the lap ends for increasing bar diameters at constant cover values c_y.

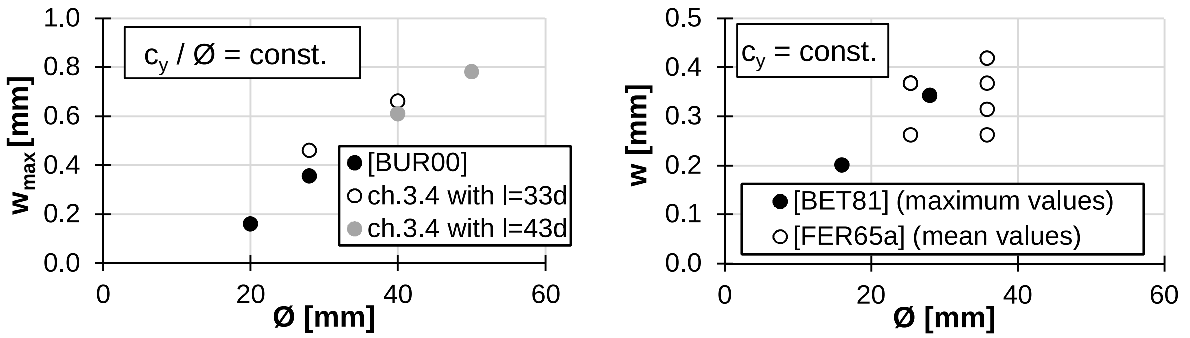

Figure 6-4 Influence of bar diameter Ø on maximum crack width for constant bottom cover ratios c_y / Ø (left) and on maximum width (mean crack width, respectively) for constant bottom cover values c_y (right) at 320 MPa

6.2.5 Transverse Reinforcement

FERGUSON [FER65a] and BURKHARDT [BUR00] did not observe an effect of transverse reinforcement on the crack width at lap ends. This finding conforms to the own test results described in chapter 3.4.

6.2.6 Concrete Strength

The tests in REHM AND ELIGEHAUSEN [REH77] indicate an increase in crack width for smaller concrete strength at constant lap length to bar diameter ratios l_0 / Ø.

6.3 Summary

The crack widths in structural members with continuous reinforcement are influenced by the reinforcement ratio in the effective height, the concrete cover, the bar diameter and the concrete strength. In undisturbed members with continuous reinforcement as well as at lap ends, larger bottom concrete cover, larger bar diameters and smaller concrete strength lead to increased crack widths. While increasing reinforcement ratios within the effective height reduce the crack width in undisturbed members, it increases the crack width at lap ends. Transverse reinforcement neither reduces the transverse crack width in continuously reinforced members nor at lap ends.

7 Design Values for Anchorage and Lap Lengths

7.1 Eurocode Reliability Management

The Eurocodes on structural design are based on a semi-probabilistic safety concept defined in EUROCODE 0 [EC0]. For higher consequence of failure, the probability of failure depending on action effects E_d and resistance R_d of a structure shall decrease. The probability of failure of a structure or member corresponds with the reliability index β by

$$P_f = \Phi(-\beta) \tag{7-1}$$

With

P_f failure probability for a certain time period

Φ cumulative distribution function of the standardised normal distribution.

The relationship between failure probability P_f and reliability index β is given in Table 7-1. The probability of failure implies that in one in 10^i instances failure occurs.

Table 7-1 Relation between P_f and β

P_f	10^{-1}	10^{-2}	10^{-3}	10^{-4}	10^{-5}	10^{-6}	10^{-7}
β	1.28	2.32	3.09	3.72	4.27	4.75	5.20

A certain reliability of structures can be achieved by preventative measures, design, quality management, efficient execution and inspection. [EC0] defines three levels of reliability that apply to the structure as a whole or to its components. The complexity of design increases with the level applied. The classes are based on the assumed consequences of failure and the exposure of the construction works to hazard. [EC0] differentiates between high, medium and low consequence regarding loss of human life as well as economic, social or environmental impact. The reliability classes are associated with three consequence classes as shown in Table 7-2.

Table 7-2 Reliability classes according to [EC0] associated with consequence classes and recommended minimum values for reliability index β

Reliability Class	Description of consequence	Minimum values for reliability index β	
		1 year reference period	50 years reference period
RC3	High consequence	5.2	4.3
RC2	Medium consequence	4.7	3.8
RC1	Low consequence	4.2	3.3

The reliability index β included in the partial safety factors is distinguished for the limit states, the reference period, the consequences of failure and the cost of safety measures. Table 7-3 gives the target reliability index β at different design situations and reference periods for medium consequences of failure at reliability class RC2.

Table 7-3 Target reliability index β for reliability class RC2 according to [EC0] (medium consequence of failure)

Limit State	Target reliability index β	
	1 year reference period	50 years reference period
Ultimate	4.7	3.8
Fatigue	-	1.5 to 3.8
Serviceability (irreversible)	2.9	1.5

[EC0] distinguishes three levels of probabilistic methods. Full probabilistic methods (level III) consider exact distributions and eventually given statistical dependencies of action and resistance parameters. Examples of such stochastic simulation methods are Monte-Carlo or Monte-Carlo importance sampling. In Monte-Carlo simulation, partial safety factors are not obtained from empirical data, but from simulated tests. An algorithm generates random values for a defined limit state function and proves whether the simulated tests are within the failure or survival zone. In the course of this procedure, an abundant number of realisations must be calculated to find exact results for small failure probabilities. For the required failure probabilities defined for structural elements, 10 to 1000 million test simulations are necessary. Therefore, this method was refined to Monte-Carlo importance sampling with a reduced number of necessary iterations [RIC09], [RAC06].

The first-order reliability method (FORM), the mean-value-first-order-second-moment procedure and the algorithm given in appendix D of [EC0] are examples of level II methods. All standard deviations and mean values of the influencing parameters are considered at this level.

The target reliability can be achieved by applying the partial safety concept according to [EC0]. The partial safety factors were obtained by first order reliability methods or full probabilistic methods denominated level II and level III methods, respectively. The application of the partial safety factors according to [EC0] is a level I method including a reliability index β greater than 3.8 for a 50 year reference period.

The probability of failure P_f can be expressed by the limit state function g. The function describes the limit state being the boundary between failure and survival of a structure, where structures survive if g > 0 (cf. Figure 7-1).

The probability of failure P_f is

$$P_f = \text{prob}\ (g \leq 0) \tag{7-2}$$

The reliability of a structure P_s is

$$P_s = 1 - P_f = 1 - P[Z = g \leq 0] \tag{7-3}$$

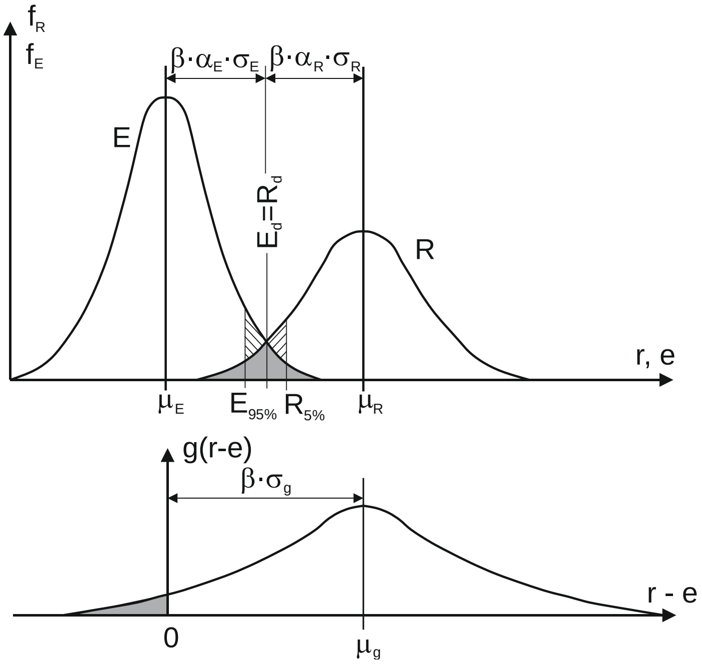

Figure 7-1 Distribution of action effects E and resistance R (top) and distribution of limit state function g (bottom) (reproduced from [ZIL10])

If R is the resistance and E the action effects, the limit state function g is:

$$g = R - E \tag{7-4}$$

The central safety zone is the area between the mean values of action effects μ_E and resistance μ_R. This area is divided by the limit state function μ_G.

$$\mu_g = \mu_R - \mu_E \tag{7-5}$$

The reliability index β describes the distance from the mean value of the limit state function μ_G to the origin as a multiple of the standard deviation σ_G with

$$\mu_g = \beta \cdot \sigma_g \tag{7-6}$$

and

$$\mu_R - \beta \cdot \alpha_R \cdot \sigma_R = \mu_E + \beta \cdot \alpha_E \cdot \sigma_E \tag{7-7}$$

The weighting factors α_E and α_R describe the influences of the random values E and R on the failure probability. The values α_E = -0.7 and α_R = 0.8 according to [EC0] give

$$\sqrt{\alpha_E^2 + \alpha_R^2} = \sqrt{(-0.7)^2 + 0.8^2} = 1 \tag{7-8}$$

Thus, the reliability index β defined in equation (7-9) is the ratio of the mean value of the limit state function to the standard deviation of the limit state function.

$$\beta = \frac{\mu_g}{\sigma_g} = \frac{\mu_R - \mu_E}{\sqrt{\sigma_R^2 + \sigma_E^2}} = \frac{\mu_R - \mu_E}{\alpha_E \cdot \sigma_E + \alpha_R \cdot \sigma_R} \tag{7-9}$$

with

$$\sigma_g^2 = \sigma_R^2 + \sigma_E^2 \tag{7-10}$$

Structures and structural elements conform to the [EC0] safety concept, where

$$E_d < R_d = R\,\{X_{d1}, X_{d2}, \ldots, a_{d1}, a_{d2}, \ldots, \theta_{d1}, \theta_{d2}, \ldots\} \tag{7-11}$$

with

R resistance of the structure

X_{di} material properties (stochastically independent random variables)

a_{di} geometrical properties

θ_{di} model uncertainties

The probability of finding a resistance R smaller than the design resistance R_d shall be:

$$P(R \le R_d) = \Phi\,(-\,\alpha_R \cdot \beta) = \Phi\,(-\,0.8 \cdot \beta) \tag{7-12}$$

7.2 General Derivation of Design Values

7.2.1 Characteristic Values

Design values can be obtained by deterministic methods based on empirical data or by probabilistic methods. The following methods may be used to calculate design resistances from mean test results according to [EC0]. At an interim stage, characteristic values defined as 5% fractiles of empirical data must be calculated.

The p-quantile R_P of a resistance R is

$$R_P = \mu_R - k_R \cdot \sigma_R = \mu_R \cdot (1 - k_R \cdot \sigma_{R\,/}\,\mu_R) \tag{7-13}$$

For a log-normal distribution, R_P is

$$R_P = \exp\,(\mu_R \cdot (1 - k_R \cdot \sigma_R / \mu_R)) \tag{7-14}$$

The coefficient k_R describes the statistical distribution, the level of confidence and the fractile value. Equation (7-15) gives 5%-fractiles for test numbers above 100.

$$R_{5\%} = \mu_R - 1.645 \cdot \sigma_R = \mu_R \cdot (1 - 1.645 \cdot \sigma_{R\,/}\,\mu_R) \tag{7-15}$$

For the log-normal distribution, the 5%-fractile can be obtained from equation (7-16).

$$R_{5\%} = \exp\,(\mu_R \cdot (1 - 1.645 \cdot \sigma_R / \mu_R)) \tag{7-16}$$

7.2.2 Partial Safety Factors in Codes

Partial safety factors for structural resistance describe the ratio of characteristic resistance values to the design point of the limit state function g in Figure 7-1. Presuming a normal distribution, the partial safety factor for the resistance of concrete in [EC2] is

$$\gamma_R = \frac{R_k}{R_d} = \frac{R_{5\%}}{R_d} = \frac{\mu_R \cdot \left(1 - k_n \cdot V_R\right)}{\mu_R \cdot \left(1 - \alpha_R \cdot \beta \cdot V_R\right)} = \frac{\left(1 - 1.645 \cdot 0.172\right)}{\left(1 - 0.8 \cdot 3.8 \cdot 0.172\right)} = 1.5 \tag{7-17}$$

with

V_R coefficient of variation of resistance $V_R = \sigma_R / \mu_R$

The partial safety factor for resistance γ_R shall include the material uncertainties, geometric uncertainties and model uncertainties. According to [EC0], the factor γ_R - denominated γ_M - includes a safety factor γ_m for the uncertainty in material properties and a factor γ_{Rd} for the model uncertainty in structural resistance. The factor γ_M is defined as:

$$\gamma_M = \gamma_m \cdot \gamma_{Rd} \tag{7-18}$$

The resulting partial safety factor depends on the coefficient of variation (COV) of the resistance V_R as shown in equation (7-17). Since most design models comprise several influencing parameters with different statistical distributions, the coefficients of variation have to be summarised for the derivation of design values. [EC0] gives two possibilities for the addition of coefficients of variation for product functions of the form

$$R = \{X_1 \cdot X_2 \cdot \ldots \cdot X_i\} \cdot \theta \tag{7-19}$$

with
X_i basic variables
θ model uncertainty

The general model for the consideration of multiple coefficients of variation is

$$V_r^2 = \left(V_\theta^2 + 1\right) \cdot \left[\Pi\left(V_{Xi}^2 + 1\right)\right] - 1 \tag{7-20}$$

For small values of V_θ^2 and V_{xi}^2, V_r^2 may be simplified to

$$V_r^2 = V_\theta^2 + \sum V_{Xi}^2 \tag{7-21}$$

If the resistance function g_{rt} is a more complex function, the COV may be obtained from

$$V_{rt}^2 = \frac{1}{g_{rt}^2\left(X_m\right)} \cdot \sum_{i=1}^{j} \left(\frac{dg_{rt}}{dX_i}\sigma_i\right)^2 \tag{7-22}$$

Most design models for structural concrete members comprise the concrete strength f_{ck}. Hence, at least the coefficients of variation of the model uncertainty and of the concrete strength must be combined.

The previous German code for structural concrete DIN 1045 [DEU88] applied global safety factors γ_{gl} for ductile and robust failure. For brittle failure, the safety factor for resistance was

$$\gamma_R = \frac{\gamma_{gl}}{\gamma_F} = \frac{2.1}{1.4} = 1.50 \tag{7-23}$$

with

γ_{gl} global safety factor

γ_F safety factor for action effects

ACI 318 [ACI14] provides the necessary level of safety by coefficients applied to the loads and by strength reduction factors ϕ_{ACI} applied to the nominal strength. The coefficients ϕ_{ACI} account for the probability of understrength due to variations of in-place material strengths and dimensions, the effect of simplifying assumptions in the design equations, the degree of ductility, the potential failure mode of the member, the required reliability, the significance of failure and the existence of alternative load paths for the member in the structure [ACI03], [DAR98].

7.2.3 Consideration of Model Uncertainties

During structural design, assumptions must be made on the structural systems, cross-sections, materials, joints, foundations and many more [SPA92]. The model uncertainty describes the difference between design model and actual structural resistance. This uncertainty results from stochastic effects not sufficiently captured by the design model. It comprises the model uncertainty itself and uncertainties of the test (instrumentation, test-setup and undocumented tolerances of geometric values).

The model uncertainty is taken into account by introducing its COV for the determination of design values. The statistic values of the model uncertainty for the resistance model may be derived from a comparison of theoretical resistance to experimental resistance obtained in tests as representative as possible. The most accurate consideration of model uncertainties is the introduction of one model uncertainty per base variable, but often a global design-model uncertainty is added or multiplied [SPA92].

Therefore, the design strength of structural elements accounts for the deviation of material strength and dimensions as well as for the model uncertainty. The model uncertainty is either accounted for within the design model by a value θ in equation (7-24) or by a partial safety factor γ_{Rd} in equation (7-25). The partial safety concept according to [EC0] applies equation (7-25) without actually defining the model uncertainty γ_{Rd}. Only the product $\gamma_M = \gamma_m \cdot \gamma_{Rd}$ is defined in [EC2].

$$R_d = R\ \{\eta \cdot X_k / \gamma_m;\ a_d \ldots, \theta\} \tag{7-24}$$

$$R_d = R\ \{\eta \cdot X_k / \gamma_m;\ a_d \ldots\} / \gamma_{Rd} \tag{7-25}$$

with

R_d design strength

η conversion factor

γ_m partial safety factor for uncertainty in material properties

γ_{Rd} partial safety factor for model uncertainty in structural resistance

a_d design values of geometrical data

Appendix D of [EC0] provides a procedure to calculate the model uncertainties δ using the correction factor b described in chapter 7.2.5 (cf. Table 7-5). After a mean value correction of the limit state function, the standard deviation and coefficient of correlation of the model uncertainty can be obtained. For the uncertainties of testing, [EC0] defines a COV of about 5%.

The PROBABILISTIC MODEL CODE [JOI00] recommends the assumption of log-normal distributed model uncertainties for design equations. The mean value of the model uncertainty is 1.0, while the COV shall be calculated or defined. [JOI00] gives partial safety factors including model and material uncertainties for the design models for shear and bending, but not for bond strength.

7.2.4 Consideration of Material Uncertainties

The partial safety factor for material uncertainties γ_m comprises the uncertainty in the ratio between the material in structures and the concrete samples tested. Sometimes, a specific model uncertainty is not covered by a partial safety factor γ_{Rd}, but is included in the partial safety factor for material uncertainties. Additionally, the effect of deviations in cross-sectional dimensions is often covered by the material factor [SPA92].

The difference between characteristic concrete strength and mean concrete strength is constantly 8 MPa according to [EC2]. This is equivalent to

$$f_{ck} = f_{cm} - 8\ \text{MPa} = f_{cm} - 1.645 \cdot \sigma_{fc} \rightarrow \sigma_{fc} = 8\ \text{MPa} / 1.645 = 4.86\ \text{MPa} \tag{7-26}$$

The COV is therefore not constant, but decreases with increasing concrete class. Table 7-4 shows examples of coefficients of variation V_{fc} for different concrete classes.

The COV of 0.172 that is given in equation (7-17) and corresponds to $\gamma_R = 1.5$ approximately equals the COV for class C20/25 concrete $V_{C20/25} = 0.174$. Calculating the partial safety factor for C20/25 with $V_{fc} = 0.174$ gives a material uncertainty $\gamma_m = 1.5$ and a partial safety factor for model uncertainty $\gamma_{Rd} = 1.0$. Thus, for C20/25, the entire COV is “consumed” by the concrete strength. In case higher concrete strength is applied, the coefficients of variation of the material decrease and the partial safety factor γ_{Rd} is greater than 1.0. For C30/37, a COV of V_{fc} = 0.128 gives a partial safety factor for material uncertainty of γ_m = 1.30 and a partial safety factor for the model uncertainty of γ_{Rd} = 1.15. This means that a constant partial safety factor of γ_M = 1.5 includes an increasing model uncertainty for increasing concrete strength, since the material uncertainty decreases.

Table 7-4 Mean values f_{cm}, standard deviation σ_{fc} and coefficients of variation for concrete strength

	f_{ck}	f_{cm}	σ_{fc}	V_{fc}
	[MPa]	[MPa]	[MPa]	[-]
C20/25	20	28	4.86	0.174
C25/30	25	33	4.86	0.147
C30/37	30	38	4.86	0.128
C40/50	40	48	4.86	0.101

7.2.5 Design Values According to Eurocode 0

<u>Application of Partial Safety Factors</u>

EUROCODE 0 [EC0] gives two models for the calculation of design values. The first model (method A) requires a characteristic value divided by the partial safety factor for material γ_m. In this case, the model uncertainty is incorporated by the COV of the model V_x.

$$X_d = \frac{\eta_d}{\gamma_m} X_{k(n)} = \frac{\eta_d}{\gamma_m} \cdot \mu_x \cdot (1 - k_n \cdot V_x) = \frac{\eta_d}{\gamma_m} \cdot \mu_x \cdot (1 - 1.645 \cdot V_x) \qquad (7\text{-}27)$$

Where η_d is the design value of a conversion factor for volume and scale effects, effects of moisture and temperature and any other relevant parameter [EC0].

Alternatively, design values may be obtained directly by accounting for the reliability required with $k_{d,n}$-factors (method B). The $k_{d,n}$-factors given in [EC0] are based on the assumption that the design value corresponds to an index of reliability β = 3.8 with $k_{d,n} = \alpha_R \cdot \beta = 0.8 \cdot 3.8 = 3.04$.

$$X_d = \eta_d \cdot X_{od} = \eta_d \cdot \mu_x \cdot (1 - k_{d,n} \cdot V_x) = \eta_d \cdot \mu_x \cdot (1 - 0.8 \cdot 3.8 \cdot V_x) \qquad (7\text{-}28)$$

The equations for design values according to [EC0] use BAYESIAN procedures with vague prior distributions and lead to almost the same results as classical statistics with confidence levels equal to 0.75.

[EC0] also gives a procedure for the calibration of resistance models and for the derivation of design values from tests (cf. Table 7-5). A resistance function r_t (statistical formulation) must be established for the design model g_{rt} (X). The resistance function r_t is a function of a number of independent variables X_i. All relevant geometrical and material properties shall be measured. There must not be any correlation between the variables in the resistance function.

Table 7-5 Calculation of design values according to [EC0] and [LEO05]

1	Development of a design model for the theoretical resistance $r_t = g_{rt}(X_i)$
2	Calculation of theoretical values r_{ti} for the design model
3	Estimation of the mean value correction factor b, which is the slope of the least-squares best fit line $b = \frac{\Sigma r_{ei} \cdot r_{ti}}{\Sigma r_{ti}^2}$ Where r_{ei} are the experimental results
4	Statistical Evaluation of the error terms δ_i that represent the model uncertainty $\delta_i = \frac{r_{ei}}{b \cdot r_{ti}}$ For the error terms a log-normal distribution is presumed. This means that the logarithmised error terms $\Delta_i = \ln(\delta_i)$ are distributed normally with a mean value $\overline{\Delta} = \frac{1}{n}\sum_{i=1}^{n} \Delta_i$ and a variance $s_\Delta^2 = \frac{1}{n-1}\sum_{i=1}^{n}\left(\Delta_i - \overline{\Delta}\right)^2$ The coefficient of variation of the error terms δ_i follows from $V_\delta = \sqrt{\exp(s_\Delta^2) - 1}$ (The statistical evaluation for the log-normal distribution is also described in chapter 2.10 for the statistical evaluation of crack widths measurements in equations (2-79) to (2-81) with different notations. For the crack width measurements the slope of the least-squares best fit line b was not taken into account)
5	Determination of the coefficients of variation V_{xi} of the basic variables, e.g. concrete strength, usually on the basis of prior knowledge
6	Coefficient of variation and standard deviation of the resistance function Where the values of V_δ^2 and V_{xi}^2 are small: $V_r^2 = V_\delta^2 + V_{rt}^2 = V_\delta^2 + \Sigma V_{xi}^2$ $Q = \sqrt{\ln(V_r^2 + 1)}$ (standard deviation)
7	Determination of the characteristic value r_k of the resistance: If a large number of tests is available, the characteristic resistance r_k may be obtained from $r_k = b \cdot g_{rt}(X_m) \cdot \exp(-k_n \cdot Q - 0.5 \cdot Q^2)$ For test numbers $n > 100$, $k_n = 1.645$ For the determination of the design value r_d of the resistance, the fractile factor k_n is replaced by the design fractile factor $k_{d,n}$ $r_d = b \cdot g_{rt}(X_m) \cdot \exp(-k_{d,n} \cdot Q - 0.5 \cdot Q^2)$ For test numbers $n > 100$, $k_{d,n} = 3.04$

The expressions for r_k and r_d are derived from the log-normally distributed resistance function r_t where μ and σ are the mean value and the standard deviation of the logarithmised values of r_t [LEO05] with

$$\ln r_k = \mu - k_n \cdot \sigma \tag{7-29}$$

$$r_k = \exp(\mu - k_n \cdot \sigma) = \exp(\mu) / \exp(k_n \cdot \sigma) \tag{7-30}$$

$$r_m = \exp(\mu + \sigma^2/2) = \exp(\mu) \cdot \exp(\sigma^2/2) \tag{7-31}$$

$$r_k = r_m / [\exp(k_n \cdot \sigma) \cdot \exp(\sigma^2/2)] = r_m \cdot \exp(- k_n \cdot \sigma - \sigma^2/2) \tag{7-32}$$

Probabilistic Methods

Alternatively, level II or level III methods can be applied for the derivation of design values. Therefore, standard deviations and mean values of all influencing parameters must be defined. The mean value and the standard deviation of the model uncertainty are obtained by a comparison of the investigated design model with a test database. The statistical characteristics of material parameters shall correspond to acceptable tolerances defined in codes. Geometric parameters are either covered by the model uncertainty or can be incorporated by tolerances [EC0].

7.3 Derivation of Design Values for Anchorages and Laps in Literature

Design values of bar stress in anchorages and laps as well as required anchorage and lap lengths were derived in [ELI79], [FIB14], [MAN17] and [DAR98]. Design values of structural resistance were obtained by division with partial safety factors in [ELI79], [FIB14]. In [MAN17] and [DAR98], the necessary coefficients for design equations were obtained by comparing the required level of reliability with probabilistic methods. The methods applied in [MAN17] give reliability indices β above 3.8 to fulfil the requirements of [EC0]. In contrast, DARWIN ET AL. [DAR98] calculate the design values for anchorages and laps according to [ACI14] with $\beta = 3.5$. Figure 7-2 shows an overview of the applied methods for the derivation of design bar stress in anchorages and laps.

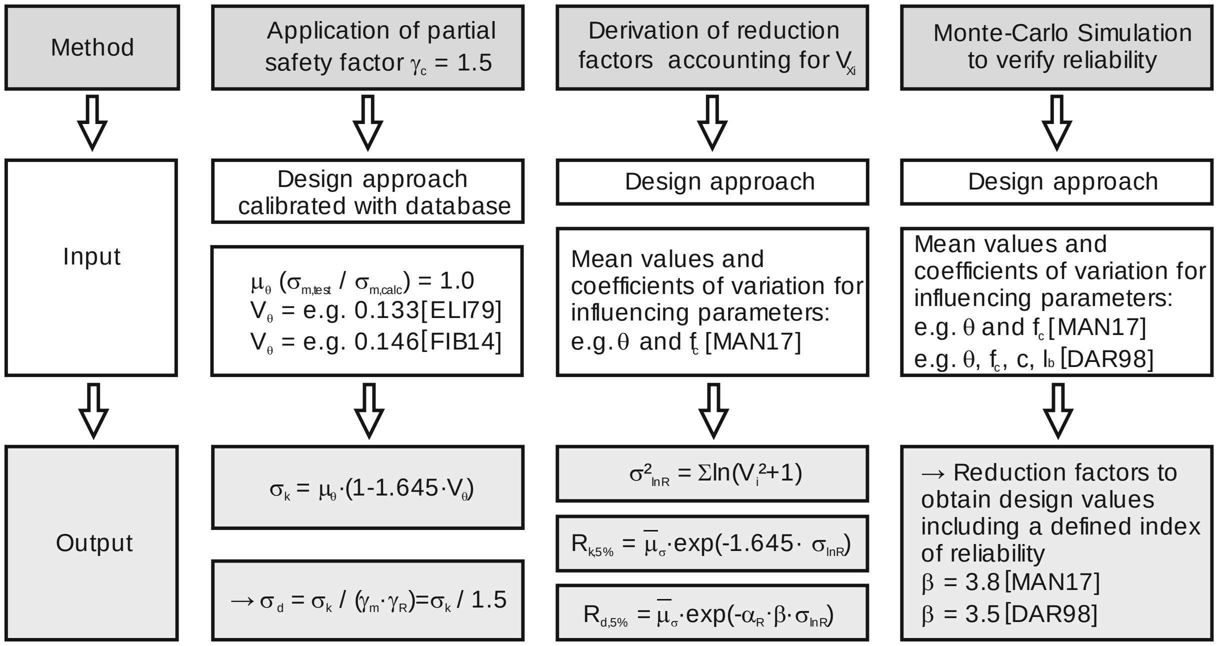

Figure 7-2 Applied methods for the derivation of design bar stress in anchorages and laps

7.3.1 ELIGEHAUSEN

ELIGEHAUSEN [ELI79] obtains design values by applying the safety factor according to [DEU88] on the characteristic lap strength σ_{sk}. This global safety factor ($\gamma_{c,DIN1045} = 2.1$) includes both the safety factor for action effects and for resistance. Evaluating the proposed design equation, ELIGEHAUSEN [ELI79] finds a COV equal to 0.133. Equations (7-33) to (7-35) show the derivation of calibration factors for characteristic and design values according to [ELI79]. The design model is described in chapter 2.9.8.

$$\sigma^c_{sm} = 5.8 \cdot \left(\frac{2 \cdot c_x}{c_y}\right)^{1/4} \cdot \left(\frac{c_y}{Ø}\right)^{1/2} \cdot f^{1/2}_{c,cube} \cdot \left(\frac{l_0}{Ø}\right)^{2/3} \cdot k = 5.8 \cdot c^*_{Elig.} \cdot f^{1/2}_{c,cube} \tag{7-33}$$

$$\sigma^c_{sk} = 5.8 \cdot (1 - 1.645 \cdot 0.133) \cdot c^*_{Elig.} \cdot f^{1/2}_{c,cube} = 4.53 \cdot c^*_{Elig.} \cdot f^{1/2}_{c,cube} \tag{7-34}$$

$$\sigma^c_{sd} = 4.53 / 2.1 \cdot c^*_{Elig.} \cdot f^{1/2}_{c,cube} = 2.2 \cdot c^*_{Elig.} \cdot f^{1/2}_{c,cube} \tag{7-35}$$

7.3.2 FIB TASK GROUP BOND

The fib task group on bond conducted a statistical analysis of the existing database [FIB05] differentiating between laps and anchorages both with and without links and derived statistical characteristics for the proposed design model [FIB14]. The obtained 5% characteristic ratios are approximately 0.76, corresponding with a COV V_x of 0.146 with

$$r_{5\%} = \frac{\mu_x \cdot (1 - 1.645 \cdot V_x)}{\mu_x} = (1 - 1.645 \cdot 0.146) = 0.76 \tag{7-36}$$

The coefficient used in equation (2-26) for the mean anchored and lapped bar stress is consequently changed from 54 to 54 · 0.76 = 41.

$$f_{stm} = 54 \cdot \left(\frac{f_{cm}}{25}\right)^{0.25} \cdot \left(\frac{25}{Ø}\right)^{0.2} \cdot \left(\frac{l_0}{Ø}\right)^{0.55} \cdot \left[\left(\frac{c_{min}}{Ø}\right)^{0.25} \cdot \left(\frac{c_{max}}{c_{min}}\right)^{0.1} + k_m \cdot K_{tr}\right] \leq f_{ym} \qquad (2\text{-}26)$$

$$f_{stk} = 41 \cdot \left(\frac{f_{cm}}{25}\right)^{0.25} \cdot \left(\frac{25}{Ø}\right)^{0.2} \cdot \left(\frac{l_0}{Ø}\right)^{0.55} \cdot \left[\left(\frac{c_{min}}{Ø}\right)^{0.25} \cdot \left(\frac{c_{max}}{c_{min}}\right)^{0.1} + k_m \cdot K_{tr}\right] \leq f_{yk} \qquad (7\text{-}37)$$

The task group verifies the derived coefficient by a detailed statistical analysis, where a target probability of failure p_f not exceeding 10^{-6} is chosen for a brittle concrete splitting mode. This probability of failure implies that in all but one in 10^6 instances, the reinforcement would reach yield before a bond failure occurs. The statistical analysis accounts for the independent statistical distribution of the parameters within the expression and of the yield strength of the reinforcement. The coefficient obtained by the simpler model is confirmed by the detailed statistical analysis [FIB14].

The task group derives the bond strength for MODEL CODE 2010 [MC2010] from rearranging equation (7-37) for f_{st} = 500 MPa / 1.15 with

$$\frac{l_{b,k}}{Ø} = \left(\frac{500/1.15}{41}\right)^{1.82} \cdot \left(\frac{f_c}{25}\right)^{-0.45} \cdot \left(\frac{25}{Ø}\right)^{-0.36} \qquad (7\text{-}38)$$

The corresponding characteristic bond strength is

$$f_{bk,0} = \frac{f_{yd} \cdot Ø}{4 \cdot l_{b,k}} = 1.5 \cdot \left(\frac{f_c}{25}\right)^{0.45} \cdot \left(\frac{25}{Ø}\right)^{0.36} \qquad (7\text{-}39)$$

For the definition of minimum confining reinforcement and rounded exponents, the coeffiecient of the characteristic bond strength is increased from 1.5 to 1.75 in equation (7-40).

$$f_{bk} = 1.75 \cdot \left(\frac{f_c}{25}\right)^{0.5} \cdot \left(\frac{25}{Ø}\right)^{0.3} \cdot (\alpha_2 + \alpha_3) \qquad (7\text{-}40)$$

The design bond strength is derived by division with the partial safety factor for concrete resistance γ_c = 1.5.

$$f_{bd} = 1.75 \cdot \left(\frac{f_c}{25}\right)^{0.5} \cdot \left(\frac{25}{Ø}\right)^{0.3} \cdot (\alpha_2 + \alpha_3)/1.5 \qquad (7\text{-}41)$$

The method applied in equations (7-38) to (7-41) for the derivation of design values for [MC2010] implies that the partial safety factor γ = 1.5 is applied to the bond length and not to the bar stress. Concurrently, the design model in [MC2010] becomes conservative by introducing the bond strength neglecting the exponential decrease in required lap length with decreasing bar stress.

According to [MC2010], the partial safety factor $\gamma_M = \gamma_m \cdot \gamma_{Rd}$ is a partial safety factor for material properties also accounting for the model uncertainties and dimensional variations. For concrete, the partial safety factor γ_M (also denominated γ_C) covers the deviations of structural dimensions not considered as basic variables and includes a conversion factor for the ratio of the strength obtained in test specimens to the strength in the actual structure. The value of γ_C should be increased if the geometrical tolerances defined in [MC2010] are not fulfilled.

Furthermore, in [FIB14] the following acceptance criteria for the suitability of equation (2-26) are defined:

- The 5% characteristic value should not lie below 1.0
- The number of results with a ratio of measured to estimated strength below 1.0 should not exceed 5%
- No individual ratio of measured to estimated strength should fall below 2/3, as lower values are not covered by the safety factor of 1.5

7.3.3 MANCINI ET AL.

MANCINI ET AL. [MAN17] evaluate the original fib database [FIB05] and derive characteristic and design values for the design model according to [FIB14]. For concrete strength and model uncertainty, log-normal distributions are verified [MAN17]. A COV of 0.15 for concrete strength and a mean concrete strength f_{cm} are applied. The evaluation distinguishes between new and existing structures. The variation in concrete strength and concrete cover is broader for existing structures, therefore, the coefficients of variation are slightly higher. For the model uncertainty of new structures, a COV $V_\theta = 0.126$ and a mean value $\theta = 0.98$ are used. The lap and anchorage resistance according to [FIB14] given in equation (2-26) is summarised to

$$R(\theta, f) = \theta \cdot f_{cm}^{0.25} \cdot A \tag{7-42}$$

Where

θ model uncertainty with $\theta = \dfrac{f_{st,test}}{f_{stm,calc}}$

A coefficient including all influencing parameters except the concrete strength f_{cm}

MANCINI ET AL. [MAN17] choose a constant value of 0.15 for the COV of concrete strength independent from the concrete class. This assumption is contrary to [EC2], which defines a constant standard deviation of 4.86 MPa and a COV depending on the concrete strength $V_{fc} = 4.86$ MPa / f_{cm}. The statistical characteristics defined in [MAN17] are summarised in Table 7-6.

Table 7-6 Statistical characteristics of concrete strength and model uncertainty according to [MAN17]

Parameter	distribution	COV V_i	Mean value μ_i
f_c	log-normal	0.15	f_{cm}
θ	log-normal	0.124	0.98

The mean value of the resistance μ_R is calculated with

$$\mu_R = \mu_\theta \cdot \mu_f^{0.25} \cdot A \tag{7-43}$$

and the variance follows from

$$\sigma_{\ln R}^2 = \ln(V_R^2 + 1) = \ln(V_\theta^2 + 1) + 0.25^2 \cdot \ln(V_{fc}^2 + 1) \tag{7-44}$$

The mean concrete strength is given by

$$\mu_f = f_{cm} = f_{ck} \cdot \exp(1.645 \cdot \sigma_{fc}) = f_{ck} \cdot \exp\left(1.645 \cdot \sqrt{\ln(V_{fc}^2 + 1)}\right) \tag{7-45}$$

Subsequently, the characteristic resistance $R_{k,5\%}$ includes the transformation from mean to characteristic concrete strength given in equation (7-45) plus the consideration of the statistical distribution of concrete strength and model uncertainty (7-44) with

$$\begin{aligned} R_{k,5\%} &= \zeta_k \cdot \bar{\theta} \cdot f_{ck}^{0.25} = 0.83 \cdot \bar{\theta} \cdot f_{ck}^{0.25} = \\ &= \bar{\theta} \cdot 54 \cdot f_{ck}^{0.25} \cdot \exp\left(-1.645 \cdot \left(\sqrt{\ln(V_\theta^2 + 1) + 0.0625 \cdot \ln(V_{fc}^2 + 1)} + \sqrt{\ln(V_{fc}^2 + 1)}\right)\right) \end{aligned} \tag{7-46}$$

The design resistance R_d is

$$\begin{aligned} R_d &= \zeta_d \cdot \bar{\theta} \cdot f_{ck}^{0.25} = 0.69 \cdot \bar{\theta} \cdot f_{ck}^{0.25} = \\ &= \bar{\theta} \cdot 54 \cdot f_{ck}^{0.25} \cdot \exp\left(-\alpha_R \cdot \beta \cdot \left(\sqrt{\ln(V_\theta^2 + 1) + 0.0625 \cdot \ln(V_{fc}^2 + 1)} + \sqrt{\ln(V_{fc}^2 + 1)}\right)\right) \end{aligned} \tag{7-47}$$

The calibration factors necessary for mean, characteristic and design values are described by the ratios ζ_i. For new structures, MANCINI ET AL. derive a characteristic ratio of $\zeta_k = 0.83$ and a ratio of design strength to mean strength of $\zeta_d = 0.69$ for an index of reliability $\beta = 3.8$ [MAN17]. Characteristic and design bond strengths are derived and the resulting partial safety factors are subsequently verified by a Monte-Carlo simulation [MAN17].

With the strength reduction factor $\zeta_k = 0.83$, the characteristic length is

$$\frac{l_{b,k}}{Ø}=\left(\frac{f_{std}}{\zeta_k \cdot 54}\right)^{1/0.55}\cdot\left(\frac{f_{ck}}{25}\right)^{-0.45}\cdot\left(\frac{25}{Ø}\right)^{-0.36}=\left(\frac{f_{std}}{0.83\cdot 54}\right)^{1/0.55}\cdot\left(\frac{f_{ck}}{25}\right)^{-0.45}\cdot\left(\frac{25}{Ø}\right)^{-0.36} \quad (7\text{-}48)$$

The design anchorage length l_{bd} / Ø is given for the calculated strength reduction factor $\zeta_d = 0.69$ with

$$\frac{l_{b,d}}{Ø}=\left(\frac{f_{std}}{\zeta_d \cdot 54}\right)^{1/0.55}\cdot\left(\frac{f_{ck}}{25}\right)^{-0.45}\cdot\left(\frac{25}{Ø}\right)^{-0.36}=\left(\frac{f_{std}}{0.69\cdot 54}\right)^{1/0.55}\cdot\left(\frac{f_{ck}}{25}\right)^{-0.45}\cdot\left(\frac{25}{Ø}\right)^{-0.36} \quad (7\text{-}49)$$

The reduction factor ζ_d is applied to the strength that is accounted for with an exponent of 1 / 0.55 < 1.0. Therefore, the applied safety factor is actually $\gamma_M = 1.4$ instead of $\gamma_M = 1.5$ with

$$\gamma_M=\frac{l_{b,d}}{l_{b,k}}=\left(\frac{1/\zeta_d}{1/\zeta_k}\right)^{1/0.55}=\left(\frac{1/0.69}{1/0.83}\right)^{1/0.55}=1.40 \quad (7\text{-}50)$$

For the reference parameters without transverse reinforcement, a characteristic concrete strength $f_{ck} = 25$ MPa, reinforcing bar diameters Ø 25 mm and a minimum concrete cover $c_{min} = 1.5 \cdot Ø$, the following design bar stress

$$f_{st,d}=0.69\cdot 54\cdot\left(\frac{f_{ck}}{25}\right)^{0.25}\cdot\left(\frac{25}{Ø}\right)^{0.2}\cdot\left(\frac{l_b}{Ø}\right)^{0.55}\cdot\left[\left(\frac{c_{min}}{Ø}\right)^{0.25}\cdot\left(\frac{c_{max}}{c_{min}}\right)^{0.1}+k_m\cdot K_{tr}\right] \quad (7\text{-}51)$$

$$f_{st,d}=0.69\cdot 54\cdot(1.0)^{0.25}\cdot(1.0)^{0.2}\cdot\left(\frac{l_b}{Ø}\right)^{0.55}\cdot[1.11]=41.3\cdot\left(\frac{l_b}{Ø}\right)^{0.55}$$

The design bond length according to [MAN17] for the reference parameters equals

$$l_{bd}=\left(\frac{500\text{ MPa}/1.15}{41.3}\right)^{1.82}\cdot Ø=72.5\cdot Ø \quad (7\text{-}52)$$

7.3.4 DARWIN ET AL.

In [DAR98] , DARWIN ET AL. investigate the reliability of the design model given in [DAR95b], which is the basis of the design model according to [ACI14]. The design model is based on the analysis of 299 lap and anchorage tests. The model has a mean test to prediction ratio of 1.0 and a COV V_x of 0.107 for anchorages and laps without transverse reinforcement and a COV of 0.125 with transverse reinforcement. Strength reduction factors for bond ϕ_b are derived to allow for the transfer from mean values to design values. The strength reduction factors are verified with a Monte-Carlo simulation and a target index of reliability β of 3.5. An index of reliability β of 3.0 is usually chosen for beams and columns. To insure that bond failure is less likely than an overall failure of the structural member, the index of reliability was increased for anchorages and laps. A strength reduction factor of 0.9 is obtained for the calculation of design anchorage and lap lengths [DAR98].

The derivation of strength reduction factors requires mean values of the action effects and resistance variables as well as coefficients of variation. The analysis includes the test-to-predicted load random variable $V_{T/P}$ given in equation (7-53) based on a comparison of test results with the calculated values. The COV of the test to prediction ratio $V_{T/P}$ (0.107 without confining reinforcement / 0.125 with confining reinforcement) comprises the COV V_m associated with the design model itself (0.081 without confining reinforcement / 0.102 with confining reinforcement) and the COV accounting for uncertainties in the measured loads and differences in the actual material and geometric properties of the specimens V_{ts} = 0.07. For unknown relative rib areas in some tests conducted, DARWIN ET AL. [DAR98] introduce an additional COV V_R = 0.02 for the test to prediction ratio for test specimens with confining reinforcement.

$$V_{T/P}^2 = V_m^2 + V_{ts}^2 + V_R^2 \tag{7-53}$$

Where

$V_{T/P}$ COV of the test to prediction ratio

V_m COV of the design model itself

V_{ts} COV of uncertainties in the measured loads and differences in the actual material and geometric properties of the specimens

V_R COV for unknown relative rib areas

An overview of the coefficients of variation and the mean values of the variables for the Monte-Carlo simulation described in [DAR98] is given in Table 7-7.

Table 7-7 Statistical characteristics for Monte-Carlo simulation according to [DAR98]

Number	Parameter	distribution	COV	Mean value
X(1)	Model uncertainty	normal	V_m = 0.081 / 0.102[1)]	1.0
X(4)	Concrete strength	normal	$((\sigma_{ccyl}/f_{cr}')^2+0.008)^{0.5}$	$0.89f_{c35}'(1+0.08\log(f_c))$
X(5)	Lap length	normal	0.61 [in.]/l_b	l_b
X(6)	Bottom cover	normal	0.23 [in.]/c_b	c_b
X(7)	Side cover	normal	0.19 [in.]/c_{s0}	c_{s0}
X(8)	Beam width	normal	0.013 / 0.017	b + 0.0625 [in.]
X(9)	Relative rib area	normal	0.124	0.0727

1) With confining reinforcement

Where

σ_{ccyl} assumed standard deviation for standard laboratory cylinders (3.8 MPa)

f_{cr} required average compressive strength of concrete

f_{c35} compressive strength at 35 psi/sec

7.3.5 Summary of Parameters Taken into Account

Table 7-8 summarises the COVs taken into account for the derivation of design stress for anchorages and laps in the publications described. All publications take the COV of the model uncertainty θ and of the concrete strength f_c into account. Only [DAR98] describes a full probabilistic analysis of the bond equation and takes the statistical distributions of model uncertainty θ, concrete strength f_c, bond length l_b, cover c_y and c_x, bar spacing c_s as well as the relative rib area f_R into account.

To derive design values from the own model for mean stress developed by bond in chapter 5.6, the statistical distribution of model uncertainty θ and material f_c are considered. The geometric parameters bond length, cover, spacing and rib area are neglected in the derivation of design values in chapter 0. Instead, the following derivation of design models presumes the geometric parameters to be covered by the COV of the model uncertainty.

Table 7-8 Summary of parameters taken into account for the derivation of design values for anchorages and laps (θ = model uncertainty)

Publication	$\sigma_{s,m} \rightarrow \sigma_{s,k}$	$\sigma_{s,k} \rightarrow \sigma_{s,d}$	$\sigma_{s,m} \rightarrow \sigma_{s,d}$	Uncertainties taken into account
[EC0]	θ, f_c	θ, f_c	θ, f_c	The factor γ_m in $\gamma_M = \gamma_m \cdot \gamma_R$ accounts for the distribution of material and permissible deviations in dimensions, γ_R accounts for the model uncertainty
[ELI79]	θ	θ, f_c	-	
[FIB14]	θ	θ, f_c	-	
[MAN17]	θ, f_c	θ, f_c	-	Model and material uncertainty
[DAR98]	-	-	θ, f_c, l_b, c_y, c_x, c_s, f_R	Uncertainty of the design model, uncertainties in the measured loads and differences in the actual material and geometric properties of the specimens

7.4 Own Derivation of Design Values for Anchorage and Lap Length

7.4.1 Method for the derivation of design values for anchorage and lap length

The applied method to derive design anchorage and lap lengths is given in Figure 7-3.

Method for derivation of design anchorage and lap length l_{bd}

↓

Derivation of mean bar stress in bond zones f_{stm} (f_{cm}, l_{bm}, Ø, c, A_{st}, p_{tr}) from database

↓

Determination of statistical data for model uncertainty θ and concrete strength f_{cm}

↓

Consideration of concrete strength f_{cm} in mean strength f_{stm} and f_{ck} in design strength f_{std}

↓

Derivation of design values according to annex D in [EC0]

↓

Rearrangement of bar stress in bond zones f_{std} for design anchorage and lap length l_{bd}

↓

Comparison of design values f_{std} with acceptance criteria

↓

Evaluation of reliability of design values f_{std} and l_{bd}

↓

Comparison of design anchorage and lap length l_{bd} for standard parameters

Figure 7-3 Method for the derivation of design anchorage and lap length l_{bd} based on database

7.4.2 Mean Values for Anchorage and Lap Length

The design values for anchorage and lap lengths are derived from the equations for mean bar stress given in chapter 5.6.

<u>Own Design Model Based on [FIB14]</u>

The own model based on [FIB14] given in equation (5-26) sums up the contribution by concrete cover (equation (5-27)) and the own proposal for the contributions of transverse reinforcement (equation (5-28)) and transverse pressure (equation (5-29)).

$$f_{stm,mod} = 54 \cdot \left(\frac{f_{cm}}{25}\right)^{0.25} \cdot \left(\frac{25}{Ø}\right)^{0.2} \cdot \left(\frac{l_b}{Ø}\right)^{0.55} \cdot \left[\alpha_c + \alpha_{tr} + \alpha_{tp}\right] \quad (5\text{-}26)$$

$$\alpha_c = \left(\frac{c_{min}}{Ø}\right)^{0.25} \cdot \left(\frac{c_{max}}{c_{min}}\right)^{0.1} \quad (5\text{-}27)$$

$$\alpha_{tr} = k_m \cdot \rho_{conf} = k_m \cdot \frac{A_{st}}{Ø \cdot s_{st}} \leq k_m \cdot 0.05 \tag{5-28}$$

$$\alpha_{tp} = 0.32 \cdot p_{tr}^{0.4} \tag{5-29}$$

Where

$f_{ck} = f_{cm} - 8$ MPa

$A_{st} \cdot n_{st} \geq A_s$ (for $\sigma_s \approx 0.5 \cdot f_{yd}$: $A_{st} \cdot n_{st} \geq 0.5 \cdot A_s$)

$k_m = 7$ or 4 according to Figure 5-54

Rearranging for the mean anchorage and lap length gives

$$\frac{l_{bm}}{Ø} = 45 \cdot \left(\frac{\sigma_s}{435}\right)^{1.82} \cdot \left(\frac{25}{f_{cm}}\right)^{0.455} \cdot \left(\frac{Ø}{25}\right)^{0.36} \cdot \left[\alpha_c + \alpha_{tr} + \alpha_{tp}\right]^{-1.82} \tag{7-54}$$

Design Model According to [PT18] with Own Calibration Factors

The model given in [PT18] was rearranged for the calculation of bar stress developed by bond and own calibration factors were derived from the database to obtain the smallest possible COV of the model uncertainty V_θ resulting in the following equation

$$f_{stm,PT} = 435 \cdot \left(\frac{f_{cm}}{25\text{ MPa}}\right)^{\frac{1}{3}} \cdot \left(\frac{20}{Ø}\right)^{\frac{2}{9}} \cdot \left(\frac{l_b}{31 \cdot Ø}\right)^{\frac{2}{3}} \cdot \left(\frac{c_{d,conf}}{1.5 \cdot Ø}\right)^{\frac{1}{3}} \tag{5-30}$$

With

$$c_{d,conf} = c_d + \left(60 \cdot k_{conf} \cdot \frac{n_l \cdot A_{st}}{n_b \cdot Ø \cdot s_{st}} + 8 \cdot \sigma_{ctd} / \sqrt{f_{ck}}\right) \cdot Ø \leq 3.75 \cdot Ø \tag{5-31}$$

k_{conf} see chapter 2.9.7

The mean anchorage and lap length is

$$\frac{l_{bm,PT}}{Ø} = 31 \cdot \left(\frac{\sigma_s}{435}\right)^{3/2} \cdot \left(\frac{25}{f_{cm}}\right)^{1/2} \cdot \left(\frac{Ø}{20}\right)^{1/3} \cdot \left(\frac{1.5 \cdot Ø}{c_{d,conf}}\right)^{1/2} \tag{7-55}$$

Comparison of the Two Design Models

In the following derivation of design values, the [EC0] notation is used. The statistical values for the two design models are given in Table 7-9. The least-squares best fit slope according to [EC0] of the own model is b = 1.00 and of the model according to [PT18] with own calibration factors b = 0.96.

Table 7-9 Statistical data (presuming a log-normal distribution) for models for mean bar stress in bond zones calculated with equations (5-26) and (5-30) under consideration of the least-squares best fit slope b

$\sigma_{test}/\sigma_{calc}$	Own model based on [FIB14]	Model according to [PT18] with own calibration factors
Mean value of error terms δ	1.00	1.04
Standard deviation	0.145	0.180
COV V_δ	0.144	0.173
Minimum	0.53	0.56
5% characteristic ratio	0.79	0.77
b	1.00	0.96
Number of results	669	669

Both equations were calibrated to best-fit the test results in the database. For the definition of the mean anchorage and lap strength according to [EC0], the least-squares best-fit slope b and the mean value of the error terms have to be taken into account.

$$r_m = b \cdot g_{rt}(X_m) \cdot \delta \tag{7-56}$$

$$r_{m,own} = 1.00 \cdot f_{stm,own} \cdot 1.00 = f_{stm,own} \tag{7-57}$$

$$r_{m,PT} = 0.96 \cdot f_{stm,PT} \cdot 1.04 = f_{stm,PT} \tag{7-58}$$

These equations are compared for the following standard values

- $f_{ck} = 25$ MPa and $f_{cm} = f_{ck} + 8$ MPa $= 33$ MPa
- $\sigma_s = 435$ MPa and $\sigma_s = 250$ MPa
- $Ø = 25$ mm
- $c_{min} = 1.5 \cdot Ø$
- $c_{max} = c_{min}$
- $A_{st} = 0$ or $\Sigma A_{st} = A_s$

Taking the value $b \cdot \delta = 1.0$ in the own model for the mean bar stress into account, does not change the calibration factors. The mean anchorage and lap length according to the own model without transverse reinforcement for the standard parameters is

$$\frac{l_{bm,own}}{Ø} = 45 \cdot \left(\frac{\sigma_s}{435}\right)^{1.82} \cdot 0.73 \tag{7-59}$$

If transverse reinforcement with $\Sigma A_{st} = A_s$ is positioned, the required bond length is

$$\frac{l_{bm,own}}{Ø} = 45 \cdot \left(\frac{\sigma_s}{435}\right)^{1.82} \cdot 0.59 \qquad (7\text{-}60)$$

The equation according to [PT18] with own calibration factors for the calculation of mean bar stress is to be multiplied with $b \cdot \delta = 1.04 \cdot 0.96 = 1.0$. For the standard parameters, the mean anchorage and lap length according to [PT18] with own calibration factors without transverse reinforcement is

$$\frac{l_{bm,PT}}{Ø} = 31 \cdot \left(\frac{\sigma_s}{435}\right)^{3/2} \cdot 0.94 \qquad (7\text{-}61)$$

Where transverse reinforcement is positioned, the anchorage and lap length is

$$\frac{l_{bm,PT}}{Ø} = 31 \cdot \left(\frac{\sigma_s}{435}\right)^{3/2} \cdot 0.82 \qquad (7\text{-}62)$$

The resulting mean bond lengths for both models are listed in Table 7-10.

Table 7-10 Mean lap and anchorage length for standard parameters according to own model and model according to [PT18] with own calibration factors

f_{ck} = 25 MPa, f_{cm} = 33 MPa, Ø = 25 mm, $c_{min} = 1.5 \cdot Ø$, $c_{max} = c_{min}$	$l_{bm,own}$	$l_{bm,PT}$
σ_s = 435 MPa, A_{st} = 0	33 · Ø	29 · Ø
σ_s = 435 MPa, $A_{st} = A_s$	27 · Ø	25 · Ø
σ_s = 250 MPa, A_{st} = 0	12 · Ø	13 · Ø

For these parameters, the mean lap and anchorage lengths shown in Figure 7-3 result.

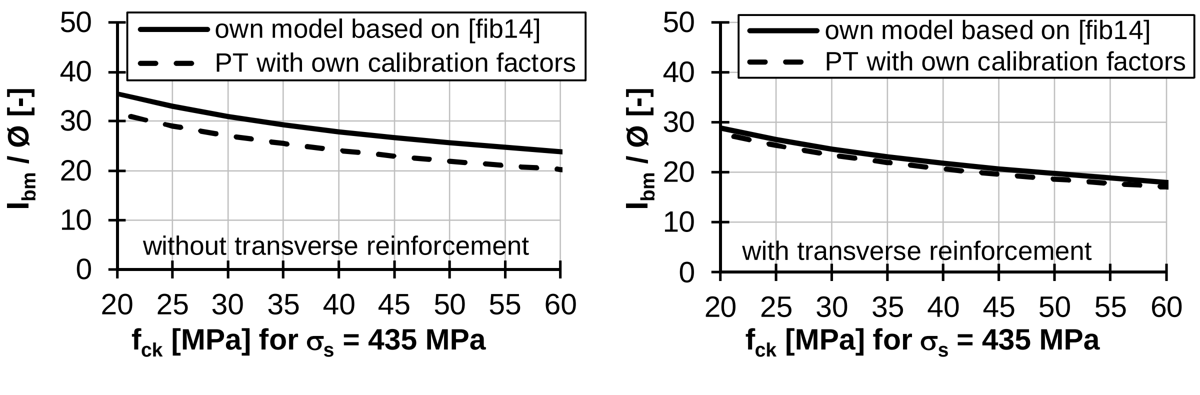

Figure 7-4 Mean bond length $l_{bm}/Ø$ vs. characteristic concrete strength f_{ck} obtained for the own model and the modified model according to [PT18] with own calibration factors for $\Sigma A_{st} = 0$ (left) and $\Sigma A_{st} = A_s$ (right) (σ_s = 435 MPa, Ø = 25 mm, $c_{min} = 1.5 \cdot Ø$)

7.4.3 Statistical Data for Derivation of Design Values

For the derivation of design values, the statistical scatter of all influencing parameters must be defined.

In [JOI00], [MC2010] and [EC2], tolerances for width and depth of structural elements as well as for the cross-sectional area of the reinforcing bars are given. In DIN EN 13670 [DEU11], the tolerable deviation – conforming with the COV – of lap length are defined as 6 % of the lap length. The concrete cover has a tolerance of +2 mm to +5 mm according to [JOI00]. The GUIDELINES FOR REINFORCING WORKS OF THE GERMAN BUILDING INDUSTRY [BAU08] give a tolerance of 10 mm for stirrup spacing. Thus, the standard deviation of the stirrup spacing has a constant value of 10 mm, while the COV of stirrup spacing increases with decreasing stirrup spacing.

The undocumented tolerances of the test specimens' dimensions, including deviations in concrete cover, stirrup spacing and lap length, may be included in the model uncertainty itself or considered with their intrinsic statistical distribution. The following evaluation of reliability is based on the assumption that the statistical distribution of the dimensions is covered by the model uncertainty. Therefore, only the model uncertainty and the scatter in concrete strength are taken into account.

The COV of the model uncertainty in the design model for anchorages and laps was derived from the database described in chapter 5. Table 7-11 gives an overview of the statistical data of the main influencing parameters for lap and anchorage strength.

Table 7-11 Statistical characteristics of dimensions for derivation of design values (the values in brackets are not taken into account in the following derivation of design values)

	Concrete strength	Lap length	Cover	Stirrup spacing
Mean value	f_{cm}	(l_b)	(c)	(s_{st})
Standard deviation	4.9 MPa	($0.06 \cdot l_b$)	(3.5 mm)	(10 mm)
COV V_i	$4.9 / f_{cm}$	(0.06)	(3.5 mm / c)	(10 mm / s_{st})

The mean values of the model uncertainty θ and the COV of the model uncertainty V_θ for [EC2], [EC2/NA], the own model based on [FIB14] and for [PT18] with own calibration factors are given in Table 7-12.

Table 7-12 Statistical characteristics of design models for derivation of design values for anchorage and lap length including the least-squares best fit slope b

	[EC2]	[EC2/NA]	own	[PT18]
Mean value θ	1.02	1.26	1.0	1.04
Standard deviation	0.324	0.381	0.145	0.180
COV V_θ	0.316	0.303	0.144	0.173

7.4.4 Consideration of Concrete Strength

The design models for the mean bar stress in bond zones f_{stm} include the mean concrete strength f_{cm}. In contrast, the design bond length shall include the characteristic concrete strength f_{ck}. Therefore, the statistical distribution of the concrete strength as well as of the model uncertainty has to be taken into account.

The procedure given in [EC0] to obtain design values does not comprise an unambiguous approach for the consideration of concrete strength. [EC2] is valid for concrete classes C12/15 to C90/105. Since the standard deviation σ_{fc} = 4.86 MPa (cf. chapter 7.2.4) is constant for all concrete classes, the COV is most unfavourable for C12/15 with V_{fc} = 4.86 MPa / 20 MPa = 0.243. This COV is taken into account in the following derivation of design values.

The characteristic and design resistance functions r_k and r_d are defined with mean values of the resistance parameters X_m in [EC0] (cf. step 7 in Table 7-5).

$$r_k = b \cdot g_{rt}(X_m) \cdot \exp(-k_n \cdot Q - 0.5 \cdot Q^2) \tag{7-63}$$

Since X_m would conform to f_{cm}, while the design lap and anchorage length shall include the characteristic concrete strength f_{ck}, this change is incorporated into the own model by the introduction of f_{ck} divided by the factor for the 5%-fractile value for a log-normal distribution.

$$r_k = b \cdot g_{rt}(f_{cm}^{0.25}) \cdot \exp(-k_n \cdot Q - 0.5 \cdot Q^2) =$$

$$= b \cdot g_{rt}\left(\left(\frac{f_{ck}}{\exp(-1.645 \cdot V_{fc} - 0.5 \cdot V_{fc}^2)}\right)^{0.25}\right) \cdot \exp(-k_n \cdot Q - 0.5 \cdot Q^2) \tag{7-64}$$

In this case, the smallest possible COV V_{fc} leads to conservative design lap and anchorage lengths with V_{fc} = 4.86 MPa / 98 MPa = 0.05

$$\begin{aligned} r_k &= b \cdot g_{rt}\left(\left(\frac{f_{ck}}{\exp(-1.645 \cdot 0.05 - 0.5 \cdot 0.05^2}\right)^{0.25}\right) \cdot \exp(-k_n \cdot Q - 0.5 \cdot Q^2) = \\ &= b \cdot 1.02 \cdot g_{rt}(f_{ck}) \cdot \exp(-k_n \cdot Q - 0.5 \cdot Q^2) \end{aligned} \tag{7-65}$$

For the model according to [PT18] with own calibration factors, the change from mean to characteristic concrete strength f_{ck} is incorporated by

$$r_k = b \cdot g_{rt}(f_{cm}^{1/3}) \cdot \exp(-k_n \cdot Q - 0.5 \cdot Q^2) =$$

$$= b \cdot g_{rt}\left(\left(\frac{f_{ck}}{\exp(-1.645 \cdot V_{fc} - 0.5 \cdot V_{fc}^2)}\right)^{1/3}\right) \cdot \exp(-k_n \cdot Q - 0.5 \cdot Q^2) \tag{7-66}$$

Inserting V_{fc} = 4.86 MPa / 98 MPa = 0.05 gives

$$r_k = b \cdot g_{rt}\left(\left(\frac{f_{ck}}{\exp(-1.645 \cdot 0.05 - 0.5 \cdot 0.05^2}\right)^{1/3}\right) \cdot \exp(-k_n \cdot Q - 0.5 \cdot Q^2) = \qquad (7\text{-}67)$$

$$= b \cdot 1.03 \cdot g_{rt}(f_{ck}) \cdot \exp(-k_n \cdot Q - 0.5 \cdot Q^2)$$

7.4.5 Design Values for Anchorage and Lap Length according to [EC0]

In chapter 5, the coefficients of variation were derived for the mean level of different design models for anchorage and lap length without consideration of the least-squares best fit slope b. In the following derivation of design values, the least-squares best fit slope b as well as the COV of the concrete strength are taken into account.

Design Values for the Own Model Based on [FIB14] According to [EC0]

The total COV for the own model follows from V_{fc} = 0.243 for concrete class C12/15 (cf. Table 7-4), the COV of the model uncertainty V_θ = 0.144 and

$$\ln\left(V_r^2 + 1\right) = 0.25^2 \cdot \ln\left(V_{fc}^2 + 1\right) + \ln\left(V_\theta^2 + 1\right) \rightarrow V_r = 0.156 \qquad (7\text{-}68)$$

The standard deviation of the resistance function is

$$Q = \sqrt{\ln\left(V_r^2 + 1\right)} = \sqrt{\ln\left(0.156^2 + 1\right)} = 0.155 \qquad (7\text{-}69)$$

The characteristic values are obtained by multiplication with the reduction factor

$$\exp(-1.645 \cdot Q - 0.5 \cdot Q^2) = \exp(-0.27) = 0.77 \qquad (7\text{-}70)$$

For design values, the reduction factor follows from

$$\exp(-3.04 \cdot Q - 0.5 \cdot Q^2) = \exp(-0.48) = 0.62 \qquad (7\text{-}71)$$

Under consideration of the concrete strength with the factor 1.02 according to chapter 7.4.4, the design bar stress in laps and anchorages is

$$f_{std,own} = 1.02 \cdot 54 \cdot 0.62 \cdot \left(\frac{f_{ck}}{25}\right)^{0.25} \cdot \left(\frac{25}{Ø}\right)^{0.2} \cdot \left(\frac{l_b}{Ø}\right)^{0.55} \cdot \left[\alpha_c + \alpha_{tr} + \alpha_{tp}\right] \qquad (7\text{-}72)$$

With $f_{std,own} = \sigma_{sd}$, the design anchorage and lap length is

$$\frac{l_{bd,own}}{Ø} = \left(\frac{435}{1.02 \cdot 54 \cdot 0.62}\right)^{1.82} \cdot \left(\frac{\sigma_{sd}}{435}\right)^{1.82} \cdot \left(\frac{25}{f_{ck}}\right)^{0.455} \cdot \left(\frac{Ø}{25}\right)^{0.36} \cdot \left[\alpha_c + \alpha_{tr} + \alpha_{tp}\right]^{-1.82}$$

$$\frac{l_{bd,own}}{Ø} = 103 \cdot \left(\frac{\sigma_{sd}}{435}\right)^{1.82} \cdot \left(\frac{25}{f_{ck}}\right)^{0.455} \cdot \left(\frac{Ø}{20}\right)^{0.36} \cdot \left[\alpha_c + \alpha_{tr} + \alpha_{tp}\right]^{-1.82} \qquad (7\text{-}73)$$

The partial safety factor γ_M of the anchorage and lap length is

$$\gamma_{M,own} = \frac{l_{bd}}{l_{bk}} = \left(\frac{1/0.62}{1/0.77}\right)^{1.82} = \left(\frac{0.77}{0.62}\right)^{1.82} = 1.48 \tag{7-74}$$

Since the partial safety factor is smaller than 1.5, the reliability of the design models is evaluated in chapter 7.4.7.

For the standard parameters defined in chapter 7.4.1 (f_{ck} = 25 MPa, f_{cm} = 33 MPa, Ø = 25 mm, c_{min} = 1.5 · Ø), the design anchorage and lap length according to the own model without transverse reinforcement is

$$\frac{l_{bd,own}}{Ø} = 103 \cdot 0.83 \cdot \left(\frac{\sigma_{sd}}{435}\right)^{1.82} = 85 \cdot \left(\frac{\sigma_{sd}}{435}\right)^{1.82} \tag{7-75}$$

Where transverse reinforcement with $\Sigma A_{st} = A_s$ is positioned, the design anchorage and lap length is

$$\frac{l_{bd,own}}{Ø} = 103 \cdot 0.67 \cdot \left(\frac{\sigma_{sd}}{435}\right)^{1.82} = 69 \cdot \left(\frac{\sigma_{sd}}{435}\right)^{1.82} \tag{7-76}$$

Design Values for the Model According to [PT18] with Own Calibration Factors According to [EC0]

For the model according to [PT18] with own calibration factors and concrete class C12/15, the total COV follows from $V_{fc} = 0.243$, $V_\theta = 0.173$ and

$$\ln\left(V_r^2 + 1\right) = 0.33^2 \cdot \ln\left(V_{fc}^2 + 1\right) + \ln\left(V_\theta^2 + 1\right) \rightarrow V_r = 0.191 \tag{7-77}$$

The standard deviation of the resistance function is

$$Q = \sqrt{\ln\left(V_r^2 + 1\right)} = \sqrt{\ln\left(0.191^2 + 1\right)} = 0.189 \tag{7-78}$$

The characteristic value follows from multiplication with the reduction factor

$$\exp(-1.645 \cdot Q - 0.5 \cdot Q^2) = \exp(-0.33) = 0.72 \tag{7-79}$$

The design values are obtained by multiplication with the reduction factor

$$\exp(-3.04 \cdot Q - 0.5 \cdot Q^2) = \exp(-0.59) = 0.55 \tag{7-80}$$

The design bar stress in anchorages and laps is

$$f_{std,PT} = 1.03 \cdot 435 \cdot 0.55 \cdot \left(\frac{f_{ck}}{25}\right)^{\frac{1}{3}} \cdot \left(\frac{20}{Ø}\right)^{\frac{2}{9}} \cdot \left(\frac{l_b}{Ø \cdot 31}\right)^{\frac{2}{3}} \cdot \left(\frac{c_{d,conf}}{1.5 \cdot Ø}\right)^{\frac{1}{3}} \tag{7-81}$$

And the design length for $f_{std,PT} = \sigma_s$ follows from

$$\frac{l_{bd,PT}}{Ø} = \frac{31}{(1.03 \cdot 0.55)^{3/2}} \cdot \left(\frac{\sigma_s}{435}\right)^{3/2} \cdot \left(\frac{25}{f_{ck}}\right)^{1/2} \cdot \left(\frac{Ø}{20}\right)^{1/3} \cdot \left(\frac{1.5 \cdot Ø}{c_{d,conf}}\right)^{1/2} \tag{7-82}$$

$$\frac{l_{bd,PT}}{Ø} = 73 \cdot \left(\frac{\sigma_s}{435}\right)^{3/2} \cdot \left(\frac{25}{f_{ck}}\right)^{1/2} \cdot \left(\frac{Ø}{20}\right)^{1/3} \cdot \left(\frac{1.5 \cdot Ø}{c_{d,conf}}\right)^{1/2} \tag{7-83}$$

The partial safety factor γ_M equals

$$\gamma_{M,PT} = \frac{l_{bd}}{l_{bk}} = \left(\frac{1/0.55}{1/0.72}\right)^{3/2} = \left(\frac{0.72}{0.55}\right)^{3/2} = 1.49 \tag{7-84}$$

The mean anchorage and lap length according to the [PT18] model with own calibration factors without transverse reinforcement for the standard parameters (f_{ck} = 25 MPa, f_{cm} = 33 MPa, Ø = 25 mm, $c_{min} = 1.5 \cdot Ø$) is

$$\frac{l_{bd,PT}}{Ø} = 73 \cdot 1.08 \cdot \left(\frac{\sigma_{sd}}{435}\right)^{3/2} = 79 \cdot \left(\frac{\sigma_{sd}}{435}\right)^{3/2} \tag{7-85}$$

Where transverse reinforcement is positioned, the design anchorage and lap length is reduced to

$$\frac{l_{bd,PT}}{Ø} = 73 \cdot 0.94 \cdot \left(\frac{\sigma_{sd}}{435}\right)^{3/2} = 69 \cdot \left(\frac{\sigma_{sd}}{435}\right)^{3/2} \tag{7-86}$$

Comparison of Derived Design Values

The resulting design lengths of the own model and the model according to [PT18] with own calibration factors are compared to the design lengths according to [EC2], [EC2/NA] and [MC2010] in Table 7-13.

Table 7-13 Comparison of design lap lengths for standard parameters (f_{ck} = 25 MPa, f_{cm} = 33 MPa, Ø = 25 mm, $c_{min} = 1.5 \cdot Ø$, $\alpha_{6,EC} = 1.5$, $\alpha_{6,NAD} = 2.0$)

	$l_{bd,own}$	$l_{bd,PT}$	$l_{bd,EC}$	$l_{bd,NAD}$	$l_{bd,MC}$
σ_s = 435 MPa, $\Sigma A_{st} = 0$	85 · Ø	79 · Ø	56 · Ø	81 · Ø	76 · Ø
σ_s = 435 MPa, $\Sigma A_{st} = A_s$	69 · Ø	69 · Ø	50 · Ø	73 · Ø	73 · Ø
σ_s = 250 MPa, $\Sigma A_{st} = 0$, $\alpha_6 = 1.0$	31 · Ø	34 · Ø	21 · Ø	23 · Ø	44 · Ø
σ_s = 250 MPa, $\Sigma A_{st} = 0.5 \cdot A_s$, $\alpha_6 = 1.0$	24 · Ø	29 · Ø	19 · Ø	21 · Ø	38 · Ø
σ_s = 250 MPa, $\Sigma A_{st} = 0.5 \cdot A_s$, $\alpha_6 = 1.0$, p=5 MPa (e.g. at beam ends)	12 · Ø	22 · Ø	15 · Ø	14 · Ø	15 · Ø

The design lap length according to [EC2/NA] exceeds the design lap length calculated according to [EC2], since the lap factor $\alpha_{6,NAD}$ is 2.0 in contrast to $\alpha_{6,EC2}$ = 1.5. The design lap lengths according to [MC2010], [EC2/NA], the own model and [PT18] with own calibration factors are approximately 40 % greater than the length according to [EC2] (cf. Figure 7-5, left).

The comparison for the design approaches at σ_s = 250 MPa (cf. Figure 7-5, right) is conducted assuming an anchorage at a beam end with p = 5 MPa. In this case, the lap factor α_6 equals 1.0 for σ_s = 250 MPa in the graphs according to [EC2] and [EC2/NA]. For laps without transverse pressure at σ_s = 250 MPa, the values according to the own model and the model according to [PT18] with own calibration factors are close to the values according to [EC2] with α_6 = 1.5, but smaller than the values according to [EC2/NA] with α_6 = 2.0.

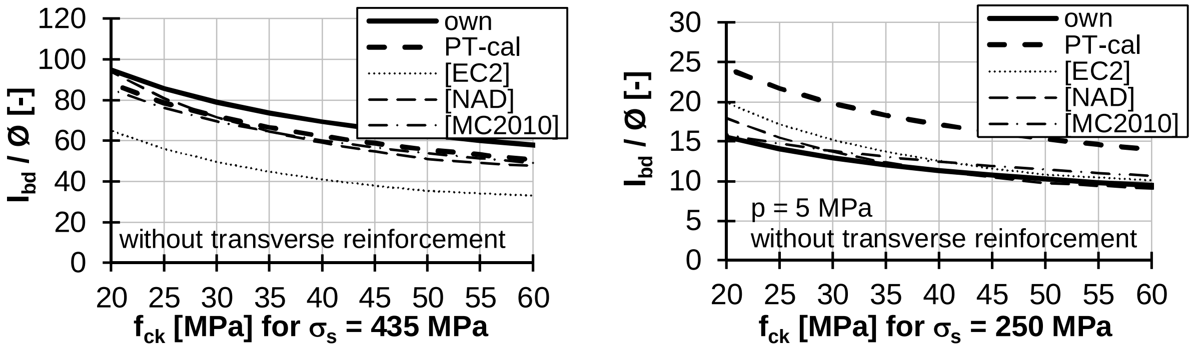

Figure 7-5 Design anchorage length l_{bd} / Ø vs. characteristic concrete strength f_{ck} obtained for the own model, the model according to [PT18] with own calibration factors and according to [EC2], [EC2/NA] and [MC2010] for σ_s = 435 MPa (left) and for σ_s = 250 MPa, α_6 = 1.0, p = 5 MPa (right) (Ø = 25 mm, c_{min} = 1.5 · Ø, ΣA_{st} = 0, f_{cm} = f_{ck} + 8 MPa)

The design lap lengths decrease where transverse reinforcement is positioned. The resulting design lap length calculated from the own model and the model according to [PT18] with own calibration factors are in the range of [EC2/NA] (cf. Figure 7-6, left). The minimum transverse reinforcement in the design model according to [EC2] and [EC2/NA] was taken into account with $\Sigma A_{st,min}$ = 1.0 · A_s at σ_s = 435 MPa and with $\Sigma A_{st,min}$ = 0.5 · A_s at σ_s = 250 MPa.

At σ_s = 250 MPa and the assumption of an anchorage at a beam end with transverse pressure (with α_6 = 1.0), transverse reinforcement influences the design bond length stronger in the own model than in the models according to [EC2], [EC2/NA] and [MC2010] (cf. Figure 7-6, right). For the defined limit in equation (2-43), additional transverse reinforcement does not decrease the design lengths according to [PT18] with own calibration factors.

For a direct comparison, the design lengths at f_{ck} = 25 MPa are given in Table 7-13.

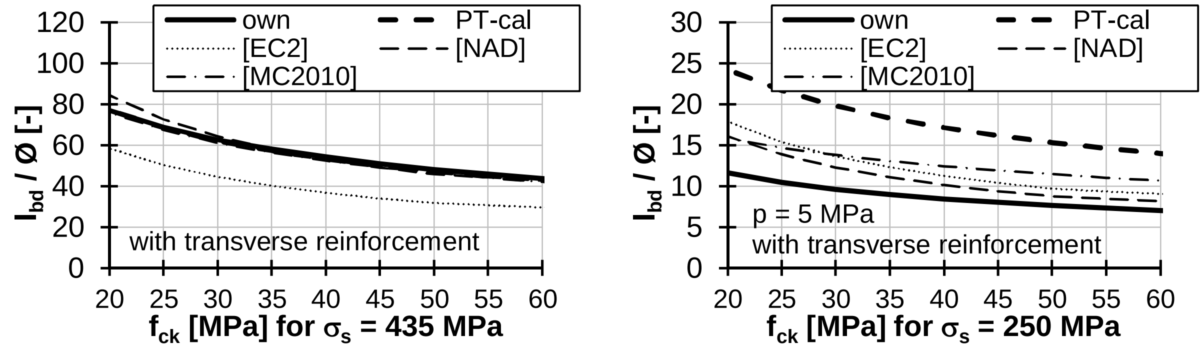

Figure 7-6 Design anchorage length l_{bd} / Ø vs. characteristic concrete strength f_{ck} obtained for the own model, the model according to [PT18] with own calibration factors and according to [EC2], [EC2/NA] and [MC2010] for $\sigma_s = 435$ MPa and $\Sigma A_{st} = 1.0 \cdot A_S$ (left) and for $\sigma_s = 250$ MPa, $\alpha_6 = 1.0$, p = 5 MPa and $\Sigma A_{st} = 0.5 \cdot A_S$ (right) (Ø = 25 mm, $c_{min} = 1.5 \cdot$ Ø, $f_{cm} = f_{ck} + 8$ MPa)

7.4.6 Comparison of Design Values with Acceptance Criteria

The design anchorage and lap lengths are assessed with their statistical characteristics obtained from the database presuming a log-normal distribution given in Table 7-14. For both models, the 5 % characteristic value of σ_{test} / $\sigma_{sd,calc}$ is larger than 1.0. The proportion of measured to estimate strength below 1.0 does not exceed 5 % and no individual ratio falls below 0.7.

Table 7-14 Statistical evaluation of ratio of measured strength to design strength σ_{test} / $\sigma_{sd,calc}$ for the own model and the model according to [PT18] with own calibration factors

σ_{test} / $\sigma_{sd,calc}$	Own Model	Model according to [PT18] with own calibration factors
Number	669	669
Mean value θ	1.60	1.84
Standard deviation	0.230	0.318
Coefficient of variation V_θ	0.144	0.173
Minimum value	0.84	0.98
5% characteristic value	1.25	1.37
Percentage of σ_{test} / $\sigma_{sd,calc}$ < 1.0	0.6 %	0.1 %

7.4.7 Reliability of Design Lengths for Anchorages and Laps

A reliability analysis of the own design model based on [FIB14] and of the design model according to [PT18] with own calibration factors is conducted. Therefore, statistical data for the influencing parameters are defined.

The index of reliability β = 3.8 describes both the reliability of action effects and of the resistance of a structure. The distance between the mean resistance of the design model and the design point equals the product of the reliability β, a factor α_R and the standard deviation of the resistance with $\alpha_R \cdot \beta \cdot \sigma_R$ (cf. Figure 7-1). For the analysis of the reliability of a resistance model only, the value $\alpha_R \cdot \beta = 3.04$ shall be obtained by comparison of the mean value of the resistance with the design point $E_d = R_d$.

In this thesis, the design point is $E_d = R_d = \sigma_{sd} = 435$ MPa and the target index of reliability is 3.04 (cf. Figure 7-7).

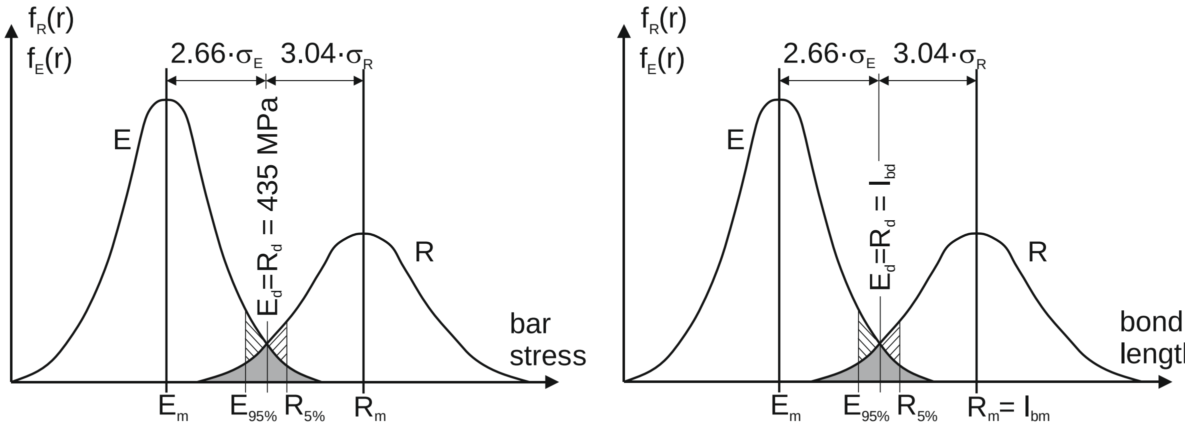

Figure 7-7 Visualisation of mean and design values for bar stress (left) and bond length (right) for an index of reliability $\beta = 3.8$ with α_E and α_R according to [EC0]

The reliability of the design models is also analysed including the statistical distribution of the action effects with $E_d = (G + Q) \cdot 435/2$. The scatter of the action effects is evaluated with a COV for the dead load $V_G = 0.10$ and a COV for the live load $V_Q = 0.20$ according to [RIC09] and a presumed ratio of $G / Q = 1.0$. The mean value of the dead load G equals 1.0 and the mean value of the live loads Q equals 0.7 [RIC09]. For a more general evaluation, the ratio G / Q must be varied.

The reliability is evaluated for the own equation, the model according to [PT18] with own calibration factors, [EC2] and [EC2/NA]. The parameters l_{bm}, Ø, c, A_{st} and p_{tr} are presumed to be deterministic and are not considered in the resistance function g (cf. Table 7-11). Table 7-15 gives the statistical characteristics taken into account.

Table 7-15 Mean value, COV of model uncertainty and least-squares best fit slope b of own model, model according to [PT18] with own calibration factors, concrete strength f_{cm}, dead load G and live load Q

	own	[PT18] cal.	[EC2]	[EC2/NA]	f_{cm}	G / Q
Mean value	1.00	1.04	1.02	1.26	20 / 33 / 43 / 58	1.0 / 0.7
COV V_i	0.144	0.173	0.316	0.303	4.86 / f_{cm}	0.10 / 0.20
b	1.00	0.96	- [1]	- [1]	- [1]	- [1]

[1] Least-squares best fit slope b not taken into account

The resulting index of reliability was obtained by a first-order reliability method (FORM) with the software COMREL. The FORM and the derivation of limit state functions for reliability investigations are described in [RIC09]. A comparison of results of the FORM and a Monte-Carlo simulation with 1,000,000 samples give rather similar values for β (cf. Table 7-16).

Table 7-16 Values for β for the design model according to [EC2] calculated with FORM and Monte-Carlo simulation

	FORM	Monte-Carlo simulation
[EC2] (f_{ck} = 12 MPa)	1.628	1.575
[EC2] (f_{ck} = 50 MPa)	2.367	2.367

Limit State Function for the own Design Model for Anchorage and Lap Length

For the limit state functions, the statistical distribution of the model uncertainty and the concrete strength are taken into account. The parameters are defined as Ø = 25 mm and $[\alpha_c + \alpha_{tr} + \alpha_{tp}] = 1$. Since the statistical distribution of these parameters is not taken into account, their values do not influence the resulting reliability. For f_{cm} = 20 MPa and σ_{sd} = 435 MPa = E_d = R_d, the design model for mean bar stress can be simplified to

$$f_{stm,own} = \theta_{own} \cdot 460 \cdot \left(\frac{f_{cm}}{25}\right)^{0.25} = \theta_{own} \cdot 435\,\text{MPa} \tag{7-87}$$

For the mean concrete strength values 33 MPa, 43 MPa and 58 MPa, the calibration factor 460 is modified. The design value is obtained by multiplication with the factor 0.62 (cf. equation (7-71)). For the resistance only, the limit state function for f_{cm} = 20 MPa is

$$g_{E+R,\sigma,own} = R_m - R_d = \theta_{own} \cdot 460 \cdot \left(\frac{f_{cm}}{25}\right)^{0.25} / 0.62 - 435 \tag{7-88}$$

Taking the statistical distribution of the action effects into account, the limit state function is given by

$$g_{E+R,\sigma,own} = R_m - R_d = \theta_{own} \cdot 460 \cdot \left(\frac{f_{cm}}{25}\right)^{0.25} / 0.62 - (G+Q) \cdot \frac{435}{2} \tag{7-89}$$

The reliability of the design models for bond lengths is also evaluated. For the design anchorage and lap lengths according to equation (7-73), the following limit state function is defined

$$g_{R,lb,own} = \left(\frac{435 \cdot \theta_{own}}{54 \cdot 0.62}\right)^{1.82} \cdot \left(\frac{25}{f_{cm}}\right)^{0.455} - \left(\frac{435}{54}\right)^{1.82} \cdot \left(\frac{25}{20}\right)^{0.455} \tag{7-90}$$

Taking the action effects into account leads to the limit state function for anchorage and lap lengths

$$g_{R+E,lb,own} = \left(\frac{435\cdot\theta_{own}}{54\cdot 0.62}\right)^{1.82}\cdot\left(\frac{25}{f_{cm}}\right)^{0.455} - \left(\frac{(G+Q)\cdot 435}{2\cdot 54}\right)^{1.82}\cdot\left(\frac{25}{20}\right)^{0.455} \tag{7-91}$$

For all limit state functions, the target value is 0.8 · 3.8 = 3.04. The mean values and COVs of the parameters considered are given in Table 7-15.

<u>Limit State Function for the Design Model for Anchorage and Lap Length According to [PT18] with Own Calibration Factors</u>

Accordingly, the reliability was evaluated for the design model according to [PT18] with own calibration factors including the least-squares best fit slope b = 0.96 with

$$f_{stm,PT} = 0.96\cdot\theta_{PT}\cdot 468.5\cdot\left(\frac{f_{cm}}{25}\right)^{1/3} = 0.96\cdot\theta_{PT}\cdot 435 \tag{7-92}$$

$$g_{R,\sigma,PT} = R_m - R_d = 0.96\cdot\theta_{PT}\cdot 468.5\cdot\left(\frac{f_{cm}}{25}\right)^{1/3} / 0.55 - 435 \tag{7-93}$$

Taking the statistical distribution of the action effects into account, the limit state function for f_{cm} = 20 MPa and $E_d = R_d = \sigma_{sd}$ = 435 MPa is

$$g_{R+E,\sigma,PT} = R_m - R_d = 0.96\cdot\theta_{PT}\cdot 468.5\cdot\left(\frac{f_{cm}}{25}\right)^{1/3} / 0.55 - (G+Q)\cdot\frac{435}{2} \tag{7-94}$$

The limit state functions for the design anchorage and lap lengths according to this model (cf. equation (7-82)) follow from

$$g_{R,lb,PT} = 31\cdot\left(\frac{0.96\cdot\theta_{PT}}{0.55}\right)^{1.5}\cdot\left(\frac{25}{f_{cm}}\right)^{0.5} - 31\cdot\left(\frac{435}{435}\right)^{1.5}\cdot\left(\frac{25}{20}\right)^{0.5} \tag{7-95}$$

$$g_{R+E,lb,PT} = 31\cdot\left(\frac{0.96\cdot\theta_{PT}}{0.55}\right)^{1.5}\cdot\left(\frac{25}{f_{cm}}\right)^{0.5} - 31\cdot\left(\frac{(G+Q)}{2}\right)^{1.5}\cdot\left(\frac{25}{20}\right)^{0.5} \tag{7-96}$$

<u>Limit State Function for Design Model According to [EC2] and [EC2/NA]</u>

For [EC2], the evaluation is conducted with the following limit state functions and the statistical data given in Table 7-15. The design tensile concrete strength according to [EC2] is $f_{ctd} = 0.7 \cdot f_{ctm} / 1.5 = 0.7 \cdot 0.3 \cdot f_{ck}^{2/3} / 1.5$. For a mean concrete strength f_{cm} = 20 MPa:

$$f_{std,EC2} = \theta_{EC2}\cdot 83\cdot(f_{cm}-8)^{2/3} = 435\,\text{MPa} \tag{7-97}$$

$$g_{R,\sigma,EC2} = R_m - R_d = \theta_{EC2}\cdot 83\cdot 1.5/0.7\cdot(f_{cm}-8)^{2/3} - 435 \tag{7-98}$$

Where the action effects are taken into account, the limit state function for [EC2] is defined as follows

$$g_{R+E,\sigma,EC2} = R_m - R_d = \theta_{EC2} \cdot 83 \cdot 1.5 / 0.7 \cdot \left(f_{cm} - 8\right)^{2/3} - \left(G + Q\right) \cdot \frac{435}{2} \quad (7\text{-}99)$$

The limit state functions for the design anchorage and lap lengths without $g_{R,lb,EC2}$ and with $g_{R+E,lb,EC2}$ action effects are

$$g_{R,lb,EC2} = \frac{\theta_{EC2} \cdot 435}{4 \cdot 2.25 \cdot 0.7 \cdot 0.3 \cdot \left(f_{cm} - 8\right)^{2/3} / 1.5} - \frac{435}{4 \cdot 2.25 \cdot 0.3 \cdot 12^{2/3}} \quad (7\text{-}100)$$

$$g_{R+E,lb,EC2} = \frac{\theta_{EC2} \cdot 435}{4 \cdot 2.25 \cdot 0.7 \cdot 0.3 \cdot \left(f_{cm} - 8\right)^{2/3} / 1.5} - \frac{\left(G + Q\right) \cdot 435 / 2}{4 \cdot 2.25 \cdot 0.3 \cdot 12^{2/3}} \quad (7\text{-}101)$$

Since the lap factor α_6 is larger in [EC2/NA] than in [EC2], the database analysis gave different statistical values for [EC2] and [EC2/NA], although the design model is very similar. The reliability of the design model according to [EC2/NA] was evaluated with the limit state functions (7-98) to (7-101) with the statistical characteristics of the model uncertainty θ_{NAD} instead of θ_{EC2}.

Comparison of Reliability Indices Obtained for Different Design Models

The indices of reliability β obtained by the FORM evaluation of the design models for bar stress with constant action effects described by the limit state functions (7-88), (7-93) and (7-98) are shown in Figure 7-8 (left). The results of the FORM evaluation of the design models taking the statistical variation of the action effects into account by limit state functions (7-89), (7-94) and (7-99) are shown in Figure 7-8 (right). In both cases, the target value is $\alpha_R \cdot \beta = 0.8 \cdot 3.8 = 3.04$.

The reliability increases with increasing concrete strength, since the standard deviation of the concrete strength is constant according to [EC2] and the COV consequently decreases with increasing concrete strength.

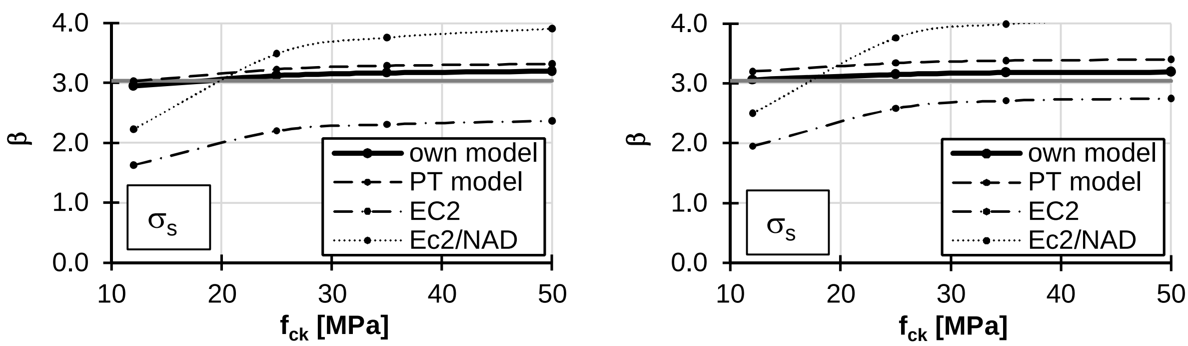

Figure 7-8 Indices of reliability $\alpha_R \cdot \beta$ of the own design model for bar stress, the model according to [PT18] with own calibration factors, according to [EC2] and [EC2/NA] obtained with FORM for constant action effects (left) and for statistically distributed action effects (right), target value $\alpha_R \cdot \beta = 3.04$

When evaluating the limit state functions for anchorage and lap lengths at constant action effects, the indices of reliability given in Figure 7-9 (left) result. Where the statistical distribution of the action effects is considered with $G_m = 1.0$, and $Q_m = 0.7$, $V_G = 0.10$ and $V_Q = 0.20$, the β values shown in Figure 7-9 (right) were obtained. For the design bar stress σ_{sd} and the design bond length l_{bd}, the target value $\alpha_R \cdot \beta = 3.04$ is accomplished with and without consideration of the action effects.

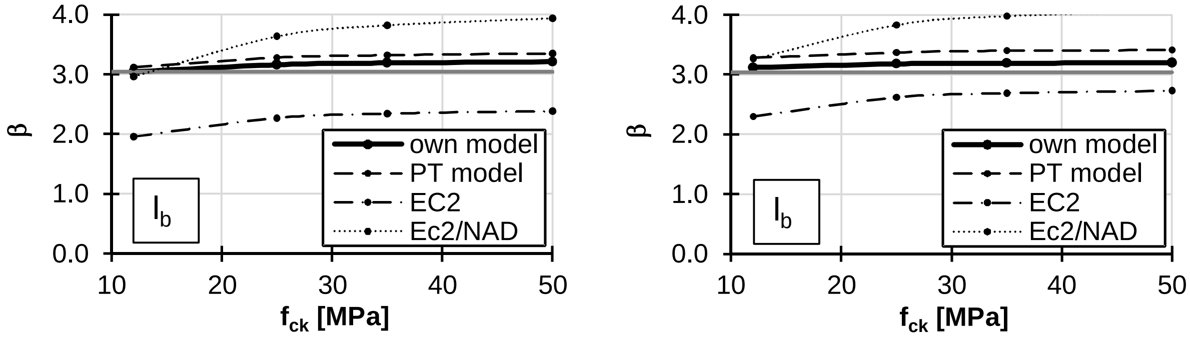

Figure 7-9 Indices of reliability $\alpha_R \cdot \beta$ of the own design model for bond length, the model according to [PT18] with own calibration factors, according to [EC2] and [EC2/NA] obtained with FORM for constant action effects (left) and for statistically distributed action effects (right), target value $\alpha_R \cdot \beta = 3.04$

Partial Safety Factor for Bond

Bond failure in anchorages and laps is rather splitting failure than pull-out failure. Therefore, the partial safety factor shall reflect the influence of tensile concrete failure. Presuming a log-normal distribution of concrete failure under tension with a COV $V_{fc} = 4.86$ MPa / 20 MPa = 0.243, the partial safety factor is $\gamma_c = 1.4$ with

$$\gamma_c = \frac{\exp(-3.04 \cdot Q - 0.5 \cdot Q^2)}{\exp(-1.645 \cdot Q - 0.5 \cdot Q^2)} = \frac{\exp(-3.04 \cdot 0.243 - 0.5 \cdot 0.243^2)}{\exp(-1.645 \cdot 0.243 - 0.5 \cdot 0.243^2)} = 1.4 \qquad (7\text{-}102)$$

Instead, [EC2] defines a conservative partial safety factor $\gamma_c = 1.5$. The partial safety factor for the bar stress developed in bond zones may be smaller than $\gamma_c = 1.5$ at the same reliability. Firstly, since the influence of concrete strength on bar stress developed in anchorages and laps is small, as it is described with an exponent 0.25 or 1/3, respectively. Secondly, the statistical scatter of the design equations for bar stress in bond zones is smaller than for concrete strength. Therefore, the total scatter of the design model including the concrete strength is smaller than the scatter of concrete strength and a partial safety factor smaller than 1.5 leads to the same reliability.

The partial safety factors for the bar stress in bond zones are $\gamma_{s,own} = 0.77 / 0.62 = 1.24$ for the own model and $\gamma_{s,PT} = 0.72 / 0.55 = 1.31$ for the model according to [PT18] with own calibration factors. According to equations (7-74) and (7-84), the partial safety factors for bond length reach the value 1.5.

7.5 Possible Reduction of Design Anchorage and Lap Length

The design lengths derived in chapter 7.4.5 without transverse pressure are longer than the design lengths according to [EC2]. To allow for a definition of shorter design lengths in future codes, different measures are considered.

The maximum bar stress in bond zones increases where transverse reinforcement is positioned. Therefore, the values for necessary design lengths can be reduced by the definition of minimum transverse reinforcement. Secondly, laps could only be permitted in zones with bar stresses well below the yield stress. In this case, the necessary bond lengths decrease significantly. Furthermore, staggered anchorages or laps slightly increase the bearing capacity of bond zones for increasing concrete cover. Design values can also be reduced by a reduction of database scatter, since smaller coefficients of variation are taken into account.

To reduce the required anchorage and lap length, it is eventually most effective to take the bar stress into account during design and to position transverse reinforcement that also provides robustness.

7.5.1 Reduction of Bond Length for Minimum Transverse Reinforcement

The database includes anchorages and laps with an without transverse reinforcement. Not all tests with transverse reinforcement fulfil the minimum reinforcement requirement with $\Sigma A_{st,min} = 1.0 \cdot A_s$, but have transverse reinforcement ratios $\Sigma A_{st} / A_s$ between 0.2 and 3.3. Taking only laps with minimum transverse reinforcement $\Sigma A_{st,min} = 1.0 \cdot A_s$ into account, leaves only 35 of 231 lap tests with transverse reinforcement in the dataset. Just three anchorage tests in the database fulfil the requirement $\Sigma A_{st,min} = 0.5 \cdot A_s$.

The exclusion of tests with transverse reinforcement smaller than the minimum transverse reinforcement gives a mean value of the model uncertainty $\theta = 1.03$ and a COV of 0.175 for the remaining 35 tests if evaluated with the own design model. The total COV of the model uncertainty for the own model is $V_\theta = 0.153$ for 473 tests instead of $V_\theta = 0.144$ for 669 tests. Since this COV exceeds the value ($V_\theta = 0.144$) considered in the derivation of design values in chapter 7.4.5, this method would even increase the design anchorage and lap length.

A reduction of the calibration factors on the basis of smaller coefficients of variation for minimum transverse reinforcement is therefore not possible. Still, the resulting lap and anchorage lengths according to the proposed design equations are smaller if transverse reinforcement is positioned (cf. Figure 7-6).

7.5.2 Reduction of Bond Length for Small Utilization of Bars

EUROCODE 2 [EC2] recommends not to locate laps in areas of high moments and bar forces. Where reinforcing bars are only utilized up to about 60 % (250 MPa / 435 MPa), the anchorage and lap lengths given in Table 7-13 for

σ_s = 250 MPa are sufficient. For the own model, the necessary bond length is reduced by 63 % to $l_{bd,own}$ = 31 · Ø for the standard parameters (f_{ck} = 25 MPa, f_{cm} = 33 MPa, Ø = 25 mm, c_{min} = 1.5 · Ø). According to the [PT18] model with own calibration factors, the necessary bond length is reduced by 57 % to $l_{bd,PT}$ = 34 · Ø for σ_s = 250 MPa and the standard parameters (cf. Figure 7-5).

7.5.3 Reduction of Bond Length for Staggering

The investigations described in [CAI14a] and [MET15] show that staggering has no positive effect on the ultimate bar stress (cf. chapter 8.2). Only the increasing anchorage or lap spacing contributes to the confinement to the bond zone, where laps are staggered. Often, the lap spacing c_s is not considered during design, because most codes account for the minimum cover c_{min} = {c_y / Ø; c_x / Ø; c_s / (2 · Ø)}. Since the values of the vertical cover c_y and the horizontal cover c_x are often decisive, the lap spacing c_s is not taken into account.

To account for the effect of bar spacing in the own model according to equation (5-26), the following change could be made for the concrete contribution

$$\alpha_c = \left(\frac{c_{min}}{Ø}\right)^{0.25} \cdot \left(\frac{c_{max}}{c_{min}}\right)^{0.1} \cdot \left(\frac{c_s}{2 \cdot Ø}\right)^{0.1} \tag{7-103}$$

With
c_{min} = min {c_y / Ø; c_x / Ø}

Applying this cover contribution in equation (5-26) gives the ratio of bar stress obtained in the tests comprised in the database σ_{test} to calculated results σ_{own} shown in Figure 7-10 (left).

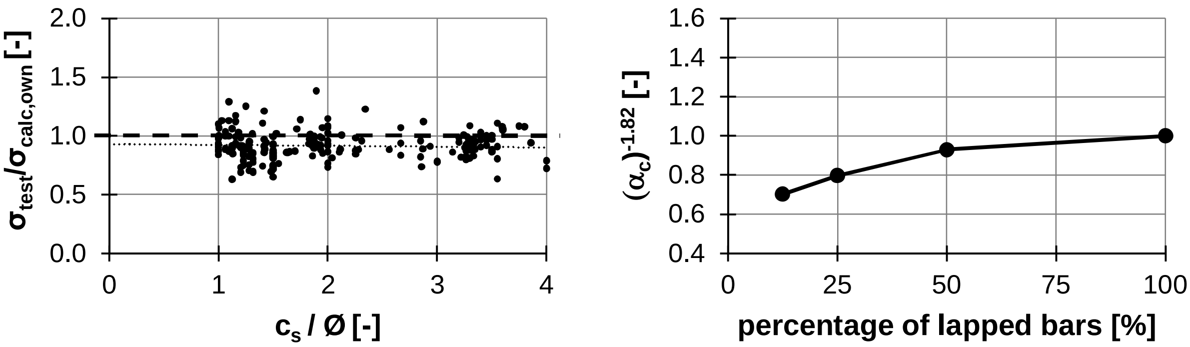

Figure 7-10 Ratio of bar stress obtained in tests σ_{test} to calculated bar stress according to equations (5-26) and (7-103) over bar-spacing to bar-diameter ratio c_s / Ø (left) and increase in necessary lap length at increasing percentage of lapped bars (right)

The minimum lap spacing according to [EC2] is c_s = 2 · Ø, while the minimum bar spacing is 1 · Ø. Accordingly, the minimum lap spacing is 2 · Ø where 100 % bars are lapped. In case, 50 % bars are lapped, the minimum allowable lap spacing is 3 · Ø and for 25 % bars lapped, the lap spacing increases to at least 7 · Ø (cf. Figure 7-11).

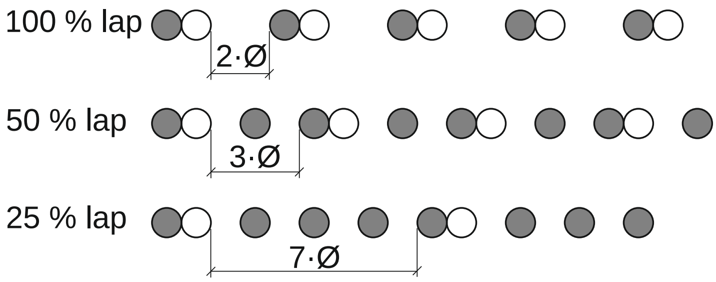

Figure 7-11 Minimum permissible lap spacing for different percentages of lapped bars

Applying these values to equations (5-26) and (7-103) gives a bar stress increase by 4 % for 50 % laps and by 13 % for 25 % laps. For laps without confinement by transverse reinforcement and transverse pressure, f_{ck} = 25 MPa, Ø = 25 mm and c_{min} / Ø = 1.0, the necessary lap length decreases at increasing lap spacing by $\alpha_c^{-1.82}$ with

$$\frac{l_{bd,own}}{Ø} = 103 \cdot \left(\frac{\sigma_s}{435}\right)^{1.82} \cdot \left[\alpha_c\right]^{-1.82} = 103 \cdot \left(\frac{\sigma_s}{435}\right)^{1.82} \cdot \left[\left(\frac{c_s}{2 \cdot Ø}\right)^{0.1}\right]^{-1.82} \qquad (7\text{-}104)$$

The design anchorage length can therefore be reduced by the factor 0.93 for the 50 % lap ($c_s = 3 \cdot Ø$) and 0.8 for the 25 % lap ($c_s = 7 \cdot Ø$) (cf. Figure 7-10 (right)).

Contrarily, tests do not show a positive effect for percentages of lapped bars below 100 %, but the post-peak behaviour of the test specimens is enhanced as continuous bars provide robustness to laps [MET15], [HEG18].

7.5.4 Classification of Bar Stress in Database

For the own model based on [FIB14], the design lap and anchorage length was derived on the basis of a COV of the model uncertainty V_θ = 0.144. If the COV were reduced, the resulting design lengths according to [EC0] were also smaller. To investigate a possible bond length reduction by smaller COVs, classes for the measured bar stress were defined. Table 7-17 gives the COV of the model uncertainty obtained from the database described in chapter 5 for different bar-stress classes.

Table 7-17 Coefficients of variation (COV) for different bar stress classes according to own model

	COV V_θ	Mean value θ	Test number n
200 MPa < σ_s < 300 MPa	0.155	1.05	73
300 MPa < σ_s < 400 MPa	0.125	1.03	194
400 MPa < σ_s < 500 MPa	0.128	1.03	228
σ_s < 1.2 f_{ym}	0.144	1.00	669

For the bar stress 400 MPa < σ_s < 500 MPa, the total COV for the own model follows from V_{fc} = 0.243 and V_θ = 0.128 with

$$\ln\left(V_r^2+1\right)=0.25^2\cdot\ln\left(V_{fc}^2+1\right)+\ln\left(V_\theta^2+1\right)\rightarrow V_r=0.142 \tag{7-105}$$

The standard deviation of the resistance function is

$$Q=\sqrt{\ln\left(V_r^2+1\right)}=\sqrt{\ln\left(0.142^2+1\right)}=0.141 \tag{7-106}$$

The reduction factors for characteristic and design values are

$$\exp(-1.645\cdot Q-0.5\cdot Q^2)=0.785 \tag{7-107}$$

and

$$\exp(-3.04\cdot Q-0.5\cdot Q^2)=\exp(-0.48)=0.645 \tag{7-108}$$

The design bar stress in laps and anchorages with 400 MPa < σ_s < 500 MPa is

$$f_{std,own}=1.02\cdot 54\cdot 0.645\cdot\left(\frac{f_{ck}}{25}\right)^{0.25}\cdot\left(\frac{25}{Ø}\right)^{0.2}\cdot\left(\frac{l_b}{Ø}\right)^{0.55}\cdot\left[\alpha_c+\alpha_{tr}+\alpha_{tp}\right] \tag{7-109}$$

With $f_{std,own}=\sigma_s$, the reduced design anchorage and lap length is

$$\frac{l_{bd,own}}{Ø}=\left(\frac{435}{1.02\cdot 54\cdot 0.645}\right)^{1.82}\cdot\left(\frac{\sigma_s}{435}\right)^{1.82}\cdot\left(\frac{25}{f_{ck}}\right)^{0.455}\cdot\left(\frac{Ø}{25}\right)^{0.36}\cdot\left[\alpha_c+\alpha_{tr}+\alpha_{tp}\right]^{-1.82}$$

$$\frac{l_{bd,own}}{Ø}=95.5\cdot\left(\frac{\sigma_s}{435}\right)^{1.82}\cdot\left(\frac{25}{f_{ck}}\right)^{0.455}\cdot\left(\frac{Ø}{25}\right)^{0.36}\cdot\left[\alpha_c+\alpha_{tr}+\alpha_{tp}\right]^{-1.82} \tag{7-110}$$

In this case, the partial safety factor γ_M of the anchorage and lap length is

$$\gamma_{M,own}=\frac{l_{bd}}{l_{bk}}=\left(\frac{1/0.645}{1/0.785}\right)^{1.82}=\left(\frac{0.785}{0.645}\right)^{1.82}=1.43 \tag{7-111}$$

Table 7-13 shows that the calibration of the own design model after classification for 400 MPa < σ_s < 500 MPa with a COV of 0.128 instead of 0.144 would enable to a reduction in design anchorage and lap lengths by 7 %. The same method can be applied for stress values from 300 MPa to 500 MPa resulting in a similar reduction.

Table 7-18 Comparison of design lap lengths for standard parameters (f_{ck} = 25 MPa, f_{cm} = 33 MPa, Ø = 25 mm, c_{min} = 1.5 · Ø) for the own model with V_θ = 0.144 and V_θ (400 MPa < σ_s < 500 MPa) = 0.128

	$l_{bd,own}$	$l_{bd,own}$ (400<σ_s<500)	$l_{bd,EC}$	$l_{bd,NAD}$	$l_{bd,MC}$
σ_s = 435 MPa, ΣA_{st} = 0	85 · Ø	79 · Ø	56 · Ø	81 · Ø	76 · Ø
σ_s = 435 MPa, ΣA_{st} = A_s	69 · Ø	64 · Ø	51 · Ø	73 · Ø	73 · Ø
σ_s = 250 MPa, ΣA_{st} = 0	31 · Ø	29 · Ø	21 · Ø	23 · Ø	44 · Ø

7.6 Difference Between Anchorages and Laps

The governing difference between anchorages and laps lies in the stress state of the bars. While the maximum bar stress at beam ends of simply supported beams is usually much smaller than the yield strength, laps must transfer bar forces up to the yield strength. Accordingly, the necessary lap lengths must be longer than anchorages. The increase in lap or anchorage strength and developable bar force respectively does not increase linearly with the bond length. Therefore, the lap length must be increased by a certain factor in case the bond strength is presumed constant over bond length. This is done in [EC2] by the lap factor α_6. When the non-linear effect of bond length is taken into account within the design equation as in [FIB14], [MC2010], [ELI79], [BUR00], [LET06a] and [CAN05]) a lap factor for the increase in anchorage length is not necessary. In contrast, a factor is necessary in [EC2], [EC2/NA] and [ACI14].

Where a linear relationship is presumed, the ratio of the required bond length $l_{b,lin}$ at 500 MPa to the reqired bond length $l_{b,lin}$ at 250 MPa is

$$l_{b,lin}(500) / l_{b,lin}(250) = \frac{Ø \cdot 500}{4 \cdot \tau} / \frac{Ø \cdot 250}{4 \cdot \tau} = 2.0 \tag{7-112}$$

Where the non-linearity of the bond length effect is accounted for, e.g. with the exponent 0.5, the ratio of the required bond length $l_{b,non\text{-}lin}$ at 500 MPa to the reqired bond length $l_{b,non\text{-}lin}$ at 250 MPa is

$$l_{b,non-lin}(500) / l_{b,non-lin}(250) = \frac{Ø \cdot 500^2}{(4 \cdot \tau)^2} / \frac{Ø \cdot 250^2}{(4 \cdot \tau)^2} = 4.0 \tag{7-113}$$

Where design models neglect the non-linear relationship, a lap factor 4.0 / 2.0 = 2.0 is required. [EC2] gives lap factors α_6 up to 1.5 and [EC2/NA] up to 2.0. The necessary lap factor – that is only needed in design models if the bar stress is considered linearly – actually depends on the bar stresses. Subsequently, anchorages that transfer the same reinforcing bar stress as laps require the same length as laps.

8 Anchorage and Lap Detailing

8.1 General

The definition of design models strongly correlates with the detailing provisions defined. Minimum cover values, bars spacing, the permissible percentage of bars lapped and minimum transverse reinforcement requirements influence the resulting coefficients of variation obtained in the database analysis and consequently the design anchorage length.

8.2 Percentage of Bars Anchored or Lapped at a Section

Where laps are staggered or adjacent to continuous bars, the percentage of lapped bars is lower than 100 %. Tests with staggered laps have rarely been conducted [SCH88], [CAI14a] since their realisation requires substantial lengths, especially when subjected to bending. The required length becomes smaller in case reinforcing bars with maximum stresses are tested well below the yield strength [CAI14a]. The original ACI [ACI01] and fib databases [FIB05] hardly include tests with less than 100 % lapped bars. The tests documented in [FER69], [STO77], [THO79] had 50 % and 67 % laps, but only three tests fulfilled the filter criteria defined in chapter 5.1. Due to the limited experimental expressiveness, all tests with continuous bars were excluded from the database for this thesis.

The presence of continuous bars increases the spacing between anchored or lapped bars and accordingly, the strength of the bond zone (cf. chapter 7.5.3). Where laps are staggered or combined with continuous bars, the stress in the surrounding concrete is not superimposed by the stress state of adjacent anchored or lapped bars. A reduced percentage of bars lapped at a section additionally contributes to the robustness of the structural member [CAI14a], [MET15].

Staggering adjacent lap centres by $1.0 \cdot l_b$ is unfavourable, since the highly stressed ends of the laps are still positioned at the same cross-section [STO77]. The large crack widths at lap ends are not reduced for this lap positioning. If laps are staggered by a distance of $0.5 \cdot l_b$, the highly utilised lap ends are positioned adjacent to the lower utilised lap centres. According to REHM [REH79], this positioning is preferable. In [DEU88], staggering of lap centres by $1.3 \cdot l_b$ was recommended. Where lap centres were staggered by $0.5 \cdot l_b$, less transverse reinforcement was required. The described longitudinal distances of the lap centres are shown in Figure 8-1.

[EC2] recommends that lapped bars should normally be staggered and that laps should not be located in areas of high moments or forces. The longitudinal distance between two adjacent laps should not be less than 0.3 times the lap length l_b.

[EC2/NA] permits a maximum percentage of lapped bars of 50 % for large diameter bars. In this case, laps are defined as staggered, for a longitudinal distance between lap centres of at least $1.5 \cdot l_b$.

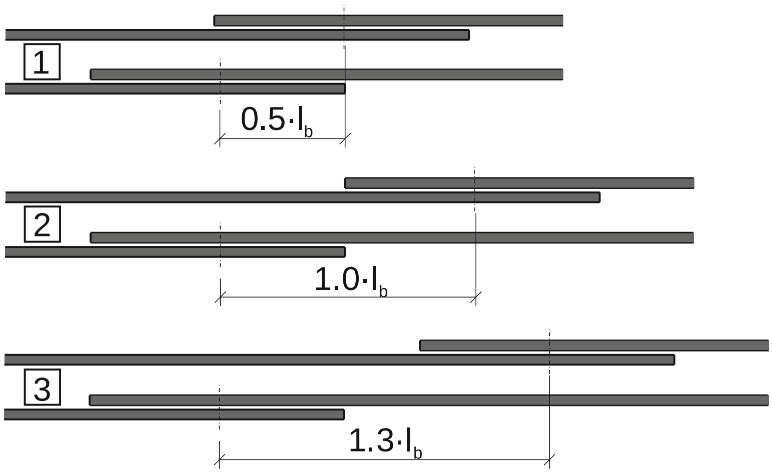

Figure 8-1 Laps centres staggered by $0.5 \cdot l_b$ (1), $1.0 \cdot l_b$ (2) and $1.3 \cdot l_b$ (3)

CAIRNS [CAI14a] describes the strain state in staggered lapped joints. If the positive effect of increased lap spacing is taken into account, an increase in lap strength could not be found. For equilibrium, the steel strain at lap centres increases where less than 100 % of the reinforcing bars are lapped at a section. The compatibility of deformations in lapped and continuous bars must be fulfilled within the lap length. But compatibility is only given if lapped-bar strains at the beginning of the lap are greater than those in continuous bars. CAIRNS [CAI14a] recommends longitudinal distances of staggered lap centres by $0.5 \cdot l_b$, where 50 % of the bars are lapped.

Summarising the effects described, the following detailing rules for staggered laps are recommended:

- Where the longitudinal distance of lap centres is greater or equal to $1.3 \cdot l_b$, laps may be considered staggered and the lap length may be reduced for the increased bar spacing
- Laps staggered by $0.5 \cdot l_b$ also increase the lap strength. Since this effect was not extensively analysed yet, the application of this distance is recommended at highly utilised laps, although the effect may not be considered in design

8.3 Minimum Anchorage and Lap Length

The minimum lap length accepted in the database was $15 \cdot Ø$ (cf. chapter 5.1). This value conforms with the minimum lap length defined in [EC2]. For the anchorage length, no limit was defined for the database evaluation. For the parameters $Ø = 25$ mm, $f_{ck} = 25$ MPa and $[\alpha_c + \alpha_{tr} + \alpha_{tp}] = 1.0$, the design lap length $l_{bd} = 15 \cdot Ø$ would enable a longitudinal bar stress of 150 MPa according to

$$\frac{l_{bd}}{Ø} = 103 \cdot \left(\frac{\sigma_s}{435}\right)^{1.82} \cdot 1.0 \cdot 1.0 \cdot 1.0 = 15 \rightarrow \sigma_s = 150\,\mathrm{MPa} \tag{8-1}$$

The minimum anchorage and lap lengths defined in [MC2010] approximately equal the minimum values defined in [EC2].

The minimum anchorage length is

$$l_{b,min,EC} = \max\left\{0.3 \cdot \frac{Ø \cdot f_{yd}}{4 \cdot f_{bd}}; 10 \cdot Ø; 100\ \text{mm}\right\} \tag{8-2}$$

And the minimum lap length follows from

$$l_{0,min,EC} = \max\left\{0.3 \cdot \alpha_3 \cdot \frac{Ø \cdot f_{yd}}{4 \cdot f_{bd}}; 15 \cdot Ø; 200\ \text{mm}\right\} \tag{8-3}$$

The values of minimum length depending on the bar diameter (10 · Ø and 15 · Ø, respectively) were defined to account for execution inaccuracies during reinforcing works. For safety reasons, in case the anchorage length is reduced by the term $A_{s,req} / A_{s,prov}$ according to [EC2], the application of at least 30 % of the design yield strength represents an additional lower limit.

When applying the design model derived in chapter 7, the following minimum values for anchorages and laps with minimum transverse reinforcement are recommended

$$l_{b,min} = \max\left\{Ø \cdot 70 \cdot \left(\frac{0.3 \cdot f_{yd}}{435}\right)^{1.82}; 20 \cdot Ø \cdot \left(\frac{\sigma_{sd}}{435}\right)^{1.82}; 100\ \text{mm}\right\} \tag{8-4}$$

The coefficient 70 accounts for confinement by concrete cover and minimum transverse reinforcement. The second value was defined in accordance with the own tests, where a bar stress of approximately 200 MPa was developed with $l_b = 5 \cdot Ø$ ($= 20 \cdot Ø \cdot (200 / 435)^{1.82}$). For laps at σ_{sd} = 435 MPa, this minimum bond length conforms with an increase in comparison to [EC2] by 20 · Ø / 15 · Ø = 1.33. The database evaluation shows that the design model for lap length according to [EC2] overestimates the developable bar stress, while the design model according to [EC2/NA] with an increased lap factor α_6 meets the test results better. The proposed increase in minimum bond length corresponds to the ratio of the lap factors with $\alpha_{6NAD} / \alpha_{6EC} = 2.0 / 1.5 = 1.33$.

8.4 Laps of Bars with Different Bar Diameters

The tests described in chapter 3.4 showed an increase in ultimate lap strength, where Ø 40 mm bars were lapped with Ø 28 mm bars. One lap test was conducted conforming with the requirements according to [EC2] for the Ø 40 mm bar ($l_b = 33 \cdot Ø_{40}$). The second lap test had a reduced lap length designed in accordance with [EC2] for the Ø 28 mm bar ($l_b = 23 \cdot Ø_{40} = 33 \cdot Ø_{28}$), but with additional surface reinforcement. In both cases, the yield strength of the Ø 40 mm bar was reached.

Since this effect was neither evaluated on the basis of larger test numbers nor of the database, it is advisable to neglect this positive effect for the time being. For laps of bars with different bar diameters, the anchorage length of both bars shall be calculated. In case bars with different bar diameters but equal cross-sectional areas are lapped, the bar with the larger bar diameter is decisive. If the bar number is equal, the smaller bar has a smaller cross-sectional area, develops higher bar stress than the bar with the larger diameter and is thus governing.

8.5 Anchorages and Laps in Several Layers

[EC2] allows for laps with up to 100 % lapped bars in a single layer, but only up to 50 % in case several layers are positioned. This requirement was justified by increased loads and the lack of experimental data [REH79]. [FIB14] finds no argument in favour of modifying bond length where there is more than a single layer of reinforcement.

In anchorage tests with a double layer of bonded bars, JIRSA ET AL. [JIR95] observed that the bond resistance of the well confined inner layer increased after failure, while the resistance of the outer layer dropped sharply.

For the confinement of anchorages and laps in several layers, additional transverse reinforcement is required. [EC2] defines increasing transverse reinforcement parallel to the tension face for anchorages of large diameter bars in several layers. Additionally, [EC2/NA] requires additional edge reinforcement of at least $0.18 \cdot A_{sl}$ [cm²/m], where A_{sl} is the cross-sectional area of the lapped reinforcement. This value originates from the requirements for Ø 50 mm bars that were defined in [JUN77].

The own lap tests showed that the confinement by transverse surface reinforcement with U-shaped bars, which were not adequately anchored in the compression zone, did not confine the bond zone sufficiently. It is therefore recommended to mind proper anchorage of transverse reinforcement for the upper layers as well. U-shaped horizontal edge reinforcement is recommended that encloses the longitudinal bars in the upper layers. This reinforcement crosses the potential splitting plane for side and face splitting of the bars in the upper layer.

8.6 Casting Position

The position of reinforcement during casting influences the quality of bond between reinforcing bars and concrete. In case bars are positioned at the top of the cross-sectional height, their bond strength is often smaller than for bottom cast bars. Furthermore, the bond conditions of bars positioned horizontally during casting differ from bars positioned vertically during casting. MARTIN AND NOAKOWSKI [MAR81] found that the bond strength of vertical bars was up to twice as high as the bond strength of horizontal bars. This bond strength reduction is due to slump and pore formation below reinforcing bars. The loss in circumference contributing to bond caused by poor bond conditions is limited to 50 % [REH61]. While pores can form below all horizontal reinforcing bars, bars at the top of a member's height are most likely to suffer from concrete slump. Therefore, bars at top of the cross-sectional height develop significantly smaller bond strength than bars positioned at the bottom of the structural member during casting. Top cast laps at low slump showed a bond strength reduction by 20 % in tests, while top cast laps at high concrete slump showed a bond strength reduction by 60 % [HAM98].

DIN 1045 [DEU88] defined a bond strength reduction by 50% for anchorages and by 30% for laps. Since splitting failures are usually decisive in both cases, the reduction was harmonised in the following codes. While [EC2], [MC90] and [MC2010] define a bond strength reduction by 30 % for poor bond conditions, the proposal for the next generation of EUROCODE 2 [PT18] gives a smaller strength decrease for anchorages and laps by 20 %.

The range of reduction factors for poor bond conditions given in literature varies widely, since the effect strongly depends on the concrete characteristics. While the reduction is up to 50 % in pull-out failures, the reduction is only 30 % for splitting failures that rather depend on the tensile strength of the surrounding concrete [ELI79]. ACI COMMITTEE 408 [ACI03] gives a comprehensive overview of publications on bond strength reduction caused by unfavourable casting positions.

The original fib lap database [FIB05] comprises several lap tests in the top cast position (e.g. [AZI93], [FER69], [FER62], [FER71], [HAM98], [HES93], [STO77], [TRE89], [ZEK81]). However, the single investigations often focused on other influencing parameters or showed contradictory results for the effect of casting position.

8.7 Transverse Reinforcement

The positioning of minimum transverse reinforcement in laps and anchorages is strongly recommended. Transverse reinforcement effectively controls the longitudinal crack width if the tensile strength of the confining concrete cover is exceeded in bond zones. This effect implies that transverse reinforcement is not necessary where small bars with large concrete cover are anchored. The recommended minimum reinforcement is $\Sigma A_{st} = 1.0 \cdot A_s$. If the longitudinal bar stress is well below the yield stress, the minimum reinforcement may be reduced to $\Sigma A_{st} = 0.5 \cdot A_s$. Lower longitudinal bar stresses are reached e.g. at supports of simply supported beams. The additional transverse reinforcement for anchorages of large diameter bars defined in [EC2] is covered by the afore mentioned values. The bond securing transverse reinforcement required along the entire beam length for bars with large diameters defined in [EC2/NA] is only covered in anchorages and laps. Anyhow, tests conducted with Ø 40 mm bars proved that longitudinal cracks only occurred in bond zones.

8.8 Surface Reinforcement

According to [EC2], the crack control of reinforced concrete members with large diameter bars can be accomplished either by direct calculation of crack width or by positioning of surface reinforcement. Tests conducted with direct tension members reinforced with Ø 40 mm bars ([HEG15], [HEG18]) showed that crack calculation can be omitted where surface reinforcement is positioned, which is equal to 2 % of the tensile area outside the stirrups $A_{s,surf} = 0.02 \cdot A_{c,ext}$ and where the crack width limit w_{lim} is 0.2 mm. For a crack width limit w_{lim} of 0.3 mm, the required cross-sectional area of the surface reinforcement may be reduced to $A_{s,surf} = 0.01 \cdot A_{c,ext}$ [HEG15], [HEG18].

Alternatively, the necessary cross-sectional area of the surface reinforcement may be calculated following the originally proposed design equation for surface reinforcement that was derived by JUNGWIRTH [JUN77] for bars with a diameter of Ø 50 mm.

The measured crack widths in the lap tests described in chapter 3.4 conform with the calculated values according to [EC2]. When taking the equivalent bar diameter $Ø_{eq}$, the increased reinforcement ratio ρ_{eff} and the decreasing bar stress σ_s into account, the crack widths measured in the tests with surface reinforcement also agree with the calculated values. In most test specimens, the maximum crack widths at the lap ends were smaller than the 95%-fractile values of the beam increased by 25 %.

The lap tests also showed that the 95%-fractile values of the crack widths along the beam length were larger than 0.4 mm. The crack widths decreased to values below 0.2 mm, in case surface reinforcement with $A_{s,surf} = 0.02 \cdot A_{c,ext}$ was positioned.

The test results in chapter 3.4 show that the attainment of the yield stress in lap tests with Ø 40 mm bars without surface reinforcement was only possible where the lap length was long (44 · Ø) and transverse reinforcement was present. Still, robust failures were only enabled by surface reinforcement in the conducted lap tests.

8.9 Robustness of Anchorages and Laps

Robustness in structures is given where certain deformability is enabled. The robustness of structural concrete elements can be defined by the ratio of deformation – such as deflection or rotation – at the ultimate strength Δ_{max} to the yield point of the structure Δ_y. The displacement ductility ratio defined by AZIZINAMINI ET AL. [AZI99] for lap tests in high strength concrete is given in Figure 8-2 (left).

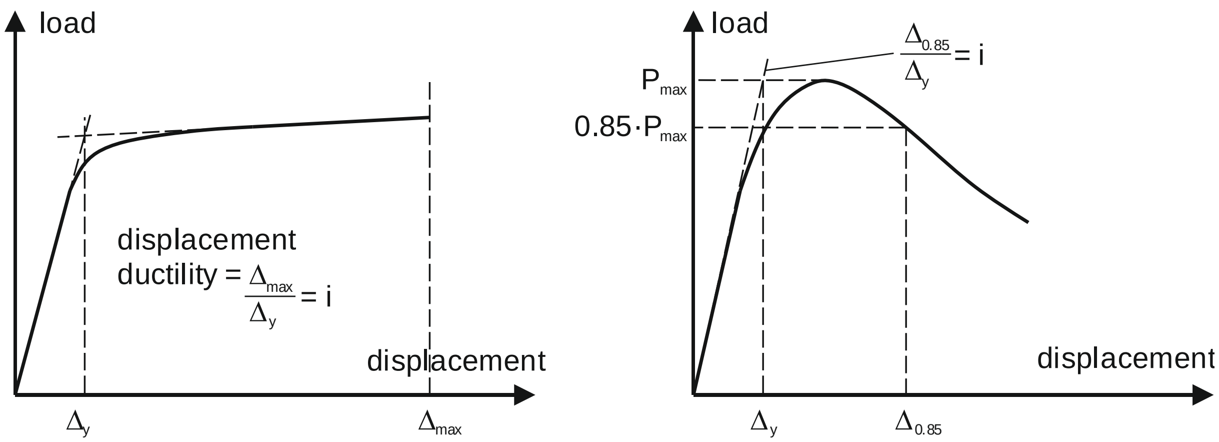

Figure 8-2 Displacement ductility ratio according to AZIZINAMINI [AZI99] (left) and COHN AND BARTLETT [COH82] (right)

Alternatively, robustness can be described by the ratio of displacement corresponding to a percentage (e.g. 85 %) of the maximum load to the displacement at the intersection of maximum load and tangent of the initial load-displacement curve corresponding to the first yield displacement of a structure [COH82] (cf. Figure 8-2, right).

If possible, anchorages and laps should not be placed in cross-sectional areas with maximum reinforcing bar stress. Robustness is given where continuous reinforcing bars in zones with high utilisation yield before anchorages and laps outside these zones fail. Transverse reinforcement, continuous longitudinal bars and long bond lengths contribute to the robustness of anchorages and laps.

In [FIB14], minimum amounts of confining reinforcement are recommended to reduce the brittleness of splitting failure. Smaller stirrup sizes and spacing result in increased robustness [RAK14]. However, even if transverse reinforcement is provided and splitting cracks are crossed by links, experimental evidence shows that links will not be capable to provide a fully ductile failure [FIB14].

In case of staggered laps, the ductility index increases for greater stagger-distance to lap-length ratios (cf. Figure 8-1). CAIRNS [CAI14a] finds that brittleness is reduced if laps are staggered, while the additional positive effect of positioned transverse reinforcement was not clearly distinguishable. The own tests also showed that percentages of lapped bars below 100 % increased the robustness of the test specimens at failure.

Surface reinforcement in the directions parallel and orthogonal to the longitudinal reinforcement effectively contributes to the robustness of laps and anchorages. The positioning of surface reinforcement is advisable for large diameter bars if all bars are to be lapped at one section, the concrete cover and bar spacing are small, the reinforcement shall reach its yield strength and substantial ductility is required.

Another possibility for providing robustness to anchorages and laps are long bond lengths to reach the yield strength of the reinforcing bars. Therefore, the PT1 WORKING DRAFT [PT18] recommends the design of tension laps for $1.2 \cdot \sigma_{sd}$ at plastic hinges and in sections where maximum effcts are expected.

9 Summary and Conclusions

9.1 Summary

Anchorages and laps of reinforcing bars are required in most structural concrete members. The characteristics of bond between concrete and reinforcement also determine the crack formation in structural concrete members. The bond between reinforcement and surrounding concrete has therefore been subject to research over the last decades. Numerous investigations on the bond behaviour between different kinds of reinforcement, concrete characteristics and anchorage types have been published. Still, bond mechanisms in reinforced concrete are not fully understood and different models for the structural design of bond zones exist. For large diameter reinforcing bars above Ø 32 mm, additional detailing rules – mostly regarding the bond behaviour – are defined in [EC2]. Large diameter bars are especially suitable for heavily reinforced concrete members with high reinforcement ratios. In this case usually only little cover and bar spacing contribute to the confinement of the bond zone.

European [EC2] and American [ACI14] codes as well as MODEL CODE 2010 [MC2010] comprise different design models for bond zones. The design model for anchorages and laps in the proposal for the next generation of EUROCODE 2 [PT18] differs from the model currently applied in [EC2]. For this new model, suitable calibration factors for the contributions of concrete cover, transverse reinforcement and transverse pressure had not been validated.

To investigate the bond behaviour of large diameter bars in structural elements, beam-end tests and simply supported beams were tested. Beam-end tests were conducted to obtain bond strength slip relationships for the investigated Ø 40 mm bars. The significance of the rather simple beam-end test specimens was analysed by variation of several test parameters. Subsequently, their influence was compared to the effects observed in the simply supported beams. The applicability of this test specimen for the investigation of the effects of confinement by concrete cover, transverse reinforcement and transverse pressure was confirmed.

The question whether design rules are equally applicable to anchorages and laps had not been resolved, yet. Hence, 17 four-point bending tests with laps in the constant moment zone were conducted to investigate the ultimate strength and crack development in laps with large diameter bars. While the focus of the research programme was set on Ø 40 mm bars, two lap tests with Ø 28 mm bars were executed to compare the bond behaviour of bars below and above the defined value of large diameter bars according to [EC2] (> Ø 32 mm).

To investigate the bond behaviour of anchorages with Ø 40 mm bars, six simply supported beams were tested at each side. The anchorage lengths (5 · Ø to 11 · Ø) were much shorter than the lap lengths applied in the four-point bending tests (33 · Ø to 44 · Ø). Another major difference to the lap tests was the presence of transverse pressure provided by the support. In contrast to the beam-end test specimens, which had been developed for the testing of single reinforcing bars, anchorage tests in simply supported beams allow for the positioning of adjacent longitudinal reinforcing bars with very small bar spacing.

The ultimate stress in the lapped reinforcing bars reached the design yield strength (435 MPa), where the laps were designed according to [EC2]. In case the lap length was increased by 30 %, the stress obtained was above the actual yield strength (about 570 MPa). Surface reinforcement positioned in the lap tests effectively reduced longitudinal and transverse cracks and increased the ultimate strength.

Since the stress to be developed in anchorages was much lower than in laps, the tested anchorage lengths were much smaller. The conducted anchorage tests revealed that the anchorage length at the ends of simply supported beams actually extends over the length of the support plus the distance to the bending crack next to the support. This distance adds a certain safety to anchorages at beam ends. But beam-end tests are generally suitable to characterise the bond behaviour of single bars. In case two or more bars are anchored, the load application has some issues. Thus, actual anchorage tests are favourable for the investigation of groups of anchored bars at beam ends.

Since the known mechanisms of bond behaviour are equally applicable to large diameter bars, additional rules for these bars are not necessary where a thorough crack control is provided. In case the crack width cannot be verified by direct calculation, surface reinforcement is recommended.

A bond test database with more than 1200 lap and anchorage tests was compiled to analyse the influence of single parameters and the applicability of design models given in literature. Originally, partly coinciding databases were compiled by ACI COMMITTEE 308 [ACI01], FIB TASK GROUP 2.5 [FIB05] and AMIN [AMI09]. Many tests were excluded from the combined database in this thesis, since the test parameters were not state of the art, poor bond conditions were tested or only single bars were anchored or lapped. After filtering, the database comprised 669 anchorage and lap tests including 123 tests with bar diameters above Ø 32 mm.

In this thesis, single parameter influences were analysed for the entire database and – since comparability is only given where the remaining parameters are equal – for selected test series. The analysis revealed very good conformity for the effects of concrete strength, anchorage length, bar diameter and concrete cover with the design model proposed in [FIB14]. However, this design model was modified for the contributions by transverse reinforcement and transverse pressure. The proposed own design model on the basis of [FIB14] is the sum of the three contributions by concrete cover, transverse reinforcement and transverse pressure.

In the PT1 WORKING DRAFT for the next generation of EUROCODE 2 [PT18] a design model for anchorage and lap length based on the design model according to [FIB14] was proposed. In this thesis, calibration factors for the proposal were derived on the basis of the database.

Since the design model according to [FIB14] shall be adopted in the next generation of EUROCODE 2, design values were derived for the own modified model and for the model defined in [PT18] with own calibration factors. The design values were derived according to annex D in [EC0]. To verify the desired index of reliability $\beta = 3.8$, a reliability analysis applying the first-order reliability method was conducted.

If minimum transverse reinforcement is positioned, the resulting lap lengths are similar to the lap lengths according to [EC2/NA] at $\sigma_s = 435$ MPa. The design bond lengths at $\sigma_s = 250$ MPa exceed the values according to [EC2] and [EC2/NA] if calculated with $\alpha_6 = 1.0$. The design lengths according to the own model and the [PT18] model with own calibration factors are smaller when the values according to [EC2] and [EC2/NA] are calculated with $\alpha_6 = 1.5$ and $\alpha_6 = 2.0$, respectively.

The key findings of this investigation are:

- Beam-end tests are suitable to characterise the parameter effects in lap and anchorage tests
- The effect of bar diameter on crack width strongly depends on the increasing concrete cover with increasing bar diameter
- Surface reinforcement effectively reduces the crack width in members with large diameter bars and provides robustness
- The design model according to [FIB14] captures the parameter effects very well, only for transverse reinforcement and pressure, modifications are proposed
- The contribution of transverse pressure was defined considering the non-linear effects of transverse pressure and bond length
- The contribution of transverse reinforcement was modified to a factor that neither includes the leg number of the transverse reinforcement nor the number of lapped or anchored bars
- Calibration factors were derived for the design model proposed in [PT18] model, the calibration factor for design bond length shall be 73 instead of 40
- The design models are equally applicable to large diameter bars
- Design values for anchorages and laps were derived applying the method in [EC0]. The partial safety factors for bar stress developed in bond zones are smaller than 1.5, while the desired reliability $\beta = 3.8$ is accomplished
- Design anchorage and lap lengths can be calculated with the own design model based on [FIB14] or – with simplified exponents – with the design model according to [PT18] with own calibration factors

9.2 Design Anchorage and Lap Length

Own Design Model Based on [FIB14]

The own model based on [FIB14] given in equation (5-26) sums up the contribution by concrete cover (equation (5-27)) as well as the own proposals for the contribution of transverse reinforcement (equation (5-28)) and transverse pressure (equation (5-29)).

$$\frac{l_{bd,own}}{Ø} = 103 \cdot \left(\frac{\sigma_{sd}}{435}\right)^{1.82} \cdot \left(\frac{25}{f_{ck}}\right)^{0.455} \cdot \left(\frac{Ø}{25}\right)^{0.36} \cdot \left[\alpha_c + \alpha_{tr} + \alpha_{tp}\right]^{-1.82} \quad (5\text{-}26)$$

$$\alpha_c = \left(\frac{c_{min}}{Ø}\right)^{0.25} \cdot \left(\frac{c_{max}}{c_{min}}\right)^{0.1} \quad (5\text{-}27)$$

$$\alpha_{tr} = k_m \cdot \rho_{conf} = k_m \cdot \frac{A_{st}}{Ø \cdot s_{st}} \leq k_m \cdot 0.05 \quad (5\text{-}28)$$

$$\alpha_{tp} = 0.32 \cdot p_{tr}^{0.4} \quad (5\text{-}29)$$

Where $f_{ck} = f_{cm} - 8$ MPa, $A_{st} \cdot n_{st} \geq A_s$ (for $\sigma_s \approx 0.5 \cdot f_{yd}$: $A_{st} \cdot n_{st} \geq 0.5 \cdot A_s$) and $k_m = 7$ or 4 according to Figure 5-54.

Robustness in anchorages and laps is provided by transverse reinforcement, little bar stress utilisation and by continuous longitudinal reinforcement. The minimum bond length is

$$l_{b,min} = \max\left\{Ø \cdot 70 \cdot \left(\frac{0.3 \cdot f_{yd}}{435}\right)^{1.82}; 20 \cdot Ø \cdot \left(\frac{\sigma_s}{435}\right)^{1.82}; 100\text{ mm}\right\} \quad (9\text{-}1)$$

Design Model According to [PT18] with Own Calibration Factors

The model given in [PT18] was rearranged for the calculation of bar stress developed by bond and own calibration factors were derived from the database for the mean bar stress. The design values for bond length were derived applying the method according to [EC0]. The derived calibration factor for the design bond length is 73 in contrast to the value 40 in the current proposal [PT18].

$$\frac{l_{bd,PT}}{Ø} = 73 \cdot \left(\frac{\sigma_s}{435}\right)^{3/2} \cdot \left(\frac{25}{f_{ck}}\right)^{1/2} \cdot \left(\frac{Ø}{20}\right)^{1/3} \cdot \left(\frac{1.5 \cdot Ø}{c_{d,conf}}\right)^{1/2} \quad (5\text{-}30)$$

$$c_{d,conf} = c_d + \left(60 \cdot k_{conf} \cdot \frac{n_l \cdot A_{st}}{n_b \cdot Ø \cdot s_{st}} + 8 \cdot \sigma_{ctd} / \sqrt{f_{ck}}\right) \cdot Ø \leq 3.75 \cdot Ø \quad (5\text{-}31)$$

With k_{conf} according to 2.9.7

Summary of Design Bond Lengths

For the standard confinement parameters ($c = 1.5 \cdot Ø$, $\Sigma A_{st} = A_s$ and $p_{tr} = 0$), the design anchorage and lap lengths are given in Table 9-1.

Table 9-1 Comparison of design lap lengths for $c_{min} = 1.5 \cdot Ø$, $\Sigma A_{st} = A_s$, $p_{tr} = 0$

σ_s	$l_{bd,own}$ / Ø	$l_{bd,PT}$ / Ø
$0.8 \cdot f_{yd} = 350$ MPa	$46 \cdot \left(\frac{25}{f_{ck}}\right)^{0.455} \cdot \left(\frac{Ø}{25}\right)^{0.36}$	$46 \cdot \left(\frac{25}{f_{ck}}\right)^{1/2} \cdot \left(\frac{Ø}{20}\right)^{1/3}$
$1.0 \cdot f_{yd} = 435$ MPa	$69 \cdot \left(\frac{25}{f_{ck}}\right)^{0.455} \cdot \left(\frac{Ø}{25}\right)^{0.36}$	$63 \cdot \left(\frac{25}{f_{ck}}\right)^{1/2} \cdot \left(\frac{Ø}{20}\right)^{1/3}$
$1.2 \cdot f_{yd} = 520$ MPa	$95 \cdot \left(\frac{25}{f_{ck}}\right)^{0.455} \cdot \left(\frac{Ø}{25}\right)^{0.36}$	$83 \cdot \left(\frac{25}{f_{ck}}\right)^{1/2} \cdot \left(\frac{Ø}{20}\right)^{1/3}$

9.3 Necessity of Additional Rules for Large Diameter Bars

The derived design equations for lap and anchorage length are equally applicable to large diameter bars up to Ø 40 mm. Additional rules for the bond behaviour these bars are not necessary where a thorough crack control in the longitudinal and transverse direction is provided. A lap test without surface reinforcement designed according to [EC2] except for an increased lap length by the factor 2.0 / 1.5 = 1.33 only just reached the yield strength before lap failure (T3). Therefore, certain provisions are recommended to provide robustness. The following findings for large diameter bars shall be incorporated in future codes:

- The additional rule according to [EC2] that permits laps in members with dimensions above 1.0 m may be removed
- The positioning of transverse reinforcement that sufficiently confines the bond zone is necessary to allow for laps of Ø 40 mm bars
- This transverse reinforcement for large diameter bars shall be covered by the minimum confining reinforcement in anchorages and laps for all bar diameters
- The percentage of lapped bars may exceed 50 %
- Robustness in laps may be obtained by transverse reinforcement, surface reinforcement and small utilisation such as $\sigma_s \leq 0.8 \cdot f_{yd}$
- In laps with large diameter bars, bar stresses well above the yield strength may only be obtained by a percentage of bars lapped at a section below 100 % or by additional continuous bars such as surface reinforcement
- Where surface reinforcement is provided, the additional rule that excludes laps with bar stresses above $0.8 \cdot f_{yd}$ may be removed

The crack widths in beams with large diameter bars with and without surface reinforcement can be calculated with the [EC2] equations for crack widths. However, the measured and calculated 95%-fractile values were larger than 0.4 mm. Where additional reinforcement with smaller bar diameters for crack control such as surface reinforcement is positioned, this value may be reduced. Surface reinforcement with a cross sectional area equal to 2% of the cross-sectional concrete area under tension outside the stirrups according to [EC2] leads to a crack width reduction of the 95%-fractile values below 0.2 mm.

The cracks at lap ends have the largest crack widths along structural concrete members independent from the bar diameter. In contrast, crack widths within laps are smaller than outside laps, since the reinforcement ratio is increased along the lap length. Since crack width limits are not maximum values, but 95%-fractile values along the entire structural member, large crack widths at lap ends are acceptable and do not require additional rules.

Not all additional rules for large diameter bars defined in [EC2/NA] were investigated, such as rules concerning curtailed reinforcement or shear. But under consideration of the detailing recommendations defined for all bar diameters in [EC2], the additional rules for large diameter bars in [EC2/NA] do not seem necessary.

9.4 Proposal for Future Research

During the analysis of the database, the small number of anchorage tests in structural elements subjected to bending, such as anchorages at beam-ends with transverse pressure as well as curtailed reinforcement was apparent. This fact is probably due to the lower costs of simplified tests. To investigate reinforcing bar stresses up to the yield strength, other test setups have to be used. Still, to derive design models and recommendations for detailing for anchorages, such structural member tests are advisable. Anchorage tests with transverse pressure and Ø 40 mm bars were tested within the test programme described in this thesis, but tests with conventional bar diameters have hardly been tested. Although the design model according to [FIB14] was calibrated with a large number of lap tests and validated with anchorage tests, the validity of these simplified, mainly one-bar anchorage tests should be reviewed on the basis of anchorages in actual beams. Especially anchorages with low transverse pressure up to the tensile strength of concrete should be validated.

The number of available tests with reinforcement lapped at the same position is sufficient for the statistical analysis of design models and for the derivation of necessary detailing rules. But certain special anchorage and lap parameters only exist in small numbers and were excluded from the database. Laps with staggered reinforcing bars are one example of deviating test setups. If the lap end of one lap ends right at the beginning of the following lap, the crack width presumably equals the crack width at 100 % laps. For detailing rules in codes, such crack analysis of staggered laps is recommended.

The tests performed by the author and the tests included in the database were performed under short term monotonic loading. Investigations have shown that the crack widths at lap ends subjected to sustained and cyclic loads depend on the lap length, since the bond strength decreases under such loads. Therefore, the influence of sustained or fatigue load on the required bond length should be analysed. An investigation would clarify whether an increased lap length or additional reinforcement such as surface reinforcement contributes to crack control under sustained or cyclic loads more effectively.

The effect of poor bond conditions was only briefly discussed in this thesis. The compilation of a database including the effects of slump and porosity below horizontal reinforcing bars is recommended. To define reduction factors for lap and anchorage strength for the next generation of EUROCODE 2 and MODEL CODE, a more profound review of this effect is advisable.

The non-linear strain development in laps was derived from discrete strain measurements in several lap investigations in the past. For anchorages, this measurement becomes increasingly difficult to accomplish, since anchorage lengths are usually small and strain gauges shall not impair the entire bond zone. Therefore, continuous measurements of the strain development in anchorages and laps – such as distributed fibre-optic strain measurements – would contribute to the understanding of bond behaviour to a great extent.

10 Additional publications in database

The described database includes further publications not cited within the thesis but within annex A.3:

AHLBORG [AHL02], ATKINS [ATK97], BEEBY, BRUFFEL AND GOUGH [BEE73], CHAMBERLIN [CHA56], [CHA58], [CHA87], HAMAD [HAM90], [HAM95], [HAM96], HASAN AND CLEARY [HAS96] , HWANG [HWA94], [HWA96] , MORITA AND FUJI [MOR82], PERRY AND JUNDI [PER69], REZANSOFF, AKANNI AND SPARLING [REZ93]

11 Literature

[ACI01] ACI 408: *ACI 408 bond database*, www.concrete.org/Store/ProductDetail.aspx?ItemID=408DB, 2001.

[ACI03] ACI COMMITTEE 408: *Bond and development of straight reinforcing bars in tension*. American Concrete Institute, Farmington Hills, MI, 2003.

[ACI14] 318-14: *Building Code Requirements for Structural Concrete*. American Concrete Institute, Farmington Hills, MI,

[AHL02] AHLBORG, T.; DEN HARTIGH, T.: *A comparative bond study of MMFX reinforcing steel in concrete*. Final Report, Michigan Technological University, 2002.

[AL-90] AL-SULAIMANI, G. J.; KALEEMULLAH, M.; BASUNBUL, I. A.; Rasheeduzzafar: *Influence of Corrosion and Cracking on Bond Behavior and Strength of Reinforced Concrete*. ACI Structural Journal. Vol. 87, Issue 2, pp. 220–231, 1990.

[AMI09] AMIN, R. S.: *End Anchorage at simple supports in reinforced concrete*. Dissertation, South Bank University London, 2009.

[AST15] ASTM A 944-10(2015): *Test Method for Comparing Bond Strength of Steel Reinforcing Bars to Concrete Using Beam-End Specimens*. ASTM International, Subcommittee A01.05, West Conshohocken, PA, 2015.

[ATK97] ATKINS, W. S.: *Deteriorated Structures*. Phase 2 A Report to the Highways Agency, 1997.

[AZI93] AZIZINAMINI, A.; STARK, M.; ROLLER, J. J.; GHOSH, S. K.: *Bond Performance of Reinforcing Bars Embedded in High-Strength Concrete*. ACI Structural Journal. Vol. 90, Issue 5, pp. 554–561, 1993.

[AZI95] AZIZINAMINI, A.; CHISALA, M.; GHOSH, S. K.: *Tension development length of reinforcing bars embedded in high-strength concrete*. Engineering Structures. Vol. 17, Issue 7, pp. 476–540, 1995.

[AZI99] AZIZINAMINI, A.; PAVEL, R.; HATFIELD, E.; GHOSH, S. K.: *Behavior of lap-spliced reinforcing bars embedded in high-strength concrete*. ACI Structural Journal. Vol. 96, Issue 5, pp. 826–835, 1999.

[BAT93] BATAYNEH, M. K.: *The effects of lateral compression on bond between deformed reinforcing bars and concrete*. Dissertation, Oxford Brookes University, 1993.

[BAU08] Die Deutsche Bauindustrie: *Richtlinienentwurf: Qualität der Bewehrungsarbeiten*, https://www.bauindustrie.de/media/documents/Bewehrungsarbeiten-RichtlinienentwurfQualitaetderBewehrung.pdf, 2008.

[BEE73] BEEBY, A. W.; BRUFFELL, S.; GOUGH, D.: *Bond - Project Report No. 4*. Research Seminar, Cement and Concrete Association. Vol. 1, Issue 1, pp. 15–20, 1973.

[BER99] BERGMEISTER, K.: *Risse im Konstruktionsbeton*. Beton- und Stahlbetonbau. Vol. 94, Issue 6, pp. 245–253, 1999.

[BET80] BETZLE, M.: *Experimentelle und theoretische Untersuchungen zum Tragverhalten von Vollstößen bei Überreifung von zugbeanspruchten Rippenstählen*. Dissertation, Technical University of Munich, 1980.
[BET81] BETZLE, M.: *Vollstöße durch Übergreifung von zugbeanspruchten Rippenstählen in Normalbeton*. DAfStb publication series, issue 319, Wilhelm Ernst & Sohn, Berlin, 1981.
[BUR00] BURKHARDT, C. J.: *Zum Tragverhalten von Übergreifungsstößen in hochfestem Beton*. Dissertation, Institute for Structural Concrete, RWTH Aachen University, 2000.
[CAB94] CABRERA, J. G.; GHODDOUSSI, P.: *Influence of Fly Ash on the Resistivity and Rate of Corrosion of Reinforced Concrete*. ACI Special Publication. Vol. 145, Issue 1, pp. 229–244, 1994.
[CAI02] CAIRNS, J.; PLIZZARI, G. A.: *Do we need a standard test for bond?* International Conference on Bond in Concrete - from research to standards, Budapest, 2002.
[CAI03] CAIRNS, J.; PLIZZARI, G. A.: *Towards a harmonised European bond test*. Materials and Structures. Vol. 36, Issue 8, pp. 498–506, 2003.
[CAI14a] CAIRNS, J.: *Staggered lap joints for tension reinforcement*. Structural Concrete. Vol. 15, Issue , pp. 45–54, 2014.
[CAI14b] CAIRNS, J.; ELIGEHAUSEN, R.: *Evaluation of EC 2 rules for design of tension lap joints*. The Structural Engineer. Vol. 92, Issue 9, pp. 44–52, 2014.
[CAI96] CAIRNS, J.; JONES, K.: *An Evaluation of the Bond-Splitting Action of Ribbed Bars*. ACI Materials Journal. Vol. 93, Issue 1, pp. 10–19, 1996.
[CAN05] CANBAY, E.; FROSCH, R. J.: *Bond Strength of Lap-Spliced Bars*. ACI Structural Journal. Vol. 102, Issue 4, pp. 605–614, 2005.
[CAN06] CANBAY, E.; FROSCH, R. J.: *Design of Lap-Spliced Bars*. ACI Structural Journal. Vol. 103, Issue 3, pp. 444–451, 2006.
[CHA56] CHAMBERLIN, S. J.: *Spacing of Reinforcement in Beams*. ACI Journal. Vol. 53, Issue 7, pp. 113–134, 1956.
[CHA58] CHAMBERLIN, S. J.: *Spacing of Spliced Bars in Beams*. ACI Journal Proceedings. Vol. 54, Issue 8, pp. 689–698, 1958.
[CHA87] Chapman, Ralph, A.; Shah, Surendra, P.: *Early-age bond strength in reinforced concrete*. ACI Materials Journal. Vol. 84, Issue 6, pp. 501–510, 1987.
[CHI55] CHINN, J.; FERGUSON, P. M.; THOMPSON, J. N.: *Lapped Splices in Reinforced Concrete Beams*. ACI Journal Proceedings. Vol. 52, Issue 2, pp. 201–214, 1955.
[CHO91] CHOI, O. C.; HADJE-GHAFFARI, H.; DARWIN, D.; MCCABE, S. L.: *Bond of Epox-Coated Reinforcement: Bar Parameters*. ACI Materials Journal. Vol. 88, Issue 2, pp. 207–217, 1991.
[COH82] COHN, M. Z.; BARTLETT, M.: *Computer-Simulated Flexural Tests of Partially Prestressed Concrete Sections*. ASCE Journal of Structural Division. Vol. 108, Issue 1, pp. 2747–2765, 1982.

[COR12] CORONELLI, D.; HANJARI, K. Z.; LUNDGREN, K.: *Bond Strength of Highly Corroded Reinforcement and Cover Delamination*. International Conference on Bond in Concrete 2012 - General Aspects of Bond, Brescia, 2012.

[CYL06] CYLLOK, M. K.: *Zugbeanspruchte Übergreifungsstöße in Beton mit rezyklierter Gesteinskörnung: Rissbildung, Tragfähigkeit und umweltökonomischer Nutzen*. Dissertation, Institute for Structural Concrete, Technical University of Munich, 2006.

[DAR95a] DARWIN, D.; THOLEN, M. L.; IDUN, E. K.; ZUO, J.: *Splice Strength of High Relative Rib Area Reinforcing Bars*. Report, University of Kansas Center for Research, 1995.

[DAR95b] DARWIN, D.; ZUO, J.; THOLEN, M.; IDUN, E.: *Development Length Criteria for Conventional and High Relative Rib Area Reinforcing Bars*. Report, University of Kansas Center for Research, 1995.

[DAR98] DARWIN, D.; IDUN, E. K.; ZUO, J.; THOLEN, M. L.: *Reliability-Based Strength Reduction Factor for Bond*. ACI Structural Journal. Vol. 95, Issue 4, pp. 434–443, 1998.

[DEU06] DEUTSCHER BETON- UND BAUTECHNIKVEREIN E.V.: *Begrenzung der Rissbildung im Stahlbeton- und Spannbetonbau*. Merkblatt, Berlin, 2006.

[DEU08] DIN 1045-1: *Tragwerke aus Beton, Stahlbeton und Spannbeton - Teil 1: Bemessung und Konstruktion*. Deutsches Institut für Normung e.V., Beuth Verlag, Berlin, 2008-08.

[DEU09] DIN 488-1: *Betonstahl - Teil 1: Stahlsorten, Eigenschaften, Kennzeichnung*. Deutsches Institut für Normung e.V., Beuth Verlag, Berlin, 2009-08.

[DEU11] DIN EN 13670: *Ausführung von Tragwerken aus Beton*. Deutsches Institut für Normung e.V., 2011-03.

[DEU12] DEUTSCHER AUSSCHUSS FÜR STAHLBETON: *Erläuterungen zu DIN EN 1992-1-1 und DIN EN 1992-1-1/NA (Eurocode 2)*. DAfStb publication series, issue 600, Beuth Verlag, Berlin, 2012.

[DEU14] ISO 16269-6: *Statistische Auswertung von Daten - Teil6: Ermittlung von statistischen Anteilsbereichen*. Deutsches Institut für Normung e.V., Beuth Verlag, Berlin, 2014-01.

[DEU88] DIN 1045: *Beton und Stahlbeton - Bemessung und Ausführung*. Deutsches Institut für Normung e.V., Beuth Verlag, Berlin, 1988-07.

[DEV91] DeVries, Moehle, Hester: *Lap Splice Strength of Plain and Epoxy-coated Reinforcements*. Report, Structural Engineering Mechanics and Materials, University of California, 1991.

[EC0] DIN EN 1990: *Eurocode: Grundlagen der Tragwerksplanung; Deutsche Fassung EN 1990: 2002-A1:2055-A1:2005/AC:2010*. Deutsches Institut für Normung e.V., Beuth Verlag, Berlin, 2012-12.

[EC2/NA] DIN EN 1992-1-1/NA: *Nationaler Anhang Eurocode 2: Bemessung und Konstruktion von Stahlbeton- und Spannbetontragwerken - Teil 1-1: Allgemeine Bemessungsregeln und Regeln für den Hochbau*. Deutsches Institut für Normung e.V., Beuth Verlag, Berlin, 2011-01.

[EC2] DIN EN 1992-1-1:2011-01: *Eurocode 2: Bemessung und Konstruktion von Stahlbeton- und Spannbetontragwerken - Teil 1-1: Allgemeine Bemessungsregeln und Regeln für den Hochbau; Fassung EN 1992-1-1: 2004 + AC:2010*. Deutsches Institut für Normung e.V., Beuth Verlag, Berlin, 2011-01.

[ELI79] ELIGEHAUSEN, R.: *Übergreifungsstöße zugbeanspruchter Rippenstäbe mit geraden Stabenden*. DAfStb publication series, issue 301, Wilhelm Ernst & Sohn, Berlin, 1979.

[ELI83] ELIGEHAUSEN, R.; POPOV, E. P.; BERTERO, V. V.: *Local Bond Stress-Slip Relationships of Deformed Bars under Generalized Excitations*. Report, UCB/EERC-83/23, Earthquake Engineering Research Center, College of Engineering, University of California, 1983.

[EMP16] EMPELMANN, M.; BUSSE, D.: *Vergleich der Nachweiskonzepte zur Rissbreitenbegrenzung nach EN 1992-1-1, DIN EN 1992-1-1/NA sowie Model Code 2010*. Report, Nr. P02-19-1A (AG: Initiative Praxisgerechte Regelwerke im Bauwesen e.V.), iBMB Fachgebiet Massivbau, Technical University Braunschweig, 2016.

[EUR91] ENV 1992-1-1: *Eurocode 2*. European Committee for Standardization, 1991.

[FER54] FERGUSON, P. M.; TURPIN, R. D.; THOMPSON, J. N.: *Minimun Bar Spacing as a Function of Bond and Shear Strength*. ACI Journal Proceedings. Vol. 50, Issue 6, pp. 869–887, 1954.

[FER62] FERGUSON, P. M.; THOMPSON, J. N.: *Development Length of High Strength Reinforcing Bars in Bond*. ACI Journal Proceedings. Vol. 59, Issue 7, pp. 887–922, 1962.

[FER65a] FERGUSON, P. M.; BREEN, J. E.: *Lapped Splices For High Strength Reinforcing Bars*. ACI Journal Proceedings. Vol. 62, Issue 9, pp. 1063–1078, 1965.

[FER65b] FERGUSON, P. M.; THOMPSON, J. N.: *Development Length for Large High Strength Reinforcing Bars*. ACI Journal Proceedings. Vol. 62, Issue 1, pp. 71–94, 1965.

[FER65c] FERGUSON, P. M.; BREEN, J. E.; THOMPSON, J. N.: *Pullout Tests on High Strength Reinforcing Bars*. ACI Journal Proceedings. Vol. 62, Issue 8, pp. 933–950, 1965.

[FER69] FERGUSON, P. M.; BRICENO, E. A.: *Tensile Lap Splices - Part 1: Retaining Wall Type, Varying Moment Zone*. Report, Center for Highway Research, University of Texas, 1969.

[FER71] FERGUSON, P. M.; KRISHNASWAMY, C. N.: *Tensile Lap Splices - Part 2: Design Recommendation for Retaining Wall Splices and Large Bar Splices*. Research Report No. 113-2, Center for Highway Research, The University of Texas at Austin, 1971.

[FIB05] fib TG 4.5: *Bond test database*, fibtg45.dii.unile.it/files%20scaricabili/Database_splicetest%20Stuttgart%20sept%202005.xls, 2005.

[FIB10] INTERNATIONAL FEDERATION FOR STRUCTURAL CONCRETE: *Bond of reinforcement in concrete: State-of-art report*. fib Bulletin 10, Lausanne, 2000.

[FIB14] INTERNATIONAL FEDERATION FOR STRUCTURAL CONCRETE: *Bond and anchorage of embedded reinforcement: Background to the fib Model Code for Concrete Structures 2010*. fib Bulletin 72, Lausanne, Switzerland, 2014.

[GHA90] GHAGHEI, P.: *Influence of transverse pressure on bond strength in reinforced concrete*. Dissertation, Polytechnic of Central London, 1990.

[GIL12] GILBERT, R. I.; MAZUMDER, M.; CHANG, Z.-T.: *Bond, slip and cracking within the anchorage length of deformed reinforcing bars in tension*. International Conference on Bond in Concrete 2012 - General Aspects of Bond, Brescia, 2012.

[HAM90] HAMAD, B. S.; JIRSA, J. O.: *Influence of Epoxy Coating on Stress Transfer from Steel to Concrete*. First Materials Engineering Congress, New York, 1990.

[HAM95] HAMAD, B. S.: *Bond strength improvement of reinforcing bars with specially designed rib geometries*. ACI Structural Journal. Vol. 92, Issue 1, pp. 3–13, 1995.

[HAM96] HAMAD, B. S.; MANSOUR, M.: *Bond Strength of Noncontact Tension Lap Splices*. ACI Structural Journal. Vol. 93, Issue 3, pp. 1–11, 1996.

[HAM98] HAMAD, B. S.; ITANI, M. S.: *Bond STrength of REinforcement in High-Performance Concrete: The Role of Silica Fume, Casting Position and Superplasticizer Dosage*. ACI Materials Journal. Vol. 95, Issue 5, pp. 499–511, 1998.

[HAS96] HASAN, H. O.; CLEARY, D. E. A.B.: *Performance of Concrete Bridge Decks and Slabs reinforced with Epoxy-Coated Steel under Repeated Loading*. ACI Structural Journal. Vol. 93, Issue , pp. 397–403, 1996.

[HEG15] HEGGER, J.; EMPELMANN, M.; SCHNELL, J.: *Weiterentwicklung von Bemessungs- und Konstruktionsregeln bei großen Stabdurchmessern (> 32 mm, B500)*. Report, https://www.isb-ev.de/wp-content/uploads/2014/05/AiF-16992-Schlussbericht.pdf, Institute of Structural Concrete, RWTH Aachen University, 2015.

[HEG18] HEGGER, J.; EMPELMANN, M.; SCHNELL, J.: *Bemessungs- und Konstruktionsregeln bei großen Stabdurchmessern und hohen Bewehrungsgraden*. Report, Institute of Structural Concrete, RWTH Aachen University, 2018.

[HES93] HESTER, C. J.; SALAMIZAVAREGH, S. E. A.: *Bond of Epoxy-Coated Reinforcement: Splices*. ACI Structural Journal. Vol. 90, Issue , pp. 89–102, 1993.

[HWA94] HWANG, L.: *Effect of Silica Fume on the Splice Strength of Deformed Bars of High-Performance Concrete*. ACI Structural Journal. Vol. , Issue , 1994.

[HWA96] HWANG, L.: *Tensile Bond Strengths of Deformed Bars of High-Strength Concrete*. ACI Structural Journal. Vol. , Issue , 1996.

[JAN86] JANOVIC, K.: *Verbundverhalten von Bewehrungsstählen unter Dauerbelastung in Normal- und Leichtbeton*. DAfStb publication series, issue 367, Ernst und Sohn, Berlin, 1986.

[JEN82] JENSEN, J. H.: *Forkammede armeringsstængers forankring, specielt ved vederlag*. Report, Department of Structural Engineering, Technical University of Denmark, 1982.

[JIR95] JIRSA, J. O.; CHEN, W. E. A.: *Development of Bundled Reinforcing Steel, Research Report No. 1363*. Report, Center for Transportation Research, University of Texas, 1995.

[JOI00] JOINT COMMITTEE ON STRUCTURAL SAFETY: *Probabilistic Model Code*. Technical University of Denmark, Lyngby, 2000.

[JUN77] JUNGWIRTH, D.; KERN, G.: *Verwendung von Bewehrungsstäben mit großen Durchmessern bzw. hohen Festigkeiten am Beispiel des Dywidag-Gewindestabs*. Beton- und Stahlbetonbau. Vol. 72, Issue 10, pp. 237–243, 1977.

[KAD94] Kadoriku: *Study on Behaviour of lap splices in Hogh-Strength Reinforced Concrete Members*. Dissertation, Kobe University, 1994.

[KEM79] KEMP, E. L.; WILHELM, W. J.: *Investigation of the parameters influencing bond cracking*. ACI Journal. Vol. 76, Issue 1, pp. 47–71, 1979.

[KOE96] KÖNIG, G.; TUE, N. V.: *Grundlagen und Bemessungshilfen für die Rissbreitenbeschränkung im Stahlbeton und Spannbeton - sowie Kommentare, Hintergrundinformationen und Anwendungsbeispiele zu den Regelungen nach DIN 1045, EC2 und Model Code 90*. DAfStb publication series, issue 466, Beuth Verlag, Berlin, 1996.

[KOK72] KOKUBU, M.; OKAMURA, H.: *Use of Large-Sized Deformed Bars in Reinforced Concrete*. Faculty of Engineering, University of Tokyo, Tokyo, 1972.

[KRE89] KRELLER, H.: *Zum nichtlinearen Trag- und Verformungsverhalten von Stahlbetonstabtragwerken unter Last- und Zwangeinwirkung*. Dissertation, University of Stuttgart, 1989.

[LEO05] Leonardo da Vinci Pilot Project CZ/02/B/F/PP-134007: *Development of Skills Facilitating Implementation of Eurocodes, Reliability Backgrounds - Handbook 2*, http://eurocodes.jrc.ec.europa.eu/showpublication.php?id=63, 2005.

[LET06a] LETTOW, S.: *Ein Verbundelement für nichtlineare Finite-Elemente-Analysen - Anwendung auf Übergreifungsstöße*. Dissertation, University of Stuttgart, 2006.

[LET06b] LETTOW, S.; ELIGEHAUSEN, R.: *Formulation of application rules for lap splices*. Meeting of TG 4.5 - bond models, fédération internationale du beton (fib), 2006.

[LUK82] LUKOSE, K.; GERGELY, P. E. A.: *Behavior of Reinforced Concrete Lapped Splices for Inelastic Cyclic Loading*. ACI Journal Proceedings. Vol. 79, Issue 5, pp. 355–365, 1982.

[LUN15] LUNDGREN, K.; TAHERSHAMI, M.; ZANDI, K.; PLOS, M.: *Tests on anchorage of naturally corroded reinforcement in concrete*. Materials and Structures. Vol. 48, Issue 7, pp. 2009–2022, 2015.

[MAN17] MANCINI, G.; CARBONE, V. I.; BERTAGNOLI, G.; GINO, D.: *Reliability-based evaluation of bond strength for tensed lapped joints and anchorages in new and existing reinforced concrete structures*. Structural Concrete. Vol. online, Issue 1-14, 2017.

[MAR15] MARX, C.: *Erstellung und Auswertung einer Datenbank zum Tragverhalten von Übergreifungsstößen in Stahlbetonbauteilen*. Master Thesis, Institute for Structural Concrete, RWTH Aachen University, 2015.

[MAR73] MARTIN, H.: *Zusammenhang zwischen Oberflächenbeschaffenheit, Verbund und Sprengwirkung*. DAfStb publication series, issue 228, Verlag Ernst & Sohn, Berlin, 1973.

[MAR80] MARTIN, H.; SCHIEßL, P.; SCHWARZKOPF, M.: *Berechnungsverfahren für Rissbreiten aus Lastbeanspruchung*. Forschung Straßenbau und Straßenverkehrstechnik. Vol. 309, Issue 1, pp. 34–65, 1980.

[MAR81] MARTIN, H.; NOAKOWSKI, P.: *Verbundverhalten von Betonstählen - Untersuchungen auf der Grundlage von Ausziehversuchen*. DAfStb publication series, issue 319, 1981.

[MAS90] MASLEHUDDIN, M.; ALLAM, I. A.; Al-Sulaimani, Ghazi, J.; AL-MANA, A.; ABDULJAUWAD, S. N.: *Effect of Rusting of Reinforcing Steel on its Mechanical Properties and Bond with Concrete*. ACI Materials Journal. Vol. 87, Issue 5, pp. 496–502, 1990.

[MAT61] MATHEY, R.; WATSTEIN, D.: *Investigation of Bond in Beam and Pull-Out Specimens with High-Yield-Strength Deformed Bars*. ACI Journal Proceedings. Vol. 32, Issue 9, pp. 1071–1090, 1961.

[MC2010] INTERNATIONAL FEDERATION FOR STRUCTURAL CONCRETE: *fib Model Code for Concrete Structures 2010*. Ernst & Sohn (Wiley), Lausanne, Switzerland, 2013.

[MC90] EURO-INTERNATIONAL COMMITTEE FOR CONCRETE: *CEB-FIP Model Code 1990*. Design code, Telford, London, 1993.

[MET15] METELLI, G.; CAIRNS, J.; PLIZZARI, G. A.: *The influence of percentage of bars lapped on performance of splices*. Materials and Structures. Vol. , Issue 48, pp. 2983–2996, 2015.

[MOR82] MORITA, S.; FUJI, S.: *Bond capacity of deformed bars due to splitting of surrounding concrete.* International Conference on Bond in Concrete, Paisley, Scotland, 1982.

[OLS90] OLSEN, N. H.: *The strength of overlapped deformed tensile reinforcement splices in high-strength concrete*. Report, Technical University of Denmark, Lyngby, 1990.

[ORA77] ORANGUN, C. O.; JIRSA, J. O.; BREEN, J. E.: *A Reevaulation of Test Data on Development Length and Splices*. ACI Journal Proceedings. Vol. 74, Issue 3, pp. 114–122, 1977.

[PER69] PERRY, E. S.; JUNDI, N.: *Pullout bond stress distribution under static and dynamic repeated loadings*. ACI Journal. Vol. 66, Issue 5, pp. 377–380, 1969.

[PLI98] PLIZZARI, G. A.; DELDOSSI, M. A.; MASSIMO, S.: *Transverse Reinforcement Effects in Anchored Deformed Bars*. Magazine of Concrete Research. Vol. 50, Issue 2, pp. 161–177, 1998.

[PT18] PT.SC2.T1: *PT1 working draft prEN 1992-1-1:2018*. European Committee for Standardization; CEN, European Committee for Standardization, 2018.

[RAC06] RACKWITZ, R.: *Zuverlässigkeit und Lasten im konstruktiven Ingenieurbau*. Lecture Notes, Technical University of Munich, 2006.

[RAK14] RAKHSHANIMEHR, M.; ESFAHANI, M. R.; KIANOUSH, M. R.; MOHAMMADZADEH, B. A.; MOUSAVI, S. R.: *Flexural ductility of reinforced concrete beams with lap-spliced bars*. Canadian Journal of Civil Engineering. Vol. 41, Issue 7, pp. 594–604, 2014.

[RAT72] RATHKJEN, A.: *Forankringsstyrker af armeringsjern ved bjælkeunderstotninger*. Report 7203, Renog Anvendt Mekanik, Civil Engineering Academy of Denmark, 1972.

[REG97] REGAN, P. E.: *Tests of slabs with fully or partly exposed main reinforcement*. Report to W.S. Atkins / The Highways Agency, School of Architecture and Engineering, University of Westminster, 1997.

[REH61] REHM, G.: *Über die Grundlagen des Verbundes zwischen Stahl und Beton*. DAfStb publication series, issue 138, Verlag Ernst & Sohn, Berlin, 1961.

[REH68] REHM, G.; MARTIN, H.: *Zur Frage der Rissbegrenzung im Stahlbetonbau*. Beton- und Stahlbetonbau. Vol. 63, Issue 8, pp. 175–182, 1968.

[REH75a] REHM, G.: *Vorbericht über Versuche mit GEWI-Stahl BSt 42/50, d = 50 mm und entsprechenden Muffenverbindungen*. Report 1415, Institute of Structural Concrete, Technical University of Munich, 1975.

[REH75b] REHM, G.: *Rippenstäbe mit d = 50 mm als Bewehrung in Stahlbetonbauteilen*. Report, University of Stuttgart, 1975.

[REH77] REHM, G.; ELIGEHAUSEN, R.: *Übergreifungsstöße von Rippenstäben unter schwellender Belastung*. DAfStb publication series, issue 291, Wilhelm Ernst & Sohn, Berlin, 1977.

[REH79] REHM, G.; ELIGEHAUSEN, R.; NEUBERT, B.: *Erläuterung der Bewehrungsrichtlinien DIN 1045, Abschnitt 18, Ausgabe 12/78*. DAfStb publication series, issue 300, Beuth, Berlin, 1979.

[REY82] REYNOLDS, G.; BEEBY, A. W.: *Bond Strength of deformed Bars*. International Conference on Bond in Concrete, Paisley, 1982.

[REZ92] REZANSOFF, T.; KONKANKAR, U. S.; FU, Y. C.: *Confinement Limits for Tension Lap Splices under Static Loading*. Canadian Journal of Civil Engineering. Vol. 19, Issue 3, pp. 447–453, 1992.

[REZ93] REZANSOFF, T.; AKANNI, A.; SPARLING, B.: *Tensile Lap Splices under Static Loading: A Review of the proposed ACI 318 Code Provisions*. ACI Structural Journal. Vol. 90, Issue 4, pp. 374–384, 1993.

[RIC09] RICKER, M.: *Zur Zuverlässigkeit der Bemessung gegen Durchstanzen bei Einzelfundamenten*. Dissertation, Institute for Structural Concrete, RWTH Aachen University, 2009.

[RIC84] RICHTER, T.: *Untersuchungen zur Verankerung von Betonrippenstahl*. Dissertation, Fakultät für Bau-, Wasser- und Forstwesen, TU Dresden, 1984.

[RIL82] RILEM: *RILEM Recommendations RC5 : bond test for reinforcement steel. 1. Beam test. TC9-RC*. RILEM, Paris, 1982.

[RIL83] RILEM: *RILEM Recommendations RC6: bond test for reinforcement steel. 2. Pull-out test. TC9-RC*. RILEM, Paris, 1983.

[ROB82] ROBINS, P. J.; STANDISH, I. G.: *Effect of Lateral Pressure on bond of Reinforcing Bars in Concrete*. International Conference on Bond in Concrete, Paisley, 1982.

[SCH14] SCHEIBE, M.; HUDE, F.; HEGGER, J.; SCHOENING, J.: *High-strength reinforcement in reinforced concrete construction - Identification of potential fields of application, development of design principles and determination of potential economic savings*. Fraunhofer IRB Verlag, 2014.

[SCH88] SCHMIDT-THRÖ; G.; STÖCKL, S.; KUPFER, H.: *Verankerugn der Bewehrung am Endauflager bei einachsiger Querpressung und Einfluss einer einachsigen Querpressung und der Verankerungslänge auf das Verbundverhalten von Rippenstählen im Beton*. DAfStb publication series, issue 389, Verlag Ernst & Sohn, Berlin, 1988.

[SCH98a] SCHIEßL, P.: *Grundlagen der Neuregelung zur Beschränkung der Rissbreite*. DAfStb publication series, issue 400, Beuth Verlag, Berlin, 1998.

[SCH98b] SCHENKEL, M.: *Zum Verbundverhalten von Bewehrung bei kleiner Betondeckung*. Dissertation, ETH Zurich, 1998.

[SPA92] SPAETHE, G.: *Die Sicherheit tragender Baukonstruktionen*. Springer, Wien New York, 1992.

[STE07] STEUCK, K. P.; PANG, J. B. K.; EBERHARD, M. O.; STANTON, J. F.: *Anchorage of large-diameter reinforcing bars grouted into ducts - Draft Research Report*. Washington State Transportation Center (TRAC), 2007.

[STO77] STÖCKL, S.; MENNE, B.; KUPFER, H.: *Versuche an zugbeanspruchten Übergreifungsstöen von Rippenstählen*. DAfStb publication series, issue 276, Wilhelm Ernst & Sohn, Berlin, 1977.

[TEP73] TEPFERS, R.: *A theory of bond applied to overlapped tensile reinforcement splices for deformed bars*. Dissertation, Division of Concrete Structures, Chalmers University of Technology, 1973.

[THO75] THOMPSON, M. A.; JIRSA, J. O.; et al.: *The Behaviour of Multiple Lap Splices in Wide Sections*. Report No. 154-1; Project 3-5-72-154, University of Texas, 1975.

[THO79] THOMPSON, M. A.; Jirsa, J. O. et al.: *Behavior of Multiple Lap Splices in Wide Sections*. ACI Journal Proceedings. Vol. 76, Issue 2, pp. 227–248, 1979.

[TRE89] TREECE, R. A.; JIRSA, J. O.: *Bond Strength of Epoxy-Coated Reinforcing Bars*. ACI Materials Journal. Vol. 86, Issue 167-174, 1989.

[UED86] UEDA, T.; LIN, I.; HAWKINS, N. M.: *Beam Bar Anchorage in Exterior Column-Beam Connections*. ACI Journal. Vol. 83, Issue 3, pp. 412–422, 1986.

[UNT65] UNTRAUER, R. E.; HENRY, R. L.: *Influence of Normal Pressure on Bond Strength*. ACI Journal Proceedings. Vol. 62, Issue 5, pp. 577–586, 1965.

[VIW79] VIWATHANATEPA, S.; POPOV, E. P.; BERTERO, V. V.: *Effects of generalized loadings on bond of reinforcing bars embedded in confined concrete blocks*. Report to National Science Foundation, Earthquake Engineering Research Center, College of Engineering, University of California, 1979.

[WIL13] WILDERMUTH, A.: *Untersuchungen zum Verbundverhalten von Bewehrungsstäben mittels vereinfachter Versuchskörper*. DAfStb publication series, issue 609, Beuth Verlag, Berlin, 2013.

[ZEK81] ZEKANY, A. J.: *The Influence of Shear on Lapped Splices in Reinforced Concrete*. Report, Center for Highway Research, University of Texas, 1981.

[ZIL10] ZILCH, K.; ZEHETMAIER, G.: *Bemessung im konstruktiven Ingenieurbau*. Springer, Berlin Heidelberg, 2010.

[ZUO00] ZUO, J.; DARWIN, D.: *Splice Strength of Conventional and High Relative Rib Area Bars in Normal and High-Strength Concrete*. ACI Structural Journal. Vol. 97, Issue 4, pp. 630–641, 2000.

[ZUO98] ZUO, J.; DARWIN, D.: *Bond Strength of High Relative Rib Area Reinforcing Bars*. Report, University of Kansas, 1998.

Annex

A.1. Design Approaches for Anchorages and Laps

	FIB BULLETIN 72 [FIB14]	MODEL CODE 2010 [MC2010]
l_b		$\frac{\sigma_s \cdot Ø}{4 \cdot 0.35 \cdot \sqrt{f_c} \cdot (\alpha_2 + \alpha_3)}$
σ_s	$54 \cdot \left(\frac{f_{cm}}{25}\right)^{1/4} \cdot \left(\frac{25}{Ø}\right)^{1/5} \cdot \left(\frac{l_b}{Ø}\right)^{0.55} \cdot \left[A(c_{min}) + A(K_{tr})\right]$ $A(c_{min}) = \left(\frac{c_{min}}{Ø}\right)^{1/4} \cdot \left(\frac{c_{max}}{c_{min}}\right)^{1/10}$ $A(K_{tr}) = k_m \cdot K_{tr}$	$\frac{l_b \cdot 4 \cdot 0.35 \cdot \sqrt{f_c}}{Ø} \cdot (\alpha_2 + \alpha_3)$
σ_s^c	$54 \cdot \left(\frac{f_{cm}}{25}\right)^{1/4} \cdot \left(\frac{25}{Ø}\right)^{1/5} \cdot \left(\frac{l_b}{Ø}\right)^{0.55} \cdot A(c_{min})$	$\frac{l_b \cdot 4 \cdot 0.35 \cdot \sqrt{f_c}}{Ø} \cdot \left[\left(\frac{c_{min}}{Ø}\right)^{0.5} \cdot \left(\frac{c_{max}}{c_{min}}\right)^{0.15}\right]$
σ_s^{st}	$54 \cdot \left(\frac{f_{cm}}{25}\right)^{1/4} \cdot \left(\frac{25}{Ø}\right)^{1/5} \cdot \left(\frac{l_b}{Ø}\right)^{0.55} \cdot k_m \cdot K_{tr}$ $= 54 \cdot \frac{f_{cm}^{1/4} \cdot 1.9 \cdot l_b^{0.55}}{2.23 \cdot Ø^{3/4}} \cdot 12 \cdot \frac{n_l \cdot n_{st} \cdot A_{st}}{l_b \cdot Ø \cdot n}$ $= 552 \cdot \frac{f_{cm}^{1/4} \cdot l_b^{0.55}}{Ø^{3/4}} \cdot \frac{n_l \cdot A_{st}}{s \cdot Ø \cdot n}$	$\frac{l_b \cdot 4 \cdot 0.35 \cdot \sqrt{f_c}}{Ø} \cdot k_d \cdot \left(\frac{n_l \cdot A_{st}}{n \cdot Ø \cdot s_t} - \frac{0.5 \cdot Ø}{1250}\right)$
Units	SI	SI
σ_s^{st} [SI]	$552 \cdot \frac{f_{cm}^{1/4} \cdot l_b^{0.55}}{Ø^{3/4}} \cdot \frac{n_l \cdot A_{st}}{s \cdot Ø \cdot n}$	See above
σ_s^{st} [SI]	$\frac{n_l \cdot A_{st} \cdot l_b \cdot \sqrt{f_c}}{Ø^2 \cdot s \cdot n} \cdot 3.86$ (with $l_0 = 33 \cdot Ø$)	$\frac{A_{st} \cdot n_l \cdot l_b \cdot \sqrt{f_c}}{Ø^2 \cdot s \cdot n} \cdot 2.32$ (with $f_c^{1/2}$[MPa]=5.48 instead $f_c^{1/2}$[psi]=66)
with	With n_l k_m = effectiveness factor for confinement 12 where the bar is less than 5d or 125 mm from the stirrup leg, 6 where the bar is further apart and 0 for slabs without vertical transverse reinforcement and for transverse bars behind the longitudinal bars $(25/Ø)^{0.2}$ $c_{min} = \min\{c_s/2; c_x; c_y\}$ $c_{max} = \max\{c_s/2; c_x\}$ $c_y = c_{vert}$ $c_x = c_{hori}$ c_s = clear bar spacing $0.5 \leq c_{min}/Ø \leq 3.5$ $c_{max} / c_{min} \leq 5.0$ $l_b \geq 10 \cdot Ø$ $K_{tr} = \frac{n_l \cdot n_{st} \cdot A_{st}}{l_b \cdot Ø \cdot n} \leq 0.05$	f_c and f_y in [MPa] Transverse reinforcement factor: $\alpha_3 = k_d \cdot (K_{tr} - \alpha_t/50) \geq 0$ $K_{tr} = n_t \cdot A_{st} / (n_b \cdot Ø \cdot s_t) \leq 0.05$ (this was derived from the semi-empirical expression from fib bulletin 72 where the denotation is $k_m \cdot K_{tr}$) Note: α_2 is always added to α_3 $f_{bd} = (\alpha_2+\alpha_3) \cdot f_{bd,0} - 2 \cdot p_{tr}/\gamma_c$ and for bars ≥ 20 mm $\Sigma A_{st} \geq \alpha_t \cdot \alpha_1 \cdot \Sigma A_s$ n_l = number of legs crossing a potential splitting failure surface A_{st} = are of one leg n_b = number of anchored or lapped bars k_d = factor for efficiency ΣA_s = area of a single bar for straight transverse bars ΣA_s = total area of all bars for transverse links $\alpha_t = 0.5 \cdot Ø/25$ $\alpha_1 = A_{s,req} / A_{s,prov.} \leq 1{,}0$ $\eta_3 = (25/Ø)^{0.3}$ for Ø > 25 mm $c_{min} = \min(c_s/2; c_x, c_y)$ $c_{max} = \max(c_s/2; c_x; c_y)$ $c_{s,min} = 2 \cdot Ø$ $\alpha_2 = (c_{min}/Ø)^{0.5} \cdot (c_{max}/c_{min})^{0.15}$ $0.5 \leq c_{min}/Ø \leq 3.5$ $1.0 \leq c_{max}/c_{min} \leq 5.0$

	EUROCODE 2: 2011 [EC2]	BURKHARDT [BUR00]

l_b	$\frac{\phi \cdot \sigma_s}{4 \cdot 0.675 \cdot f_c^{2/3}} \cdot (1 - k \cdot \left(\frac{\Sigma A_{st} - A_{st,min}}{A_s}\right)$	
σ_s	$\frac{4 \cdot l_b \cdot 0.675 \cdot f_c^{2/3}}{\phi} \cdot \frac{1}{1 - k \cdot \left(\frac{\Sigma A_{st} - A_{st,min}}{A_s}\right)}$	
σ_s^c	$\frac{4 \cdot l_b \cdot 0.675 \cdot f_c^{2/3}}{\phi} \cdot \frac{0.15 \cdot (c_{min} - \phi)/\phi}{1 - 0.15 \cdot (c_{min} - \phi)/\phi}$	$38 \cdot f_c^{1/4} \cdot \left(\frac{l_b}{\phi}\right)^{1/2} \cdot \left(\frac{c_{min}}{\phi}\right)^{1/5} \cdot \left(\frac{10}{\phi}\right)^{1/2} \cdot \frac{2}{1 + \frac{\sigma_{s,min}}{\sigma_{s,max}}}$
σ_s^{st}	$\frac{4 \cdot l_b \cdot 0.675 \cdot f_c^{2/3}}{\phi} \cdot \frac{k \cdot \left(\frac{n_{st} \cdot A_{st}}{A_s} - 0.25\right)}{1 - k \cdot \left(\frac{n_{st} \cdot A_{st}}{A_s} - 0.25\right)}$	$4.2 \cdot f_c^{1/4} \cdot \sqrt{\frac{l_b \cdot n_l \cdot A_{st} \cdot f_{yt}}{s \cdot n \cdot A_s}}$
Units	SI	SI
σ_s^{st} [SI]	See above	See above
σ_s^{st} [SI]	See above	$4.74 \cdot \sqrt{\frac{f_c^{1/2} \cdot l_b \cdot n_l \cdot A_{st} \cdot f_{yt}}{s \cdot n \cdot \phi^2}}$ with f_{yst} = 300 MPa: $82 \cdot \sqrt{\frac{f_c^{1/2} \cdot l_b \cdot n_l \cdot A_{st}}{s \cdot n \cdot \phi^2}}$ For the IMB constellation $\frac{A_{tr} \cdot l_b \cdot \sqrt{f_c}}{\phi^2 \cdot s \cdot n} \cdot 7.2$ (with f_c = 435 MPa)
with	A_s = one bar $0.7 \leq \alpha_3 = 1 - K \cdot \frac{\Sigma A_{st} - \Sigma A_{st,min}}{A_s} \leq 1.0$ $0.7 \leq \alpha_2 = 1 - 0.15 \cdot (c_d - Ø)/Ø \leq 1.0$ $\Sigma A_{st,min}$ = 0.25 for anchorages $\Sigma A_{st,min}$ = 1.0 for laps The transverse reinforcement should be positioned at the outer thirds of the lap c_s = clear bar spacing η_2 = (132 – Ø) / 100 c_d = min {c_s/2; c_x; c_y} n_l is not considered	With n_l With $f_{yt} \leq 300$ MPa σ_s^{st} is added to the concrete contribution σ_s^c n_l = number of legs per stirrup orthogonal to the lap plane n_s = number of lapped bars s_t = clear spacing of stirrups A_s = area of one lapped bar Burkhardt only tested beams where side splitting was most likely $0.75 \leq K = (10/Ø)^{1/2} \leq 1.0$ c_m = min {c_x,c_y,c_s/2}

	ELIGEHAUSEN [ELI79]	LETTOW [LET06B]
l_b		
σ_s	Equations for corner laps, for laps without lateral influence of cover and for beams with a combination of both	$11.1 \cdot f_c^{2/5} \cdot \left(\frac{l_b}{\phi}\right)^{3/5} \cdot 1.0 \cdot 1.1 \cdot \left(\frac{l_b}{s}\right)^{1/10}$ Factor 1.0 for concrete cover Where no stirrups are present, $1.1 \cdot \left(\frac{l_b}{s}\right)^{1/10} = 1.0$
σ_s^c	$\sigma_c = 2.2 \cdot \left(\frac{e_s}{c_y}\right)^{1/2} \cdot \left(\frac{c_y}{Ø}\right) \cdot f_c^{1/2} \cdot \left(\frac{l_b}{Ø}\right)^{2/3} \cdot \left(\frac{10}{Ø}\right)^{0.5} \cdot \frac{2}{1+\frac{\min\sigma}{\max\sigma}}$ 1.0 für good bond, otherwise 0.8	$11.1 \cdot f_c^{2/5} \cdot \left(\frac{l_b}{\phi}\right)^{3/5} \cdot \left[\left(\frac{c_x}{\phi}\right)^{1/4} \cdot \left(\frac{c_y}{\phi}\right)^{1/2}\right]$
σ_s^{st}	$6 \cdot \sqrt{\frac{n_{st} \cdot A_{st}}{A_s} \cdot f_{yt}}$	$11.1 \cdot f_c^{2/5} \cdot \left(\frac{l_b}{Ø}\right)^{3/5} \cdot 1.0 \cdot \left(1.1 \cdot \left(\frac{l_b}{s}\right)^{1/10} - 1\right)$
Units	SI	SI
σ_s^{st} [SI]	See above	See above
σ_s^{st} [SI]	$118 \cdot \sqrt{\frac{l_0 \cdot A_{st}}{s_t \cdot \phi^2}}$ For the IMB constellation $\frac{A_{st} \cdot l_b \cdot \sqrt{f_c}}{\phi^2 \cdot s \cdot n} \cdot 4.8$ (with f_c = 435 MPa)	For the IMB constellation $\frac{A_{tr} \cdot l_b \cdot \sqrt{f_c}}{\phi^2 \cdot s \cdot n} \cdot 6.4$ (with f_c = 435 MPa)
with	f_c and f_y in [MPa], f_c obtained in cube tests With $f_{yt} \leq 300$ MPa No other boundaries for transverse reinforcement σ_s^{st} is added to the concrete contribution σ_s^c for stirrups around one bar: $\alpha_{Q,m} = 6.0 \cdot \sqrt{2}$, $\alpha_{Q,d} = 3.2$ for stirrups around two bars: $\alpha_{Q,m} = 6.0$, $\alpha_{Q,d} = 2,3$ for straight transverse reinforcement outside the lap: $\alpha_{Q,m} = 1.8$, $\alpha_{Q,d} = 1,0$ for transverse reinforcement inside the lap: $\alpha_Q = 0$ A_s = area of one lapped bar $K = k_d \cdot k_q \cdot k_v$ $0.75 \leq k_d = 10/Ø \leq 1.0$ $k_q = 2 / (1+k_1)$ $k_1 = \min\sigma_e / \max\sigma_e \geq 0.6$ k_v = 1,0 for bond condition I $c_y = c_{vert}$ e_s = clear width of the crack plane per lap $e_s = 2\ c_x$ (bars with side effect) $\leq 8 \cdot c_y$ $e_s = 2\ e_l$ (bars without side effect) $\leq 3.4 \cdot c_y$ c_x = side cover e_l = half clear bar distance $2 \cdot e_l$ = clear bar distance	f_c and f_y in [MPa] $\alpha_3 = 1/(\ 1.1 \cdot (l_0 / s_t)^{1/10}\ )$ $c_x = c_{hori}$ $c_y = c_{vert}$ No factor for bar diameter No boundaries defined

	ACI 318 [ACI14]	ORANGUN [ORA77]
l_b	$\dfrac{3\cdot\sigma_s\cdot\phi}{40\cdot\sqrt{f_c}\cdot\left(\dfrac{c_{min}}{\phi}+\dfrac{40\cdot n_l\cdot A_{st}}{\phi\cdot s\cdot n}\right)}$	$\dfrac{\phi\cdot\left(\dfrac{\sigma_s}{4\cdot\sqrt{f_c}}-50\right)}{1{,}2+\dfrac{3\cdot c}{\phi}+\dfrac{n_l\cdot A_{st}\cdot f_{yt}}{500\cdot n\cdot s\cdot\phi}}$
σ_s	$\dfrac{40\cdot l_b}{3\cdot\phi}\cdot\sqrt{f_c}\cdot\left(\dfrac{c_{min}}{\phi}+\dfrac{40\cdot n_l\cdot A_{st}}{\phi\cdot s\cdot n}\right)$	$\left[1{,}2+\dfrac{3\cdot C}{\phi}+\dfrac{50\cdot\phi}{l_b}+\dfrac{n_l\cdot A_{st}\cdot f_{yt}}{500\cdot n\cdot s\cdot\phi}\right]\cdot\dfrac{4\cdot l_b\cdot\sqrt{f_c}}{\phi}$
σ_s^c	$\dfrac{40\cdot l_b}{3\cdot\phi}\cdot\sqrt{f_c}\cdot\dfrac{c_{min}}{\phi}$ With cover values to bar centres	$\left[1{,}2+\dfrac{3\cdot C}{\phi}+\dfrac{50\cdot\phi}{l_b}\right]\cdot\dfrac{4\cdot l_b\cdot\sqrt{f_c}}{\phi}$
σ_s^{st}	$\dfrac{40\cdot l_b}{3\cdot\phi}\cdot\sqrt{f_c}\cdot\dfrac{40\cdot n_l\cdot A_{st}}{\phi\cdot s\cdot n}$	$\dfrac{n_l\cdot A_{st}\cdot f_{yt}}{500\cdot n\cdot s\cdot\phi}\cdot\dfrac{4\cdot l_b\cdot\sqrt{f_c}}{\phi}$
units	$\dfrac{in.\cdot psi}{in.}\cdot\dfrac{in.^2}{in.^2}=psi$	$\dfrac{in.\cdot psi}{in.}\cdot\dfrac{in.^2\cdot psi}{in.^2}=psi^2$
σ_s^{st} [SI]	$\dfrac{40^2\cdot l_b}{3\cdot\phi}\cdot\sqrt{f_c}\cdot\dfrac{6.895\cdot n_l\cdot A_{tr}}{1000\cdot\phi\cdot s\cdot n}$	$\dfrac{n_l\cdot A_{st}\cdot f_{yt}}{500\cdot n\cdot s\cdot\phi}\cdot\dfrac{6.895\cdot 4\cdot l_b\cdot\sqrt{f_c}}{1000\cdot\phi}$
σ_s^{st} [SI]	$\dfrac{n_l\cdot A_{st}\cdot l_b\cdot\sqrt{f_c}}{\phi^2\cdot s\cdot n}\cdot 3.68$	$\dfrac{n_l\cdot A_{st}\cdot l_b\cdot\sqrt{f_c}}{\phi^2\cdot s\cdot n}\cdot 3.31$ (with f_{yt} = 60000)
with	A_{tr} is the total cross sectional area of all transverse reinforcement within the spacing s that crosses the potential plane of splitting through the reinforcement being developed f_c and f_y in [psi] $\dfrac{\phi}{c_{min}+K_{tr}}\geq\dfrac{1}{2.5}=0.4$ (For other values, pull-out failure is expected) ψ_s = 0.8 for d ≤ #6 ψ_s = 1.0 for other cases (c_b+K_{tr}) / Ø ≤ 2,5 C_{min} = min {c_x, c_y; $c_s/2$} The values c_x and c_y are the distances to the bar center c_s = center to center spacing c_{min} = 1/1/2 [in.] = 38 mm	$A_{tr}=\dfrac{A_{st}\cdot n_l}{n}$ A_{st} = cross sectional area of the single stirrup, n_l = number of legs and n = number of lapped bars, f_c and f_y in [psi] design model including f_{yt} c_b = c_y c_s = half clear spacing or half available concrete width per bar c = min {c_b, c_s} both values do not include half the bar diameter like ACI 318 does no reduction factor for bar diameter c/Ø ≤ 2.5 $K_{tr}=\dfrac{A_{tr}\cdot f_{yt}}{600\cdot s\cdot\phi}\leq 2.5$

	ZUO / DARWIN [ZUO00]	CANBAY / FROSCH [CAN06]
l_b		
σ_s	$\left[59.8\cdot l_b\cdot(c_{min}+0.5\cdot\phi)+2350\cdot A_s\right]$ $\cdot\left(0.1\frac{c_{max}}{c_{min}}+0.9\right)\cdot\frac{f_c^{1/4}}{A_s}$ $+\left(31.14\cdot\frac{N\cdot A_{st}}{n}+3.99\right)\cdot\frac{f_c^{3/4}}{A_s}$	
σ_s^c	$\left[59.8\cdot l_b\cdot(c_{min}+0.5\cdot\phi)+2350\cdot A_s\right]$ $\cdot\left(0.1\frac{c_{max}}{c_{min}}+0.9\right)\cdot\frac{f_c^{1/4}}{A_s}$	$\frac{388\cdot l_s^{1/2}\cdot f_c^{1/4}}{n\cdot\phi\cdot\tan\beta}\cdot\left(c_x^{1/2}+(n-1)\cdot\left(\frac{c_s}{2}\right)^{1/2}\right)$ (side) $\frac{388\cdot l_s^{1/2}\cdot f_c^{1/4}\cdot c_y^{1/2}}{n\cdot\phi\cdot\tan\beta}\cdot\left(0.1\cdot\frac{c_x}{c_y}+0.9+(n-1)\cdot\left(0.1\cdot\frac{c_s/2}{c_y}+0.9\right)\right)$ (face)
σ_s^{st}	$\left(31.14\cdot\frac{N\cdot A_{st}}{n}+3.99\right)\cdot\frac{f_c^{3/4}}{A_s}=$ $31.14\cdot\frac{l_b\cdot A_{st}}{s\cdot n}\cdot\frac{f_c^{3/4}}{A_s}$	$\frac{n_{st}\cdot n_1\cdot A_{st}\cdot f_{yt}\cdot n_s\cdot f_c^{1/2}}{n_s\cdot\tan\beta\cdot A_s\cdot 170}=\frac{n_1\cdot A_{st}\cdot f_{yt}\cdot l_b\cdot\sqrt{f_c}}{s\cdot 48\cdot\phi^2}$ (side) with $\beta = 20°$ $\frac{n_{st}\cdot A_{st}\cdot f_{yt}\cdot n_s\cdot f_c^{1/2}}{n_s\cdot\tan\beta\cdot A_s\cdot 170}=\frac{A_{st}\cdot f_{yt}\cdot l_b\cdot\sqrt{f_c}}{s\cdot 48\cdot\phi^2}$ (face), this equ. included n_s
units	$\frac{in.\cdot psi}{in.}\cdot\frac{in.^2}{in.^2}=psi$	$\frac{in.\cdot psi}{in.}\cdot\frac{in.^2\cdot psi}{in.^2}=psi^2$
σ_s^{st} [SI]	$31.14\cdot\frac{l_b\cdot A_{st}}{s\cdot n}\cdot\frac{f_c^{3/4}}{A_s}\cdot\frac{6.895}{1000}$	$\frac{n_1\cdot A_{st}\cdot f_{yt}\cdot l_b\cdot\sqrt{f_c}}{s\cdot 48\cdot\phi^2}\cdot\frac{6.895}{1000}$ (side) $\frac{A_{st}\cdot f_{yt}\cdot l_b\cdot\sqrt{f_c}}{s\cdot 48\cdot\phi^2}\cdot\frac{6.895}{1000}$ (face)
σ_s^{st} [SI]	$\frac{A_{st}\cdot l_b\cdot\sqrt{f_c}}{\phi^2\cdot s\cdot n}\cdot 2.22$ (mit $f_c^{3/4}$ / $f_c^{1/2}$ = 8.1)	$\frac{n_1\cdot A_{st}\cdot l_b\cdot\sqrt{f_c}}{\phi^2\cdot s\cdot n}\cdot 1.29$ (mit f_{yt} = 9000 and n = 3)
with	With N = number of stirrups = l_b/s A_{st} = cross sectional area of the single stirrup n = number of lapped bars f_c and f_y in [psi] the f_c exponent remains unclear t_d = coefficient for the effect of bar diameter $t_d = 0.03\cdot\phi+0.22$ [SI] c = (c_{min} + 0.5·Ø)·(0.1c_{max} / c_{min} + 0.9) c_s = min (c_{si}+0,25in.; c_{so}) c_{si} = clear spacing divided by 2 = c_s c_{so} = side cover = c_x c_b = bottom cover = c_y c_{min}, c_{max} = minimum or maximum value of c_s or c_b c_{max} / c_{min} ≤ 3.5 (c+K_{tr}) / Ø ≤ 4.0	f_c and f_y in [psi] Design model including f_y Mote: $f_{yt,m}$ = 9000 psi = 62 MPa only. This is a mean value along the splice. The factor $\frac{n\cdot\sqrt{f_c}}{170}$ may be omitted The factor equals 1.0 for n=3 and f_c = 22 MPa With n_l No factor for bar diameter c_b is the bottom cover (c_y) c_{so} is the side cover (c_x) c_{si} is half the bar spacing (c_s/2 in fib notation) Canbay and Frosch have two publications. In one (2005) they give effective covers: $c_i^* = c_i\cdot 0{,}77/\sqrt{(c_i/d)}$ where i stands for b, so and si. Other boundaries were not found. In the 2006 publication they give weighted cover dimensions with: $c_s = (2\cdot c_{s0}+2\cdot(n-1)c_{si}\ /\ (2\cdot n)$ that's the mean concrete cover for each lap or anchored bar. Canbay investigated bars from 9.5 to 35.8 mm, larger diameters than 35.8 mm were not considered as laps are not permitted according to ACI 318-05 (12.14.2.1)

A.2. Additional Information on Experimental Programme

A.2.1. Material

Table A 1 Mean concrete properties of the lap tests

Test	Mean cylinder strength f_{cm}	Mean cube strength $f_{cm,cube}$	Splitting tensile strength $f_{ct,spalt}$	Mean cube strength 28d $f_{cm,cube,28d}$	Young's modulus E_{cm}
	[MPa]	[MPa]	[MPa]	[MPa]	[MPa]
T1	40.2	44.4	2.8	48.2	27041
T2	32.5	39.6	3.1	41.4	25008
T3	33.0	41.5	2.8	45.3	25328
T4	54.8	74.9	3.8	78.3	28890
T5	34.6	40.4	2.7	47.9	25819
T6	39.2	46.0	-	48.8	25718
T7	34.5	43.6	3.1	49.7	24377
T8	36.8	43.6	3.2	50.4	25850
T9	37.6	49.5	3.1	47.8	25275
T10	40.8	46.6	3.4	48.2	24473
T11	37.3	43.4	2.9	44.1	24201
T12	33.6	36.8	2.8	47.1	24632
T13	32.5	37.8	2.7	45.6	24137
T15	38.4	43.2	2.8	46.8	23133
T16	34.4	43.9	2.8	47.6	24611
T17	38.3	45.1	3.2	46.2	25041
T18	39.6	45.0	3.0	44.4	24717

Table A 2 Mean concrete properties of the beam end tests

Test	Mean cylinder strength f_{cm}	Mean cube strength $f_{cm,cube}$	Splitting tensile strength $f_{ct,spalt}$	Mean cube strength 28d $f_{cm,cube,28d}$	Young's modulus E_{cm}
	[MPa]	[MPa]	[MPa]	[MPa]	[MPa]
BET-1(1+2)	29.4	36.5	2.5	41.6	24829
BET-1(3+4)	26.4	29.3	2.7	39.6	21675
BET-2	55.4	70.3	3.7	71.9	30525
BET-3	104.0	116.4	-	139.3	37388
BET-4(1+2)	28.6	34.0	2.5	42.4	23543
BET-4(3+4)	32.5	39.6	3.1	41.4	25008
BET-5(1+2)	29.7	35.7	2.8	42.4	24383
BET-5 (3)	32.5	36.5	3.1	41.4	25008
BET-6	29.9	35.9	2.9	42.4	24539
BET-7	32.0	37.3	2.7	41.8	24663
BET-8	34.3	40.8	2.7	42.2	24936
BET-9	38.2	43.0	3.2	48.2	25296
BET-10 (1+2)	33.5	36.4	3.1	43.7	24052
BET-10 (3+4)	36.9	41.8	2.9	48.8	25792
BET-11	37.3	42.9	2.8	48.8	24378
BET-12	29.5	34.7	2.8	44.0	24540
BET-13	30.5	35.4	2.7	44.0	20912
BET-14	50.5	63.1	4.1	59.1	27193
BET-15	50.4	632.7	4.1	59.1	28315
BET-16	31.1	36.8	2.6	47.1	24173
BET-17	31.1	36.8	2.6	47.1	24173
BET-18	50.5	63.1	4.1	59.1	27193
BET-19	50.5	63.1	4.1	59.1	27193
BET-20	37.7	44.1	3.0	46.8	22877
BET-21	37.7	44.1	3.0	46.8	22877
BET-22	50.4	62.7	4.0	59.1	28315

Table A 3 Mean concrete properties of the anchorage tests

Test	Mean cylinder strength f_{cm}	Mean cube strength $f_{cm,cube}$	Splitting tensile strength $f_{ct,spalt}$	Mean cube strength 28d $f_{cm,cube,28d}$	Young's modulus E_{cm}
	[MPa]	[MPa]	[MPa]	[MPa]	[MPa]
V1-1	38.3	44.2	3.2	-	24641
V1-2	39.8	45.0	3.6	-	24399
V2-1	-	73.6	3.7	85.8	-
V2-2	60.4	74.5	4.1	85.8	31233
V3-1	35.2	39.1	3.0	45.1	23277
V3-2	35.2	39.3	-	45.1	-
V4-1	34.2	38.8	3.1	45.7	23694
V4-2	34.6	39.7	3.1	45.7	23495
V5-1	37.0	42.5	2.7	44.7	23820
V5-2	37.0	40.0	3.2	44.7	23909
V6-1	31.9	35.5	3.0	42.3	22225
V6-2	32.0	37.3	3.1	42.3	22487

Table A 4 Relative rib area of the tested reinforcing bars

Rolling Mill	Measurement	Bar diameter	Relative rib area f_R
-	-	10 mm	0.052
Hennigsdorfer Elektrostahlwerke	-	20 mm	0.056
Stahlwerk Annahütte	ibac	40 mm	0.064
Stahlwerk Annahütte	ibac	50 mm	0.067
Badische Stahlwerke	Rolling mill	40 mm	0.079

Table A 5 Steel properties of the tested reinforcing bars

Bar	Area A_s	Yield strength	Tensile strength	Tensile strength/ yield strength	Young's Modulus
[mm]	[mm²]	[MPa]	[MPa]	[-]	[MPa]
10	80	535	637	1.19	206446
20	314	570	661	1.16	195267
40	1257	572	690	1.21	201170
50	1964	540	627	1.16	196430
40 (BSW)	1257	583	694	1.19	-

A.2.2. Beam-End Tests: Reinforcement and Instrumentation

A.2.2.1. BET-1, BET-13 and BET-2

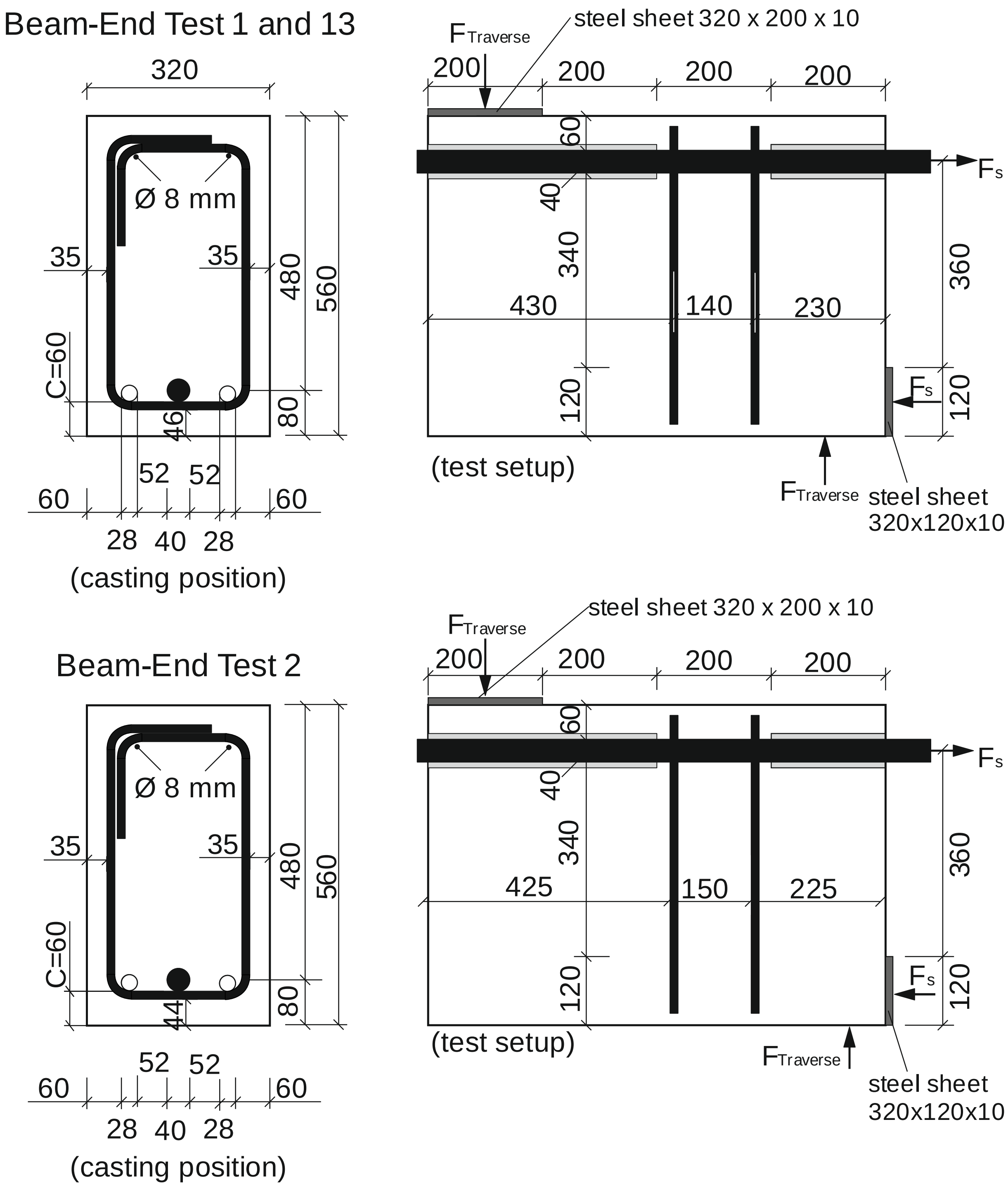

Figure A 1 Reinforcement layout of Beam-End Tests 1, 13 and 2

A.2.2.2. BET-3 and BET-4

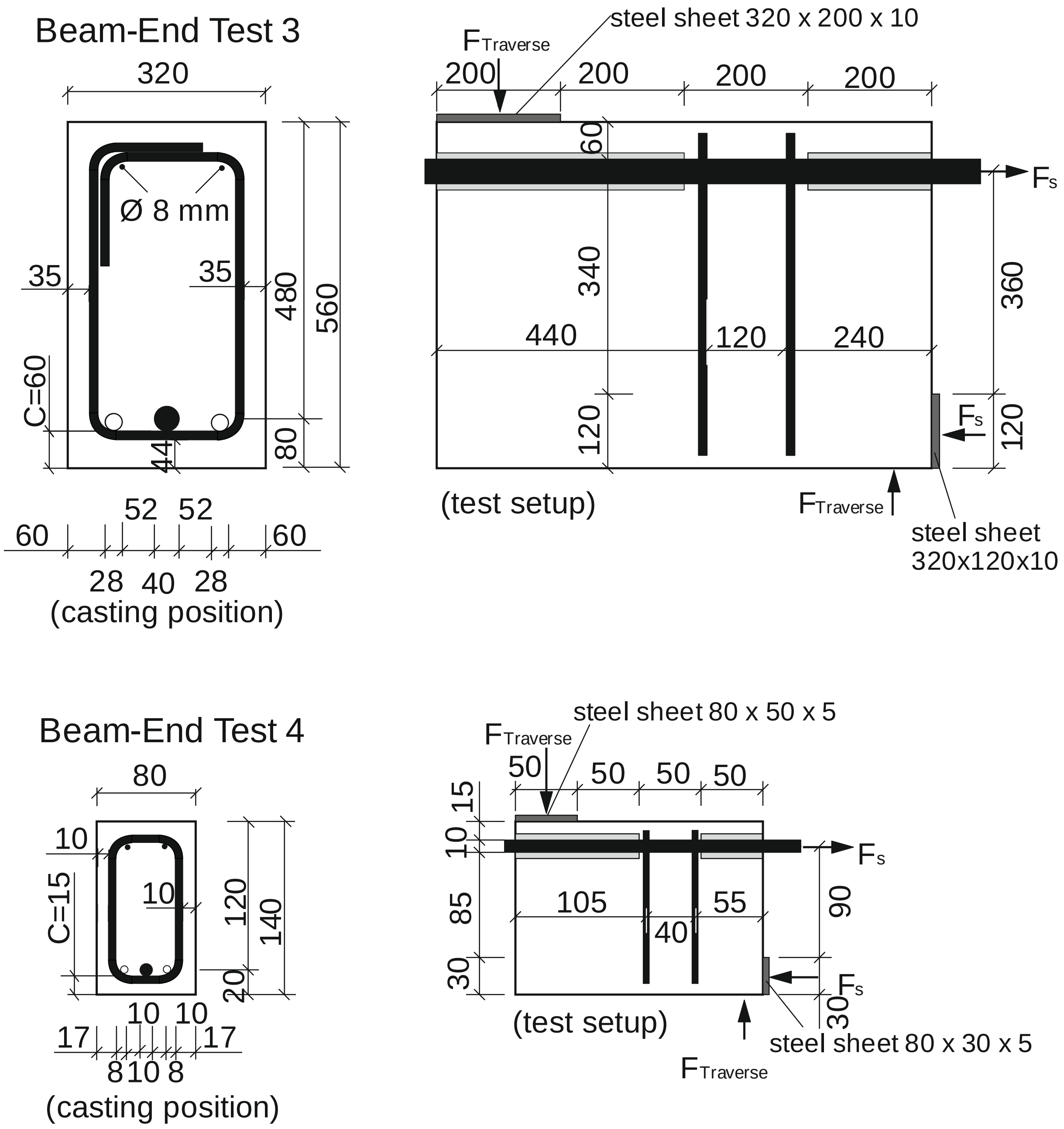

Figure A 2 Reinforcement layout of Beam-End Tests 3 and 4

A.2.2.3. BET-5 and BET-6

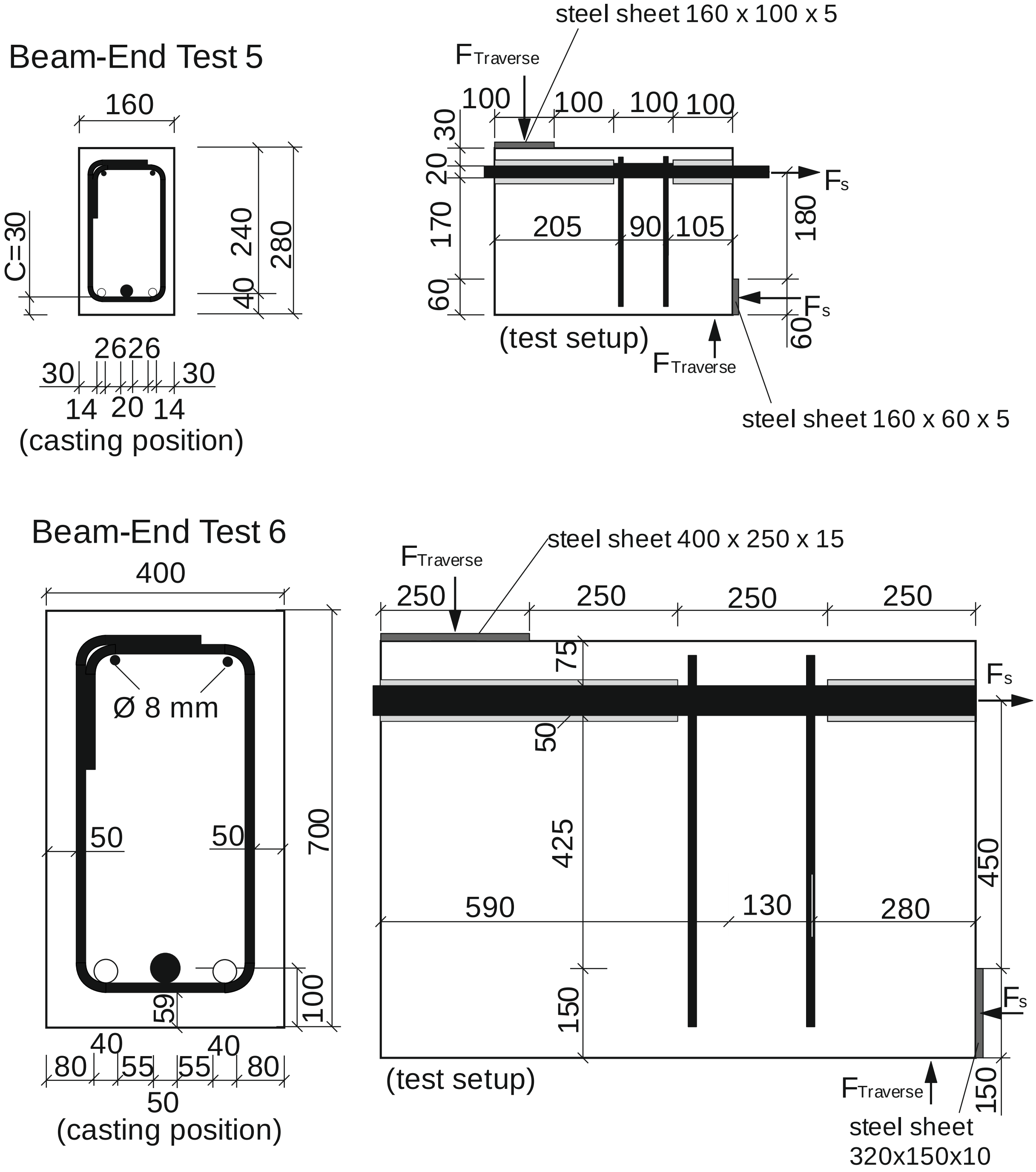

Figure A 3 Reinforcement layout of Beam-End Tests 5 and 6

A.2.2.4. BET-7 and BET-8

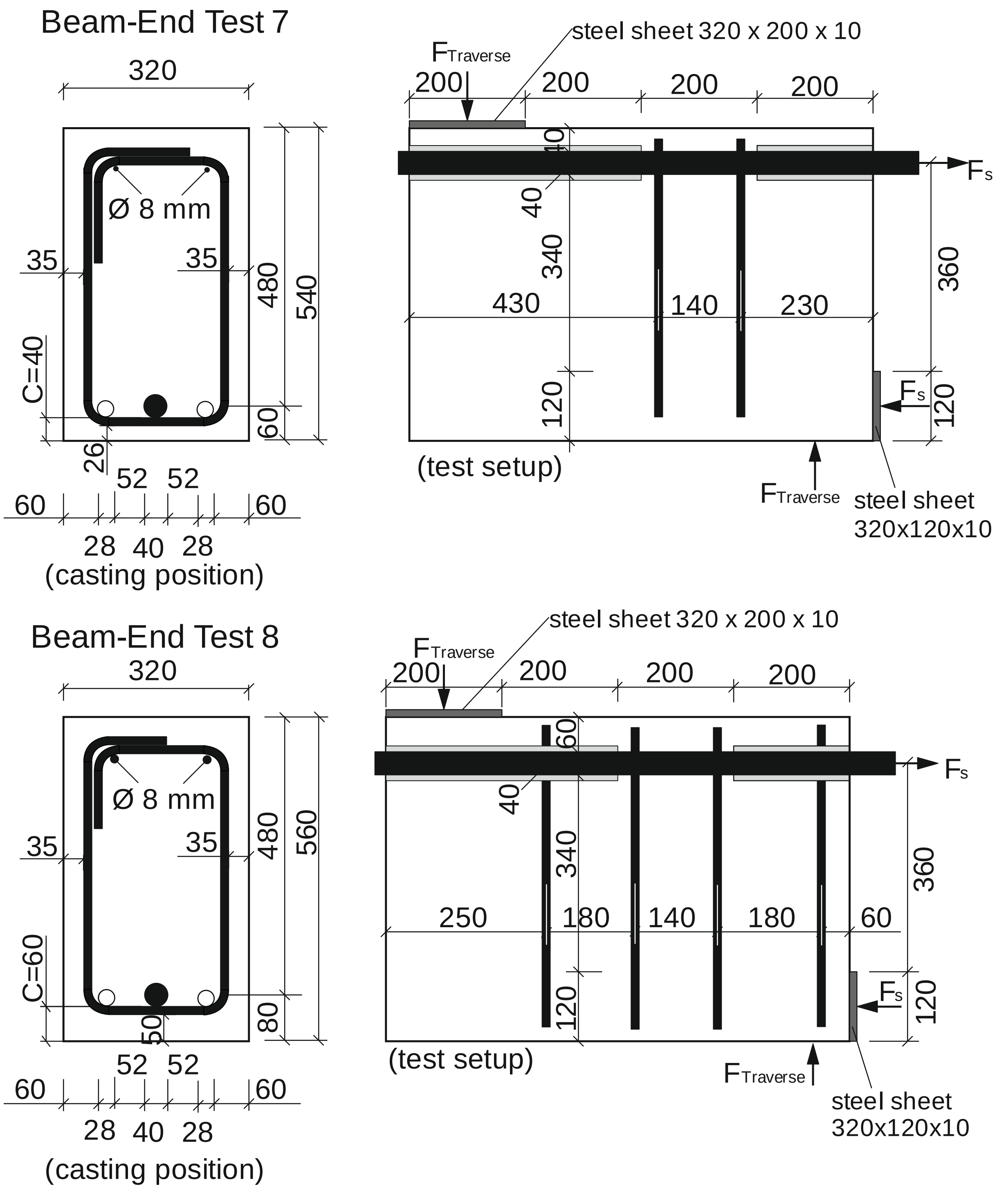

Figure A 4 Reinforcement layout of Beam-End Tests 7 and 8

A.2.2.5. BET-9 and BET-10

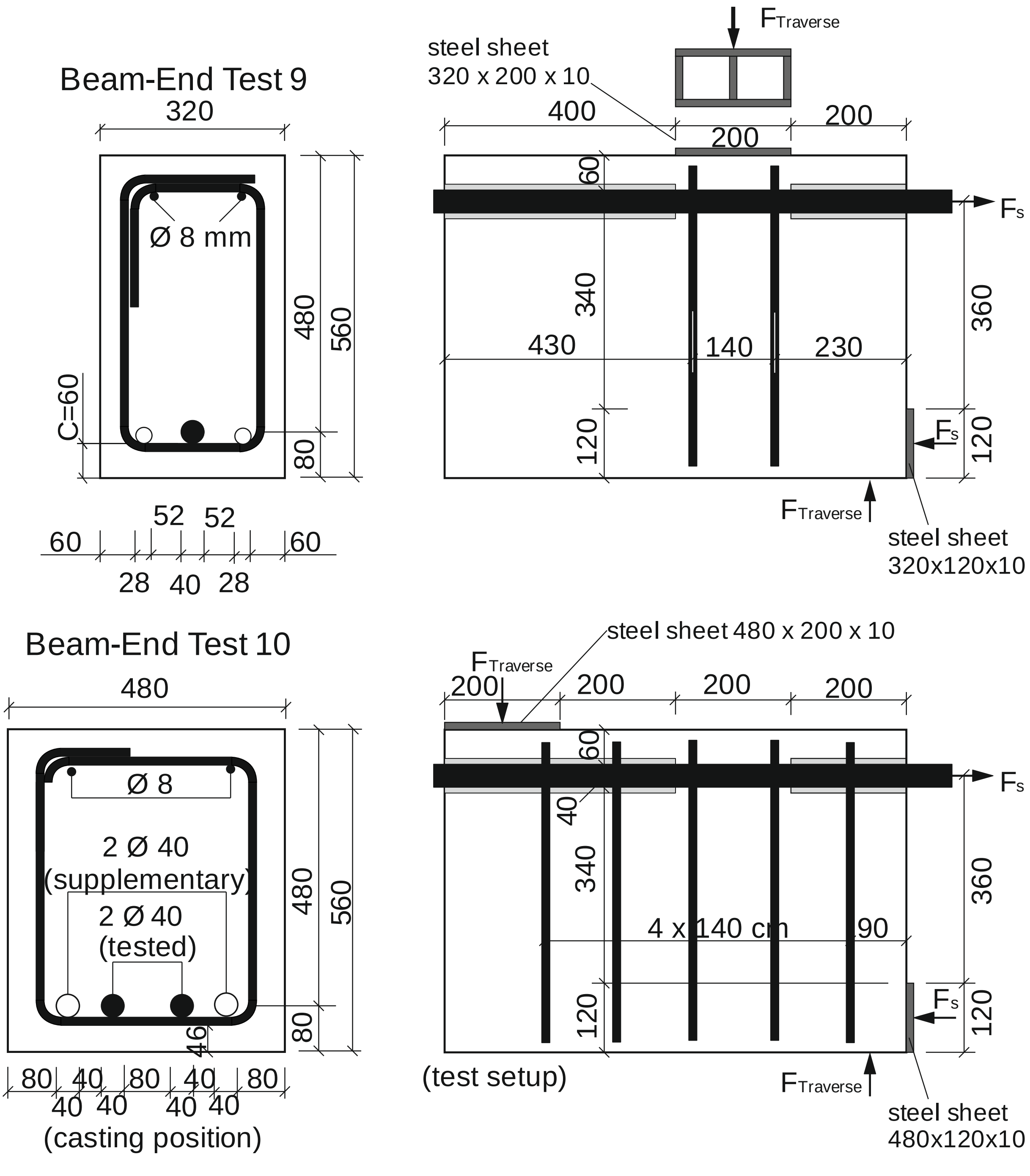

Figure A 5 Reinforcement layout of Beam-End Tests 9 and 10

A.2.2.6. BET-11 and BET-12

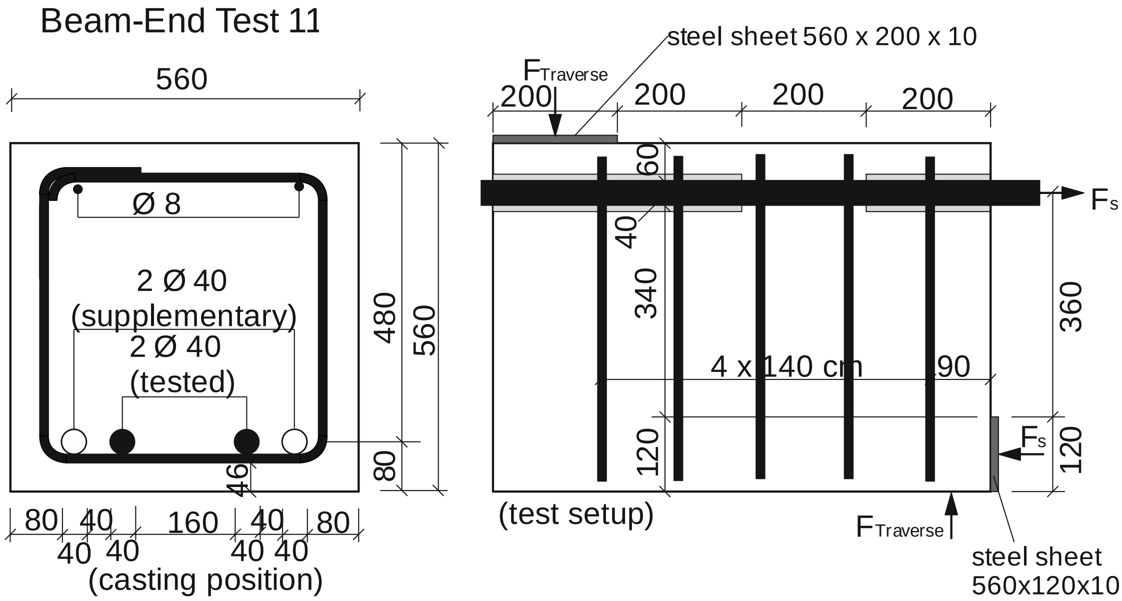

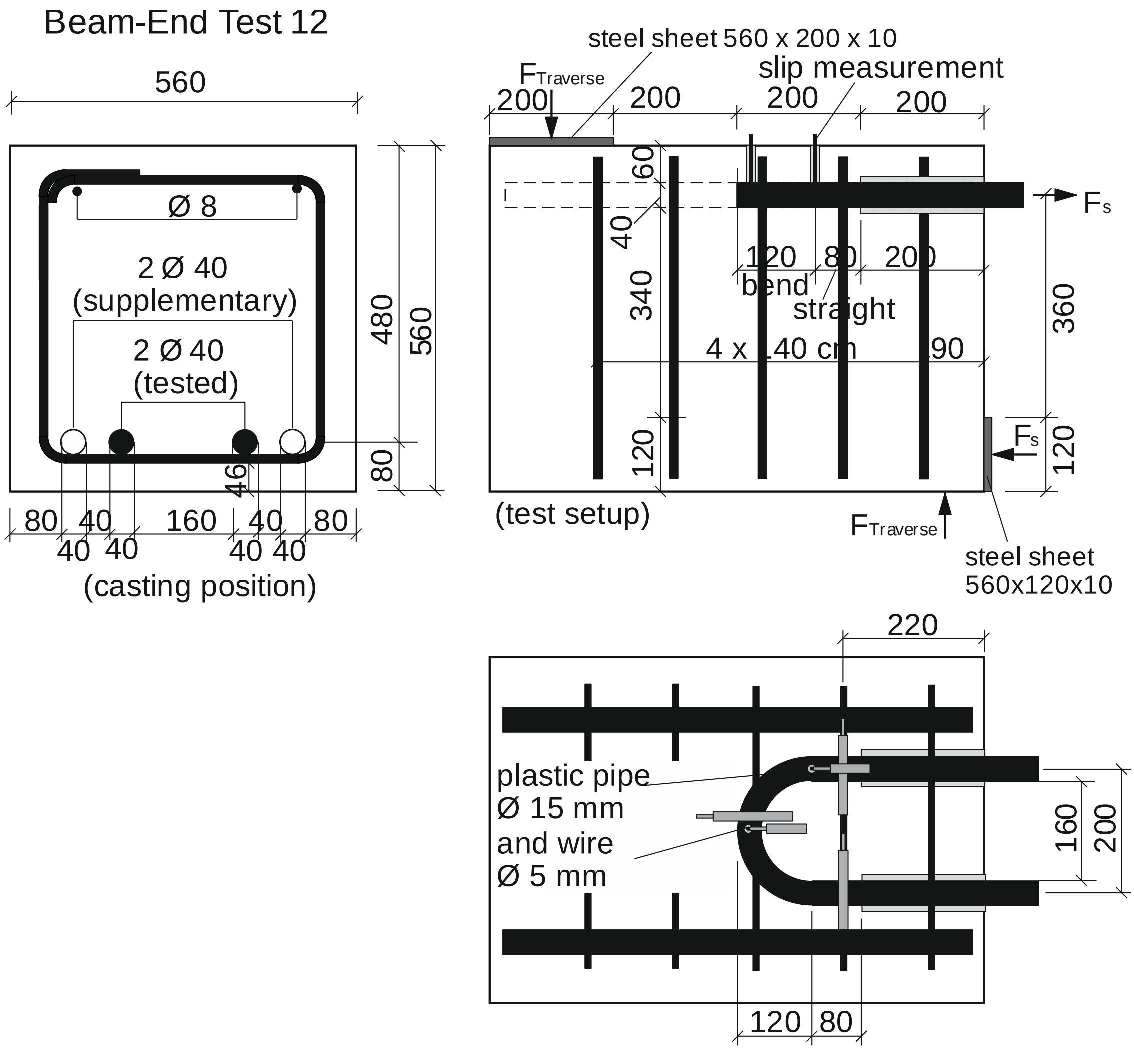

Figure A 6 Reinforcement layout of Beam-End Tests 11 and 12

A.2.2.7. BET-14 and BET-15

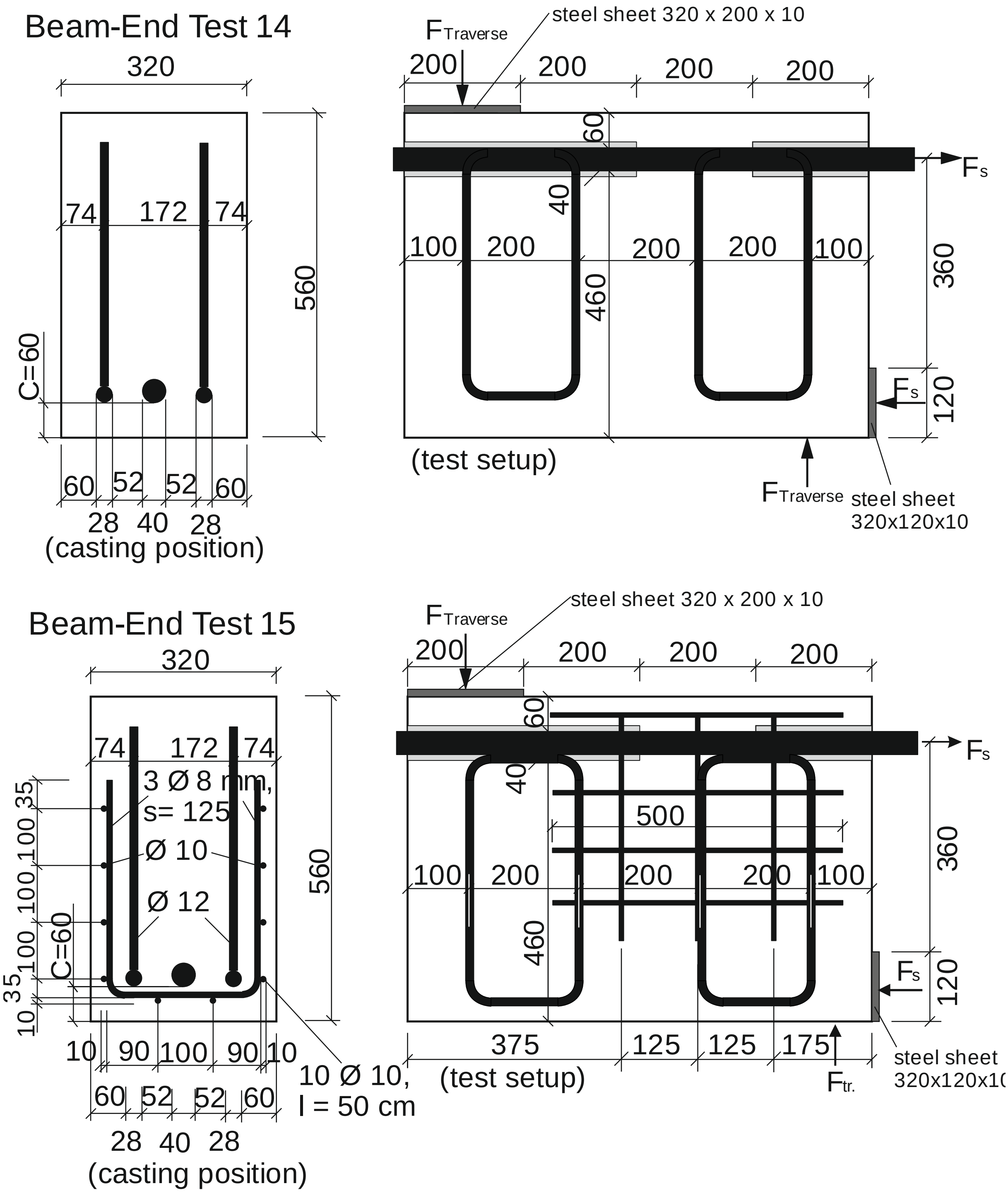

Figure A 7 Reinforcement layout of Beam-End Tests 14 and 15

A.2.2.8. BET-16

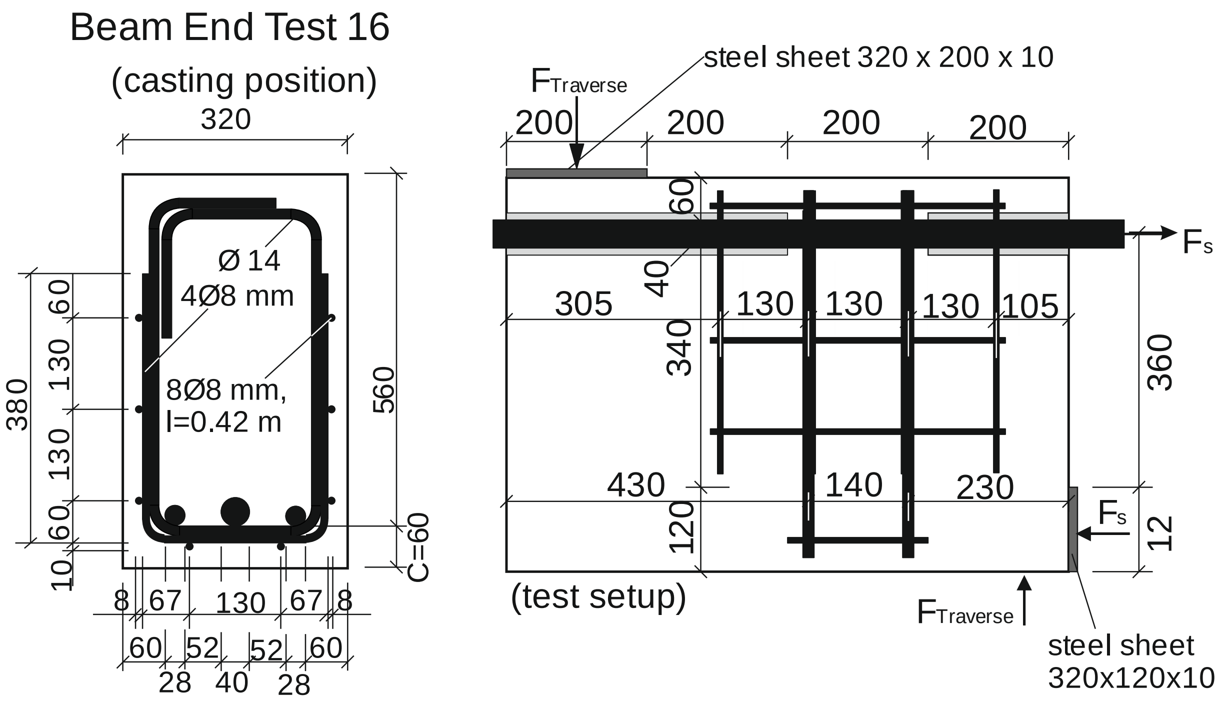

Figure A 8 Reinforcement layout of Beam-End Tests 16

A.2.2.9. BET-17 and BET-18

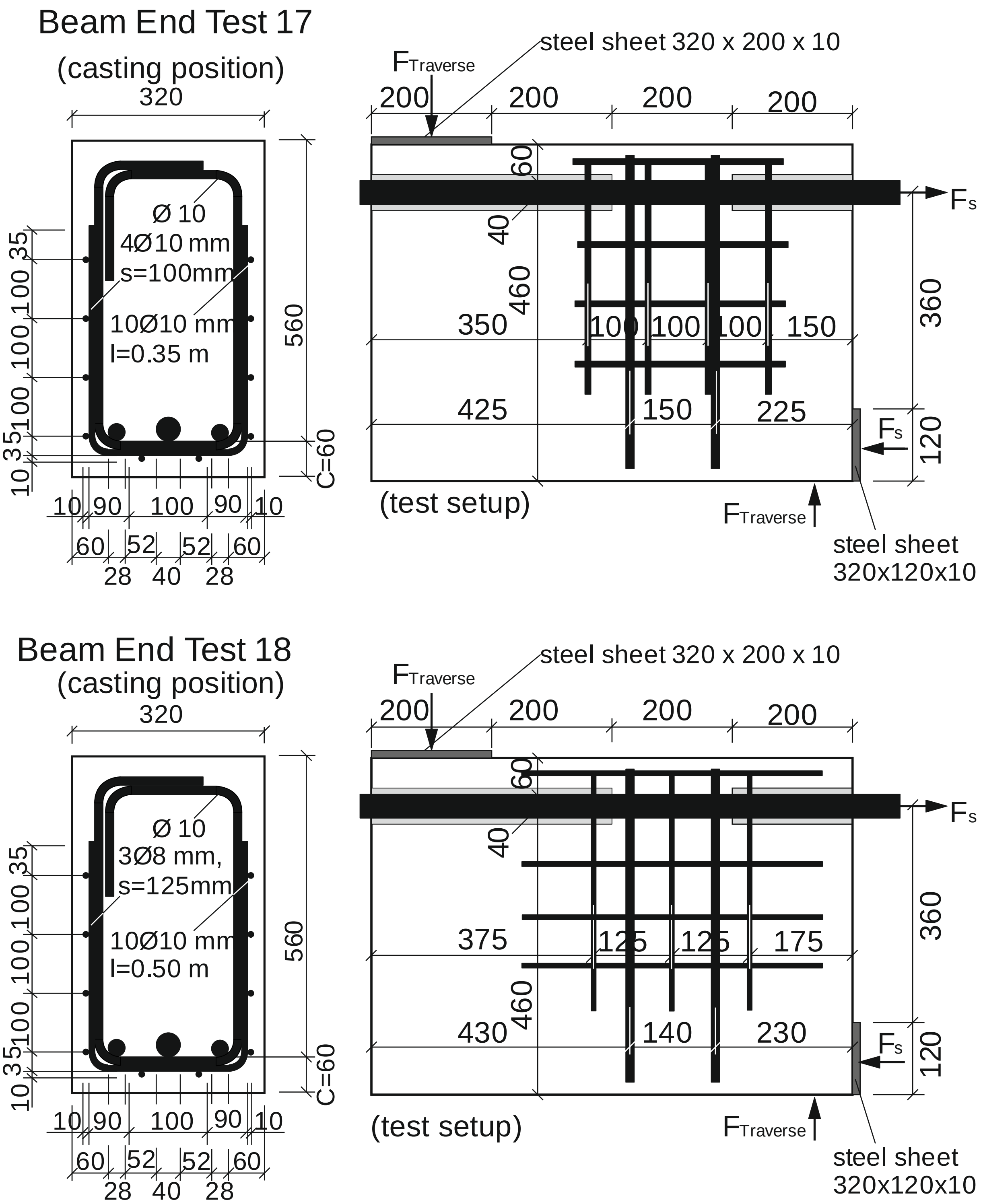

Figure A 9 Reinforcement layout of Beam-End Tests 17 and 18

A.2.2.10. BET-19 and BET-20

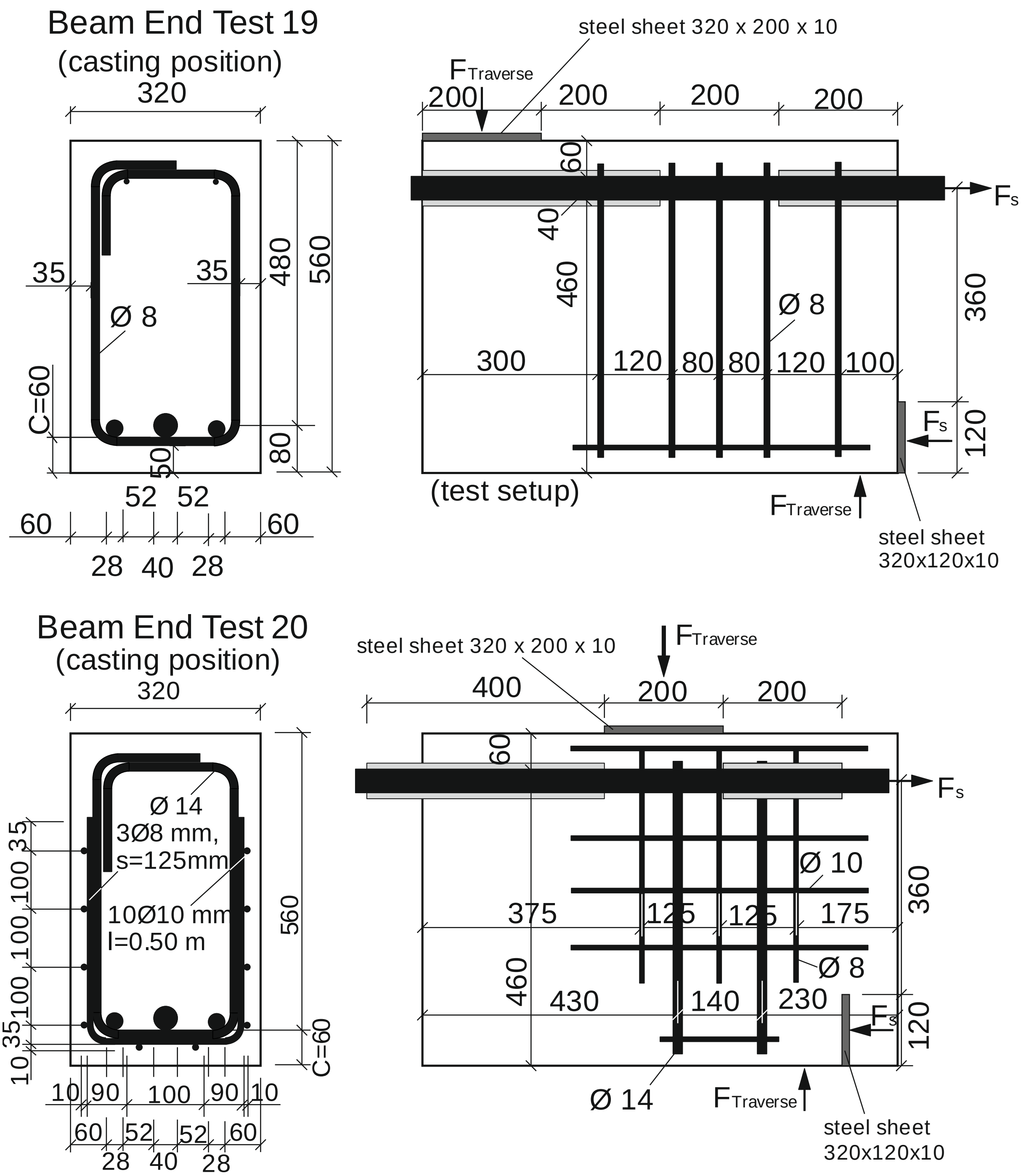

Figure A 10 Reinforcement layout of Beam-End Tests 19 and 20

A.2.2.11. BET-21 and BET-22

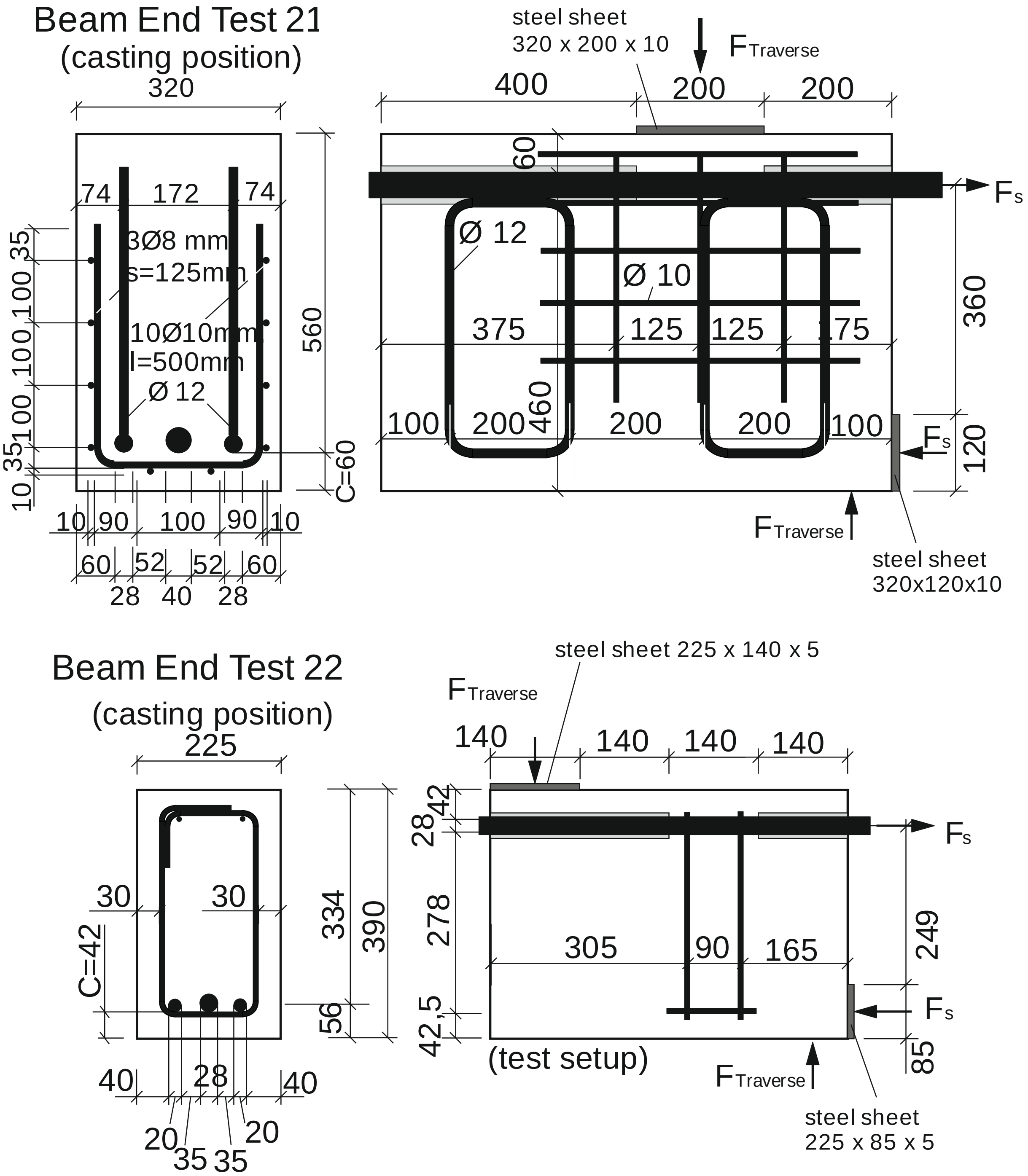

Figure A 11 Reinforcement layout of Beam-End Tests 21 and 22

A.2.2.12. Instrumentation of Beam-End Tests

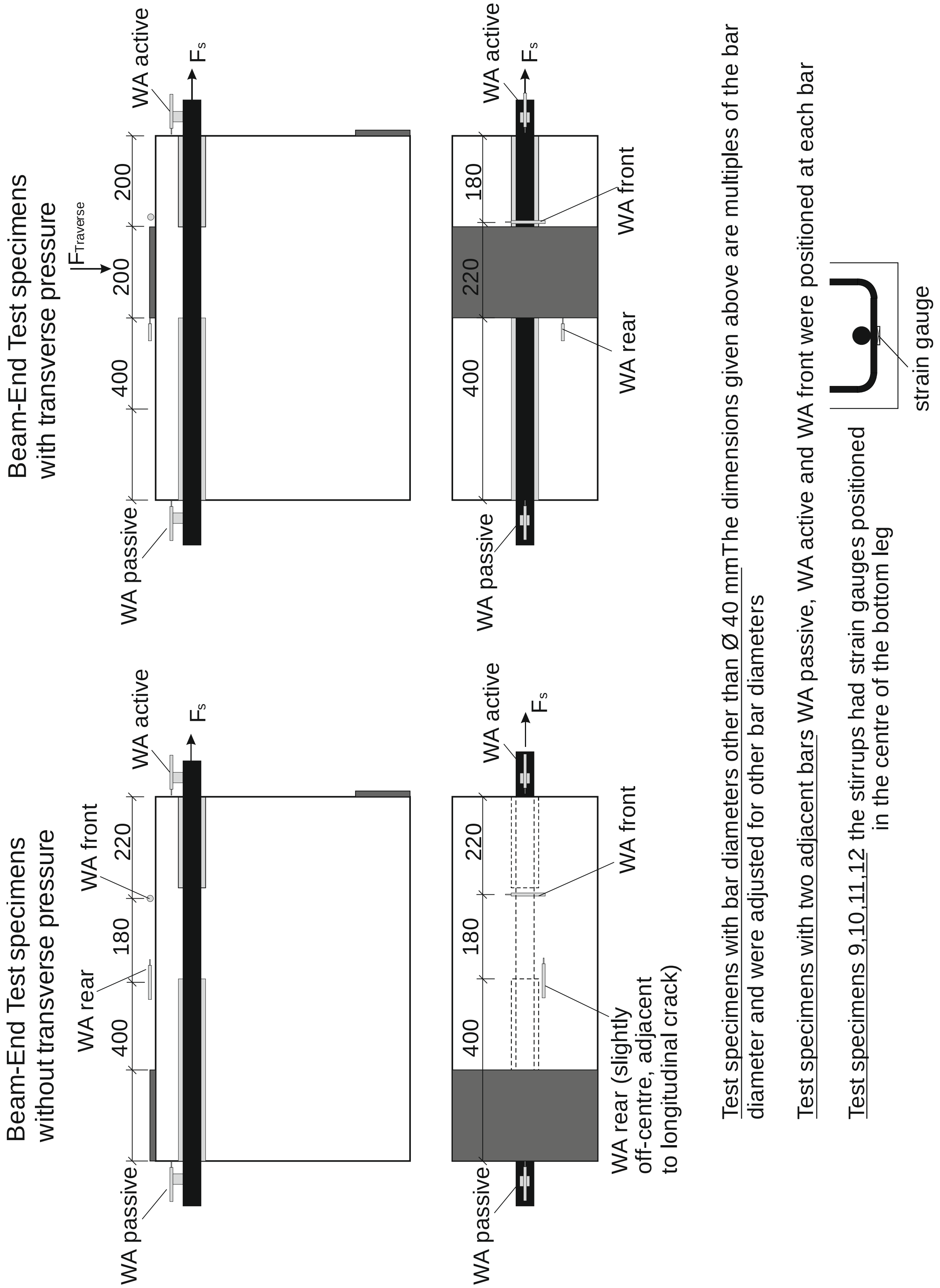

A.2.3. Lap Tests: Reinforcement and Instrumentation

A.2.3.1. Lap Test T1

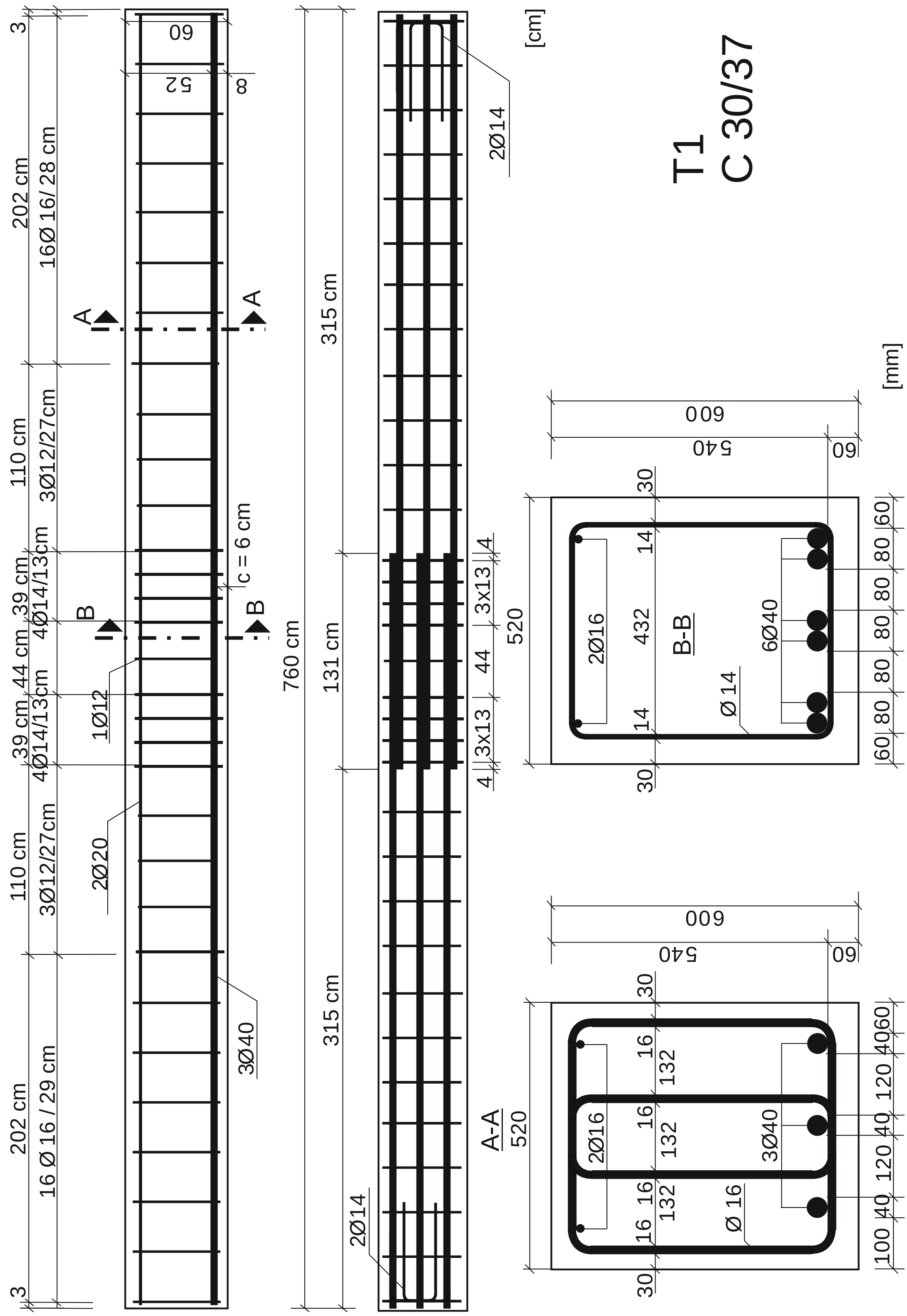

Figure A 12 Reinforcement layout lap test T1

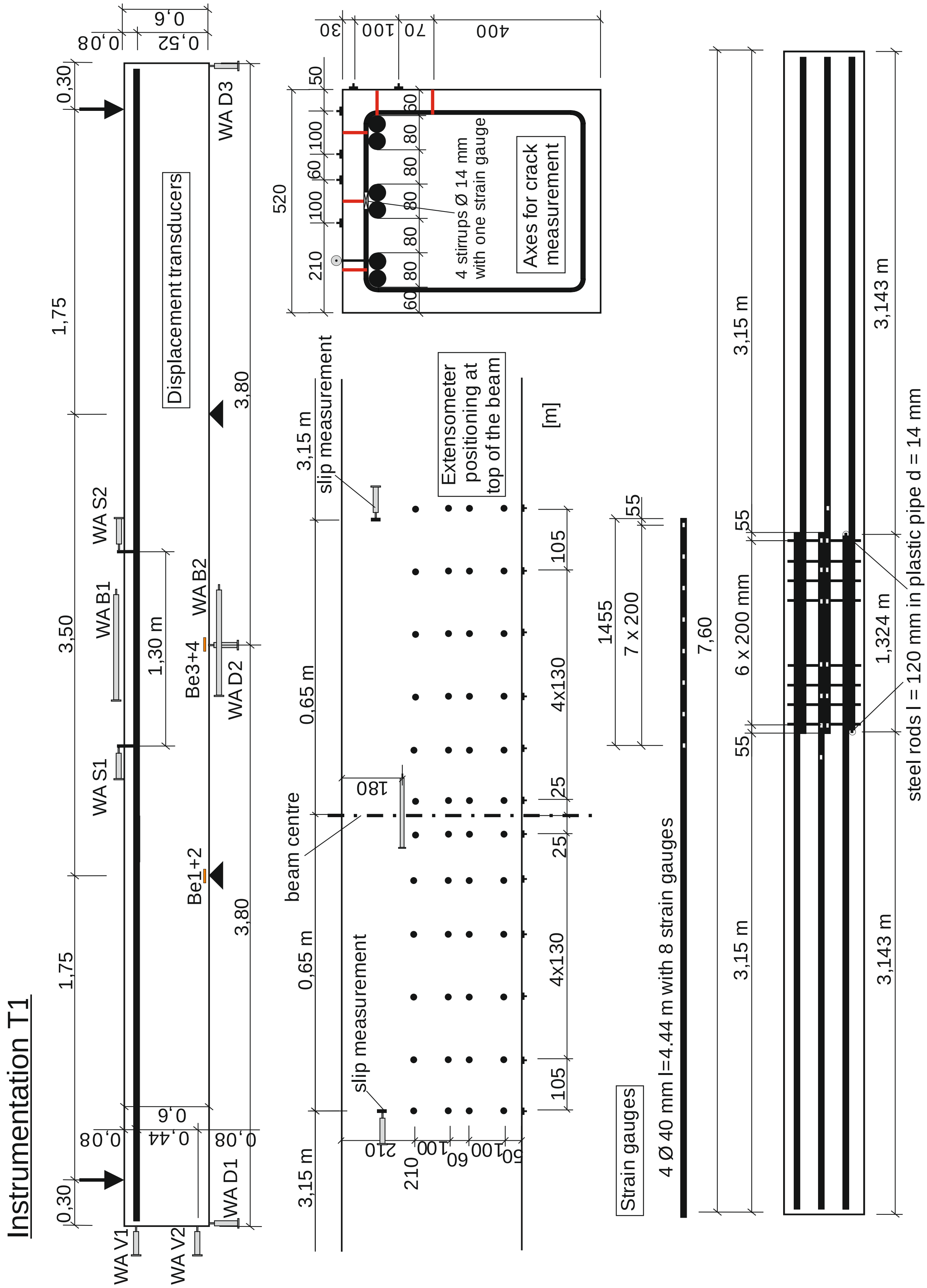

Figure A 13 Instrumentation lap test T1

A.2.3.2. Lap Test T2

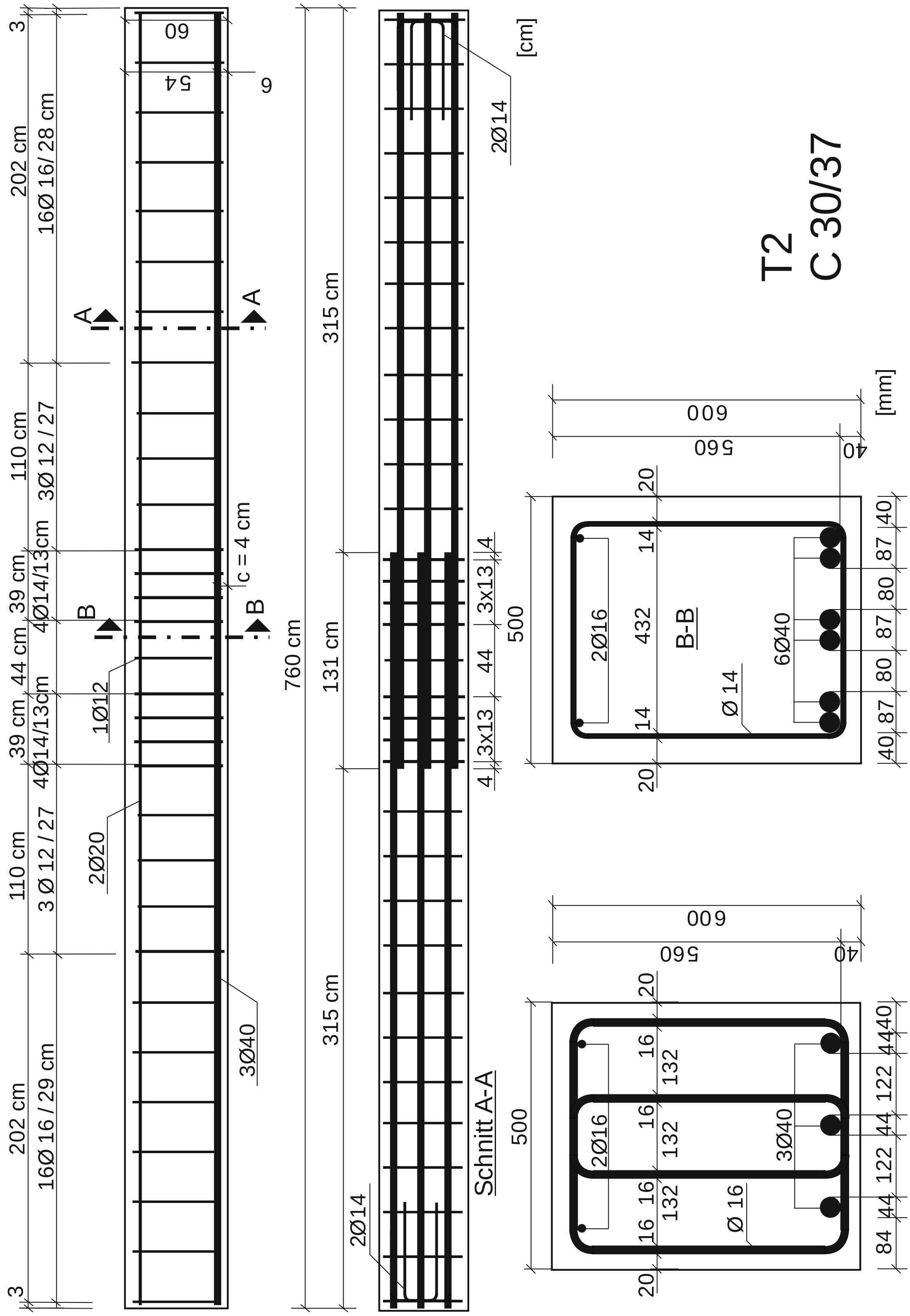

Figure A 14 Reinforcement layout lap test T2

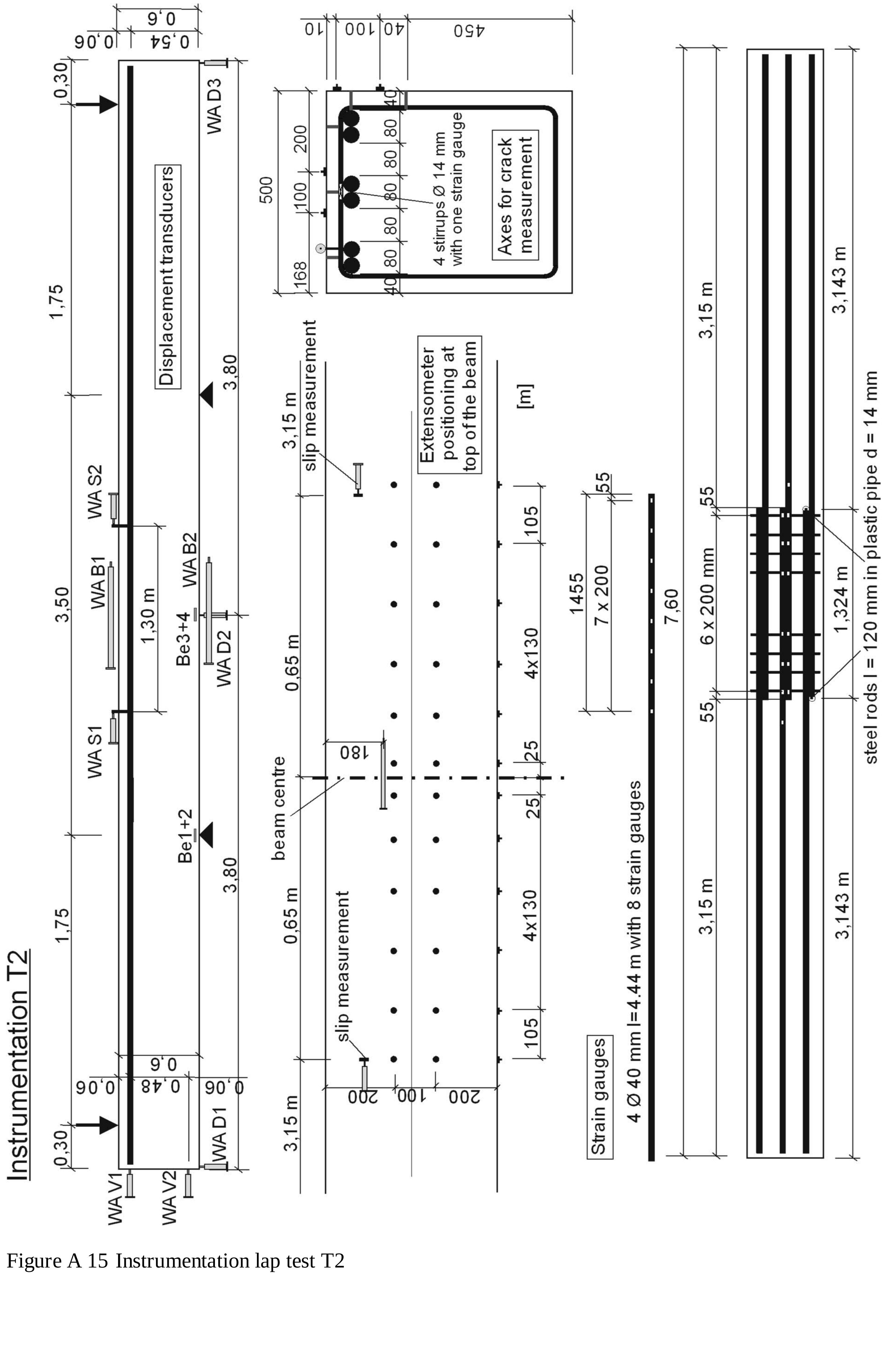

Figure A 15 Instrumentation lap test T2

A.2.3.3. Lap Test T3

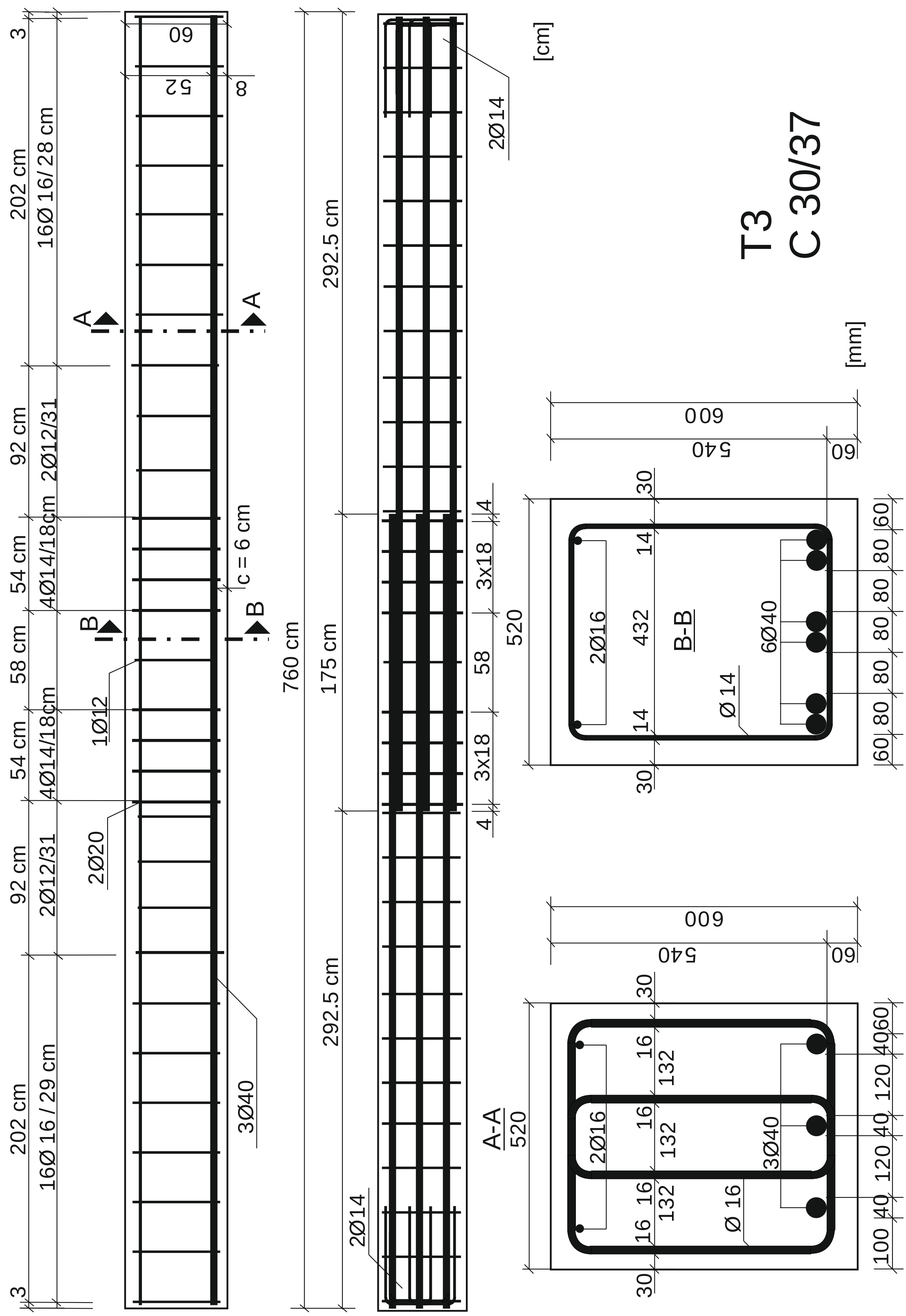

Figure A 16 Reinforcement layout lap test T3

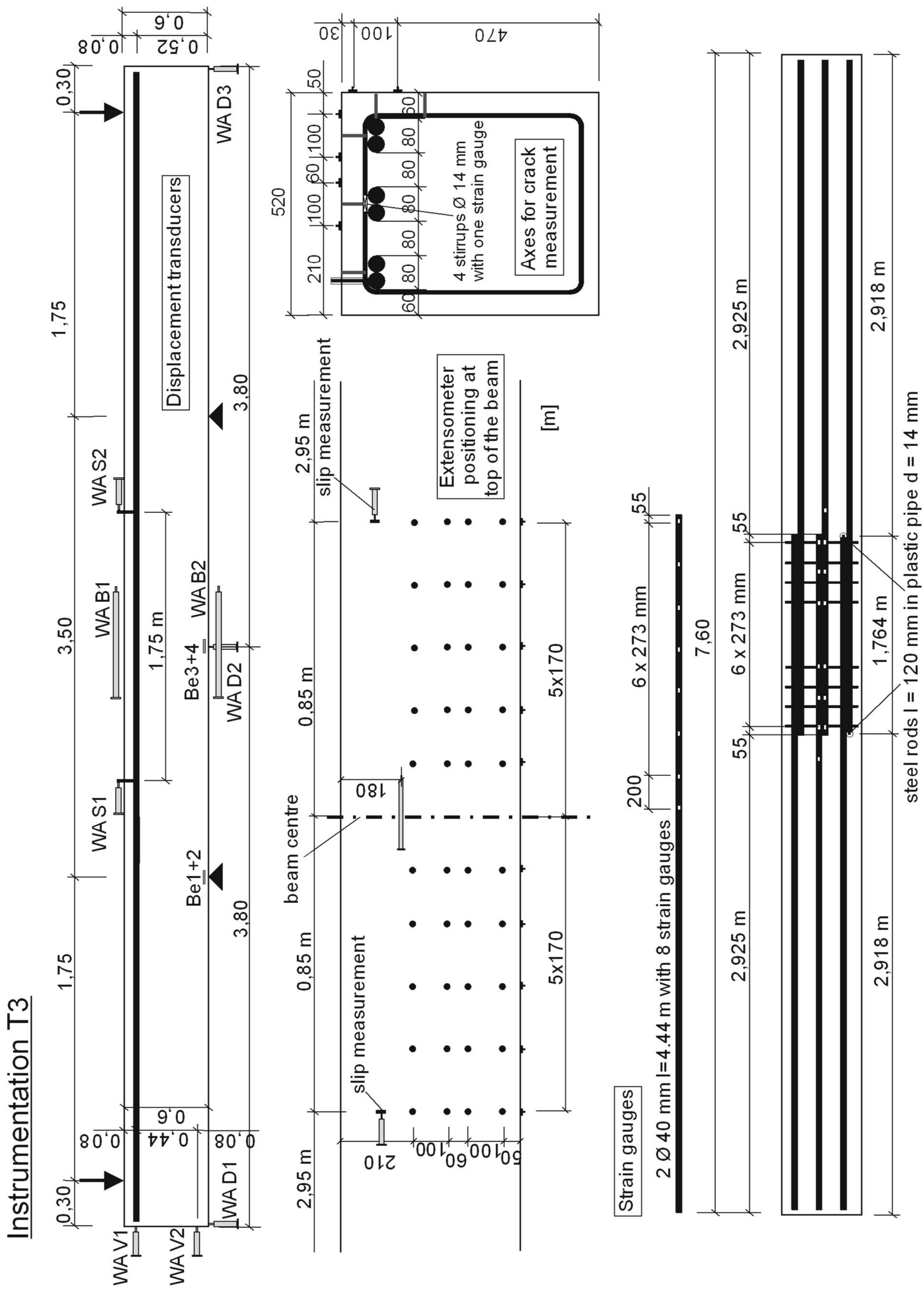

Figure A 17 Instrumentation lap test T3

A.2.3.4. Lap Test T4

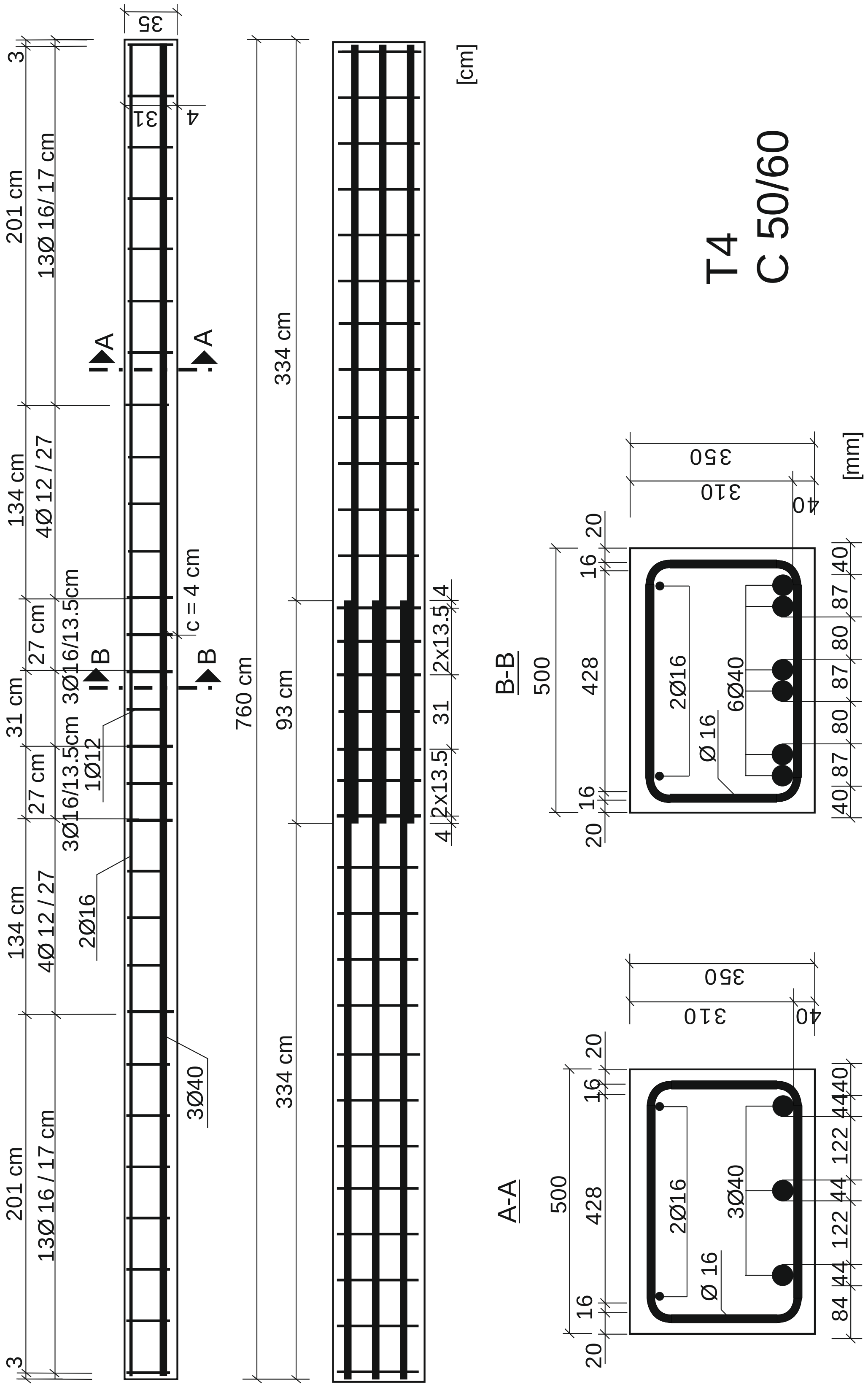

Figure A 18 Reinforcement layout lap test T4

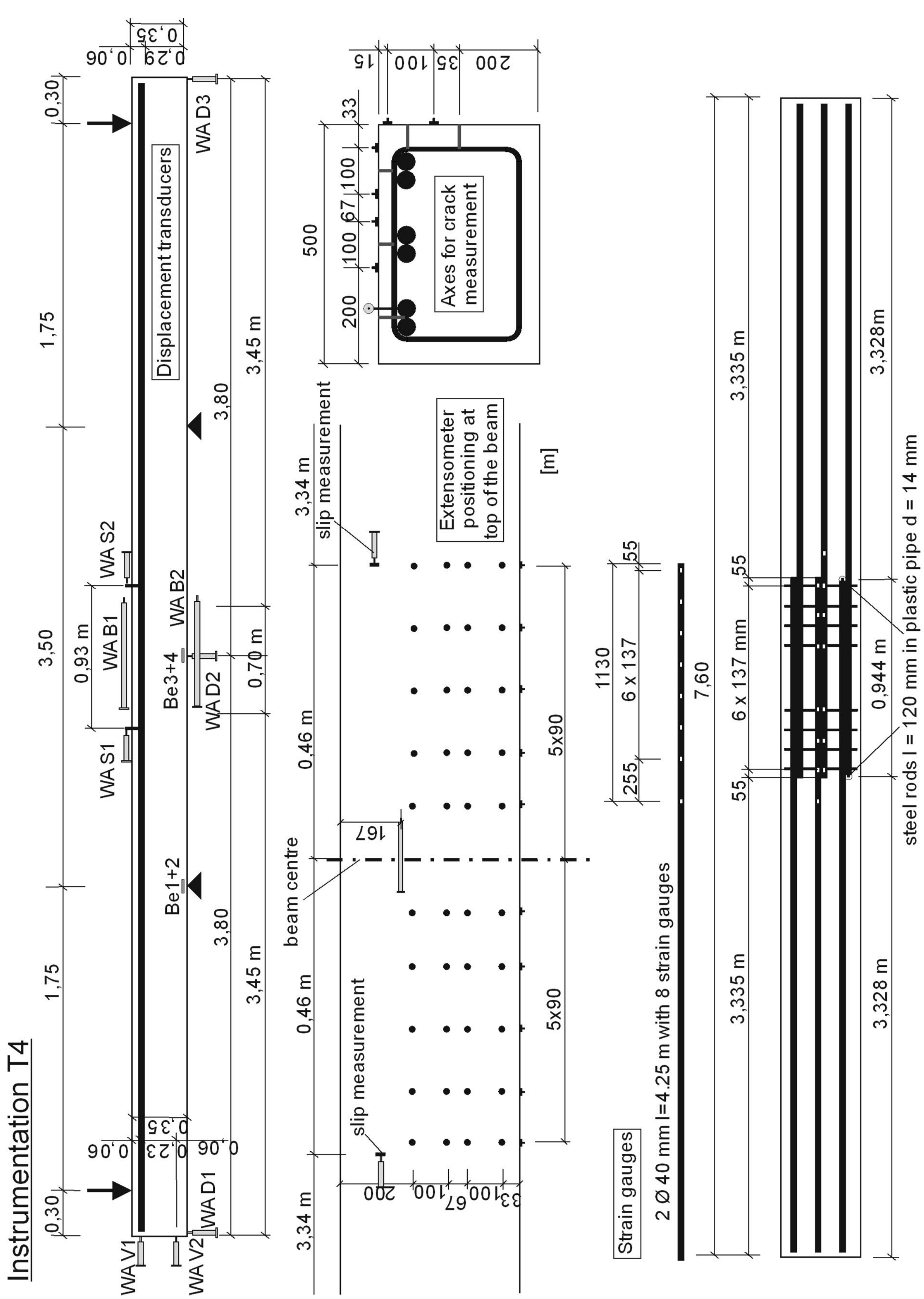

Figure A 19 Instrumentation lap test T4

A.2.3.5. Lap Test T5

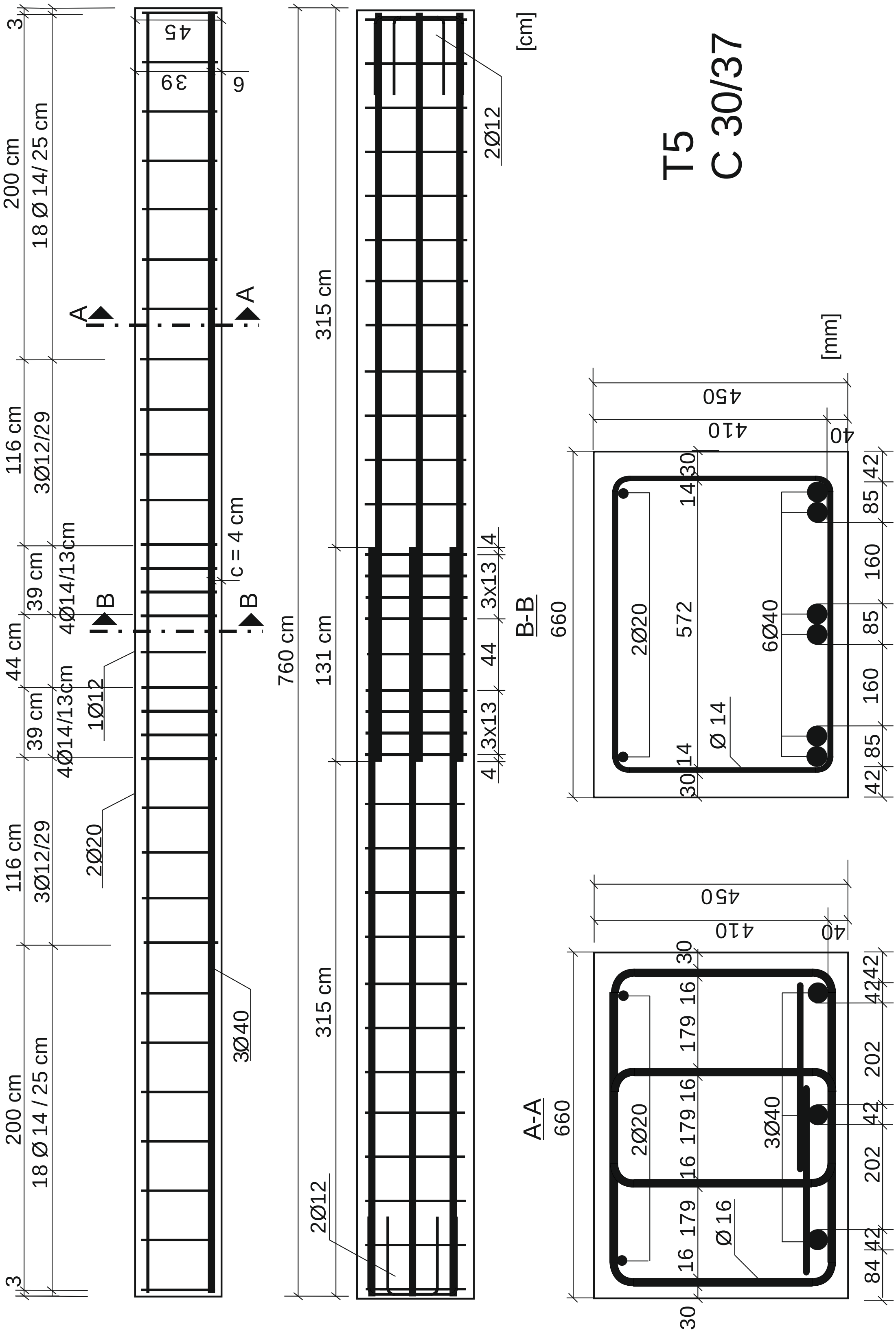

Figure A 20 Reinforcement layout lap test T5

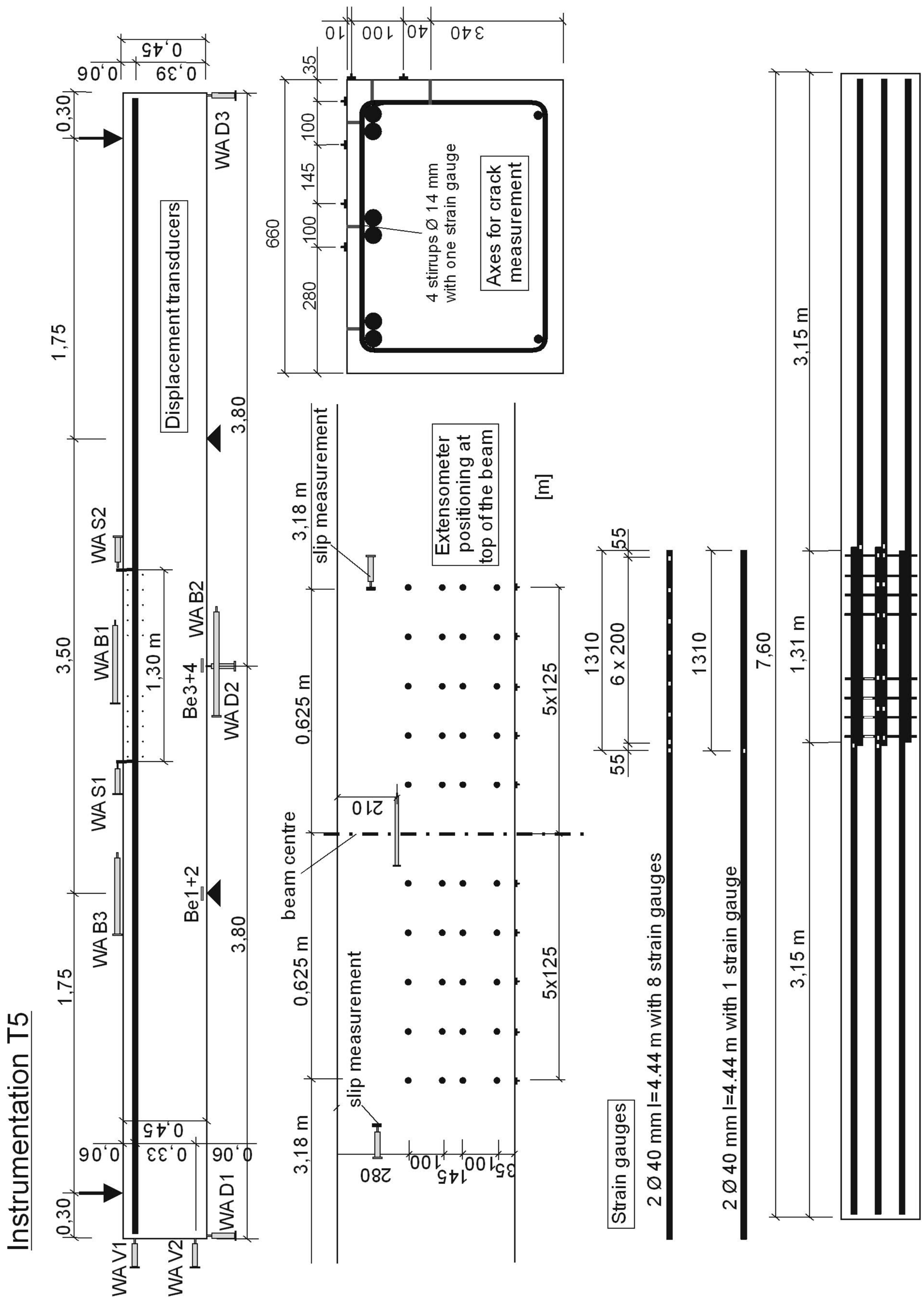

Figure A 21 Instrumentation lap test T5

A.2.3.6. Lap Test T6

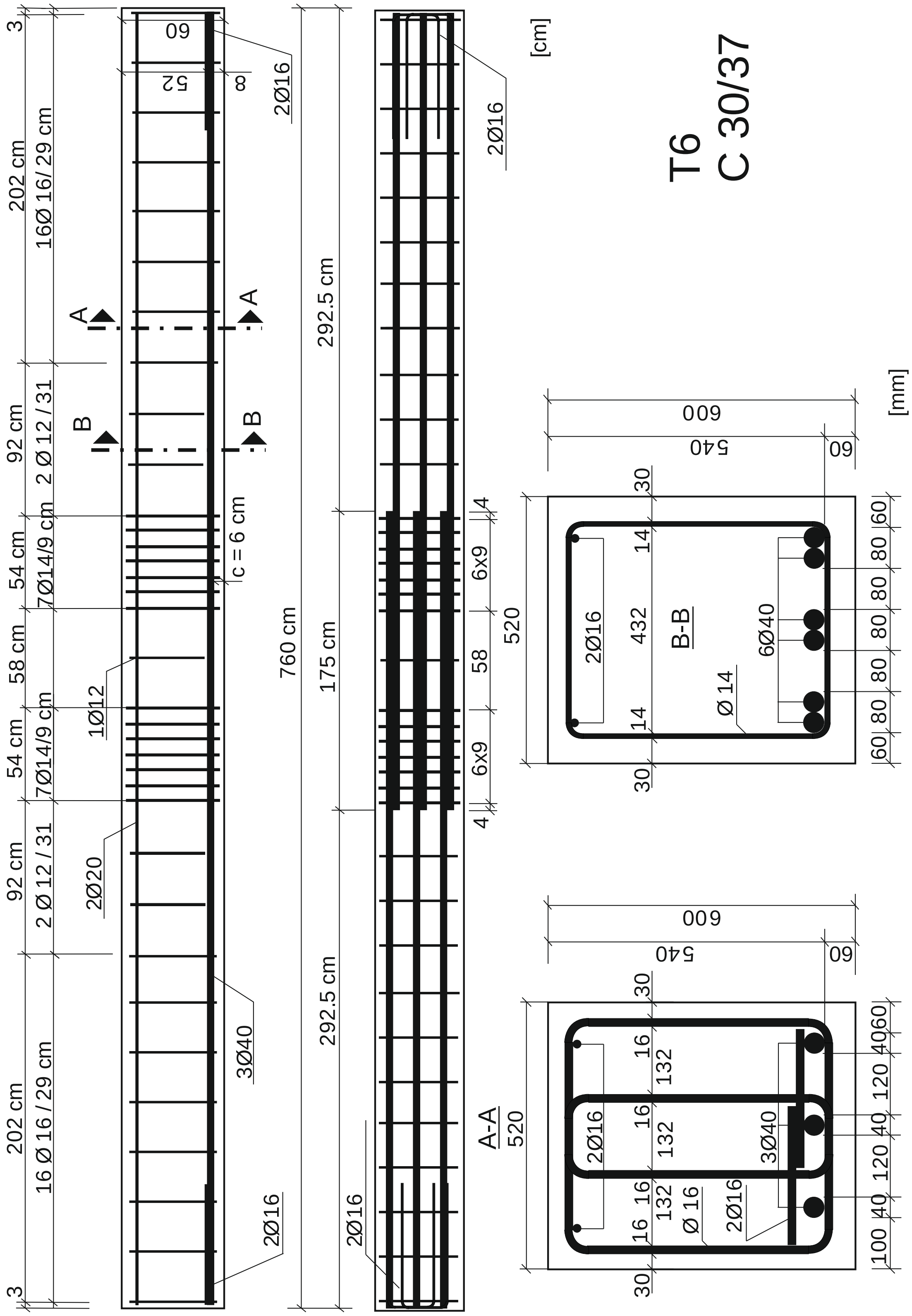

Figure A 22 Reinforcement layout lap test T6

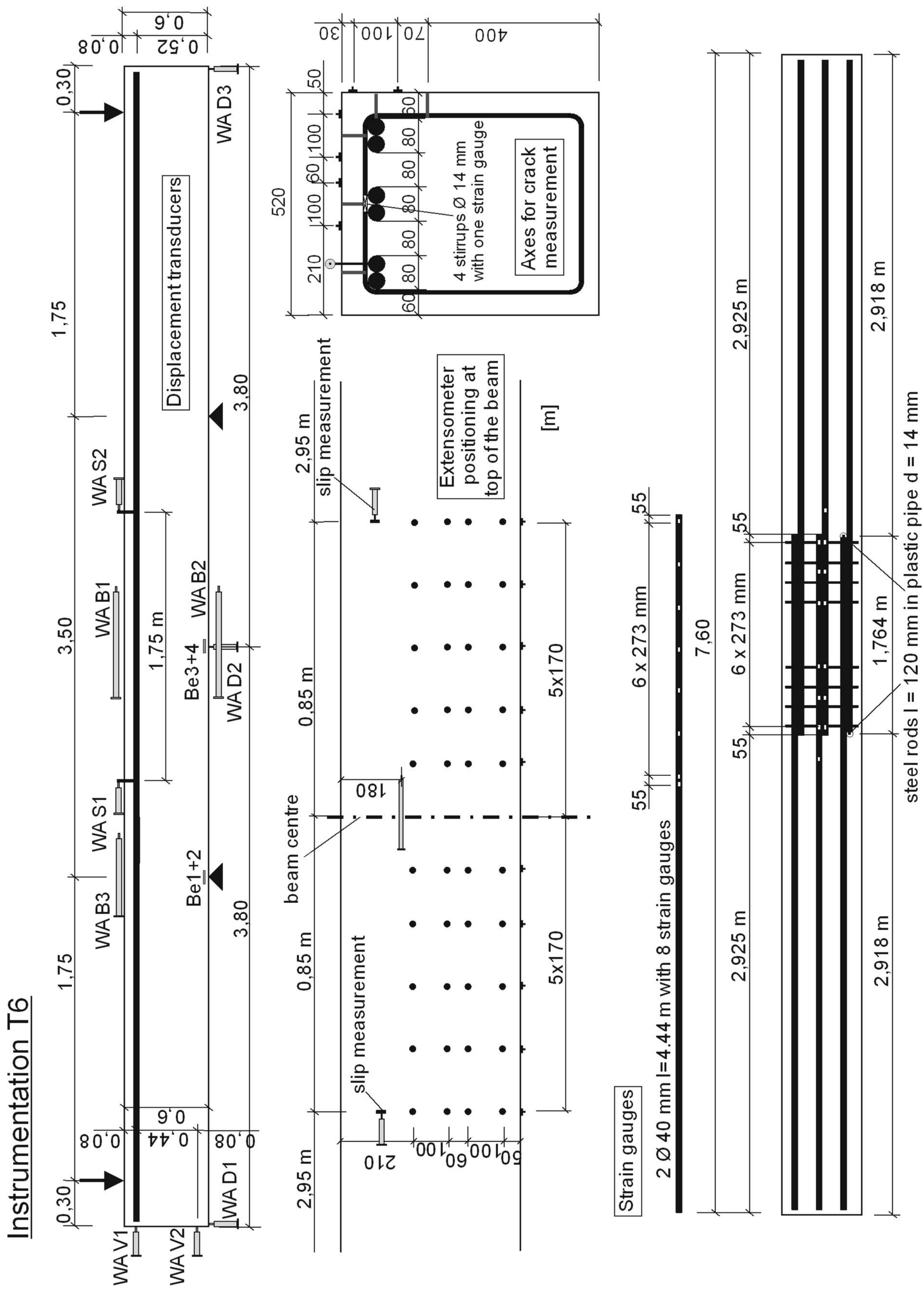

Figure A 23 Instrumentation lap test T6

A.2.3.7. Lap Test T7

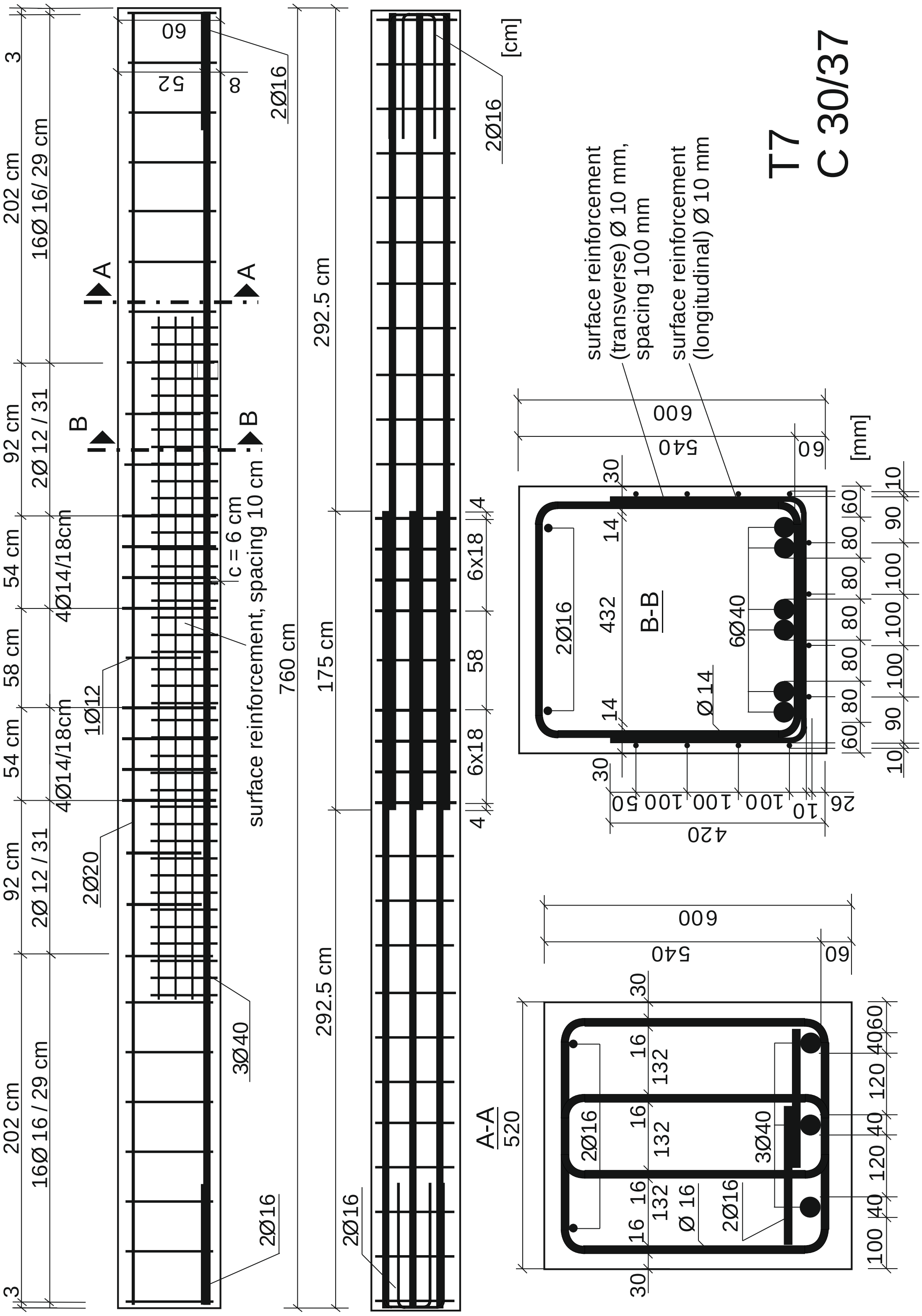

Figure A 24 Reinforcement layout lap test T7

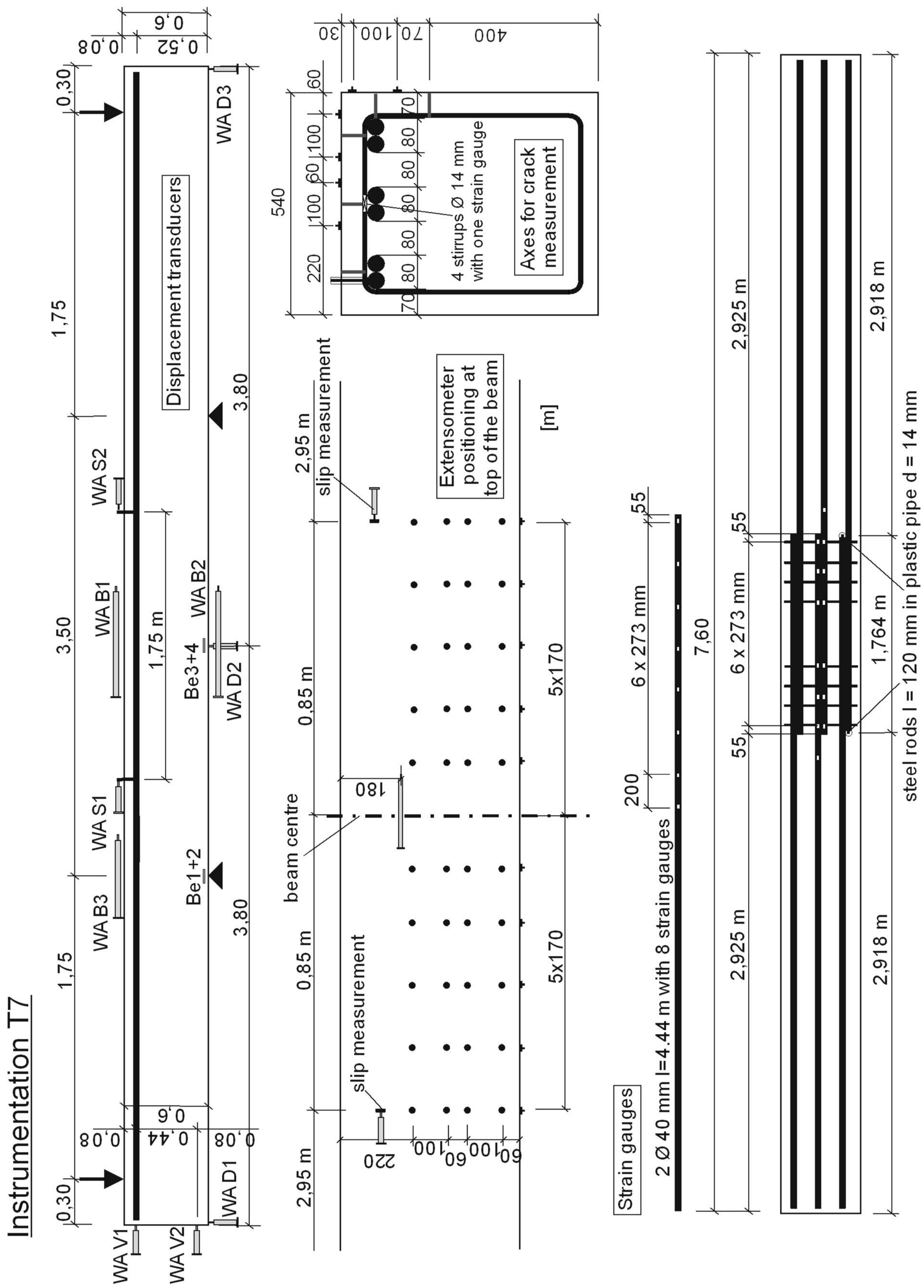

Figure A 25 Instrumentation lap test T7

A.2.3.8. Lap Test T8

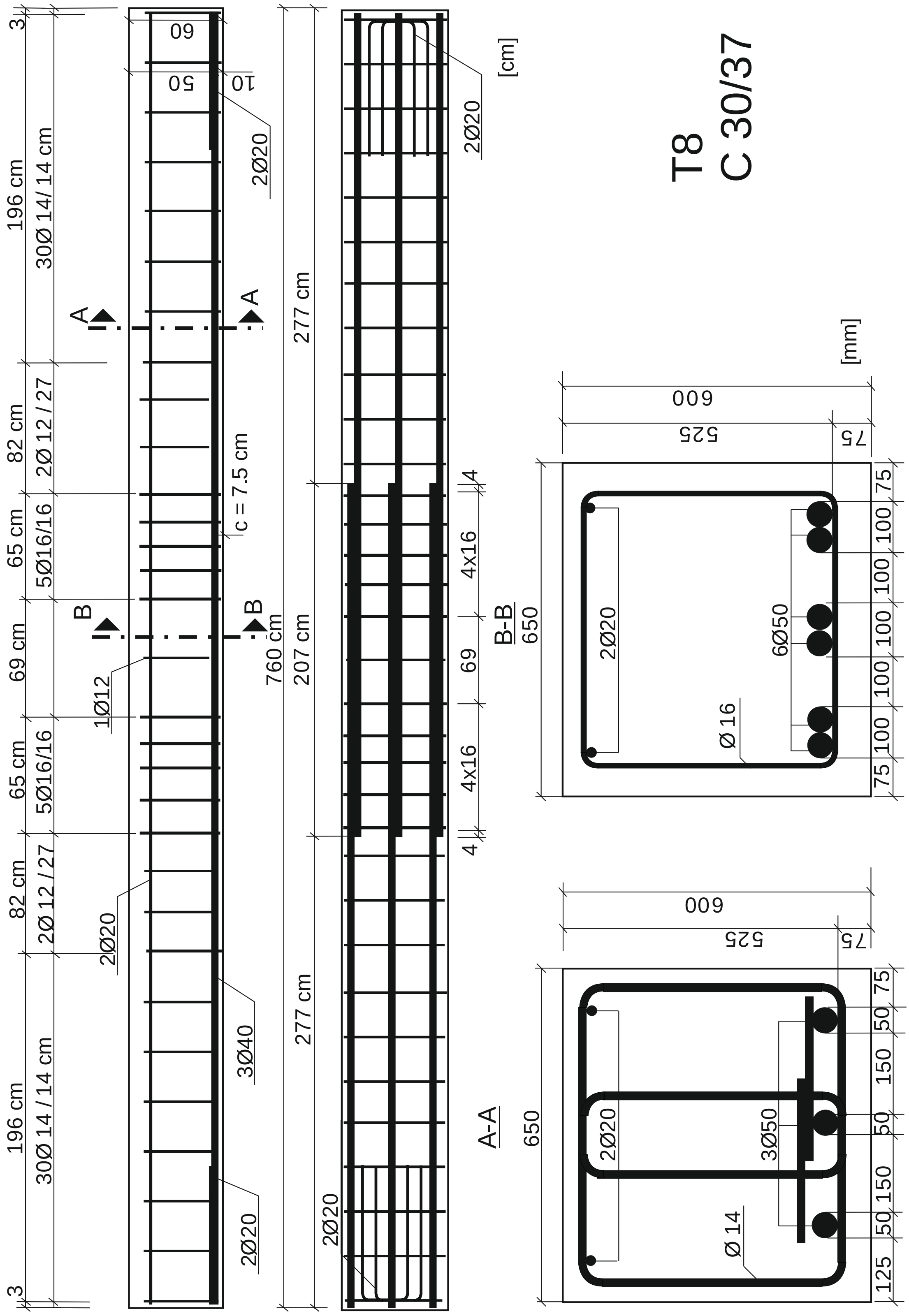

Figure A 26 Reinforcement layout lap test T8

A.2.3.9. Lap Test T9

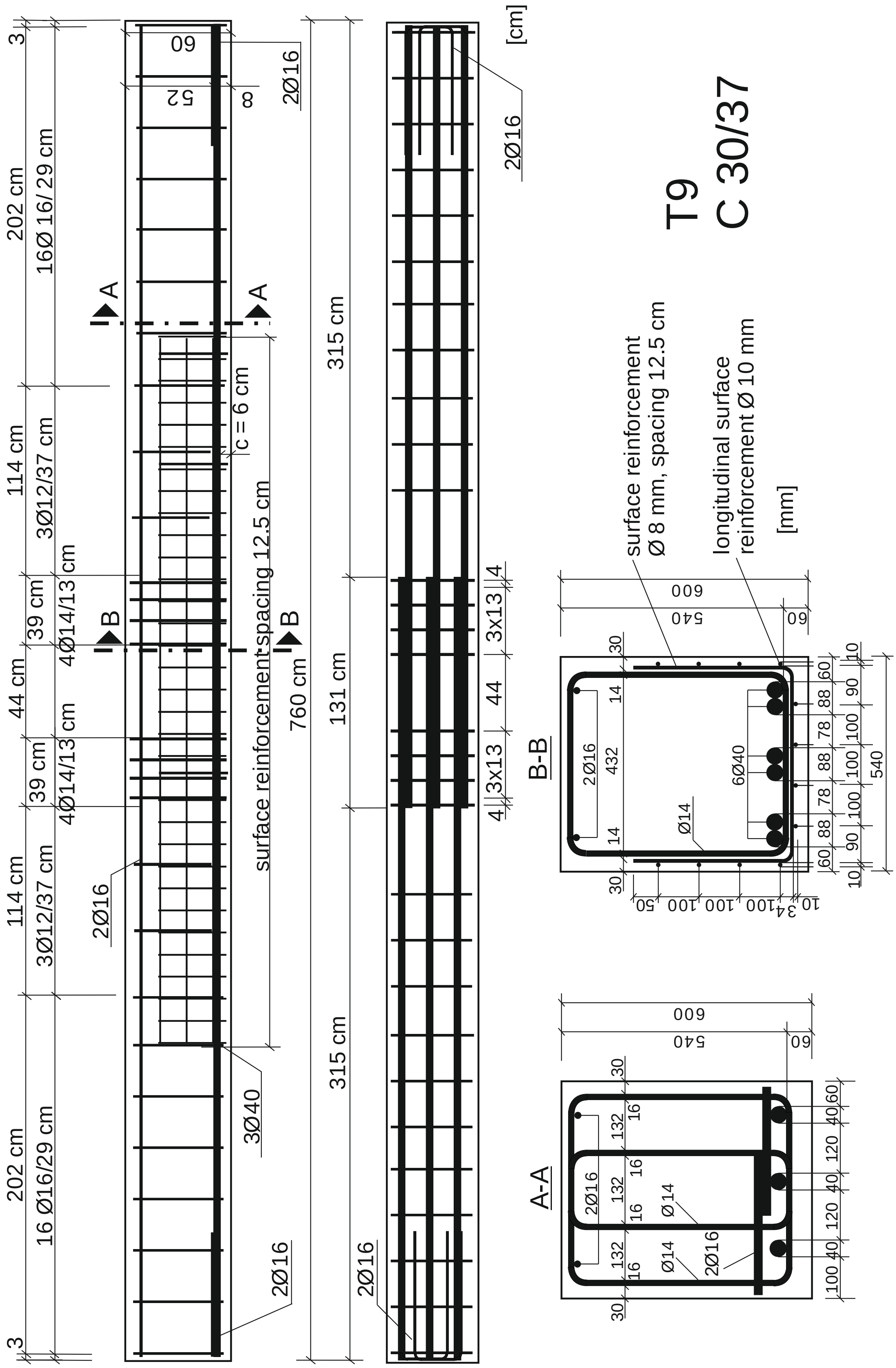

Figure A 27 Reinforcement layout lap test T9

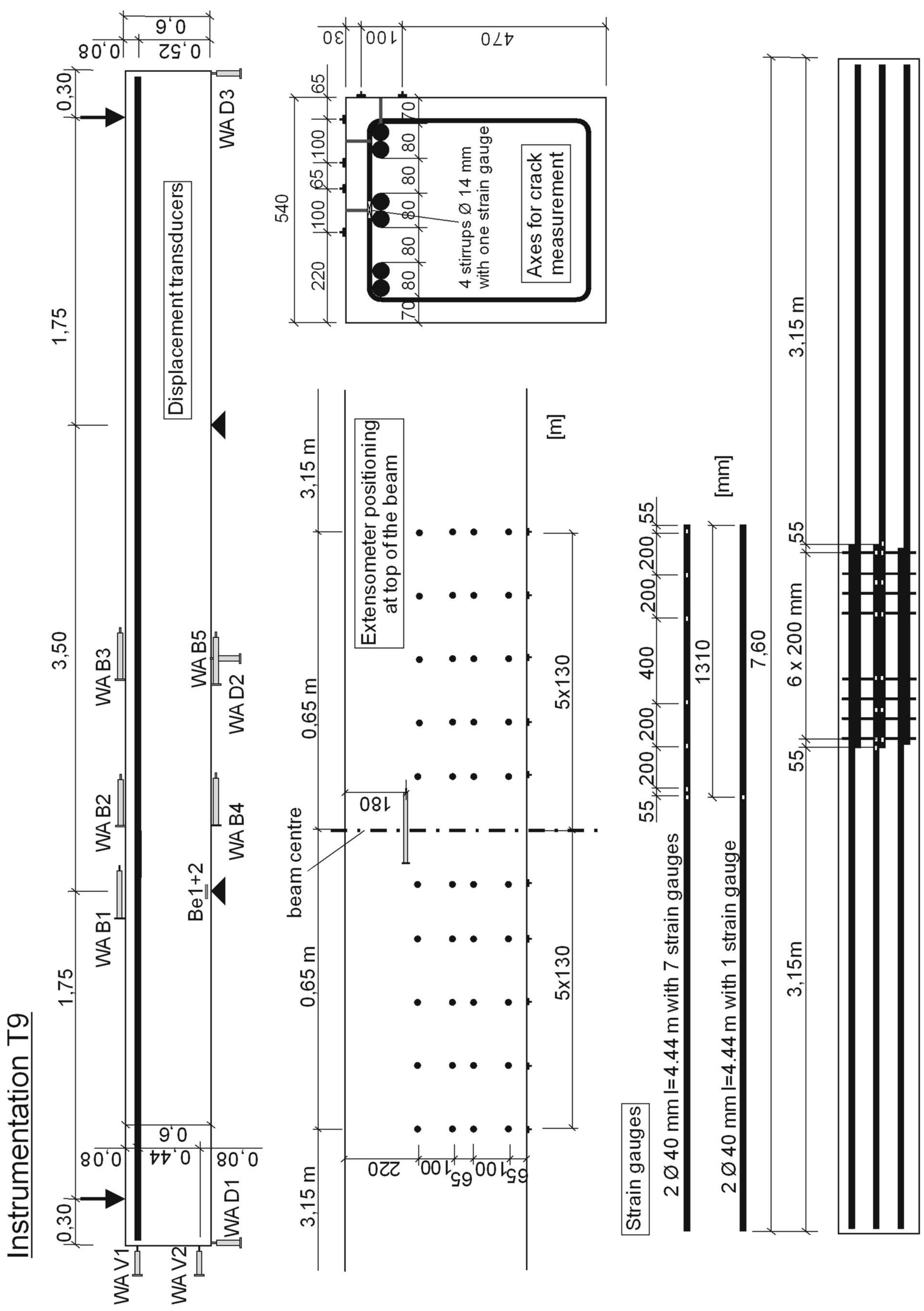

Figure A 28 Instrumentation lap test T9

A.2.3.10. Lap Test T10

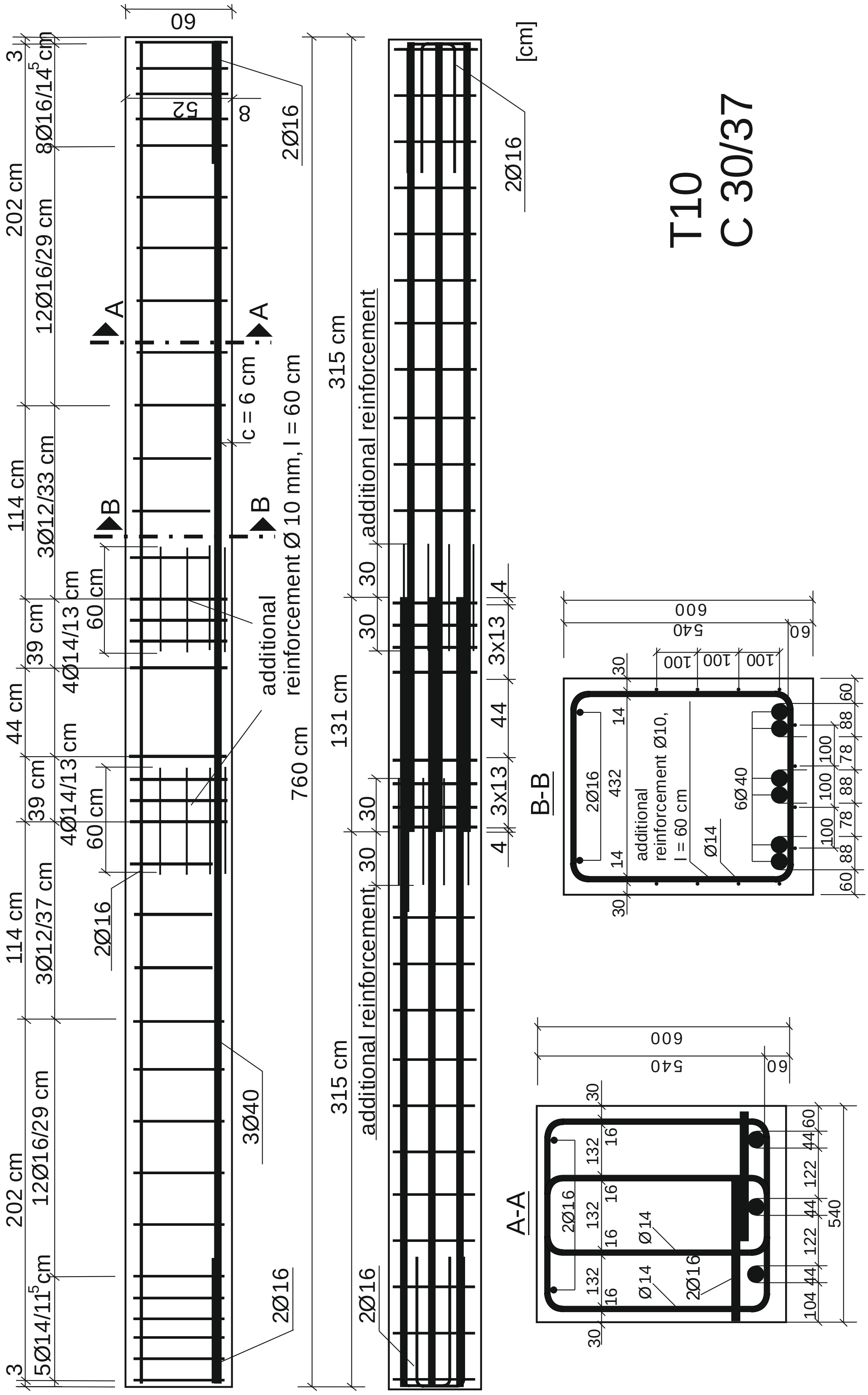

Figure A 29 Reinforcement layout lap test T10

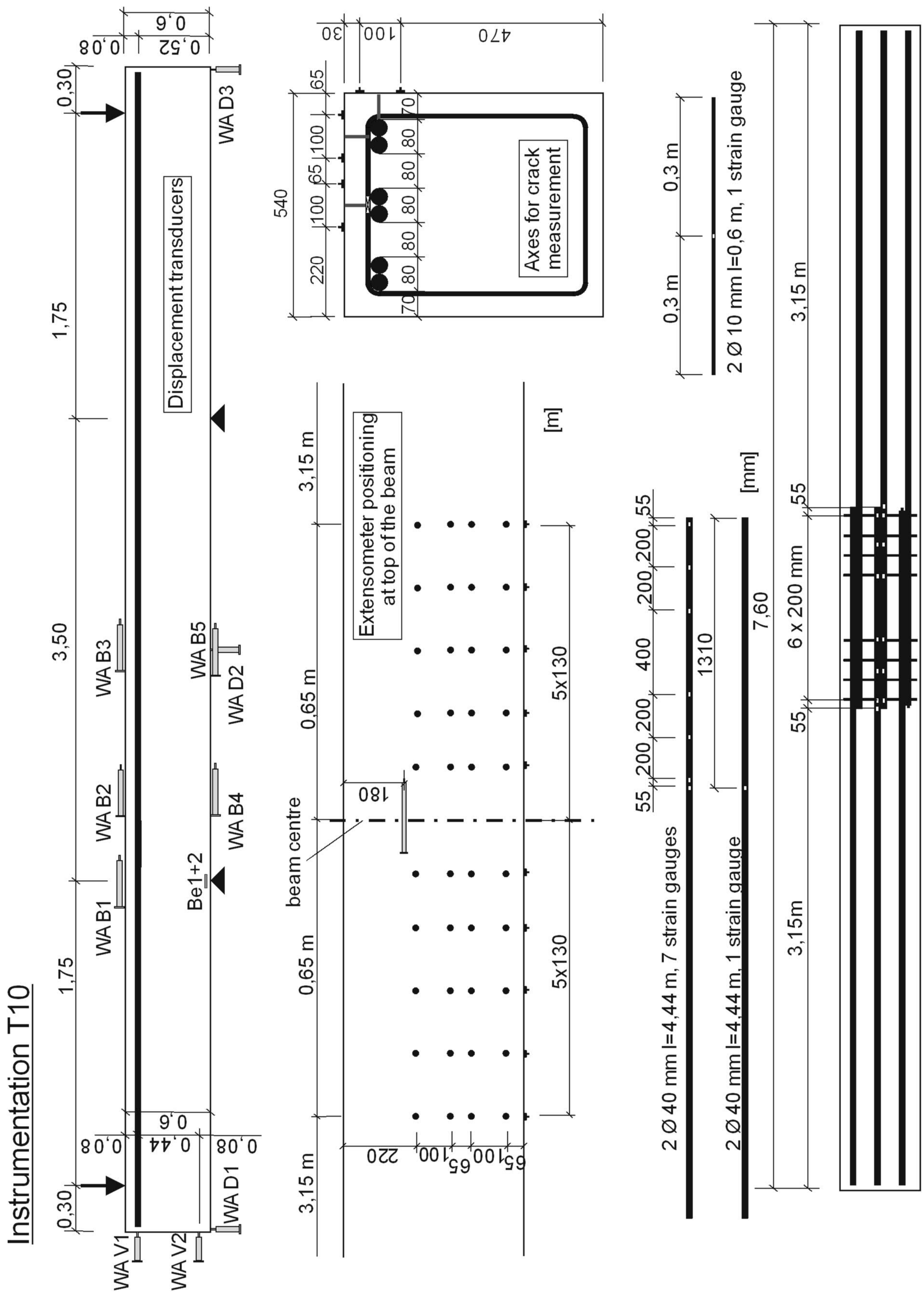

Figure A 30 Instrumentation lap test T10

A.2.3.11. Lap Test T11

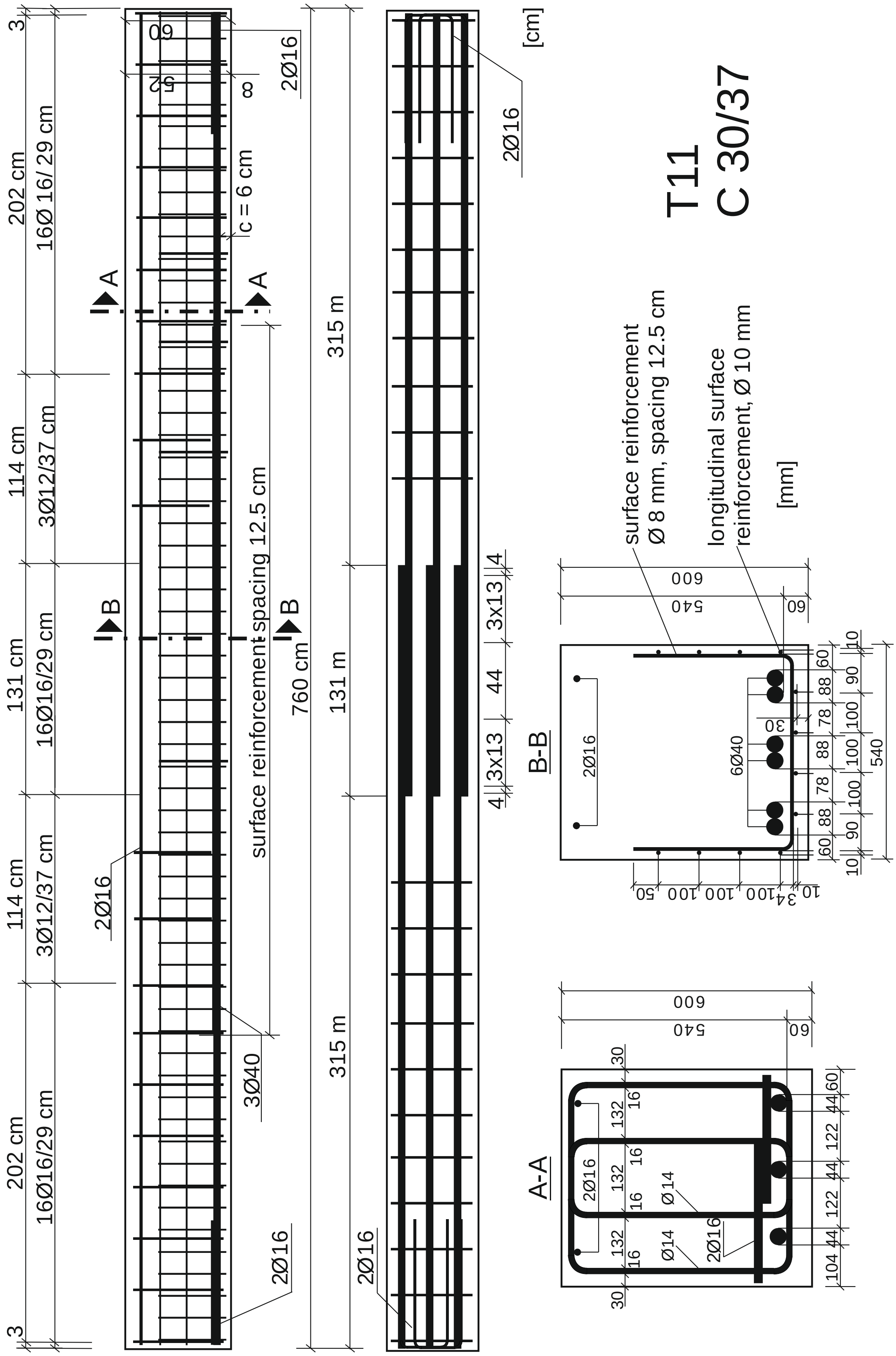

Figure A 31 Reinforcement layout lap test T11

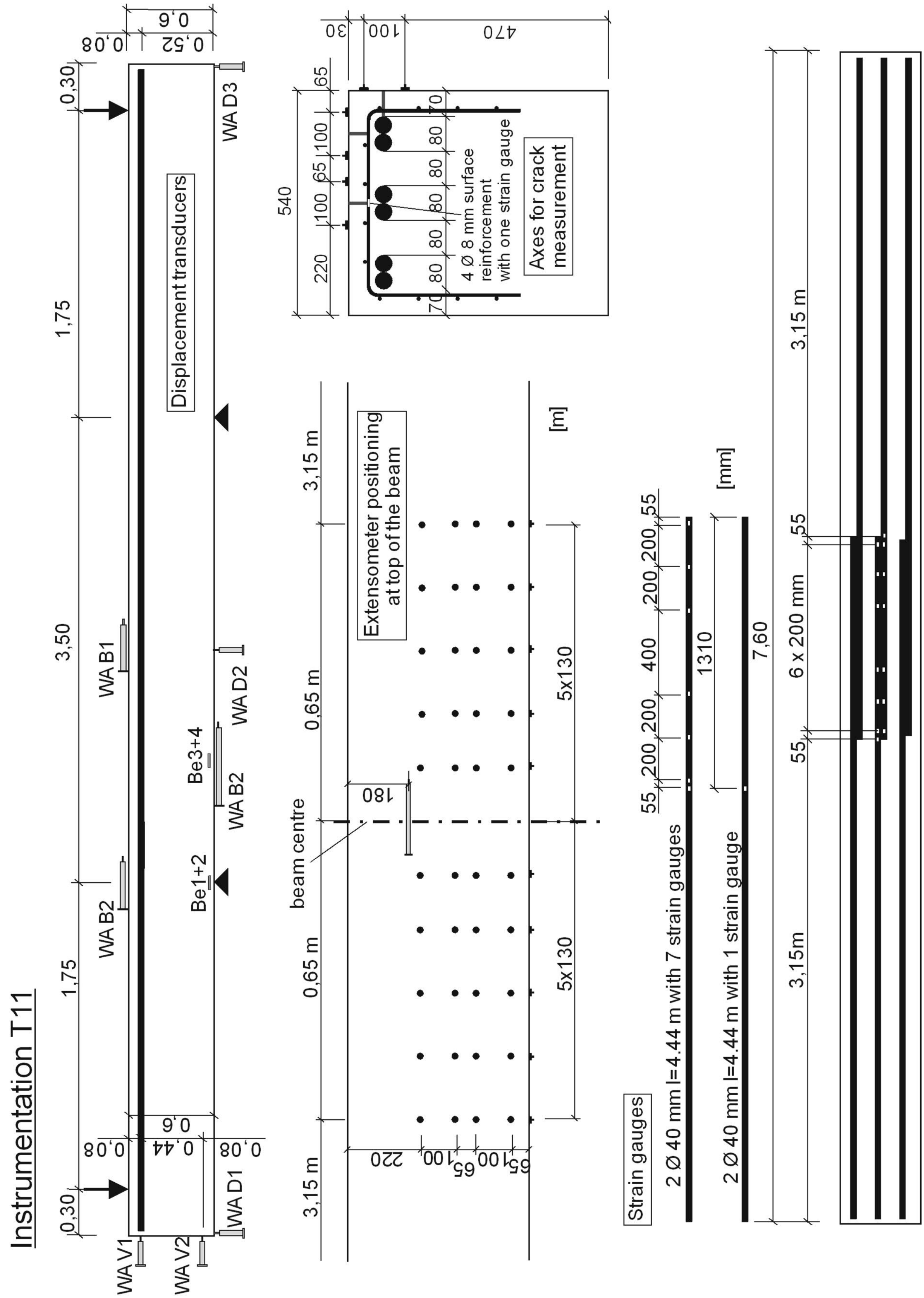

Figure A 32 Instrumentation lap test T11

A.2.3.12. Lap Test T12

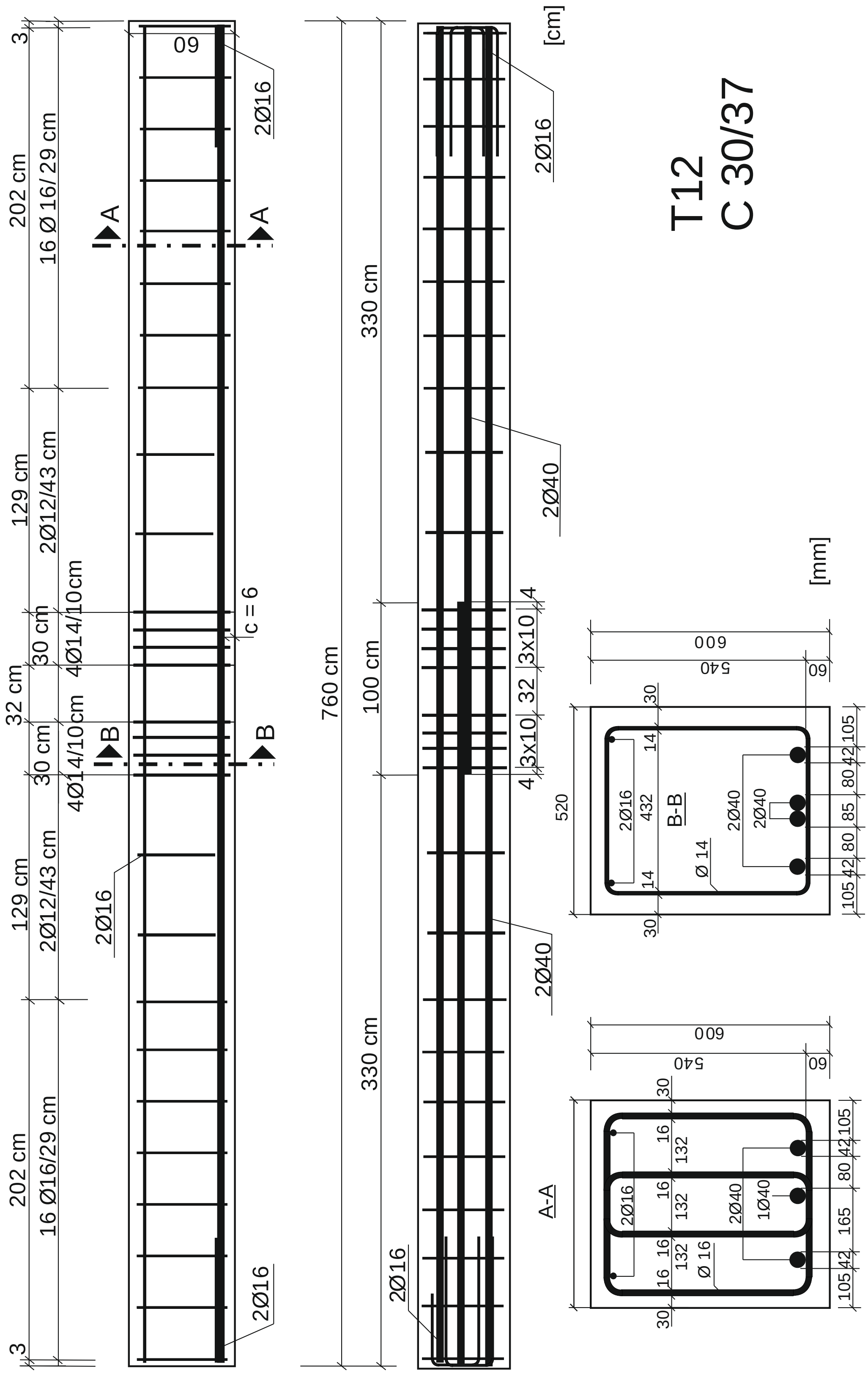

Figure A 33 Reinforcement layout lap test T12

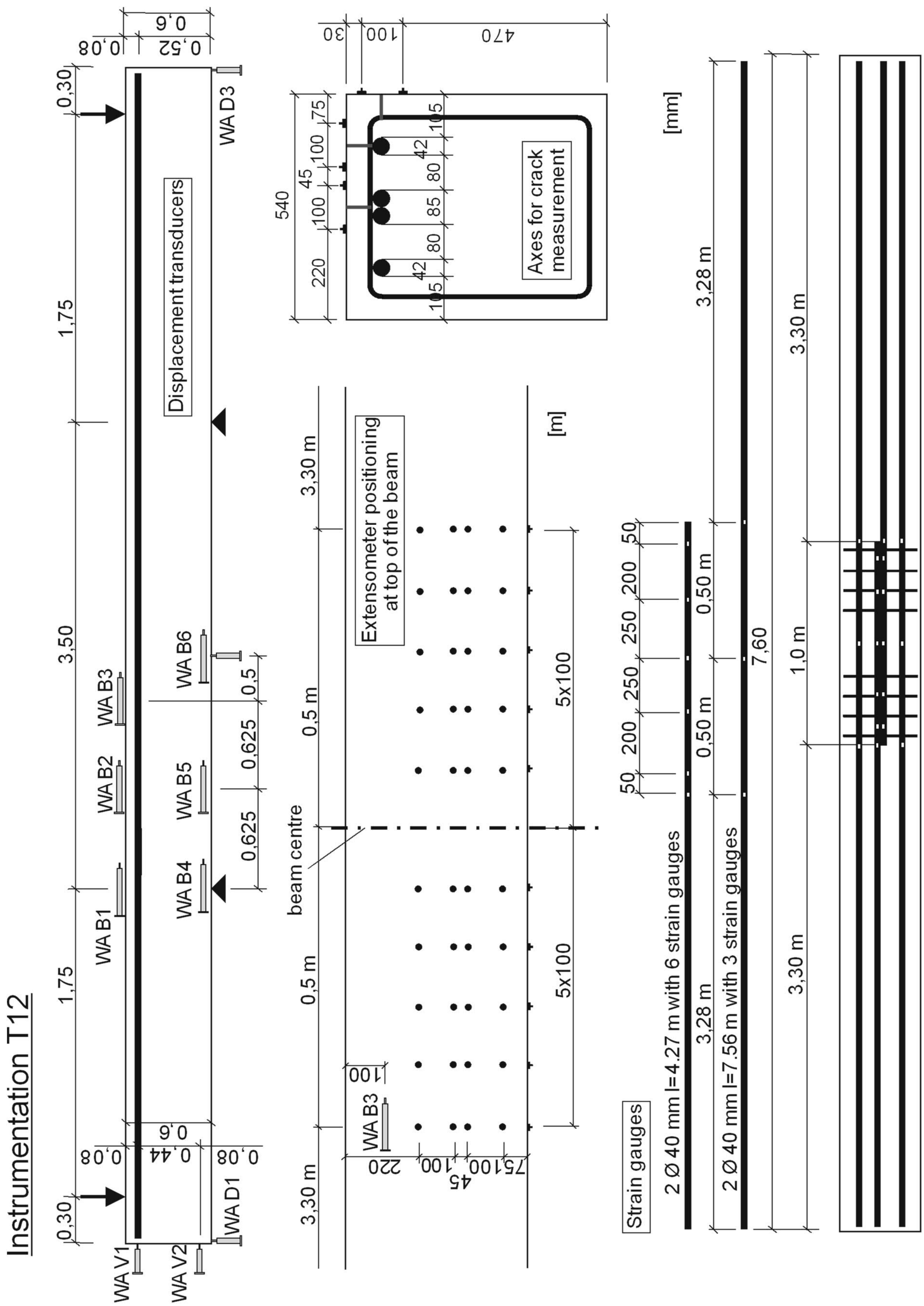

Figure A 34 Instrumentation lap test T12

A.2.3.13. Lap Test T13

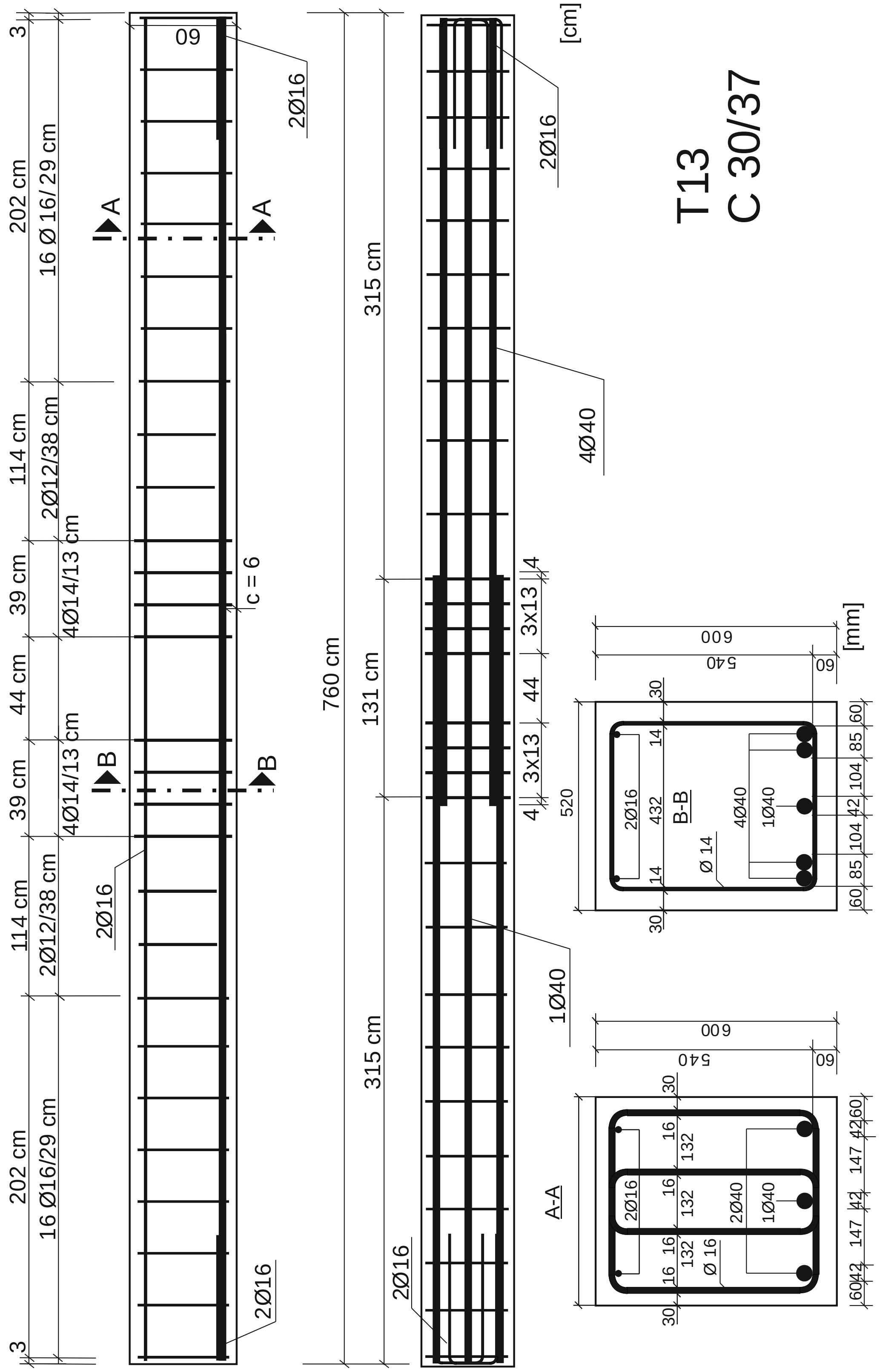

Figure A 35 Reinforcement layout lap test T13

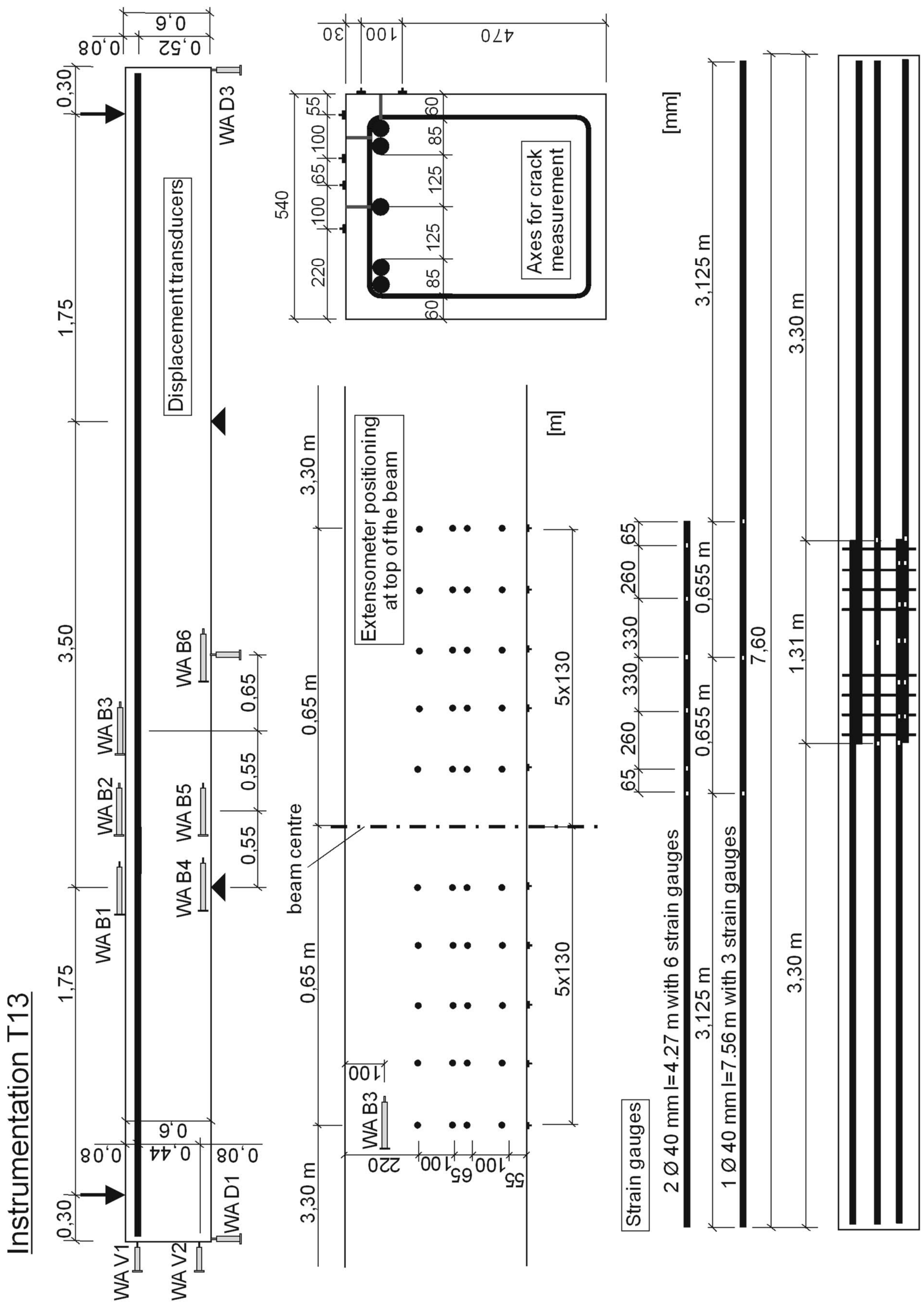

Figure A 36 Instrumentation lap test T13

A.2.3.14. Lap Test T15

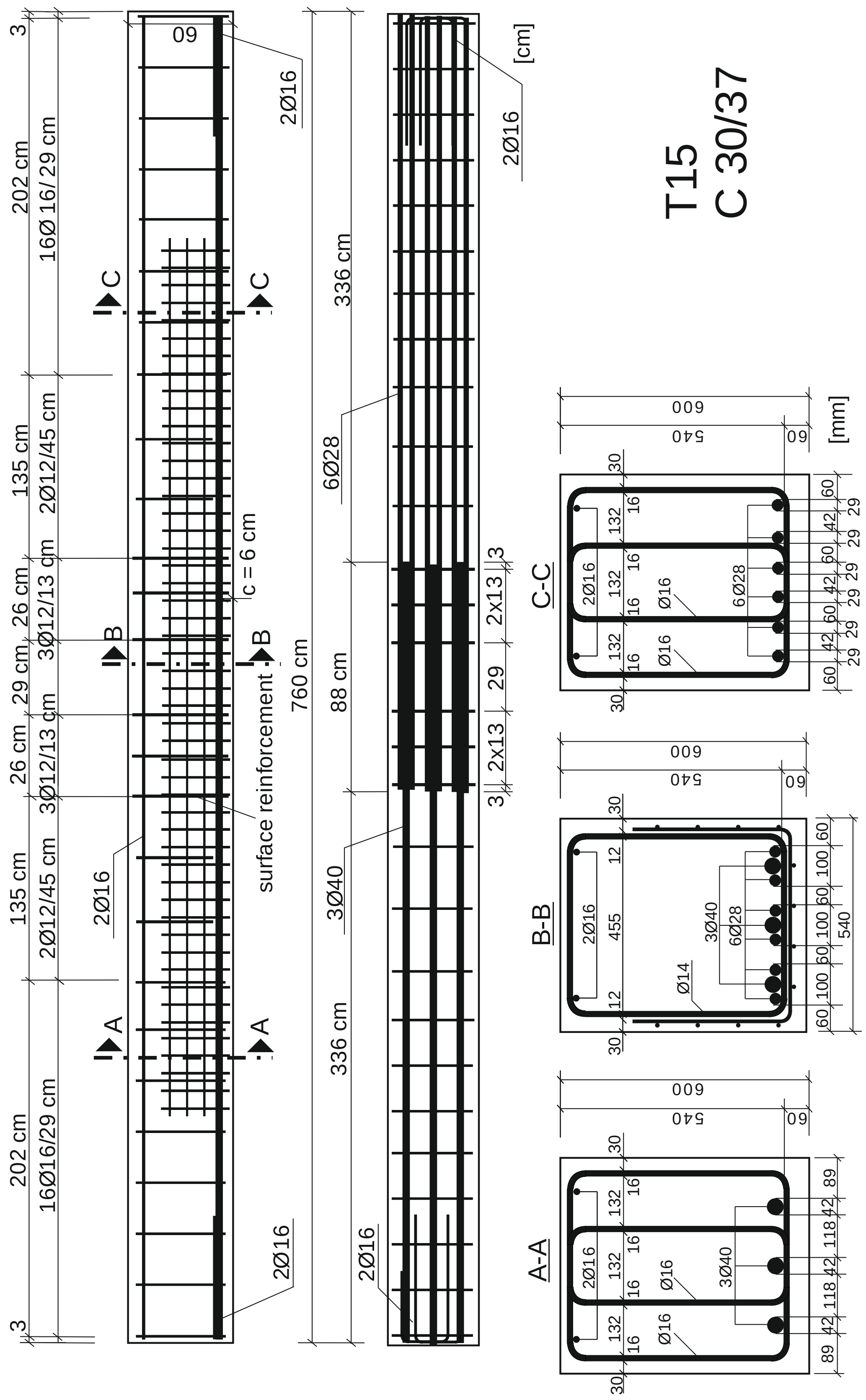

Figure A 37 Reinforcement layout lap test T15

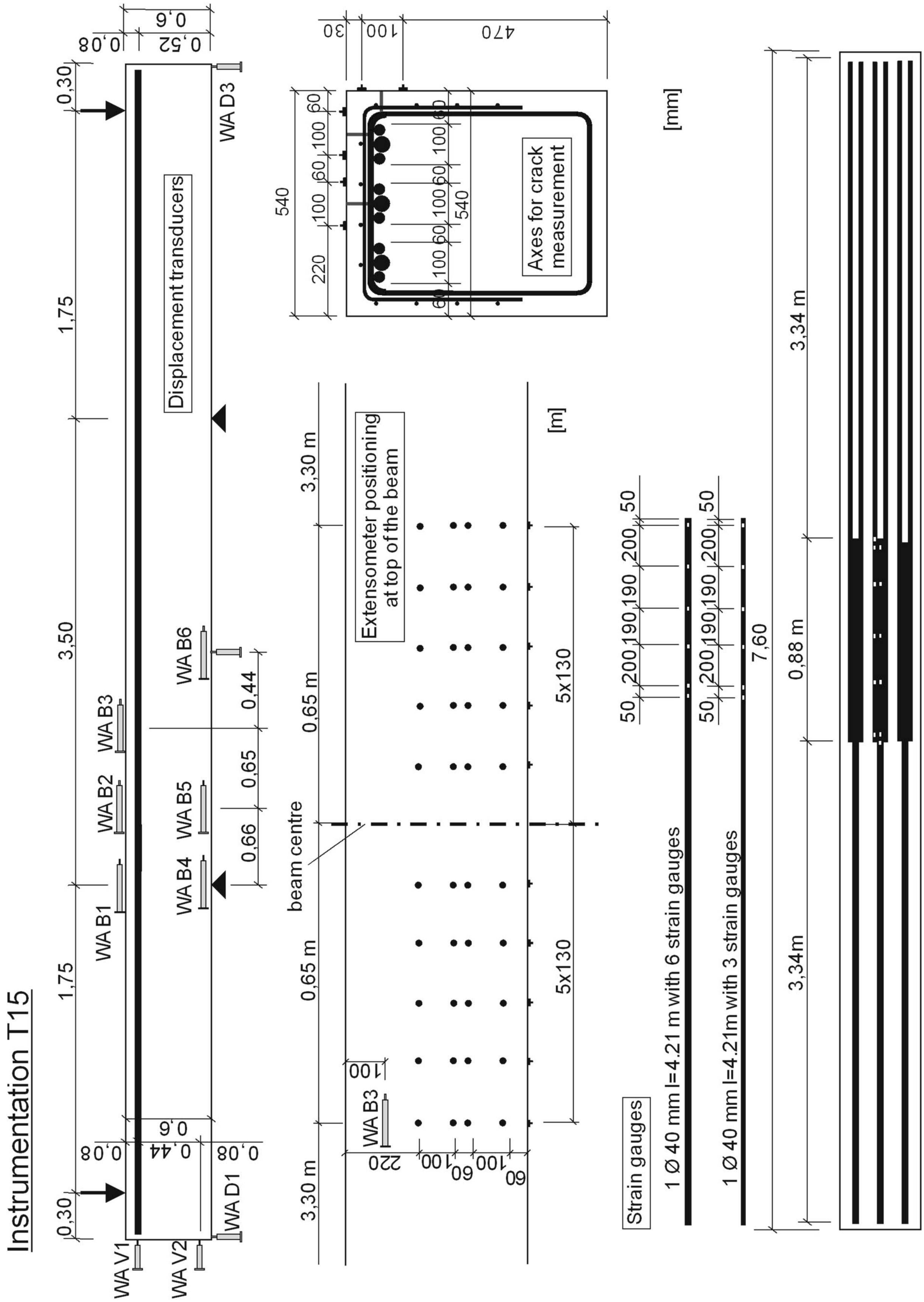

Figure A 38 Instrumentation lap test T15

A.2.3.15. Lap Test T16

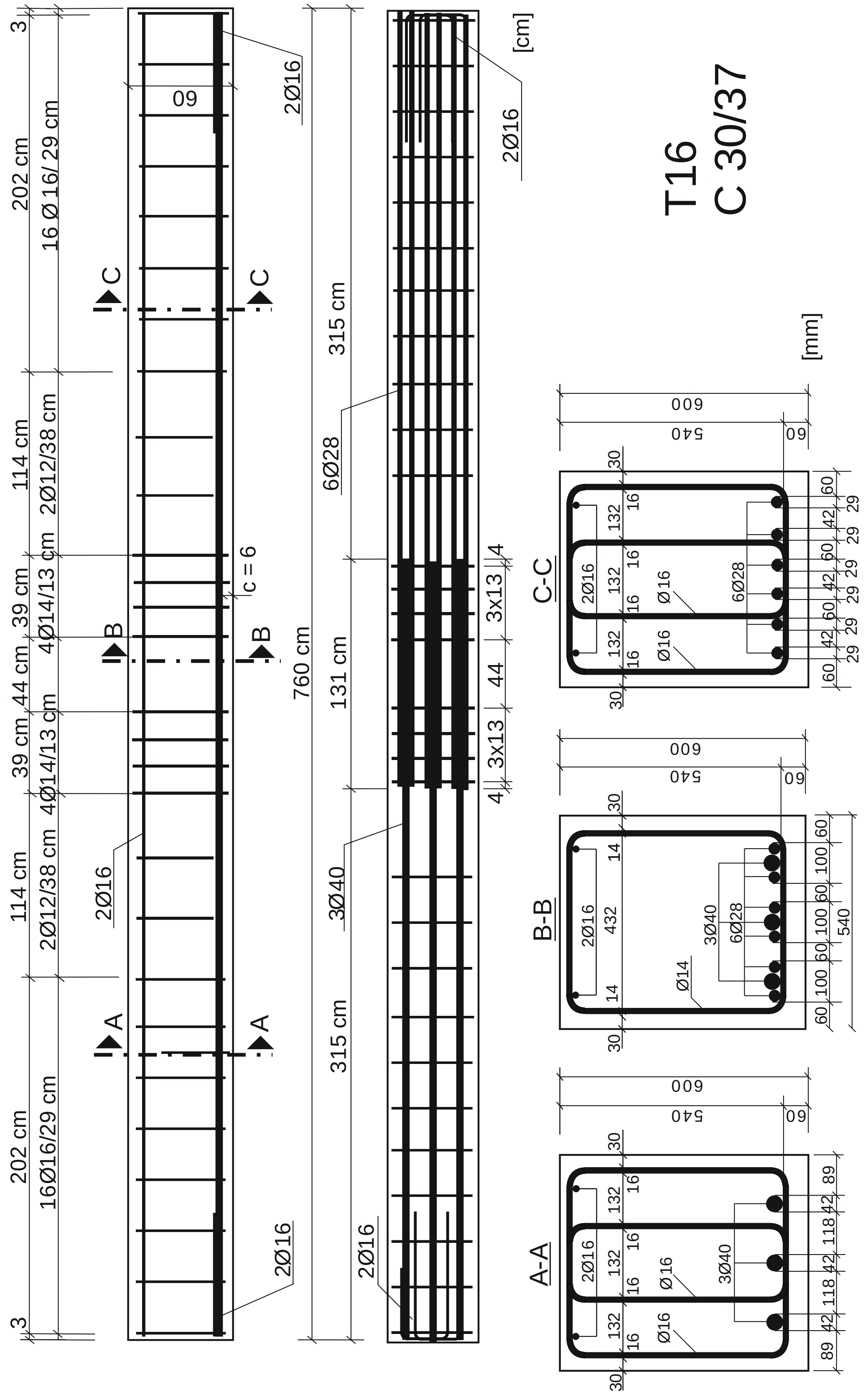

Figure A 39 Reinforcement layout lap test T16

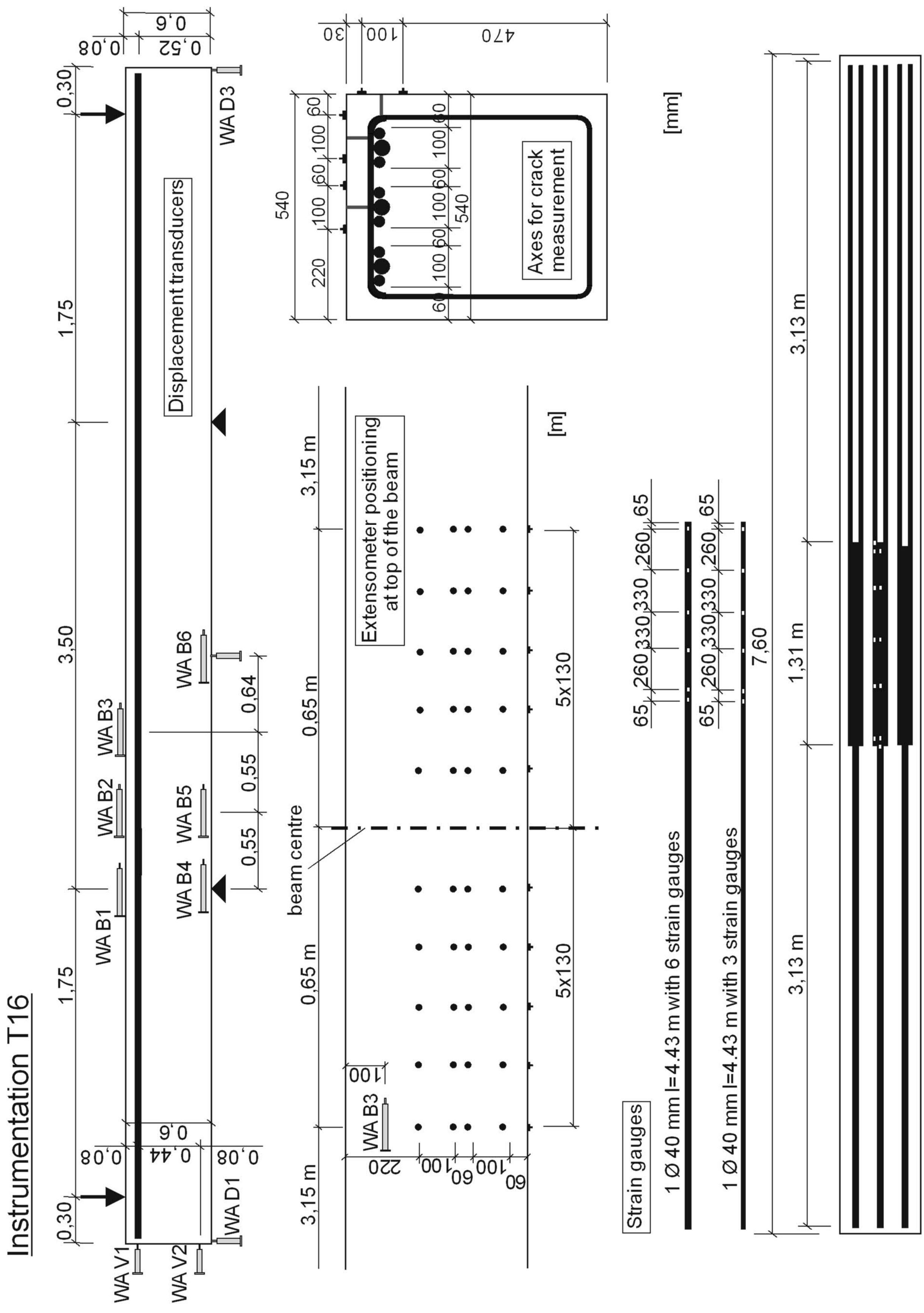

Figure A 40 Instrumentation lap test T16

A.2.3.16. Lap Test T17

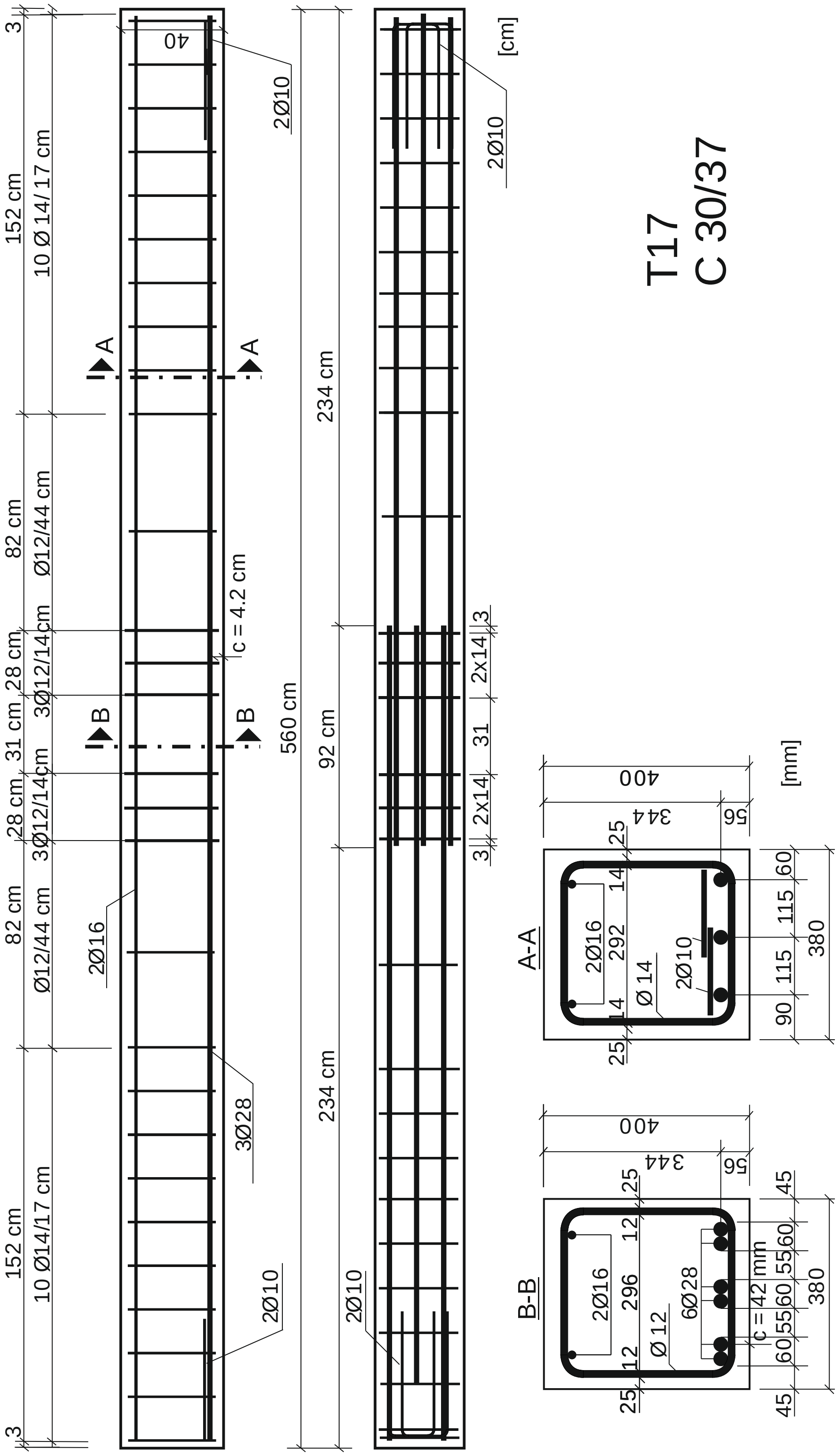

Figure A 41 Reinforcement layout lap test T17

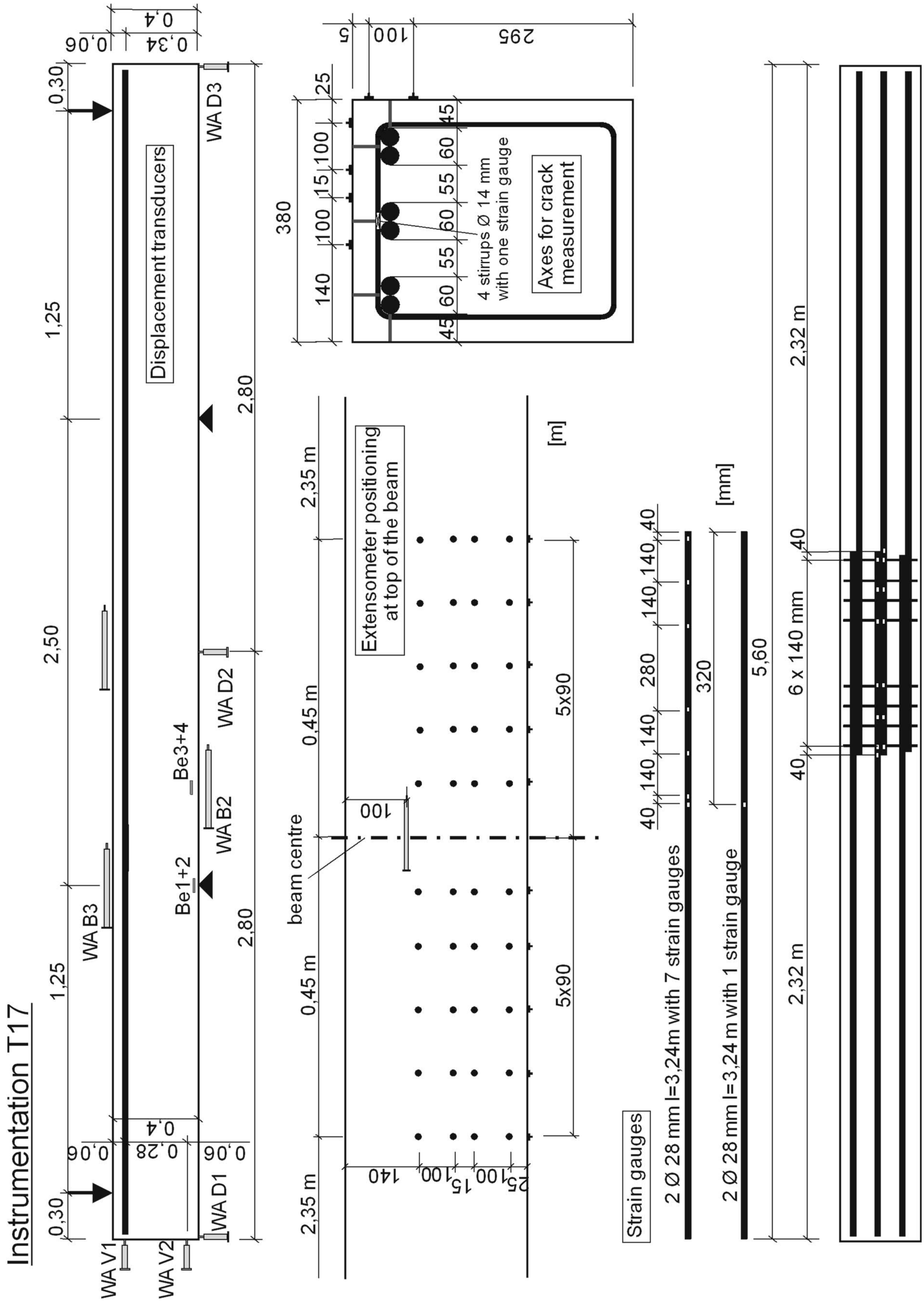

Figure A 42 Instrumentation lap test T17

A.2.3.17. Lap Test T18

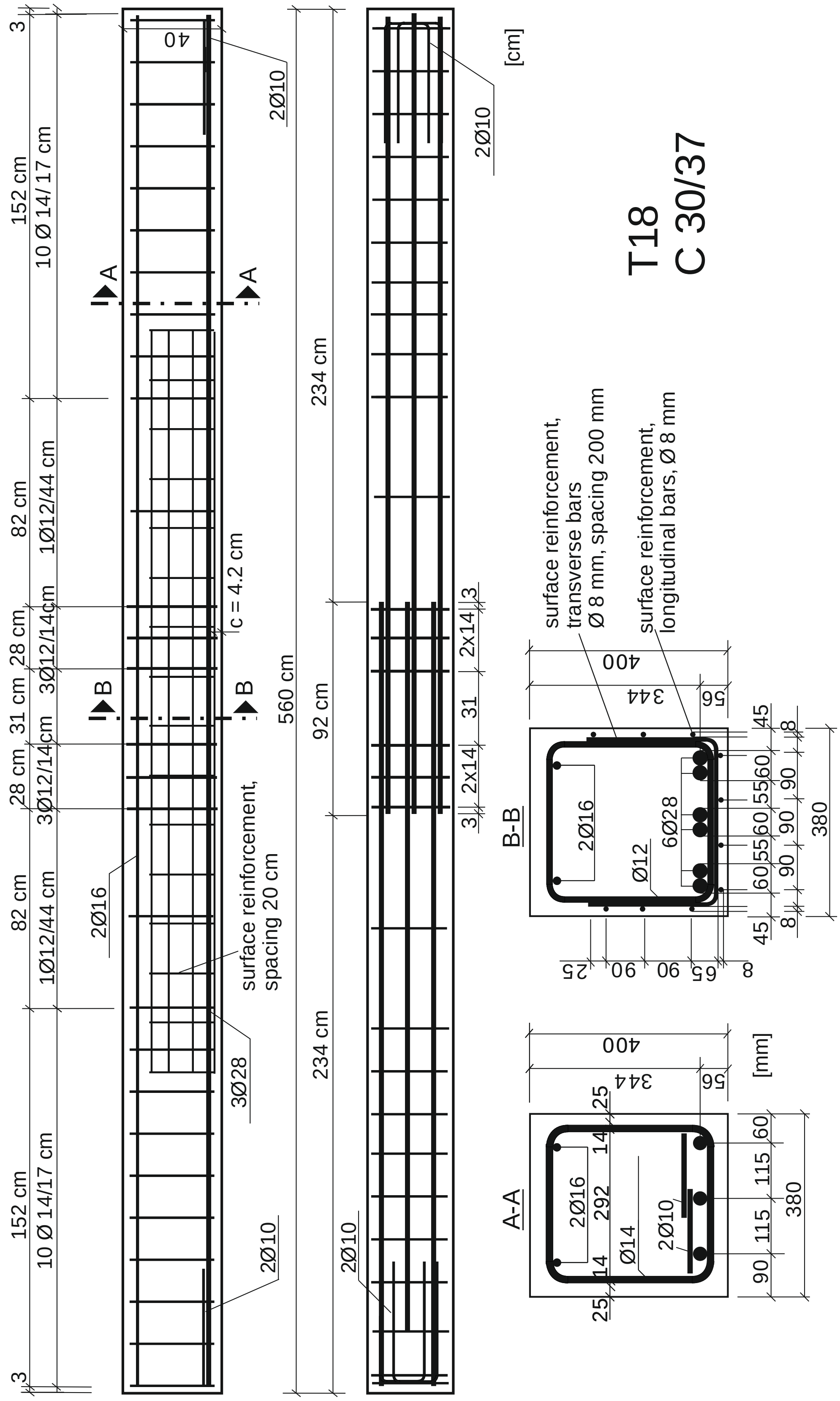

Figure A 43 Reinforcement layout lap test T18

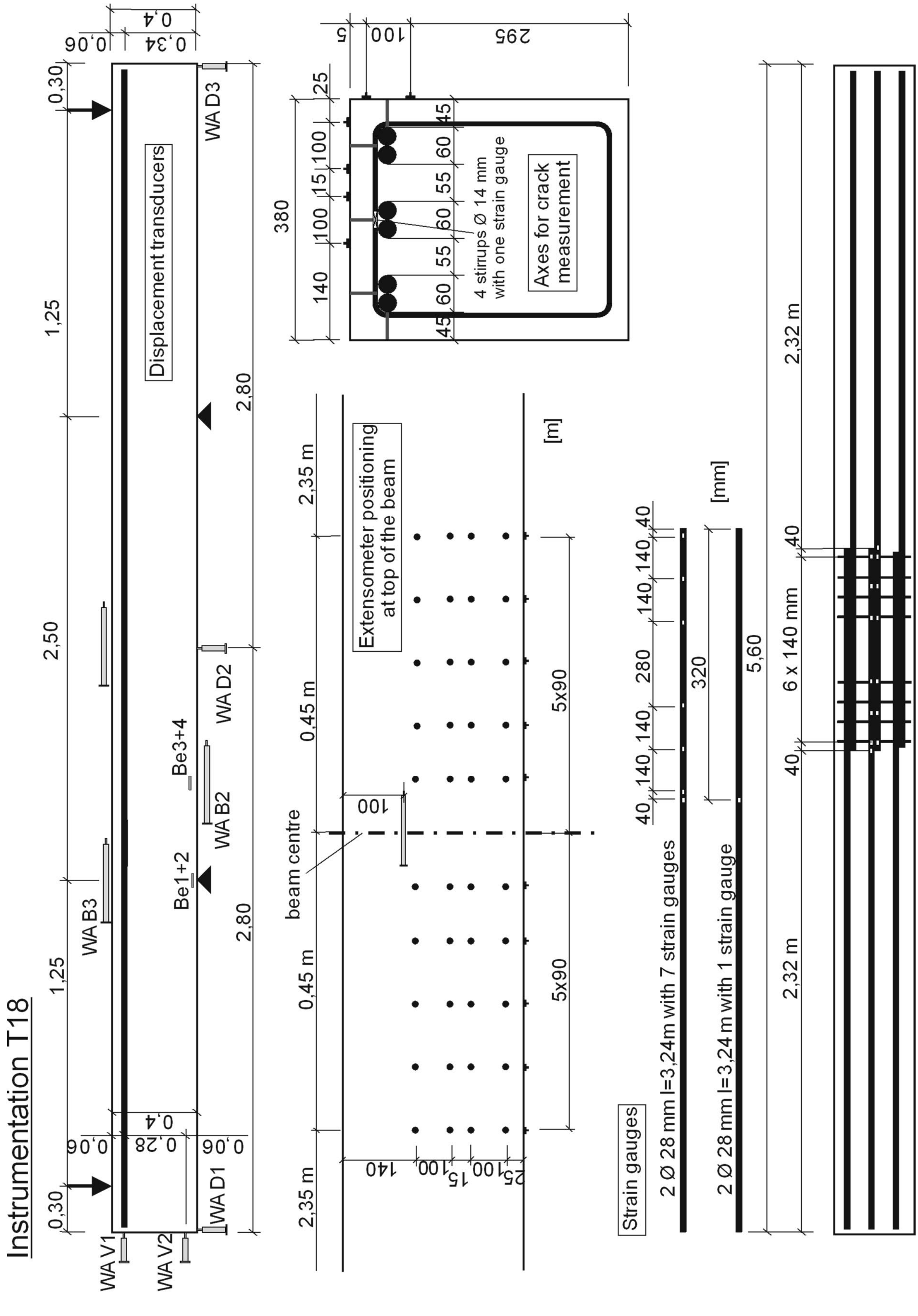

Figure A 44 Instrumentation lap test T18

A.2.4. Anchorage Tests: Reinforcement and Instrumentation

A.2.4.1. Anchorage test V1

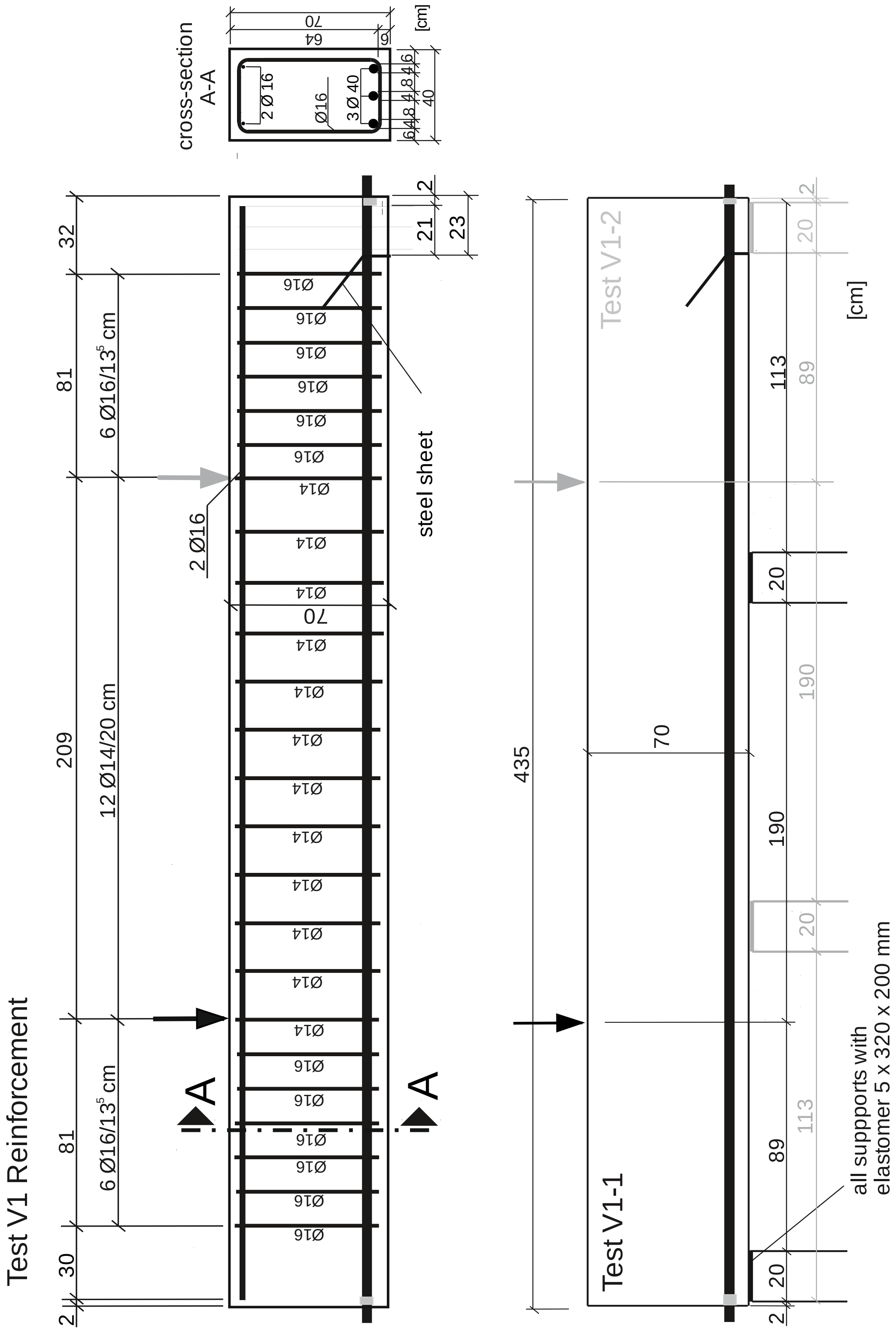

Figure A 45 Reinforcement layout anchorage test V1

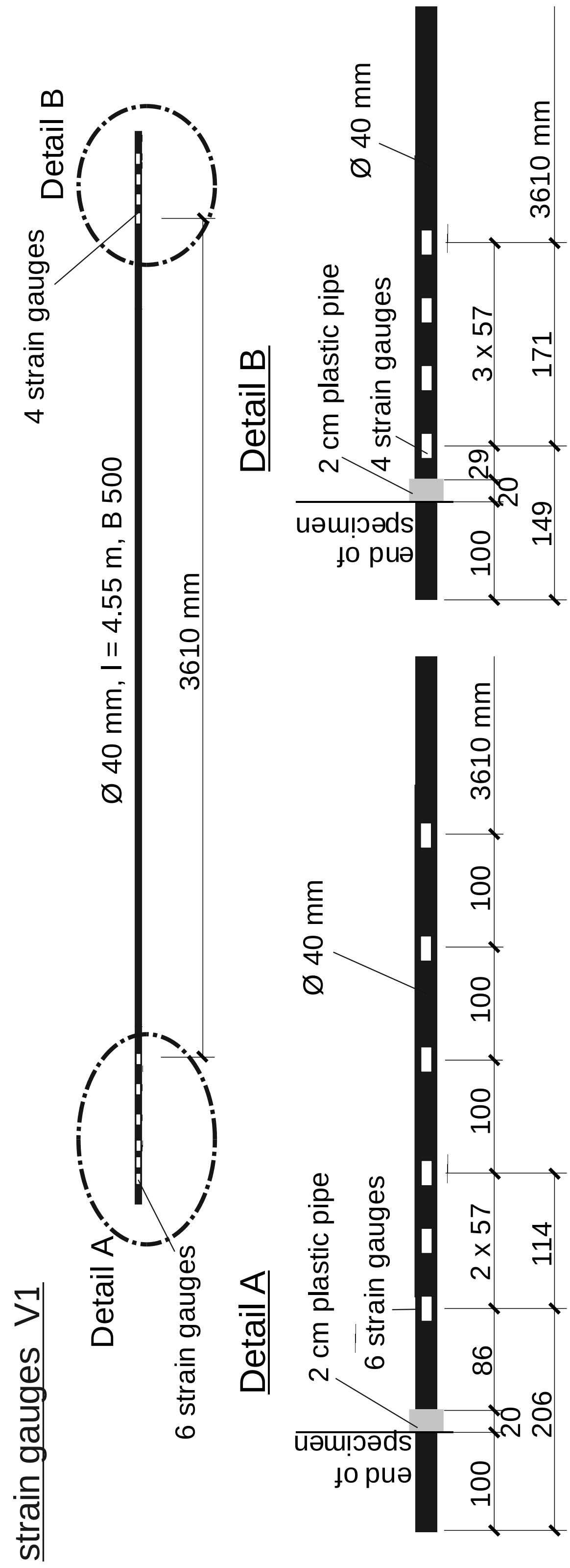

Figure A 46 Instrumentation anchorage test V1

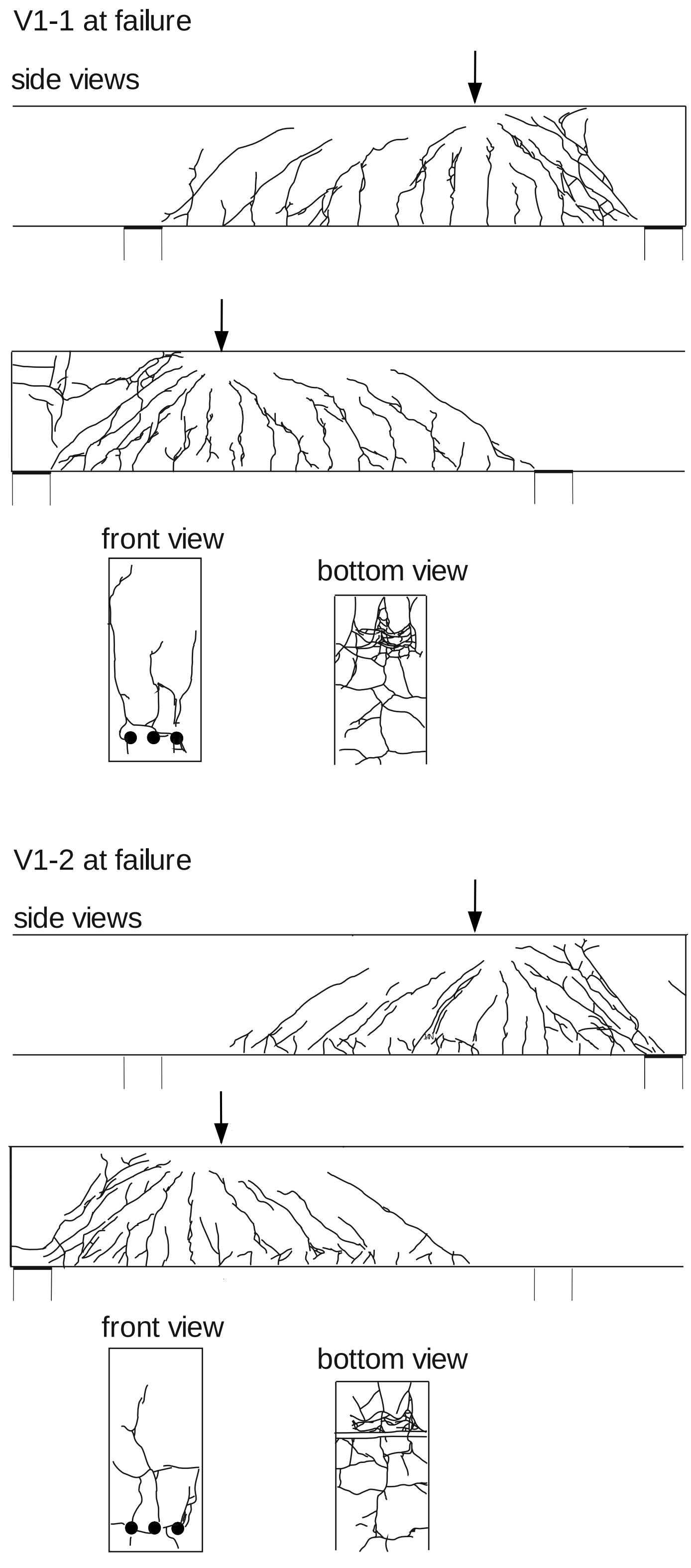

Figure A 47 Crack development in anchorage tests V1-1 and V1-2

A.2.4.2. Anchorage test V2

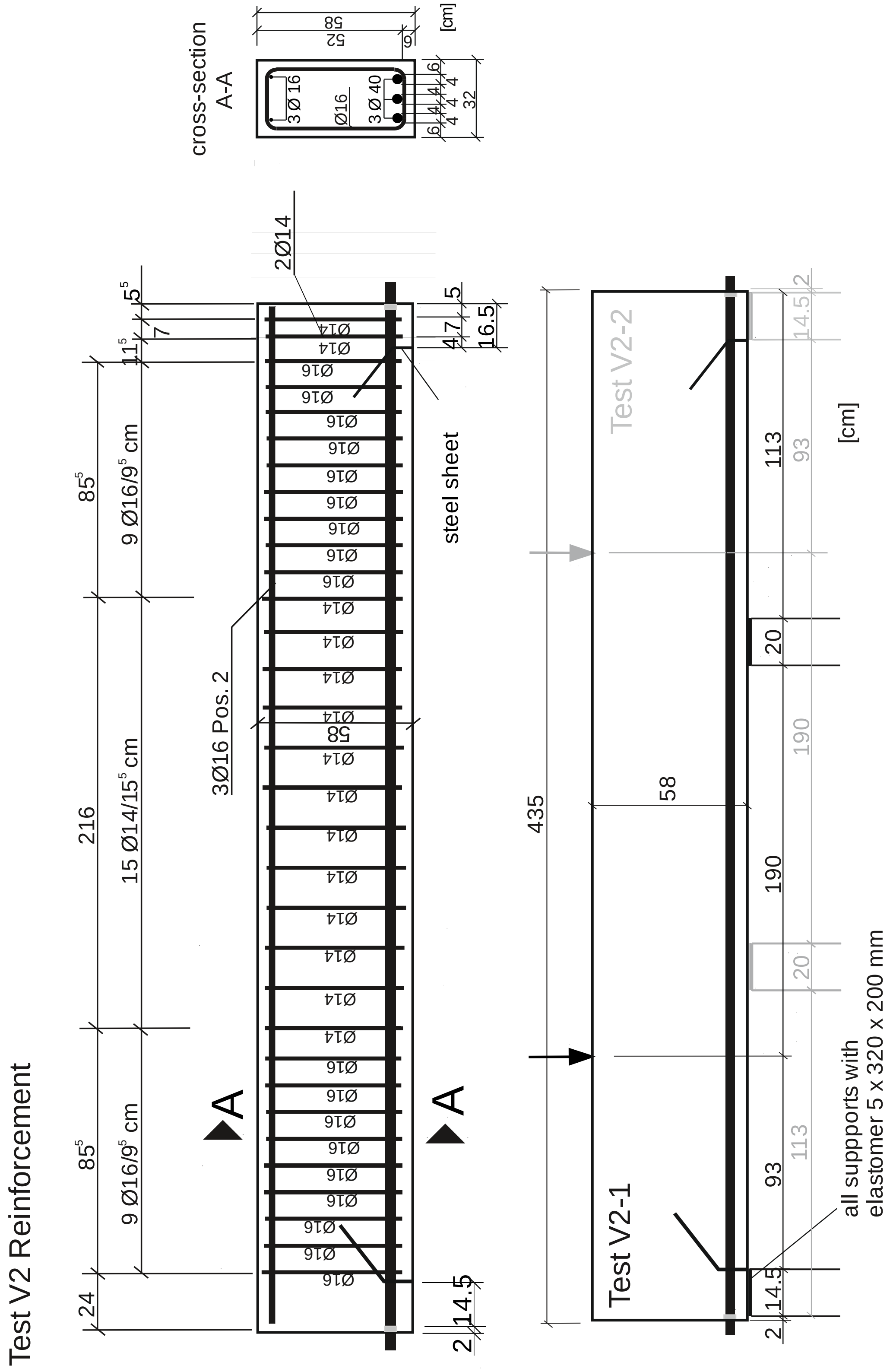

Figure A 48 Reinforcement layout anchorage test V2

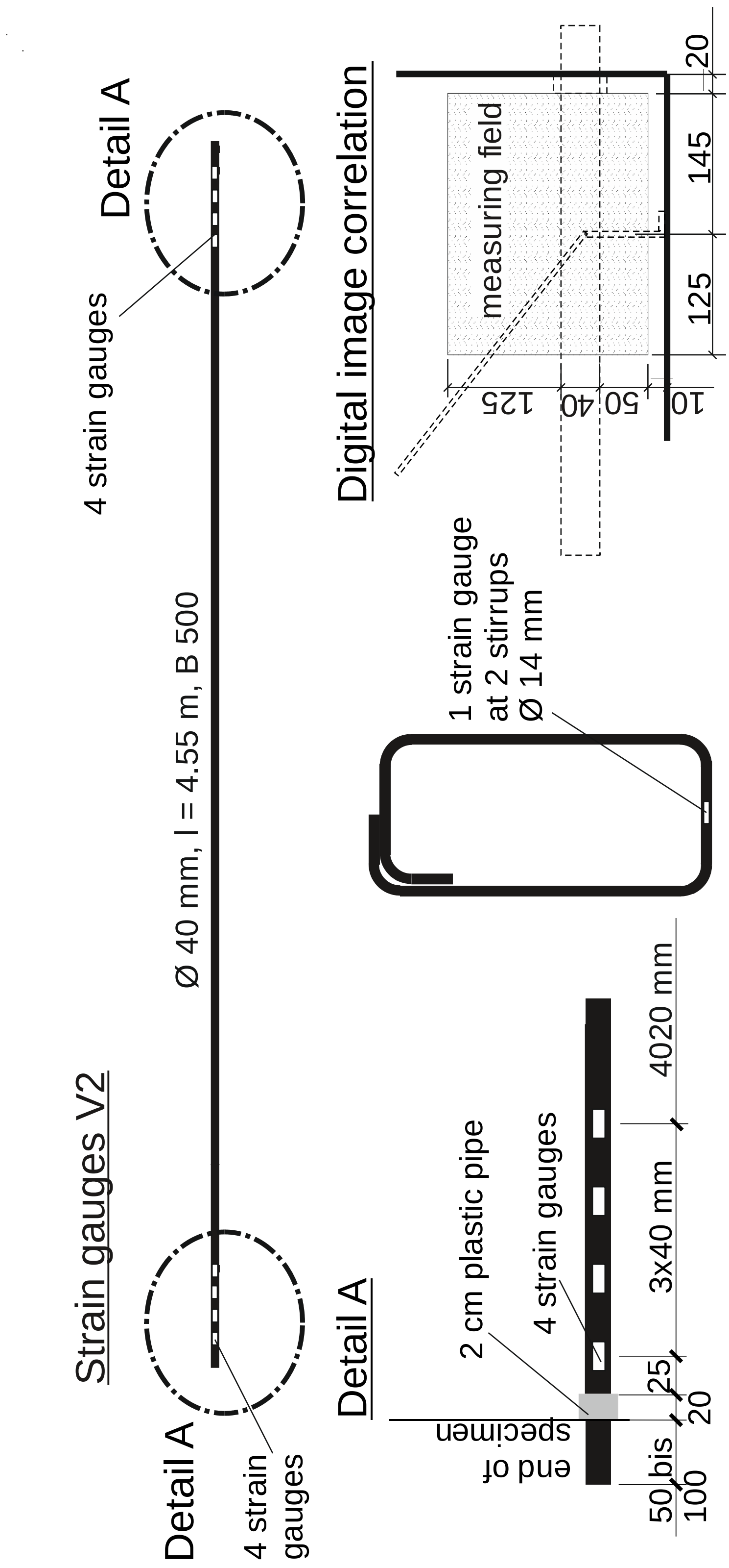

Figure A 49 Instrumentation anchorage test V2

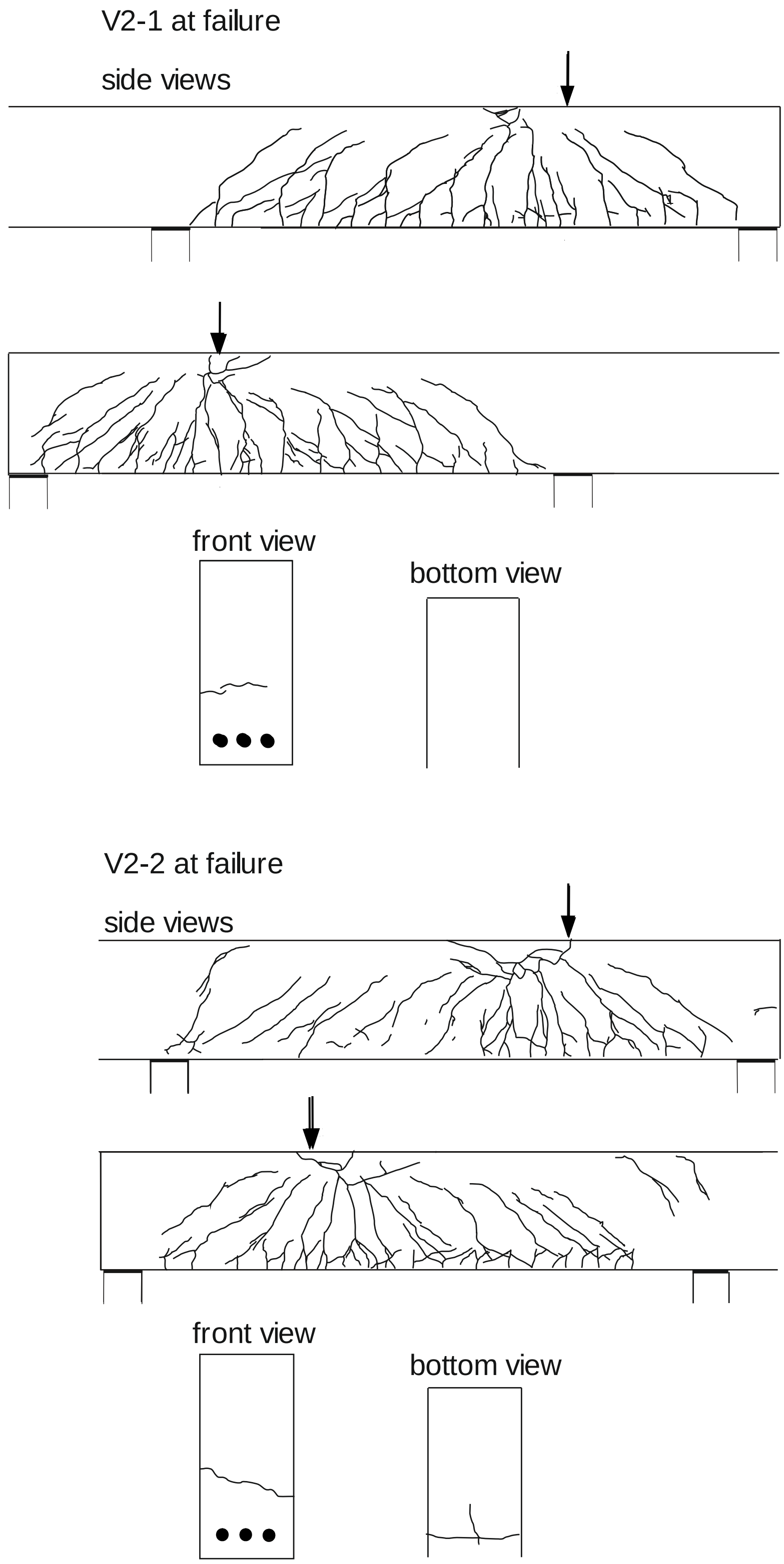

Figure A 50 Crack development in anchorage tests V2-1 and V2-2

A.2.4.3. Anchorage test V3

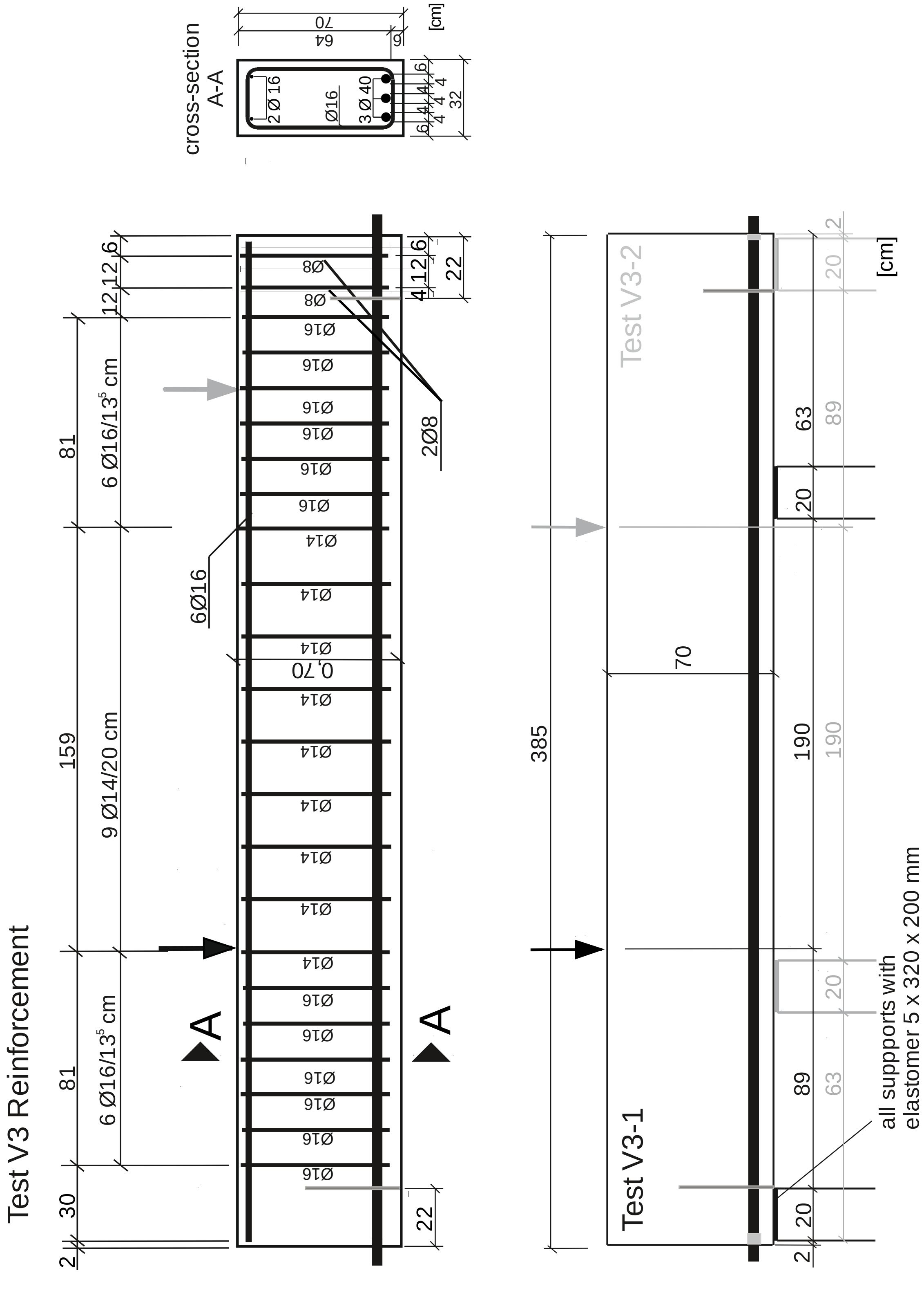

Figure A 51 Reinforcement layout anchorage test V3

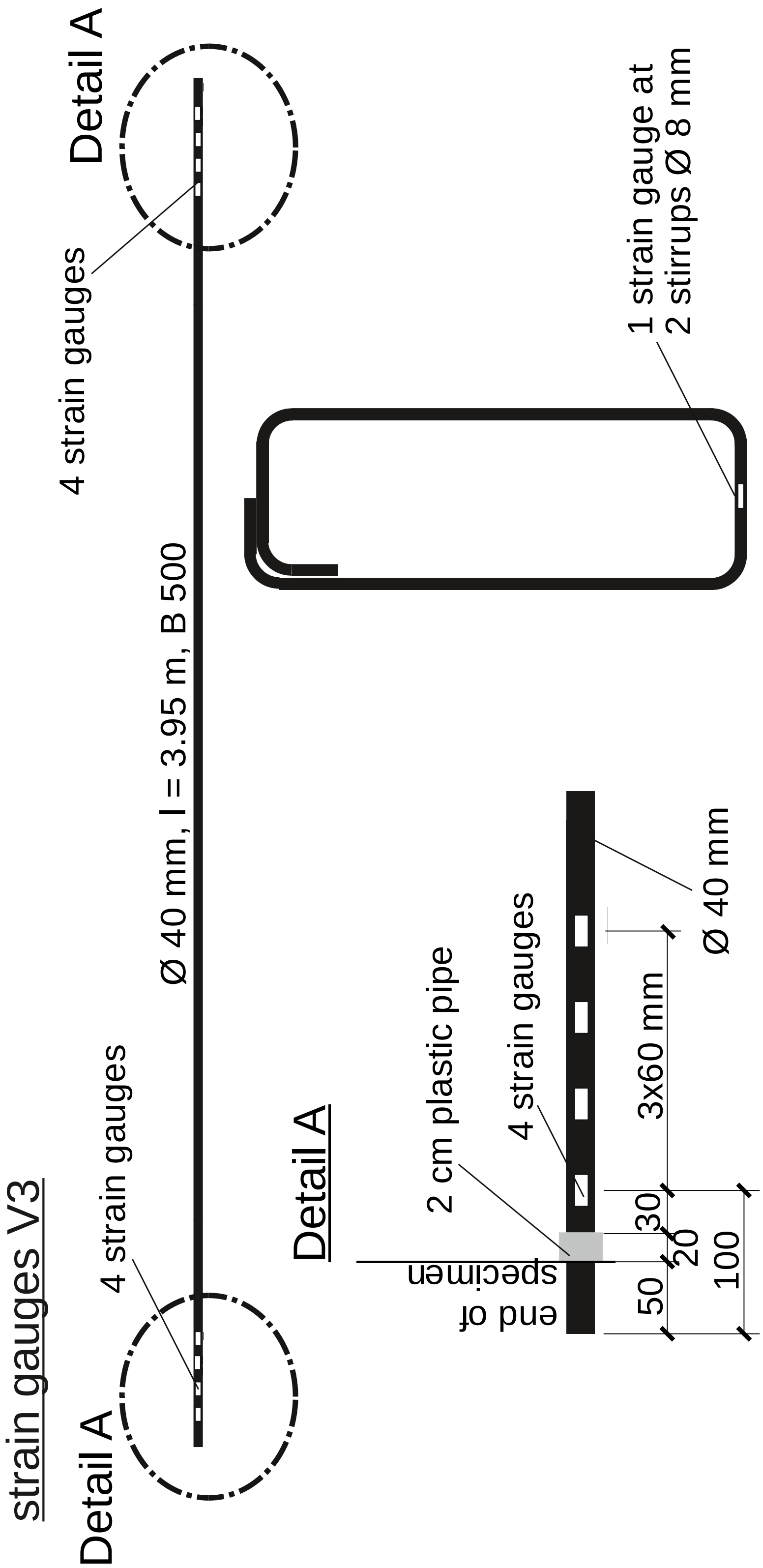

Figure A 52 Instrumentation anchorage test V3

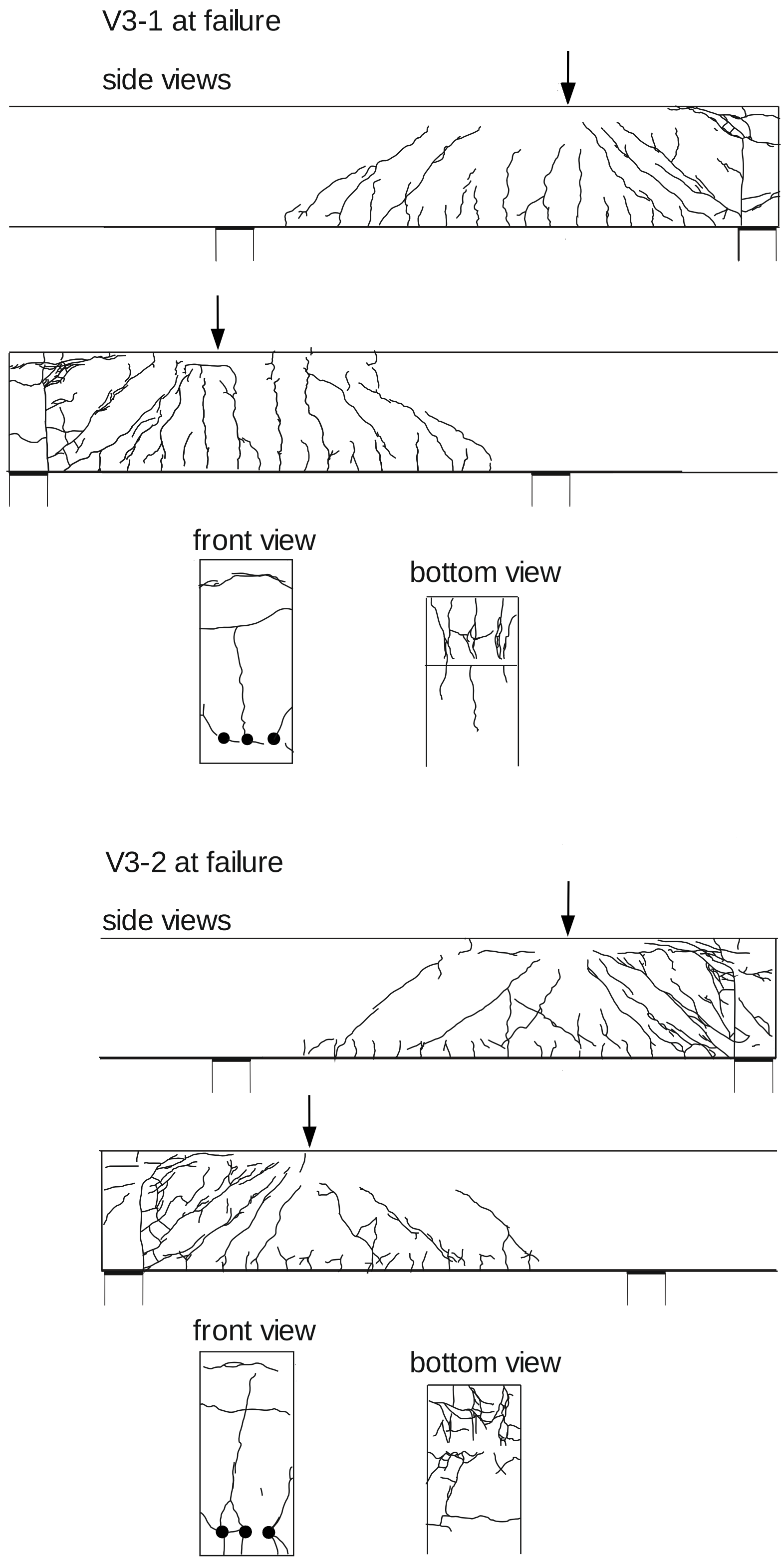

Figure A 53 Crack development in anchorage tests V3-1 and V3-2

A.2.4.4. Anchorage test V4

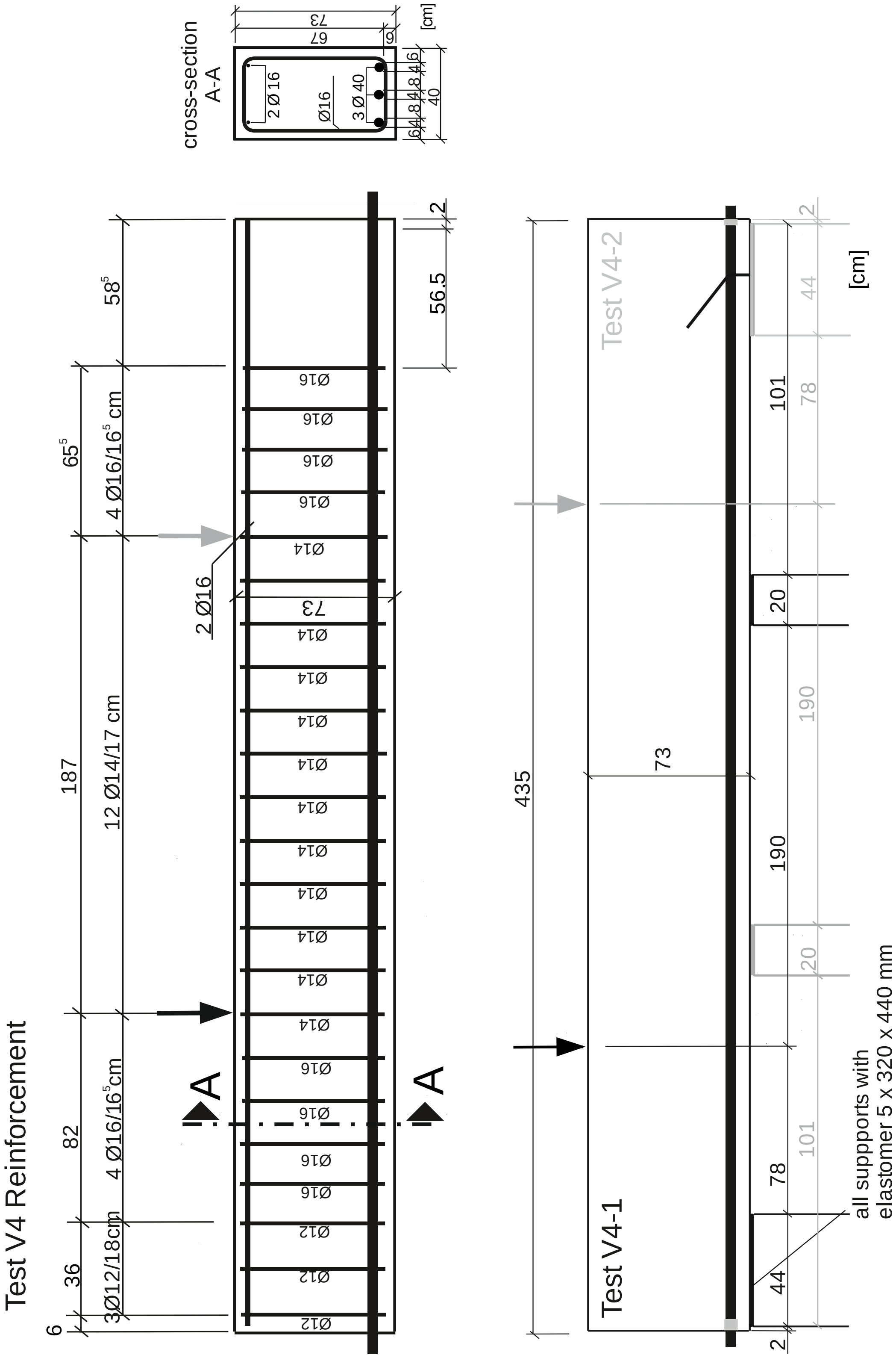

Figure A 54 Reinforcement layout anchorage test V4

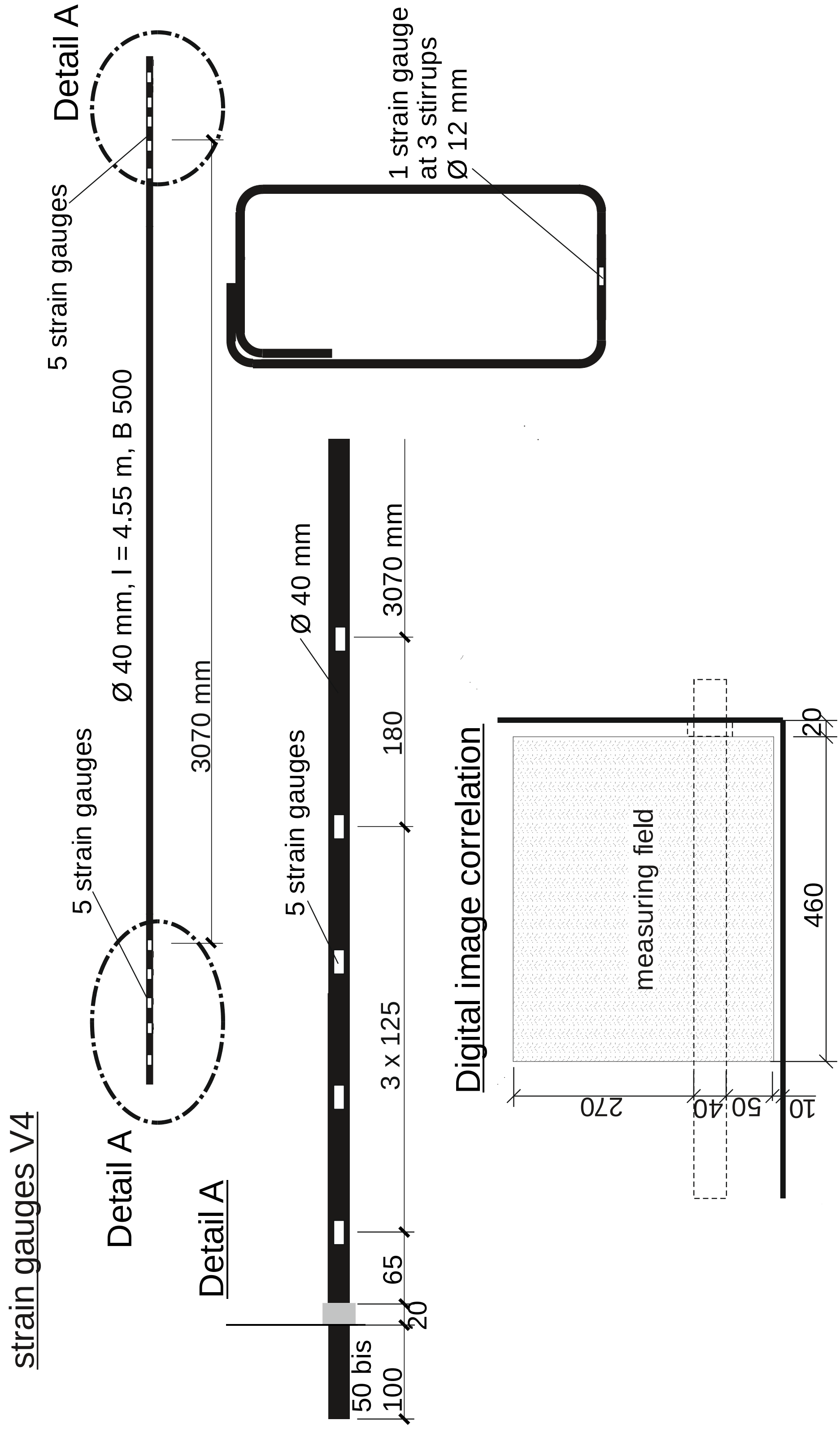

Figure A 55 Instrumentation anchorage test V4

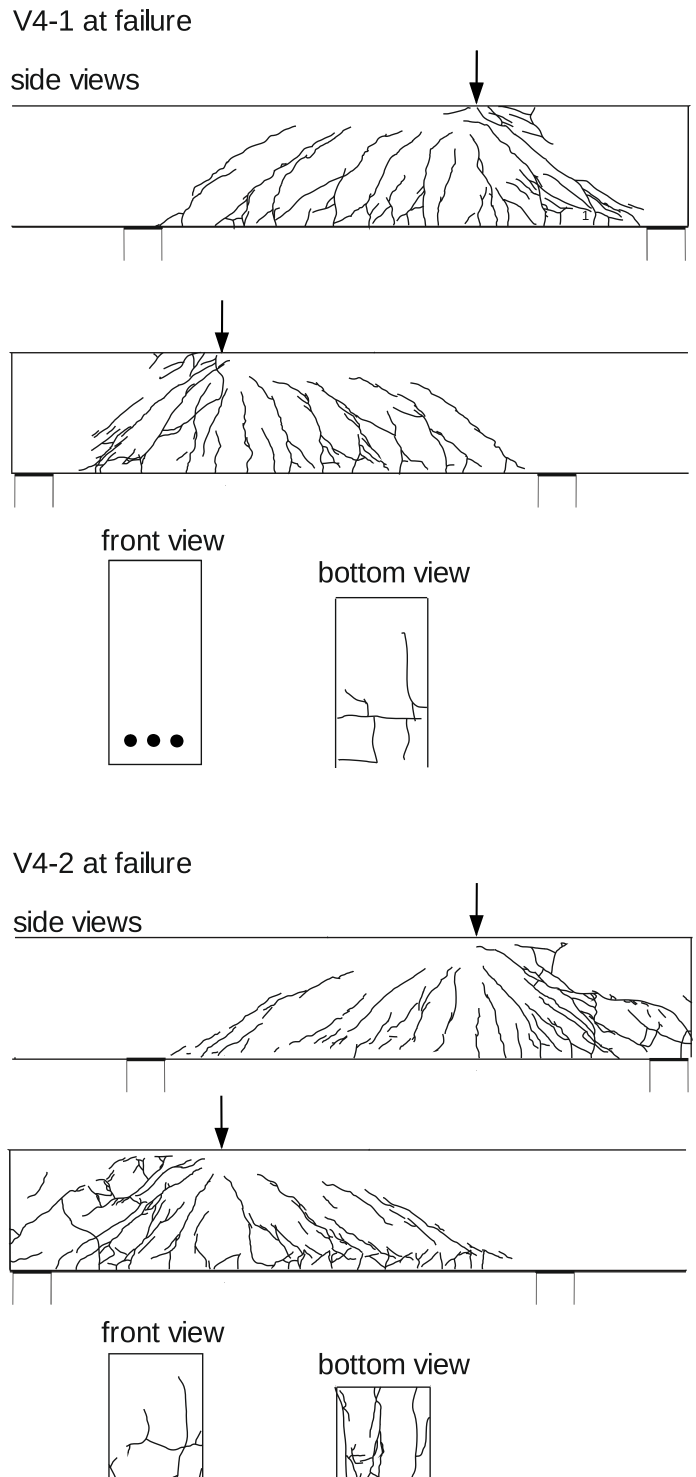

Figure A 56 Crack development in anchorage tests V4-1 and V4-2

A.2.4.5. Anchorage test V5

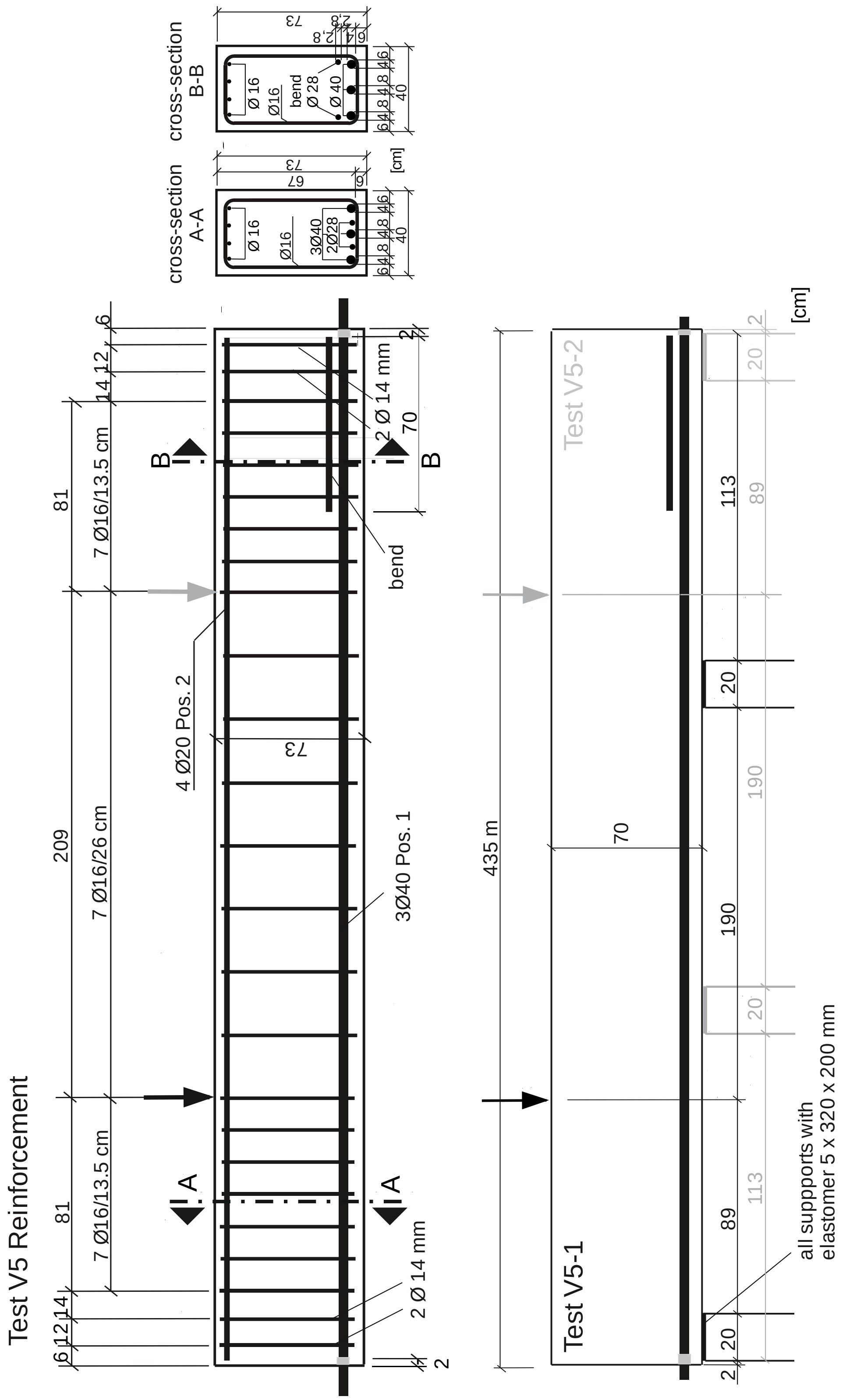

Figure A 57 Reinforcement layout anchorage test V5

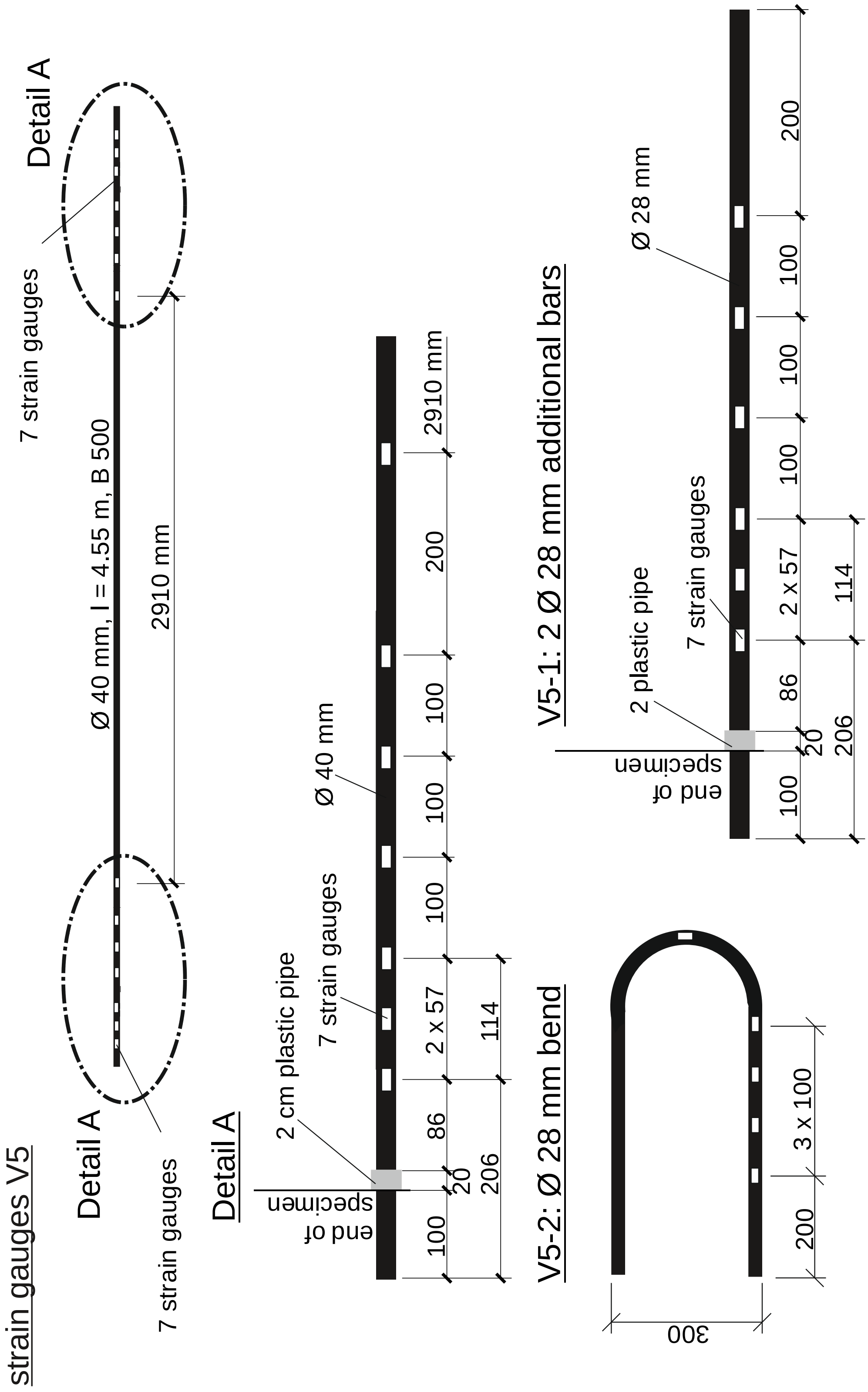

Figure A 58 Instrumentation anchorage test V5

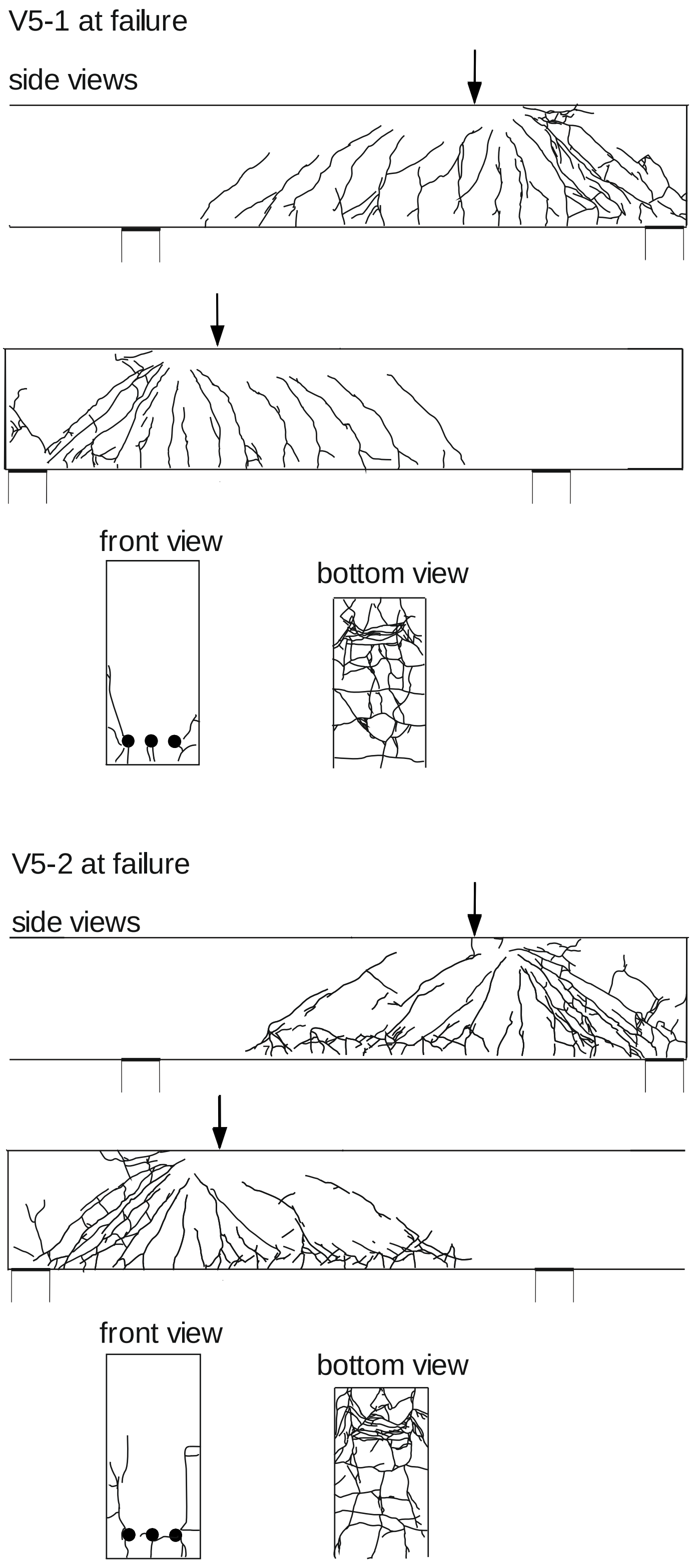

Figure A 59 Crack development in anchorage tests V5-1 and V5-2

A.2.4.6. Anchorage test V6

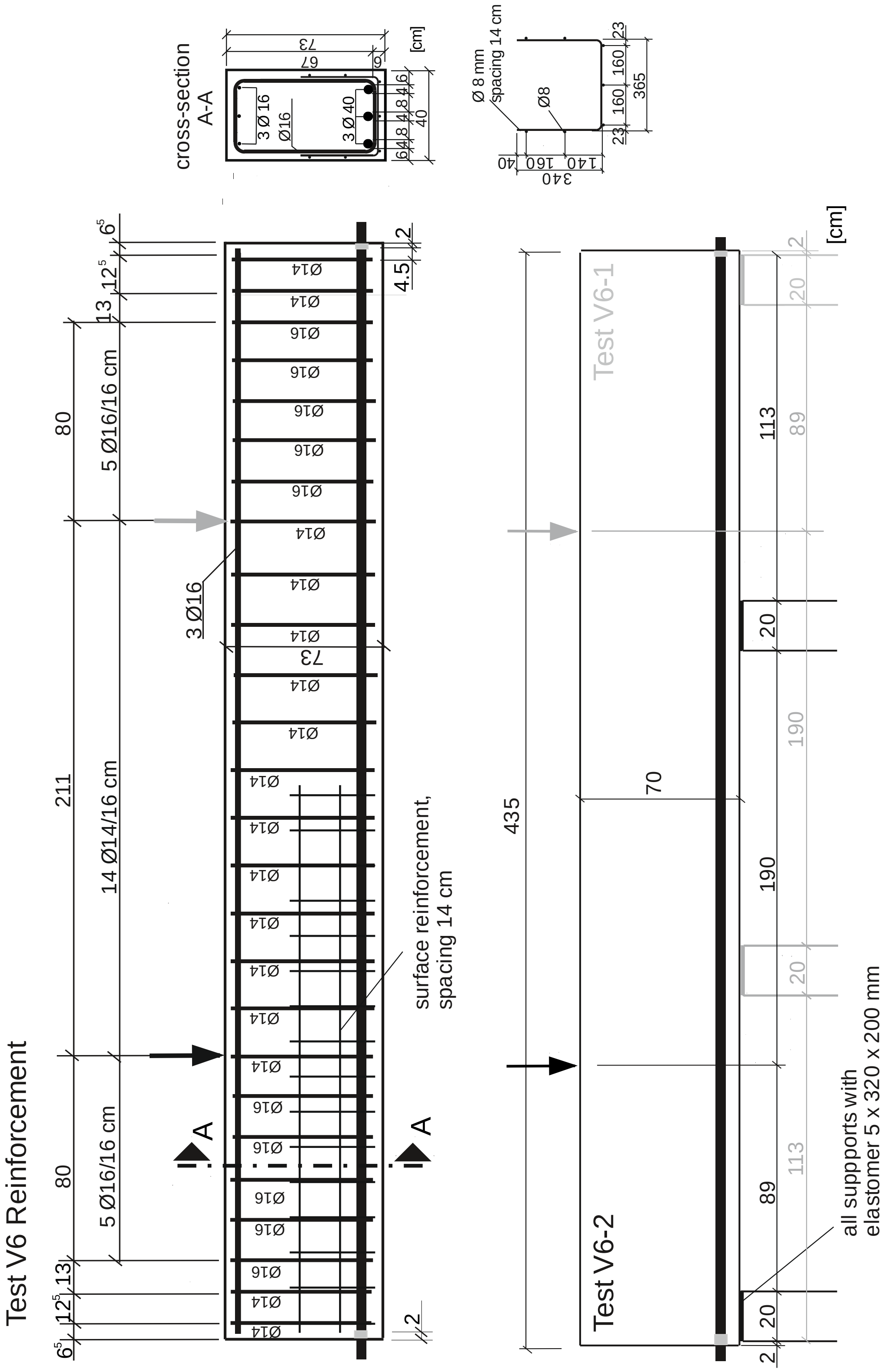

Figure A 60 Reinforcement layout anchorage test V6

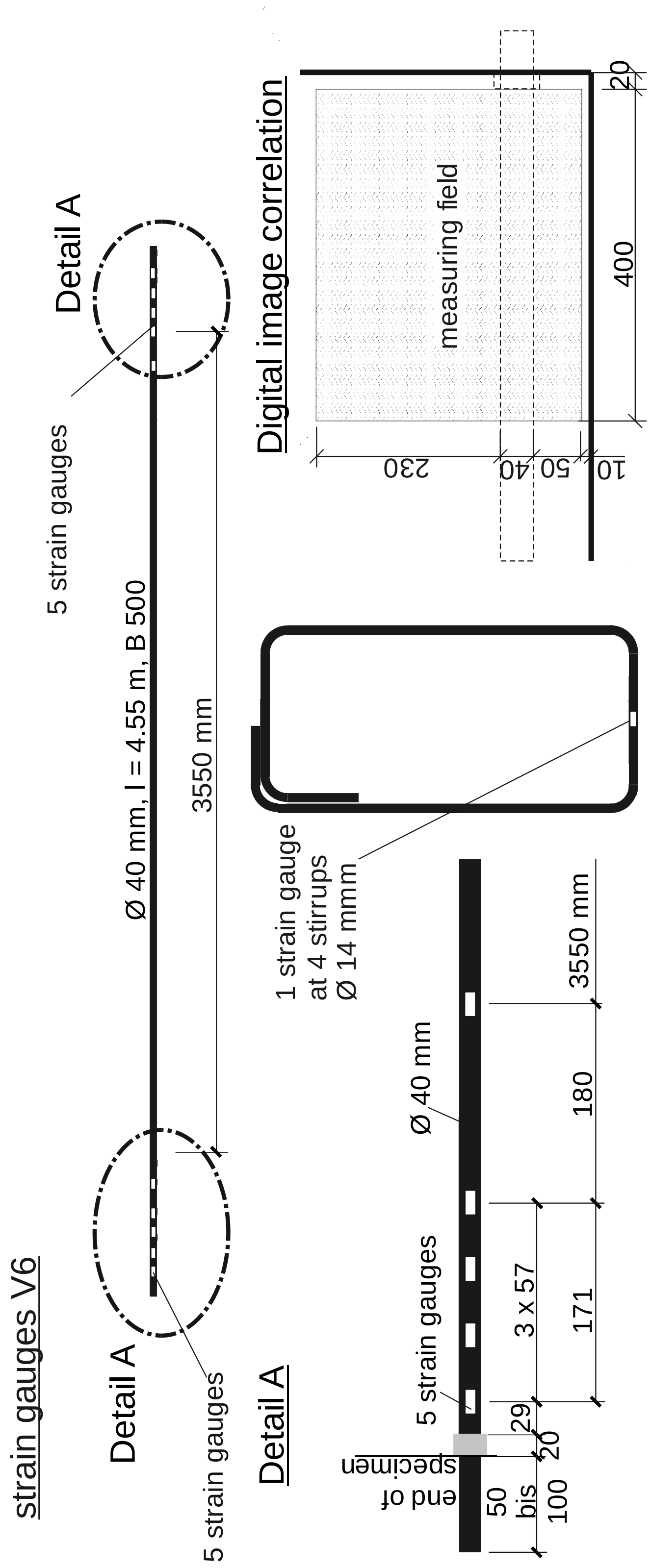

Figure A 61 Instrumentation anchorage test V6

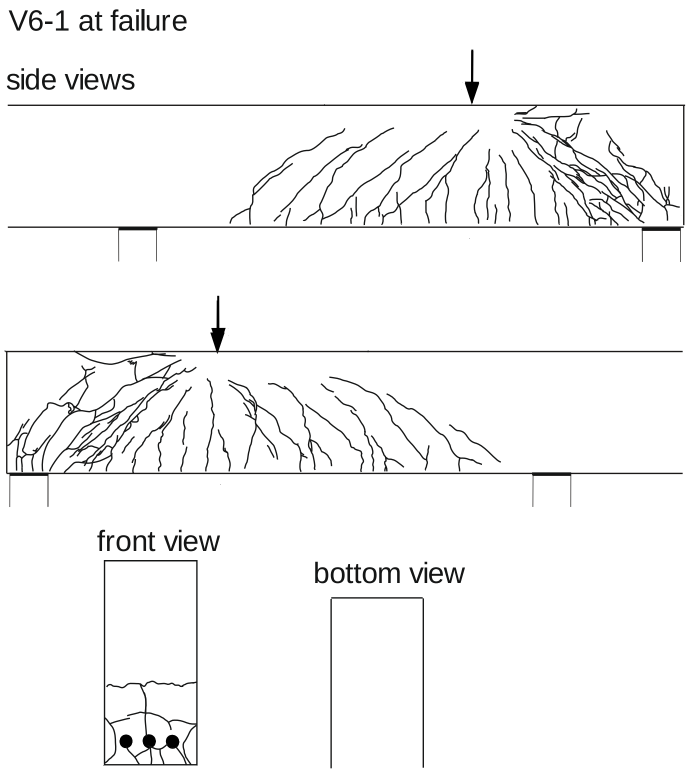

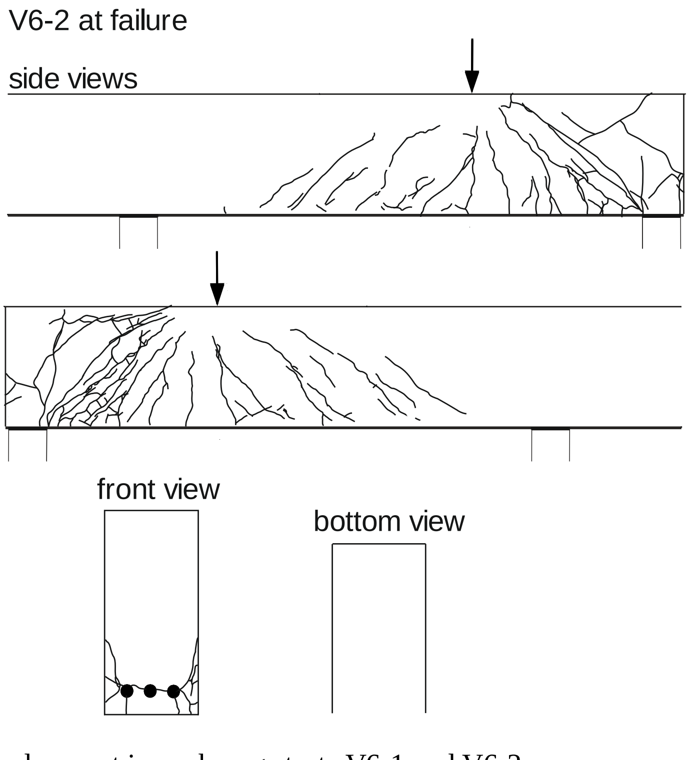

Figure A 62 Crack development in anchorage tests V6-1 and V6-2

A.2.4.7. Strain Measurements in Anchorage Tests

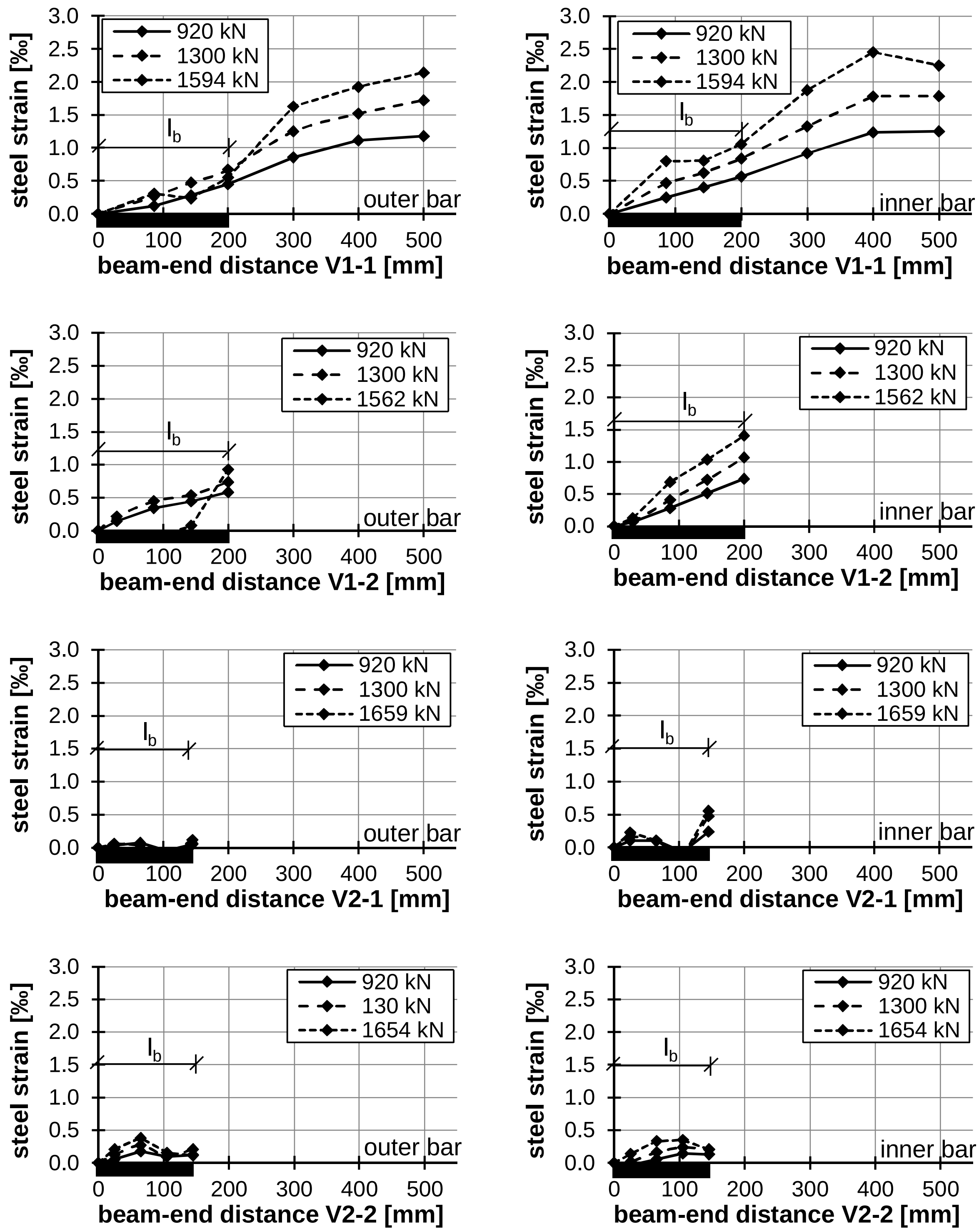

Figure A 63 Strain measurements along the anchorage length in tests V1-1, V1-2, V2-1 and V2-2

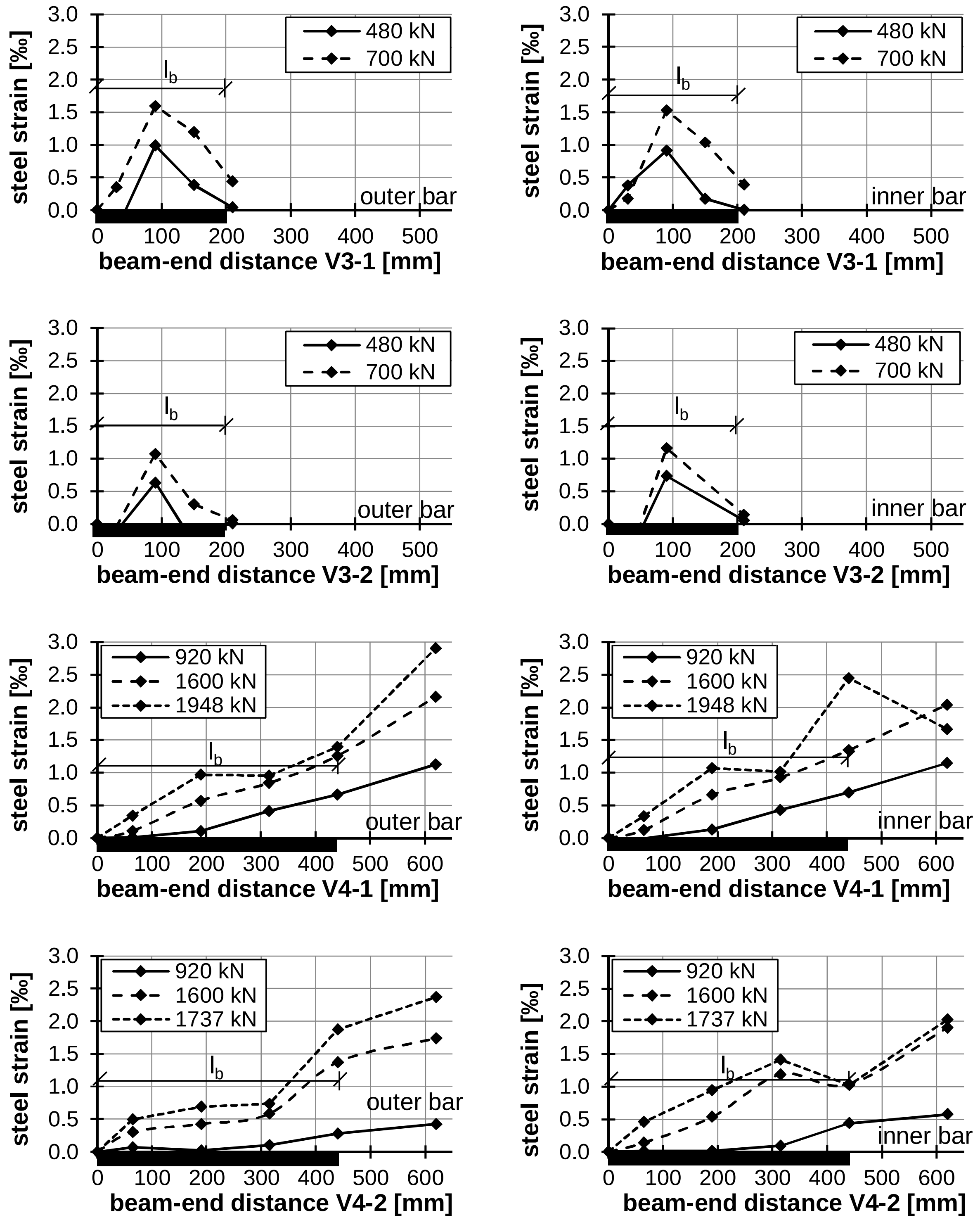

Figure A 64 Strain measurements along the anchorage length in tests V3-1, V3-2, V4-1 and V4-2

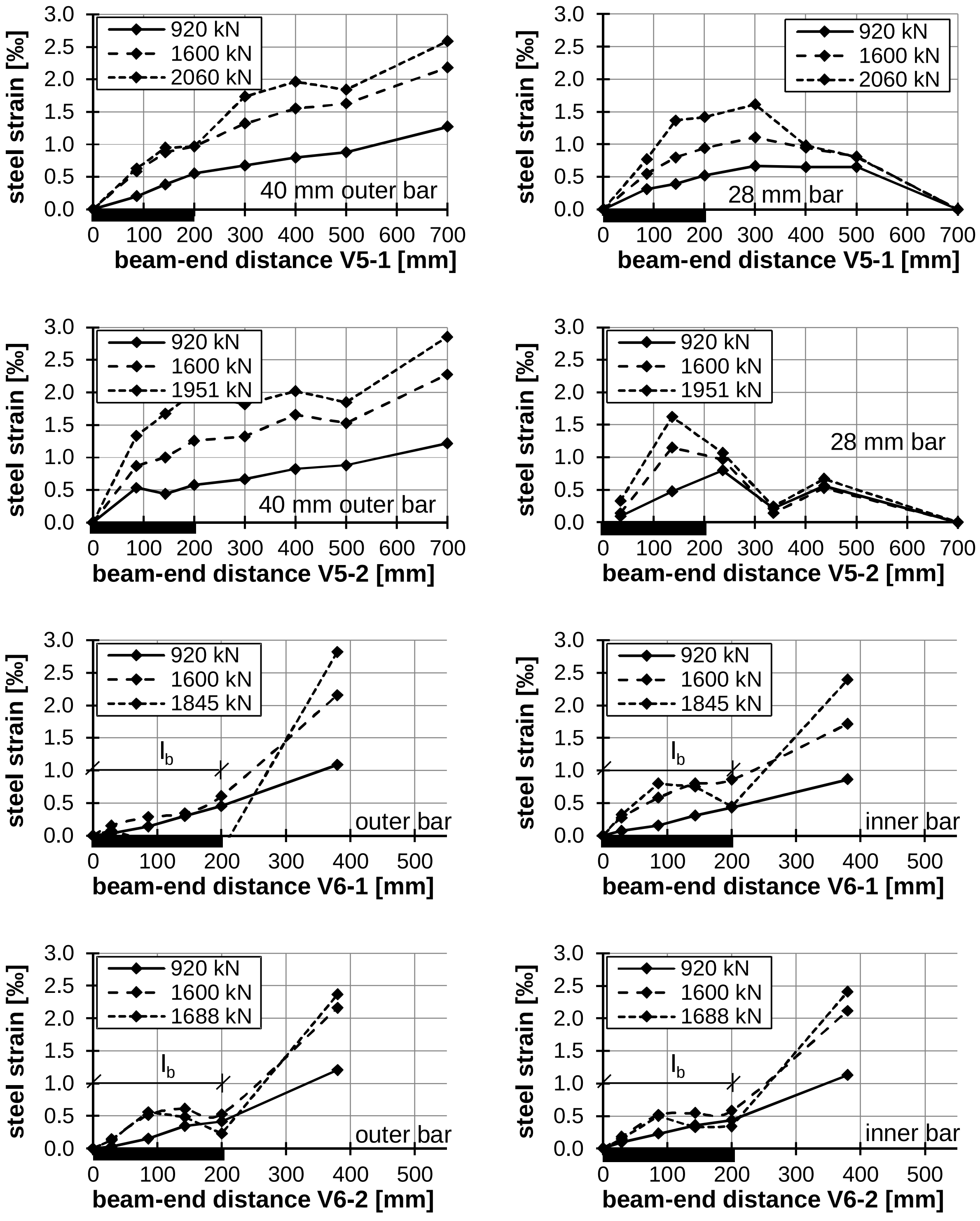

Figure A 65 Strain measurements along the anchorage length in tests V5-1, V5-2, V6-1 and V6-2

A.3. Test series included in lap database

A.3.1. General

Numbers given in Table 2-1:

1 Tests with transverse reinforcement

2 Tests without transverse reinforcement

3 fib database 2005 [FIB05]

4 fib database 2006 with filter

5 ACI database 2001 [ACI01] (bottom bars only)

6 LETTOW database 2006 [LET06a]

7 own database 2018

8 own database 2018, filtered:
laps only, l_0 / Ø > 14.5, f_{cm} > 20 MPa, c_{min} > 0.95, $\sigma_s < 1.2 \cdot f_y$

9 fib bulletin 72, filtered:
l_0 / Ø >15, f_{cm} > 20 MPa, c_{min} > 0.95, $\sigma_s < 1.2 \cdot f_y$

10 CAIRNS AND ELIGEHAUSEN [CAI14], filtered:
f_c > C20/25, c_{min} > Ø, $\sigma_s < 1.2 \cdot f_y$

[1] cantilever

[2] tension member

Table A 6 Considered lap tests in the different evaluations of the database

	1	2	3	4	5	6	7	8	9	10
Total test number	807	555	494	793	807	507	781	457	807	555
Number with transverse reinforcement	370	370	253	391	402	251	388	231	370	370
Number without transverse reinforcement	437	437	241	402	405	256	393	226	437	437
Author										
[AZI95]	7	0	x		-		x	x		
[AZI97]	25	32	x		x		x	x		
[AZI93]	0	18	x		-		x	x		
[BET80]	5	0	x		-		x	x		
[CHA56]	0	11	x		x		x	x		
[CHA58]	0.0	6.0	x		x		x	x		
[CHI55]	0.0	32.0	x		x		x	x		
[CHO91]	0	8	x		x		x	x		
[DAR95]	60	13	x		x		x	x		
[DEV91]	10	0	x		x		x	x		
[ELI79]	0	8	x		-		x	x		
[FER65b]	9	26	x		x		x	x		
[FER65a][1]	0	4	x		x		x	x		
[FER69]			-							
[FER62]			-							
[FER71]			-							
[HAM99]	0	8	x		x		x	x		
[HAM96]	0	17	x		-		x	x		
[HAM90]			-							
[HAS96]	2	0	x		x		x	x		
[HEG99]	5	4	x		-		x	x		
[HES93]	10	7	x		x		x	x		
[HWA94]	4	4	x		-		x	x		
[HWA96]	8	2	x		-		x	x		
[KAD94]	34	0	x		x		x	x		
[MAT61]	0	14	x		x		x	x		
[OLS90][2]	21	0	x		-		x	x		
[REH77]	19	1	x		-		x	x		
[REZ93]	11	4	x		x		x	x		
[REZ92]	0	34	x		x		x	x		
[STO77][2]	25	0	x		-		x	x		
[TEP73]	12	169	x		-		x	x		
[THO75]	4	11	x		x		x	x		
[TRE89]			-							
[ZEK81]	10	2	x		x		x	x		
[ZUO98]	63	28	x		x		x	x		
[HEG15] [HEG18]	16	1	-		-		x	x		

A.3.2. AHLBORG [AHL02]

Author	Test	l_0	n_b	Ø	c_x	c_s	c_y	f_{cm}	$Ø_{st}$	n_{st}	s_t	n_l	f_R	f_y	$\sigma_{s,max}$
		[mm]	-	[mm]	[mm]	[mm]	[mm]	[MPa]	[mm]	-	[mm]	-	-	[MPa]	[MPa]
[55]	MMFX1	153	1	19.1	38.2	0	82.7	37.9	-	-	-	-	*	500	252
[55]	MMFX2	153	1	19.1	38.2	0	82.7	37.9	-	-	-	-	*	500	300
[55]	MMFX3	153	1	19.1	38.2	0	82.7	37.9	-	-	-	-	*	500	300
[55]	MMFX4	153	1	19.1	38.2	0	82.7	37.9	-	-	-	-	*	500	305
[55]	MMFX5	153	1	19.1	38.2	0	82.7	37.9	-	-	-	-	*	500	311
[55]	MMFX6	153	1	19.1	38.2	0	82.7	37.9	-	-	-	-	*	500	315
[55]	MMFX7	204	1	19.1	38.2	0	82.7	37.9	-	-	-	-	*	500	394
[55]	MMFX8	204	1	19.1	38.2	0	82.7	37.9	-	-	-	-	*	500	405
[55]	MMFX9	204	1	19.1	38.2	0	82.7	37.9	-	-	-	-	*	500	381
[55]	MMFX10	204	1	19.1	38.2	0	82.7	37.9	-	-	-	-	*	500	391
[55]	MMFX11	204	1	19.1	38.2	0	82.7	37.9	-	-	-	-	*	500	363
[55]	MMFX12	204	1	19.1	38.2	0	82.7	37.9	-	-	-	-	*	500	389
[55]	MMFX13	255	1	19.1	38.2	0	82.7	37.9	-	-	-	-	*	500	378
[55]	MMFX14	255	1	19.1	38.2	0	82.7	37.9	-	-	-	-	*	500	381
[55]	MMFX15	255	1	19.1	38.2	0	82.7	37.9	-	-	-	-	*	500	423
[55]	MMFX16	255	1	19.1	38.2	0	82.7	37.9	-	-	-	-	*	500	440
[55]	MMFX17	255	1	19.1	38.2	0	82.7	37.9	-	-	-	-	*	500	361
[55]	MMFX18	306	1	19.1	38.2	0	82.7	37.9	-	-	-	-	*	500	378
[55]	MMFX19	306	1	19.1	38.2	0	82.7	37.9	-	-	-	-	*	500	418
[55]	MMFX20	306	1	19.1	38.2	0	82.7	37.9	-	-	-	-	*	500	382
[55]	MMFX21	306	1	19.1	38.2	0	82.7	37.9	-	-	-	-	*	500	413
[55]	MMFX22	306	1	19.1	38.2	0	82.7	37.9	-	-	-	-	*	500	382
[55]	MMFX23	306	1	19.1	38.2	0	82.7	37.9	-	-	-	-	*	500	371

A.3.3. Amin [AMI09]

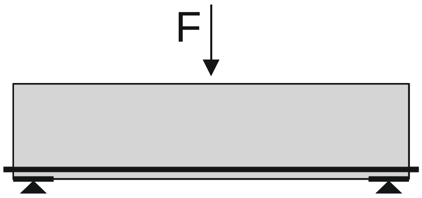

type I

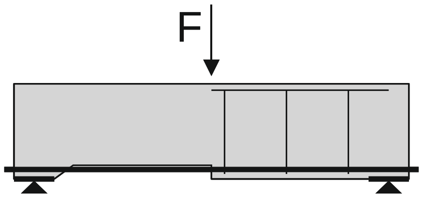

type II

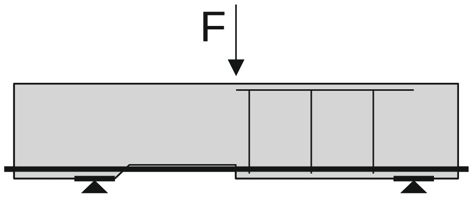

type III

Author	Test	l_0	n_b	Ø	c_x	c_s	c_y	f_{cm}	$Ø_{st}$	n_{st}	s_t	n_l	f_R	f_y	$\sigma_{s,max}$
		[mm]	-	[mm]	[mm]	[mm]	[mm]	[MPa]	[mm]	-	[mm]	-	-	[MPa]	[MPa]
[43]	Bs4	150	2	16	25	247	25	28.2	-	0	-	-	*	521	202
[43]	Bs5	160	2	16	25	247	25	27.6	-	0	-	-	*	521	102
[43]	Bs6	240	2	16	25	247	25	22.4	-	0	-	-	*	521	196
[43]	Bs7	320	2	16	25	247	25	21.6	-	0	-	-	*	521	175
[43]	Bs8	160	2	16	55	243	25	21.6	-	0	-	-	*	521	151
[43]	Bs9	240	2	16	55	243	25	21.6	-	0	-	-	*	521	240
[43]	Bs10	150	2	16	55	243	25	22.4	-	0	-	-	*	521	231
[43]	Bs11	100	2	16	25	247	25	23.9	-	0	-	-	*	521	155
[43]	Bs12	100	2	16	55	243	25	23.9	-	0	-	-	*	521	239
[43]	Bs13	150	2	16	25	247	25	27.5	-	0	-	-	*	521	127
[43]	Bs14	150	2	16	55	243	25	27.5	-	0	-	-	*	521	210
[43]	Bs15	150	2	16	25	247	25	27.5	-	0	-	-	*	521	134
[43]	Bs16	150	2	16	55	243	25	26.4	-	0	-	-	*	521	146
[43]	Bs17	240	2	16	25	247	25	26.4	-	0	-	-	*	521	189
[43]	Bs18	240	2	16	55	243	25	26.4	-	0	-	-	*	521	255
[43]	Bs19	100	2	16	25	247	25	31.6	-	0	-	-	*	521	131
[43]	Bs20	100	2	16	25	247	25	31.6	-	0	-	-	*	521	166
[43]	Bs21	95	2	16	25	197	25	40.48	-	0	-	-	*	560	149
[43]	Bs22	150	2	16	25	197	25	29.28	-	0	-	-	*	560	160
[43]	Bs23	150	2	16	25	197	16	25.52	-	0	-	-	*	560	183
[43]	Bs24	100	2	16	25	197	25	31.44	6	2	100	2	*	560	170
[43]	Bs25	150	2	16	25	197	25	26.96	-	0	-	-	*	560	177
[43]	Bs26	150	2	16	25	197	16	30.4	-	0	-	-	*	560	167
[43]	Bs27	100	1	16	67	0	16	30.8	-	0	-	-	*	560	333
[43]	Bs28	100	1	16	67	0	16	30.8	-	0	-	-	*	560	542
[43]	Bs29	150	1	16	67	0	16	34.56	-	0	-	-	*	560	488
[43]	Bs30	150	1	16	0	0	16	34.56	6	2	100	2	*	560	580
[43]	Bs31	100	2	16	25	197	25	34.56	-	0	-	-	*	560	114
[43]	Bs32	150	2	16	25	197	25	31.84	-	0	-	-	*	560	159
[43]	Bs33	150	2	16	25	197	25	27.36	-	0	-	-	*	560	156
[43]	Bs34	150	2	16	25	197	25	31.92	6	2	100	2	*	560	189
[43]	Bs35	100	2	16	25	197	25	25.52	-	0	-	-	*	560	85
[43]	Bs36	100	2	16	16	198	25	28.72	-	0	-	-	*	560	88
[43]	Bs37	150	2	16	16	198	25	32.8	-	0	-	-	*	560	165

A.3.4. ATKINS [ATK97]

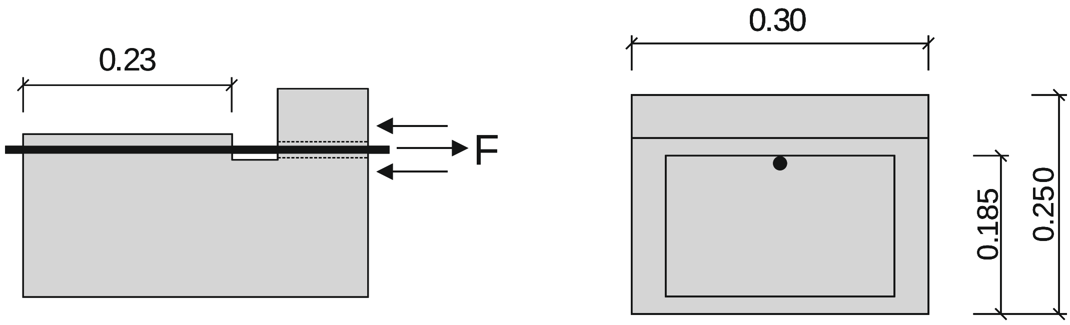

Author	Test	l_0	n_b	Ø	c_x	c_s	c_y	f_{cm}	$Ø_{st}$	n_{st}	s_t	n_l	f_R	f_y	$\sigma_{s,max}$
		[mm]	-	[mm]	[mm]	[mm]	[mm]	[MPa]	[mm]	-	[mm]	-	-	[MPa]	[MPa]
[56]	B7	230	1	20	10	0	140	36.2	-	-	-	-	*	500	270
[56]	B8	230	1	20	20	0	140	36.2	-	-	-	-	*	500	318
[56]	B9	230	1	20	30	0	140	36.2	-	-	-	-	*	500	382
[56]	B10	230	1	20	10	0	140	36.2	-	-	-	-	*	500	334
[56]	B11	230	1	20	20	0	140	36.2	-	-	-	-	*	500	334
[56]	B12	230	1	20	30	0	140	36.2	-	-	-	-	*	500	366

A.3.5. AZIZINAMINI; CHISALA; GHOSH[AZI95]

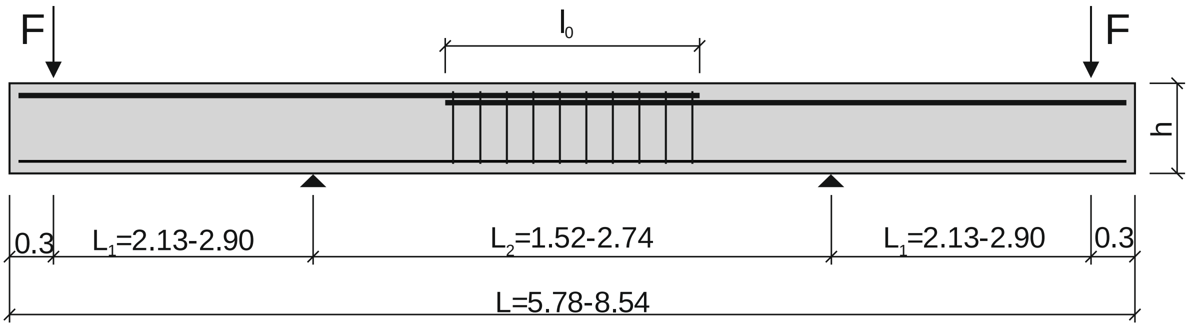

Author	Test	l_0	n_b	Ø	c_x	c_s	c_y	f_{cm}	$Ø_{st}$	n_{st}	s_t	n_l	f_R	f_y	$\sigma_{s,max}$
		[mm]	-	[mm]	[mm]	[mm]	[mm]	[MPa]	[mm]	-	[mm]	-	-	[MPa]	[MPa]
[01]	57.5S-50	1461	2	35	35	70	35	104	6	6	254	2	*	508	513
[01]	57.5S-60	1461	3	35	35	70	35	114	10	5	305	2	0.06	488	504
[01]	57.5S-100	1461	3	345	35	70	35	104	10	9	178	2	*	488	552
[01]	57.5S-150	1461	3	345	35	70	35	104	10	12	127	2	*	488	548
[01]	45S-60	1143	3	35	35	70	35	103	10	4	305	2	0.06	488	521
[01]	45S-100	1143	3	35	35	70	35	102	10	6	203	2	0.06	488	523
[01]	40S-150	1016	3	35	35	70	35	109	10	8	127	2	0.06	488	508

A.3.6. AZIZINAMINI; PAVEL; HATFIELD; GHOSH [AZI99]

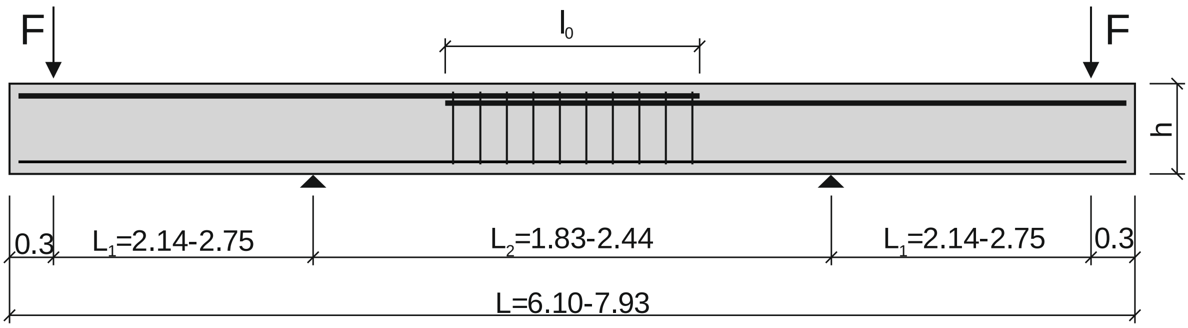

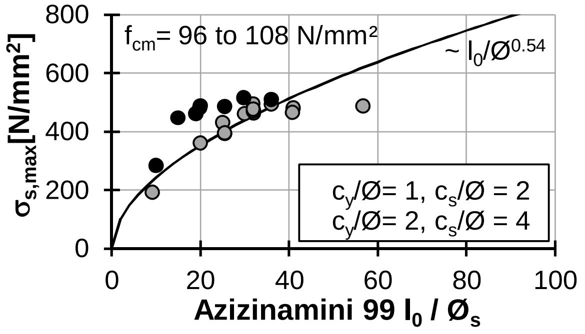

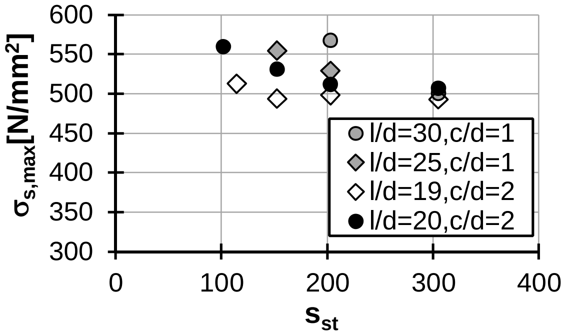

Author	Test	l_0	n_b	Ø	c_x	c_s	c_y	f_{cm}	$Ø_{st}$	n_{st}	s_t	n_l	f_R	f_y	$\sigma_{s,max}$
		[mm]	-	[mm]	[mm]	[mm]	[mm]	[MPa]	[mm]	-	[mm]	-	-	[MPa]	[MPa]
[02]	1	1041	2	25.4	25	76	25	104	-	-	-	-	*	537	481
[02]	2	914	3	25.4	25	51	25	100	-	-	-	-	0.074	497	494
[02]	3	813	2	25.4	25	76	25	107	-	-	-	-	0.074	497	475
[02]	4	813	2	25.4	25	76	25	107	-	-	-	-	0.074	497	462
[02]	5	762	3	25.4	25	51	25	104	-	-	-	-	0.074	497	461
[02]	6	635	2	25.4	25	76	25	106	-	-	-	-	0.074	497	430
[02]	7	584	2	25.4	25	76	25	36	-	-	-	-	*	537	308
[02]	8	508	2	25.4	25	76	25	106	-	-	-	-	0.074	497	361
[02]	16	914	2	25.4	51	102	51	100	-	-	-	-	0.074	497	510
[02]	17	508	2	25.4	51	102	51	104	-	-	-	-	0.074	497	488
[02]	18	483	2	25.4	51	102	51	107	-	-	-	-	0.074	497	460
[02]	19	483	2	25.4	51	102	51	107	-	-	-	-	0.074	497	463
[02]	20	381	2	25.4	51	102	51	106	-	-	-	-	0.074	497	447
[02]	21	254	2	25.4	51	102	51	106	-	-	-	-	0.074	497	283
[02]	29	2032	2	36	35	92	35	104	-	-	-	-	*	508	488
[02]	30	1461	2	36	35	92	35	96	-	-	-	-	*	508	465
[02]	31	1143	3	36	35	86	35	109	-	-	-	-	0.086	493	495
[02]	32	1143	2	36	35	92	35	107	-	-	-	-	0.086	493	471
[02]	33	1143	2	36	35	92	35	107	-	-	-	-	0.059	488	478
[02]	34	1143	3	36	35	86	35	75	-	-	-	-	0.059	488	336
[02]	36	1016	2	36	35	92	35	90	-	-	-	-	*	488	403
[02]	37	1016	3	36	35	86	35	94	-	-	-	-	0.059	488	314
[02]	39	1016	2	36	35	92	35	35	-	-	-	-	*	488	297
[02]	40	914	3	36	35	86	35	100	-	-	-	-	0.059	488	393
[02]	42	914	3	36	35	86	35	100	-	-	-	-	0.059	488	395
[02]	43	914	3	36	35	86	35	43	-	-	-	-	0.059	488	322
[02]	45	610	2	36	35	92	35	88	-	-	-	-	*	488	306
Author	Test	l_0	n_b	Ø	c_x	c_s	c_y	f_{cm}	$Ø_{st}$	n_{st}	s_t	n_l	f_R	f_y	$\sigma_{s,max}$
		[mm]	-	[mm]	[mm]	[mm]	[mm]	[MPa]	[mm]	-	[mm]	-	-	[MPa]	[MPa]

[02]	46	610	2	36	35	92	35	35	-	-	-	-	*	488	205
[02]	48	330	2	36	35	92	35	99	-	-	-	-	*	508	192
[02]	58	1067	2	36	76	162	76	104	-	-	-	-	0.086	493	516
[02]	59	914	2	36	76	162	76	100	-	-	-	-	0.059	493	486
[02]	60	711	2	36	76	162	76	104	-	-	-	-	0.086	493	481
[02]	10	635	2	25.4	25	76	25	110	10	5	152	2	0.074	499	554
[02]	11	635	2	25.4	25	76	25	108	10	4	203	2	0.074	499	529
[02]	14	813	2	25.4	25	76	25	108	10	3	305	2	0.074	499	556
[02]	15	813	2	25.4	25	76	25	101	10	3	381	2	0.074	491	523
[02]	22	381	2	25.4	51	102	51	108	10	5	76	2	0.074	499	529
[02]	23	381	2	25.4	51	102	51	108	10	4	114	2	0.074	499	465
[02]	24	381	2	25.4	51	102	51	108	10	3	165	2	0.074	499	448
[02]	25	483	2	25.4	51	102	51	110	10	5	114	2	0.074	497	512
[02]	26	483	2	25.4	51	102	51	110	10	4	152	2	0.074	497	494
[02]	27	483	2	25.4	51	102	51	108	10	3	203	2	0.074	499	498
[02]	28	483	2	25.4	51	102	51	101	10	2	305	2	0.074	491	493
[02]	49	1016	3	36	35	86	35	109	10	8	127	2	0.059	488	480
[02]	52	1143	3	36	35	86	35	102	10	6	203	2	0.059	488	567
[02]	53	1143	3	36	35	86	35	103	10	4	305	2	0.059	488	501
[02]	56	1461	2	36	35	92	35	104	6	6	254	2	*	508	490
[02]	61	508	2	36	76	162	76	105	10	8	64	2	0.086	517	490
[02]	62	508	2	36	76	162	76	110	10	5	114	2	0.086	493	456
[02]	63	508	2	36	76	162	76	110	10	4	152	2	0.086	493	403
[02]	64	610	2	36	76	162	76	105	10	10	64	2	0.086	517	521
[02]	65	610	2	36	76	162	76	101	10	5	127	2	0.086	493	449
[02]	66	610	2	36	76	162	76	101	10	4	178	2	0.086	493	459
[02]	67	711	2	36	76	162	76	106	10	7	102	2	0.086	517	560
[02]	68	711	2	36	76	162	76	106	10	5	152	2	0.086	517	531
[02]	69	711	2	36	76	162	76	108	10	4	203	2	0.086	493	512
[02]	70	711	2	36	76	162	76	108	10	3	305	2	0.086	493	507

A.3.7. AZIZINAMINI; STARK [AZI93]

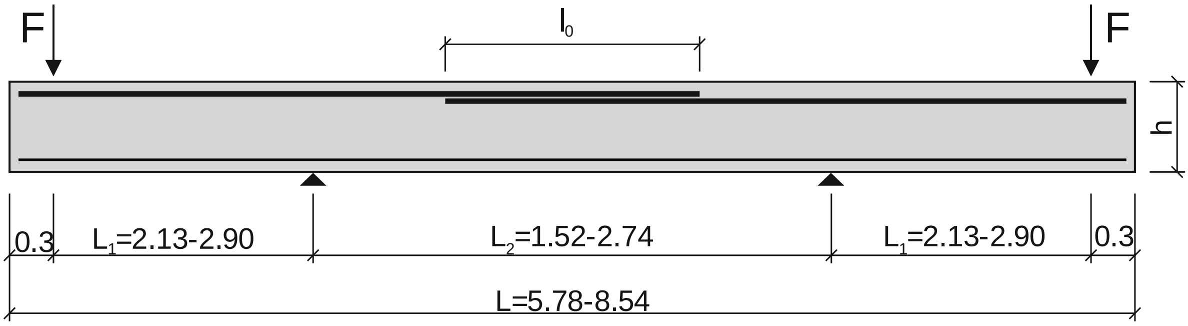

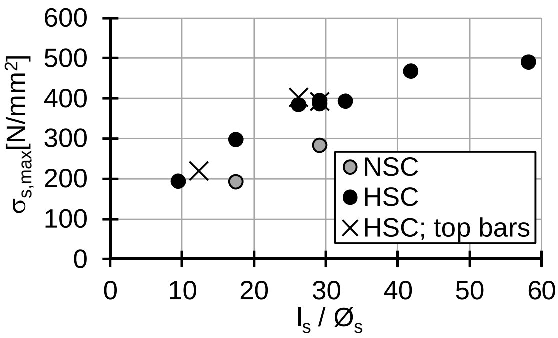

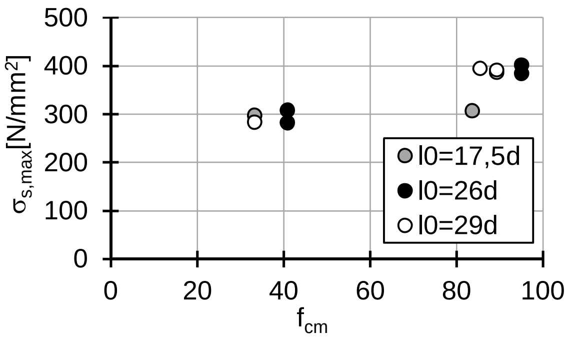

Author	Test	l_0	n_b	Ø	c_x	c_s	c_y	f_{cm}	$Ø_{st}$	n_{st}	s_t	n_l	f_R	f_y	$\sigma_{s,max}$
		[mm]	-	[mm]	[mm]	[mm]	[mm]	[MPa]	[mm]	-	[mm]	-	-	[MPa]	[MPa]
[03]	BB-11-5-24	610	2	34.93	35	92	35	33	-	-	-	-	*	488	192
[03]	BB-11-5-40	1016	2	34.93	35	92	35	33	-	-	-	-	*	488	283
[03]	BB-11-12-24	610	2	34.93	35	92	35	84	-	-	-	-	*	488	297
[03]	BB-11-12-40	1016	2	34.93	35	92	35	86	-	-	-	-	*	488	394
[03]	BB-11-11-45	1143	3	34.93	35	86	35	71	-	-	-	-	*	488	393
[03]	BT-11-11-45	1143	3	34.93	35	86	35	71	-	-	-	-	*	488	348
[03]	BB-11-15-36	914	3	34.93	35	86	35	95	-	-	-	-	*	488	384
[03]	BT-11-15-36	914	3	34.93	35	86	35	95	-	-	-	-	*	488	402
[03]	BB-11-5-36	914	3	34.93	35	86	35	41	-	-	-	-	*	488	308
[03]	BT-11-5-36	914	3	34.93	35	86	35	41	-	-	-	-	*	488	282
[03]	BB-11-13-40	1016	3	34.93	35	86	35	89	-	-	-	-	*	488	386
[03]	BT-11-13-40	1016	3	34.93	35	86	35	89	-	-	-	-	*	488	392
[03]	BB-11-15-3	330	2	34.93	35	92	35	99	-	-	-	-	*	508	194
[03]	BT-11-15-17	432	2	34.93	35	92	35	99	-	-	-	-	*	508	219
[03]	AB83-11-15-57.5	1461	2	34.93	35	92	35	96	-	-	-	-	*	508	468
[03]	AB89-11-15-80	2032	2	34.93	35	92	35	104	-	-	-	-	*	508	490
[03]	BB-8-5-23	584	2	25.4	25	76	25	36	-	-	-	-	*	537	307
[03]	AB83-8-15-41	1041	2	25.4	25	76	25	104	-	-	-	-	*	537	482

A.3.8. BATAYNEH [BAT93]

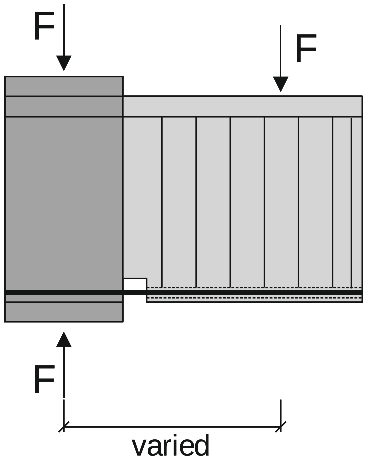

Beam test

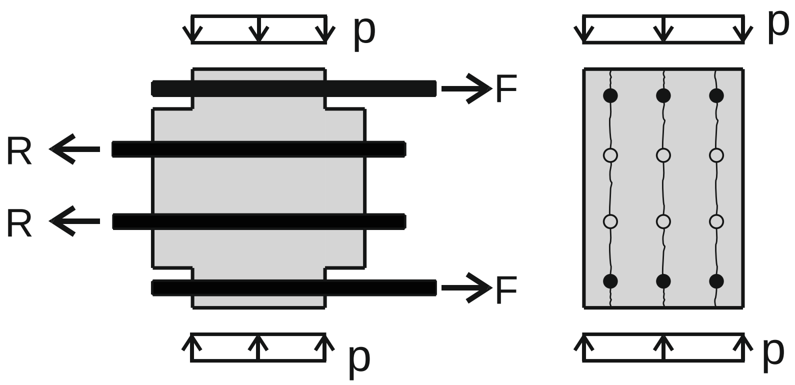

Pull-out

Author	Test	l_0	n_b	Ø	c_x	c_s	c_y	f_{cm}	$Ø_{st}$	n_{st}	s_t	n_l	f_R	f_y	$\sigma_{s,max}$
		[mm]	-	[mm]	[mm]	[mm]	[mm]	[MPa]	[mm]	-	[mm]	-	-	[MPa]	[MPa]
[44]	S8-B21	120	2	8	16	227	16	15.2	-	-	-	-	*	500	407
[44]	S8-B22	120	2	8	16	227	16	15.2	-	-	-	-	*	500	385
[44]	S8-C21	120	2	8	16	227	16	23	-	-	-	-	*	500	590
[44]	S8-C22	120	2	8	16	227	16	23	-	-	-	-	*	500	592
[44]	S8-C23	120	2	8	16	227	16	23	-	-	-	-	*	500	565
[44]	S8-B31	120	2	8	24	211	24	14.8	-	-	-	-	*	500	503
[44]	S8-B32	120	2	8	24	211	24	14.8	-	-	-	-	*	500	400
[44]	S8-B33	120	2	8	24	211	24	14.8	-	-	-	-	*	500	453
[44]	S8-C31	120	2	8	24	211	24	17.4	-	-	-	-	*	500	478
[44]	S8-C32	120	2	8	24	211	24	17.4	-	-	-	-	*	500	446
[44]	P8-2F21	80	2	8	16	227	16	25.7	-	-	-	-	*	500	376
[44]	P8-2F22	80	2	8	16	227	16	25.7	-	-	-	-	*	500	412
[44]	P8-2F23	80	2	8	16	227	16	25.7	-	-	-	-	*	500	402
[44]	P8-4F21	80	2	8	16	227	16	25.7	-	-	-	-	*	500	448
[44]	P8-4F22	80	2	8	16	227	16	25.7	-	-	-	-	*	500	453
[44]	P8-2K21	80	2	8	16	227	16	33.3	-	-	-	-	*	500	511
[44]	P8-2K22	80	2	8	16	227	16	33.3	-	-	-	-	*	500	516
[44]	P8-2K23	80	2	8	16	227	16	33.3	-	-	-	-	*	500	511
[44]	P8-4K21	80	2	8	16	227	16	36.6	-	-	-	-	*	500	536
[44]	P8-4K22	80	2	8	16	227	16	36.6	-	-	-	-	*	500	542
[44]	P8-4K23	80	2	8	16	227	16	36.6	-	-	-	-	*	500	531
[44]	S12-B11	180	2	12	12	227	12	19.4	-	-	-	-	*	500	269
[44]	S12-B12	180	2	12	12	227	12	19.4	-	-	-	-	*	500	298
[44]	S12-B13	180	2	12	12	227	12	19.4	-	-	-	-	*	500	286
[44]	S12-C11	180	2	12	12	227	12	17.7	-	-	-	-	*	500	397
[44]	S12-C12	180	2	12	12	227	12	17.7	-	-	-	-	*	500	415
[44]	S12-C13	180	2	12	12	227	12	17.7	-	-	-	-	*	500	363
[44]	S12-B21	180	2	12	24	203	24	18.6	-	-	-	-	*	500	461
[44]	S12-B22	180	2	12	24	203	24	18.6	-	-	-	-	*	500	462
[44]	S12-B23	180	2	12	24	203	24	18.6	-	-	-	-	*	500	472
[44]	S12-C21	180	2	12	24	203	24	16	-	-	-	-	*	500	506
[44]	S12-C22	180	2	12	24	203	24	16	-	-	-	-	*	500	468
[44]	S12-C23	180	2	12	24	203	24	16	-	-	-	-	*	500	523
[44]	S12-B31	180	2	12	36	179	36	19.2	-	-	-	-	*	500	481
[44]	S12-B32	180	2	12	36	179	36	19.2	-	-	-	-	*	500	488
[44]	S12-B33	180	2	12	36	179	36	19.2	-	-	-	-	*	500	557
[44]	S12-C31	180	2	12	36	179	36	21.7	-	-	-	-	*	500	558
Author	Test	l_0	n_b	Ø	c_x	c_s	c_y	f_{cm}	$Ø_{st}$	n_{st}	s_t	n_l	f_R	f_y	$\sigma_{s,max}$
		[mm]	-	[mm]	[mm]	[mm]	[mm]	[MPa]	[mm]	-	[mm]	-	-	[MPa]	[MPa]

[44]	S12-C32	180	2	12	36	179	36	21.7	-	-	-	-	*	500	565
[44]	S12-C33	180	2	12	36	179	36	21.7	-	-	-	-	*	500	537
[44]	P12-2F21	120	2	12	24	203	24	27.2	-	-	-	-	*	500	428
[44]	P12-2F22	120	2	12	24	203	24	27.2	-	-	-	-	*	500	354
[44]	P12-2F23	120	2	12	24	203	24	27.2	-	-	-	-	*	500	392
[44]	P12-4F21	120	2	12	24	203	24	28.4	-	-	-	-	*	500	466
[44]	P12-4F22	120	2	12	24	203	24	28.4	-	-	-	-	*	500	456
[44]	P12-2K21	120	2	12	24	203	24	33.5	-	-	-	-	*	500	415
[44]	P12-2K22	120	2	12	24	203	24	33.5	-	-	-	-	*	500	450
[44]	P12-2K23	120	2	12	24	203	24	33.5	-	-	-	-	*	500	456
[44]	P12-4K21	120	2	12	24	203	24	34.4	-	-	-	-	*	500	520
[44]	P12-4K22	120	2	12	24	203	24	34.4	-	-	-	-	*	500	525
[44]	P12-4K23	120	2	12	24	203	24	34.4	-	-	-	-	*	500	498
[44]	S16-B11	240	2	16	16	211	16	15.2	-	-	-	-	*	500	368
[44]	S16-B12	240	2	16	16	211	16	15.2	-	-	-	-	*	500	366
[44]	S16-C11	240	2	16	16	211	16	20.2	-	-	-	-	*	500	396
[44]	S16-C12	240	2	16	16	211	16	20.2	-	-	-	-	*	500	446
[44]	S16-C13	240	2	16	16	211	16	20.2	-	-	-	-	*	500	410
[44]	S16-B21	240	2	16	32	179	32	17.9	-	-	-	-	*	500	450
[44]	S16-B22	240	2	16	32	179	32	17.9	-	-	-	-	*	500	450
[44]	S16-B23	240	2	16	32	179	32	17.9	-	-	-	-	*	500	486
[44]	S16-C21	240	2	16	32	179	32	17.6	-	-	-	-	*	500	516
[44]	S16-C22	240	2	16	32	179	32	17.6	-	-	-	-	*	500	510
[44]	S16-B31	240	2	16	48	147	48	21.1	-	-	-	-	*	500	534
[44]	S16-B33	240	2	16	48	147	48	21.1	-	-	-	-	*	500	540
[44]	S16-C31	240	2	16	48	147	48	21	-	-	-	-	*	500	536
[44]	S16-C32	240	2	16	48	147	48	21	-	-	-	-	*	500	516
[44]	S16-C33	240	2	16	32	64	32	21	-	-	-	-	*	500	546
[44]	P16-2F21	160	2	16	32	64	32	29.3	-	-	-	-	*	500	471
[44]	P16-2F22	160	2	16	16	211	16	29.3	-	-	-	-	*	500	459
[44]	P16-2F23	160	2	16	16	211	16	29.3	-	-	-	-	*	500	466
[44]	P16-4F21	160	2	16	32	179	32	27.3	-	-	-	-	*	500	425
[44]	P16-4F22	160	2	16	32	179	32	27.3	-	-	-	-	*	500	439
[44]	P16-4F23	160	2	16	32	179	32	27.3	-	-	-	-	*	500	467
[44]	P16-2K21	160	2	16	32	179	32	34.8	-	-	-	-	*	500	488
[44]	P16-2K22	160	2	16	32	179	32	34.8	-	-	-	-	*	500	478
[44]	P16-2K23	160	2	16	32	179	32	34.8	-	-	-	-	*	500	499
[44]	P16-4K21	160	2	16	12	77	12	35.2	-	-	-	-	*	500	515
[44]	P16-4K22	160	2	16	12	77	12	35.2	-	-	-	-	*	500	515
[44]	P16-4K23	160	2	16	16	211	16	35.2	-	-	-	-	*	500	502
[44]	beam01	180	2	12	12	77	12	13.9	-	-	-	-	*	500	200
[44]	beam21	180	2	12	12	77	12	21.7	-	-	-	-	*	500	366
[44]	beam11	180	2	12	12	77	12	21.8	-	-	-	-	*	500	464
[44]	beam02.1	180	2	12	50	118	24	20.2	-	-	-	-	*	500	416
[44]	beam02.2	180	2	12	50	118	24	18.2	-	-	-	-	*	500	396
[44]	S8-A21	120	2	8	16	32	16	18.5	-	-	-	-	*	500	233
[44]	S8-A22	120	2	8	16	32	16	18.5	-	-	-	-	*	500	229
[44]	S8-A31	120	2	8	24	48	24	21.2	-	-	-	-	*	500	360
[44]	S8-A32	120	2	8	24	48	24	21.2	-	-	-	-	*	500	382
[44]	S8-A33	120	2	8	24	48	24	21.2	-	-	-	-	*	500	364
[44]	S12-A11	180	2	12	12	24	12	19.4	-	-	-	-	*	500	194
[44]	S12-A12	180	2	12	12	24	12	19.4	-	-	-	-	*	500	212
[44]	S12-A13	180	2	12	12	24	12	19.4	-	-	-	-	*	500	232
[44]	S12-A22	180	2	12	24	48	24	16.6	-	-	-	-	*	500	256
[44]	S12-A23	180	2	12	24	48	24	16.6	-	-	-	-	*	500	267
Author	**Test**	l_0	n_b	**Ø**	c_x	c_s	c_y	f_{cm}	$Ø_{st}$	n_{st}	s_t	n_l	f_R	f_y	$\sigma_{s,max}$
		[mm]	-	[mm]	[mm]	[mm]	[mm]	[MPa]	[mm]	-	[mm]	-	-	[MPa]	[MPa]
[44]	S12-A31	180	2	12	36	72	36	16.5	-	-	-	-	*	500	317
[44]	S12-A33	180	2	12	36	72	36	16.5	-	-	-	-	*	500	319

[44]	S16-A11	240	2	16	16	32	16	20	-	-	-	-	*	500	228
[44]	S16-A12	240	2	16	16	32	16	20	-	-	-	-	*	500	186
[44]	S16-A21	240	2	16	32	64	32	21.9	-	-	-	-	*	500	282
[44]	S16-A23	240	2	16	32	64	32	21.9	-	-	-	-	*	500	264
[44]	S16-A31	240	2	16	48	96	48	20.2	-	-	-	-	*	500	325
[44]	S16-A32	240	2	16	48	96	48	20.2	-	-	-	-	*	500	326
[44]	S16-A51	240	2	16	80	160	80	19.3	-	-	-	-	*	500	301
[44]	S16-A52	240	2	16	80	160	80	19.3	-	-	-	-	*	500	289
[44]	P8-OF21	80	2	8	16	32	16	30.2	-	-	-	-	*	500	284
[44]	P8-OF22	80	2	8	16	32	16	30.2	-	-	-	-	*	500	289
[44]	P8-OF23	80	2	8	16	32	16	30.2	-	-	-	-	*	500	287
[44]	P12-OF21	120	2	12	24	48	24	31.8	-	-	-	-	*	500	308
[44]	P12-OF22	120	2	12	24	48	24	31.8	-	-	-	-	*	500	265
[44]	P12-OF23	120	2	12	24	48	24	31.8	-	-	-	-	*	500	274
[44]	P16-OF21	160	2	16	32	64	32	28.5	-	-	-	-	*	500	284
[44]	P16-OF22	160	2	16	32	64	32	28.5	-	-	-	-	*	500	288
[44]	P16-OF23	160	2	16	32	64	32	28.5	-	-	-	-	*	500	288
[44]	P8-OK21	80	2	8	16	32	16	33.6	-	-	-	-	*	500	372
[44]	P8-OK22	80	2	8	16	32	16	33.6	-	-	-	-	*	500	360
[44]	P8-OK23	80	2	8	16	32	16	33.6	-	-	-	-	*	500	368
[44]	P12-OK21	120	2	12	24	48	24	34	-	-	-	-	*	500	297
[44]	P12-OK22	120	2	12	24	48	24	34	-	-	-	-	*	500	282
[44]	P16-OK21	160	2	16	32	64	32	30.8	-	-	-	-	*	500	245
[44]	P16-OK22	160	2	16	32	64	32	30.8	-	-	-	-	*	500	249

A.3.9. BEEBY: BRUFFEL; GOUGH [BEE73]

Author	Test	l_0	n_b	Ø	c_x	c_s	c_y	f_{cm}	$Ø_{st}$	n_{st}	s_t	n_l	f_R	f_y	$\sigma_{s,max}$
		[mm]	-	[mm]	[mm]	[mm]	[mm]	[MPa]	[mm]	-	[mm]	-	-	[MPa]	[MPa]
[51]	1	230	2	16	16	136	16	36	-	-	-	-	*	500	267
[51]	2	230	2	16	32	72	32	36	-	-	-	-	*	500	316

A.3.10. BETZLE [BET80]

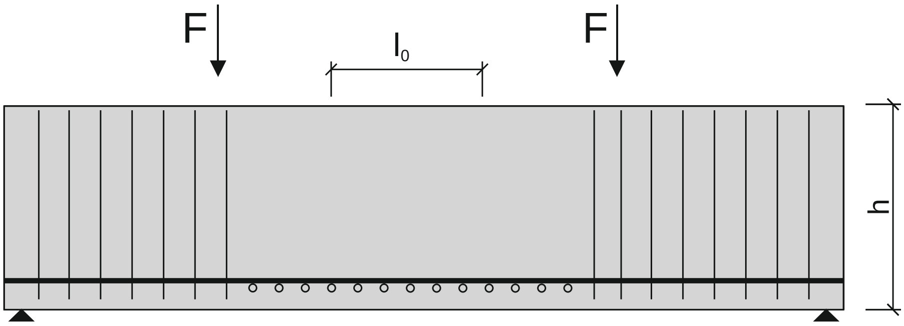

Author	Test	l_0	n_b	Ø	c_x	c_s	c_y	f_{cm}	$Ø_{st}$	n_{st}	s_t	n_l	f_R	f_y	$\sigma_{s,max}$
		[mm]	-	[mm]	[mm]	[mm]	[mm]	[MPa]	[mm]	-	[mm]	-	-	[MPa]	[MPa]
[04]	B1	1900	5	28	28	56	50	20	16	9	205	-	0.075	440	450
[04]	B2	1530	5	28	56	56	90	22	16	8	200	-	0.075	440	440
[04]	B3	1210	2	28	84	168	50	22	12	7	200	-	0.072	440	510
[04]	B4	640	10	16	48	32	50	24	10	5	125	-	0.078	420	380
[04]	B5	420	5	16	80	160	30	22	6	5	135	-	0.078	420	320

A.3.11. CHAMBERLIN [CHA56]

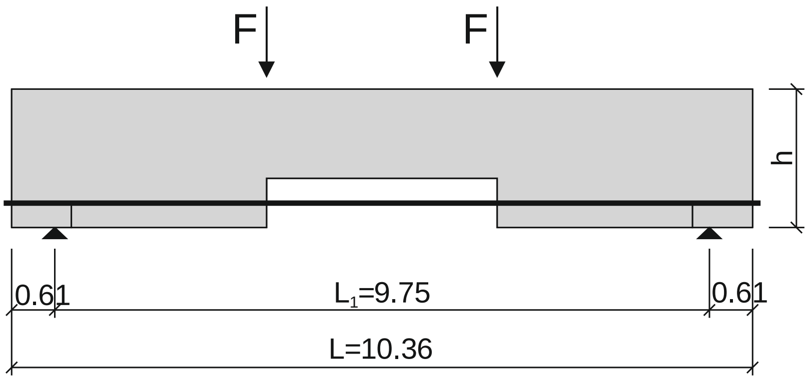

Author	Test	l_0	n_b	Ø	c_x	c_s	c_y	f_{cm}	$Ø_{st}$	n_{st}	s_t	n_l	f_R	f_y	$σ_{s,max}$
		[mm]	-	[mm]	[mm]	[mm]	[mm]	[MPa]	[mm]	-	[mm]	-	-	[MPa]	[MPa]
[05]	SIII15	152	1	12.7	12.7	0	25.4	30.8	-	-	-	-	*	*	238
[05]	SIII16	152	1	12.7	19.1	0	25.4	30.8	-	-	-	-	*	*	263
[05]	SIII31	152	1	12.7	12.7	0	25.4	40.5	-	-	-	-	*	*	273
[05]	SIII32	152	1	12.7	19.1	0	25.4	40.5	-	-	-	-	*	*	320
[05]	SIII33	152	1	12.7	25.4	0	25.4	40.5	-	-	-	-	*	*	334
[05]	SII11	152	1	12.7	12.7	0	25.4	25.4	-	-	-	-	*	*	285
[05]	SIII27	152	1	12.7	12.7	0	25.4	40.5	-	-	-	-	*	*	320
[05]	SIII28	152	1	12.7	19.1	0	25.4	40.5	-	-	-	-	*	*	340
[05]	SIII29	152	1	12.7	25.4	0	25.4	40.5	-	-	-	-	*	*	340
[05]	SIV53	152	2	12.7	50.8	25.4	25.4	31.3	-	-	-	-	*	*	325
[05]	SIII23	229	1	19.1	19.1	0	25.4	30.8	-	-	-	-	*	*	289
[05]	II5	25.4	1	12.7	6.35	0	6.35	25.4	-	-	-	-	*	*	212
[05]	II6	38.1	1	12.7	12.7	0	12.7	25.4	-	-	-	-	*	*	253
[05]	II7	50.8	1	12.7	19.1	0	19.1	25.4	-	-	-	-	*	*	292
[05]	II8	63.5	1	12.7	25.4	0	25.4	25.4	-	-	-	-	*	*	337
[05]	III1	25.4	1	12.7	6.35	0	6.35	30.8	-	-	-	-	*	*	161
[05]	III2	38.1	1	12.7	12.7	0	12.7	30.8	-	-	-	-	*	*	223
[05]	III3	50.8	1	12.7	19.1	0	19.1	30.8	-	-	-	-	*	*	249
[05]	III5	25.4	1	12.7	6.35	0	6.35	30.8	-	-	-	-	*	*	76
[05]	III6	38.1	1	12.7	12.7	0	12.7	30.8	-	-	-	-	*	*	1127
[05]	III7	50.8	1	12.7	19.1	0	19.1	30.8	-	-	-	-	*	*	1617
[05]	III9	38.2	1	12.7	6.35	0	6.35	30.8	-	-	-	-	*	*	2437
[05]	III10	57.2	1	12.7	12.7	0	12.7	30.8	-	-	-	-	*	*	277
[05]	III13	25.4	1	12.7	6.35	0	6.35	40.4	-	-	-	-	*	*	259
[05]	III17	25.4	1	12.7	6.35	0	6.35	40.4	-	-	-	-	*	*	210
[05]	III18	38.1	1	12.7	12.7	0	12.7	40.4	-	-	-	-	*	*	241
[05]	III19	50.8	1	12.7	19.1	0	19.1	40.4	-	-	-	-	*	*	291
[05]	III21	25.4	1	12.7	6.35	0	6.35	40.4	-	-	-	-	*	*	105
[05]	III22	38.1	1	12.7	12.7	0	12.7	40.4	-	-	-	-	*	*	121
[05]	III23	50.8	1	12.7	19.1	0	19.1	40.4	-	-	-	-	*	*	145

A.3.12. CHAMBERLIN [CHA58]

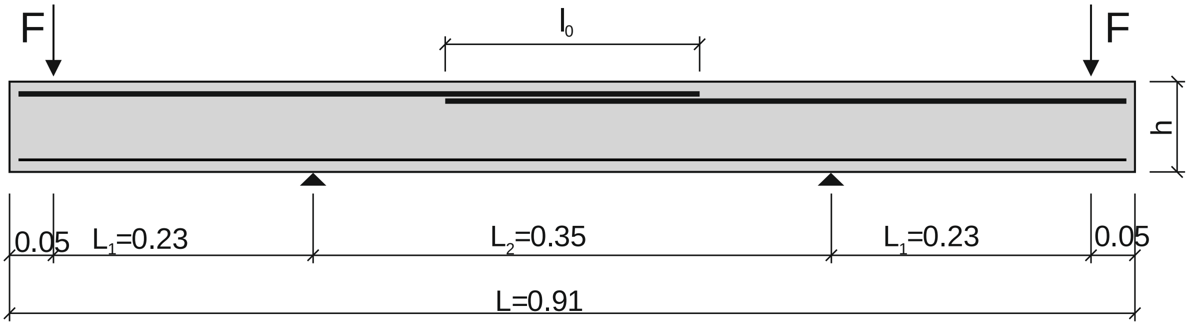

Author	Test	l_0	n_b	Ø	c_x	c_s	c_y	f_{cm}	$Ø_{st}$	n_{st}	s_t	n_l	f_R	f_y	$\sigma_{s,max}$
		[mm]	-	[mm]	[mm]	[mm]	[mm]	[MPa]	[mm]	-	[mm]	-	-	[MPa]	[MPa]
[06]	3a	152	2	12.7	13	76	25	31	-	-	-	-	*	345	227
[06]	3b	152	2	12.7	13	51	25	31	-	-	-	-	*	345	228
[06]	3c	152	2	12.7	13	25	25	31	-	-	-	-	*	345	231
[06]	4a	152	1	12.7	64	-	25	30	-	-	-	-	*	345	294
[06]	4b	152	1	12.7	57	-	25	30	-	-	-	-	*	345	303
[06]	4c	152	1	12.7	51	-	25	30	-	-	-	-	*	345	299

A.3.13. CHAMBERLIN [CHA87]

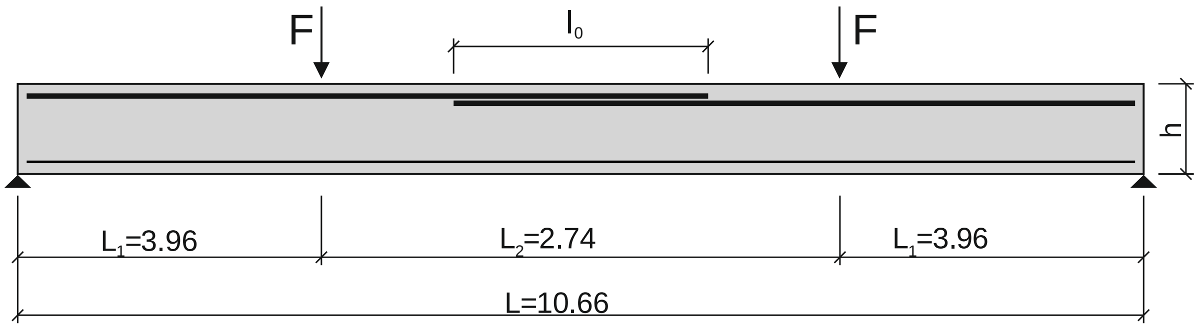

Author	Test	l_0	n_b	Ø	c_x	c_s	c_y	f_{cm}	$Ø_{st}$	n_{st}	s_t	n_l	f_R	f_y	$\sigma_{s,max}$
		[mm]	-	[mm]	[mm]	[mm]	[mm]	[MPa]	[mm]	-	[mm]	-	-	[MPa]	[MPa]
[57]	R3	76	1	9.5	58.7	0	58.7	19.8	-	-	-	-	*	414	313
[57]	W3	76	1	9.5	58.7	0	58.7	21.7	-	-	-	-	*	414	254
[57]	T5	76	1	9.5	58.7	0	58.7	25	-	-	-	-	*	414	297
[57]	W7	76	1	9.5	58.7	0	58.7	30.7	-	-	-	-	*	414	305
[57]	V10	76	1	9.5	58.7	0	58.7	28.6	-	-	-	-	*	414	291
[57]	V14	76	1	9.5	58.7	0	58.7	29.2	-	-	-	-	*	414	282
[57]	S28	76	1	9.5	58.7	0	58.7	29.2	-	-	-	-	*	414	322
[57]	Q28	76	1	9.5	58.7	0	58.7	31.3	-	-	-	-	*	414	377
[57]	R28	76	1	9.5	58.7	0	58.7	37.4	-	-	-	-	*	414	412
[57]	B2	127	1	9.5	58.7	0	58.7	19.2	-	-	-	-	*	414	416
[57]	T5	127	1	9.5	58.7	0	58.7	19.6	-	-	-	-	*	414	344
[57]	E5	127	1	9.5	58.7	0	58.7	21.2	-	-	-	-	*	414	376
[57]	M5	127	1	9.5	58.7	0	58.7	21.4	-	-	-	-	*	414	369
[57]	O17	127	1	9.5	58.7	0	58.7	27.3	-	-	-	-	*	414	453
[57]	F28	127	1	9.5	58.7	0	58.7	29.8	-	-	-	-	*	414	425
[57]	R3	177	1	9.5	58.7	0	58.7	19.8	-	-	-	-	*	414	488
[57]	V10	177	1	9.5	58.7	0	58.7	28.6	-	-	-	-	*	414	455

A.3.14. CHINN; FERGUSON; THOMPSON [CHI55]

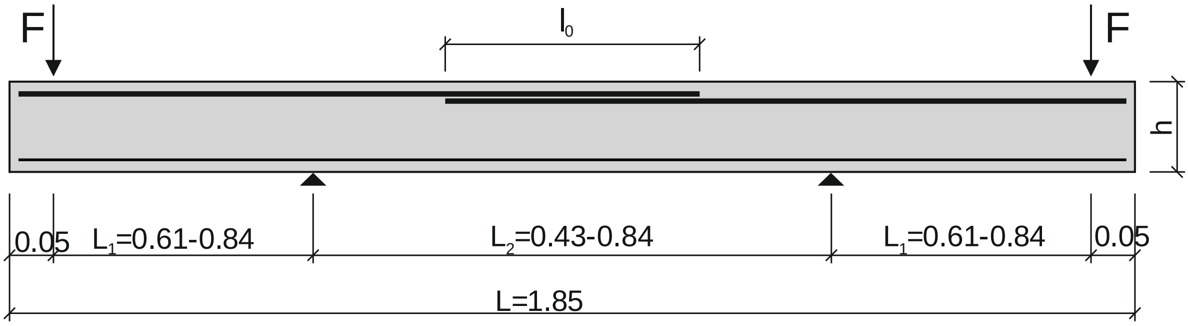

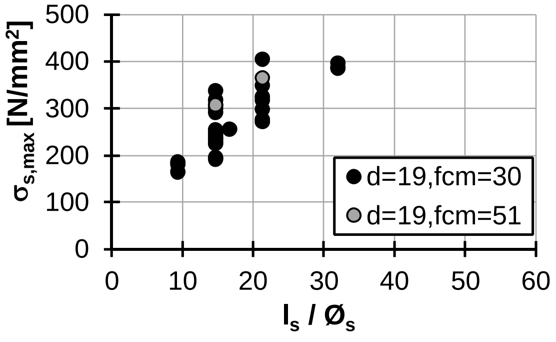

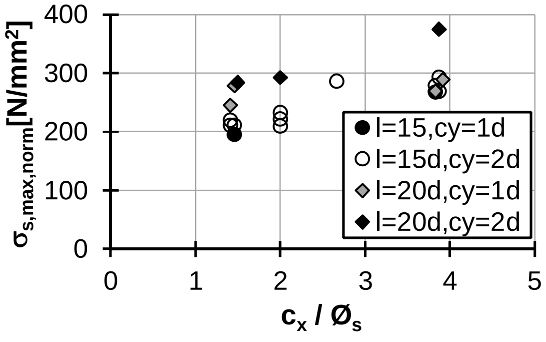

Author	Test	l_0	n_b	Ø	c_x	c_s	c_y	f_{cm}	$Ø_{st}$	n_{st}	s_t	n_l	f_R	f_y	$σ_{s,max}$
		[mm]	-	[mm]	[mm]	[mm]	[mm]	[MPa]	[mm]	-	[mm]	-	-	[MPa]	[MPa]
[07]	D31	140	1	9.53	37	-	21	32	-	-	-	-	*	545	417
[07]	D36	140	1	9.53	37	-	14	30	-	-	-	-	*	545	338
[07]	D10	178	1	19.05	27	-	38	30	-	-	-	-	*	393	182
[07]	D20	178	1	19.05	29	-	36	29	-	-	-	-	*	393	186
[07]	D22	178	1	19.05	28	-	20	31	-	-	-	-	*	393	165
[07]	D13	279	1	19.05	74	-	37	33	-	-	-	-	*	393	338
[07]	D14	279	1	19.05	28	-	21	33	-	-	-	-	*	393	226
[07]	D15	279	1	19.05	73	-	16	30	-	-	-	-	*	393	292
[07]	D21	279	1	19.05	74	-	37	31	-	-	-	-	*	393	300
[07]	D29	279	1	19.05	28	-	35	52	-	-	-	-	*	393	308
[07]	D3	279	2	19.05	38	25	38	30	-	-	-	-	*	393	255
[07]	D32	279	1	19.05	73	-	37	32	-	-	-	-	*	393	318
[07]	D38	279	1	19.05	40	-	39	22	-	-	-	-	*	393	195
[07]	D39	279	1	19.05	28	-	40	22	-	-	-	-	*	393	192
[07]	D5	279	1	19.05	51	-	38	29	-	-	-	-	*	393	307
[07]	D6	279	2	19.05	38	32	29	30	-	-	-	-	*	393	230
[07]	D7	279	1	19.05	27	-	32	31	-	-	-	-	*	393	234
[07]	D8	279	2	19.05	38	32	38	32	-	-	-	-	*	393	249
[07]	D9	279	1	19.05	27	-	37	30	-	-	-	-	*	393	242
[07]	D34	318	1	19.05	27	-	38	26	-	-	-	-	*	393	256
[07]	D12	406	1	19.05	29	-	41	31	-	-	-	-	*	393	317
[07]	D17	406	1	19.05	28	-	20	25	-	-	-	-	*	393	277
[07]	D19	406	1	19.05	74	-	43	29	-	-	-	-	*	393	405
[07]	D23	406	1	19.05	27	-	20	31	-	-	-	-	*	393	272
[07]	D24	406	1	19.05	73	-	21	31	-	-	-	-	*	393	298
[07]	D30	406	1	19.05	28	-	40	52	-	-	-	-	*	393	365
[07]	D4	406	2	19.05	38	25	38	31	-	-	-	-	*	393	325
[07]	D40	406	1	19.05	75	-	19	36	-	-	-	-	*	393	349
[07]	D25	610	1	19.05	27	-	39	35	-	-	-	-	*	393	397
[07]	D26	610	1	19.05	28	-	19	35	-	-	-	-	*	393	388
[07]	D35	610	1	19.05	27	-	37	26	-	-	-	-	*	393	386
[07]	D33	514	1	35.81	51	-	39	33	-	-	-	-	*	393	196

A.3.15. CHOI; HADJE-GHAFFARI; DARWIN; MCCABE [CHO91]

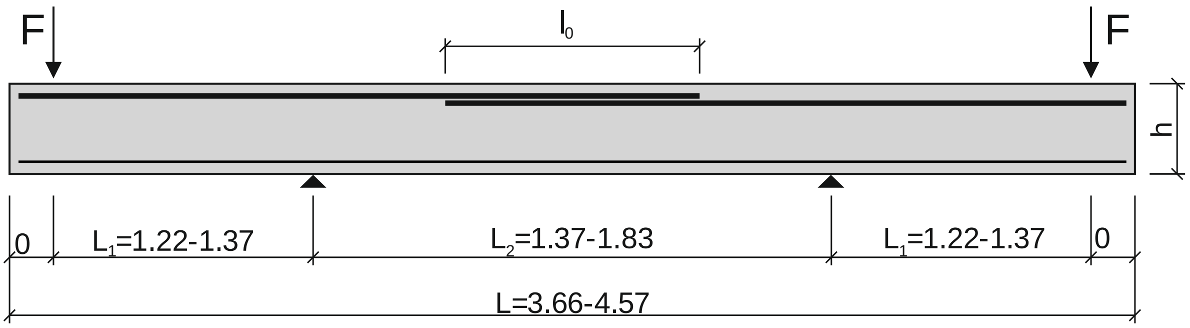

Author	Test	l_0	n_b	Ø	c_x	c_s	c_y	f_{cm}	$Ø_{st}$	n_{st}	s_t	n_l	f_R	f_y	$\sigma_{s,max}$
		[mm]	-	[mm]	[mm]	[mm]	[mm]	[MPa]	[mm]	-	[mm]	-	-	[MPa]	[MPa]
[08]	1-5N0-12-0-U	305	2	15.875	51	102	25	37	-	-	-	-	0.086	440	424
[08]	1-5N0-12-0-U	305	3	15.875	51	102	25	37	-	-	-	-	0.086	440	441
[08]	2-6C0-12-0-U	305	2	19.05	51	102	25	41	-	-	-	-	0.079	476	354
[08]	2-6S0-12-0-U	305	2	19.05	51	102	25	41	-	-	-	-	0.06	490	315
[08]	3-8N0-16-0-U	406	2	25.4	51	102	38	41	-	-	-	-	0.08	440	297
[08]	3-8S0-16-0-U	406	2	25.4	51	102	38	41	-	-	-	-	0.064	490	295
[08]	4-11C0-24-0-U	610	2	36	51	102	51	40	-	-	-	-	0.069	476	261
[08]	4-11S0-24-0-U	610	2	36	51	102	51	40	-	-	-	-	0.071	490	278

A.3.16. DARWIN, THOLEN; IDUN [DAR95]

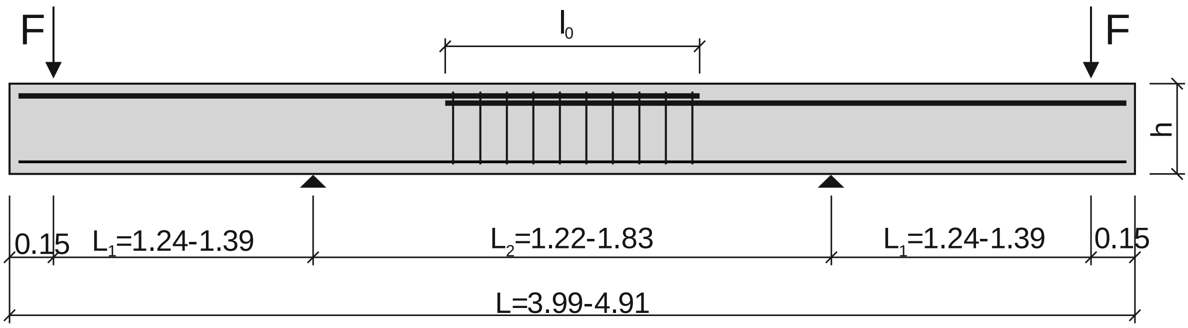

Author	Test	l_0	n_b	Ø	c_x	c_s	c_y	f_{cm}	$Ø_{st}$	n_{st}	s_t	n_l	f_R	f_y	$\sigma_{s,max}$
		[mm]	-	[mm]	[mm]	[mm]	[mm]	[MPa]	[mm]	-	[mm]	-	-	[MPa]	[MPa]
[09]	1.1	406	2	25.4	75	149	75	35	-	-	-	-	0.101	414	356
[09]	1.2	406	2	25.4	52	116	49	35	-	-	-	-	0.101	414	308
[09]	1.3	406	3	25.4	52	73	49	35	-	-	-	-	0.101	414	311
[09]	2.4	610	2	25.4	51	97	33	36	-	-	-	-	0.14	517	374
[09]	2.5	610	2	25.4	52	94	46	36	-	-	-	-	0.14	517	406
[09]	4.5	610	2	25.4	52	98	47	28	-	-	-	-	0.101	414	354
[09]	6.5	610	2	25.4	51	97	50	29	-	-	-	-	0.14	517	371
[09]	8.3	610	2	25.4	51	99	51	26	-	-	-	-	0.072	545	427
[09]	10.2	660	2	25.4	52	95	49	29	-	-	-	-	0.119	558	424
[09]	13.4	406	3	15.875	53	52	34	28	-	-	-	-	0.109	441	414
[09]	14.3	432	3	15.875	52	52	33	29	-	-	-	-	0.109	441	430
[09]	15.5	1016	2	36	78	152	48	36	-	-	-	-	0.127	558	374
[09]	16.2	1016	2	36	77	151	48	36	-	-	-	-	0.127	558	362
[09]	12.1	254	4	15.875	48	26	34	28	13	2	254	2	0.082	448	314
[09]	12.2	254	4	15.875	50	26	33	28	13	2	254	2	0.109	441	314
[09]	12.3	254	3	15.875	52	53	33	28	10	1	254	2	0.082	448	335
[09]	12.4	254	3	15.875	52	52	32	28	10	1	254	2	0.109	441	359
[09]	13.1	305	3	15.875	39	65	33	28	10	1	305	2	0.109	441	386
[09]	13.2	305	3	15.875	40	64	33	28	10	1	305	2	0.082	448	388
[09]	14.5	305	2	15.875	40	160	31	29	10	2	305	2	0.082	448	415
[09]	14.6	305	2	15.875	39	162	32	29	10	2	305	2	0.109	441	432
[09]	1.5	406	3	25.4	52	70	49	35	13	5	102	2	0.101	414	361
[09]	1.6	406	3	25.4	52	73	49	35	13	3	203	2	0.101	414	360
[09]	2.1	610	2	25.4	57	87	34	36	10	7	102	2	0.071	483	432
[09]	2.2	610	2	25.4	54	91	36	36	10	7	102	2	0.14	517	536
[09]	2.3	610	2	25.4	54	90	50	36	10	4	203	2	0.14	517	509
[09]	3.4	610	2	25.4	54	94	51	35	10	4	203	2	0.085	-	386
[09]	3.5	711	3	25.4	25	49	48	26	10	8	102	2	0.085	-	362
[09]	4.1	610	2	25.4	52	98	32	28	13	6	122	2	0.071	483	434
[09]	4.2	610	2	25.4	53	94	33	28	10	8	87	2	0.14	517	503
[09]	4.4	610	2	25.4	52	100	31	28	10	4	203	2	0.101	414	408
[09]	5.1	610	3	25.4	51	97	32	29	10	7	102	2	0.065	-	448
[09]	5.2	610	3	25.4	53	95	35	29	10	7	102	2	0.14	517	454
[09]	5.3	610	2	25.4	52	94	33	29	10	7	102	2	0.14	517	471
[09]	5.4	610	2	25.4	50	101	32	29	10	7	102	2	0.065	-	408
[09]	5.5	610	2	25.4	52	97	36	29	10	4	203	2	0.085	-	321
[09]	5.6	559	2	25.4	53	92	33	29	13	5	140	2	0.14	517	460
[09]	6.1	610	3	25.4	52	21	48	29	13	8	87	2	0.065	-	441
[09]	6.2	610	3	25.4	51	22	51	29	13	8	87	2	0.14	517	521
[09]	6.3	406	2	25.4	51	97	34	29	10	2	406	2	0.14	517	319
[09]	6.4	406	2	25.4	53	94	34	29	10	2	406	2	0.085	-	253
[09]	7.1	406	2	25.4	53	91	48	29	10	2	406	2	0.14	517	323
Author	Test	l_0	n_b	Ø	c_x	c_s	c_y	f_{cm}	$Ø_{st}$	n_{st}	s_t	n_l	f_R	f_y	$\sigma_{s,max}$

		[mm]	-	[mm]	[mm]	[mm]	[mm]	[MPa]	[mm]	-	[mm]	-	-	[MPa]	[MPa]
[09]	7.2	457	2	25.4	37	129	33	29	13	5	114	2	0.101	414	387
[09]	7.5	610	3	25.4	52	20	51	29	13	8	87	2	0.14	517	512
[09]	7.6	406	2	25.4	52	100	49	29	10	2	406	2	0.101	414	307
[09]	8.1	610	3	25.4	52	23	50	26	13	8	87	2	0.069	545	489
[09]	8.2	610	3	25.4	52	22	50	26	13	8	87	2	0.119	558	547
[09]	8.4	406	2	25.4	52	96	48	26	10	2	406	2	0.119	558	339
[09]	9.1	610	2	25.4	52	95	50	29	10	2	610	2	0.119	558	440
[09]	9.2	457	2	25.4	52	94	33	29	10	6	91	2	0.14	517	479
[09]	9.3	610	2	25.4	53	97	46	29	10	2	610	2	0.069	545	383
[09]	9.4	610	2	25.4	51	96	49	29	10	2	610	2	0.14	517	451
[09]	10.3	660	2	25.4	53	94	46	29	10	2	660	2	0.069	545	408
[09]	10.4	508	2	25.4	53	95	49	29	13	5	127	2	0.069	545	430
[09]	11.1	457	3	25.4	51	23	49	30	13	6	91	2	0.14	517	467
[09]	11.2	457	2	25.4	53	94	48	30	13	4	152	2	0.069	545	429
[09]	11.3	457	2	25.4	52	94	49	30	13	4	152	2	0.119	558	433
[09]	11.4	610	2	25.4	53	94	49	30	10	2	610	2	0.14	517	433
[09]	14.1	914	3	25.4	52	25	48	29	10	3	457	2	0.101	414	418
[09]	14.2	533	3	25.4	51	24	48	29	13	7	89	2	0.101	414	438
[09]	15.1	686	2	36	38	76	48	36	13	9	86	2	0.127	558	470
[09]	15.2	686	2	36	41	75	49	36	13	9	86	2	0.072	441	438
[09]	15.3	1016	2	36	39	78	46	36	10	10	113	2	0.072	441	433
[09]	15.4	1016	2	36	40	75	48	36	10	10	113	2	0.127	558	537
[09]	16.3	1016	2	36	77	151	45	36	10	4	339	2	0.127	558	426
[09]	16.4	1016	2	36	78	152	47	36	10	4	339	2	0.07	483	424
[09]	17.3	965	2	36	77	152	48	32	10	8	138	2	0.127	558	479
[09]	17.4	965	2	36	79	152	47	32	10	8	138	2	0.07	483	457
[09]	17.5	762	2	36	78	152	48	32	13	7	127	2	0.07	483	406
[09]	17.6	762	2	36	78	151	49	32	13	7	127	2	0.127	558	479
[09]	18.1	1016	2	36	38	229	47	32	10	10	113	2	0.127	558	557
[09]	18.3	1016	2	36	77	152	49	32	10	6	203	2	0.127	558	482
[09]	18.4	1016	2	36	77	154	48	32	10	6	203	2	0.07	483	459

A.3.17. DE VRIES: MOEHLE; HESTER [DEV91]

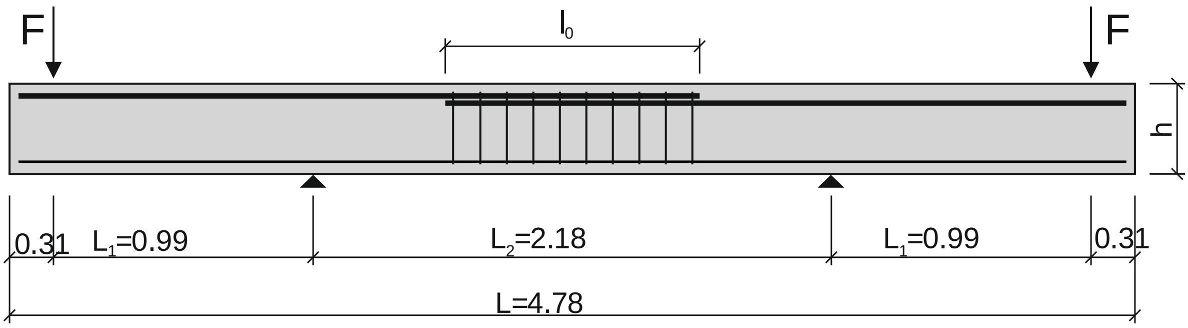

Author	Test	l_0	n_b	Ø	c_x	c_s	c_y	f_{cm}	$Ø_{st}$	n_{st}	s_t	n_l	f_R	f_y	$σ_{s,max}$
		[mm]	-	[mm]	[mm]	[mm]	[mm]	[MPa]	[mm]	-	[mm]	-	-	[MPa]	[MPa]
[10]	8G-9B-P6	229	2	19.05	48	108	29	61	10	3	114	2	*	528	485
[10]	8N-9B-P6	229	2	19.05	41	124	32	57	10	3	114	2	*	528	389
[10]	8G-22B-P9	559	2	28.6512	38	89	29	51	10	4	186	2	*	458	364
[10]	8N-18B-P9	457	2	28.6512	35	98	38	53	10	3	229	2	*	485	356
[10]	8G-16B-P9	406	2	28.6512	35	95	27	51	10	3	203	2	*	458	292
[10]	8G-18B-P9	457	2	28.6512	43	79	32	59	10	3	229	2	*	485	361
[10]	10N-12B-P9	305	2	28.6512	49	66	30	67	10	3	152	2	*	485	258
[10]	10G-12B-P9	305	2	28.6512	41	82	32	67	10	3	152	2	*	485	258
[10]	15G-12B-P9	305	2	28.6512	35	98	30	111	10	3	152	2	*	485	337
[10]	15N-12B-P9	305	2	28.6512	38	92	32	93	10	3	152	2	*	485	349

A.3.18. ELIGEHAUSEN [ELI79]

Eligehausen, R.: *Übergreifungsstöße zugbeanspruchter Rippenstäbe mit geraden Stabenden. In:* DAfStb, 1979.

Author	Test	l_0	n_b	Ø	c_x	c_s	c_y	f_{cm}	$Ø_{st}$	n_{st}	s_t	n_l	f_R	f_y	$σ_{s,max}$
		[mm]	-	[mm]	[mm]	[mm]	[mm]	[MPa]	[mm]	-	[mm]	-	-	[MPa]	[MPa]
[11]	H1A	612	2	20	40	160	40	28	-	-	-	-	*	550	402
[11]	H2A	299	2	12	24	48	40	28	-	-	-	-	*	550	441
[11]	S60A1	600	2	20	40	60	140	31	-	-	-	-	*	550	344
[11]	S60A2	600	2	20	40	60	140	31	-	-	-	-	*	550	311
[11]	S60A3	600	2	20	40	60	140	31	-	-	-	-	*	550	353
[11]	S120A1	600	2	20	40	120	140	31	-	-	-	-	*	550	421
[11]	S120A2	600	2	20	40	120	140	31	-	-	-	-	*	550	417
[11]	S120A3	600	2	20	40	120	140	31	-	-	-	-	*	550	416

A.3.19. FERGUSON; BRICENO [FER69]

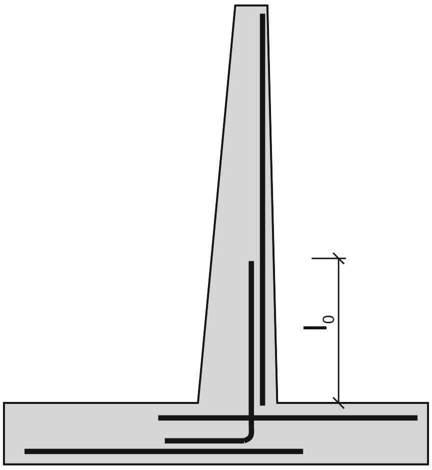

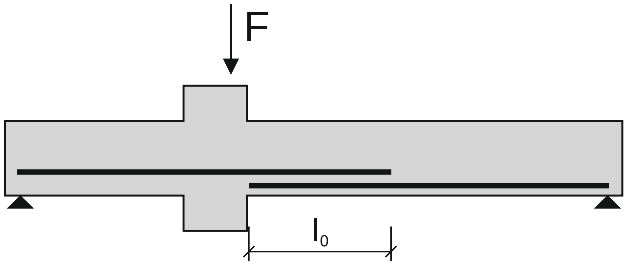

Author	Test	l_0	n_b	Ø	c_x	c_s	c_y	f_{cm}	$Ø_{st}$	n_{st}	s_t	n_l	f_R	f_y	$\sigma_{s,max}$
		[mm]	-	[mm]	[mm]	[mm]	[mm]	[MPa]	[mm]	-	[mm]	-	-	[MPa]	[MPa]
[13]	24	146	2	36	23	47	51	25	6	8	188	2	*	448	448
[13]	25	107	3	36	23	50	51	23	10	8	152	2	*	448	439
[13]	26	107	3	36	29	54	51	22	10	8	152	2	*	483	415
[13]	17	127	2	36	73	143	51	24	-	-	-	-	*	448	410
[13]	22	127	2	36	57	175	51	27	-	-	-	-	*	448	531
[13]	14	84	2	36	73	143	51	21	-	-	-	-	*	448	283
[13]	13	112	2	36	54	111	51	23	-	-	-	-	*	448	386
[13]	16	112	2	36	56	108	51	21	-	-	-	-	*	448	379
[13]	15	165	2	36	56	108	51	23	-	-	-	-	*	448	497
[13]	28	112	2	36	56	108	51	23	-	-	-	-	*	483	414
[13]	12	165	2	36	39	75	51	29	-	-	-	-	*	448	492
[13]	2a	81	2	25	38	76	51	27	-	-	-	-	*	483	407
[13]	27	107	2	36	88	65	51	23	-	-	-	-	*	483	276
[13]	1a	119	2	25	25	51	51	19	-	-	-	-	*	483	352
[13]	7	146	2	36	23	47	51	20	-	-	-	-	*	448	308
[13]	11	216	2	36	22	47	51	22	-	-	-	-	*	448	410
[13]	19	146	2	36	23	43	51	26	-	-	-	-	*	448	410
[13]	20	146	1	36	23	43	51	22	-	-	-	-	*	448	386
[13]	1	216	2	36	22	43	51	19	-	-	-	-	*	448	317
[13]	9	216	2	36	22	43	51	21	-	-	-	-	*	448	407
[13]	5	216	2	36	21	43	51	27	-	-	-	-	*	448	417
[13]	3a	107	2	25	17	30	51	26	-	-	-	-	*	483	438
[13]	4a	107	2	25	15	28	51	30	-	-	-	-	*	483	410

A.3.20. FERGUSON; THOMPSON [FER62]

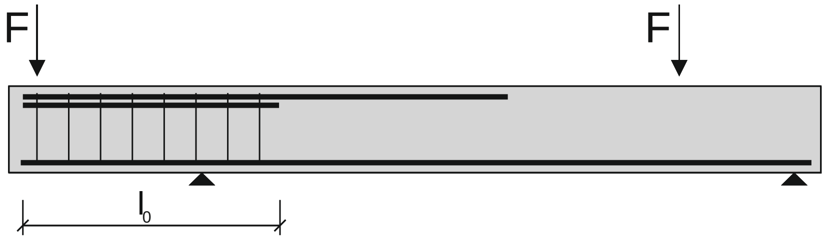

Author	Test	l_0	n_b	Ø	c_x	c_s	c_y	f_{cm}	$Ø_{st}$	n_{st}	s_t	n_l	f_R	f_y	$\sigma_{s,max}$
		[mm]	-	[mm]	[mm]	[mm]	[mm]	[MPa]	[mm]	-	[mm]	-	-	[MPa]	[MPa]
[14]	B13	400	1	22	44	0	44	26	-	-	-	-	*	417	416
[14]	B19	400	1	22	42	0	43	20	-	-	-	-	*	383	380
[14]	B20	400	1	22	43	0	43	37	-	-	-	-	*	541	541
[14]	B46	533	1	22	37	0	37	28	-	-	-	-	*	517	513
[14]	B47	533	1	22	41	0	41	18	-	-	-	-	*	398	400
[14]	B16	533	1	22	20	0	20	27	-	-	-	-	*	433	434
[14]	B27	533	1	22	38	0	39	41	-	-	-	-	*	617	616
[14]	B34	533	1	22	65	0	65	16	-	-	-	-	*	457	458
[14]	B38	533	1	22	66	0	66	25	-	-	-	-	*	595	593
[14]	B45	533	1	22	38	0	38	24	-	-	-	-	*	400	400
[14]	B14	579	1	22	43	0	43	32	-	-	-	-	*	561	557
[14]	B21	579	1	22	42	0	42	33	-	-	-	-	*	540	539
[14]	B35	710	1	22	61	0	62	20	-	-	-	-	*	623	623
[14]	B36	710	1	22	65	0	65	22	-	-	-	-	*	678	678
[14]	B37	710	1	22	19	0	20	20	-	-	-	-	*	474	473
[14]	B39	710	1	22	68	0	68	23	-	-	-	-	*	630	645
[14]	B40	710	1	22	23	0	23	26	-	-	-	-	*	595	591
[14]	B44	710	1	22	42	0	42	21	-	-	-	-	*	506	517
[14]	B24	710	1	22	40	0	40	25	-	-	-	-	*	630	631
[14]	B15	710	1	22	39	0	39	23	-	-	-	-	*	511	508
[14]	B17	710	1	22	37	0	37	19	-	-	-	-	*	479	478
[14]	B22	710	1	22	35	0	35	39	-	-	-	-	*	643	641
[14]	B7	710	1	22	42	0	42	18	-	-	-	-	*	485	485
[14]	B42	888	1	22	42	0	42	20	-	-	-	-	*	610	606
[14]	B4	888	1	22	20	0	20	23	-	-	-	-	*	535	532
[14]	B3	888	1	22	42	0	42	19	-	-	-	-	*	561	563
[14]	B1	888	1	22	53	0	53	24	-	-	-	-	*	651	651
[14]	B43	888	1	22	24	0	24	25	-	-	-	-	*	609	606
[14]	A4	304	1	9.5	31	0	31	18	-	-	-	-	*	671	663
[14]	A1	380	1	9.5	17	0	17	17	-	-	-	-	*	628	723
[14]	C1	1172	1	35.8	37	0	37	41	-	-	-	-	*	322	331
[14]	C8	1172	1	35.8	40	0	40	16	-	-	-	-	*	361	370
[14]	C9	1172	1	35.8	70	0	70	23	-	-	-	-	*	404	416
[14]	C5	1757	1	35.8	44	0	44	27	-	-	-	-	*	466	465

A.3.21. Ferguson; Breen; Thompson [FER65a]

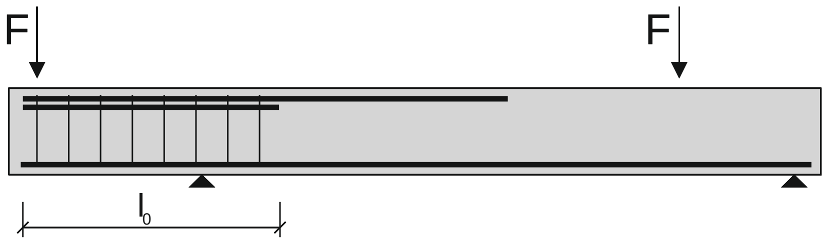

Author	Test	l_0	n_b	Ø	c_x	c_s	c_y	f_{cm}	$Ø_{st}$	n_{st}	s_t	n_l	f_R	f_y	$\sigma_{s,max}$
		[mm]	-	[mm]	[mm]	[mm]	[mm]	[MPa]	[mm]	-	[mm]	-	-	[MPa]	[MPa]
[15]	C26M	1289	2	36	118	308	76	19	-	-	-	-	*	614	564
[15]	C23M	1289	2	36	118	307	38	20	-	-	-	-	*	614	477

A.3.22. Ferguson; Thompson [FER65b]

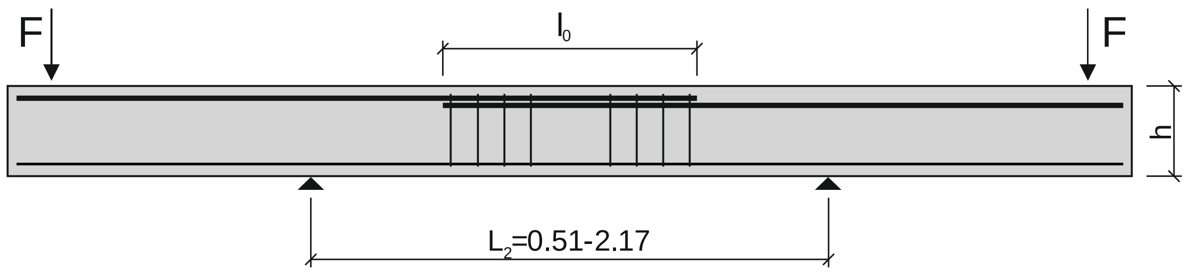

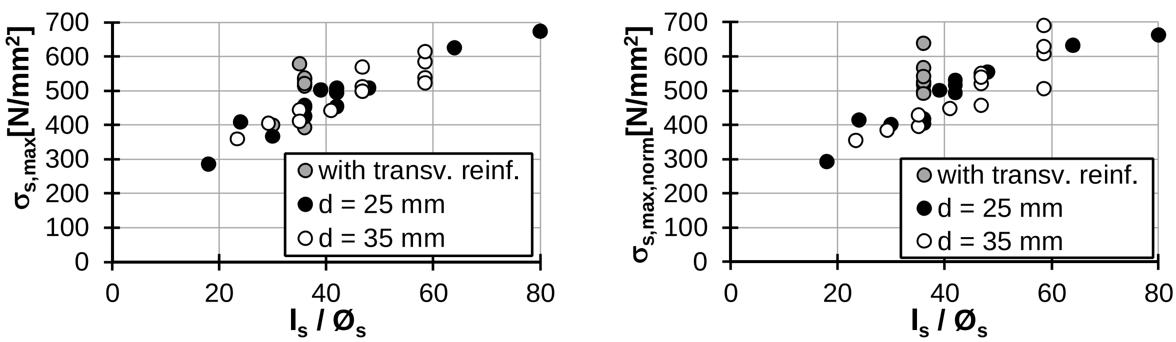

Author	Test	l_0	n_b	Ø	c_x	c_s	c_y	f_{cm}	$Ø_{st}$	n_{st}	s_t	n_l	f_R	f_y	$\sigma_{s,max}$
		[mm]	-	[mm]	[mm]	[mm]	[mm]	[MPa]	[mm]	-	[mm]	-	-	[MPa]	[MPa]
[12]	11R36a	1257	2	36	117	235	51	21	10	11	126	2	*	641	578
[12]	8F36c	914	2	25.4	83	167	37	19	6	6	183	2	*	510	427
[12]	8F36d	914	2	25.4	83	167	39	25	6	10	102	2	*	510	514
[12]	8F36e	914	2	25.4	83	168	37	29	6	6	183	2	*	510	533
[12]	8F36f	914	2	25.4	83	167	38	26	6	10	102	2	*	510	537
[12]	8F36g	914	2	25.4	83	166	39	21	6	6	183	2	*	510	521
[12]	8F36h	914	2	25.4	83	166	40	13	6	14	70	2	*	510	393
[12]	8F36j	914	2	25.4	83	168	38	13	6	14	70	2	*	510	452
[12]	8F30b	762	2	25.4	83	166	38	18	6	6	152	2	*	510	400
[12]	8R18a	457	2	25.4	83	166	44	24	-	-	-	-	*	683	286
[12]	8R24a	610	2	25.4	83	168	42	24	-	-	-	-	*	683	408
[12]	8F30a	762	2	25.4	83	167	39	21	-	-	-	-	*	510	366
[12]	8F36a	914	2	25.4	83	169	36	32	-	-	-	-	*	438	457
[12]	8F36b	914	2	25.4	83	164	36	26	-	-	-	-	*	510	425
[12]	8F36k	914	2	25.4	36	72	35	24	-	-	-	-	*	510	381
[12]	8F39a***	991	2	25.4	83	167	39	25	-	-	-	-	*	438	503
[12]	8F42a***	1067	2	25.4	83	170	38	18	-	-	-	-	*	438	455
[12]	8F42b***	1067	2	25.4	83	169	37	26	-	-	-	-	*	438	507
[12]	8R42a	1067	2	25.4	83	170	40	23	-	-	-	-	*	683	494
[12]	8R48a	1219	2	25.4	83	166	38	21	-	-	-	-	*	683	508
[12]	8R64a	1626	2	25.4	83	167	39	24	-	-	-	-	*	683	625
[12]	8R80a	2032	2	25.4	83	166	38	26	-	-	-	-	*	683	672
[12]	11R24a	838	2	36	117	235	42	26	-	-	-	-	*	641	359
[12]	11R30a	1048	2	36	117	235	33	28	-	-	-	-	*	641	405
[12]	11F36a	1257	2	36	117	235	38	32	-	-	-	-	*	503	444
[12]	11F36b	1257	2	36	117	234	37	23	-	-	-	-	*	448	411
[12]	11F42a	1467	2	36	117	233	38	24	-	-	-	-	*	448	442
[12]	11F48a	1676	2	36	117	235	39	22	-	-	-	-	*	503	512
[12]	11F48b	1676	2	36	117	237	40	23	-	-	-	-	*	448	498
[12]	11R48a	1676	2	36	117	237	38	39	-	-	-	-	*	641	569
[12]	11R48b	1676	2	36	117	239	52	21	-	-	-	-	*	641	499
[12]	11F60a	2096	2	36	117	232	40	18	-	-	-	-	*	503	585
[12]	11F60b	2096	2	36	117	233	38	28	-	-	-	-	*	448	538
[12]	11R60a	2096	2	36	117	233	36	19	-	-	-	-	*	641	523
[12]	11R60b	2096	2	36	117	232	44	24	-	-	-	-	*	641	614

A.3.23. FERGUSON; KRISHNASWAMY [FER71]

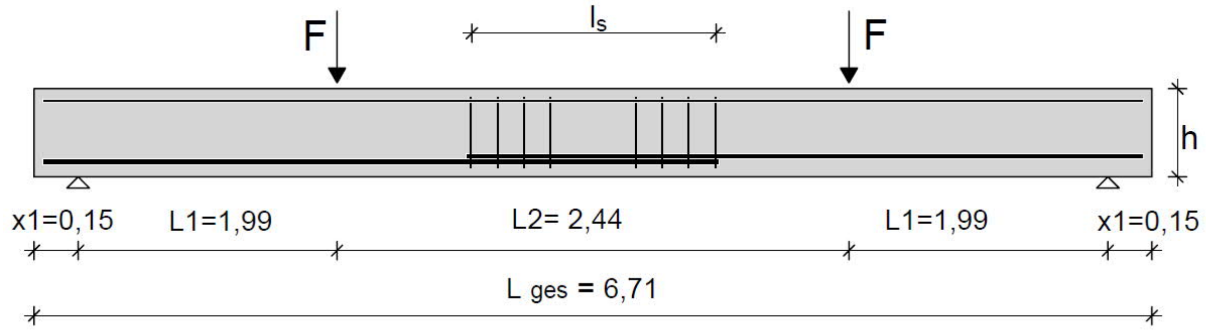

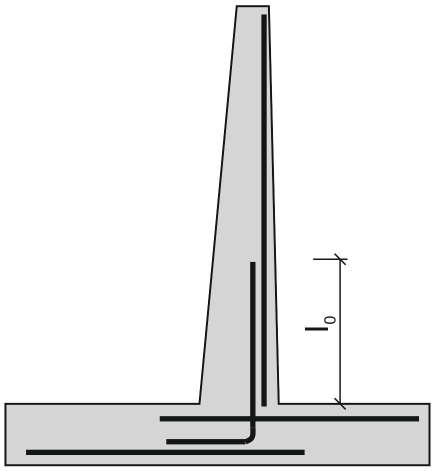

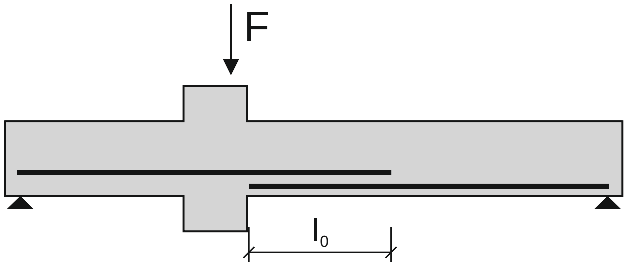

Author	Test	l_0	n_b	Ø	c_x	c_s	c_y	f_{cm}	$Ø_{st}$	n_{st}	s_t	n_l	f_R	f_y	$\sigma_{s,max}$
		[mm]	-	[mm]	[mm]	[mm]	[mm]	[MPa]	[mm]	-	[mm]	-	-	[MPa]	[MPa]
[16]	14S2	1137	2	43	86	177	60	23	6	19	76	2	*	410	427
[16]	14S3	76	2	43	86	174	60	21	6	13	64	2	*	269	277
[16]	14S4	76	2	43	86	177	60	22	6	13	64	4	*	345	354
[16]	14S6	91	2	43	86	177	60	25	6	16	61	4	*	414	425
[16]	18S1+++	183	2	57	114	231	76	19	10	13	152	2	*	452	506
[16]	18S2	152	2	57	114	231	76	18	10	13	127	4	*	363	375
[16]	18S3	183	2	57	114	231	76	32	6	13	152	4	*	410	417
[16]	18S4	152	2	57	114	233	76	27	13	20	80	2	*	455	465
[16]	18S13	122	2	57	114	234	76	23	10	16	81	4	*	410	420
[16]	18S11	152	2	57	114	234	76	22	10	10	169	4	*	429	440
[16]	18S15	249	2	57	114	228	67	20	-	-	-	-	*	423	367
[16]	18S12	152	2	57	114	234	76	22	-	-	-	-	*	423	320
[16]	SP34	91	1	36	287	-	19	23	-	-	-	-	*	466	373
[16]	SP33+++	140	1	36	287	-	19	23	-	-	-	-	*	466	510
[16]	SP32	127	1	36	287	-	32	23	-	-	-	-	*	466	489
[16]	SP35	51	1	36	287	-	51	23	-	-	-	-	*	466	263
[16]	SP36	61	1	36	204	-	51	24	-	-	-	-	*	466	325
[16]	SP40	38	2	16	32	64	21	22	-	-	-	-	*	503	297
[16]	SP37+++	114	3	36	143	105	51	22	-	-	-	-	*	466	508
[16]	SP39	114	3	36	54	106	51	22	-	-	-	-	*	494	368
[16]	SP38	102	2	36	36	71	51	20	-	-	-	-	*	466	312
[16]	14S1	114	2	43	86	177	60	19	-	-	-	-	*	421	325

A.3.24. GHAGHEI [GHA90]

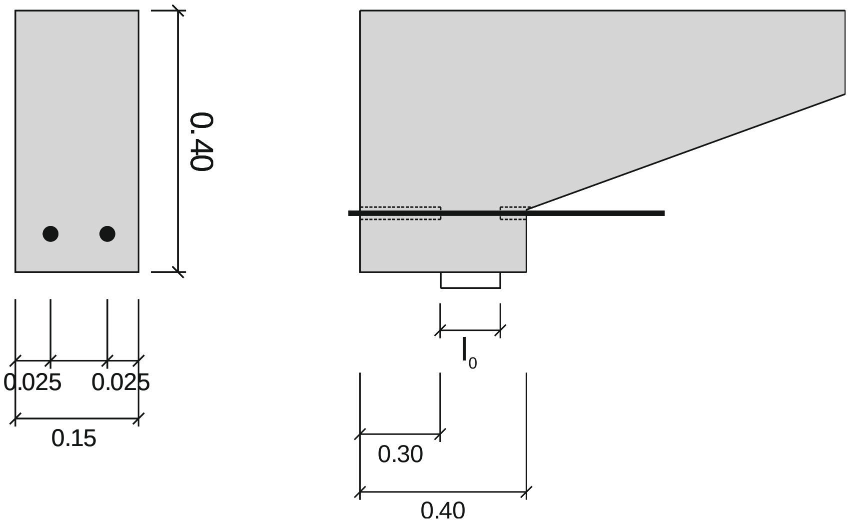

Author	Test	l_0	n_b	Ø	c_x	c_s	c_y	f_{cm}	$Ø_{st}$	n_{st}	s_t	n_l	f_R	f_y	$\sigma_{s,max}$
		[mm]	-	[mm]	[mm]	[mm]	[mm]	[MPa]	[mm]	-	[mm]	-	-	[MPa]	[MPa]
[49]	4*	200	2	25	25	50	25	35.5	-	-	-	-	*	495	362
[49]	6	100	2	25	25	50	25	33	-	-	-	-	*	495	149
[49]	7	100	2	25	25	50	25	32.8	-	-	-	-	*	495	215
[49]	8	100	2	25	25	50	25	29.6	-	-	-	-	*	495	164
[49]	9	100	2	25	25	50	25	29.4	-	-	-	-	*	495	165

A.3.25. HAMAD; ITANI [HAM98]

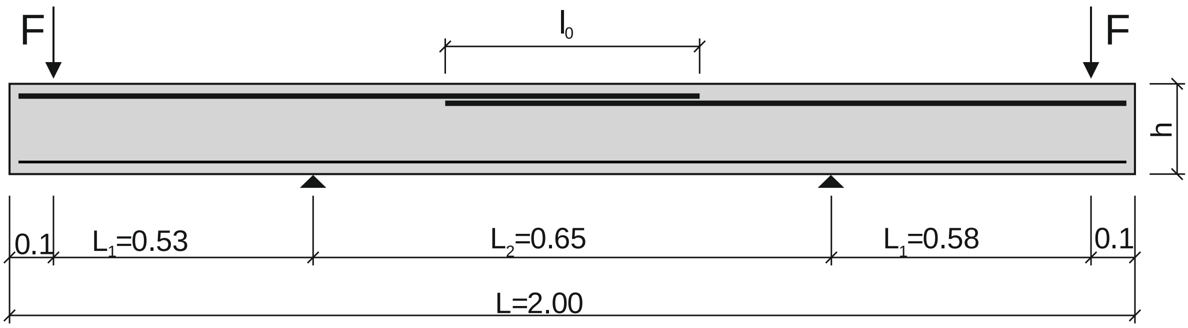

Author	Test	l_0	n_b	Ø	c_x	c_s	c_y	f_{cm}	$Ø_{st}$	n_{st}	s_t	n_l	f_R	f_y	$\sigma_{s,max}$
		[mm]	-	[mm]	[mm]	[mm]	[mm]	[MPa]	[mm]	-	[mm]	-	-	[MPa]	[MPa]
[17]	PC-00-B-SP2	305	2	25	38	80	38	66	-	-	-	-	*	426	370
[17]	SC-05-B-SP2	305	2	25	38	80	38	77	-	-	-	-	*	426	391
[17]	SC-10-B-SP2	305	2	25	38	80	38	77	-	-	-	-	*	426	356
[17]	SC-15-B-SP2	305	2	25	38	80	38	76	-	-	-	-	*	426	379
[17]	SC-20-B-SP2	305	2	25	38	80	38	74	-	-	-	-	*	426	388
[17]	PC-00-B-SP4	305	2	25	38	80	38	52	-	-	-	-	*	426	317
[17]	SC-10-B-SP4	305	2	25	38	80	38	71	-	-	-	-	*	426	339
[17]	SC-20-B-SP4	305	2	25	38	80	38	76	-	-	-	-	*	426	267

A.3.26. HAMAD [HAM90]

Author	Test	l_0	n_b	Ø	c_x	c_s	c_y	f_{cm}	$Ø_{st}$	n_{st}	s_t	n_l	f_R	f_y	$\sigma_{s,max}$
		[mm]	-	[mm]	[mm]	[mm]	[mm]	[MPa]	[mm]	-	[mm]	-	-	[MPa]	[MPa]
[18]	6P3-18-3-U ++	46	3	19	51	32	51	26	10	3	229	2	*	470	502
[18]	11P3-30-3-U	76	2	36	51	98	51	26	10	3	381	2	*	441	179
[18]	11P-30-6-U	76	2	36	51	98	51	28	10	6	152	2	*	441	305
[18]	11P3-30-6-U	76	3	36	51	39	51	28	10	6	152	2	*	441	242
[18]	6P3180U	46	3	19	51	32	51	26	-	-	-	-	*	470	452
[18]	11P3300U	76	2	36	51	98	51	26	-	-	-	-	*	441	247

A.3.27. HAMAD [HAM95]

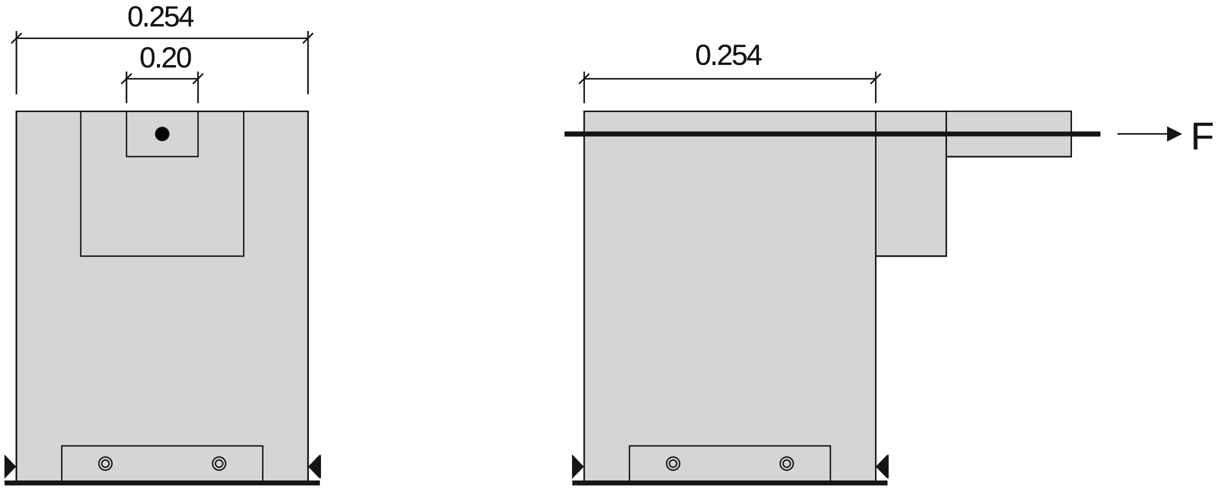

Author	Test	l_0	n_b	Ø	c_x	c_s	c_y	f_{cm}	$Ø_{st}$	n_{st}	s_t	n_l	f_R	f_y	$\sigma_{s,max}$
		[mm]	-	[mm]	[mm]	[mm]	[mm]	[MPa]	[mm]	-	[mm]	-	-	[MPa]	[MPa]
[54]	3.45-0.5-0.04	248	1	18.6	23.8	0	128	22.4	-	-	-	-	*	500	273
[54]	3.45-0.50.04r	248	1	18.6	23.8	0	128	22.4	-	-	-	-	*	500	259
[54]	6-45-0.5-0.04	248	1	18.6	23.8	0	128	43.1	-	-	-	-	*	500	439
[54]	6-45-0.50.04r	248	1	18.6	23.8	0	128	43.1	-	-	-	-	*	500	405

A.3.28. Hamad; Mansour [HAM96]

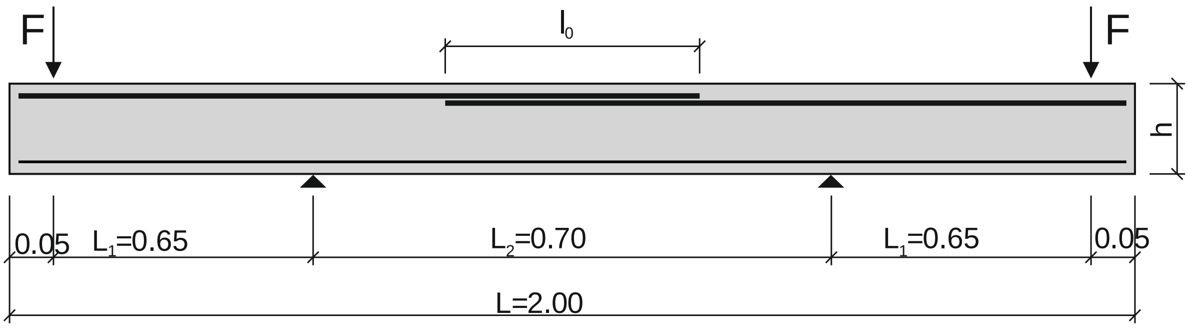

Author	Test	l_0	n_b	Ø	c_x	c_s	c_y	f_{cm}	$Ø_{st}$	n_{st}	s_t	n_l	f_R	f_y	$\sigma_{s,max}$
		[mm]	-	[mm]	[mm]	[mm]	[mm]	[MPa]	[mm]	-	[mm]	-	-	[MPa]	[MPa]
[19]	S1-14-300-0	300	3	14	20	238	20	23	-	-	-	-	0.056	469	379
[19]	S2-14-300-30	300	3	14	20	208	20	22	-	-	-	-	0.056	469	393
[19]	S3-14-300-60	300	3	14	20	178	20	23	-	-	-	-	0.056	469	406
[19]	S4-14-300-90	300	3	14	20	148	20	21	-	-	-	-	0.056	469	402
[19]	S5-14-300-120	300	3	14	20	118	20	21	-	-	-	-	0.056	469	371
[19]	S6-14-300-150	300	3	14	20	88	20	22	-	-	-	-	0.056	469	363
[19]	S7-16-300-0	300	3	16	20	232	20	22	-	-	-	-	0.056	476	331
[19]	S8-16-300-30	300	3	16	20	202	20	21	-	-	-	-	0.056	476	338
[19]	S9-16-300-60	300	3	16	20	172	20	22	-	-	-	-	0.056	476	350
[19]	S10-16-300-90	300	3	16	20	142	20	23	-	-	-	-	0.056	476	363
[19]	S11-16-300-120	300	3	16	20	112	20	22	-	-	-	-	0.056	476	331
[19]	S12-16-300-150	300	3	16	20	82	20	23	-	-	-	-	0.056	476	321
[19]	S13-20-350-0	350	3	20	20	220	20	20	-	-	-	-	0.056	474	340
[19]	S14-20-350-35	350	3	20	20	185	20	19	-	-	-	-	0.056	474	363
[19]	S15-20-350-70	350	3	20	20	150	20	21	-	-	-	-	0.056	474	370
[19]	S16-20-350-105	350	3	20	20	115	20	24	-	-	-	-	0.056	474	374
[19]	S17-20-350-140	350	3	20	20	80	20	22	-	-	-	-	0.056	474	347

A.3.29. Hasan; Cleary [HAS96]

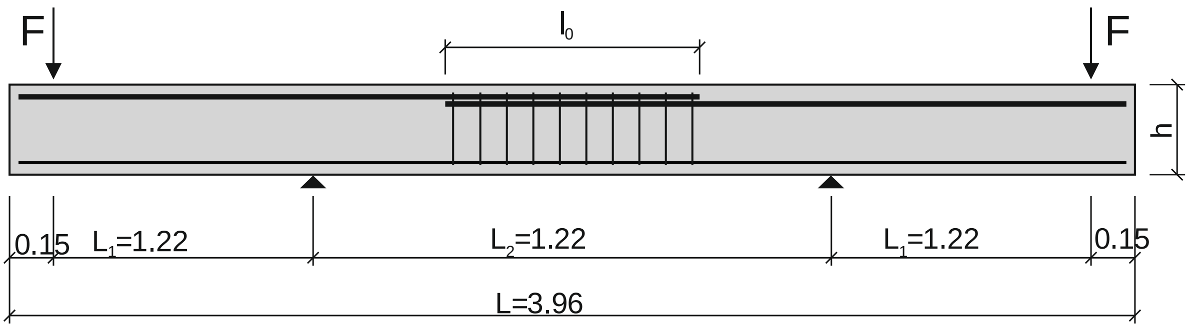

Author	Test	l_0	n_b	Ø	c_x	c_s	c_y	f_{cm}	$Ø_{st}$	n_{st}	s_t	n_l	f_R	f_y	$\sigma_{s,max}$
		[mm]	-	[mm]	[mm]	[mm]	[mm]	[MPa]	[mm]	-	[mm]	-	-	[MPa]	[MPa]
[20]	U7STAT	305	3	22.225	117	121	64	27	10	2	152	2	*	276	290

A.3.30. HEGGER; BURKHARDT [HEG99]

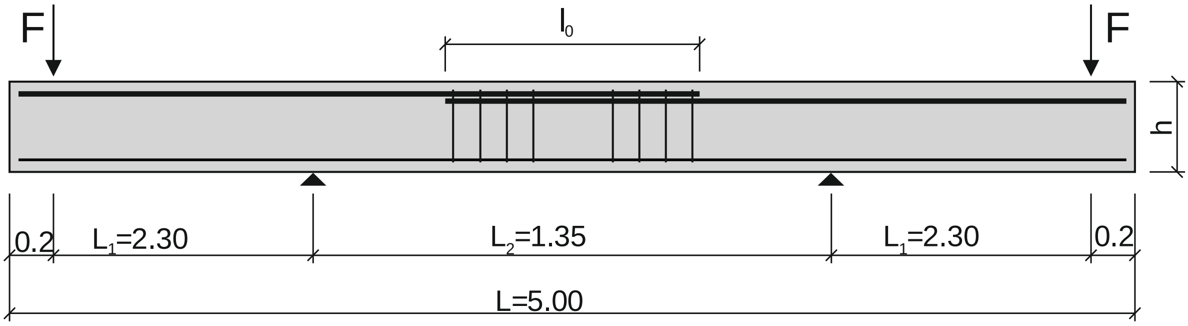

Author	Test	l_0	n_b	Ø	c_x	c_s	c_y	f_{cm}	$Ø_{st}$	n_{st}	s_t	n_l	f_R	f_y	$\sigma_{s,max}$
		[mm]	-	[mm]	[mm]	[mm]	[mm]	[MPa]	[mm]	-	[mm]	-	-	[MPa]	[MPa]
[21]	B 1	750	2	20	20	40	20	90	8	7	75	2	0.056	570	570
[21]	B 2	300	2	20	20	40	20	80	8	6	50	2	0.056	570	565
[21]	B 3	750	2	20	20	40	20	80	-	-	-	-	0.058	589	540
[21]	B 4	750	2	20	20	40	20	100	-	-	-	-	0.058	589	510
[21]	B 5	850	2	20	20	40	20	85	-	-	-	-	0.058	589	564
[21]	B 6	750	2	20	40	40	40	85	-	-	-	-	0.058	589	589
[21]	B 7	750	2	20	20	40	20	84	8	2	700	2	0.058	589	580
[21]	B 8	420	2	28	30	56	30	80	10	8	50	2	0.06	557	557
[21]	B 9	300	4	20	20	40	20	89	8	6	50	2	0.058	591	591

A.3.31. HESTER; SALAMIZAVAREGH; DARWIN; MCCABE [HES93]

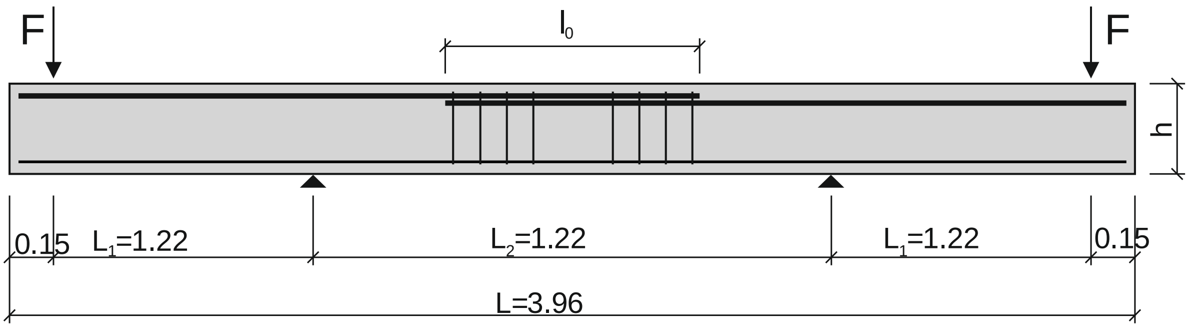

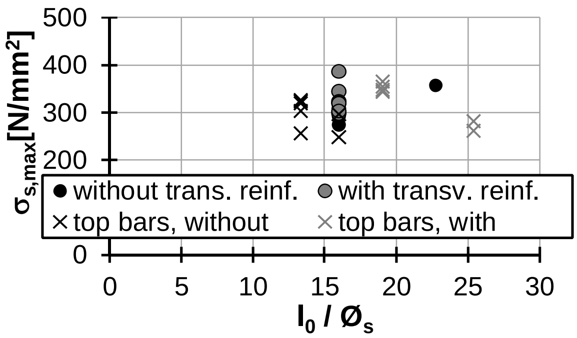

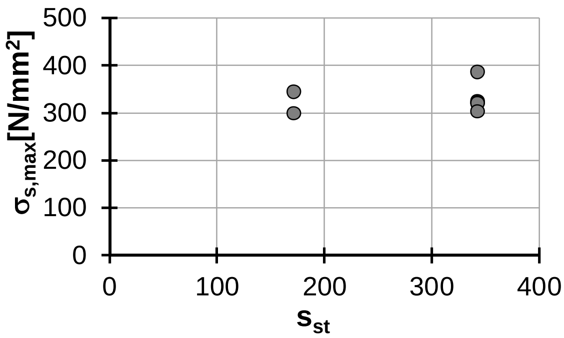

Author	Test	l_0	n_b	Ø	c_x	c_s	c_y	f_{cm}	$Ø_{st}$	n_{st}	s_t	n_l	f_R	f_y	$\sigma_{s,max}$
		[mm]	-	[mm]	[mm]	[mm]	[mm]	[MPa]	[mm]	-	[mm]	-	-	[MPa]	[MPa]
[23]	7-8C3-16-3-U	406	2	25.4	51	203	52	36	10	3	171	2	0.071	476	355
[23]	4-8S3-16-2-U	406	3	25.4	51	76	52	44	10	2	342	2	0.07	490	324
[23]	4-8S3-16-3-U	406	3	25.4	51	76	53	44	10	3	171	2	0.07	490	345
[23]	5-8C3-16-2-U	406	3	25.4	51	76	52	38	10	2	342	2	0.071	476	321
[23]	6-8C3-22 3/4-3-U	578	3	25.4	51	76	55	40	10	3	257	2	0.071	476	390
[23]	1-8N3-16-2-U	406	3	25.4	51	76	51	41	10	2	342	2	0.078	440	387
[23]	6-8C3-22 3/4-4-U	578	3	25.4	51	76	55	40	10	4	171	2	0.071	476	385
[23]	5-8C3-16-3-U	406	3	25.4	51	76	52	38	10	3	171	2	0.071	476	299
[23]	3-8S3-16-2-U	406	3	25.4	51	76	53	42	10	2	342	2	0.07	490	321
[23]	2-8C3-16-2-U	406	3	25.4	51	76	46	43	10	2	342	2	0.071	476	303
[23]	1-8N3-16-0-U	406	3	25.4	51	76	51	41	-	-	-	-	0.078	440	345
[23]	2-8C3-16-0-U	406	3	25.4	51	76	47	43	-	-	-	-	0.071	476	319
[23]	3-8S3-16-0-U	406	3	25.4	51	76	52	42	-	-	-	-	0.07	490	323
[23]	4-8S3-16-0-U	406	3	25.4	51	76	53	44	-	-	-	-	0.07	490	292
[23]	5-8C3-16-0-U	406	3	25.4	51	76	52	38	-	-	-	-	0.071	476	275
[23]	7-8C3-16-0-U	406	2	25.4	51	203	54	36	-	-	-	-	0.071	476	313
[23]	6-8C3-22-0-U	578	3	25.4	51	76	55	40	-	-	-	-	0.071	476	358

A.3.32. HWANG [HWA94]

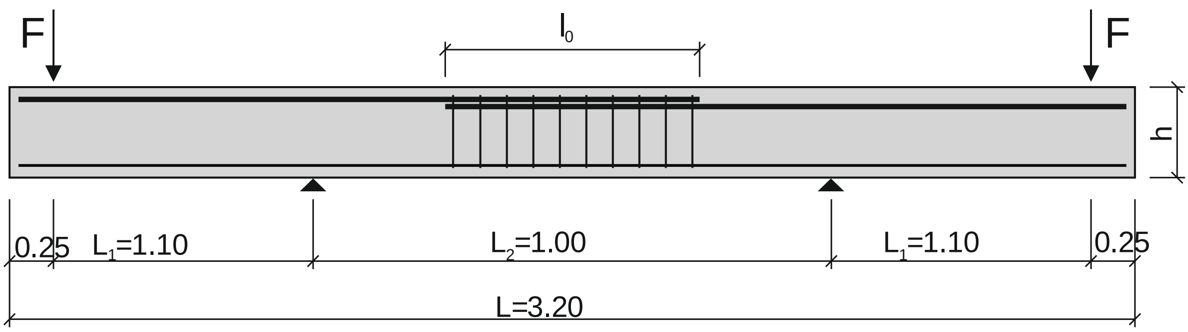

Author	Test	l_0	n_b	Ø	c_x	c_s	c_y	f_{cm}	$Ø_{st}$	n_{st}	s_t	n_l	f_R	f_y	$σ_{s,max}$
		[mm]	-	[mm]	[mm]	[mm]	[mm]	[MPa]	[mm]	-	[mm]	-	-	[MPa]	[MPa]
[24]	S28-S-M	300	2	28.7	29	57	29	81	10	3	100	2	0.1	478	367
[24]	P28-S-M	300	2	28.7	29	57	29	77	10	3	100	2	0.1	478	420
[24]	S28-N-M	300	2	28.7	29	57	29	84	-	-	-	-	0.1	478	305
[24]	P28-N-M	300	2	28.7	29	57	29	71	-	-	-	-	0.1	478	298
[24]	S33-S-U	300	2	28.7	29	57	29	69	10	3	100	2	0.1	478	379
[24]	P33-S-U	300	2	28.7	29	57	29	62	10	3	100	2	0.1	478	379
[24]	S33-N-U	300	2	28.7	29	57	29	71	-	-	-	-	0.1	478	277
[24]	P33-N-M	300	2	28.7	29	57	29	64	-	-	-	-	0.1	478	307

A.3.33. HWANG [HWA96]

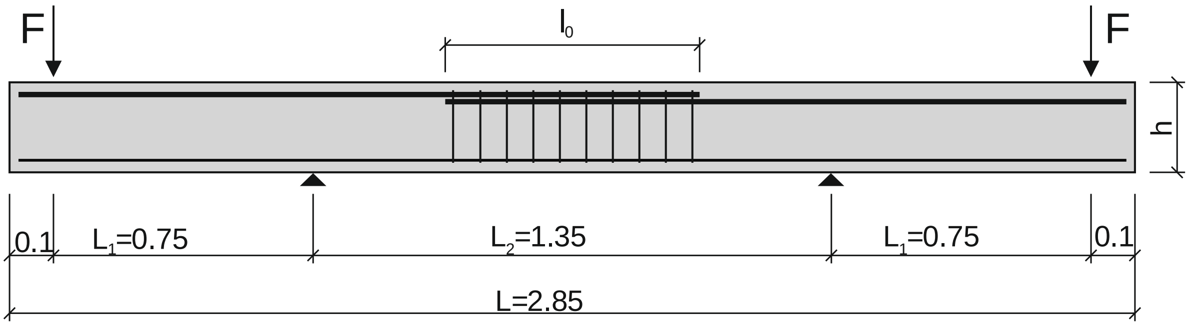

Author	Test	l_0	n_b	Ø	c_x	c_s	c_y	f_{cm}	$Ø_{st}$	n_{st}	s_t	n_l	f_R	f_y	$σ_{s,max}$
		[mm]	-	[mm]	[mm]	[mm]	[mm]	[MPa]	[mm]	-	[mm]	-	-	[MPa]	[MPa]
[25]	70-L300-9S1	300	2	28.7	50	85	50	69	10	5	63	2	*	519	492
[25]	70-L300-9N1	300	2	28.7	50	85	50	62	-	-	-	-	*	519	320
[25]	70-L300-9N2	300	2	28.7	50	85	50	67	-	-	-	-	*	519	320
[25]	70-L200-9S1	200	2	28.7	50	85	50	60	10	3	70	2	*	519	429
[25]	70-L200-9S2	200	2	28.7	50	85	50	70	10	3	70	2	*	519	325
[25]	55-L300-9S1	300	2	28.7	50	85	50	58	10	5	63	2	*	519	377
[25]	55-L300-9S2	300	2	28.7	50	85	50	53	10	5	63	2	*	519	439
[25]	55-L200-9S1	200	2	28.7	50	85	50	56	10	3	70	2	*	519	347
[25]	55-L150-9S1	150	2	28.7	50	85	50	55	10	3	58	2	*	519	283
[25]	40-L300-9S1	300	2	28.7	50	85	50	47	10	5	63	2	*	519	361

A.3.34. JENSEN [JEN82]

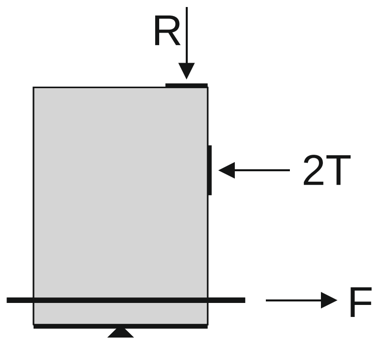

Author	Test	l_0	n_b	Ø	c_x	c_s	c_y	f_{cm}	$Ø_{st}$	n_{st}	s_t	n_l	f_R	f_y	$σ_{s,max}$
		[mm]	-	[mm]	[mm]	[mm]	[mm]	[MPa]	[mm]	-	[mm]	-	-	[MPa]	[MPa]
[45]	251301	128	2	16	50	118	24	23.1	-	-	-	-	*	900	271
[45]	251302	128	2	16	50	118	24	23.1	-	-	-	-	*	900	269

[45]	351301	128	2	16	50	118	24	29.3	-	-	-	-	*	900	324
[45]	351302	128	2	16	50	118	24	29.3	-	-	-	-	*	900	324
[45]	451301	128	2	16	50	118	24	38.4	-	-	-	-	*	900	378
[45]	451302	128	2	16	50	118	24	40.4	-	-	-	-	*	900	405
[45]	451303	128	2	16	50	118	24	40.4	-	-	-	-	*	900	381
[45]	151311	128	2	16	50	118	24	12.4	-	-	-	-	*	900	218
[45]	151312	128	2	16	50	118	24	12.4	-	-	-	-	*	900	218
[45]	201311	128	2	16	50	118	24	26.9	-	-	-	-	*	900	327
[45]	201312	128	2	16	50	118	24	26.9	-	-	-	-	*	900	327
[45]	221311	128	2	16	50	118	24	23.2	-	-	-	-	*	900	306
[45]	221312	128	2	16	50	118	24	23.2	-	-	-	-	*	900	327
[45]	251311	128	2	16	50	118	24	17.5	-	-	-	-	*	900	322
[45]	251312	128	2	16	50	118	24	17.5	-	-	-	-	*	900	292
[45]	301311	128	2	16	50	118	24	30.8	-	-	-	-	*	900	355
[45]	301312	128	2	16	50	118	24	30.8	-	-	-	-	*	900	355
[45]	351311	128	2	16	50	118	24	31.4	-	-	-	-	*	900	328
[45]	351312	128	2	16	50	118	24	31.4	-	-	-	-	*	900	328
[45]	401311	128	2	16	50	118	24	43.2	-	-	-	-	*	900	409
[45]	401312	128	2	16	50	118	24	43.2	-	-	-	-	*	900	413
[45]	401313	128	2	16	50	118	24	31.6	-	-	-	-	*	900	300
[45]	401314	128	2	16	50	118	24	31.6	-	-	-	-	*	900	328
[45]	451311	128	2	16	50	118	24	44.1	-	-	-	-	*	900	423
[45]	451312	128	2	16	50	118	24	44.1	-	-	-	-	*	900	398
[45]	451313	128	2	16	50	118	24	38.4	-	-	-	-	*	900	482
[45]	151321	128	2	16	50	118	24	13.7	-	-	-	-	*	900	318
[45]	151322	128	2	16	50	118	24	13.7	-	-	-	-	*	900	296
[45]	251321	128	2	16	50	118	24	19	-	-	-	-	*	900	351
[45]	251322	128	2	16	50	118	24	19	-	-	-	-	*	900	324
[45]	351321	128	2	16	50	118	24	23.9	-	-	-	-	*	900	324
[45]	351322	128	2	16	50	118	24	23.9	-	-	-	-	*	900	326
[45]	451321	128	2	16	50	118	24	33.2	-	-	-	-	*	900	379
[45]	451322	128	2	16	50	118	24	33.2	-	-	-	-	*	900	378
[45]	251331	128	2	16	50	118	24	17	-	-	-	-	*	900	487
[45]	251332	128	2	16	50	118	24	17	-	-	-	-	*	900	433
[45]	251333	128	2	16	50	118	24	23.1	-	-	-	-	*	900	432
[45]	251334	128	2	16	50	118	24	23.1	-	-	-	-	*	900	432
[45]	351331	128	2	16	50	118	24	29.3	-	-	-	-	*	900	488
[45]	351332	128	2	16	50	118	24	29.3	-	-	-	-	*	900	460
[45]	451331	128	2	16	50	118	24	33.2	-	-	-	-	*	900	488
Author	**Test**	l_0	n_b	**Ø**	c_x	c_s	c_y	f_{cm}	$Ø_{st}$	n_{st}	s_t	n_l	f_R	f_y	$\sigma_{s,max}$
		[mm]	-	[mm]	[mm]	[mm]	[mm]	[MPa]	[mm]	-	[mm]	-	-	[MPa]	[MPa]
[45]	451332	128	2	16	50	118	24	33.2	-	-	-	-	*	900	437
[45]	451333	128	2	16	50	118	24	40.4	-	-	-	-	*	900	596
[45]	451334	128	2	16	50	118	24	40.4	-	-	-	-	*	900	537
[45]	151901	192	2	16	50	118	24	16.9	-	-	-	-	*	900	378
[45]	151902	192	2	16	50	118	24	16.9	-	-	-	-	*	900	378
[45]	251901	192	2	16	50	118	24	20.8	-	-	-	-	*	900	432
[45]	251902	192	2	16	50	118	24	20.8	-	-	-	-	*	900	460
[45]	351901	192	2	16	50	118	24	33.5	-	-	-	-	*	900	487
[45]	351902	192	2	16	50	118	24	33.5	-	-	-	-	*	900	460
[45]	451901	192	2	16	50	118	24	33.2	-	-	-	-	*	900	453
[45]	451902	192	2	16	50	118	24	33.2	-	-	-	-	*	900	460
[45]	151911	192	2	16	50	118	24	12.4	-	-	-	-	*	900	323
[45]	151912	192	2	16	50	118	24	12.4	-	-	-	-	*	900	300
[45]	201911	192	2	16	50	118	24	26.9	-	-	-	-	*	900	543
[45]	201912	192	2	16	50	118	24	26.9	-	-	-	-	*	900	491
[45]	221911	192	2	16	50	118	24	23.2	-	-	-	-	*	900	464
[45]	221912	192	2	16	50	118	24	23.2	-	-	-	-	*	900	464
[45]	251911	192	2	16	50	118	24	17.5	-	-	-	-	*	900	437

[45]	251912	192	2	16	50	118	24	17.5	-	-	-	-	*	900	437
[45]	301911	192	2	16	50	118	24	30.8	-	-	-	-	*	900	519
[45]	301912	192	2	16	50	118	24	30.8	-	-	-	-	*	900	519
[45]	351911	192	2	16	50	118	24	31.4	-	-	-	-	*	900	492
[45]	351912	192	2	16	50	118	24	31.4	-	-	-	-	*	900	464
[45]	401911	192	2	16	50	118	24	43.2	-	-	-	-	*	900	572
[45]	401912	192	2	16	50	118	24	43.2	-	-	-	-	*	900	572
[45]	401913	192	2	16	50	118	24	31.6	-	-	-	-	*	900	519
[45]	401914	192	2	16	50	118	24	31.6	-	-	-	-	*	900	464
[45]	451912	192	2	16	50	118	24	44.1	-	-	-	-	*	900	654
[45]	151921	192	2	16	50	118	24	15.1	-	-	-	-	*	900	436
[45]	151922	192	2	16	50	118	24	15.1	-	-	-	-	*	900	464
[45]	351921	192	2	16	50	118	24	35.9	-	-	-	-	*	900	596
[45]	351922	192	2	16	50	118	24	35.9	-	-	-	-	*	900	651
[45]	451921	192	2	16	50	118	24	45	-	-	-	-	*	900	760
[45]	451922	192	2	16	50	118	24	45	-	-	-	-	*	900	707
[45]	152611	256	2	16	50	118	24	13.7	-	-	-	-	*	900	407
[45]	152612	256	2	16	50	118	24	13.7	-	-	-	-	*	900	436
[45]	252611	256	2	16	50	118	24	19	-	-	-	-	*	900	492
[45]	352611	256	2	16	50	118	24	23.9	-	-	-	-	*	900	463
[45]	352612	256	2	16	50	118	24	23.9	-	-	-	-	*	900	491
[45]	452611	256	2	16	50	118	24	33.2	-	-	-	-	*	900	570
[45]	152621	256	2	16	50	118	24	15.1	-	-	-	-	*	900	569
[45]	152622	256	2	16	50	118	24	15.1	-	-	-	-	*	900	542
[45]	252621	256	2	16	50	118	24	17	-	-	-	-	*	900	633
[45]	2013H1	128	2	16	50	118	24	15.1	-	-	-	-	*	900	288
[45]	2013H2	128	2	16	50	118	24	15.1	-	-	-	-	*	900	259
[45]	2013V1	128	2	16	50	138	24	17	-	-	-	-	*	900	241
[45]	2013V2	128	2	16	50	138	24	15.1	-	-	-	-	*	900	241
[45]	2019H1	128	2	16	50	118	24	15.1	-	-	-	-	*	900	234
[45]	2019H2	128	2	16	50	118	24	17	-	-	-	-	*	900	215
[45]	2019V1	128	2	16	50	118	24	15.1	-	-	-	-	*	900	234
[45]	2019V2	128	2	16	50	118	24	15.1	-	-	-	-	*	900	234

A.3.35. Kemp; Wilhelm [KEM79]

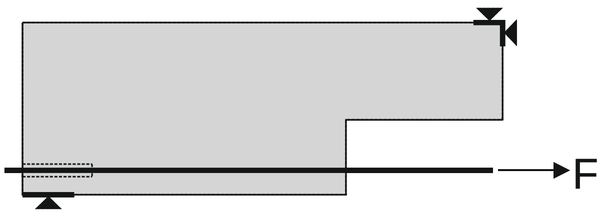

Author	Test	l_0	n_b	Ø	c_x	c_s	c_y	f_{cm}	$Ø_{st}$	n_{st}	s_t	n_l	f_R	f_y	$\sigma_{s,max}$
		[mm]	-	[mm]	[mm]	[mm]	[mm]	[MPa]	[mm]	-	[mm]	-	-	[MPa]	[MPa]
[52]	E210-1	406	2	35.8	96.7	264	25.4	29.1	-	-	-	-	*	414	176
[52]	E210-2	406	2	35.8	96.7	264	25.4	29.1	-	-	-	-	*	414	177
[52]	E220-1	406	2	35.8	96.7	264	50.8	30.4	-	-	-	-	*	414	232
[52]	E220-2	406	2	35.8	96.7	264	50.8	30.4	-	-	-	-	*	414	217
[52]	E230-1	406	2	35.8	96.7	264	76.3	30.6	-	-	-	-	*	414	255
[52]	E230-2	406	2	35.8	96.7	264	76.3	30.6	-	-	-	-	*	414	269
[52]	E310-1	406	2	35.8	58	171	25.4	29.2	-	-	-	-	*	414	172
[52]	E310-2	406	2	35.8	58	171	25.4	29.2	-	-	-	-	*	414	172
[52]	E320-1	406	2	35.8	58	171	50.8	30.1	-	-	-	-	*	414	209
[52]	E320-2	406	2	35.8	58	171	50.8	30.1	-	-	-	-	*	414	214
[52]	E330-1	406	2	35.8	58	171	76.3	26.4	-	-	-	-	*	414	232
[52]	E330-2	406	2	35.8	58	171	76.3	26.4	-	-	-	-	*	414	228

A.3.36. KADORIKU [KAD94]

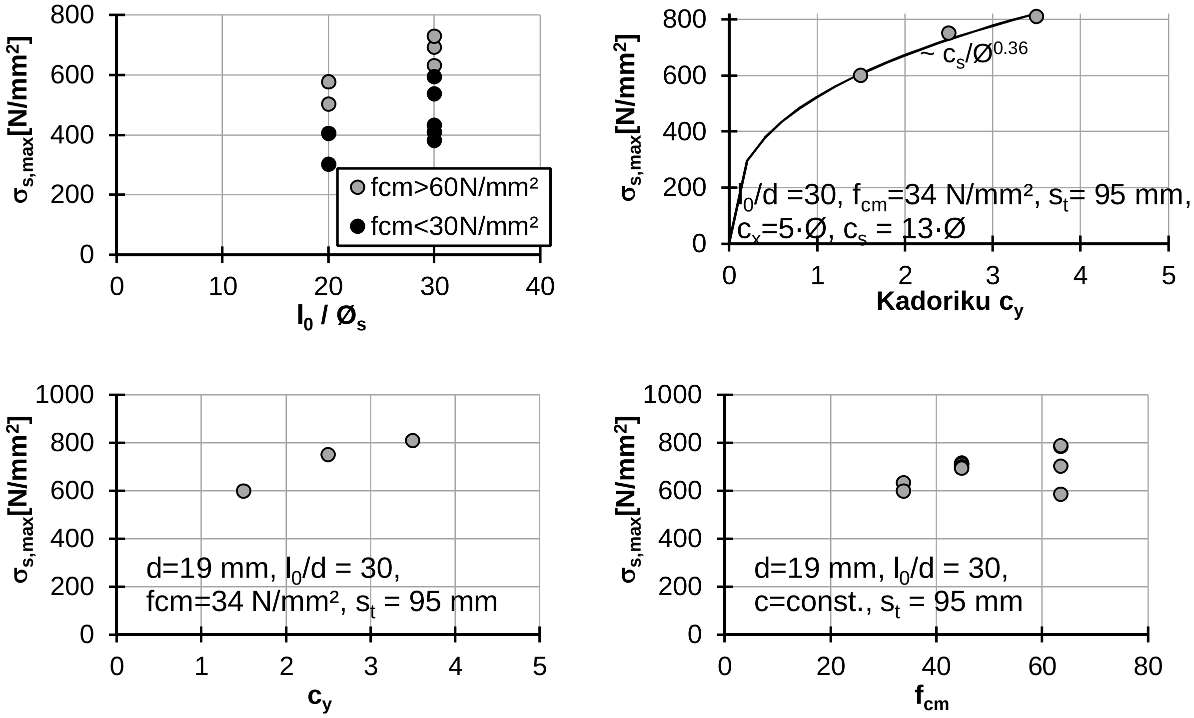

Author	Test	l_0	n_b	Ø	c_x	c_s	c_y	f_{cm}	$Ø_{st}$	n_{st}	s_t	n_l	f_R	f_y	$\sigma_{s,max}$
		[mm]	-	[mm]	[mm]	[mm]	[mm]	[MPa]	[mm]	-	[mm]	-	-	[MPa]	[MPa]
[26]	PB-01	380	2	19	36	152	29	62	9	2	380	2	*	708	576
[26]	PB-02	570	2	19	36	152	29	62	9	3	285	2	*	708	693
[26]	PB-04	570	2	19	36	152	29	22	9	3	285	2	*	708	433
[26]	PB-05	760	2	19	36	152	29	22	9	4	253	2	*	708	558
[26]	PB-06***	950	2	19	36	152	29	22	9	5	238	2	*	708	757
[26]	PB-15	570	2	19	36	152	29	76	9	3	285	2	*	725	730
[26]	PB-16	570	2	19	36	152	29	61	9	3	285	2	*	656	632
[26]	PB-19	570	2	19	36	152	29	28	9	3	285	2	*	725	593
[26]	PB-20	570	2	19	36	152	29	28	9	3	285	2	*	530	538
[26]	PB-21	380	2	19	36	152	29	28	9	2	380	2	*	530	405
[26]	PB-23	570	2	19	36	152	29	21	9	3	285	2	*	530	382
[26]	PB-24	570	2	19	36	152	29	21	9	3	285	2	*	442	410
[26]	PB-25	380	2	19	36	152	29	21	9	2	380	2	*	442	302
[26]	PB-27	570	2	19	36	112	29	61	9	3	285	2	*	656	646
[26]	PB-31	380	2	19	36	152	29	61	9	4	127	2	*	530	503
[26]	S1-01	570	2	19	90	244	29	64	6	7	95	2	*	843	784
[26]	S1-02	570	2	19	90	244	29	64	6	7	95	2	*	843	788
[26]	S1-03	570	2	19	90	244	29	64	6	7	95	2	*	843	704
[26]	S1-04	570	2	19	90	244	29	64	6	7	95	2	*	843	585
[26]	S2-01	570	2	19	90	244	29	45	6	7	95	2	*	843	712
[26]	S2-02	570	2	19	90	244	29	45	6	7	95	2	*	843	715
[26]	S2-03	570	2	19	90	244	29	45	6	7	95	2	*	843	709
[26]	S2-04	570	2	19	90	244	29	45	6	7	95	2	*	843	699
[26]	S2-05	570	2	19	90	244	29	45	6	7	95	2	*	843	694
[26]	S3-01	570	2	19	90	244	29	34	6	7	95	2	*	843	633
[26]	S3-03	570	2	19	90	244	48	34	6	7	95	2	*	843	750
[26]	S3-04	570	2	19	90	244	67	34	6	7	95	2	*	843	810
[26]	S3-05	570	2	19	90	244	29	34	6	7	95	2	*	843	599
[26]	PB-10	570	2	19	29	166	29	61	6	6	113	2	*	725	707
[26]	PB-16	570	2	19	29	166	29	61	10	2	484	2	*	656	632
[26]	PB-11	570	2	19	29	166	29	61	10	4	170	2	*	725	719
[26]	PB-13	570	2	19	29	166	29	21	6	6	113	2	*	725	426
[26]	PB-24	570	2	19	29	166	29	21	10	2	484	2	*	442	410
[26]	PB-14	570	2	19	29	166	29	21	10	4	170	2	*	725	480

A.3.37. MATHEY; WATSTEIN [MAT61]

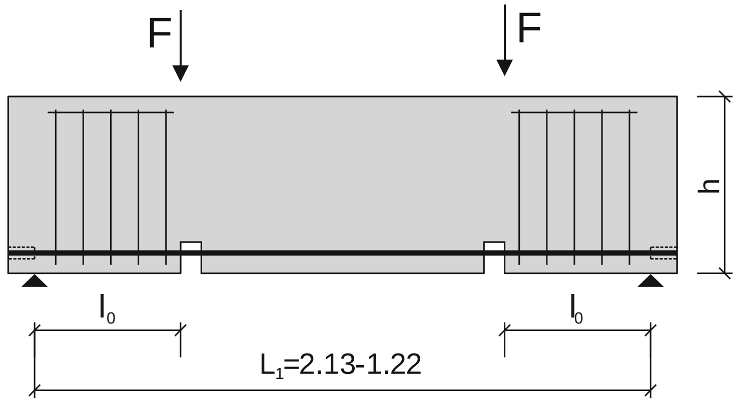

Author	Test	l_0	n_b	Ø	c_x	c_s	c_y	f_{cm}	$Ø_{st}$	n_{st}	s_t	n_l	f_R	f_y	$\sigma_{s,max}$
		[mm]	-	[mm]	[mm]	[mm]	[mm]	[MPa]	[mm]	-	[mm]	-	-	[MPa]	[MPa]
[27]	4-7-2	178	1	12.7	95	0	44	29	13	2	178	2	0.096	791	611
[27]	4-7-1	178	1	12.7	95	0	44	29	13	2	178	2	0.096	791	635
[27]	4-10.5-3	267	1	12.7	95	0	44	25	13	3	133	2	0.096	791	783
[27]	4-10.5-2	267	1	12.7	95	0	44	28	13	3	133	2	0.096	791	794
[27]	4-14-2	356	1	12.7	95	0	44	26	13	4	119	2	0.096	791	693
[27]	8-21-1	533	1	25.4	89	0	38	29	13	5	133	2	0.088	669	427
[27]	8-28-1	711	1	25.4	89	0	38	31	13	7	119	2	0.088	669	534
[27]	8-28-2	711	1	25.4	89	0	38	26	13	7	119	2	0.088	669	498
[27]	8-34-1	864	1	25.4	89	0	38	26	13	9	108	2	0.088	669	640
[27]	8-14-1	356	1	25.4	89	0	38	25	13	4	119	2	0.088	669	231
[27]	8-34-2	864	1	25.4	89	0	38	26	13	9	108	2	0.088	669	623
[27]	8-14-2	356	1	25.4	89	0	38	28	13	4	119	2	0.088	669	293
[27]	8-7-1	178	1	25.4	89	0	38	28	13	2	178	2	0.088	669	197
[27]	8-21-2	533	1	25.4	89	0	38	24	13	5	133	2	0.088	669	368

A.3.38. MORITA; FUJI [MOR82]

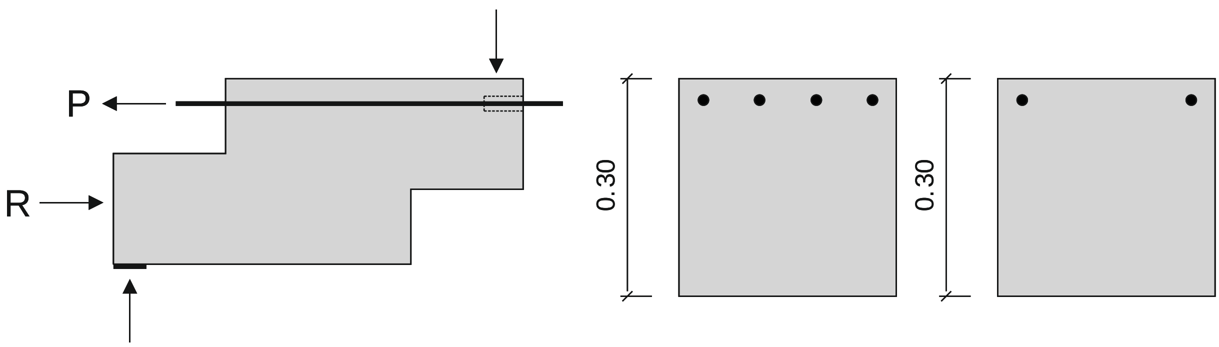

Author	Test	l_0	n_b	Ø	c_x	c_s	c_y	f_{cm}	$Ø_{st}$	n_{st}	s_t	n_l	f_R	f_y	$\sigma_{s,max}$
		[mm]	-	[mm]	[mm]	[mm]	[mm]	[MPa]	[mm]	-	[mm]	-	-	[MPa]	[MPa]
[53]	5	500	2	19	30	202	30	22.3	-	-	-	-	*	500	383
[53]	6	500	4	19	30	54.7	30	22.3	-	-	-	-	*	500	232

A.3.39. OLSEN [OLS90]

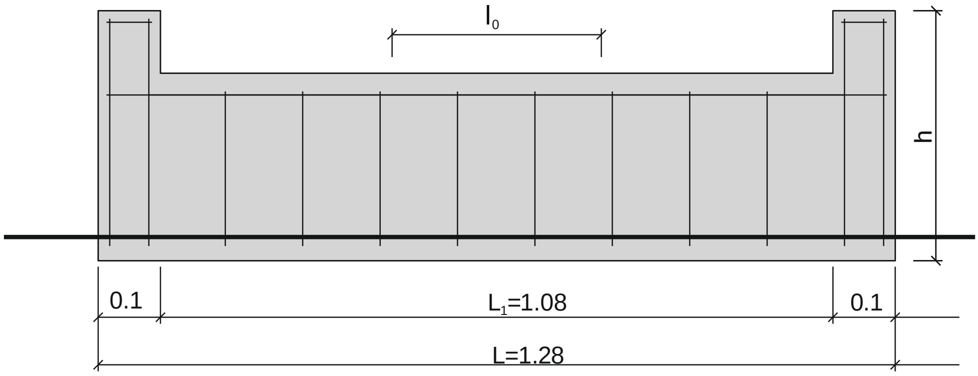

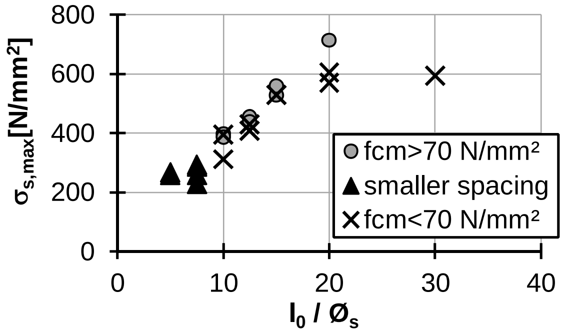

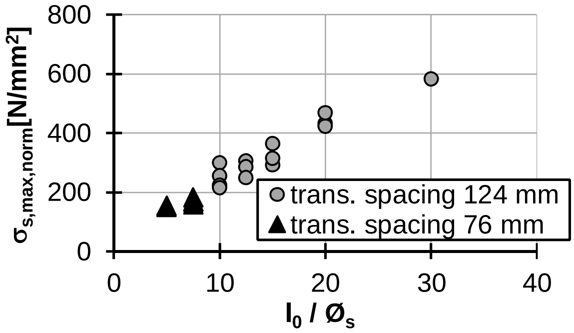

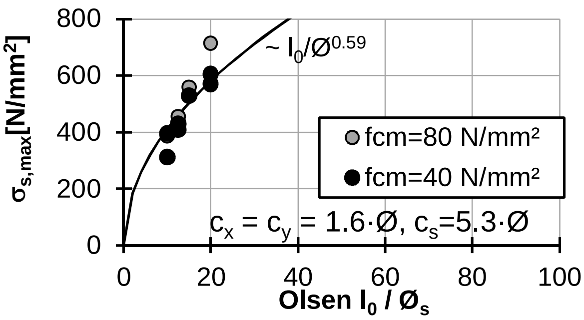

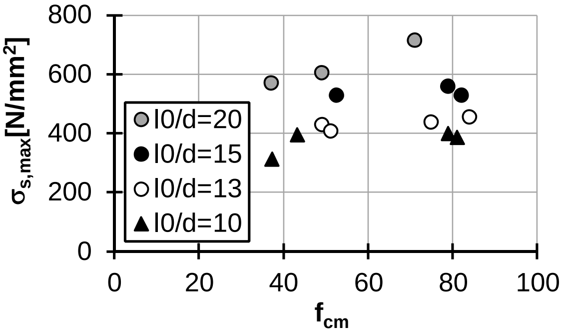

Author	Test	l_0	n_b	Ø	c_x	c_s	c_y	f_{cm}	$Ø_{st}$	n_{st}	s_t	n_l	f_R	f_y	$σ_{s,max}$
		[mm]	-	[mm]	[mm]	[mm]	[mm]	[MPa]	[mm]	-	[mm]	-	-	[MPa]	[MPa]
[28]	90/15	240	2	16	26	84	26	82	6	2	124	2	*	647	529
[28]	70/20	320	2	16	26	84	26	71	6	3	124	2	*	647	714
[28]	50/20	320	2	16	26	84	26	49	6	3	124	2	*	647	605
[28]	30/30	480	2	16	26	84	26	26	6	4	124	2	*	647	594
[28]	90/05	80	2	16	26	84	26	75	6	2	76	2	*	647	259
[28]	70/05	80	2	16	26	84	26	75	6	2	76	2	*	647	266
[28]	50/10	160	2	16	26	84	26	43	6	2	124	2	*	647	395
[28]	30/10	160	2	16	26	84	26	37	6	2	124	2	*	647	311
[28]	90/10	160	2	16	26	84	26	79	6	2	124	2	*	647	397
[28]	70/10	160	2	16	26	84	26	81	6	2	124	2	*	647	386
[28]	30/20	320	2	16	26	84	26	37	6	3	124	2	*	647	570
[28]	70/15	240	2	16	26	84	26	79	6	2	124	2	*	647	559
[28]	90/12.5	200	2	16	26	84	26	84	6	2	124	2	*	647	455
[28]	90/07.5	120	2	16	26	84	26	77	6	2	76	2	*	647	293
[28]	70/12.5	200	2	16	26	84	26	75	6	2	124	2	*	647	438
[28]	70/07.5	120	2	16	26	84	26	82	6	2	76	2	*	647	285
[28]	40/15	240	2	16	26	84	26	53	6	2	124	2	*	647	528
[28]	50/12.5	200	2	16	26	84	26	49	6	2	124	2	*	647	429
[28]	50/07.5	120	2	16	26	84	26	50	6	2	76	2	*	647	257
[28]	30/12.5	200	2	16	26	84	26	51	6	2	124	2	*	647	408
[28]	30/07.5	120	2	16	26	84	26	45	6	2	76	2	*	647	227

A.3.40. Perry; Jundi [PER69]

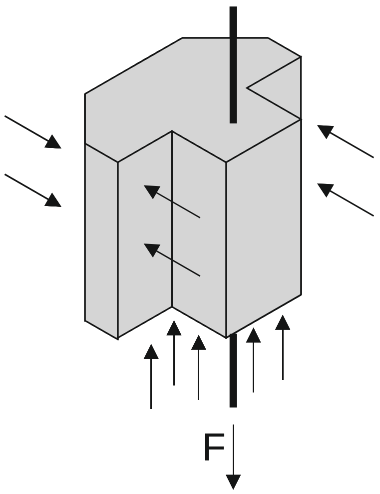

Author	Test	l_0	n_b	Ø	c_x	c_s	c_y	f_{cm}	$Ø_{st}$	n_{st}	s_t	n_l	f_R	f_y	$\sigma_{s,max}$
		[mm]	-	[mm]	[mm]	[mm]	[mm]	[MPa]	[mm]	-	[mm]	-	-	[MPa]	[MPa]
[50]	co.1	229	1	19.1	54.1	0	19.1	15.2	-	-	-	-	*	500	149
[50]	co.2	229	1	19.1	54.1	0	19.1	23.2	-	-	-	-	*	500	179
[50]	co.3	229	1	19.1	54.1	0	19.1	27.8	-	-	-	-	*	500	204
[50]	co.4	229	1	19.1	54.1	0	19.1	34.9	-	-	-	-	*	500	243
[50]	co.5	229	1	19.1	54.1	0	19.1	18.6	-	-	-	-	*	500	139
[50]	co.6	229	1	19.1	54.1	0	19.1	17.9	-	-	-	-	*	500	120
[50]	co.7	229	1	19.1	54.1	0	19.1	20.7	-	-	-	-	*	500	192
[50]	co.8	229	1	19.1	54.1	0	19.1	31.7	-	-	-	-	*	500	161
[50]	co.9	229	1	19.1	54.1	0	19.1	35.2	-	-	-	-	*	500	211

A.3.41. RATHKJEN [RAT72]

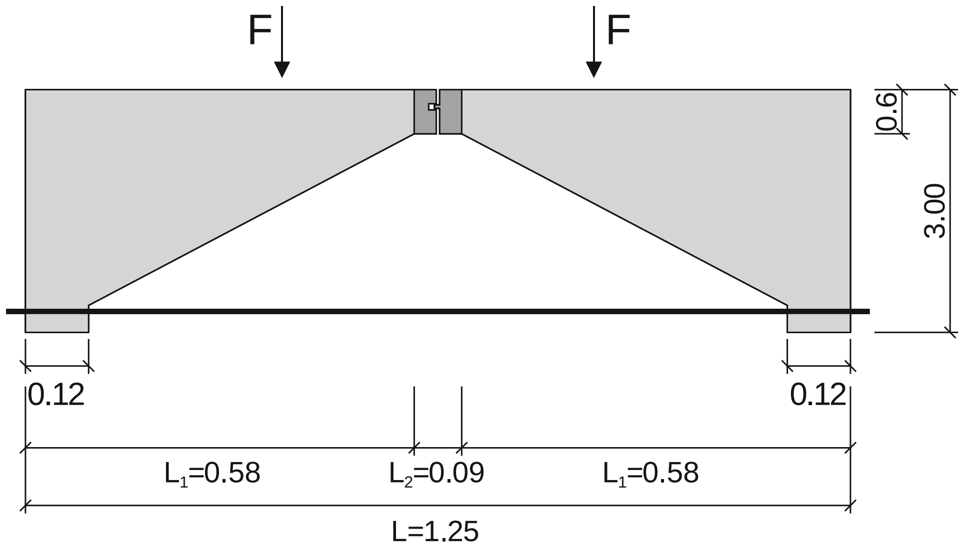

Author	Test	l_0	n_b	Ø	c_x	c_s	c_y	f_{cm}	$Ø_{st}$	n_{st}	s_t	n_l	f_R	f_y	$\sigma_{s,max}$
		[mm]	-	[mm]	[mm]	[mm]	[mm]	[MPa]	[mm]	-	[mm]	-	-	[MPa]	[MPa]
[46]	13	120	1	14	63	0	20	26.4	-	-	-	-	*	560	380
[46]	14	120	1	14	63	0	20	25.1	-	-	-	-	*	560	349
[46]	15	120	1	14	63	0	20	25.3	-	-	-	-	*	560	362
[46]	16	120	1	14	63	0	20	24.1	-	-	-	-	*	560	355
[46]	17	120	1	14	63	0	20	28.1	-	-	-	-	*	560	310
[46]	18	120	1	14	63	0	20	29.5	-	-	-	-	*	560	318
[46]	19	120	1	14	63	0	20	20.1	-	-	-	-	*	560	190
[46]	20	120	1	14	63	0	20	22.2	-	-	-	-	*	560	325
[46]	21	120	1	14	63	0	20	18.6	-	-	-	-	*	560	249
[46]	36	120	1	14	63	0	20	18.1	-	-	-	-	*	560	287
[46]	37	120	1	14	63	0	20	19.2	-	-	-	-	*	560	294
[46]	38	120	1	14	63	0	20	19.2	-	-	-	-	*	560	346
[46]	39	120	1	14	63	0	20	18.9	-	-	-	-	*	560	256
[46]	52	120	1	14	63	0	20	21.6	-	-	-	-	*	560	385
[46]	53	120	1	14	63	0	20	22.2	-	-	-	-	*	560	210
[46]	54	120	1	14	63	0	20	24.3	-	-	-	-	*	560	249
[46]	57	120	1	14	63	0	20	25.1	-	-	-	-	*	560	305
[46]	107	120	1	14	63	0	20	18.5	-	-	-	-	*	560	162
[46]	22	120	2	14	30	52	20	32.3	-	-	-	-	*	560	364
[46]	23	120	2	14	30	52	20	33.1	-	-	-	-	*	560	314
[46]	24	120	2	14	30	52	20	17.6	-	-	-	-	*	560	225
[46]	25	120	2	14	30	52	20	19	-	-	-	-	*	560	224
[46]	26	120	2	14	30	52	20	19.4	-	-	-	-	*	560	212
[46]	27	120	2	14	30	52	20	19.1	-	-	-	-	*	560	237
[46]	28	120	2	14	30	52	20	18.5	-	-	-	-	*	560	198
[46]	29	120	2	14	30	52	20	18	-	-	-	-	*	560	269
[46]	30	120	2	14	30	52	20	27.4	-	-	-	-	*	560	334
[46]	31	120	2	14	30	52	20	26.7	-	-	-	-	*	560	256
[46]	32	120	2	14	30	52	20	27.6	-	-	-	-	*	560	326
[46]	33	120	2	14	30	52	20	26.3	-	-	-	-	*	560	313
[46]	34	120	2	14	30	52	20	28.5	-	-	-	-	*	560	410
[46]	35	120	2	14	30	52	20	29.5	-	-	-	-	*	560	417
[46]	110	120	3	10	32	23	22	14.4	-	-	-	-	*	560	384
[46]	111	120	3	10	32	23	22	14.4	-	-	-	-	*	560	396
[46]	112	120	3	10	32	23	22	14.9	-	-	-	-	*	560	380
Author	Test	l_0	n_b	Ø	c_x	c_s	c_y	f_{cm}	$Ø_{st}$	n_{st}	s_t	n_l	f_R	f_y	$\sigma_{s,max}$
		[mm]	-	[mm]	[mm]	[mm]	[mm]	[MPa]	[mm]	-	[mm]	-	-	[MPa]	[MPa]

[46]	113	120	3	10	32	23	22	14.9	-	-	-	-	*	560	312
[46]	114	120	3	10	32	23	22	21.2	-	-	-	-	*	560	370
[46]	115	120	3	10	32	23	22	21.2	-	-	-	-	*	560	380
[46]	116	120	3	10	32	23	22	18.2	-	-	-	-	*	560	505
[46]	117	120	3	10	32	23	22	18.2	-	-	-	-	*	560	479
[46]	118	120	3	10	32	23	22	20.6	-	-	-	-	*	560	384
[46]	119	120	3	10	32	23	22	20.6	-	-	-	-	*	560	367
[46]	120	120	3	10	32	23	22	20.9	-	-	-	-	*	560	572
[46]	121	120	3	10	32	23	22	17.6	-	-	-	-	*	560	423
[46]	122	120	3	10	32	23	22	17.6	-	-	-	-	*	560	332
[46]	123	120	3	10	32	23	22	18.3	-	-	-	-	*	560	495
[46]	124	120	3	10	32	23	22	19.5	-	-	-	-	*	560	356
[46]	125	120	3	10	32	23	22	19.5	-	-	-	-	*	560	330
[46]	A1	120	2	10	32	46	22	20	-	-	-	-	*	560	352
[46]	A2	120	2	10	32	46	22	20	-	-	-	-	*	560	335
[46]	A3	120	2	10	32	46	22	20	-	-	-	-	*	560	369
[46]	A4	120	2	10	32	46	22	20	-	-	-	-	*	560	369
[46]	A5	120	2	10	32	46	22	20	-	-	-	-	*	560	369

A.3.42. REGAN [REG97]

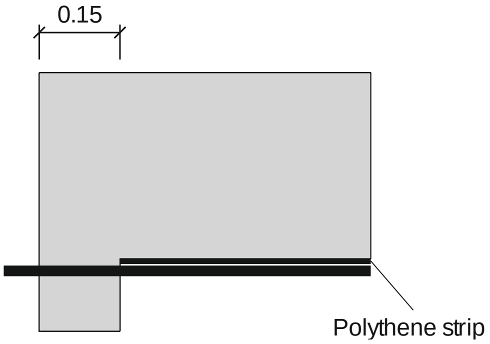

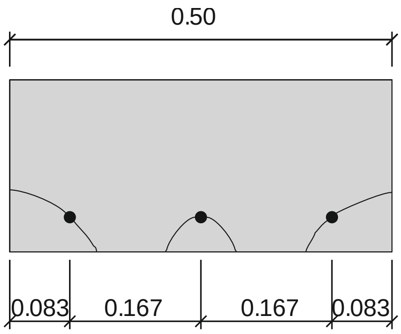

Author	Test	l_0	n_b	Ø	c_x	c_s	c_y	f_{cm}	$Ø_{st}$	n_{st}	s_t	n_l	f_R	f_y	$\sigma_{s,max}$
		[mm]	-	[mm]	[mm]	[mm]	[mm]	[MPa]	[mm]	-	[mm]	-	-	[MPa]	[MPa]
[47]	6	150	3	20	73	147	20	37.9	-	-	-	-	*	500	271
[47]	7	150	3	20	73	147	20	37.5	-	-	-	-	*	500	267
[47]	9edge	150	3	20	73	147	20	35.2	-	-	-	-	*	500	316
[47]	10	150	3	20	73	147	20	35.2	-	-	-	-	*	500	343

A.3.43. REHM; ELIGEHAUSEN [REH77]

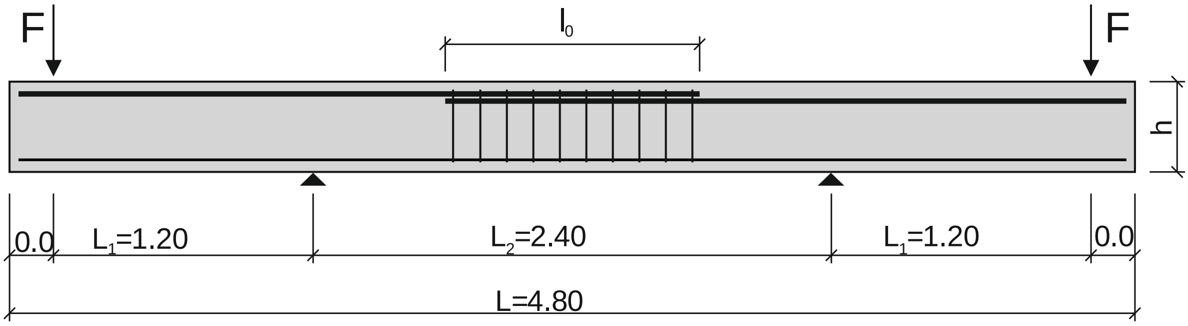

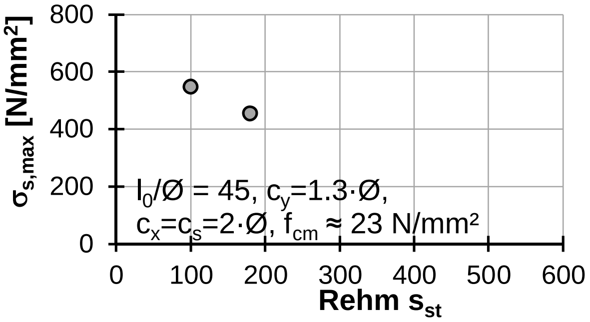

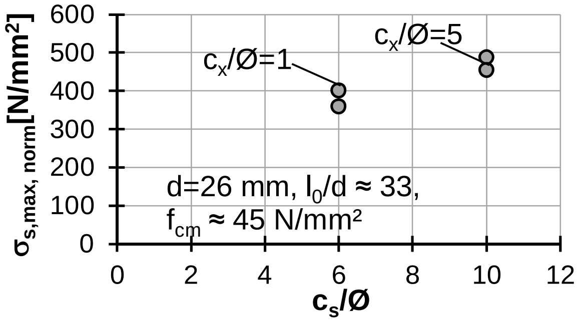

Author	Test	l_0	n_b	Ø	c_x	c_s	c_y	f_{cm}	$Ø_{st}$	n_{st}	s_t	n_l	f_R	f_y	$\sigma_{s,max}$
		[mm]	-	[mm]	[mm]	[mm]	[mm]	[MPa]	[mm]	-	[mm]	-	-	[MPa]	[MPa]
[29]	S1.2	1020	5	14	86	172	15	24	6	6	200	2	0.072	426	532
[29]	S1.3	610	5	14	86	172	15	19	6	4	200	2	0.069	423	544
[29]	S1.4	610	5	14	29	28	18	21	8	3	180	2	0.069	423	456
[29]	S1.5	820	5	14	29	56	18	21	8	5	180	2	0.068	440	544
[29]	S1.6	820	5	14	29	28	18	19	8	5	180	2	0.071	421	492
[29]	S1.7	570	5	14	29	28	18	53	8	3	180	2	0.07	422	515
[29]	S1.8	420	4	14	14	28	18	45	8	3	180	2	0.07	415	446
[29]	S1.9	660	5	14	29	28	18	24	8	7	100	2	0.071	439	548
[29]	S1.11	210	5	14	29	28	18	43	8	5	50	2	0.07	447	393
[29]	S1.12	320	5	14	29	28	18	42	8	6	56	2	0.074	420	373
[29]	S2.1	910	5	26	26	52	27	50	12	6	150	2	0.069	404	471
[29]	S2.2	830	4	26	130	260	25	42	10	6	150	2	0.075	466	555
[29]	S2.3	810	5	28	28	56	28	36	12	6	150	2	0.07	561	252
[29]	S2.4	1140	5	26	26	52	27	55	10	7	160	2	0.076	425	457
[29]	S2.5	910	5	26	26	156	26	48	10	7	150	2	0.075	428	424
[29]	S2.6	830	4	26	130	260	25	46	10	6	150	2	0.071	448	531
[29]	S2.7	910	5	26	26	52	27	49	12	6	150	2	0.075	467	455
[29]	S2.8	910	5	26	26	156	26	46	10	7	150	2	0.092	429	467
[29]	S2.9	1100	5	28	28	56	27	20	10	9	150	2	0.086	561	433

A.3.44. REZANSOFF; KONKANAR; FU [REZ92]

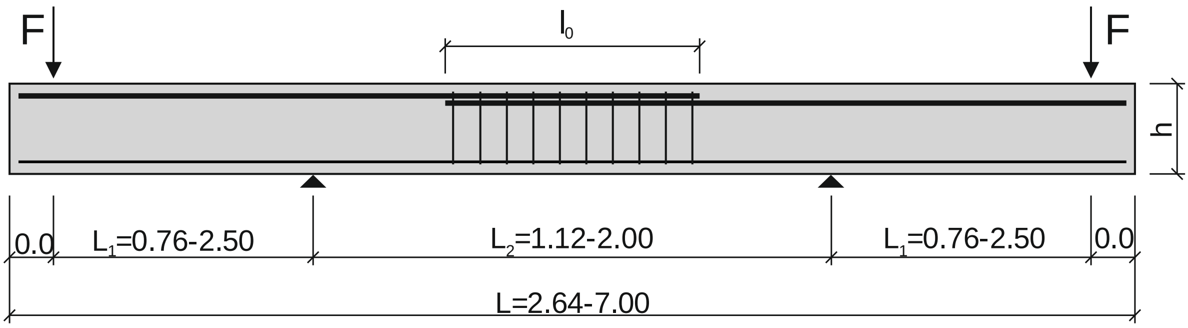

Author	Test	l_0 [mm]	n_b -	Ø [mm]	c_x [mm]	c_s [mm]	c_y [mm]	f_{cm} [MPa]	$Ø_{st}$ [mm]	n_{st} -	s_t [mm]	n_l -	f_R -	f_y [MPa]	$\sigma_{s,max}$ [MPa]
[31]	20-6-2	461	2	19.5	25	151	25	29	8	5	115	2	0.08	500	486
[31]	20-6-3	391	2	19.5	25	151	25	27	8	6	78	2	0.08	500	520
[31]	20-6-1	561	2	19.5	25	151	25	28	8	3	280	2	0.08	500	539
[31]	20-8-11	415	2	25.2	25	129	25	31	8	13	35	2	*	452	517
[31]	20-8-9	475	2	25.2	38	103	38	29	8	9	59	2	*	452	418
[31]	20-8-10	384	2	25.2	38	103	38	30	8	12	35	2	*	452	445
[31]	20-8-1	475	2	25.2	25	129	25	36	8	13	40	2	*	452	490
[31]	20-8-12	415	2	25.2	38	103	38	30	8	11	42	2	*	452	447
[31]	20-8-2	553	2	25.2	25	129	25	40	8	11	55	2	*	452	449
[31]	20-8-3	663	2	25.2	25	129	25	38	8	9	83	2	*	452	443
[31]	20-8-6	663	2	25.2	25	129	25	33	8	9	83	2	*	452	520
[31]	20-8-7	663	2	25.2	38	103	38	31	8	4	221	2	*	452	426
[31]	20-8-8	553	2	25.2	38	103	38	30	8	7	92	2	*	452	414
[31]	20-8-5	553	2	25.2	25	129	25	33	8	11	55	2	*	452	524
[31]	20-8-4	475	2	25.2	25	129	25	30	8	13	40	2	*	452	496
[31]	20-8-21	390	2	25.2	32	115	38	23	8	7	65	2	*	420	318
[31]	20-8-13	729	2	25.2	30	119	25	24	8	4	243	2	*	444	356
[31]	20-8-14	587	2	25.2	30	119	25	23	8	6	117	2	*	444	372
[31]	20-8-15	516	2	25.2	30	119	25	25	8	7	86	2	*	444	381
[31]	20-8-16	729	2	25.2	30	119	25	23	8	4	243	2	*	420	383
[31]	20-8-18	443	2	25.2	30	119	25	23	8	8	63	2	*	420	382
[31]	20-8-19	550	2	25.2	32	115	38	22	8	4	183	2	*	420	310
[31]	20-8-17	516	2	25.2	30	119	25	24	8	7	86	2	*	420	419
[31]	20-8-20	440	2	25.2	32	115	38	23	8	6	88	2	*	420	313
[31]	20-11-4	480	2	35.7	51	85	38	30	11	10	53	2	*	456	329
[31]	20-11-2	675	2	35.7	51	85	58	30	11	11	68	2	*	476	486
[31]	20-11-1	965	2	35.7	51	85	58	33	11	5	241	2	*	476	474
[31]	20-11-3	676	2	35.7	51	85	38	31	11	7	113	2	*	456	363
[31]	20-11-8	871	2	35.7	51	86	25	23	11	10	97	2	*	456	430
[31]	20-11-5	686	2	35.7	51	86	51	25	11	9	86	2	*	456	447
[31]	20-11-6	882	2	35.7	51	86	51	25	11	6	176	2	*	456	380
[31]	20-11-7	691	2	35.7	51	86	25	23	11	12	63	2	*	456	358
[31]	20-9-1	500	2	29.9	51	109	38	24	11	7	83	2	*	464	408
[31]	20-9-2	650	2	29.9	51	109	38	23	11	5	163	2	*	464	452

A.3.45. REZANSOFF; AKANNI; SPARLING [REZ93]

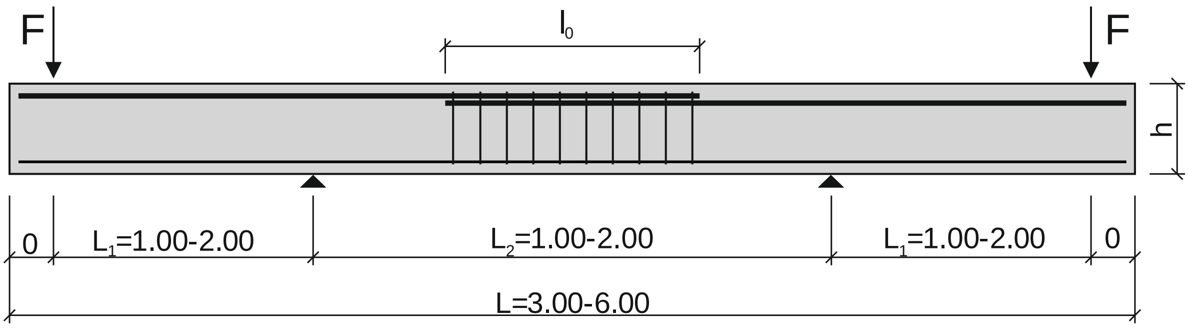

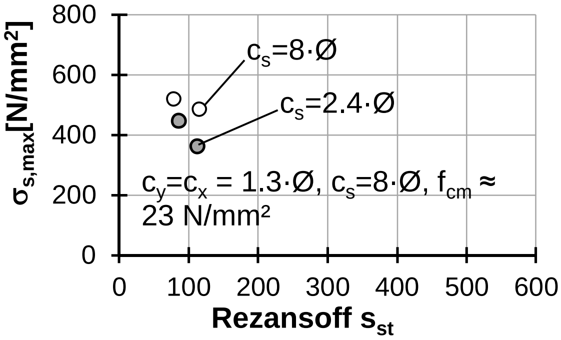

Author	Test	l_0	n_b	Ø	c_x	c_s	c_y	f_{cm}	$Ø_{st}$	n_{st}	s_t	n_l	f_R	f_y	$σ_{s,max}$
		[mm]	-	[mm]	[mm]	[mm]	[mm]	[MPa]	[mm]	-	[mm]	-	-	[MPa]	[MPa]
[30]	6	560	3	25.2	46	26	51	25	8	8	80	2	*	445	356
[30]	1b	750	2	25.2	46	26	51	26	6	6	150	2	*	445	481
[30]	1a	750	2	25.2	46	26	51	27	6	6	150	2	*	445	511
[30]	7	375	3	25.2	46	26	51	25	16	4	125	2	*	445	326
[30]	3a	750	3	25.2	46	26	51	27	6	6	150	2	*	445	481
[30]	3b	750	3	25.2	46	26	51	26	6	6	150	2	*	445	416
[30]	8	300	3	25.2	46	50	51	25	16	3	150	2	*	445	236
[30]	4b	1125	3	29.9	46	29	51	26	6	5	281	2	*	475	471
[30]	9	850	3	29.9	46	29	51	27	11	10	94	2	*	475	527
[30]	10	560	3	29.9	46	29	51	28	16	7	93	2	*	475	489
[30]	4a	900	3	29.9	46	29	51	28	6	4	300	2	*	475	426
[30]	2a	750	3	25.2	46	50	51	27	-	-	-	-	*	445	410
[30]	2b	750	3	25.2	46	50	51	26	-	-	-	-	*	445	411
[30]	5a	900	3	29.9	46	60	51	28	-	-	-	-	*	475	390
[30]	5b	1125	3	29.9	46	60	51	26	-	-	-	-	*	475	460

A.3.46. Richter [RIC84]

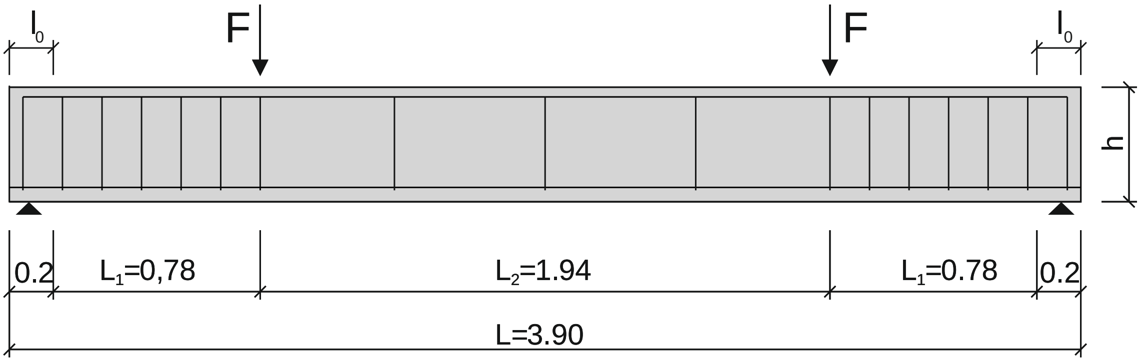

Author	Test	l_0	n_b	Ø	c_x	c_s	c_y	f_{cm}	$Ø_{st}$	n_{st}	s_t	n_l	f_R	f_y	$\sigma_{s,max}$
		[mm]	-	[mm]	[mm]	[mm]	[mm]	[MPa]	[mm]	-	[mm]	-	-	[MPa]	[MPa]
[39]	2.1	200	2	16	15	30	15	33.8	8	2	120	2	*	412	254
[39]	2.2	200	2	16	15	30	15	38.3	8	2	120	2	*	412	296
[39]	2.3	200	2	16	15	30	15	32.1	8	2	120	2	*	412	302

A.3.47. Schießl [SCH88]

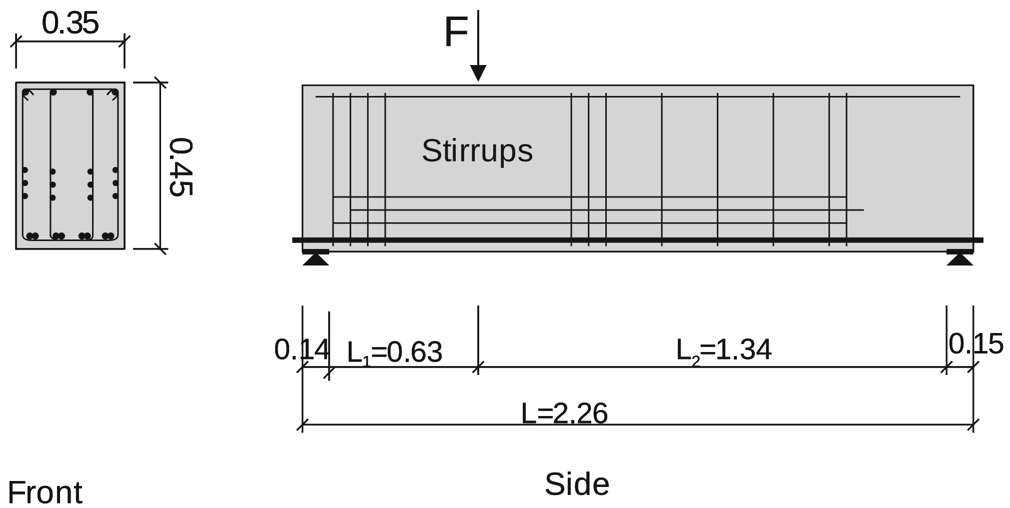

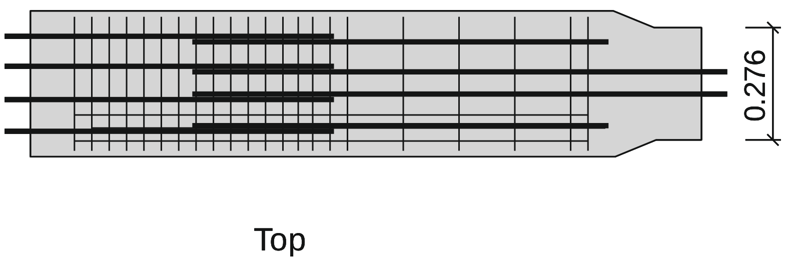

Author	Test	l_0	n_b	Ø	c_x	c_s	c_y	f_{cm}	$Ø_{st}$	n_{st}	s_t	n_l	f_R	f_y	$\sigma_{s,max}$
		[mm]	-	[mm]	[mm]	[mm]	[mm]	[MPa]	[mm]	-	[mm]	-	-	[MPa]	[MPa]
[58]	1	140	4	16	47	64	25	43	-	-	-	-	*	420	
[58]	2	110	2	16	90	64	25	43	-	-	-	-	*	420	

A.3.48. STÖCKL; MENNE; KUPFER [STO77]

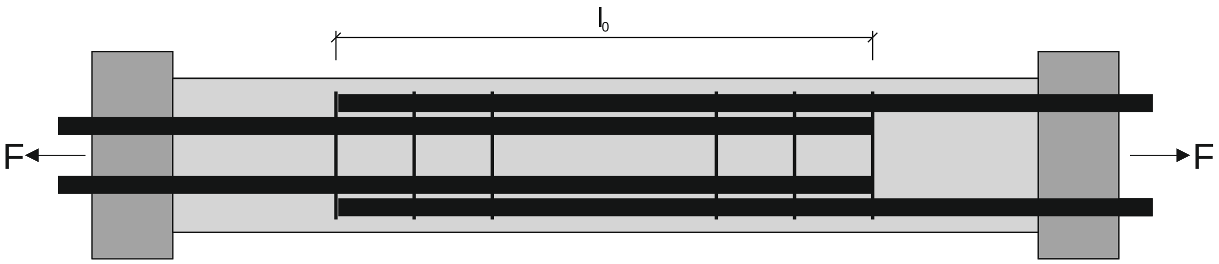

Author	Test	l_0	n_b	Ø	c_x	c_s	c_y	f_{cm}	$Ø_{st}$	n_{st}	s_t	n_l	f_R	f_y	$\sigma_{s,max}$
		[mm]	-	[mm]	[mm]	[mm]	[mm]	[MPa]	[mm]	-	[mm]	-	-	[MPa]	[MPa]
[32]	I-1	1900	1	26	26	104	23	29	8	17	115	-	0.068	465	525
[32]	I-2	1900	1	26	130	416	23	19	8	17	115	-	0.07	465	573
[32]	I-3	1900	1	26	18	52	23	18	8	17	115	2	0.07	465	566
[32]	II-9	1900	1	26	26	52	23	18	8	17	115	-	0.07	465	489
[32]	II-14	1560	1	26	26	52	23	21	8	14	115	-	0.07	465	468
[32]	II-8	1900	1	26	130	260	23	19	8	17	115	-	0.07	465	576
[32]	II-4	1300	1	26	130	260	23	20	8	11	115	-	0.07	465	530
[32]	II-6	1300	1	26	130	260	23	19	8	11	115	-	0.07	465	480
[32]	II-5	1900	1	26	18	52	23	20	8	17	115	2	0.07	465	576
[32]	II-7	1300	1	26	18	52	23	20	8	11	115	2	0.07	465	485
[32]	III-13	1900	2	26	26	52	23	19	8	17	115	-	0.07	465	485
[32]	III-12	1300	2	26	130	260	23	22	8	11	115	-	0.07	465	552
[32]	III-11	1130	2	26	169	338	23	17	8	10	115	-	0.07	465	446
[32]	IV-17	1560	1	26	78	52	23	21	8	14	115	-	0.07	465	540
[32]	IV-18	1560	1	26	26	52	23	21	8	14	115	-	0.07	465	470
[32]	IV-10	1900	1	26	130	260	23	19	8	17	115	-	0.07	465	562
[32]	IV-19	1900	1	26	26	52	25	19	10	6	253	-	0.07	465	425
[32]	IV-24	1560	1	26	26	52	25	25	10	6	208	-	0.07	465	509
[32]	IV-23	780	1	26	130	260	25	20	10	6	104	-	0.07	465	338
[32]	IV-20	1300	1	26	104	156	23	21	8	11	115	-	0.07	465	530
[32]	IV-15	1560	1	26	26	52	16	21	8	14	115	-	0.07	465	458
[32]	IV-16	1260	1	18	50	36	23	19	8	11	115	-	0.07	444	465
[32]	IV-21	1900	2	26	119	52	23	20	8	17	115	-	0.07	465	422
[32]	IV-22	1900	2	26	28	234	23	23	8	17	115	2	0.07	465	562

A.3.49. TEPFERS [TEP73]

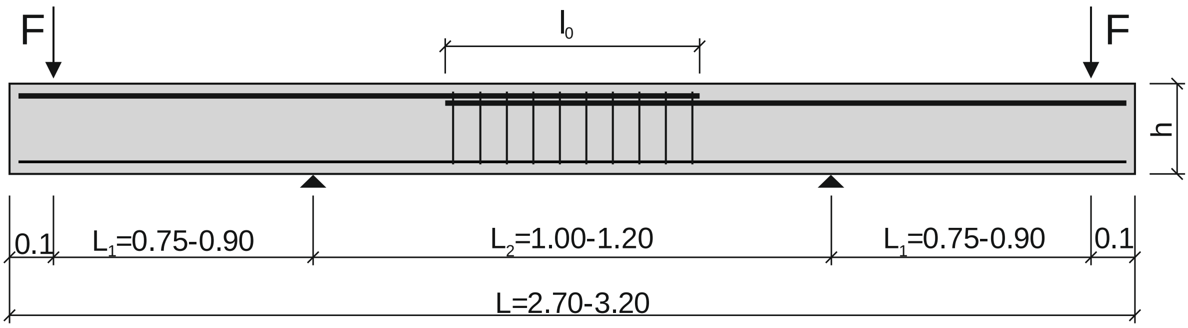

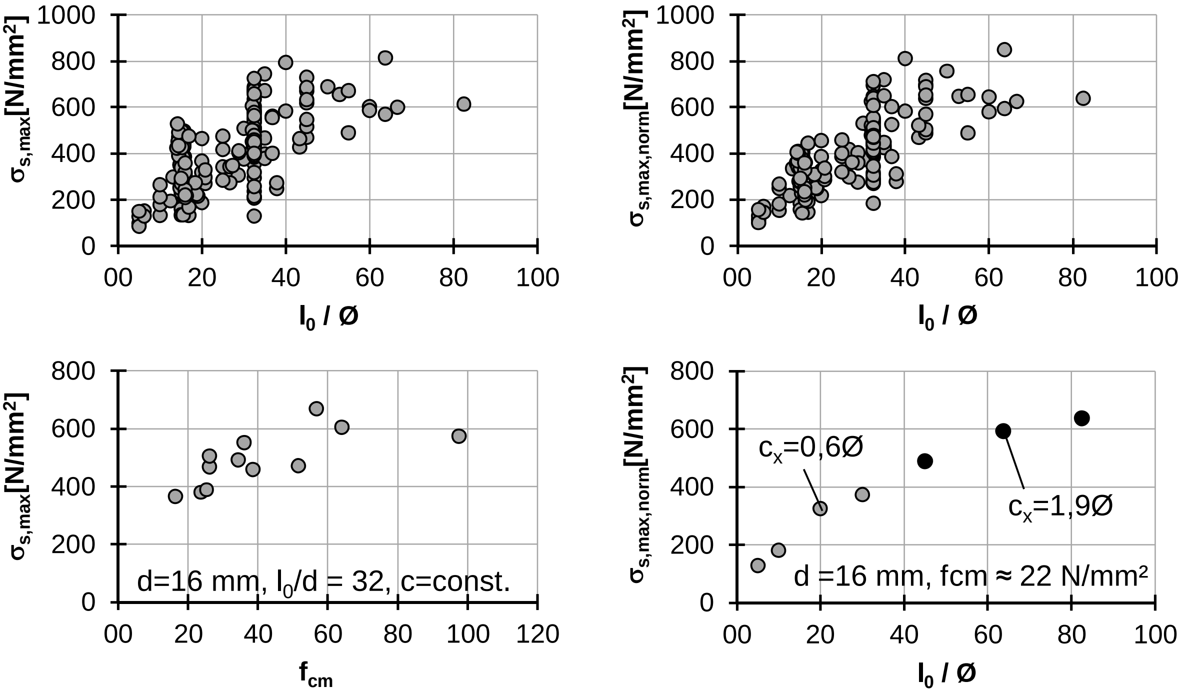

Author	Test	l_0	n_b	Ø	c_x	c_s	c_y	f_{cm}	$Ø_{st}$	n_{st}	s_t	n_l	f_R	f_y	$\sigma_{s,max}$
		[mm]	-	[mm]	[mm]	[mm]	[mm]	[MPa]	[mm]	-	[mm]	-	-	[MPa]	[MPa]
[33]	123-s1	240	2	16	40	16	25	22	-	-	-	-	0.12	589	271
[33]	123-s2	400	2	16	40	16	25	29	-	-	-	-	0.12	589	417
[33]	123-s3	560	2	16	40	16	25	29	-	-	-	-	0.12	589	466
[33]	123-s4	720	2	16	40	16	25	28	-	-	-	-	0.12	589	516
[33]	123-s7	960	2	16	40	16	25	29	-	-	-	-	0.12	804	603
[33]	657-1	520	2	16	30	36	20	21	-	-	-	-	0.12	903	385
[33]	657-2	720	2	16	30	36	20	21	-	-	-	-	0.12	903	469
[33]	657-3	1020	2	16	30	36	20	21	-	-	-	-	0.12	903	569
[33]	657-4	1320	2	16	30	36	20	21	-	-	-	-	0.12	912	612
[33]	657-13	720	2	16	32	31	39	21	-	-	-	-	0.12	883	546
[33]	657-14	720	2	16	25	46	10	21	-	-	-	-	0.12	883	437
[33]	657-15	720	2	16	47	49	34	22	-	-	-	-	0.12	883	618
[33]	657-16	720	2	16	57	74	41	22	-	-	-	-	0.12	883	632
[33]	657-22	60	2	12	10	62	20	20	-	-	-	-	0.12	667	149
[33]	657-23	120	2	12	10	62	20	24	-	-	-	-	0.12	667	264
[33]	657-24	240	2	12	10	62	20	27	-	-	-	-	0.12	682	464
[33]	657-25	360	2	12	10	62	20	21	-	-	-	-	0.12	652	508
[33]	657-25A	660	2	12	10	62	20	28	-	-	-	-	0.12	594	671
[33]	657-37	80	2	16	10	46	20	23	-	-	-	-	0.12	736	126
[33]	657-38	160	2	16	10	46	20	24	-	-	-	-	0.12	746	179
[33]	657-39	320	2	16	10	46	20	23	-	-	-	-	0.12	741	318
[33]	657-40	480	2	16	10	46	20	26	-	-	-	-	0.12	746	377
[33]	657-40A	880	2	16	10	46	20	25	-	-	-	-	0.12	574	490
[33]	715-52	520	2	16	40	50	5	26	-	-	-	-	0.12	625	481
[33]	715-53	520	2	16	40	54	15	27	-	-	-	-	0.12	625	547
[33]	715-54	520	2	16	40	55	35	27	-	-	-	-	0.12	591	563
[33]	715-55	520	2	16	40	56	50	34	-	-	-	-	0.12	591	657
[33]	732-1	520	2	16	32	34	19	16	-	-	-	-	0.12	607	365
[33]	732-2	520	2	16	32	34	24	22	-	-	-	-	0.12	607	392
[33]	732-3	520	2	16	32	34	18	34	-	-	-	-	0.12	613	492
[33]	732-4	520	2	16	32	33	21	45	-	-	-	-	0.12	603	590
[33]	732-5	520	2	16	29	40	16	57	-	-	-	-	0.12	589	669
[33]	732-6	520	2	16	33	32	17	64	-	-	-	-	0.12	589	604
[33]	732-7	520	2	16	28	41	23	8	-	-	-	-	0.12	618	206
[33]	732-9	520	2	16	30	37	23	20	-	-	-	-	0.12	589	488
[33]	732-10	520	2	16	26	45	22	26	-	-	-	-	0.12	589	511
[33]	732-11	520	2	16	33	31	21	15	-	-	-	-	0.12	589	389
[33]	732-12	520	2	16	32	32	21	7	-	-	-	-	0.12	589	210
[33]	732-13	520	2	16	35	26	26	9	-	-	-	-	0.06	438	215
[33]	732-14	520	2	16	35	27	26	12	-	-	-	-	0.06	438	257
[33]	732-15	520	2	16	36	26	23	27	-	-	-	-	0.06	423	411
[33]	732-16	520	2	16	37	25	26	32	-	-	-	-	0.06	421	440
[33]	732-17	520	2	16	30	39	21	45	-	-	-	-	0.06	421	481
[33]	732-18	520	2	16	30	37	20	32	-	-	-	-	0.12	621	535
[33]	732-19	520	2	16	36	26	21	33	-	-	-	-	0.12	621	537
[33]	732-20	520	2	16	30	36	17	26	-	-	-	-	0.12	610	468
[33]	732-21	520	2	16	33	30	19	26	-	-	-	-	0.12	610	505
[33]	732-33	520	2	16	30	36	21	29	-	-	-	-	0.12	589	295
[33]	732-34	520	2	16	30	37	20	37	-	-	-	-	0.12	589	579
[33]	732-35	520	2	16	32	35	19	36	-	-	-	-	0.12	589	551
[33]	732-36	520	2	16	30	38	19	98	-	-	-	-	0.12	589	574
[33]	732-37	520	2	16	37	27	18	91	-	-	-	-	0.12	589	438
Author	Test	l_0	n_b	Ø	c_x	c_s	c_y	f_{cm}	$Ø_{st}$	n_{st}	s_t	n_l	f_R	f_y	$\sigma_{s,max}$
		[mm]	-	[mm]	[mm]	[mm]	[mm]	[MPa]	[mm]	-	[mm]	-	-	[MPa]	[MPa]

[33]	732-38	320	2	8	18	94	13	25	-	-	-	-	0.06	451	584
[33]	732-39	320	2	8	18	96	16	23	-	-	-	-	0.12	726	794
[33]	732-40	320	2	10	22	77	18	21	-	-	-	-	0.06	412	500
[33]	732-41	320	2	10	26	76	15	22	-	-	-	-	0.12	647	605
[33]	732-42	320	2	19	26	72	36	33	-	-	-	-	0.06	429	475
[33]	732-43	520	2	19	40	43	39	21	-	-	-	-	0.12	623	348
[33]	732-44	520	2	16	32	34	57	21	-	-	-	-	0.12	589	459
[33]	732-45	520	2	16	31	36	49	19	-	-	-	-	0.12	589	477
[33]	732-46	520	2	16	82	30	1	26	-	-	-	-	0.12	589	388
[33]	732-47	520	2	16	83	28	18	17	-	-	-	-	0.12	589	355
[33]	732-48	520	2	16	101	32	17	19	-	-	-	-	0.12	589	439
[33]	732-49	520	2	16	36	24	1	16	-	-	-	-	0.12	589	380
[33]	732-50	520	2	16	3	32	74	18	-	-	-	-	0.12	589	318
[33]	732-51	520	2	16	32	35	19	25	-	-	-	-	0.06	505	388
[33]	732-52	520	2	16	31	35	19	24	-	-	-	-	0.06	505	380
[33]	732-53	520	2	16	30	39	20	11	-	-	-	-	0.06	488	236
[33]	732-54	520	2	16	32	37	17	39	-	-	-	-	0.06	482	459
[33]	732-55	520	2	16	33	34	18	52	-	-	-	-	0.06	476	471
[33]	732-56	320	2	10	22	83	18	14	-	-	-	-	0.06	418	414
[33]	732-57	320	2	10	19	86	15	16	-	-	-	-	0.06	418	450
[33]	732-59	720	2	19	37	10	24	15	-	-	-	-	0.12	714	273
[33]	732-60	320	2	19	36	12	26	15	-	-	-	-	0.12	714	168
[33]	732-61	720	2	19	38	7	19	16	-	-	-	-	0.06	442	247
[33]	732-62	320	2	19	38	62	21	16	-	-	-	-	0.06	442	131
[33]	732-63	220	2	12	24	62	19	16	-	-	-	-	0.12	638	274
[33]	732-64	320	2	12	23	65	17	12	-	-	-	-	0.12	638	343
[33]	732-65	420	2	12	26	60	16	16	-	-	-	-	0.12	643	378
[33]	732-66	520	2	12	25	61	20	16	-	-	-	-	0.12	643	463
[33]	732-67	220	2	12	22	66	15	18	-	-	-	-	0.06	437	231
[33]	732-68	320	2	12	19	72	14	18	-	-	-	-	0.06	437	275
[33]	732-69	420	2	12	21	68	14	17	-	-	-	-	0.06	446	397
[33]	732-70	520	2	12	28	55	12	17	-	-	-	-	0.06	440	427
[33]	732-71	520	2	16	72	41	23	20	-	-	-	-	0.12	719	408
[33]	732-72	520	2	16	100	35	24	22	-	-	-	-	0.12	656	498
[33]	732-73	520	2	16	127	32	25	23	-	-	-	-	0.12	637	432
[33]	732-74	520	2	16	27	41	66	21	-	-	-	-	0.12	648	427
[33]	732-75	520	2	16	29	37	83	21	-	-	-	-	0.12	625	449
[33]	732-76	520	2	16	28	38	96	6	-	-	-	-	0.12	727	129
[33]	732-77	520	2	16	28	39	95	13	-	-	-	-	0.12	701	401
[33]	732-84	520	2	16	44	16	23	32	-	-	-	-	0.12	725	687
[33]	732-85	520	2	16	63	35	24	30	-	-	-	-	0.12	725	667
[33]	732-86	520	2	16	111	75	29	27	-	-	-	-	0.12	725	724
[33]	732-87	520	2	16	152	115	24	31	-	-	-	-	0.12	719	673
[33]	732-88	520	2	16	167	134	24	31	-	-	-	-	0.12	719	577
[33]	732-90	520	2	16	33	31	23	46	-	-	-	-	0.12	589	634
[33]	732-100	50	2	8	11	99	12	16	-	-	-	-	0.12	702	151
[33]	732-101	105	2	8	15	89	9	16	-	-	-	-	0.12	1058	297
[33]	732-102	150	2	8	14	93	8	16	-	-	-	-	0.12	702	252
[33]	732-103	200	2	8	19	80	10	16	-	-	-	-	0.12	702	342
[33]	732-104	50	2	8	15	90	13	16	-	-	-	-	0.06	479	129
[33]	732-105	100	2	8	14	93	10	16	-	-	-	-	0.06	479	193
[33]	732-106	150	2	8	14	92	11	16	-	-	-	-	0.06	479	224
[33]	732-107	200	2	8	15	90	12	16	-	-	-	-	0.06	479	284
[33]	732-112	50	2	10	13	85	15	13	-	-	-	-	0.06	402	85
[33]	732-113	100	2	10	13	85	13	13	-	-	-	-	0.06	762	212
Author	**Test**	**l_0**	**n_b**	**Ø**	**c_x**	**c_s**	**c_y**	**f_{cm}**	**$Ø_{st}$**	**n_{st}**	**s_t**	**n_l**	**f_R**	**f_y**	**$\sigma_{s,max}$**
		[mm]	-	[mm]	[mm]	[mm]	[mm]	[MPa]	[mm]	-	[mm]	-	-	[MPa]	[MPa]
[33]	732-114	150	2	10	13	85	10	13	-	-	-	-	0.06	402	133
[33]	732-115	200	2	10	14	83	13	13	-	-	-	-	0.06	402	186

[33]	732-116	50	2	10	15	81	12	14	-	-	-	-	0.12	646	97
[33]	732-117	100	2	10	17	77	10	14	-	-	-	-	0.12	646	131
[33]	732-118	150	2	10	15	80	10	14	-	-	-	-	0.12	646	159
[33]	732-119	190	2	10	10	91	13	14	-	-	-	-	0.12	646	216
[33]	732-124	160	2	10	20	71	17	22	-	-	-	-	0.12	647	244
[33]	732-125	160	2	10	39	34	15	22	-	-	-	-	0.12	638	308
[33]	732-127	160	2	10	20	71	25	22	-	-	-	-	0.12	638	318
[33]	732-128	160	2	10	40	27	32	20	-	-	-	-	0.12	638	220
[33]	732-131	160	2	10	39	28	2	20	-	-	-	-	0.06	412	178
[33]	732-132	155	2	10	1	109	13	20	-	-	-	-	0.06	412	133
[33]	732-133	155	2	10	17	77	11	20	-	-	-	-	0.06	412	195
[33]	732-134	153	2	10	41	30	13	20	-	-	-	-	0.06	419	215
[33]	732-135	160	2	10	3	105	29	20	-	-	-	-	0.06	419	209
[33]	732-136	160	2	10	21	70	27	24	-	-	-	-	0.06	419	358
[33]	732-137	150	2	10	40	31	28	24	-	-	-	-	0.06	419	292
[33]	732-138	160	2	10	20	66	14	16	-	-	-	-	0.12	633	283
[33]	732-139	160	2	10	20	72	14	16	-	-	-	-	0.12	633	293
[33]	732-140	147	2	10	22	68	15	16	-	-	-	-	0.06	414	252
[33]	732-141	150	2	10	21	69	13	16	-	-	-	-	0.06	414	232
[33]	732-142	158	2	10	22	68	15	29	-	-	-	-	0.12	633	386
[33]	732-143	155	2	10	21	69	15	29	-	-	-	-	0.12	633	384
[33]	732-144	148	2	10	18	71	15	29	-	-	-	-	0.06	414	353
[33]	732-145	148	2	10	20	68	15	29	-	-	-	-	0.06	414	349
[33]	732-146	156	2	10	19	69	15	44	-	-	-	-	0.12	633	441
[33]	732-147	145	2	10	21	71	15	44	-	-	-	-	0.12	633	471
[33]	732-148	157	2	10	21	70	15	44	-	-	-	-	0.06	414	430
[33]	732-149	145	2	10	22	69	15	44	-	-	-	-	0.06	414	389
[33]	732-151	150	2	10	21	68	15	49	-	-	-	-	0.12	638	455
[33]	732-152	144	2	10	20	70	16	49	-	-	-	-	0.06	417	434
[33]	732-153	140	2	10	21	67	15	49	-	-	-	-	0.06	417	424
[33]	732-154	152	2	10	19	69	15	57	-	-	-	-	0.12	638	426
[33]	732-155	156	2	10	20	72	15	57	-	-	-	-	0.12	638	497
[33]	732-156	152	2	10	20	72	15	57	-	-	-	-	0.06	417	495
[33]	732-157	145	2	10	23	66	16	57	-	-	-	-	0.06	417	491
[33]	732-158	152	2	10	21	70	15	72	-	-	-	-	0.12	638	494
[33]	732-159	162	2	10	20	67	13	72	-	-	-	-	0.12	638	471
[33]	732-160	143	2	10	20	69	15	72	-	-	-	-	0.06	417	452
[33]	732-161	142	2	10	20	69	21	72	-	-	-	-	0.06	417	528
[33]	732-175	400	2	8	18	65	20	17	-	-	-	-	0.12	677	688
[33]	732-176	600	2	10	16	63	18	17	-	-	-	-	0.12	623	587
[33]	732-177	800	2	12	14	101	18	21	-	-	-	-	0.12	628	600
[33]	747-1	520	2	25	75	100	37	20	-	-	-	-	0.06	436	270
[33]	747-2	720	2	25	75	100	40	25	-	-	-	-	0.06	438	404
[33]	747-3	920	2	25	75	100	40	29	-	-	-	-	0.06	436	401
[33]	747-4	520	2	25	78	93	37	24	-	-	-	-	0.12	623	296
[33]	747-5	920	2	25	78	92	49	19	-	-	-	-	0.12	628	560
[33]	747-6	1320	2	25	74	100	36	26	-	-	-	-	0.12	625	653
[33]	747-7	520	2	32	62	95	51	36	-	-	-	-	0.06	423	217
[33]	747-8	920	2	32	65	90	38	38	-	-	-	-	0.06	422	305
[33]	747-16	520	2	25	80	93	40	23	-	-	-	-	0.06	494	329
[33]	747-17	720	2	25	74	102	41	43	-	-	-	-	0.06	502	411
[33]	747-18	920	2	25	80	92	49	31	-	-	-	-	0.06	495	554
[33]	123-s8	240	2	16	40	16	25	25	8	2	120	2	0.12	804	338
Author	**Test**	**l_0**	**n_b**	**Ø**	**c_x**	**c_s**	**c_y**	**f_{cm}**	**$Ø_{st}$**	**n_{st}**	**s_t**	**n_l**	**f_R**	**f_y**	**$\sigma_{s,max}$**
		[mm]	-	[mm]	[mm]	[mm]	[mm]	[MPa]	[mm]	-	[mm]	-	-	[MPa]	[MPa]
[33]	123-s9	400	2	16	40	16	25	29	8	2	200	2	0.12	804	474
[33]	123-s10	560	2	16	40	16	25	29	8	2	400	2	0.12	804	670
[33]	123-s13	560	2	16	40	16	25	29	8	6	90	2	0.12	804	744
[33]	123-s14	720	2	16	40	16	25	27	8	6	120	2	0.12	804	729

[33]	123-s18	720	2	16	40	16	25	24	10	6	120	2	0.12	804	685
[33]	657-5	320	2	16	30	36	20	20	6	6	100	2	0.12	844	367
[33]	657-6	520	2	16	30	35	20	20	6	6	100	2	0.12	903	508
[33]	657-7	720	2	16	30	36	20	21	4	6	100	2	0.12	883	669
[33]	657-8	1020	2	16	30	35	20	21	6	6	100	2	0.12	873	814
[33]	657-9	520	2	16	30	36	20	23	4	6	100	2	0.12	883	457
[33]	657-10	520	2	16	30	36	20	23	8	6	100	2	0.12	903	678

A.3.50. THOMPSON; JIRSA [THO79]

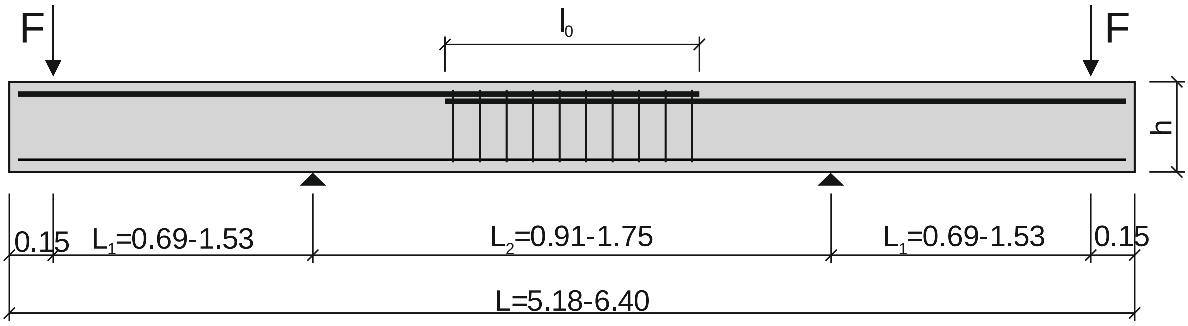

Author	Test	l_0	n_b	Ø	c_x	c_s	c_y	f_{cm}	$Ø_{st}$	n_{st}	s_t	n_l	f_R	f_y	$\sigma_{s,max}$
		[mm]	-	[mm]	[mm]	[mm]	[mm]	[MPa]	[mm]	-	[mm]	-	-	[MPa]	[MPa]
[34]	11-30-4/2/2-6/6-S5	762	6	36	51	102	51	21	10	6	152	6	*	448	329
[34]	11-20-4/2/2/-6/6-SP	508	6	36	51	102	51	22	10	7	85	6	*	464	296
[34]	11-20-4/2/2-6/6-S5	508	6	36	51	102	51	23	10	4	169	6	*	464	285
[34]	8-15-4/2/2-6/6-S5	381	6	25.4	51	102	51	24	10	3	191	6	*	421	400
[34]	6-12-4/2/2-6/6	305	6	19	51	102	51	26	-	-	-	-	*	425	398
[34]	8-18-4/3/2-6/6	457	6	25.4	51	102	76	32	-	-	-	-	*	409	390
[34]	8-18-4/3/2.5-4/6	457	4	25.4	64	102	76	20	-	-	-	-	*	409	345
[34]	8-24-4/2/2-6/6	610	6	25.4	51	102	51	21	-	-	-	-	*	409	353
[34]	11-25-6/2/3-5/5	635	5	36	76	152	51	27	-	-	-	-	*	457	307
[34]	11-30-4/2/2-6/6	762	6	36	51	102	51	20	-	-	-	-	*	417	267
[34]	11-30-4/2/4-6/6	762	6	36	102	102	51	23	-	-	-	-	*	437	311
[34]	11-30-4/2/2.7/4/6	762	4	36	69	102	51	30	-	-	-	-	*	436	400
[34]	11-45-4/1/2-6/6	1143	6	36	51	102	25	24	-	-	-	-	*	417	317
[34]	14-60-4/2/2-5/5	1524	5	43	51	102	51	20	-	-	-	-	*	398	322
[34]	14-6--4/2/4-5/5	1524	5	43	102	102	51	22	-	-	-	-	*	398	391

A.3.51. Treece; Jirsa [TRE89]

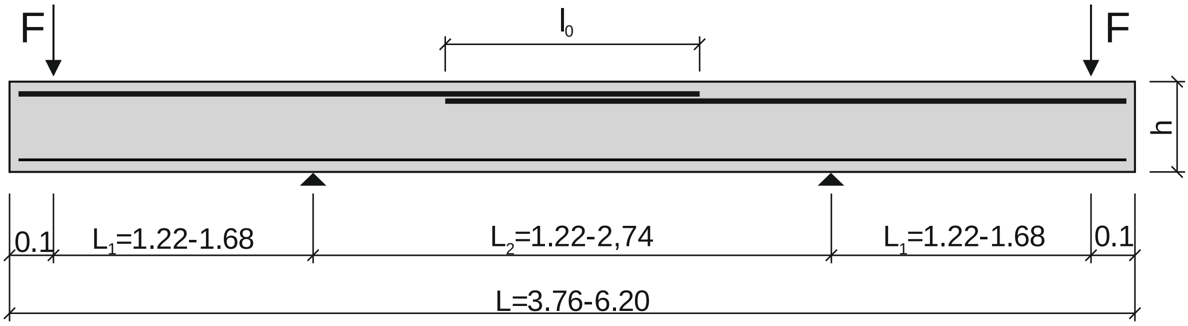

Author	Test	l_0	n_b	Ø	c_x	c_s	c_y	f_{cm}	$Ø_{st}$	n_{st}	s_t	n_l	f_R	f_y	$\sigma_{s,max}$
		[mm]	-	[mm]	[mm]	[mm]	[mm]	[MPa]	[mm]	-	[mm]	-	-	[MPa]	[MPa]
[35]	0-6-12	41	3	19	51	102	19	21	-	-	-	-	*	*	436
[35]	0-6-8	41	3	19	51	102	22	21	-	-	-	-	*	*	435
[35]	0-6-4r	61	3	19	51	102	25	32	-	-	-	-	*	*	433
[35]	0-6-4	30	3	19	51	102	51	16	-	-	-	-	*	*	364
[35]	0-11-12	46	3	36	51	102	51	13	-	-	-	-	*	*	321
[35]	0-11-4b	91	3	36	51	102	51	26	-	-	-	-	*	*	311
[35]	0-11-12b	46	3	36	51	102	51	13	-	-	-	-	*	*	295
[35]	0-11-4	91	3	36	51	102	51	16	-	-	-	-	*	*	294
[35]	0-11-8	46	3	36	51	102	54	13	-	-	-	-	*	*	276

A.3.52. UNTRAUER; HENRY [UNT65]

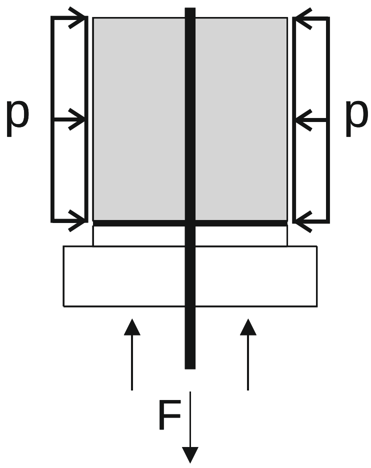

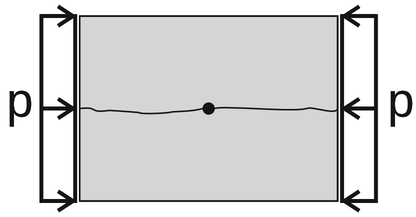

Author	Test	l_0 [mm]	n_b -	Ø [mm]	c_x [mm]	c_s [mm]	c_y [mm]	f_{cm} [MPa]	$Ø_{st}$ [mm]	n_{st} -	s_t [mm]	n_l -	f_R -	f_y [MPa]	$\sigma_{s,max}$ [MPa]
[48]	36910	151	1	28.5	61.9	0	61.9	24.9	-	-	-	-	*	500	232
[48]	36920	151	1	28.5	61.9	0	61.9	24.9	-	-	-	-	*	500	288
[48]	45905	151	1	28.5	61.9	0	61.9	30.9	-	-	-	-	*	500	233
[48]	47910	151	1	28.5	61.9	0	61.9	32.6	-	-	-	-	*	500	314
[48]	51915	151	1	28.5	61.9	0	61.9	35.1	-	-	-	-	*	500	308
[48]	51920	151	1	28.5	61.9	0	61.9	35.1	-	-	-	-	*	500	357
[48]	47925	151	1	28.5	61.9	0	61.9	32.6	-	-	-	-	*	500	408
[48]	43935	151	1	28.5	61.9	0	61.9	29.5	-	-	-	-	*	500	320
[48]	43950	151	1	28.5	61.9	0	61.9	29.5	-	-	-	-	*	500	335
[48]	47950	151	1	28.5	61.9	0	61.9	32.7	-	-	-	-	*	500	458
[48]	64905	151	1	28.5	61.9	0	61.9	44.2	-	-	-	-	*	500	290
[48]	69905	151	1	28.5	61.9	0	61.9	40.8	-	-	-	-	*	500	246
[48]	65915	151	1	28.5	61.9	0	61.9	44.6	-	-	-	-	*	500	431
[48]	69920	151	1	28.5	61.9	0	61.9	47.7	-	-	-	-	*	500	385
[48]	65930	151	1	28.5	61.9	0	61.9	44.6	-	-	-	-	*	500	466
[48]	36605	152	1	19	61.9	0	61.9	24.9	-	-	-	-	*	500	347
[48]	36625	152	1	19	66.7	0	66.7	24.9	-	-	-	-	*	500	332
[48]	47605	152	1	19	66.7	0	66.7	32.6	-	-	-	-	*	500	430
[48]	43610	152	1	19	66.7	0	66.7	29.5	-	-	-	-	*	500	399
[48]	51615	152	1	19	66.7	0	66.7	35.1	-	-	-	-	*	500	393
[48]	47620	152	1	19	66.7	0	66.7	32.6	-	-	-	-	*	500	521
[48]	51625	152	1	19	66.7	0	66.7	35.1	-	-	-	-	*	500	519
[48]	43630	152	1	19	66.7	0	66.7	29.5	-	-	-	-	*	500	458
[48]	47650	152	1	19	66.7	0	66.7	32.7	-	-	-	-	*	500	652
[48]	65610	152	1	19	66.7	0	66.7	44.6	-	-	-	-	*	500	544
[48]	64620	152	1	19	66.7	0	66.7	44.2	-	-	-	-	*	500	644
[48]	69620	152	1	19	66.7	0	66.7	47.7	-	-	-	-	*	500	469
[48]	65630	152	1	19	66.7	0	66.7	44.6	-	-	-	-	*	500	671

A.3.53. ZEKANY [ZEK81]

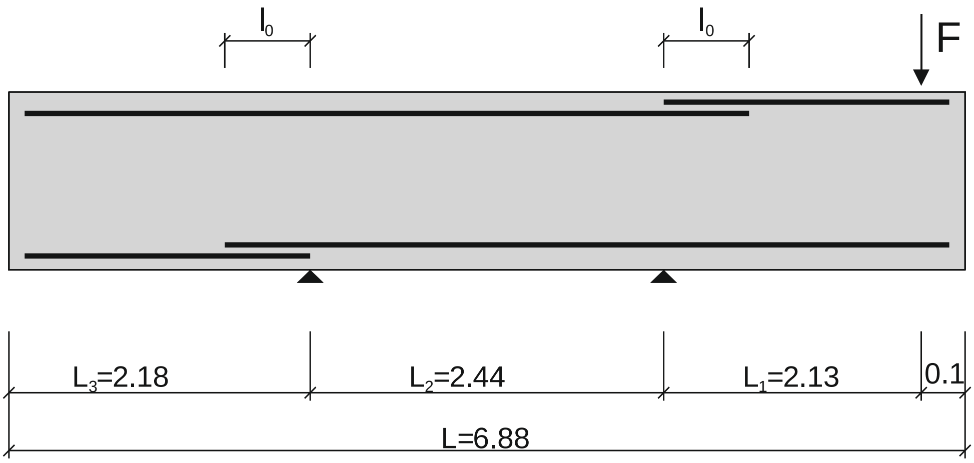

Author	Test	l_0	n_b	Ø	c_x	c_s	c_y	f_{cm}	$Ø_{st}$	n_{st}	s_t	n_l	f_R	f_y	$\sigma_{s,max}$
		[mm]	-	[mm]	[mm]	[mm]	[mm]	[MPa]	[mm]	-	[mm]	-	-	[MPa]	[MPa]
[36]	11-40-B-A	559	4	36	51	102	51	37	6	5	114	2	*	414	311
[36]	2-4.5-80-B	559	4	36	51	102	51	29	6	5	114	2	*	414	295
[36]	2-5-40-B(4)	559	4	36	51	102	51	27	6	4	114	4	*	414	289
[36]	3-5-53-B	559	4	36	51	102	51	26	10	4	127	2	*	414	274
[36]	2-4.5-53-B	559	4	36	51	102	51	28	6	5	114	2	*	414	292
[36]	11-53-B	559	4	36	51	102	51	28	6	5	114	2	*	414	294
[36]	11-40-B	559	4	36	51	102	51	35	6	5	114	2	*	414	316
[36]	11-53-B-D	559	4	36	51	102	51	28	6	5	114	2	*	414	235
[36]	3-5-40-B	559	4	36	51	102	51	26	10	4	127	2	*	414	266
[36]	9-53-B	406	5	28.6512	51	76	51	39	6	4	114	2	*	433	397
[36]	9-53-B-N	406	5	28.6512	51	72	51	39	-	-	-	-	*	433	329
[36]	N-N-80-B	559	4	36	51	94	51	26	-	-	-	-	*	414	264

A.3.54. ZUO; DARWIN [ZUO98]

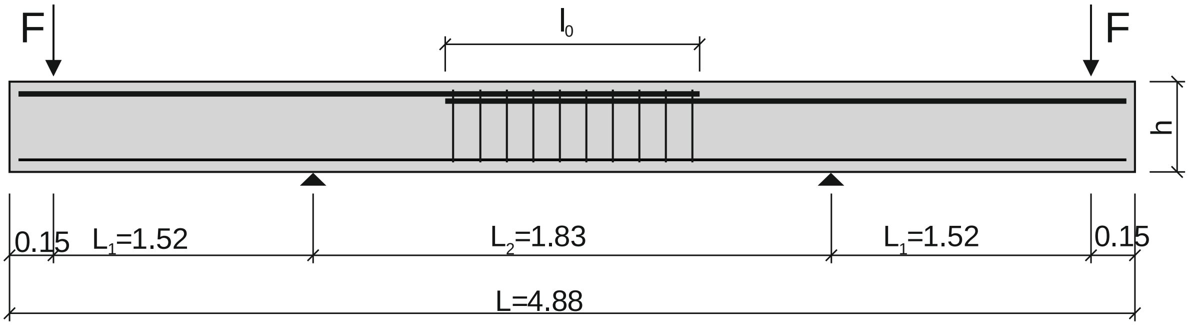

Author	Test	l_0	n_b	Ø	c_x	c_s	c_y	f_{cm}	$Ø_{st}$	n_{st}	s_t	n_l	f_R	f_y	$\sigma_{s,max}$
		[mm]	-	[mm]	[mm]	[mm]	[mm]	[MPa]	[mm]	-	[mm]	-	-	[MPa]	[MPa]
[37]	19.1-B-S-U	914	3	25.4	50	98	50	29	-	-	-	-	0.119	556	503
[37]	19.2-B-N-U^^	914	3	25.4	51	96	49	29	-	-	-	-	0.119	556	465
[37]	20.6-B-S-U	1016	3	25.4	38	34	33	35	-	-	-	-	0.119	556	392
[37]	23a.5-B-S-U	559	2	25.4	51	96	49	64	-	-	-	-	0.119	556	431
[37]	23a.6-B-S-U	737	2	25.4	52	95	49	64	-	-	-	-	0.119	556	522
[37]	23b.3-B-S-U	495	2	25.4	77	196	78	58	-	-	-	-	0.119	556	494
[37]	24.1-B-S-U	813	2	25.4	51	95	48	30	-	-	-	-	0.121	545	425
[37]	25.1-B-S-U	419	3	15.9	50	52	40	31	-	-	-	-	0.141	434	438
[37]	26.3-B-S-U	1016	3	25.4	39	33	48	34	-	-	-	-	0.121	545	428
[37]	26.5-B-S-U	1016	3	25.4	38	35	48	34	-	-	-	-	0.069	538	440
[37]	28.5-B-S-U	762	2	36	50	205	51	87	-	-	-	-	0.127	536	352
[37]	30.5-B-S-U	762	2	36	52	204	50	91	-	-	-	-	0.127	536	463
[37]	31.5-B-S-U	559	3	25.4	46	26	38	89	-	-	-	-	0.121	545	425
[37]	31.6-B-S-U	559	3	25.4	44	27	38	89	-	-	-	-	0.085	479	438
[37]	32.1-B-S-U	813	2	36	51	50	48	99	-	-	-	-	0.127	536	438
[37]	32.2-B-S-U	813	2	36	51	54	49	99	-	-	-	-	0.07	460	425
[37]	32.3-B-S-U	813	2	36	50	204	49	99	-	-	-	-	0.127	536	419
[37]	32.4-B-S-U	711	2	36	52	206	49	99	-	-	-	-	0.07	460	422
[37]	34.1-B-S-U	610	3	25.4	52	98	49	38	-	-	-	-	0.121	545	398
[37]	34.2-B-N-U^^	610	3	25.4	53	99	49	38	-	-	-	-	0.121	545	426
[37]	34.3-B-S-U	610	3	25.4	53	94	50	38	-	-	-	-	0.085	479	405
[37]	34.4-B-N-U^^	610	3	25.4	52	96	49	38	-	-	-	-	0.085	479	402
[37]	36.3-B-S-U	660	3	25.4	51	93	51	35	-	-	-	-	0.085	479	431
[37]	36.4-B-N-U^^	660	3	25.4	52	93	50	35	-	-	-	-	0.085	479	414
[37]	38.1-B-N-U^^	660	3	25.4	49	99	46	35	-	-	-	-	0.085	479	373
[37]	38.2-B-S-U	660	3	25.4	54	94	53	35	-	-	-	-	0.085	479	416
[37]	39.6-B-S-U	533	3	25.4	50	26	38	100	-	-	-	-	0.101	467	451
[37]	40.5-B-S-U	432	2	25.4	51	95	47	108	-	-	-	-	0.069	538	455
[37]	19.3-B-S-U	762	3	25.4	52	96	48	29	10	3	381	2	0.119	556	489
[37]	19.4-B-N-U^^	762	3	25.4	52	96	48	29	10	3	381	2	0.119	556	528
[37]	20.1-B-S-U	1016	3	36	51	67	47	35	13	8	145	2	0.127	536	483
[37]	20.2-B-N-U^^	1016	3	36	51	66	47	35	13	8	145	2	0.127	536	488
[37]	20.3-B-S-U	1016	3	36	51	67	46	35	13	5	254	2	0.127	536	466
[37]	20.4-B-N-U^^	1016	3	36	52	66	47	35	13	5	254	2	0.127	536	460
[37]	21.1-B-S-U	610	3	25.4	45	25	37	30	16	6	122	2	0.119	556	502
[37]	21.3-B-S-U	635	3	25.4	42	29	38	30	16	5	159	2	0.119	556	518
[37]	21.5-B-S-U	635	2	25.4	42	113	36	30	13	5	159	2	0.119	556	529
[37]	23a.1-B-S-U	533	3	25.4	55	94	49	63	10	4	178	2	0.119	556	545
[37]	23a.3-B-N-U^^	533	3	25.4	52	97	48	63	10	4	178	2	0.119	556	546
[37]	23a.4-B-S-U	533	3	25.4	51	96	49	63	10	4	178	2	0.119	556	547
Author	Test	l_0	n_b	Ø	c_x	c_s	c_y	f_{cm}	$Ø_{st}$	n_{st}	s_t	n_l	f_R	f_y	$\sigma_{s,max}$
		[mm]	-	[mm]	[mm]	[mm]	[mm]	[MPa]	[mm]	-	[mm]	-	-	[MPa]	[MPa]

[37]	23b.1-B-S-U	445	3	25.4	37	36	50	58	13	5	111	2	0.119	556	544
[37]	26.1-B-S-U^	762	3	25.4	40	33	48	34	10	6	152	2	0.121	545	442
[37]	27.1-B-S-U^	572	3	25.4	48	25	37	75	10	6	114	2	0.121	545	544
[37]	27.2-B-S-U	572	3	25.4	51	24	36	75	10	6	114	2	0.069	538	533
[37]	27.3-B-S-U^	445	3	25.4	49	23	37	75	13	5	111	2	0.121	545	537
[37]	27.4-B-S-U	445	3	25.4	51	23	37	75	13	5	111	2	0.069	538	533
[37]	27.5-B-S-U^	457	3	25.4	102	48	36	75	13	4	152	2	0.121	545	532
[37]	27.6-B-S-U	457	3	25.4	102	47	37	75	13	4	152	2	0.069	538	531
[37]	28.1-B-S-U	635	2	36	56	39	48	87	10	5	159	2	0.127	536	492
[37]	28.3-B-S-U	711	3	36	55	63	48	87	10	4	237	2	0.127	536	463
[37]	29.1-B-S-U^	508	3	25.4	45	25	37	73	10	5	127	2	0.121	545	553
[37]	29.2-B-S-U	508	3	25.4	48	25	38	73	10	5	127	2	0.069	538	576
[37]	29.3-B-S-U^	457	3	25.4	47	25	37	73	10	6	91	2	0.121	545	540
[37]	29.4-B-S-U	457	3	25.4	49	25	36	73	10	6	91	2	0.069	538	527
[37]	29.5-B-S-U^	406	3	25.4	99	49	37	73	10	4	135	2	0.121	545	523
[37]	29.6-B-S-U	406	3	25.4	99	50	36	73	10	4	135	2	0.069	538	537
[37]	30.1-B-S-U	635	2	36	60	35	48	91	10	3	318	2	0.127	536	456
[37]	30.3-B-S-U	711	3	36	50	65	48	91	10	2	711	2	0.127	536	462
[37]	31.1-B-S-U^	406	2	25.4	51	95	39	89	10	2	406	2	0.121	545	472
[37]	31.3-B-S-U	406	2	25.4	50	98	37	89	10	2	406	2	0.069	538	451
[37]	33.1-B-S-U^	457	3	25.4	52	22	50	37	13	6	91	2	0.121	545	420
[37]	33.2-B-S-U	457	3	25.4	50	20	49	37	13	6	91	2	0.085	479	421
[37]	33.3-B-S-U^	457	3	25.4	53	97	50	37	10	4	152	2	0.121	545	396
[37]	33.4-B-S-U	457	3	25.4	52	97	49	37	10	4	152	2	0.085	479	401
[37]	33.5-B-S-U^	559	2	25.4	52	95	49	36	10	2	559	2	0.121	545	388
[37]	33.6-B-S-U	559	2	25.4	53	86	48	36	10	2	559	2	0.085	479	399
[37]	35.1-B-S-U	508	2	25.4	37	121	49	37	10	5	127	2	0.14	520	470
[37]	35.3-B-S-U	508	2	25.4	38	115	49	37	10	5	127	2	0.085	479	425
[37]	36.1-B-S-U^	610	3	25.4	49	25	37	35	16	6	122	2	0.121	545	528
[37]	36.2-B-S-U^	533	3	25.4	50	25	36	35	13	7	89	2	0.121	545	463
[37]	37.4-B-S-U	533	3	25.4	51	25	38	33	13	7	89	2	0.14	520	503
[37]	38.3-B-S-U^	610	3	25.4	49	25	37	35	16	6	122	2	0.121	545	471
[37]	38.4-B-S-U^	533	3	25.4	50	25	36	35	13	7	89	2	0.121	545	419
[37]	38.5-B-S-U^	610	2	25.4	52	95	37	35	10	6	122	2	0.121	545	466
[37]	38.6-B-S-U^	660	2	25.4	50	98	45	35	10	2	660	2	0.121	545	391
[37]	39.2-B-S-U	406	3	25.4	48	26	37	100	10	4	135	2	0.101	467	477
[37]	39.3-B-S-U	406	3	25.4	48	25	38	100	10	4	135	2	0.069	538	524
[37]	40.1-B-S-U	584	2	36	52	51	37	108	10	4	195	2	0.127	536	461
[37]	40.4-B-S-U	584	2	36	51	54	37	108	10	4	195	2	0.072	452	407
[37]	41.1-B-S-U	406	2	25.4	51	94	39	70	10	2	406	2	0.119	556	457
[37]	41.2-B-S-U	406	3	25.4	48	24	38	70	16	4	135	2	0.119	556	568
[37]	41.3-B-S-U	406	3	25.4	48	23	48	70	13	4	135	2	0.119	556	547
[37]	41.4-B-S-U	406	3	25.4	48	25	37	70	16	4	135	2	0.069	538	533
[37]	41.5-B-N-U^^	406	3	25.4	51	95	50	72	10	2	406	2	0.085	479	456
[37]	41.6-B-S-U	406	3	25.4	51	95	50	72	10	2	406	2	0.085	479	452
[37]	42.1-B-S-U	406	2	25.4	51	94	47	82	10	2	406	2	0.069	538	445
[37]	42.4-B-S-U	406	3	25.4	48	25	46	82	13	4	135	2	0.069	538	488
[37]	42.5-B-S-U	406	3	25.4	48	25	37	82	16	4	135	2	0.069	538	524
[37]	43.2-B-S-U	406	2	25.4	52	95	47	79	10	2	406	2	0.119	556	449
[37]	43.3-B-S-U	406	3	25.4	47	25	47	79	13	4	135	2	0.119	556	544
[37]	43.6-B-S-U	406	3	25.4	48	25	38	79	16	4	135	2	0.119	556	564